به نام خدا

مرکز دانلود رایگان
مهندسی متالورژی و مواد

www.Iran-mavad.com

WOODHEAD PUBLISHING IN MATERIALS

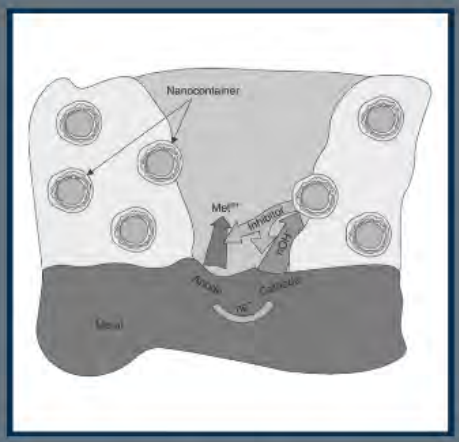

Corrosion protection and control using nanomaterials

Edited by Viswanathan S. Saji and Ronald Cook

WP
WOODHEAD PUBLISHING

Corrosion protection and control using nanomaterials

Related titles:

Laser surface modification of metals for corrosion and erosion resistance
(ISBN 978-0-85709-015-7)
Laser surface modification (LSM) offers many advantages over conventional surface engineering technologies. LSM can selectively modify surface composition and microstructure without having an adverse effect on surrounding material properties or causing serious thermal distortion. This book reviews a range of LSM techniques. Part I discusses methods for improving corrosion and cracking resistance. Part II considers techniques for improving erosion-corrosion resistance for metals exposed to hostile environmental conditions.

Gaseous hydrogen embrittlement of metals in energy technologies Volume 1: The problem, its characterisation and effects on particular alloy classes
(ISBN 978-1-84569-677-1)
This important two-volume book reviews the problem of degradation of metals and other materials exposed to hydrogen. The first part of Volume 1 begins by discussing how the problem of gaseous hydrogen embrittlement affects such sectors as the petrochemicals, automotive, nuclear and other energy industries. Part II reviews ways of characterising and testing for hydrogen-assisted fatigue and fracture. A final group of chapters analyse the ways gaseous hydrogen embrittlement affects high-performance steels, superalloys, titanium and aluminium alloys.

Gaseous hydrogen embrittlement of metals in energy technologies Volume 2: Mechanisms, modelling and future developments
(ISBN 978-0-85709-536-7)
This important two-volume book reviews the problem of degradation of metals and other materials exposed to hydrogen. The first part of Volume 2 reviews the mechanisms of hydrogen embrittlement, including absorption, diffusion and trapping of hydrogen in metals. Part II discusses ways of modelling hydrogen-induced damage and assessing service life. The final section in the book assesses future trends in research.

Details of these and other Woodhead Publishing materials books can be obtained by:

- visiting our web site at www.woodheadpublishing.com
- contacting Customer Services (e-mail: sales@woodheadpublishing.com; fax: +44 (0) 1223 832819; tel.: +44 (0) 1223 499140 ext. 130; address: Woodhead Publishing Limited, 80 High Street, Sawston, Cambridge CB22 3HJ, UK)
- contacting our US office (e-mail: usmarketing@woodheadpublishing.com; tel. (215) 928 9112; address: Woodhead Publishing, 1518 Walnut Street, Suite 1100, Philadelphia, PA 19102-3406, USA)

If you would like e-versions of our content, please visit our online platform: www.woodheadpublishingonline.com. Please recommend it to your librarian so that everyone in your institution can benefit from the wealth of content on the site.

Corrosion protection and control using nanomaterials

Edited by
Viswanathan S. Saji and Ronald Cook

Oxford Cambridge Philadelphia New Delhi

Published by Woodhead Publishing Limited,
80 High Street, Sawston, Cambridge CB22 3HJ, UK
www.woodheadpublishing.com
www.woodheadpublishingonline.com

Woodhead Publishing, 1518 Walnut Street, Suite 1100, Philadelphia, PA 19102-3406, USA

Woodhead Publishing India Private Limited, G-2, Vardaan House, 7/28 Ansari Road,
Daryaganj, New Delhi – 110002, India
www.woodheadpublishingindia.com

First published 2012, Woodhead Publishing Limited

British Library Cataloguing in Publication Data
A catalogue record for this book is available from the British Library.

Library of Congress Control Number: 2011943548

ISBN 978-1-84569-949-9 (print)
ISBN 978-0-85709-580-0 (online)

The publisher's policy is to use permanent paper from mills that operate a sustainable forestry policy, and which has been manufactured from pulp which is processed using acid-free and elemental chlorine-free practices. Furthermore, the publisher ensures that the text paper and cover board used have met acceptable environmental accreditation standards.

Typeset by RefineCatch Limited, Bungay, Suffolk, UK
Printed by TJI Digital, Padstow, Cornwall, UK

Contents

Contributor contact details

(* = main contact)

Editors

Viswanathan S. Saji
Department of Advanced Materials Chemistry
Korea University
Jochiwon
Choongnam 339-700
South Korea
E-mail: vssaji@korea.ac.kr

Ronald Cook
TDA Research, Inc.
12345 W. 52nd Avenue
Wheat Ridge, CO 80033
USA
E-mail: cookrl@tda.com

Chapter 1

Viswanathan S. Saji
Department of Advanced Materials Chemistry
Korea University
Jochiwon
Choongnam 339-700
South Korea
E-mail: vssaji@korea.ac.kr

Chapter 2

S. Roy
School of Chemical Engineering and Advanced Materials
Faculty of Science, Agriculture and Engineering
Newcastle University
Newcastle-upon-Tyne
NE1 7RU
UK
E-mail: s.roy@ncl.ac.uk

Chapter 3

X. Y. Zhang
School of Materials Science and Engineering
Chongqing University
Chongqing 400044
China
E-mail: kehen888@163.com

Chapter 4

L. Ying* and L. Liu
State Key Laboratory for Corrosion and Protection
Institute of Metal Research
Chinese Academy of Sciences
Shenyang 110016
China
E-mail: liying@imr.ac.cn

Chapter 5

D. Sobha Jayakrishnan
Electroplating and Metal Finishing Technology Division
CSIR – Central Electrochemical Research Institute
Karaikudi 630006
Tamil Nadu
India
E-mail: sobha.jayakrishnan@gmail.com

Chapter 6

R. K. Singh Raman*
Department of Mechanical and Aerospace Engineering
Department of Chemical Engineering
Monash University
Melbourne
Victoria 3800
Australia
E-mail: raman.singh@monash.edu

P. Singh
Centre for Clean Energy Engineering
University of Connecticut
44 Weavers Road
Storrs, CT 06269-5233
USA
E-mail: singh@engr.uconn.edu

Chapter 7

W. Gao* and Z. Li
Department of Chemical and Materials Engineering
The University of Auckland
Private Bag 92019
Auckland
New Zealand
E-mail: w.gao@auckland.ac.nz

Y. He
Beijing Key Laboratory for Corrosion, Erosion and Surface Technology
University of Science and Technology Beijing
Beijing 100083
China

Chapter 8

T. S. N. Sankara Narayanan
National Metallurgical Laboratory
Madras Centre
CSIR Complex
Taramani
Chennai 600 113
India
E-mail: tsnsn@rediffmail.com

Chapter 9

M. G. S. Ferreira*, M. L. Zheludkevich, J. Tedim and K. A. Yasakau
Department of Ceramics and Glass Engineering
University of Aveiro
Campus Santiago
Aveiro 3810-193
Portugal
E-mail: mgferreira@cv.ua.pt

Chapter 10

D. G. Shchukin* and D. O. Grigoriev
Max-Planck Institute of Colloids and Interfaces
Am Muehlenberg 1
14476 Potsdam-Golm
Germany
E-mail: dmitry.shchukin@mpikg.mpg.de

Chapter 11

Susai Rajendran
Corrosion Research Centre
Department of Chemistry
RVS School of Engineering and Technology
Dindigul-624 005
Tamilnadu
India
E-mail: susairajendran@gmail.com

Chapter 12

S. S. Pathak* and A. S. Khanna
Department of Metallurgical Engineering and Materials Science
Indian Institute of Technology Bombay
Mumbai 40076
India
E-mail: pathak.iitb@gmail.com; khanna@iitb.ac.in

Chapter 13

C.-J. Weng, C.-H. Chang and J.-M. Yeh*
Chung Yuan Christian University
Chung Li 32023
Taiwan
E-mail: juiming@cycu.edu.tw

Chapter 14

R. Asmatulu
Department of Mechanical Engineering
Wichita State University
1845 Fairmount
Wichita, KS 67260-0133
USA
E-mail: ramazan.asmatulu@wichita.edu

Chapter 15

M. Bobby Kannan*
Discipline of Chemical Engineering
School of Engineering and Physical Sciences
James Cook University
Townsville 4811
Australia
E-mail: bobby.mathan@jcu.edu.au

Viswanathan S. Saji*
Department of Advanced Materials Chemistry
Korea University
Jochiwon
Choongnam 339-700
South Korea
E-mail: vssaji@korea.ac.kr

Preface

We are pleased to present the book *Corrosion protection and control using nanomaterials* on the fiftieth anniversary of Richard Feynman's classic lecture, 'There's plenty of room at the bottom'. The science and technology of nanomaterials is without a doubt the major turning point in the industrial development of the twenty-first century. Most industrial sectors and biosciences are benefiting greatly from manipulation of materials at the nanometer scale. Corrosion is the biggest threat to many industries. How has nanotechnology benefited the field of corrosion prevention? What are the corrosion behaviors of nanocrystalline materials? What about their high temperature oxidation? How can nanoparticles help improve the barrier properties of a coating? There are many questions to be addressed and we have attempted to answer a few of them.

Chapter 1 provides an overview of the current understanding of the problem of corrosion. The chapter also provides a brief introduction to nanomaterials in this context. Chapter 2 discusses corrosion basics with reference to nanostructured materials. Chapter 3 addresses theoretical aspects of grain size reduction on corrosion with a model example and comparison with experimental results of nanocrystalline zirconium and its alloys. Chapter 4 provides a good account of the relevant electrochemical aspects of nanostructured materials. The nature of passive film and its correlation with nanocrystallization are explained. Chapter 5 gives a good description of fabrication of electrodeposited nanostructured materials.

Chapters 6 to 15 address the usage of nanomaterials in different corrosion prevention strategies. Chapters 6 and 7 are on the moderate and high temperature oxidation resistance of nanocrystalline materials. While Chapter 6 provides a general and current understanding on the topic and an elaborate description of the author group's hypothesis on low chromium alloys, Chapter 7 gives an overview of the research works at the University of Auckland in collaboration with the University of Science and Technology Beijing, on the development of nanostructured high temperature oxidation resistance coatings. Chapter 8 gives a detailed account of tribocorrosion and the role of nanomaterials.

Chapters 9 and 10 are on self-healing nanocoatings. Chapter 9 gives a comprehensive explanation of both self-healing conventional and recent

nanotechnology associated coatings; Chapter 10 explains specifically the nanocarriers in the coatings. Chapter 11 gives an account of nanostructured carriers and self-assembled monolayers in corrosion prevention.

Chapter 12 provides a comprehensive description of sol–gel coatings for corrosion prevention. The chapter also gives an interesting introduction to nanomaterials and corrosion. Chapter 13 discusses polymer nanocomposite coatings, which are of prime importance in barrier protection. The chapter provides a good description of the inorganic–organic hybrid technology. Currently investigated nanostructured coatings for aerospace applications are discussed in Chapter 14. Chapter 15 discusses current nanotechnological approaches to making advanced biomaterials and their impact on corrosion resistance.

We hope that this book will contribute significantly to the science and technology of corrosion control.

Viswanathan S. Saji
Ronald Cook

1

The impact of nanotechnology on reducing corrosion cost

V. S. SAJI, Korea University, South Korea

Abstract: Nanoscience and nanotechnology have revolutionized the present day scientific world, leading to the development of new tools and techniques. Materials at nanometer scale possess many advantages over their micrometer scale counterparts. The key aspect in many applications is the efficient design of nanomaterials in which the desirable pros can be distinguishably emphasized and the undesirable cons can be properly suppressed. Widespread efforts are underway to promote their effective use in the realm of corrosion control. Employing nanomaterials can enhance a material's performance significantly in certain areas of corrosion control; for example, in an advanced coating. Availability and economic synthesis strategies of nanomaterials are key points. More studies are needed to corroborate the use of nanomaterials in different areas of corrosion control and to authenticate the corrosion/oxidation performance of nanostructured materials.

Key words: nanomaterials, corrosion control, coatings.

1.1 Introduction

1.1.1 Nanostructured materials

Materials with morphological features on the nanoscale (usually smaller than 100 nm) in at least one dimension are referred to as nanomaterials (Nalwa, 2000). For convenience of discussion, they can be classified as nanosized and nanostructured materials (Fig. 1.1). A nanostructured material (also referred to as a nanocrystalline or nanophase material) can be defined as one with nanoscale morphological features constructed using a combination of nanosized (e.g. grain size, particle size, structure size, etc.), materials and/or nanoscale empty spaces. Examples include secondary structures consisting of primary nanoparticles, nanograined metals/alloys/ceramics, nanoporous structures, nanocomposites, etc. The overall property of a nanostructured material depends essentially on parameters such as the size and distribution of the constituent phases (particle, grain, phase, etc.), nature of grain boundaries and interaction between the phases. Due to the small size of the building blocks, high surface to volume ratio and the very high relative number of atoms in the grain/phase boundaries, these materials are expected to have improved and diversified properties when compared with their microstructured counterparts. Significant progress has been made in recent years in various aspects of processing nanostructured materials; for example, nanostructured coatings.

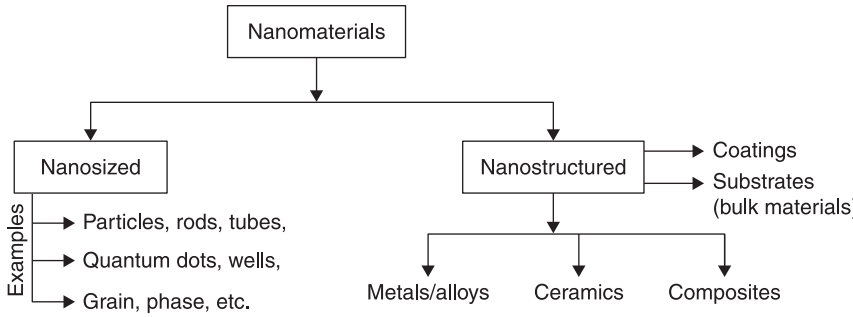

1.1 Schematic showing nanomaterials.

Nanotechnologists have achieved significant milestones in electronics, computer technology, microscopy and biotechnology, which are in commercial practice. Presently, nanomaterials are in commercial use in cosmetics, sunscreens, dental fillings, water filtration systems, catalytic systems, high sensitivity sensors, photovoltaic cells, flash drives, cutting tools, insulation materials, paints, etc. For example, the addition of nanoparticles to paint prevents dust sticking to its surface and prolongs service life through resistance to wear, tear and corrosion. There are products on the market specifically offering hard coatings and easy to clean coatings (Schmidt, 2010). According to the consumer product inventory maintained by a US-based project on emerging nanotechnologies, over 600 nanoproducts are already on the market worldwide and their value is expected to reach US$1 trillion by 2015 (PEN, 2011). Many promising projects are ongoing, both industrial and academic, which can bring huge benefits.

In spite of the dramatic increase in commercial products based on nanomaterials, there exist many challenges in the commercial application of nanotechnology in various fields. The potential adverse human health effect scenario resulting from exposure to novel nanomaterials, referred to as 'nanotoxicity', is a major concern (Brayner, 2008). In many application areas, more authentic studies are required to substantiate the efficiency of nanostructured materials. Extensive research efforts are being devoted to validating the applicability of nanomaterials in many key application areas including energy conversion (Saji, *et al*., 2011a; Saji *et al*., 2011b), biomedical (Saji *et al*., 2010), corrosion prevention (Saji and Thomas, 2007; Nik Masdek and Alfantazi, 2010), etc.

1.1.2 Cost of corrosion

In spite of much advancement in the science and technology of corrosion prevention and control, the phenomenon of corrosion (usually of metals and alloys) continues to pose a major concern to many industries around the world. The direct and indirect cost of corrosion is huge (estimated to be US$2.2 trillion

annually in direct costs worldwide) (WCO, 2011). A good portion of the loss can be avoided by proper corrosion control and monitoring.

In general, corrosion can be prevented by suitable modifications in: material (e.g. selection of corrosion resistant materials), environment (e.g. addition of inhibitors) and material surfaces (e.g. coatings). Metals can be protected cathodically (e.g. cathodic protection) as well as anodically (e.g. passivation). In practice, effective corrosion control is achieved by combining two or more of these methods. Usually, highly corrosion resistant materials are associated with a high cost factor. Even then, such materials can undergo degradation in severe environments/stress. The use of cheaper metallic materials along with proper corrosion control strategies is therefore economic for many applications.

Corrosion protection by coatings (painting, plating, anodizing, galvanizing, etc.) can be passive (providing only a barrier effect) or active (corrosion inhibitors are incorporated in coatings) or a combination of both. A passive coating works by providing a barrier of corrosion resistant material between the damaging environment and the otherwise lower cost structural material. In general, an industrial coating system (e.g. aircraft coating) usually consists of three individual layers: conversion coating/anodization layer, a second primer layer (pigmented organic resin matrix, principal provider of corrosion resistance) and a top polyurethane/polyol resin coat (principal barrier coating). The reader is referred to reference textbooks available for further reading on corrosion (Uhlig and Review, 1985; Fontana and Greene, 1986).

1.2 Nanotechnology and corrosion

When conferring corrosion control by nanomaterials, there are two main considerations. The first aspect is the understanding of corrosion behaviors of nanostructured materials; whether or not a nanostructured material possesses better corrosion resistance (e.g. corrosion/oxidation/cracking resistance of a nanostructured steel substrate/coating) when compared with the microstructured counterpart (see Section 1.3). The second aspect is how nanosized materials can be effectively employed in corrosion prevention strategies (e.g. in an automobile or aerospace coating) (see Section 1.4), an area where nanotechnology corrosion control benefits are considerable. Nanotechnological advancements are expected to improve corrosion monitoring and inspection sectors. Figure 1.2 shows a correlation between ‘nano’ and ‘corrosion’.

Enhancement of corrosion resistance can bring huge dividends, as nanostructured materials are also superior in mechanical and electronic properties. Nanostructured metals, which are expected to be stronger, harder and tougher, can provide very hard coatings that are more resistant to corrosion, useful for applications in defense armor, aerospace components, construction equipment, medical devices, sports equipment, etc. Efforts are focused on the commercialization of nanostructured alloys (steel, cobalt alloys, etc.) as well as nanostructured bulk metals (Cu, Ni, Zr, Ti, etc.). A number of leading research and development institutes and companies

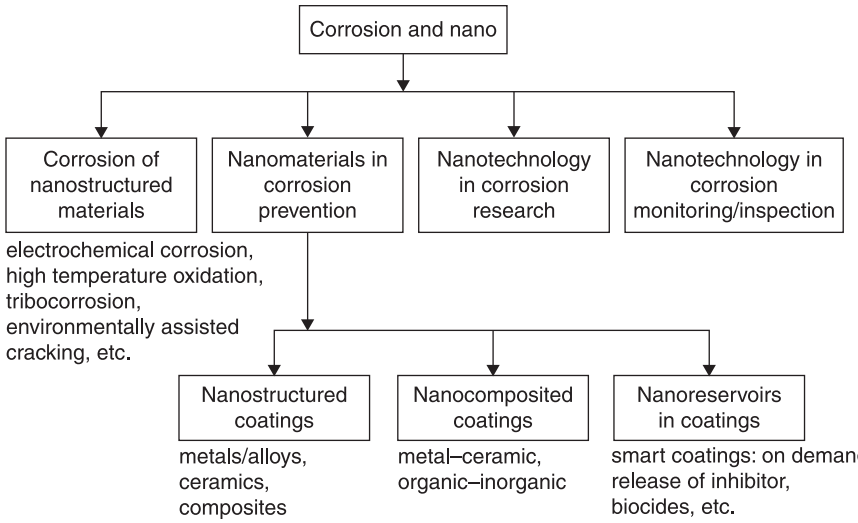

1.2 Diagram showing correlation of nanotechnology with corrosion.

are pursuing research in the area of nanostructured steels (Branagan, 2005). The negative aspect to the strength and hardness of nanostructured metals is that they tend to be less ductile.

There are various strategies available (both vacuum and non-vacuum based) for the fabrication of nanostructured materials, among which simple and economic solution-based (non-vacuum) approaches such as electrodeposition and sol–gel techniques are particularly interesting. Electrodeposition is perhaps the cheapest strategy for making nanocrystalline metals, alloys and metal matrix composites, both in bulk form and as coatings (Schwarzacher, 2006). Electrodeposited nanostructured cobalt alloys are potential replacements for hard chromium in wear and corrosion application. By modifying the plating bath chemistry and current wave forms it may be possible to promote nucleation and hinder growth of crystals to produce finer nanocrystalline materials (grain sizes down to 10 nm). Likewise, many investigations have been performed on silica, zirconia, titania and their composite sol–gel thin films for application in corrosion protection.

Nanotechnology has led to the development of paints and finishing materials with self-healing, self-cleaning and discoloration resistance in addition to the expected high scratch and wear resistance. Nanotechnology has also enabled the exploration of alternatives to chromate conversion coatings, which are hazardous because of the presence of toxic hexavalent chromium (Voevodin *et al*., 2003). In this direction, nanoparticle/nanostructured carriers have become a major area of interest in developing smart coatings with ‘on-demand releasable’ corrosion inhibitors and biocides (Cook *et al*., 2005).

Nanocomposite technology is already in commercial practice in certain application areas. Nanocomposites are proven to have enhanced properties for applications ranging from aerospace components to bioimplants. A polymer nanocomposite (e.g. polymer–nanoclay) coating can effectively combine the benefits of organic polymers, such as elasticity and water resistance, with those of advanced inorganic materials, such as hardness (Pang and Zhitomirsky, 2005; Wang *et al*., 2006). Nanostructured ceramic (nanostructured diamond, metalloceramics, hydroxyapatite, etc.) and composite coatings increase general corrosion resistance of bioimplants in addition to the expected property enhancement of bioactivity and wear resistance (Catledge *et al*., 2004). Nanoparticles of diamond and other chemical compounds used for hard coatings (SiC, ZrO_2 and $A1_2O_3$) are commercially available, with typical particle sizes in the range 4–300 nm. Nano ZrO_2 powder has been used to coat engine components by plasma spray (Jensen and Sorensen, 1996).

Studies suggest that nanocrystalline alloy coatings and composite ceramic coatings possess improved high temperature oxidation resistance (Gao and Li, 2004; Yao *et al*., 2001; Singh Raman and Gupta, 2009). However, the viability of a nanocrystalline material will ultimately depend upon the general corrosion/oxidation resistance over extended periods of service. It should be remembered that research on many nanostructured materials, such as nanostructured steel, is in its infancy, and many promising developments are expected in the near future. Many challenges remain in the processing of nanostructured bulk/coating materials.

1.3 Corrosion/oxidation behavior of nanostructured materials

A typical feature of nanocrystalline materials is the defective core structure, which is caused by the incorporation of vacancies, dislocations and grain/interphase boundaries (Nalwa, 2000). Grain boundaries are usually more active sites and can be subjected to preferential corrosion/cracking. The increased grain boundary fraction can make more anodic sites for nucleation of corrosion in a nanostructured material. Grain boundaries are associated with high diffusivity and higher electrical resistivity. The grain boundaries turn out to be more susceptible to corrosion attack if intergranular diffusion of corrosive species (for example, diffusion of nascent hydrogen) is favored. The positive aspect is that grain boundaries favor faster diffusion of passivating ions from the bulk to the surface, which can promote formation of a more effective protective layer (particularly significant in high temperature oxidation). This effect is of greatest implication in the case of materials which are highly degradation resistant by virtue of their passive film. The proven enhancement of bulk electrical resistivity of the nanostructured materials is favorable for corrosion resistance.

A material's tendency to degrade depends on many parameter (Uhlig and Review, 1985; Fontana and Greene, 1986). From the available information, a

general statement on corrosion resistance of nanostructured metals/alloys is not viable. Reported studies on electrochemical corrosion of nanocrystalline metals/alloys show variable results. Studies suggest that in both weakly acidic and alkaline media nanocrystalline materials maintain a more effective passive layer, whereas in media containing aggressive ions the passive film stability is decreased when compared microcrystalline counterparts (Saji and Thomas, 2007). Recent analysis on electrodeposited alloys suggests that, by suitably controlling alloy composition and grain size and by proper grain refining, a more effective homogeneous passive layer can be grown on nanocrystalline structure that can provide superior corrosion resistance in aggressive environments (Nik Masdek and Alfantazi, 2010).

Nanocrystalline materials show promising advantages in preventing high temperature oxide scale formation (Gao and Li, 2004; Yao *et al*., 2006; Singh Raman and Gupta, 2009). High temperature materials rely on the formation of protective oxide films such as Al_2O_3 and Cr_2O_3 to resist high temperature and corrosive environments. The high density of grain boundaries in a nanocrystalline material provides fast diffusion paths, promoting selective oxidation of protective oxide scales with better adhesion to the substrate. Consequently, the percentage of passivating elements (such as Al and Cr) in the alloy/composite that is required to form a complete protective oxide scale can be substantially reduced. Experimental results indicated that, when the grain size of Ni–20Cr–Al coatings was ~60 nm, alloys containing ~2 wt% Al could form a complete α-Al_2O_3 scale at 1000°C in air. This concentration is only one-third of the required Al% for the alloy with normal grain size (Gao and Li, 2004). More studies are needed to validate these results, especially at temperatures where substantial grain growth can happen. Tribocorrosion resistance of nanostructured materials is reported to be higher (Benea *et al*., 2002). Promising results are expected for the corrosion cracking/fatigue behavior of nanostructured materials.

It can be stated that nanostructured materials have distinctly higher corrosion/oxidation resistance in certain applications, whereas they are inferior in other areas. More plant trials are required before commercial use in different application areas. Suitable engineering design and the selection of appropriate composition may bring huge increases in the corrosion resistance of nanostructured materials. This is in contrast to the application of nanomaterials in corrosion prevention strategies (mainly in coatings) as discussed below.

1.4 Nanomaterials in corrosion prevention

Among the different corrosion prevention strategies, coatings (both passive and active) are benefited appreciably by nanomaterials. A nanocoating can be defined as having either the thickness of the coating in nanoscale or the second phase particles that are dispersed into the matrix in the nanosize range or coatings having nanosized grains/phases, etc. Thin film coatings have been available for several years. In

Table 1.1 Nanocoatings in corrosion prevention

Thin films	Nanograined coatings	Nanocomposite coatings	Smart coatings
ceramic, metallic, composite (nano/ micrograined), self-assembled monolayer	ceramic, metallic, composite (thin/thick films)	polymer–ceramic, metallic–ceramic, polymer–metallic	replacement for conversion coatings, smart polymer coatings

particular, nanocoatings can be divided into nanostructured coatings (coatings with grain sizes in the range of 100 nm) and nanocomposited coatings (Table 1.1). Nanocoatings can be made by a variety of non-vacuum and vacuum based methods such as sol–gel, electrodeposition, magnetron sputtering, electro-spark deposition, high velocity oxy-fuel thermal spray, laser beam surface treatment, etc. Specific improvements sought include higher wear, erosion, high temperature oxidation and corrosion resistance (Agarwala *et al*., 2006).

Significant research has been done on nanocomposited bulk/coatings for various applications including corrosion prevention. The incorporation of nanoparticles in paint for mechanical property improvement, wear resistance, ultraviolet protection, water repellence, gas barrier property etc., is in widespread commercial practice. For example, the scratch resistance of paints can be improved by incorporating nanoparticles of alumina or silica. The barrier performance of epoxy coatings is found to be boosted after incorporation of nanophases by effectively decreasing porosity and diffusion paths (e.g. the incorporation of clay in polymer matrix nanocomposites increases water and gas barrier properties). The intermingling of nanomaterials is said to effectively fill spaces, block entry by water and air and fill tiny flaws, providing more effective passive protection. Nanoclay-based composite coatings have prompted extensive research efforts around the world, including use in automotive parts (Fernando, 2009). The increased path length for molecular diffusion caused by the platy nature of the clay materials enhances barrier properties and corrosion resistance.

Such nanocomposites help in crack bridging, crack deflection and crack bowing and reduce the trend for the coating to blister or delaminate (Dietsche *et al*., 2000). Polypyrrole nanocomposites with montmorillonite clay showed better corrosion protection compared with undoped polypyrrole (Yeh and Chin, 2003). Electrochemical studies suggest a beneficial role of Fe_2O_3, SiO_2 and halloysite clay nanoparticles in significantly improving the corrosion resistance of epoxy coated steels. Silica nanoparticles were found to significantly improve the microstructure of the coating matrix and enhanced the anticorrosive performance of the coating (Shi *et al*. 2009). Nanoparticles can prevent epoxy disaggregation during curing, resulting in a more homogeneous coating. During the painting process, ceramic nanoparticles can float around freely in the liquid paint. When the material (for e.g.

an automobile body) is baked at a higher temperature, the ceramic nanoparticles cross-link into a dense network instead of the long molecular chains found in conventional paint. This allows the lacquer to provide a much more effective wear and tear resistance and allows the paint to retain its gloss. Nano TiO_2 and Al_2O_3 are used for developing self-cleaning paints (Shen *et al*., 2005). Such self-cleaning hydrophobic properties cause water droplets to bead off from a surface, picking up dirt and other surface contaminants. Low wettability effectively prevents water on the substrate surface and exhibits excellent corrosion resistance in wet environments. As a result of the above particulars, nanoparticle-incorporated coatings are expected to have a dramatic increase in resistance to corrosion of the substrate due to their improved hydrophilic, anti-wear, anti-friction and self-cleaning properties.

Co-deposition of ceramic nanoscaled particles (ZrO_2, Al_2O_3, ZnO, TiO_2, ferrites, etc.) during electroplating and electroless plating can bring improvements in technical properties (Euler *et al*., 2003; Agarwala and Sharma, 2003). However, the high surface energy and an agglomeration tendency of nanoparticles in highly conductive metal electrolytes will tend to impede uniform distribution of the particles. Corrosion resistance of coating may be inferior with such aggregation due to the accelerated diffusion of aggressive ions along the interfaces between the incorporated particles (Euler *et al*., 2003). Extreme care is therefore needed in processing and thus novel deposition strategies are required. On the other hand, the addition of organic additives such as saccharin during the electrodeposition process was found to promote corrosion performance by acting as a grain refiner. The beneficial effect of such a fine grain microstructure is that it can cause added effective surface passivation arising from the more homogeneous nanocrystalline structure (Nik Masdek and Alfantazi, 2010). Studies showed that bulk metallic–ceramic nanocomposites (e.g. titanium–ceramic nanocomposites) showed enhancement of mechanical and corrosion resistance properties for use as hard tissue replacement implants (Jurczyk *et al*., 2008).

It has been reported that nanocomposites of cement mortar improved chloride penetration resistance. Incorporation of Fe_2O_3, Al_2O_3, TiO_2 and SiO_2 nanoparticles and nanoclays (montmorillonite) (as low as 1 wt%) significantly increased ionic transport resistance and decreased electric capacitance of cement mortar (He and Shi, 2008). Nano-silica and nanoclays were found to be better choices. Admixing of nanomaterials not only led to denser cement mortar but also changed the morphology of cement hydration products. Considering the low cost of nanoclays, their use in concrete to reduce chloride permeability is promising.

Significant efforts are currently underway to find alternatives to chromate conversion coatings via nanotechnology. Nanosized silica has proven to be a better choice. The method of forming functionalized silica nanoparticles in an aqueous sol–gel process and then cross-linking the nanoparticles to form a thin film is an excellent example of a nanoscience approach to coatings. This self-assembled nanophase particle surface treatment based on hydrolyzed silanes containing cross-linking agents (free of organic solvents and Cr-containing compounds) promotes adhesion of overcoat layers more effectively (Zheludkevich

et al., 2005a). Highly protective films can be prepared by self-assembled monolayers; for example, by chemical modification of a carboxylate self-assembled monolayer with alkyltriethoxysilanes (Aramaki and Shimura, 2004). Scientists at Brookhaven National Laboratory have developed a method for coating metal surfaces with ultrathin film (less than 10 nm) containing nanoparticles, beneficial for applications such as aluminum components in aircraft (Sugama, 2009). The corrosion-resistant film includes an at least partially cross-linked amido-functionalized silanol component in combination with rare-earth metal oxide nanoparticles. Studies showed that sol–gel films containing zirconia nanoparticles present improved barrier properties. Doping this hybrid nanostructured sol–gel coating with cerium nitrate brings additional improvement to corrosion protection, providing prolonged release of the cerium ions (Zehludkevich *et al*., 2005b).

The most attractive approach among nanotechnology associated coatings is smart coatings. These are active coatings that can respond to an external stimulus (pH, humidity changes, distortion of the coating, electromagnetic radiation, etc.) and can prevent further corrosion by release of corrosion inhibitors, biocides, etc., that are loaded in nanoreservoirs/nanocarriers dispersed in the matrix. Smart coatings have the capacity to self-heal and are proposed as replacements for chromate conversion coatings. Chromate-free pigments available for paints and coatings today (phosphates, silicates, borates, molybdates or cyanamides of Zn, Ca, Sr, Al, Ba, Mg or Ce) are not effective in many applications, such as in thin organic coatings with limited barrier functionality (e.g. coil and aircraft coatings). Organic inhibitors are very soluble in water, or are volatile, and are usually not preferred. The addition of inhibitors to sol–gel coatings (which are proposed as substitutes for chromate conversion coatings) often results in detrimental properties. The inhibitors incorporated directly into the sol–gel matrix may lose their activity quickly (Saji, 2011c).

The concept of smart coatings has thus attracted huge interest. Inherently conducting polymer films containing inhibiting anions as the dopant anions can release them when the film is subjected to a breach in the coating. However, conducting polymers have several limitations for use in industrial coatings. The film-forming properties of the polymers are not ideal and they have high cost and limited solubility. As an alternative, McGee *et al.* patented a non-electrically conducting film-forming copolymer-based coating. The polymer backbone contains a nitrogen-containing functional group and a metallate anion bonded to nitrogen in the functional group by ion pairing through Coulomb attraction. The metallate anion (of Mo,W, etc.) will release from the nitrogen functional group once the pH rises above a limit that is associated with the pKa of the nitrogen group (McGhee *et al*., 2010).

A few novel reports are available on nanoparticles/nanostructure carriers (of organic corrosion inhibitors) in smart coatings. There is a new generation of active corrosion protection coatings composed of hybrid sol–gel films doped with halloysite nanotubes able to release the entrapped corrosion inhibitors in a controllable way (Shchukin *et al*., 2008). A silica–zirconia-based hybrid film was

used in this work as an anticorrosion coating deposited on 2024 Al alloy. Halloysite nanotubes with inner voids loaded by corrosion inhibitors (2-mercaptobenzothiazole) and outer surfaces layer-by-layer covered with polyelectrolyte multi-layers were introduced into the hybrid films. Recently a Max Planck team reported development of laser-activated nanocontainers filled with corrosion inhibitors. The method relies on making sub-micron and nanocontainers sensitive to light by doping them with metal nanoparticles or organic dyes. Upon illumination with laser light, the absorption centers locally disrupt the shells of the containers (core–shell modification), thus increasing the permeability of the container walls. The corrosion inhibitor stored in the container is then released, covering and healing the corrosion area (Skorb *et al.*, 2009). These coatings can simultaneously provide continuous passivation through the controlled release of inhibitors and self-curing of the defects.

Reports are available on smart primer coatings (Katsiaryna, 2010). Katsiaryna patented a corrosion inhibiting coating comprising a primer layer as first layer. The primer layer incorporates corrosion inhibitor loaded containers capable of releasing organic corrosion inhibitors in response to electromagnetic radiation. A top second layer having no containers prevents spontaneous opening of the containers in the primer layer induced by electromagnetic radiation. The coating has the capability to release an inhibitor in response to electromagnetic irradiation

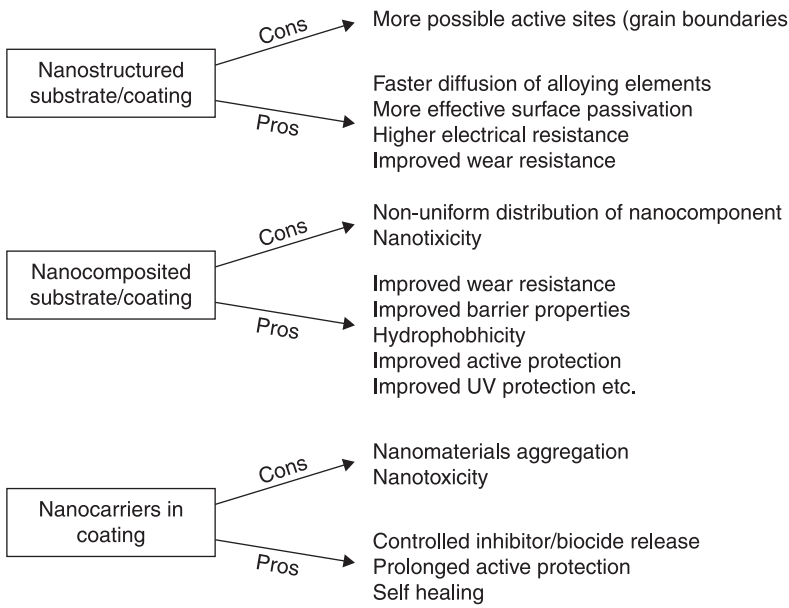

Substrate refers to bulk materials.
Depending on the material of interest and processing, cost factor can be favorable or unfavorable.
Nanomaterials aggregation/non-uniform distribution can be controlled by adopting suitable composite technologies or by nanomaterial-surface modification strategies.

1.3 Expected corrosion resistance properties of nanomaterials.

if the protective top layer develops defective areas that enable direct exposure of the containers to the electromagnetic radiation. The container has a photoactive anatase titania core. The inhibitor is present in pores and the core is enclosed in a polymer shell. The patent made use of photocatalytically active porous materials (anatase titania) which act as initiators for the release of encapsulated inhibitor only when they are exposed to electromagnetic radiation in damaged areas.

In spite of these promising results, more studies are needed in this direction for commercialization of smart coatings. Obstacles, such as cost factors and difficulty of handling, need to be overcome.

1.5 Conclusions

Materials at nanoscale are attracting huge interest due to their potential application in various fields. The applicability of nanomaterials is already established in some areas. However, challenges remain for their application elsewhere. The case with corrosion control using nanomaterials is the same. The potential practical applicability of different nanostructured materials in corrosion prevention is still in its infancy. Studies suggest that the corrosion behavior of nanostructured materials is case sensitive and depends on the constituent elements (composition) and the nature of the environment; more than that, on the dependence on grain size reduction. A nanostructured material can show huge enhancement in corrosion/oxidation resistance for a specific industrial application, provided proper measures are taken in design, composition and grain refining. Many challenges exist in the processing of various nanostructured alloys/composites of interest. Up to the present understanding, an area that is going to be benefited significantly is that of high temperature oxidation resistant materials. By employing nanostructured materials, one may be able to reduce the content of costlier and toxic elements in the alloy composition, giving a huge dividend in the materials cost.

It should be remembered that, in applications such as industrial coatings, better performance is a correlated factor thanks to the hydrophobicity, wear/scratch resistance and the mechanical properties of the coating; it is known that nanomaterials enhance these properties greatly. The availability of nanomaterials is a primary concern. Cheaper and novel deposition strategies such as those based on electrodeposition and sol–gel chemistry are attractive. Efforts being made to reduce grain size below 10 nm may bring some unexpected advantages of electrodeposited alloys/metals. In addition to different forms of coating where different nanoforms have already proven to provide better (or at least not inferior) corrosion resistance, other corrosion prevention strategies are going to be of great benefit. Smart coatings with on-demand releasable corrosion inhibitors are a major breakthrough. Figure 1.3 shows a schematic of the expected properties. The use of nanotechnology in corrosion monitoring and inspection continues to show great promise. As materials of the future, evaluation of the corrosion resistance of industrially important nanostructured bulk materials and coatings, and the creation of standards and rules, is of prime importance.

1.6 References

Agarwala, V., Agarwala, R.C., Sunder Daniel, B.S. 'Development of nanograined metallic materials by bulk and coating techniques', *Synthesis and Reactivity in Inorganic, Metal-Organic, and Nano-Metal Chemistry*, 2006, **36**, 3–16.

Agarwala, R.C., Sharma, R. 'Electroless Ni-P nanocoating technology', *Synthesis and Reactivity in Inorganic, Metal-Organic, and Nano-Metal Chemistry*, 2008, **38**, 229–36.

Aramaki, K., Shimura, T. 'Prevention of passive film breakdown on iron by coverage with one-dimensional polymer films of a carboxylate ion self-assembled monolayer modified with alkyltriethoxysilanes', *Corrosion Science*, 2004, **46**, 2563–81.

Benea, L., Bonora, P.L., Borello, A., Martelli, S. 'Wear corrosion properties of nanostructured SiC-nickel composite coatings obtained by electroplating', *Wear*, 2002, **249**, 995–1003.

Branagan, D.J. 'Enabling factors toward production of nanostructured steel on an industrial scale', *Journal of Materials Engineering and Performance*, 2005, **14**, 5–9.

Brayner, R. 'The toxicological impact of nanoparticles', *Nanotoday*, 2008, **3**, 48–55.

Catledge, S.A., Fries, M., Vohra, Y.K. 'Nanostructured surface modifications for biomedical implants', in H.S. Nalwa (ed.) *Encyclopedia of Nanoscience and Nanotechnology*. California: American Scientific Publishers, 2004, 741–62.

Cook, R.L., Myers, A.W., Elliott, J.E. 'Chromate-free on-demand releasable corrosion inhibitors for aluminum alloys', *Proc. 2005 Tri Service Corrosion Conference*, November 14–18, Florida, US Defense.

Dietsche, F., Thomann, Y., Thomann, R., Mulhaupt, R. 'Translucent acrylic nanocomposites containing anisotropic laminated nanoparticles derived from intercalated layered silicates', *Journal of Applied Polymer Science*, 2000, **75**, 396–405.

Euler, F., Jakob, C., Romanus, H., Spiess, L., Wielage, B., Lampke, T., Steinhäuser, S. 'Interface behavior in nickel composite coatings with nanoparticles of oxide ceramic', *Electrochimica Acta*, 2003, **48**, 3063–70.

Fernando, R.H. 'Nanocomposite and nanostructured coatings: recent advancements', in *Nanotechnology applications in coatings–ACS Symposium Series 1008*, Washington: American Chemical Society, 2009, 2–21.

Fontana, M.G., Greene, N.D. *Corrosion Engineering*, 3rd edn. New York: Mcgraw Hill, 1986.

Gao, W., Li, Z. 'Nanostructured alloy and composite coatings for high temperature applications', *Materials Research*, 2004, **7**, 175–82.

He, X., Shi, X. 'Chloride permeability and microstructure of Portland cement mortars incorporating nanomaterials', in *Transportation Research Record: Journal of the Transportation Research Board*, Vol. 2070, Washington: Transportation Research Board of the National Academies, 2008, 13–21.

Jensen, H., Sorensen, G. 'Ion bombardment of nanoparticle coatings', *Surface and Coating Technology*, 1996, **84**, 500–5.

Jurczyk, M., Niespodziana, K., Tulinski, M., Jurczyk, K. 'Nanoscale metallic and composite biomaterials', *Journal of Optoelectronics and Advanced Materials*, 2008, **10**, 732–6.

Katsiaryna, S. 'Corrosion inhibiting coatings controllable by electromagnetic irradiation and methods for corrosion inhibition using the same', *EU patent* 2202280, 2010.

McGee, J.D., Smith II, T.S., Bammel, B.D., Bryden, T.R. 'Release on demand corrosion inhibitor composition', *US patent* 0291307, 2010.

Nalwa, H.S. *Handbook of nanostructured materials and nanotechnology*, Vol.1, San Diego: Academic press, 2000.

Nik Masdek, N.R., Alfantazi, A. 'Review of studies on corrosion of electrodeposited nanocrystalline metals and alloys', *ECS Transactions*, 2010, **28**, 249-60.

Pang, X., Zhitomirsky, I. 'Electrodeposition of nanocomposites organic–inorganic coatings for biomedical applications', *International Journal of Nanoscience*, 2005, **4**, 409 –18.
PEN, Project on Emerging Nanotechnologies, 2011 (http://www.nanotechproject.org.)
Saji, V.S., Thomas, J. 'Nanomaterials for corrosion control', *Current science*, 2007, **92**, 51–55.
Saji, V.S, Choe, H.C., Yeung, K.W.K. 'Nanotechnolgy in biomedical applications: a review', *International Journal of Nano and Biomaterials*, 2010, **3**, 119–39.
Saji, V.S., Kim, Y.S., Kim, T.H., Cho, J., Song, H.K. 'One-dimensional (1D) nanostructured and nanocomposited $LiFePO_4$: its perspective advantages for cathode materials of lithium ion batteries', *Physical Chemistry Chemical Physics*, 2011a, **13**, 19226–237.
Saji, V.S, Choi, I.K., Lee, C.W. 'Progress in electrodeposited absorber layer for $CuIn_{(1-x)}Ga_xSe_2$ (CIGS) solar cells', *Solar Energy*, 2011b, **85**, 2666–78.
Saji, V.S. 'Contemporary developments in corrosion inhibitors: review of patents', *Recent Patents on Corrosion Science* , 2011c, **1** , 63–71.
Schmidt, H. 'Commercial success with nanomaterials', *Nano magazine*, **12**, 01/2010.
Schwarzacher, W. 'Electrodeposition: a technology for the future', *The Electrochemical Society Interface*, spring 2006, 32–3.
Shchukin, D.G., Lamaka, S.V., Yasakau, K.A., Zheludkevich, M.L., Ferreira, M.G.S., Moehwald, H. 'Active anticorrosion coatings with halloysite nanocontainers', *Journal of Physical Chemistry C*, 2008, **112**, 958–64.
Shen, G.X., Chen, Y.C., Lin, L., Lin, C.J., Scantlebury, D. 'Study on a hydrophobic nano-TiO_2 coating and its properties for corrosion protection of metals', *Electrochimica Acta*, 2005, **50**, 5083–9.
Shi, X., Nguyen, T.A., Suo, Z., Liu, Y., Avic, R. 'Effect of nanoparticles on anticorrosion and mechanical properties of epoxy coatings', *Surface and Coating Technology*, 2009, **204**, 237 –45.
Singh Raman, R.K., Gupta, R.K. 'Oxidation resistance of nanocrystalline vis-à-vis microcrystalline Fe-Cr alloys', *Corrosion Science*, 2009, **51**, 316–21.
Skorb, E.V., Skirtach, A.G., Sviridov, D.V., Shchukin, D.G., Moehwald, H. 'Laser controllable coatings for corrosion protection', *ACS Nano*, 2009, **3**, 1753–60.
Sugama, T. Corrosion resistant metal surfaces, *US patent* 7507480, 2009.
Uhlig, H.H., Review, R.W. *Corrosion and Corrosion Control: an Introduction to Corrosion Science and Engineering*, 3rd edn. New York: John Wiley and Sons, 1985.
Voevodin, N., Balbyshev, V.N., Khobaib, M., Donley, M.S. 'Nanostructured coatings approach for corrosion protection ', *Progress in Organic Coatings*, 2003, **47**, 416–23.
Wang, Y., Limb, S., Luob, J.L., Xub, Z.H. 'Tribological and corrosion behaviors of Al_2O_3/polymer nanocomposite coatings', *Wear*, 2006, **260**, 976–83.
WCO, The World Corrosion Organization, 2011 (http://www.corrosion.org.)
Yao, M., He, Y., Zhang, Y., Yang, Q. 'Al_2O_3-Y_2O_3 nano-and micro-composite coatings on Fe-9Cr-Mo alloy', *Journal of Rare Earths*, 2006, **24**, 587–590.
Yeh, J.M., Chin, C.P. 'Structure and properties of poly(omethoxyaniline) clay nanocomposites materials', *Journal of Applied Polymer Science*, 2003, **88**, 1072–78.
Zheludkevich, M.L., Miranda Salvado, I.M., Ferreira, M.G.S. 'Sol–gel coatings for corrosion protection of metals', *Journal of Materials Chemistry*, 2005a, **15**, 5099–111.
Zheludkevich, M.L., Serra, R., Montemor, M.F., Yasakau, K.A., Miranda Salvado, I.M., Ferreira, M.G.S. 'Nanostructured sol–gel coatings doped with cerium nitrate as pretreatments for AA2024-T3 corrosion protection performance', *Electrochimica Acta*, 2005b, **51**, 208–17.

2

Corrosion and nanomaterials: thermodynamic and kinetic factors

S. ROY, Newcastle University, UK

Abstract: Thermodynamics and kinetics of corrosion are key to understanding and formulating nanoscale materials and their exploitation in corrosion prevention. In particular, nanoscale dimensions may impart behaviour to these materials which is not usually observed in bulk. The relevance of using kinetic and thermodynamic considerations for galvanic corrosion is discussed with theoretical development. The application of these fundamentals to infer corrosion behaviour in alloys and nanolayers has been elucidated.

Key words: nanoscale materials, corrosion prevention, galvanic corrosion, corrosion kinetics, electrochemical thermodynamics.

2.1 Introduction

Human civilisation could not have been achieved without our ability to extract useful materials from the natural world. The importance of this ability is the classification of human technological progress into Paleo- and Neolithic (Stone) Ages, followed by metal-based Bronze and Iron Ages (Aitchison, 1960; Macdonald, 1999). The latter two ages, which led to rapid growth in human populations, show the impact of metal on human history – in both war and peace. The importance of metals in everyday life today remains as influential as it has been in the preceding 4000 years, and will continue to dominate as the human population reaches unprecedented numbers over the next 50 years (UN, 2004).

Corrosion prevention is one of the first technical uses of nanotechnology by humans. This is because almost all man-made structures rely on the stability of a 1–2-nm thick passive film which provides stability to the underlying material. For example, skyscrapers would not be able to exist if structures were not made of tough non-degrading materials capable of withstanding earthquakes. Energy distribution in the megacities relies on specialised alloys and ceramics which can withstand high temperatures encountered during electricity generation and its subsequent distribution. Even the more recent internet 'revolution' relying on optical technology would have been inconceivable if the first metal cables laid across the Atlantic had failed (Cookson, 2003). The growing demand for specialised materials which combine strength, stability and desirable physical properties can be seen by examining metal prices in the past decade (World Bank, 2006).

The search for materials providing solutions to fulfil specific needs continues undiminished. In a variety of industrial sectors over the past two decades, this has

been in the form of exploiting 'nanotechnology' and 'nanomaterials' to provide new avenues for solving problems. In the field of corrosion prevention, as in other areas, researchers have attempted to employ nanoscale techniques to either better understand the process of corrosion itself or prevent it from occurring. In this chapter we present the thermodynamic and kinetic considerations for standard corrosion reactions and how the employment of nanoscale material may change traditional theoretical analysis. In addition, technical exploitation and evidence of nanotechnology in different case studies are used to elaborate the applications of such theoretical knowledge.

A nanomaterial should be defined as a material which derives certain particular functionalities from a dimensional constraint in the nanometre range, i.e. 10^{-9} m. There has been some debate in the first decade, i.e. the 1990s, on the range (in nm) where certain differences in physical, electronic and chemical properties are observed. The current consensus is that usually a material should have a dimension smaller than 100 nm. The lower end of this 'dimension' related behaviour is of course a single molecule (or a few molecules). Since single molecules of metals, ceramics and polymers differ substantially in size, the use of the word 'nanomaterial' is somewhat arbitrary and depends on the material in question. Suffice to say that the functionality has to be derived from a cluster of molecules which imparts specific behaviour not observed in single molecules or bulk material.

In corrosion prevention, therefore, one first has to define the functionality that is required. For example, researchers have shown that corrosion properties of Zn–Ni multilayer coatings are improved when the layers are at a particular thickness – i.e. 2 μm (Fei and Wilcox, 2006). It has been shown that hard coatings used in high-speed tools requiring protection from wear can be improved by producing layers of TiN interspersed with interfaces, which provide additional hardness. Researchers showed that this occurs when interfaces are spaced at 8 nm (Bull and Jones, 1994). When the layers are thinner than this, the material reverts to its bulk behaviour.

Another example of corrosion prevention is the advantage offered by lowering grain size, and thereby imparting hardness (Ralston *et al.*, 2010; Shi, 2010). The classic prediction of hardness dependence on grain size (Hall, 1951; Petch, 1953), predicts that hardness should increase with diminishing grain size. This has been intelligently exploited by gradually reducing the grain size at the surface while retaining larger grains in the bulk material (Ralston *et al.*, 2010). Researchers have also established that no additional advantage in corrosion behaviour is gained by reducing the grain size in the bulk material (Luo *et al.*, 2010) since corrosion is a surface phenomenon.

Other uses of corrosion prevention are highlighted in intelligent 'self-repairing' coatings, which are based on the principle of encapsulating polymers within the coating that are released when a defect is generated (Hughes *et al.*, 2010). The released polymer reacts with the environment to form a protective sealant. Other

approaches include the use of proteins and adsorbates which change the surface charge of a metal by forming a monolayer, thereby preventing the ingress of aggressive ions into the material (Hodgson *et al.*, 2002). More detailed information on these approaches can be obtained in recent reviews (Saji and Thomas, 2007; Hughes *et al.*, 2010; Liu *et al.*, 2010).

Such wide exploitation of nanotechnology for corrosion prevention is derived from the fact that the stability of almost all metals and their alloys (after extraction from their ores) is due to a corrosion-resistant layer formed on their surfaces. This surface layer is usually a hydroxide, oxide, sulfide or nitride, which is impenetrable to the environment, thereby providing protection to the underlying material. Corrosion prevention, in fact, can be viewed as one of the oldest nanotechnologies used, even when the underlying science was missing. Armed with the knowledge of nanoscience, one can refine existing strategies and develop new ones to protect and preserve many materials.

In order to exploit this form of nanotechnology, however, one needs to have a good understanding of the underlying science. Corrosion, and therefore its prevention, is underpinned by materials electrochemistry. Electrochemical thermodynamics and kinetics determine 'if' and 'how fast' a metal will corrode. However, many of these theoretical considerations are derived for bulk materials and modification or adjustments may be needed to apply them to nanoscale systems. The forthcoming sections are dedicated to describing the background on why corrosion occurs, followed by electrochemical theories on thermodynamics and kinetics. The employment of these theoretical analyses to understand nanoscale materials is described by using appropriate case studies.

2.2 Corrosion

Corrosion occurs in the aqueous environment because protons and oxygen, which are readily available in nature, are reduced to more stable products. They require electrons to reduce, which are supplied by the base metals and other electropositive species. In fact, this is the reason why only few metals, such as Pt and Au, are found in their native state. These metals, therefore, are called 'noble' metals. The remaining metals exist as minerals in their oxidised state. In anoxic or anaerobic conditions, reducing agents such as sulfur and nitrate can lead to corrosion, as evidenced during microbial corrosion (Smith *et al.*, 2011).

For the metallic corrosion of iron, one can write the following chemical reactions:

$$\text{(Oxidation)} \quad Fe \rightarrow Fe^{2+} + 2e^- \qquad [2.1]$$

$$\text{(Reduction)} \quad 2H^+ + 2e^- \rightarrow H_2 \qquad [2.2]$$

$$\text{or} \quad \tfrac{1}{2} O_2 + H_2O + 2e^- \rightarrow 2OH^- \qquad [2.3]$$

A reaction-couple can also form between two different metals, leading to galvanic corrosion. For example, copper and zinc, when connected electrically, lead to corrosion damage of zinc:

$$\text{(Reduction)} \quad Cu^{2+} + 2e^{-} \rightarrow Cu \qquad [2.4]$$

$$\text{(Oxidation)} \quad Zn \rightarrow Zn^{2+} + 2e^{-} \qquad [2.5]$$

Often these reactions are presented as overall reactions:

$$Fe + \tfrac{1}{2} O_2 + H_2O \rightarrow Fe(OH)_2 \qquad [2.6]$$

$$\text{or} \quad Cu^{2+} + Zn \rightarrow Cu + Zn^{2+} \qquad [2.7]$$

Although the overall form of the reaction is deceptive in the fact that it shows that no electrons are involved, one should not forget that corrosion involves a redox couple which, in effect, includes the transfer of electrons. In the same vein, the reduction of sulfate and nitrate replaces Reactions [2.2] and [2.3] under anoxic conditions. In this regard, corrosion is an 'inevitable' process. The answer to why these processes are inherent or inevitable lies in the thermodynamics of these reactions.

2.3 Thermodynamics

If one were to accept that the degradation of the metals is caused by oxidation from their neutral valence state, then the question remains as to why they exhibit this behaviour. The reason for this is the difference in the *electrochemical potentials* of the two species. Table 2.1 shows the electrochemical series for some common metals and the comparable electrochemical potential for oxygen and proton reduction. Notably, very few metals are inherently stable in their natural state, and indeed most engineering and construction materials are unstable. Interestingly, metals such as nickel, chromium and titanium, which are considered corrosion resistant, are very reactive. In principle, then, one would never expect to see any engineering material unless there was a method for its protection.

The protection of most metallic materials in nature ('non-noble' metals) is derived from a protective layer which is impermeable to either electronic or ionic conduction. Some of these protective layers are formed by virtue of the fact that a metal reacts with the environment such that this impermeable film can be grown and maintained. In other cases, these films are formed through human intervention. The protective layer is usually of nanometre dimensions – in this regard corrosion prevention is a very early application of nanotechnology. Normally, this impermeable film is continuously produced at the metal surface, while at the other end it is dissolved into the environment, leading to an overall loss of material, often measured as a weight loss or 'corrosion loss'.

This means that the rate of corrosion loss is intricately tied to the stability and degradation of the film, and the reactivity of the metallic materials is not of much

Table 2.1 Standard electrode potentials for reduction of metals, oxygen and protons

No.	Electrode reaction	E°/V
1	$Au^{+} + e^{-} \Leftrightarrow Au$	+1.69
2	$Pt^{2+} + 2e^{-} \Leftrightarrow Pt$	+1.18
3	$Ag^{+} + e^{-} \Leftrightarrow Ag$	+0.799
4	$Cu^{+} + e^{-} \Leftrightarrow Cu$	+0.518
5	$O_2 + H_2O + 4e^{-} \Leftrightarrow 4OH^{-}$	+0.401
6	$Cu^{2+} + 2e^{-} \Leftrightarrow Cu$	+0.339
7	$2H^{+} + 2e^{-} \Leftrightarrow H_2$	0.000
8	$Sn^{2+} + 2e^{-} \Leftrightarrow Sn$	–0.141
9	$Ni^{2+} + 2e^{-} \Leftrightarrow Ni$	–0.236
10	$Co^{2+} + 2e^{-} \Leftrightarrow Co$	–0.282
11	$Fe^{2+} + 2e^{-} \Leftrightarrow Fe$	–0.440
12	$Zn^{2+} + 2e^{-} \Leftrightarrow Zn$	–0.762
13	$Cr^{3+} + 3e^{-} \Leftrightarrow Cr$	–0.74
14	$Ti^{2+} + 2e^{-} \Leftrightarrow Ti$	–1.60
15	$Al^{3+} + 3e^{-} \Leftrightarrow Al$	–1.68

Note: the stability of materials (reduced species) decreases from the top to the bottom of the table

consequence except that it should form the film. In fact, the very reactive metals in Table 2.1, such as Cr, Ti and Al, form stable and impenetrable oxide films spontaneously, which then protects the underlying material. Therefore, the exploration of corrosion prevention usually involves examining strategies of forming stable films with an ability to heal or repair themselves when they are damaged. In the next sections we examine the fundamental considerations involved in forming stable films, i.e. the thermodynamics of their formation. Thereafter, we examine the rate of formation of these films, i.e. the kinetics of growth of these films.

2.3.1 Formation of stable films

Since the main consideration of forming a stable impenetrable film is its ability to grow in a certain environment, all reaction products between a metal and its environment must be considered. A classical method of depicting the reduction reactions which can lead to metal oxidation is a Pourbaix diagram (Pourbaix, 1974). A typical pH–potential plot, which is a Pourbaix diagram, is illustrated in Fig. 2.1. In the figure, the possible products formed between copper and water (Fig. 2.1(a)) or copper, water and chloride (Fig. 2.1(b)) are shown. The dotted lines represent oxygen and hydrogen reduction reactions representative of water stability. The pH–potential diagram shows the most stable product formed by a reaction between the metal and the environment. Details of developing Pourbaix plots for numerous metals in different environments are available in Pourbaix (1974).

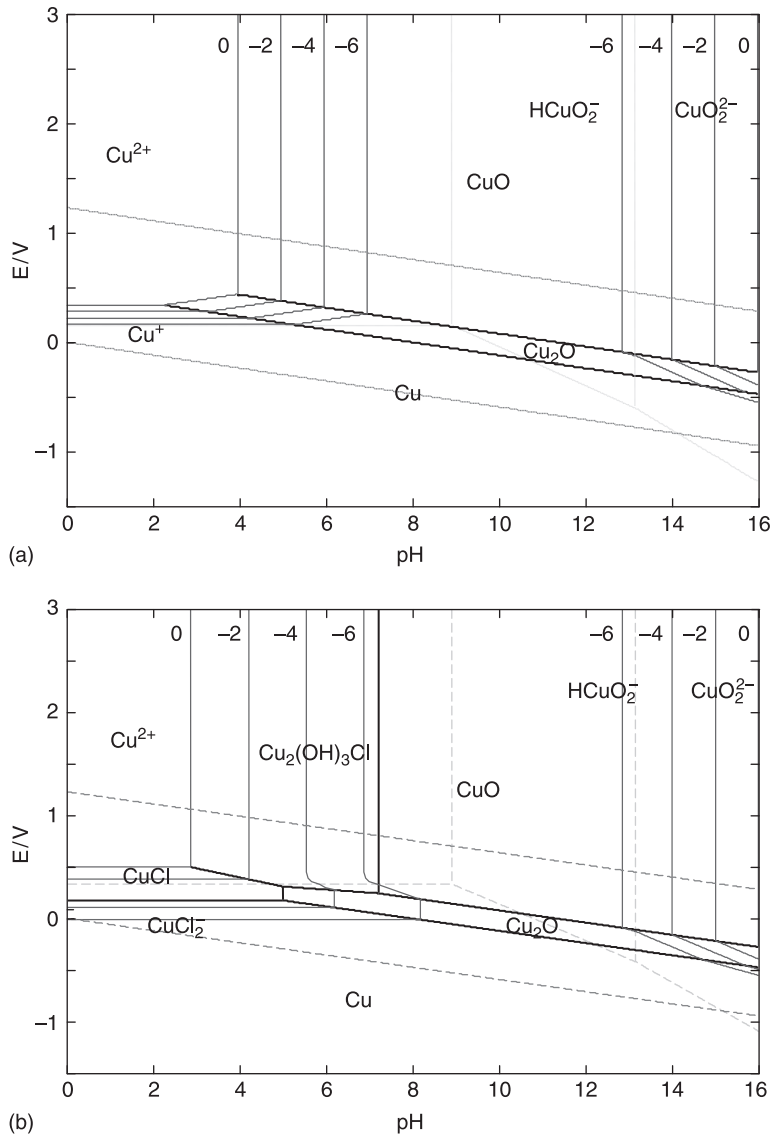

2.1 (a) Copper–water and (b) copper–chloride–water Pourbaix plots. The graphs show the different products that can exist when copper is in contact with water in the absence and presence of chloride. The regions where solid products exist are marked with bold and dissolved products are marked in normal font (reprinted with permission from author).

Figure 2.1(a) shows a Pourbaix diagram for a copper–water system and Fig. 2.1(b) shows a copper–water–chloride system (Buckle, 2007). The difference between the two plots is due to changing anion species and their concentration. If one were to examine the regions where relatively slowly dissolving products are formed in Fig. 2.1(a), such as CuO or Cu_2O, the metal can be protected from corrosion. In this region the reaction products can separate the two reactants, provided that the oxide film is of low porosity. In some cases, films may form but dissolve at a relatively fast rate, such as CuCl, which is formed when chloride is present (as in Fig. 2.1(b)) and allows the metal to dissolve at an appreciable rate. By comparing (a) and (b) from Fig. 2.1, it is clear that copper may be stable in water at moderately acidic solutions but will dissolve if chloride is added to it, due to the formation of products such as CuCl which dissolve easily in the surrounding media.

Despite their significant use in corrosion prevention, Pourbaix diagrams are only useful for predicting the stability of a metal in the long term. This is mainly because the plots are derived based on *only the most stable reaction product formed*. Intermediate products and their stability or porosity are not considered in the development of the pH–potential plots. This means that process dynamics – which define the route taken by surface reactions to attain the final stable product – are ignored. This can have quite unexpected outcomes for corrosion prevention. The overall corrosion of a material could be significant during the period before the final product is formed. A classic example is γ- and α- FeOOH formed during atmospheric corrosion. Since their protection ability is quite different (Oswin and Cohen, 1957; Kudo *et al.*, 1968), the rate of corrosion is dependent on the film porosity and stability of these two different films, which cannot be directly inferred from a Pourbaix plot.

The second issue about using Pourbaix diagrams is that free energy values used to calculate the stability of a species are based on bulk values for a given material. The free energy of formation for a cluster of 100 or 1000 atoms, however, may not be the same as that in bulk material. Since the accuracy of a Pourbaix plot is entirely dependent on the free energy data, it is important to maintain a critical view of the validity of their applicability for nanoscale materials. The final issue is that these plots do not reveal the speed (or kinetics) at which a material is degraded or lost to the environment during the process of film formation. This means that, while these graphs can provide information on whether a material will be (eventually) stable within an environment, they do not allow prediction of how much material will be lost *before it is stabilised*. In order to predict the lifetime of a certain material, the rate of dissolution, i.e. kinetics, is more important.

2.4 Kinetics

In order to understand the kinetics of corrosion, one needs to differentiate between the different regimes of dissolution that can exist in a metal. For example, in the

presence of atmospheric oxygen in water, the reduction of oxygen is accompanied by dissolution of iron to ferrous ions:

$$\text{Step 1} \qquad Fe \rightarrow Fe^{2+} + 2e^{-} \qquad [2.8]$$

There can be further heterogeneous reactions at the electrode surface leading to the formation of a precipitate at the electrode surface (Landolt, 2003):

$$\text{Step 2} \qquad 2\,Fe^{2+} + 3\,H_2O + \tfrac{1}{2}\,O_2 \rightarrow 2\,\gamma\text{-}FeOOH + 4H^{+} \qquad [2.9]$$

The oxy-hydroxide formed on the metal can react still further to form oxides (Landolt, 2003):

$$\text{Step 3} \qquad 8\,\gamma\text{-}FeOOH + Fe^{2+} + 2\,e^{-} \rightarrow 3\,Fe_3O_4 + 4\,H_2O \qquad [2.10]$$

Step 1, where the metal readily loses its electron directly to the environment without the formation of any film on its surface, is called the active dissolution region. The second reaction forming an oxy-hydroxide occurs between the metal and oxygen, which has to penetrate through the pores of an oxy-hydroxide film. Step 3 is enabled by further reaction between the metal and the oxy-hydroxide. This sequence of reactions leads to the formation of a less porous film, i.e. Fe_2O_3, which protects the metal.

Figure 2.2(a) shows the metal–solution interface for active dissolution. As shown, in this case the metal is dissolved at the surface of the electrode. The electrons released by metal dissolution are used by a counter-reaction such as proton or oxygen reduction. The formation of solid products on the surface via Reaction 4, which may be determined by the environment (for example, humidity), may lead to the formation of a film on the surface. If porous surface products are formed on the surface then the reaction products may still reach the surface by diffusion, as shown in Fig. 2.2(b).

The situation may also occur where a dense oxide film is formed on the surface, as is shown in Fig. 2.2(c). Such dense films are formed in the case of corrosion-resistant materials such as Cr and Ni and some valve metals. In this case the kinetics may be controlled by the movement of ions or electrons through the film (Schmuki, 2002), or the dissolution rate of the film at the film–electrolyte interface, as depicted in Fig. 2.2(c). Since the film thickness, film composition and thereby film formation and dissolution can change with time (Yu and Scully, 1997), it is difficult to predict the rate of corrosion in this case. More importantly, the difference between active and passive dissolution rates, i.e. corrosion loss, is due to the presence of the film, be it porous or compact.

2.4.1 Reaction equations

The rate of electrochemical metal dissolution kinetics is characterised by the corrosion current, j, which is usually measured in terms of mA/cm^2 and converted

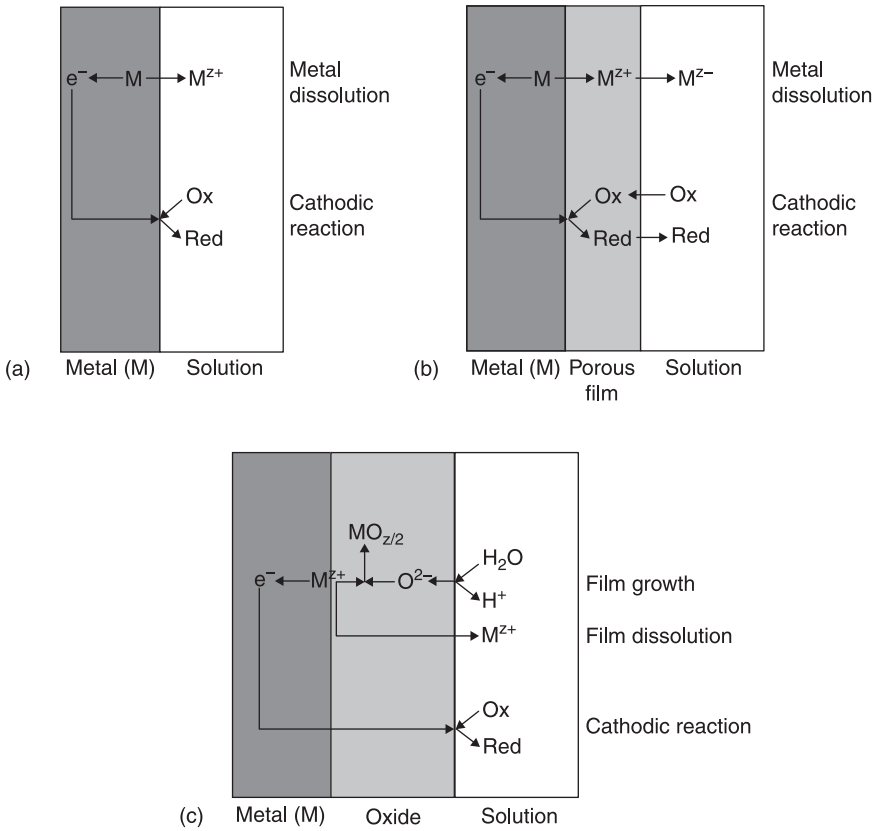

2.2 Schematic of corrosion processes: (a) in the absence of a surface film, (b) in the presence of a porous film, and (c) at a passivated surface.

to a weight loss of mm/yr. The current–potential relationship for a metal in an aqueous solution is given by a Butler–Volmer type relationship between j and the electrode potential, E,

$$j = F\,k_a\,c_M \exp\left[\frac{\alpha z F}{RT}\left(E - E_{rev}\right)\right] - F\,k_c\,c_{M^{z+}} \exp\left[-\frac{(1-\alpha) z F}{RT}\left(E - E_{rev}\right)\right] \quad [2.11]$$

The notable point about this equation is that the overall current is a summation of two currents – an anodic and a cathodic one. The anodic part is the first term on the right-hand side and the cathodic part is the second term. If the potential difference is positive, then an anodic current flows; if it is negative, then the current is cathodic. In Eq. 2.11, α is the transfer coefficient, z is the number of electrons exchanged in the reaction, F is Faraday's constant and k is the reaction rate constant. The subscripts a and c denote anodic and cathodic, respectively, *rev* stands for equilibrium and R and T are the universal gas constant and absolute temperature.

When the potential of the system is sufficiently different from E_{rev}, i.e. 100 mV, then it may be sufficient to use the cathodic or anodic term only, because the other term becomes negligibly small. In a corrosion system, the corroding material, such as iron, is dissolved electrochemically in its active state (Fig. 2.1 (a)). In this case the current–potential relationship for iron may be expressed as:

$$j_{Fe} = j_{0,Fe}\left\{\exp\left(\frac{\alpha z F}{RT}(E - E_{rev,Fe}\right)\right\} \quad [2.12]$$

where j_0 is the exchange current density (derived from the rate constants). The counter-reaction, for example oxygen reduction, can be expressed by using solely the cathodic term, since that is also far away from its equilibrium potential.

$$j_{O_2} = j_{0,O_2}\left\{-\exp\left(-\frac{(1-\alpha) z F}{RT}(E - E_{rev,O_2}\right)\right\} \quad [2.13]$$

When the current–potential relationship of the anodic branch of the corroding metal and the cathodic branch of the oxidising agent are expressed in their logarithmic form then one obtains the familiar Tafel expressions:

$$\ln j_{Fe} = \ln j_{0,Fe} + \frac{\alpha z F}{RT}(E - E_{rev,Fe}), \text{ for the anodic reaction} \quad [2.14]$$

and

$$\ln \left|j_{O_2}\right| = \ln j_{0,O_2} - \frac{(1-\alpha) z F}{RT}(E - E_{rev,O_2}), \text{ for the cathodic reaction} \quad [2.15]$$

When the counter-reaction is oxygen evolution, the rate of oxygen discharge is controlled by mass transfer rather than kinetics, due to the low solubility of oxygen in water. In that case, the rate of dissolution is governed simply by mass transfer limiting current of oxygen, which is given by:

$$|j_{O_2}| = k_{m,O_2} c_{O_2} \quad [2.16]$$

In Eq. 2.16, k_{m,O_2} is the mass transfer coefficient of oxygen for that system and c_{O_2} is the solubility of oxygen in water. When there is a porous layer on the surface of a metal, then the concentration of oxygen may be much lower at the reaction surface because it has to diffuse through the film covering the metal.

When there is a passive film on the surface, the situation is somewhat different, as is shown in Fig. 2.2(c). The oxidation, as well as the reduction reaction, occurs at the metal–oxide interface, and the dissolution, which balances the rate of film formation and film breakdown, occurs at the film–solution interface. Since passive films are not very conductive, a large potential drop can occur across a very thin film. The transport of ions across the film is governed by high field conduction (Schmuki, 2002):

$$j = A' \exp(B' \Delta\Phi_2 / t) \quad [2.17]$$

where A' and B' are potential-independent constants, $\Delta\Phi_2$ is the potential difference across the oxide film and t is the film thickness. This means that the passive region

is characterised by a low current over a large range of potentials. As soon as the passive film is broken, an extremely high active current is generated in the system, as given by Eq. 2.12. This high current then rebuilds the film, thereby repairing the damage, and once again renders it passive.

The rate of corrosion (or metal dissolution) as described in the presence of a porous or a compact film is governed by the structure and stability of this film. If film formation is rapid then re-passivation occurs quickly. This occurs in the case of Ni, Cr or Ni–Cr alloys or in valve metals such as Ti, Ta and Al. However, where re-passivation is slower, or if the passive films are less stable, such as those encountered in Cu and Fe, metal loss during the process of re-passivation can be significant. Therefore, it is important to understand how quickly passivation can be gained, which can be understood by separately analysing the kinetics of cathodic and anodic reactions and determining the rate controlling step.

2.4.2 Mixed potential system

Figure 2.3 shows the anodic and cathodic reactions occurring on a metal substrate, such as Fe. As discussed in the preceding section, the anodic dissolution rate of

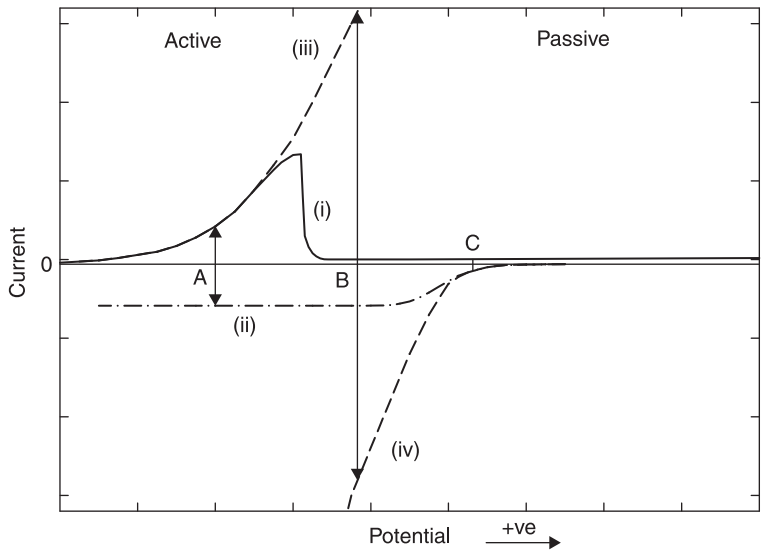

2.3 Current–potential curves for corroding systems: (i) dissolution under active or passive conditions, (ii) cathodic reaction under mass transport control. 'A' denotes the corrosion potential under active dissolution conditions and 'C' under passive conditions. 'B' denotes the potential following breakdown of the passive film where the dashed lines (iii) and (iv) are obtained by extrapolating the active dissolution lines.

Fe can be active or passive. In the active region, the current for Fe dissolution bears an exponential relationship with the potential difference, which is denoted by the solid curve (i) at low over-potentials. If the oxygen reduction is the counter-reaction, then the system will shift to a potential where the electrons required for the mass transfer controlled cathodic reaction exactly balance those generated by the dissolution of the metal. This is shown by the position 'A'.

However, if there is a passive film over the surface, the situation changes. In that case the number of electrons released during metal dissolution is lower and therefore the potential at which the balancing reaction operates shifts to 'C'. This is a much higher potential than 'A' and the metal is protected by the film. At this point the dissolution is no longer governed by mass transfer controlled oxygen reduction but by the rate for dissolution of the oxide film.

Any damage to the film will cause the surface of the metal to be in direct contact with the oxidising agent in the environment. This means that the system will slide back to the active region, the currents of which can be obtained by extrapolating the active region to the relevant over-potential region. In Fig. 2.3, this is denoted by the dotted lines for anodic and cathodic currents. Clearly this current is very high, denoted by position 'B', which should locally repair the film and render it passive in a very short time. If this does not occur, then the film cannot be repaired and corrosion will occur. However, it is possible that one of the reactants (for example, dissolved oxygen) may be present in such small quantities that the damage is unable to heal. In this case corrosion will continue at the rate oxygen reaches the damaged section, which will delay the formation of the surface layer.

Interestingly, as shown in Fig. 2.3, the system potential can lie anywhere in the passive region, depending on the film thickness and conductivity. For films of high thickness or low conductivity the system potential will lie very far to the right (on the *x*-axis), or noble potentials. If the film is damaged and the mixed potential is high, it is more likely to repair the film by passing a high current. However, in many cases, local changes or localised corrosion in the presence of aggressive anions such as Cl^- may prevail, resulting in a lack of protective film formation.

This example establishes the tenets of the mixed potential theory: (1) that the reaction surface is at the same potential, (2) that the electrons released in the anodic reaction are consumed by the reduction reaction, which means that (3) the total currents for the anodic (oxidation) and cathodic (reduction) reactions have to exactly balance each other. In this regard, one can say that the total current, *J*, of a system is equal to 0:

$$J = \sum_i j_i = 0 \qquad [2.18]$$

In Eq. 2.18, j_i is the partial current of any reaction *i*. The corresponding system potential is called the corrosion potential.

2.5 Applications

The principles described have been used to solve an interesting case of galvanic corrosion observed in compositionally modulated metal multilayers (CMMs) and alloys. The electrodeposition of copper and nickel alloys or metal multilayers has received attention due to their practical importance for corrosion protection (Jensen *et al.*, 1998; Fei and Wilcox, 2006) as well as magnetic (Foecke and Lashmore, 1992; Lenczowski *et al.*, 1995; Miyazaki *et al.*, 1999; Bakonyi *et al.*, 2002; Spray and Nowak, 2006) and mechanical (Tsalakos and Jankowski, 1986) applications. Details of the uses and fabrication are elaborated elsewhere (Roy, 2009).

Although there are several different CMM systems, Cu–Ni and Cu–Co have received more attention because they are ideal systems to study electrochemical principles and behaviour. This is because copper and nickel are separated by a wide gap in nobility, they form solid solutions and their electrochemical behaviour during co-deposition remains similar to that during the deposition of the individual metals. Cobalt and copper differ greatly in terms of nobility but the two metals are virtually immiscible. In the solid state, the behaviour of Cu–Co, therefore, is expected to be almost opposite to the behaviour of the Cu–Ni system (Madore, 1993; Roy, 2009). This allows one to examine the effect of metal ions, additives, complexants, etc, on alloy composition and properties during fabrication of these components by electroplating.

In accordance with Pourbaix diagrams, nickel is passive (shows no anodic currents during polarisation) in sulfate or citrate based media (Madore, 1993; Golodnitsky *et al.*, 2002; Roy, 2009) but does dissolve when chloride is present in solution (Correia and Machado, 2000). Cobalt shows similarly passive behaviour and has often been alloyed with nickel to achieve good corrosion behaviour (Golodnitsky *et al.*, 2002; Tury *et al.*, 2006). However, during fabrication of Cu–Ni multilayered structures using pulsing currents it was found that nickel dissolved from the deposit and that this dissolution was controlled by the mass transfer rate of cupric ions in solution, even when the alloy was deposited from a citrate electrolyte (Roy *et al.*, 1994). This is somewhat unexpected, since nickel is deemed passive in these solutions. This was found to be the case for both Cu–Ni deposition from sulfamate electrolytes (Bradley *et al.*, 1996) and Cu–Co deposition from citrate baths (Bradley and Landolt, 1999; Dulal *et al.*, 2004a), where again the less noble components are expected to remain passive and protected.

However, closer examination showed that the Cu–Ni system, immediately after the interruption of current, acquires an open circuit potential (or a mixed potential) which lies above the nickel reversible potential and below the copper reversible potential. In addition, the pH of these solutions, i.e. pH = 4, does not allow the formation of nickel oxides on the surface of the nickel. Therefore, in accordance with the mixed potential theory, copper continues to deposit at the expense of nickel dissolution, forming a classic galvanic corrosion cell. This process does not

stop immediately because the rate of surface coverage is slow, and in order to completely stop the reaction five to ten monolayers of copper have to be deposited (Roy *et al.*, 1994; Roy and Landolt, 1995; Bradley *et al.*, 1996).

The question one has to put is that, if this is the case, would copper then continue to deposit and nickel completely dissolve from the deposit? However, subsequent analysis showed that copper enrichment at the surface slowed down until the copper content reached about 80%, after which the reaction virtually stopped (Roy and Landolt, 1995; Bradley *et al.*, 1996). The galvanic corrosion is controlled by copper mass transfer through the liquid phase at the beginning, showing a linear growth of the Cu-rich layer (Roy and Landolt, 1995). Since the reaction stops due to surface enrichment of copper, the growth is inhibited quite suddenly when the thickness of the layer reaches about 10 nm (Roy and Landolt, 1995; Bradley *et al.*, 1996).

This showed that, although nickel had been presumed to be passive in the solutions, this assumption was incorrect. In fact, a few monolayers of Ni were lost due to galvanic corrosion, which then created a Cu-rich surface film which protected the underlying nickel. This phenomenon was not observed during the electrodeposition of Cu–Ni alloys because the loss of a few monolayers went undetected. In fact, corrosion measurements with an electrochemical quartz crystal nanobalance (EQCN) failed to show the loss of the base metal (Chaissang, 1997), presumably because the atomic weights of Cu, Ni and Co are similar. Since the oxidation of the less noble component is accompanied by the reduction of the noble material, galvanic corrosion could not be detected by monitoring changes in the mass of the deposit.

Further research was carried out to determine whether Ni passivated quickly when a passive potential was imposed on it. This was performed by driving the nickel potential to the regime where nickel oxide is expected to form (Meuleman *et al.*, 2002). It was found that indeed nickel dissolution was blocked after one or two monolayers of nickel were lost, due to the faster passivation kinetics (Meuleman *et al.*, 2002). It was found that the interfaces between the copper and nickel layers were sharper, which also corroborates that passivation was rapid (Meuleman *et al.*, 2004), and it has been estimated that almost 50% less nickel was lost by oxidation (Meuleman *et al.*, 2002).

Similar cases of galvanic corrosion have been observed during Cu–Co (Bradley and Landolt, 1999; Dulal *et al.*, 2004a; Dulal *et al.*, 2004b), Ni–Mo (Huang and Podlaha, 2004) and Ni–W (Franz *et al.*, 2008) deposition from citrate baths. The behaviour of the corrosion of cobalt from the deposit was somewhat different from the Cu–Ni system. Since copper and cobalt are immiscible, it was found that Cu nucleated preferentially on Cu and Co on Co. This meant that the areas that were Co-rich remained uncovered by copper (Kelley *et al.*, 2001; Dulal *et al.*, 2004b) leading to significantly more corrosion of Co than Ni. This continued dissolution from the matrix led to a porous structure of the coating and, in some cases, phase separation of cobalt and copper (Kelley *et al.*, 2001).

This unusual behaviour is not only applicable in aqueous electrolytes. Cu–Zn alloys deposited from ionic liquids have also shown galvanic corrosion (Zhu and Hussey, 2001). Metal redox reactions in these systems are very reversible and the electrolyte does not contain dissolved oxygen. This means that metal protection by passivation in solution cannot occur. In addition, many of the coatings obtained in ionic liquids are nanoporous and the electrolyte is in contact with the metallic material, leading to continued corrosion.

Recent reports on bimetallic Pt–Co catalysts used for fuel cells also exhibit galvanic corrosion during charge–discharge cycles (Hseih *et al.*, 2009; Fugier *et al.*, 2010). In these studies nanoparticles of catalysts were fabricated to obtain high surface area; however, in all cases, the surface approached platinum-type behaviour after many charge–discharge cycles due to the preferential dissolution or oxidation of the less noble component (Hseih *et al.*, 2009; Fugier *et al.*, 2010).

Since the activity of a catalyst is dependent on the stability of the material at the surface, retaining noble metal at the electrolyte–metal is a challenging problem indeed. Although corrosion aspects in catalyst design were not considered until recently, in order to develop high performance fuel cells this difficult issue will need to be addressed in the future. Earlier de-alloying studies (Kaesche, 2003) have provided methods to estimate at which atomic concentrations a less noble material will remain alloyed. These aspects should be incorporated in the design and fabrication of electrocatalysts in future.

2.6 Conclusions

The fundamental basis of corrosion has been elaborated with electrochemical thermodynamic and kinetics considerations. It has been shown that, in an aqueous environment, most metals derive stability from a nanoscale protective film formed at the surface of the material. It has been argued that corrosion loss before attainment of equilibrium can have a profound effect on the properties and performance of a material. The importance of these aspects in nanolayers, nanocoatings and nanoscale electrocatalysts has been used as illustrative case studies.

2.7 References

Aitchison, L. (1960), *A History of Metals*, Volumes 1 & 2. New York: Interscience.

Bakonyi, I., Tóth, J., Goualou, L., Becsei, T., Tóth-Kádár, E. *et al.* (2002), 'Giant magnetoresistance of electrodeposited $Ni_{81}Cu_{19}$/Cu multilayers', *J. Electrochem. Soc.*, **149**(4), C195–C200.

Bradley, P., Roy, S., and Landolt, D. (1996), 'Pulse-plating of copper-nickel alloys from a sulfamate solution', *J. Chemical Society, Faraday Transactions*, **92**, 4015–19.

Bradley, P. E. and Landolt, D. (1999), 'Pulse-plating of copper-cobalt alloys', *Electrochim. Acta*, **45**, 1077–87.

Buckle, R. (2007), 'The Recovery of Metals from Waste Solutions by Electrochemical Methods', Thesis, Newcastle University pp. 33–7 and 84–7.

Bull, S. J. and Jones, A. M. (1994) 'Multilayer coatings for improved performance', *Surf. Coatings Tech.*, **78**, 173–84.

Chaissang, E. (1997), 'In situ mass changes and stress measurements in Cu/$Fe_{20}Ni_{80}$ electrodeposited metal multilayers', *J. Electrochem. Soc.*, **144**, L328–L330.

Cookson, G. (2003) *The Cable: The Wire that Changed the World.* Stroud: Tempus.

Correia, A. N. and Machado, S. A. S. (2000), 'Electrodeposition and characterisation of thin layers of Ni-Co alloys obtained from dilute chloride baths', *Electrochim. Acta*, **45**, 1733–40.

Dulal, S. M. S. I, Charles, E. A. and Roy, S. (2004a), 'Characterisation of Co-Ni(Cu)/Cu Multilayers Deposited from a Citrate Electrolyte in a Flow Channel Cell', *Electrochim. Acta*, **49**, 2041–9.

Dulal, S. M. S. I., Charles, E. A. and Roy, S. (2004b), 'Dissolution from electrodeposited copper–cobalt–copper sandwiches', *J. Appl. Electrochem.*, **34**, 151–8.

Fei, J. Y. and Wilcox, G. D. (2006), 'Electrodeposition of zinc-nickel compositionally modulated multi-layer coatings and their corrosion behaviours', *Surf. Coatings Tech.*, **200**, 3533–9.

Foecke, T. and Lashmore, D. (1992), 'Mechanical Behaviour of Compositionally Modulated Alloys', *Scripta Metallurgica*, **27**, 651–6.

Franz, S., Marlot, A., Cavalotti, P. L. and Landolt, D. (2008), 'Pulse plating of Ni-W alloys from model electrolytes', *Trans. Inst. Metal Finishing*, **86**, 92–7.

Fugier, P., Passot, S., Anglade, C., Guétaz, L., Guillet, N. *et al.* (2010), 'Pt_xCo_y catalysts degradation in PEFC environments: mechanistic insights II. Preparation and characterisation of particles with homogeneous composition', *J. Electrochem. Soc.*, **157**, B943–C951.

Golodnitsky, D., Rosenberg, Y. and Ulus, A. (2002), 'The role of anion additives in the electrodeposition of nickel-cobalt alloys from sulfamate electrolytes', *Electrochim. Acta*, **47**, 2707–14.

Hall, E. O. (1951), 'The deformation and ageing of mild steel: III discussion of results', *Proc. Phys. Soc. B*, **64**, 747–53.

Hodgson, A. W. E., Mueller, Y., Forster, D. and Virtanen, S. (2002), 'Electrochemical characterisation of passive films on Ti alloys under simulated biological conditions', *Electrochim. Acta*, **47**, 1913–23.

Hseih, Y.-C., Wu, P.-W., Lu, Y.-J. and Chang, Y.-M. (2009), 'Displacement reaction in pulse current deposition of PtRu for methanol electro-oxidation', *J. Electrochem. Soc.*, **156**, B735–42.

Huang, Q. and Podlaha, J. (2004), 'Simulation of Pulsed Electrodeposition for Giant Magnetoresistance FeCoNiCu/Cu Multilayers', *J. Electrochem. Soc.*, **151**, C119–C126.

Hughes, A. E., Cole, I. S., Muster, T. H. and Varley, R. J. (2010), 'Designing green, self-healing coatings for metal protection', *NPG Asia Materials*, **2**(4), 143–51.

Jensen, J. D., Gabe, D. R. and Wilcox, G. D. (1998), 'The Practical Realisation of Zinc-Iron CMA Coatings', *Surf. Coatings Tech.*, **105**, 240–50.

Kaesche, H. (2003), *Corrosion of Metals: Physiochemical Principles and Current Problems.* Berlin: Springer-Verlag.

Kelley, J. J., Cantoni, M. and Landolt, D. (2001), 'Three-dimensional structuring of electrodeposited Cu-Co multilayer alloys', *J. Electrochem. Soc.*, **147**, C620–C626.

Kudo, K., Shibata, T., Okamoto, G. and Sato, N. (1968), 'Ellipsometric and radiotracer measurements of the passive oxide film on Fe in neutral solution', *Corr. Science*, **8**, 809–14.

Landolt, D. (2003), *Corrosion and Surface Chemistry of Metals.* Oxford: CRC Press; 350–5.

Lenczowski, S. K. J., Schönenberger, C., Gijs, M. A. and Jonge, W. J. M. (1995), 'Giant magnetoresistance of electrodeposited Co/Cu multilayers', *J. Magnetism and Magnetic Materials*, **148**, 455–65.

Liu, L., Li, Y. and Wang, F. (2010), 'Electrochemical corrosion behaviour of nanocrystalline materials – a review', *J. Mater. Sci. Technol.*, **26**, 1–14.

Luo, W., Xu, Y., Wang, Q., Shi, P. and Yan, M. (2010), 'Effect of grain size on corrosion of nanocrystalline copper in NaOH solution', *Corr. Science*, **52**, 3509–13.

Macdonald, D. D. (1999), 'Passivity – the key to our metals-based civilisation', *Pure Appl. Chem.*, **71**, 951–78.

Madore, C. (1993), 'Analyse théorique et réalisation pratique de nouveaux dispositifs expérimentaux pour l'étude de la distribution des courants partiels lors de l'électrodeposition d'alliage', Thesis 1189, EPFL publications.

Meuleman, W. R. A., Roy, S., Péter, L. and Varga, I. (2002), 'Effect of current and potential waveforms on sublayer thickness of electrodeposited copper-nickel multilayers', *J. Electrochem. Soc.*, **151**, C479–C486.

Meuleman, W. R. A., Roy, S., Péter, L. and Bakonyi, I. (2004), 'Effect of current and potential waveforms on GMR characteristics of electrodeposited Ni(Cu)/Cu multilayers', *J. Electrochem. Soc.*, **151**, C256–C261.

Miyazaki, K., Kainuma, S., Hisatake, K., Watanabe, T. and Fukumoro, N. (1999), 'Giant magnetoresistance in Co-Cu granular alloy films and nanowires prepared by pulsed-electrodeposition', *Electrochim. Acta*, **44**, 3713–19.

Oswin, M. G. and Cohen, M. (1957), 'Study of the cathodic reduction of oxide films on irons', *J. Electrochem. Soc.*, **104**, 9–16.

Petch, N. J. (1953), 'The cleavage strength of crystals', *J. Iron and Steel Institute*, **174**, 25–8.

Pourbaix, M. (1974), *Atlas of Electrochemical Equilibria in Aqueous Solutions*. Houston: National Association of Corrosion Engineers.

Ralston, K. D., Birbilis, A. D. and Davies, C. H. J. (2010), 'Revealing the relationship between grain size and corrosion rate of metals', *Scripta Materialia*, **63**, 1201–4.

Roy, S., Matlosz, M. and Landolt, D. (1994), 'Effect of corrosion on the composition of pulse-plated Cu-Ni alloys', *J. Electrochem. Soc.*, **141**, 1509–17.

Roy, S. and Landolt, D. (1995), 'Effect of Off-Time on the Composition of Pulse Plated Cu-Ni Alloys', *J. Electrochem. Soc.*, **142**, 3021–7.

Roy, S. (2009), 'Electrochemical Fabrication of Nanostructured, Compositionally Modulated Metal Multilayers (CMMMs)', in Schmuki, P. and Virtanen, S. (eds) *Electrochemistry at the Nanoscale*. Berlin: Springer-Verlag; 349–76.

Saji, V. S. and Thomas, J. (2007), 'Nanomaterials for corrosion control', *Current Science*, **92**(1), 51–5.

Schmuki, P. (2002), 'From Bacon to barriers: a review on the passivity of metals and alloys', *J. Solid State Electrochem.*, **6**, 145–64.

Shi, X. (2010), 'On the use of nanotechnology to manage steel corrosion', *Recent Patents on Engineering*, **4**(1), 1–6.

Smith, P. J. (2011), 'A Predictive Model for Microbiologically Influenced Corrosion (MIC) in Sub-Sea Production Pipelines', Thesis, Newcastle University.

Smith, P., Roy, S., Swailes, D., Maxwell, S., Page, D., Lawson, J. (2011), 'A Model for the corrosion of steel subjected to synthetic produced water containing sulfate, chloride and hydrogen sulphide', *Chemical Engineering Science*, **66**, 5775–5790.

Spray, J. and Nowak, U. (2006), 'Exchange bias in ferromagnetic /antiferromagnetic bilayers with imperfect interfaces', *J. Phys. D., Appl. Phys.*, **39**, 4536–9.

Tsalakos, T. and Jankowski, A. F. (1986), 'Mechanical Properties of Composition-Modulated Metallic Foils', *Annu. Rev. Mater. Sci.*, **16**, 293–313.

Tury, B., Lakatos-Varsanyi, M. and Roy, S. (2006), 'Ni-Co alloys plated by pulse currents', *Surface and Coatings Technology*, **200**, 6713–17.

United Nations (2004), *World Population to 2300*, Department of Economic and Social Affairs, Population Division, New York. Available from: http://www.un.org/esa/population/publications/longrange2/WorldPop2300final.pdf [Accessed 12 July 2011].

World Bank Group (2006), *The Outlook for Metals Markets*, Oil Gas, Mining and Chemicals Department, Washington. Available from: http://siteresources.worldbank.org/INTOGMC/Resources/outlook_for_metals_marketpdf [Accessed 12 July 2011].

Yu, S. Y. and Scully, R. J. (1997), 'Corrosion and passivity of Ti-13% Nb-13% Zr in comparison to other biomedical alloys', *Corrosion*, **53**, 965–76.

Zhu, Q. and Hussey, C. L. (2001), 'Galvanostatic pulse plating of Cu-Al alloy in a chloroaluminate molten salt: Room-temperature rotating ring disk electrode studies', *J. Electrochem. Soc.*, **148**, 395–402.

3

Understanding the corrosion resistance of nanocrystalline materials: the influence of grain size

X. Y. ZHANG, Chongqing University, China

Abstract: Zirconium and its alloys are widely used in nuclear reactors, both as structural components and as fuel cladding materials. In nuclear reactors, increasing the fuel burn-up is an effective means of decreasing cost. Waterside corrosion and the hydrogen absorption reaction of zirconium alloys are the main factors restricting further improvements to fuel burn-up rate. Once the chemical composition of an alloy has been determined, the properties of the alloy will be controlled by the processing technique selected. Several factors that affect the corrosion of nanocrystalline metals, such as grain boundary, atomic diffusion and phase interface characteristics, among others, are discussed. When the grain size of the metal is below 100 nm or in the ultra-fine range (100–1000 nm), its mechanical, physical and chemical properties, along with its microstructural characteristics, will be very different from those of metals with coarse grains.

Key words: zirconium, nanocrystalline materials, corrosion resistance, grain size.

3.1 Introduction

This chapter first discusses the relationship between the corrosion rate of nanocrystalline (NC) metals versus their grain size, then presents a computational model for the investigation of the interaction of grain size and electron activity. As an example, the corrosion rate of NC zirconium and its alloys has been calculated for the purposes of comparison with the experimental results obtained. Finally, the structural evolution of NC and polycrystalline (coarse-grained, CG) zirconium during corrosion and the role of grain boundaries (GBs) in both metals have been experimentally studied to provide insights into the corrosion behaviors of NC metals.

3.2 Grain boundary and electron movement: the corrosion mechanism of nanocrystalline metals

Many experimental results have shown that when the grain size of a metal is below 100 nm or in the ultra-fine range (100–1000 nm) its mechanical properties and microstructural characteristics will be very different from those of metals with coarse grain size, such as aluminum alloy,[1,2] steel[3] and titanium alloy.[4,5] However, the corrosion resistance of these NC materials remains relatively

unclear in terms of their corrosion characteristics and the influencing factors involved.

From a materials science perspective, the physical, chemical and mechanical properties of a material are determined by its chemical components and constitutional structure. Once the chemical composition of an alloy is established, the properties of the alloy can be determined by the processing technique used. Corrosion behavior can thus be influenced by several factors. For example, AZ91D Mg alloy[6] has a fine grain structure and second phase (β), and a die-cast sample showed that it had a higher corrosion resistance than ingot samples, indicating that the corrosion rate decreased with the grain size of the α matrix and the precipitate particle size of the β phase. Fujimoto *et al.*[7] studied the influence of grain size on the resistance of 304 stainless steel to corrosion by a NaCl + HCl solution. They found that a surface layer with a grain size of 25–30 nm has very good corrosion resistance. These authors hypothesized that this good corrosion resistance could not be attributed to the fine structure of the metal, but was instead the result of the absence of sulfide, nonmetallic elements and impurities.

Xu *et al.*[8] prepared a surface NC layer of zircaloy-4 alloy by using laser treatment and Ar ion beam bombardment. They then studied its corrosion behavior in a H_2SO_4 solution. The result indicated that the NC layer has remarkable corrosion resistance. They discussed the Gibbs free energy of the fine structure and suggested that the good corrosion resistance should be attributed to the nanostructure of the matrix and to the dispersion of the fine precipitated particles. Viana *et al.*[9] reported that, for 7075 aluminum alloy, very fine and distributed second phase particles can improve the stress corrosion resistance of the alloy. In addition, the good corrosion resistance of $Ti_{0.43}Al_{0.52}Cr_{0.03}Y_{0.02}N$ nanostructured film in both air and water was attributed to the density of the film structure.[10] Whatever the correct theory, the question remains whether the unusual corrosion characteristics discussed above are the result of the reduction in grain size.

It is generally believed that the corrosion of CG metals relates to the GBs.[11–15] Intergranular corrosion (IGC) is commonly suggested as the most important mechanism and plays a major role in the corrosion of CG metals. This means that refinement of the grain decreases the corrosion resistance because of the increase in the volume fraction of GBs, despite the fact that it enhances the strength and toughness of metals. Therefore, ultra-fine or NC metals have generally been expected to show low corrosion resistance because of the huge numbers of GBs resulting from the nanoscale grain size.[16–21] However, as mentioned above, many studies have reported that NC metals actually have superior corrosion resistance.[22–30] These conflicts suggest that it is difficult to predict the corrosion behavior of NC metals based on their CG analogs alone, and that there may be a different corrosion mechanism in NC metals.

According to the corrosion theory, a corrosion course is controlled by the activation of electrons. In most metals, the electron mean free path is approximately a few dozen nanometers. In contrast to what is observed for CG and ultra-fine

metals, in which the grain size is in the range of 100–1000 nm, the grain size of NC metals is of the same order of magnitude as the electron mean free path, or may even be smaller than the electron mean free path. Therefore, the GBs of NC metals must restrict the activity of electrons and play a different role from that of CG analogs in corrosion.

3.3 Theory of interaction between the grain boundary of nanocrystalline metals and electron movement

According to the Wagner metal oxidation theory, the metal oxidation process is controlled by the crystal lattice diffusion in the oxide phase and by diffusion along the GB. It also conforms to the parabola rule at high temperatures:

$$\frac{\partial y}{\partial t} = \frac{k}{y} \qquad [3.1]$$

Here, y is the weight gain of the oxide film, k the corrosion rate constant and t the time.

Many previous experimental results have indicated that, similarly to the oxide of zinc, the oxide of zirconium is an n-type semi-conductor. Its oxidation reaction is of the internal type.[31] Therefore, the oxidation rate constant of zirconium can be expressed as below:[32]

$$k = (1+Z)\times Z\times C_O \times D\times \left(1-\frac{C_O^{(a)}}{C_O^{(b)}}\right) \qquad [3.2]$$

Here D is the diffusion coefficient of O in an oxide film, Z is the zirconium ion valence number in the oxide phase (+4), C_O is oxygen (O) ion total concentration in ZrO_2, $C_O^{(a)}$ is the concentration of O in zirconium at the Zr/ZrO_2 interface and $C_O^{(b)}$ is the concentration of O in ZrO_2 at the ZrO_2/O_2 interface.

The diffusion coefficient D in Eq. 3.2 can be computed from the equation below:[33]

$$D = \frac{\sigma_0 k_B T}{q^2 n} \qquad [3.3]$$

Here σ_0 is the electrical conductivity of the oxide, k_B is the Boltzmann constant, n is the current carrier density, q is the electron charge and T is the temperature.

In order to discuss the relation between the electrical conductivity of oxide and the grain size of metal, the electrical conductivity of pure metal should first be considered. A correction coefficient r, which relates the electrical conductivity of pure metal to that of the oxide, can then be introduced, as follows:

$$\sigma_0 = r\sigma \qquad [3.4]$$

Here σ is the electrical conductivity of pure metal. The r is a correction coefficient, and its value is between 0 and 1.

In Eq. 3.4, σ relates to the electron structure and scattering in the metal. From the free electron theory of metal, Fermi velocity v_F is defined as the free electron movement velocity at the highest energy (E_F), and the relaxation time τ is the time between the first and second collisions of the electron. So the electron mean free path l_F nearby the Fermi surface can be expressed as $l_F = v_F\tau$. In addition, σ can be also expressed as below:[34]

$$\sigma = \frac{Nq^2 l_F}{mv_F} \qquad [3.5]$$

Here N is the electron density, l_F is the electron mean free path, v_F is the Fermi velocity and m is the electron mass.

In metals, the electron can move freely along any direction in three dimensions. However, when the grain size of the metal is in nanoscale and is smaller than the electron mean free path, the electron movement is restricted by GB. The electron quantum effect which resulted from the scatter of GBs appears in NC metal.[32,35] Therefore, for NC metal the electron mean free path can be influenced by the grain size. In this case, the electron mean free path l_F in Eq. 3.5 can be replaced by the effective electron mean free path l_{eff}, namely,

$$\sigma = \frac{Nq^2 l_{eff}}{mv_F} \qquad [3.6]$$

For further discussion, it is defined that the electron mean free path of the bulk metal is l_{bulk} and the average grain radius of NC metal is R. When $R < l_{bulk}$, the relation between the l_{bulk} and R can be expressed as below:[35]

$$\frac{1}{l_{eff}} = \frac{1}{R} + \frac{1}{l_{bulk}} \qquad [3.7]$$

Substituting the parameters of Eqs 3.2–3.4 and 3.6 into Eq. 3.1 and integrating both sides of Eq. 3.1, the following relation is obtained:

$$y^2 = r\frac{Nk_B Tl_{eff}}{mv_F n} \times (1+Z) \times Z \times C_O \times \left(1 - \frac{C_O^{(a)}}{C_O^{(b)}}\right) \times 2 \times t + C \qquad [3.8]$$

$$k = r\frac{Nk_B Tl_{eff}}{mv_F n} \times (1+Z) \times Z \times C_O \times \left(1 - \frac{C_O^{(a)}}{C_O^{(b)}}\right) \times 2 \times t \qquad [3.9]$$

Here C is the integral constant. The influence of grain size on the corrosion resistance of NC zirconium metal can be deduced from Eqs 3.7 and 3.8.

From the Zr–O phase diagram[36] it can be calculated that $C_O = 0.378$, $C_O^{(S)} = 0.333$, and $C_O^{(b)} = 0.614$. The carrier current density n is[37] 4.954×10^{28}.

In order to calculate v_F, the effective electron mass m^* and effective Fermi energy E_F^θ were considered. Zirconium is a transition metal. The electron

conduction process can also be influenced by the hole. The electron structure of zirconium is $4d^25s^2$, with an overlap between the 4d band and the 5s band. The conductivity of zirconium is therefore provided by the electron of the 5s band and the hole of the 4d band. The s electron can be scattered either to the s band or to the d band. The effective electron mass should therefore be considered. This is about 0.1–0.01 of the free electron mass.[34] The effective mass m^* of zirconium can be calculated by a simplified method as shown below:[38]

$$\frac{m}{m^*_{\pm}} = 1 \pm \frac{2E_n}{|V_n|} \qquad [3.10]$$

$$E_n = \frac{\hbar^2}{2m}\left(\frac{\pi}{a}n_1\right)^2 \qquad [3.11]$$

where α is the crystal lattice constant, $\hbar$ the Planck constant, m the electron stationary mass, n_1 the number of Brillouin zones and V_n the infinitesimal disturbance corrected value of the n step energy. From Eqs 3.10 and 3.11 it can be calculated that the effective electron mass $m^* = 1.547\times10^{-32}$ kg; $E_F^{\theta} = 1.062\times10^{-16}$ J, and $v_F^{\theta} = 1.712\times10^{9}$ m/s.

The resistance, ρ, of zirconium is $4\times10^{-7}\ \Omega$ m at 20°C.[39] At higher temperatures, its physical properties will be changed as the metal lattice undergoes thermal expansion. Zirconium has a hexagonal close-packed (hcp) structure, and the relation between the volume expansion coefficients a_V and linear expansion coefficients along the a and c axes is:

$$a_V = 2a_a + a_c \qquad [3.12]$$

Here a_a is the linear expansion coefficient along the a axis, a_c is the linear expansion coefficient along the c axis. The relation between the unit volume and temperature is:

$$V_t = V_0 \times (1 + a_V \Delta T) \qquad [3.13]$$

Here V_0 is the unit volume at 273 K, $\Delta T = T - 273$ K, and T is the Kelvin temperature.

From Eqs 3.12 and 3.13 and Eqs 3.2, 3.7 and 3.9, the relation between the effective electron mean free path l_{eff} and the grain size of zirconium at different temperatures was calculated as shown in Fig. 3.1. The relation between the corrosion rate constant k and grain size was calculated as shown in Fig. 3.2.

From Fig. 3.1 and 3.2, it can be observed that the effective electron mean free path l_{eff} and corrosion rate constant k decrease nonlinearly with decreasing grain size. These results indicate that the quantum effect resulting from GBs increases remarkably with the decrease in grain size. However, it should be noted that, when the grain size varies from a size up to 100 nm to a size below 100 nm, the physical and the chemical properties of the metal do not change abruptly. As grain size decreases, the quantum effect gradually increases. For a metal with a grain size far below 100 nm, the quantum effect has a fatal influence on the electrical

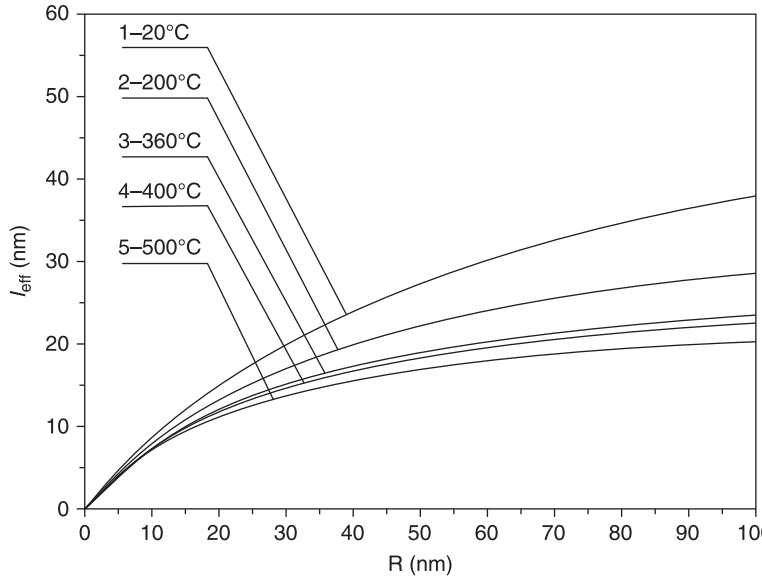

3.1 Relation of effective electronic mean free path, l_{eff}, and grain size (average grain radius R) at different temperatures (corresponding to Eq. 3.7). Effective electronic mean free path is about several tens of nanometers, indicating that grain size of NC metals can restrict electron movement.

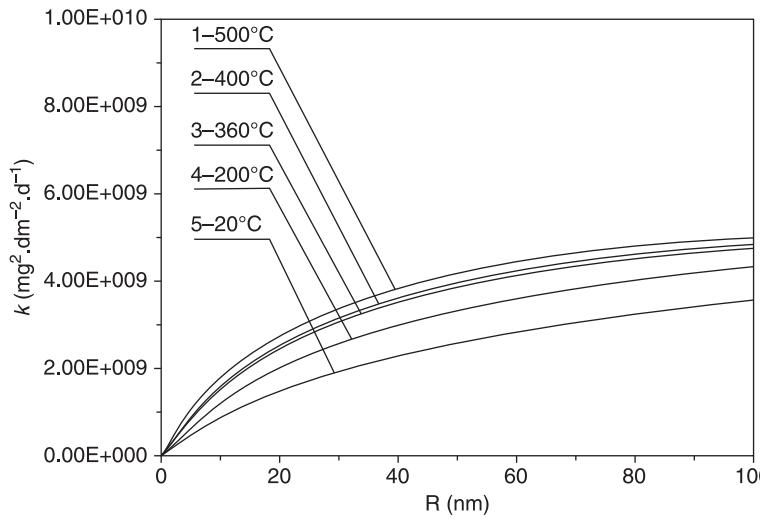

3.2 Relation of corrosion rate constant, *k*, decreases with decreasing grain size (average grain radius R) and increases with increasing temperature (corresponding to Eq. 3.9). Compared with the result of Fig. 3.1, the result indicates that GB restriction on the movement increases with decreasing grain size.

properties of the metal. Thus, the electrical conduction mechanism of the metal undergoes gradual changes between coarse grain size and NC grain size. The trend of these changes can be forecast from Fig. 3.1 and 3.2.

From Eq. 3.8, the corrosion curves of zirconium metal with different grain sizes at different temperatures were calculated as shown in Fig. 3.3. The curves of normal values in Fig. 3.3 were calculated according to the electron mean free path of zirconium with a coarse grain size of about 3–10 ηm.

The results in Fig. 3.3 show that the corrosion resistance of NC zirconium is far superior to that of zirconium with coarse grain size. On the other hand, with the decrease of grain size, the corrosion weight gain of NC zirconium metal also decreases, as does the corrosion rate constant (see Fig. 3.2). The refinement of grain size can thus remarkably improve the corrosion resistance of zirconium metal.

In general, the influence of grain size on the oxidation resistance of CG metals can be divided into negative and positive effects.[40,41] A negative example is IGC, in which the corrosion behavior of metals is controlled by the corrosion dynamic

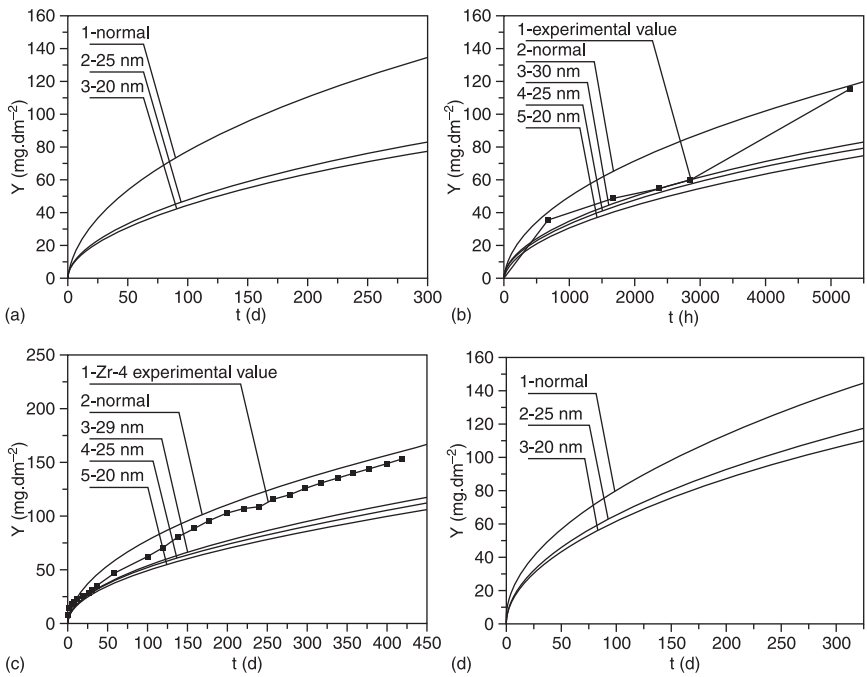

3.3 Corrosion kinetics of zirconium metal with different grain size[42,43] ('normal' means coarse grain size): (a) at 200°C; (b) annealed Zr–0.2Nb alloy in water at 360°C using static autoclave according to the ASTM G2 method; (c) zircaloy-4 alloy in steam at 400°C/10.5 MPa; (d) at 500°C.

of GBs. In this case GBs facilitate corrosion. However, for some metals, an oxide protection layer, formed in the initial stage of oxidation, can inhibit further oxidation of the metal. In this case, grain refinement can lead to an increase in the number of active atoms on the surface, accelerating the formation of the oxide protection layer. Thus, grain refinement has a positive effect on the corrosion resistance of the metal. For zirconium metal, the ratio of oxide volume to metal volume is 1.56, causing the formation of the oxide protection layer.[32] The refinement of grain size can therefore improve the corrosion resistance of zirconium metal, in accordance with the results of Fig. 3.2 and 3.3. Furthermore, it can be seen from Fig. 3.3 that temperature has an important influence on the effect of grain size on the corrosion resistance of zirconium metal. Specifically, with increasing temperature, the lattice expands and the effective electron mean free path l_{eff} varies, meaning that the grain size effect varies with the change in temperature.

3.4 Lattice distortion, Fermi energy and Fermi velocity of nanocrystalline metals

Conductivity (or resistance) is an important property of conventional metals. It has been reported that there is a difference in electrical resistivity between NC and CG metals.[44–47] This difference results from the lattice distortion of the NC materials.[48] It has also been observed that the lattice of nanoparticles with a free surface contracts as grain size decreases, because it undergoes huge surface tension.[49,50] However, although the grains of NC metals do not have an absolutely free surface, the vacancy content or solid solubility of the solute atom actually increases substantially as grain size decreases. The lattice therefore expands as grain size decreases,[51–54] meaning that the relationship between lattice distortion and electrical resistivity should also be considered. However, the means by which grain size and lattice distortion influence electrical resistivity in NC metals remains unclear.

According to the correlation between conductivity and Fermi velocity, the relation between the electrical conductivity and resistivity, the electrical resistivity can be defined as below:[55]

$$\frac{1}{\rho} = \sigma = \frac{Ne^2 l_F}{m^* V_F} \qquad [3.14]$$

where ρ is the electrical resistivity, N is the electron density, e is the electron quantity, l_F is the electron mean free path, V_F is the Fermi velocity, and m^* is the effective electron mass.

Based on the metal free electron theory, Fermi velocity V_F is defined as the free electron movement velocity at the highest energy E_F. The relation between V_F, E_F and lattice distortion η may be given by:[56]

$$V_F = \sqrt{\frac{2E_F}{m^*}} = \sqrt{\frac{2E_F^0}{m^*}}(1+\eta)^{-1} \quad [3.15]$$

where E_F is the Fermi energy, E_F^0 is the Fermi energy at ground state, and η is the lattice distortion.

Combining Eqs 3.14 and 3.15, ρ can be expressed as:

$$\rho = \frac{1}{\sigma} = \frac{\sqrt{2m^* E_F^0}}{Ne^2 l_F}(1+\eta)^{-1} \quad [3.16]$$

In light of the restriction imposed by GBs on electron movement in NC metals, when the average grain radius (R) of NC metal is less than that of the electron mean free path of bulk metal (l_{bulk}), the electron mean free path (l_F) can be replaced by the effective electron mean free path (l_{eff}), i.e. Eq. 3.13. Therefore Eq. 3.16 may be rewritten as:

$$\rho = \frac{1}{\sigma} = \frac{\sqrt{2m^* E_F^0}}{Ne^2 l_{eff}}(1+\eta)^{-1} \quad [3.17]$$

According to Eqs 3.12, 3.13 and 3.17, the relation between ρ and t may be given by:[57]

$$\rho = \frac{1}{\sigma} = \frac{\sqrt{2m^* E_F^0}}{Ne^2 l_{eff}}(1+1.01a_V t)^{1/3} \quad [3.18]$$

As discussed in Section 3.2, there is an overlap between the 4d band and the 5s band because the electron structure of zirconium is $4d^2 5s^2$. Therefore, the conductivity of zirconium is provided by the s electron of the 5s band and the hole of the 4d band. The s electron can be scattered to either the s band or the d band. For alkaline metals, the s electron can only be scattered to the s band. Thus, the resistance of transition metals is higher than that of alkaline metals. Similarly to semi-conducting materials, zirconium has a considerable band gap, which is about 1.64 eV. Therefore, the effective electron mass should be taken into account. The effective electron mass is about 0.1–0.01 of the free electron mass.[57,58]

According to Eqs 3.14–3.18, the changes in the electrical resistivity and the lattice distortion of zirconium have been calculated at 298 K, as shown in Fig. 3.4(a). The electrical resistivity increases as the lattice distortion increases. A comparison of the value of electrical resistivity of 20 nm with that of 40 nm reveals that the average value of electrical resistivity of 20 nm is about 1.62 times more than that of 40 nm. Fig. 3.4(b) shows the variation in electrical resistivity and temperature at the different grain sizes. It can be observed that the electrical resistivity increases with the temperature. The average value of electrical resistivity of 20 nm is approximately twice that of 60 nm, and about 1.45 times that of 40 nm. So it can be concluded that the smaller the grain size in zirconium, the higher the electrical resistivity that can be obtained.

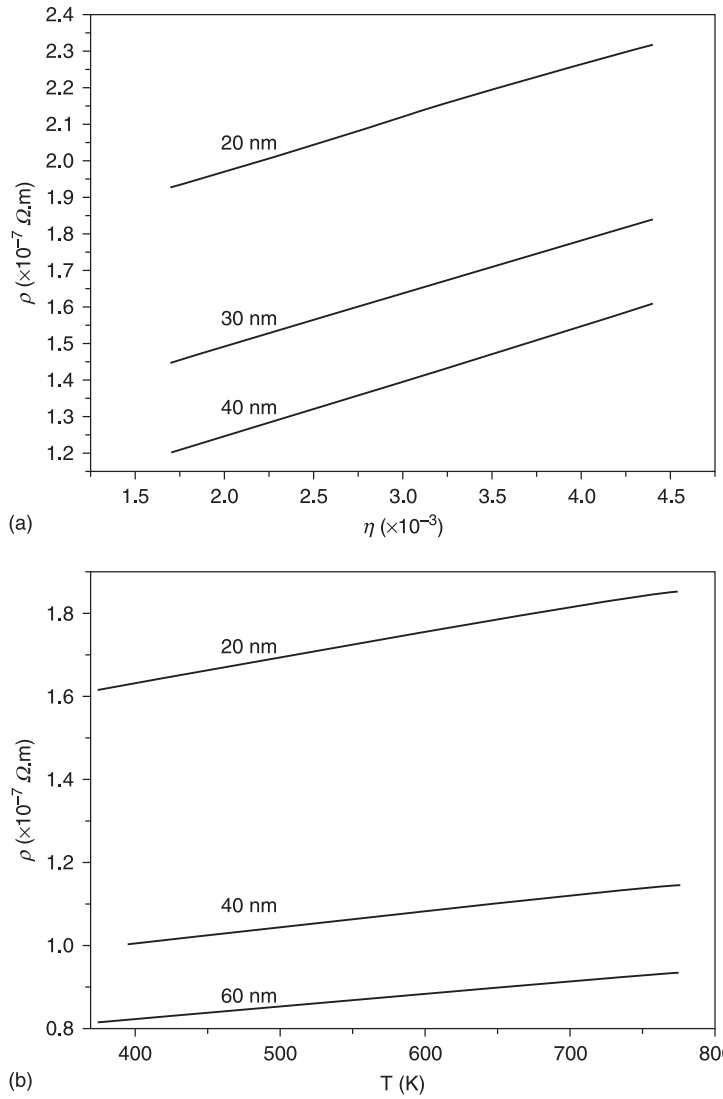

3.4 (a) Electronic resistivity as a function of lattice distortion at 298 K under different grain sizes. (b) Electronic resistivity as a function of temperature under different grain sizes.

3.5 Influence of reduction in grain size

3.5.1 Corrosion dynamics of nanocrystalline metals

Zircaloy-4 was obtained by the vacuum arc melting method. The chemical composition of the ingot is Zr–Sn (1.50 wt%) – Fe (0.20 wt%) – Cr (0.10 wt%) – O

(0.003 wt%). By hot and cold rolling and annealing treatments, the grain size in the alloy is 2–4 μm. A surface NC layer was prepared by high speed shot-peening for 60 min at room temperature (293 K). After a polishing treatment, the chemical composition of the NC is the same as that of the center part of the sample. The change in nanoscale grain size versus the distance from the sample surface is shown in Figure 3.5(a). Figure 3.5(b) shows a transmission electron microscopy (TEM) image of the microstructure near the sample surface (about 3 ηm). Figure 3.5(c) shows a diagram of the grain size distribution analyzed by the Image-Pro Plus software. The average grain size of the surface NC layer is about 20–30 nm.[26,30]

An oxidation experiment was carried out in an autoclave at 673 K/10.3 MPa and 773 K/10.3 MPa. Following different lengths of time in the autoclave, the samples were taken out and analyzed. The microstructures were examined by X-ray diffraction (XRD), scanning electron microscopy (SEM), energy dispersive spectrometer (EDS) and TEM.

Figure 3.6 shows the surface morphology of the NC and CG zircaloy-4 at 673 K/10.3 MPa for 160 days and 773 K/10.3 MPa for several hours, respectively. It can be observed that, as corrosion time increases, the surface of the CG zircaloy-4 becomes covered by oxide films of a grey–white color. The oxide films of NC zircaloy-4 present a natural metallic luster. Figure 3.7(a) shows the oxidation kinetics (oxide film thickening) curves of the NC and CG zircaloy-4 at 673 K/10.3 MPa. In the initial stages of corrosion, the thickness value of the oxide films formed on the NC substrate is equal to that of the oxide films formed on the CG substrate. As corrosion time increases, the growth rate of the oxide (ZrO_2) films formed on the NC substrate is lower than that of the oxide films formed on the CG substrate. Specifically, after 160 days at 673 K/10.3 MPa, the ZrO_2 film thickness of the NC zircaloy-4 is about 70% of that of the CG zircaloy-4. After 16 hours at 773 K/10.3 MPa (see Fig. 3.7(b)), the ZrO_2 film thickness of the NC zircaloy-4 is about 1% of that of the CG zircaloy-4, which indicates that NC refinements provide a 100-fold improvement in the corrosion resistance of the zircaloy-4. These results reveal that the corrosion resistance of a NC zircaloy is superior to that of a CG zircaloy. After surface NC treatment, the movement of electrons is affected by the grain boundary. As the grain size decreases, the grain boundary quantum effect increases, leading to a lower corrosion rate and improved corrosion resistance.

Previous studies[59,60] showed that the dominating factors that control oxidation were defects and voids during the initial stages of corrosion. As the thickness of the oxide films increased, the corrosion mechanism for zircaloy was mainly controlled by the diffusion of oxygen ions and the reaction rate of oxygen ions with metal ions at the oxide/metal interface. The oxide compact film which formed during the initial oxidation stages could impede the further diffusion of oxygen ions, leading to a lower diffusion velocity of oxygen and an abrupt decrease in oxygen content near the oxide/metal interface. The grain size of the ZrO_2 film of NC zircaloy-4 was confirmed to be smaller[27] than that of the ZrO_2 film of CG

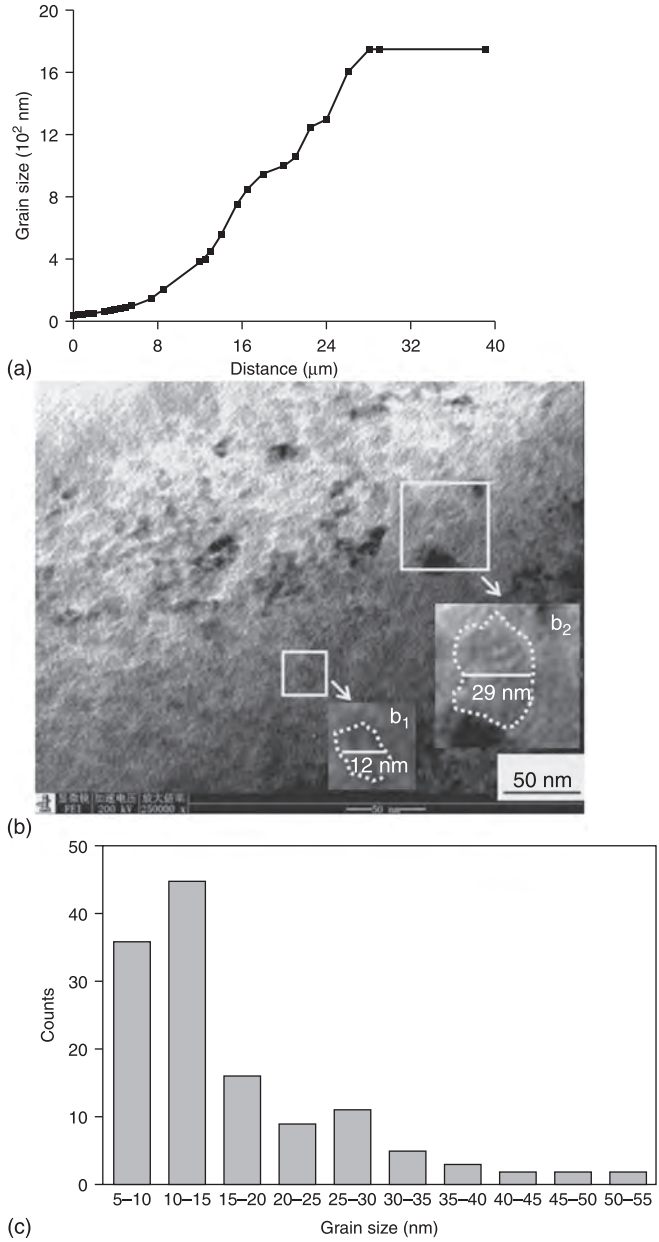

3.5 (a) The change of nanoscale grain size versus the distance from the sample surface. (b) TEM image of microstructure near the sample surface (about 3 ηm). Insets are the magnifications (b_1 and b_2) to indicate fine grains (marked by dashed lines). (c) Diagram of grain size distribution.

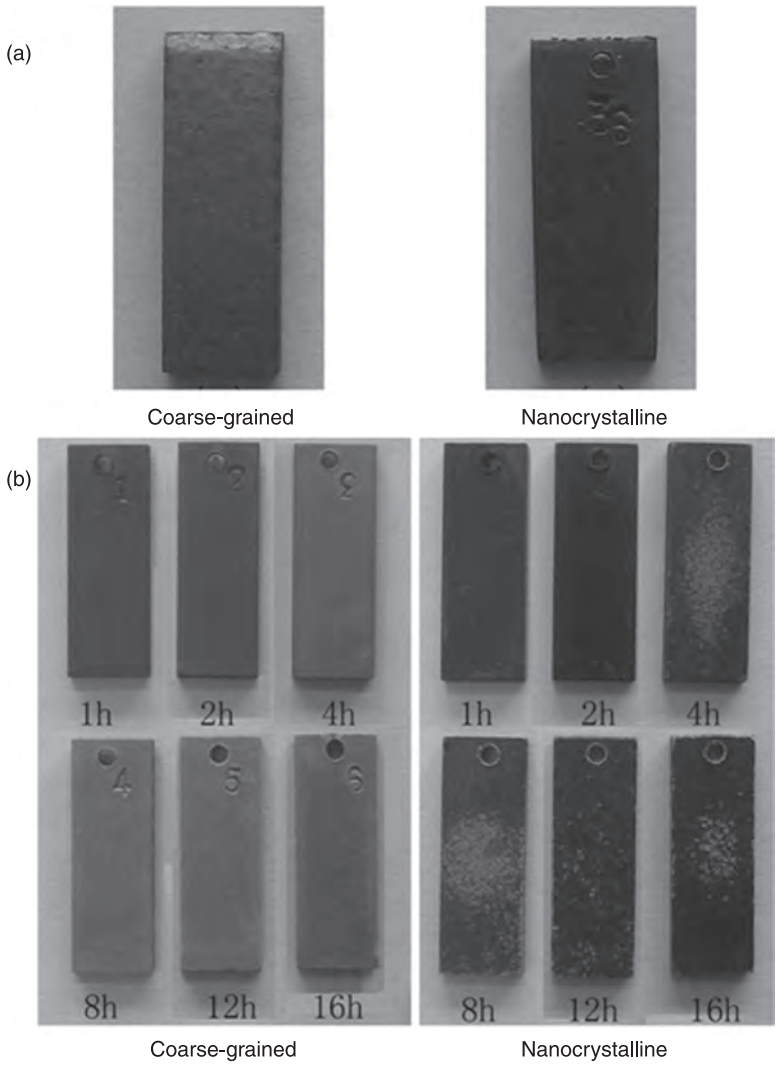

3.6 The surface morphology of CG zircaloy-4 and NC zircaloy-4 at (a) 673 K/10.3 MPa for 160 days and (b) 773 K/10.3 Mpa for up to 16 hours.

zircaloy-4. Figure 3.8 shows the oxygen content distribution of the ZrO_2 film and of metal analyzed using an EDS.[61] The samples were oxidized for 100 days at 673 K/10.3 MPa. The principal difference between Fig. 3.8(a) and 3.8(b) is that the oxygen content is higher and decreases gradually at the ZrO_2/CG metal interface, but decreases abruptly at the ZrO_2/NC metal interface. The oxidation of

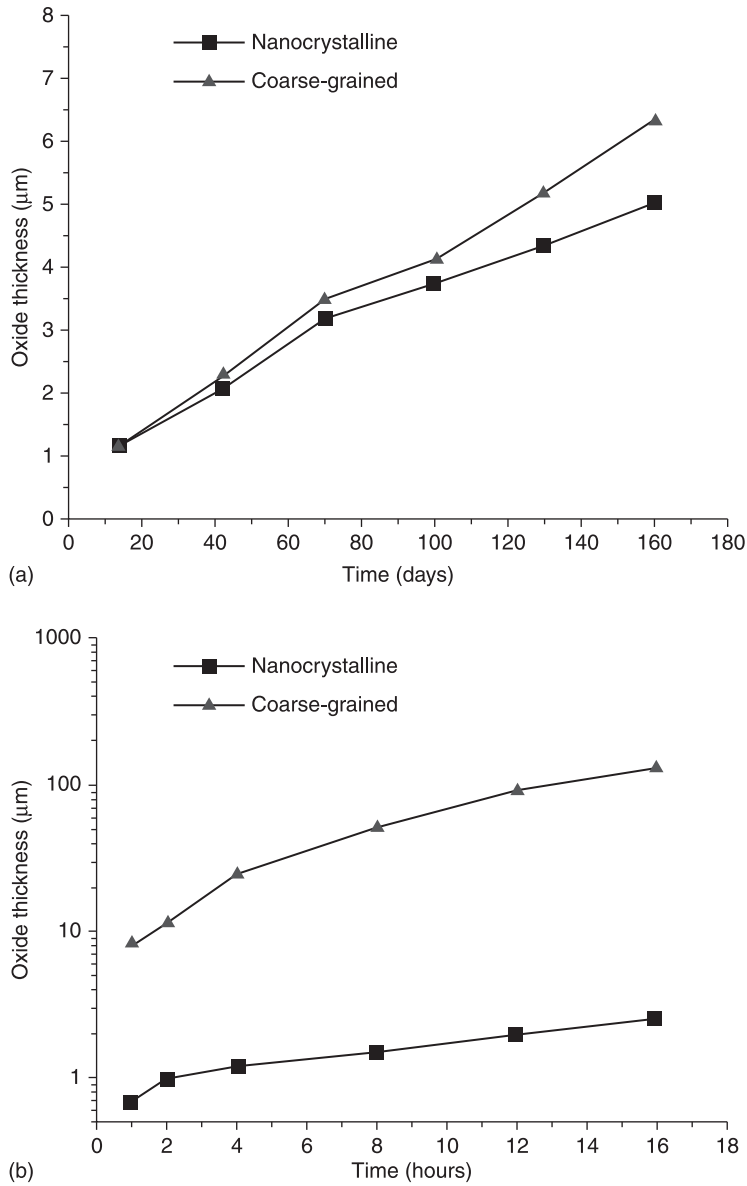

3.7 The oxidation kinetics curves of CG zircaloy-4 and NC zircaloy-4 at (a) 673 K/10.3 MPa and (b) 773 K/10.3 MPa.

zirconium was controlled by the diffusion of oxygen ions and by the reaction at the ZrO_2/metal interface.[62–64] The result of Fig. 3.8(a) implies that the diffusion velocity of the oxygen is lower than the interface reaction velocity of the ZrO_2/NC metal, resulting in an abrupt decrease in oxygen content near the interface.

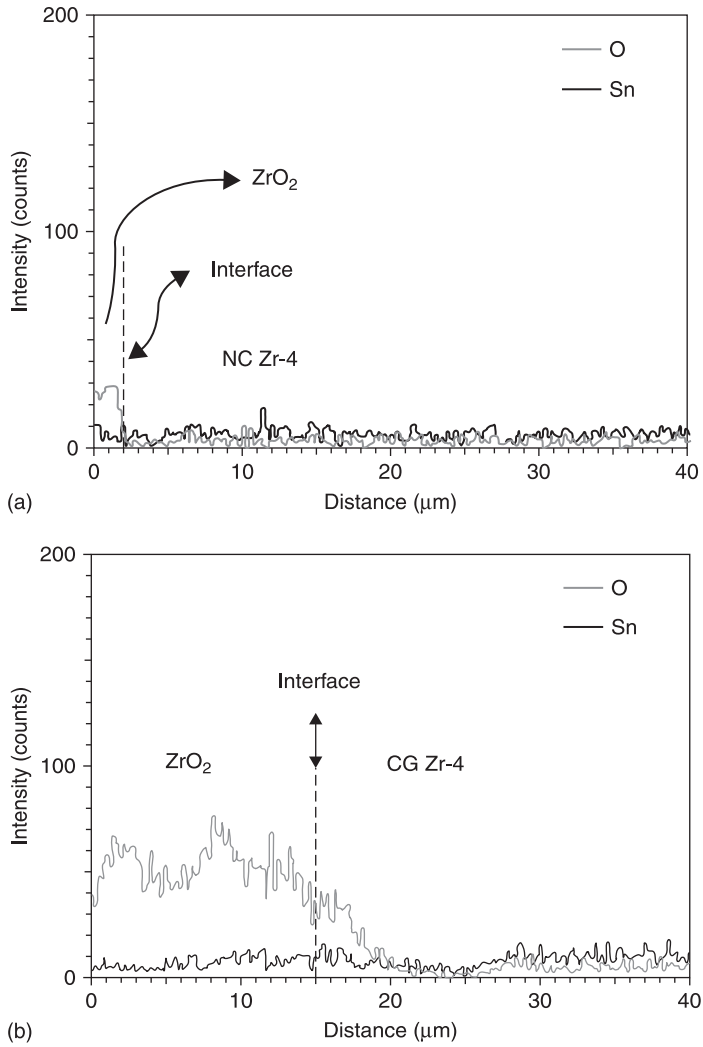

3.8 The oxygen content distribution in ZrO_2 film formed on NC substrate (a) and CG substrate (b). The samples were oxidized for 100 days at 673 K/10.3 MPa.

Turning to the oxide film of the CG zircaloy-4, this loose film cannot impede oxygen diffusion because of the transformation from tetragonal to monoclinic phase. Oxygen diffuses along the negative ion vacancies, voids and micro-cracks, and reacts with the metal matrix. The diffusion velocity of the oxygen is therefore higher than the interface reaction velocity of the ZrO_2/CG metal, resulting in a large oxygen diffusion depth (about 20 μm; see Fig. 3.8(b)) and a gradual decrease in oxygen content near the interface.

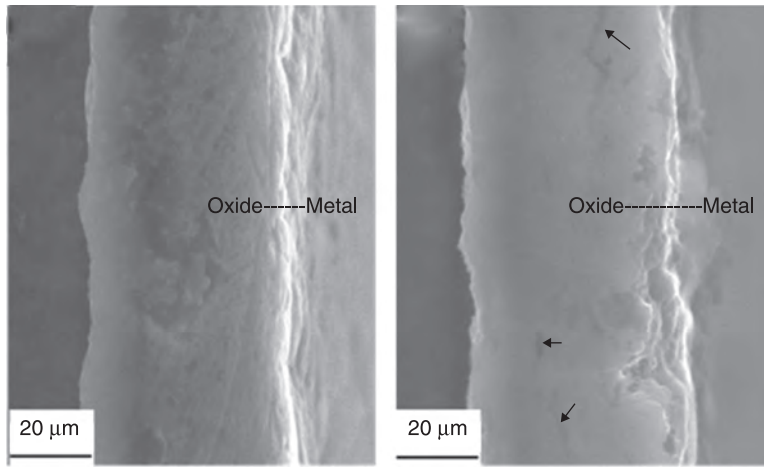

3.9 SEM cross-section images of the oxide formed on (a) NC and (b) CG after a corrosion test for 130 days.

Figure 3.9 shows SEM images of the cross-section of oxide formed on the NC and CG zircaloy-4 respectively. For CG zircaloy-4, some obvious cracks are observed in the films (as seen from the black arrows). Furthermore, the oxide/NC metal interface is more regular and smoother than the oxide/CG metal interface. Previous studies[60,65] have confirmed that, during the corrosion transition period, clusters of voids are generated in oxide films due to the invasion of oxygen ions. On the one hand, the void clusters absorb the anion vacancies in the oxide film. On the other, they can promote the reaction of the water molecules with electrons, which can in turn generate hydrogen and oxygen ions, with the latter used in the growth of oxide films. The existence of voids can thus induce an inconsistent corrosion rate, leading to an irregular oxide/metal interface. Furthermore, the accumulation and growth of voids can generate cracks, and the cracks will degenerate the combining capacity of the oxide films with the metal matrix.[66] Figure 3.9 shows that the integrity of oxide films and the combining capacity of oxide films with the metal matrix in NC zircaloy-4 are superior to those in CG zircaloy-4.

3.5.2 Structural evolution of nanocrystalline zircaloy at high temperature and pressure

The microstructure of oxide films formed on the NC zircaloy-4 was investigated by TEM. As shown in Fig. 3.10, after 42 days of corrosion, the oxide film was composed solely of tetragonal ZrO_2 (t-ZrO_2) (see diffraction pattern in

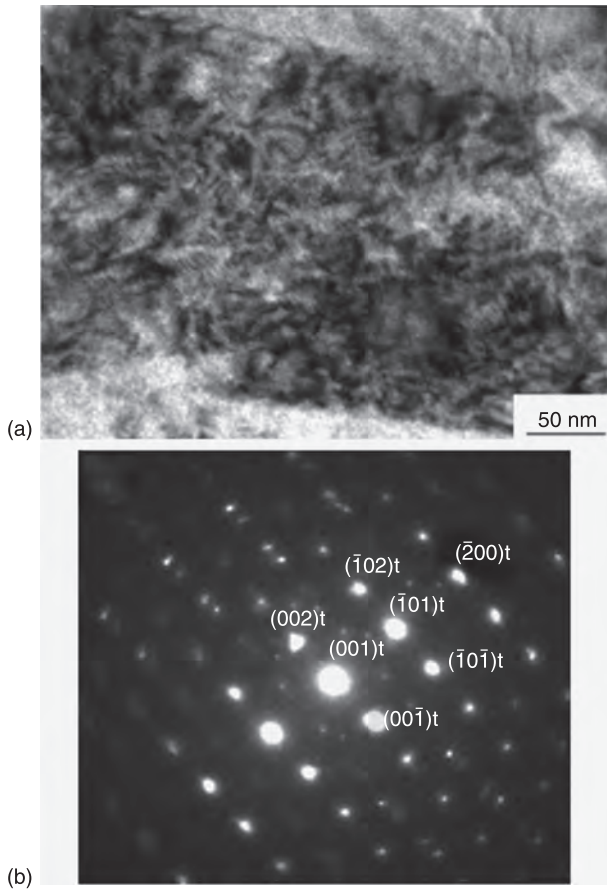

3.10 (a) TEM image of oxide film formed on NC zircaloy-4 after corrosion for 42 days, indicating that the oxide film was formed only by t-ZrO_2, as seen on diffraction pattern (b).

Fig. 3.10(b)). However, after 70 days of corrosion (see Fig. 3.11), monoclinic ZrO_2 (m-ZrO_2) can be found (see arrows in Fig. 3.11(a) and the diffraction pattern in Fig. 3.11(b)). This phenomenon implies that phase transformation from t-ZrO_2 to m-ZrO_2 has occurred and that some t-ZrO_2 has transformed into m-ZrO_2. Figure 3.12(a) shows a TEM image of an oxide film after a corrosion test lasting 130 days. Only an m-ZrO_2 phase was found, indicating that phase transformation was completed and t-ZrO_2 had disappeared (see diffraction pattern Fig 3.12(b)).

It has been observed[20,26,28,67–71] that two structures of equiaxed and columnar (monoclinic) crystals exist in the oxide films of zircaloy-4. The columnar crystal was found to be composed of m-ZrO_2, while the equiaxed crystal was found to be

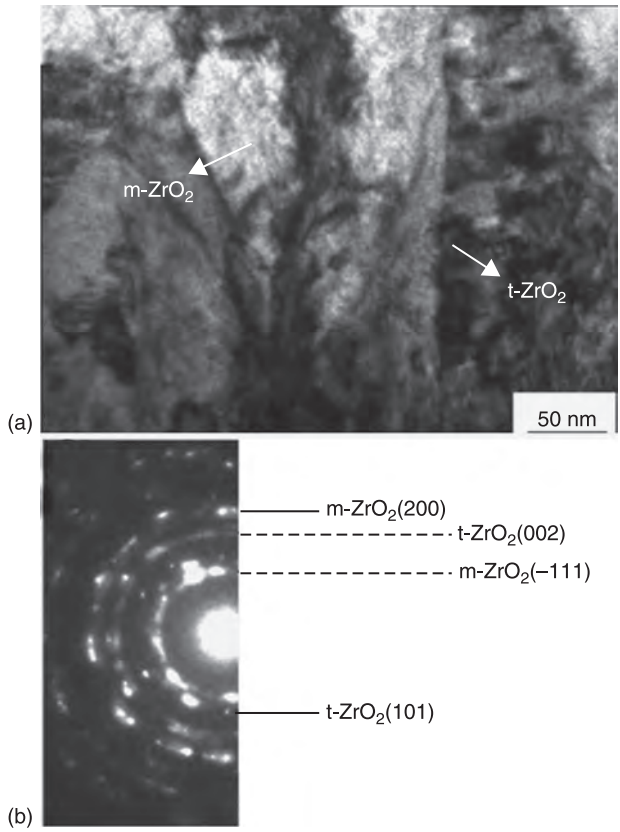

3.11 (a) TEM image of oxide film formed on NC zircaloy-4 after corrosion for 70 days, indicating that phase transformation from t-ZrO_2 to m-ZrO_2 occurred, as seen on diffraction pattern (b).

composed of t-ZrO_2.[72,73] The corrosion resistance of zircaloy-4 depends principally on the compaction and integrity of the oxide films during the initial stages of corrosion. In the early stages the oxide films were composed of t-ZrO_2.[26,74,75] The stability of the t-ZrO_2 was dependent on the compressive stress of the oxide/metal interface.[28,61,76] As the thickness of the oxide film increased, the t-ZrO_2 phase was transformed to m-ZrO_2. This was accompanied by a relaxation of the compressive stress, leading to the formation of cracks in the oxide films. The stress evolution characteristics of the oxide films of both the nanostructured and normally structured Zr-4 alloy in water were studied at 673 K/10.3 MPa.[77] The results indicate that the micro-strain of m-ZrO_2 and t-ZrO_2 formed in the nanostructure bases is larger than that formed in the CG structure bases. For the 160 day oxide sample, the compressive stress of the t-ZrO_2 formed in the CG structure bases is about 1200 MPa, and the compressive stress of the t-ZrO_2 formed in the NC bases is about 1900 MPa. This

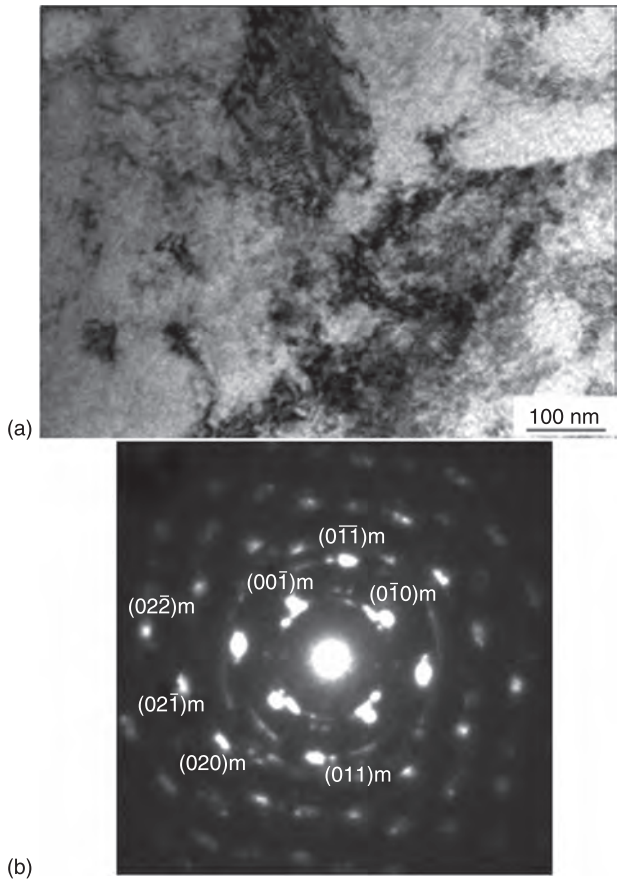

3.12 (a) TEM image of oxide film formed on NC zircaloy-4 after corrosion for 130 days. Only the m-ZrO_2 phase was found, indicating that phase transformation from t-ZrO_2 to m-ZrO_2 was complete and that t-ZrO_2 had disappeared, as seen on diffraction pattern (b).

shows that the compressive stress of the oxide film/metal interface in the NC metal is larger than that in the CG metal. A nanocrystallized treatment is beneficial for the formation of a compact oxide film (t-ZrO_2), which has a protective effect, and which can improve the corrosion resistance of the zircaloy-4.

The growth characteristics of the ZrO_2 film were calculated on the basis of the XRD results.[17,61] Figure 3.13 shows the grain size changes in ZrO_2 formed on different substrates along with the increase in time at 673 K/10.3 MPa. It can be observed that the grain size of the ZrO_2 film formed on the NC substrate is smaller than that of the ZrO_2 film formed on the CG substrate. Therefore, the growth rate of the former oxide film is slower than that of the latter oxide film. These results match those shown in Fig. 3.7, indicating that the oxidation kinetics course of the NC

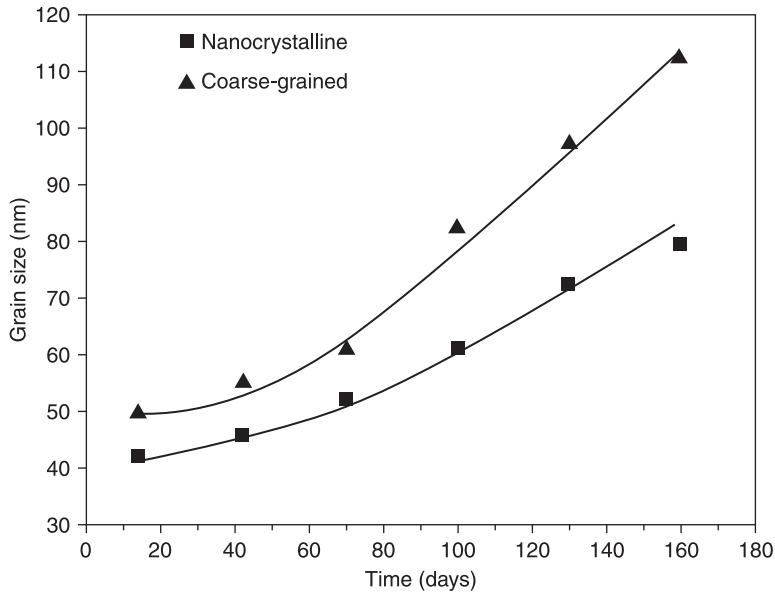

3.13 Grain size changes of ZrO_2 film over time at 673 K/10.3 MPa. The grain size of ZrO_2 film formed on the NC substrate is smaller than that of ZrO_2 film formed on the CG substrate.

zircaloy-4 is lagging. Two different stages affect the ZrO_2 film.[61,67–73,78] In the early stage, oxygen reacts with the metal to form tetragonal ZrO_2. It is compact and can impede further diffusion of the oxygen. In the second stage, the tetragonal ZrO_2 transforms into monoclinic ZrO_2. Then the oxide film becomes loose and voids and micro-cracks develop. In this case the oxygen diffuses not only through the negative ion vacancies, but also through the voids and micro-cracks, resulting in an accelerated growth of the oxide film.[62,78] Delaying the tetragonal/monoclinic phase transformation can therefore reduce oxide film growth.[62–64] The volume fractions of the tetragonal and monoclinic phases in the ZrO_2 films have also been calculated (as shown in Fig. 3.14). The results show that at 673 K/10.3 MPa the volume fraction of the tetragonal phase of the ZrO_2 film formed on the NC substrate is larger than that of the ZrO_2 film formed on the CG substrate (see Fig. 3.14(a)).

What is more interesting is that, at 773 K/10.3 MPa, XRD cannot detect the tetragonal phase in the ZrO_2 film formed on the CG substrate, which had been oxidized for only 1 hour (see the blue profile of Fig. 3.14(b)). However, the volume fraction of the tetragonal phase in the ZrO_2 film formed on the NC substrate for 16 hours is 15.83%. This significant difference reveals that in the ZrO_2 film formed on the NC substrate the transformation from tetragonal to monoclinic phase has lagged. It is assumed that, in the early oxidation stages of the NC zircaloy-4, the large volume fraction of the GBs accelerates the oxygen diffusion along the GBs

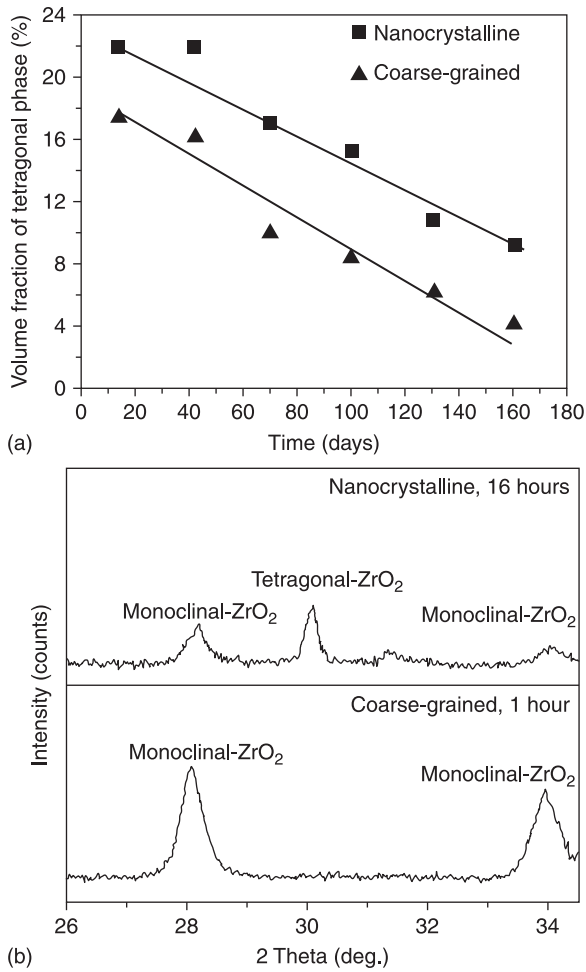

3.14 (a) Volume fraction of the tetragonal phase of ZrO_2 film formed on the NC substrate and CG substrate at 673 K/10.3 MPa. (b) XRD patterns of the ZrO_2 film formed on the NC substrate for 16 hours and the ZrO_2 film formed on the CG substrate for 1 hour at 773 K/10.3 MPa, respectively. Note that a tetragonal phase cannot be detected in ZrO_2 film formed on the CG substrate.

and results in the immediate formation of the tetragonal ZrO_2 film. The kinetic course of the oxidation is then impeded by the tetragonal ZrO_2 film.

3.6 Conclusions

This chapter has provided a detailed examination of the corrosion behavior of NC zirconium at high temperature. The corrosion mechanism of NC metals has also

been discussed: when the grain size of a metal decreases to a nanoscale, about equal in size to the electron mean free path, the grain boundary will restrict the movement of electrons. The corrosion behavior of NC metals cannot therefore be explained by the IGC mechanism, which is commonly taken to be the most important mechanism for describing the corrosion of CG metals.

A computational model of corrosion rate versus grain size of NC zirconium has been proposed, based on Wagner's theory and the electron theory of solids. Influencing factors such as conductivity, electron mean free path, grain size and lattice distortion were taken into account. Using this model the corrosion rate and weight gain of NC zirconium at different temperatures were calculated, with results showing that the corrosion resistance of NC zirconium is considerably higher than that of zirconium with coarse grain size. The corrosion rate constant and weight gain of NC zirconium both decrease with decreasing grain size.

Corrosion experiments comparing NC zircaloy-4 and CG zircaloy-4 at 673 K/10.3 MPa and 773 K/10.3 MPa in water were carried out, and the microstructure of oxide films was studied. The results indicate that the growth rate of oxide films formed on the NC zircaloy-4 is lower that that of oxide films formed on the CG zircaloy-4. The lower oxygen content and lower diffusion velocity of oxygen at the oxide/NC metal interface can hinder the reaction of oxygen ions with metal ions. The oxide/metal interface of NC zircaloy-4 is more regular and smoother than that of CG zircaloy-4, suggesting that fewer void clusters are generated in the oxide films formed on the NC zircaloy-4.

The experimental results also show that the phase transformation from t-ZrO_2 to m-ZrO_2 phase in the oxide films formed on the NC zircaloy-4 is delayed, leading to slower oxide film growth. With respect to oxidation kinetics, in the early stages of corrosion the tetragonal ZrO_2 film on NC zircaloy-4 was formed quickly by the accelerated diffusion of the oxygen along the GBs. The protective tetragonal ZrO_2 film then impedes further diffusion of the oxygen, leading to a slowing of the rate of oxygen diffusion and of the transformation from tetragonal to monoclinic phase. The oxidation kinetics course of the NC zircaloy-4 has thus lagged.

3.7 References

1. H. G. Salem, R. E. Goforth and K. T. Hartwig, *Mater. Trans.*, **34** (2003): 1153.
2. M. Mahayana, Z. Horita and K. Hono, *Acta Mater.*, **49** (2001): 21.
3. S. D. Hyuk and B. C. Kim, *Acta Mater.*, **48** (2000): 2247.
4. R. S. Mishra, V. V. Stilyrov, C. Echer, R. Z. Valiev and A. K. Mukherjee, *Mater. Sci. Eng. A*, **298** (2001): 44.
5. X. Y. Zhang, C. Jia, Z. N. Liu and J. Yi, *Rare Met. Mater. Eng.*, **35**(1) (2006): 178.
6. R. Ambat, N. N. Aung and W. W. Zhou, *Corros. Sci.*, **42** (2000): 1433.
7. S. Fujimoto, H. Hayashida and T. Shibata, *Mater. Sci. Eng. A*, **267** (1999): 314.
8. J. Xu, X. D. Bai, F. He, S. G. Wang, X. He *et al*., *J. Nucl. Mater.*, **265** (1999): 240.
9. F. Viana, A. M. P. Pinto, H. M. C. Santos and A. B. Lopes, *J. Mater. Process. Technol.*, **92** (1999): 54.

10. L. A. Donohue, D. B. Lewis, M. D. Münz, M. M. Stack, S. B. Lyon *et al.*, *Vacuum* **55** (1999): 109.
11. S. H. Kim, U. Erb, K. T. Aust and G. Palumbo, *Scri. Mater.*, **44** (2001): 835.
12. S. Zhao, D. A. Wolfe, T. S. Huang and G. S. Frankel, *J. Stati. Plan. Inference.*, **137** (2007): 2405.
13. D. N. Wasnik, V. Kain, I. Samajdar, B. Verlinden and P. K. De, *Acta Mater.*, **50** (2002): 4587.
14. M. Shimada, H. Kokawa, Z. J. Wang, Y. S. Sato and I. Karibe, *Acta Mater.* **50** (2002): 2331.
15. H. Miyamoto, K. Harada, T. Mimaki, A. Vinogradov and S. Hashimoto, *Corros. Sci.*, **50** (2008): 1215.
16. S. H. Kim, K. T. Aust and U. Erb, *Scri. Mater.*, **48** (2003), 1379.
17. A. Barbucci, G. Farne, P. Matteazzi, R. Riccieri and G. Cerisola, *Corros. Sci.*, **41** (1999): 463.
18. H. S. Kim and M. B. Bush, *Nanostruct. Mater.*, **11** (1999): 361.
19. H. Garbacz, M. Pisarek and K. J. Kurzydlowski, *Biomol. Eng.*, **24** (2007): 559.
20. B. Yu, P. Woo and U. Erb, *Scri. Mater.*, **56** (2007): 353.
21. W. Luo, C. Qian, X. J. Wu and M. Yan, *Mater. Sci. Eng. A*, **452–3** (2007): 524.
22. A. Balyanov, J. Kutnyakova and N. A. Amirkhanova, *Scri. Mater.*, **51** (2004): 225.
23. D. Zander and U. Koster, *Mater. Sci. Eng. A*, **375–7** (2004): 53.
24. L. Wang, J. Zhang, Y. Gao, Q. Xue, L. Hu *et al.*, *Scri. Mater.*, **55** (2006): 657.
25. K. T. Liu and J. G. Duh, *J. Electro. Chem.*, **618** (2008): 45.
26. X. Y. Zhang, C. Li, N. F. Liu, Q. Zhang, M. H. Shi *et al.*, *Nul. Pow. Eng.*, **28** (2007): 71.
27. X. Y. Zhang, C. Li, S. Y. Qiu, M. H. Shi, P. C. Zhang *et al.*, *Rare Metal Mater. Eng.*, **37** (2008): 112.
28. X. Y. Zhang, Y. T. Zhu, C. Li, M. H. Yu, Q. Zhang *et al.*, *Rare Metal. Mater. Eng.*, **37** (2008): 1149.
29. X. Y. Zhang, M. H. Shi, Y. T. Zhu, Q. Liu, B. F. Luan *et al.*, *Front. Eng. Power Eng. China*, **2** (2008): 386.
30. X. Y. Zhang, Y. T. Zhu, L. F. Ye, Q. Liu, C. Li *et al.*, *Rare Metal Mater. Eng.*, **38** (2009): 506.
31. B. Cox, V. G. Kritsky, C. Lemaignan, V. Polley and I. G. Ritchie, *Waterside corrosion of zirconium alloys in nuclear power plants*, IEAE-TECDOC–996. Vienna: IAEA, 1998, p. 249.
32. T. F. Li, *High-Temperature Oxidation and Corrosion of Metals*. Beijing: Chemical Industry Press, 2003, p. 167.
33. M. S. Li, *High Temperature Corrosion Metals*. Beijing: Metallurgical Industry Press, 2001, p. 152.
34. Y. F. Shen, *Basic Course in Solid State Physics*. Beijing: Chemical Industry Press, 2004, p. 410.
35. K. J. Claye Bunde, *Nanomaterials Chemistry*. Beijing: Chemical Industry Press, 2004, p. 137.
36. E. L. Dreizin, *Combustion, Explosion, Shock Waves*. New York: Springer, 2003, p. 681.
37. B. K. Xiong, W. G. Wen and X. M. Yang, *The Metallurgy of Zirconium and Hafnium*. Beijing: Metallurgical Industry Press, 2003, p. 54.
38. F. Wang and J. Dezhou, *Univer.*, **21** (2005): 40.
39. J. Ye, T. F. Li and J. L. Zhou, *Acta Metall. Sin.*, **31** (1995): B109.
40. T. F. Li and J. Chin, *Soc. Corro. Protec.*, **22** (2002): 180.

41. D. J. Yang and Z. S. Shen, *Corrosion of Metals*. Beijing: Metallurgical Industry Press, 2003, p.116.
42. Y. H. Jeong, H. G. Kim, D. J. Kim, B. K. Choi and J. H. Kim, *J. Nucl. Mater.* **3** (2003): 72.
43. E. A. Garcia and G. Beranger, *J. Nucl. Mater.* **273** (1999): 221.
44. X. D. Liu, K. Lu and B. Z. Ding, *Chinese Science Bulletin*, **39** (1994): 217.
45. X. S. Ye, J. Sha and H. Fang, *Chinese Science Bulletin*, **41** (1996): 2039.
46. L. Liu, B. Li and X. Z. Ding, *Chinese Science Bulletin*, **39** (1994): 471.
47. X. S. Ye, J. Sha, Q. Liu and J. Zhejiang, *Univer.*, **34** (2000): 1.
48. K. Heinemann and H. Poppa, *Surf. Sci. Lett.*, **156** (1985): 265.
49. C. Solliard and M. Flueli, *Sur. Sci.*, **156** (1985): 48.
50. W. Daisuke and K. Matsuo, *J. Magn. Magn. Mater.*, **310** (2007): 690.
51. S. Giorgio, C. R. Henry and C. Chapon, *J. Cryst. Growth*, **100** (1990): 254.
52. C. Goyhenex, C. R. Henry and J. Urban, *Philos. Mag: A*, **69** (1994): 1073.
53. S. K. Pradhan, T. Chakraborty and S. P. Sen Gupta, *Nano. Struc. Mater.*, **5** (1995): 53.
54. X. Y. Zhang, M. H. Shi, C. Li, N. F. Liu and Y. M. Wei, *Mater. Sci. Eng. A*, **448** (2007): 259.
55. Y. F. Shen, *Basic Course in Solid State Physics*. Beijing: Chemical Industry Press, 2004, p. 410.
56. M. H. Yu, X. Y. Zhang and Y. T. Zhu, *J. Guangxi Univer.*, **34** (2009): 238.
57. M. H. Yu, X. Y. Zhang, Y. T. Zhu and J. X. Wen, *Rare Metal Mater. Eng.*, **38** (2009): 1269.
58. F. Wang, *Journal of De Zhou Univer.*, **21** (2005): 40.
59. J. Y. Park, J. Y. Seung, B. K. Choi and Y. H. Jeong. *J. All. Comp.*, **437**(1–2), (2007): 274.
60. B. X. Zhou, Q. Li, M. Y. Yao, W. Q. Liu and Y. L. Zhu, *Nucl Power Eng.*, **26**(4), (2005): 364.
61. Y. T. Zhu and X. Y. Zhang, *Sci. China Ser. E-Tech. Sci.*, **52** (2009): 2227.
62. B. X. Zhou, in L. F. P. Van-Swam and C. M. Eucken (eds), *Zirconium in the Nuclear Industry*, Eighth International Symposium, STP 1023. Philadelphia: ASTM. Intl., 1989, p. 360.
63. D. Pecheur, J. Godlewski and J. Peybernes, in E. R. Bradley and G. P. Sabol (eds), *Zirconium in the Nuclear Industry*, Eleventh International Symposium, STP 1295. Philadelphia: ASTM. Intl., 2000, p. 793.
64. B. Cox, V. G. Kritsky, C. Lemaignan, V. Polley and I. G. Ritchie, *Waterside corrosion of zirconium alloys in nuclear power plants*, IEAE-TECDOC-996. Vienna: IAEA, 1998.
65. W. Q. Liu, W. J. Chen, Q. Li, B. X. Zhou and M. Y. Yao, *Nucl. Power Eng.*, **25** (2004): 517.
66. B. X. Zhou, in: L. F. P. Van-Swam and C. M. Eucken (eds), *Zirconium in the Nuclear Industry*, Eighth International Symposium, STP 1023. Philadelphia: ASTM. Intl., 1989, p. 360.
67. H. J. Beie, A. Mitwalsky, F. Garzarolli, H. Ruhamann and H. J. Sell, in: *Zirconium in the Nuclear Industry*, Tenth International Symposium, STP 1245. New York: ASTM. Intl. 1994, p. 615.
68. B. Wadman, Z. Lai, H. O. Andren, A. Nyström, P. Rudling *et al*., in: *Zirconium in the Nuclear Industry*, Eleventh International Symposium, STP 1295. Philadelphia: ASTM. Intl., 1996, p. 579.
69. F. Garzarolli, W. Goll and A. Seibold, in: *Zirconium in the Nuclear Industry*, Eleventh International Symposium, STP 1295. Philadelphia: ASTM. Intl., 1996, p. 541.
70. H. Anada and K. Takeda, in: *Zirconium in the Nuclear Industry*, Eleventh International Symposium, STP 1295. Philadelphia: ASTM. Intl., 1996, p. 35.
71. H. J. Beie, A. Mitwalsky and F. Garzarolli, in: *Zirconium in the Nuclear Industry*, Eleventh International Symposium, STP 1295. Philadelphia: ASTM. Intl., 1996, pp. 615–43.

72. S. Abolhassani, M. Dadras, M. Leboeuf and D. Gavillet, *J. Nucl. Mater.*, **321** (2003): 70.
73. A. Yilmazbayhan, T. Motta, R. J. Comstock, G. P. Sabol, B. Lai *et al*., *J Nucl. Mater.*, **324** (2004): 6.
74. D. Pecheur, J. Godlewski and J. Peybernes, in: *Zirconium in the Nuclear Industry*, Twelfth International Symposium, STP 1354. West Conshohocken: ASTM. Intl., 2000, p. 793.
75. T. Motta, A. Yilmazbayhan, R. J. Comstock, J. Partezana, G. P. Sabol *et al.*, *J. ASTM Int*., **2** (2005): Paper ID JAI12375.
76. J. Cox, *Nucl. Mater.*, **336** (2005): 331.
77. L. F. Ye, Y. T. Zhu, X. Y. Zhang, C. Li, Q. Zhang *et al.*, *Ordnance Mater. Sci. Eng*., **31** (2008): 38.
78. A. Yilmazbayhan, T. Motta, R. J. Comstock, G. P. Sabol, B. Lai *et al.*, *J. Nucl. Mater*., **324** (2004): 6.

4

Understanding the corrosion resistance of nanocrystalline materials: electrochemical influences

L. YING and L. LI, Chinese Academy of Sciences, China

Abstract: The small grain size and the high volume fraction of grain boundaries result in significantly different corrosion behaviors between nanocrystalline materials and corresponding coarse crystalline materials. In active dissolution, nanocrystallization accelerates the corrosion reactions. In passivation, nanocrystallization changes the composition of the passive film, improves the formation of compact film, influences the semiconductor property and possesses the different morphology and growth process of passive film. The small grain size influences the passivation depending on fast element diffusion and special adsorbed ability, all of which increase the corrosion resistance of materials. In local corrosion, nanocrystallization increases the unstable points on the surface of the materials, which increases the possibility of local corrosion. However, the excellent ability of element diffusion helps heal the local corrosion points, which inhibits the growth of the local corrosion.

Key words: nanocrystalline materials, electrochemical corrosion, passivation, semiconductive properties, pit initiation and growth.

4.1 Introduction

Corrosion is a problem of unassailable importance for the human race, one that exists in every aspect of living. Corrosion can not only cause huge losses for industry, but can also threaten the safety of people's lives and property. Therefore, corrosion is a serious scientific problem. Researchers not only study the corrosion behavior of metals/alloys in various environments, they also analyze the corrosion mechanism and aim to find the most effective ways of protecting materials.

Nanocrystallization has become a useful means of improving the performance of materials. Nanocrystalline (NC) materials are characterized by their small grain sizes (<100 nm) and high volume fraction of grain boundaries, which often give rise to unique physical, chemical and mechanical properties compared with those of their cast counterparts.[1–4] These properties have been found to be particularly useful for corrosion protection applications.

There are several methods of producing NC materials, such as chemical deposition, ultrasonic shot peening (USSP), deep rolling treatment and magnetron sputtering. The common characteristic of these methods is that they give materials nanoscale grain size. NC coatings made by magnetron sputtering have been applied in industry. The NC coating of Ni-based superalloys has been found to

greatly enhance their high-temperature oxidation resistance; this is because a continuous protective Al_2O_3 external scale is formed on the alloy surface.[1,5–7] Recently, a NC coating with the same chemistry has been applied to high-temperature alloys in order to increase their corrosion resistance. This coating can also increase their resistance to synergistic corrosion caused by solid salt and water vapor at an intermediate temperature.[8–10] Such an NC coating has a wide range of applications. Some NC coatings have been applied to aid resistance to high-temperature corrosion on ships.[11] Previous investigations have also shown that nanocrystallization can significantly influence the electrochemical behavior of metals/alloys at normal temperatures.[3,4]

In the case of normal-temperature corrosion, nearly all metals/alloys are thermodynamically reactive in most natural environments, for example in air. This is especially true when the environment is moist, polluted or hot, and in water, especially when it is saline, acid or alkaline. There are various common corrosion behaviors of metals/alloys, the familiar patterns among which are active dissolution, passivation and local corrosion. This review focuses on three kinds of corrosion behavior and discusses the effect of nanocrystallization in a liquid system. NC materials have many useful applications and therefore better understanding of their structural and chemical characteristics is of vital importance.

4.2 Active dissolution of nanocrystalline materials in a liquid system

Extensive research has been carried out into NC materials because of the need for a basic understanding of the nature of nanostructures and their potential technological applications.[12,13] The preponderance of grain boundaries in NC materials increases the ratio of surface area as well as surface energy, which also increases the chemical activity in the materials. Therefore, if the materials exhibit active dissolution in a liquid system, the dissolution rate of the corresponding NC materials will be faster than traditional coarse crystalline materials.

Y. Li *et al.*[14] produced a nanocrystallized surface on low-carbon steel using the USSP technique. The corrosion behavior of the NC materials in a 0.05 M H_2SO_4 + 0.05 M Na_2SO_4 liquid system is active dissolution and the dissolution rate of NC materials is higher than that of the corresponding coarse crystalline material. The anodic reaction process did not change, even though the low-carbon steel was nanocrystallized by USSP treatment. The anodic current density increased, however, because of the increasing amount of atoms that took part in the reaction. Through nanocrystallization, the cathode reaction has been changed from the old electrochemical control to diffusion control. Both anodic and cathodic reactions have been stimulated by nanocrystallization and therefore the active dissolution has been increased. The NC thin film on low-carbon steel (~ 40 nm) on

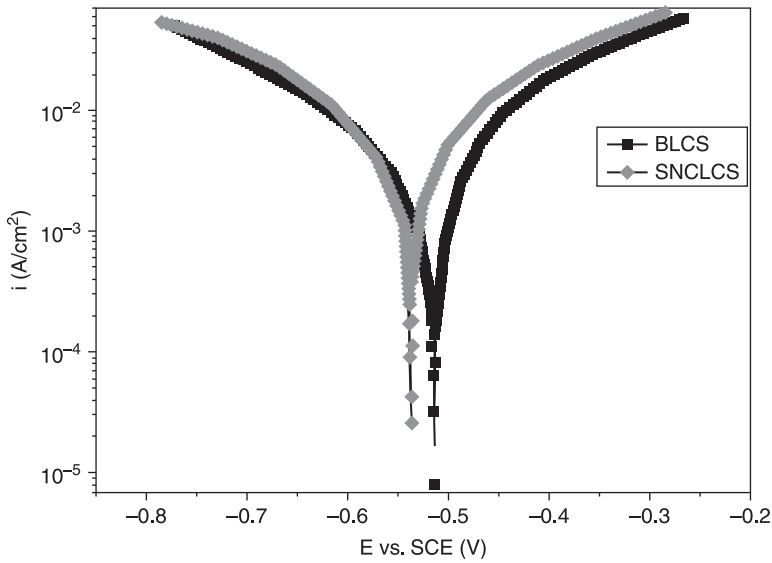

4.1 Polarization curves for surface-nanocrystallized low-carbon steel (SNCLCS (♦)) by ultrasonic shot peening and its corresponding bulk low-carbon steel (BLCS (■)) in 0.5 mol/l H_2SO_4 aqueous solution.[14]

quartz plate produced by the magnetron sputtering technique also has a higher active dissolution rate compared with the corresponding coarse crystalline material (Fig. 4.1) in a 0.5 M H_2SO_4 system. The NC bulk low-carbon steel produced by deep rolling also has the same electrochemical behavior, with the above results.

Lu *et al.*[15,16] studied the electrochemical corrosion behavior of a Cu–Zr alloy NC coating produced by magnetron sputtering (grain size 10–20 nm). The experimental results indicated that the nanocrystallization decreased the dissolutive rate of Cu–20Zr and Cu–70Zr alloys. They attributed this to the existence of large numbers of grain boundaries in the NC Cu–20Zr/Cu–70Zr films; the Cl^- might be strongly absorbed on the surface of NC films, forming a continuous insoluble copper chloride scale complex, which acted to restrain the corrosion process.[15]

According to the above results, there is a significant reverse influence of nanocrystallization on the dissolution of metals/alloys. However, the present authors theorize that nanocrystallization changes the surface condition of metals or alloys, which can effectively increase the activity of metallic atoms and accelerate the corrosion reactions. Therefore, if the corrosion products are dissoluble, the corrosion rate is increased by nanocrystallization; if the corrosion products are insoluble, the corrosion rate is decreased because the corrosion products act as a block layer to delay the dissolution.

4.3 Passivation ability of nanocrystalline materials

The corrosion behavior of NC materials has been assessed by several techniques in various environments. Zeiger *et al.*[17] reported the enhanced corrosion resistance of NC Fe-8Al in Na_2SO_4 solution (pH = 6). The authors attributed this enhanced corrosion resistance to the fast grain boundary diffusion of Al, which formed a protective oxide film. Thorpe *et al.*[18] found that the corrosion resistance of NC Fe32–Ni36–Cr14–P12–B6 was significantly greater than that of its amorphous counterpart; this was because of the observed greater Cr enrichment in the surface film via rapid interphase boundary diffusion. As a normal passive material, it is well known that the corrosion resistance of cast stainless steels is significantly improved when the Cr content reaches or exceeds 12.5%, especially in solutions containing Cl^-.

A superior localized corrosion resistance was found in the electrochemical corrosion behavior of a sputter-deposited 304 stainless steel NC coating.[4] Wang *et al.*[19] also reported improved corrosion resistance of surface NC 304 stainless steel in 3.5% NaCl solution, which was obtained by a sandblasting and annealing process. Meng *et al.*[20] studied the corrosion behavior of Fe–10Cr NC coating in acidic solution and found that the chemical stability of the passive film was increased compared with corresponding cast alloy. Ye *et al.*[21] reported that a sputter-deposited 309 stainless steel NC coating had a higher pitting resistance compared with its coarse-grained analogue. Liu *et al.*[22] also found that nanocrystallization can increase the passivation ability of an Ni-based superalloy,

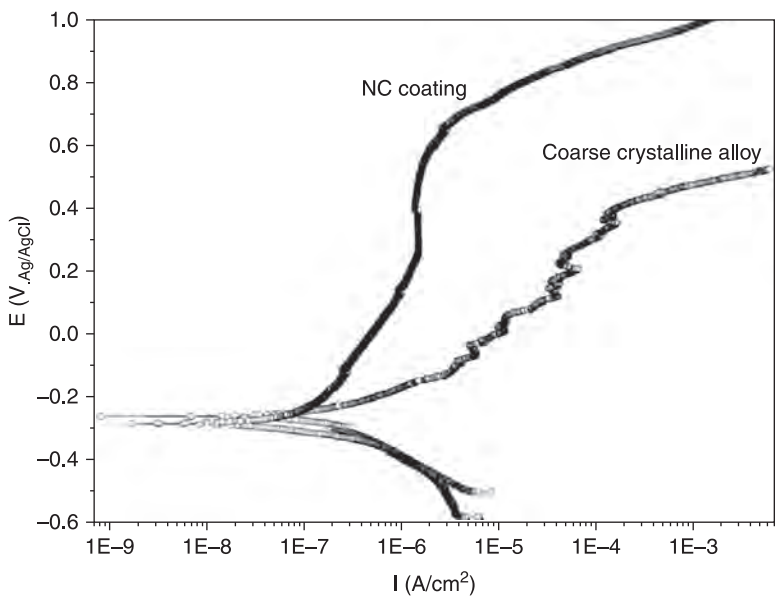

4.2 Potentiodynamic polarization plots of the conventional coarse crystalline Ni-based alloy and the corresponding NC coating in 3.5% NaCl solution.[23]

shown in Fig. 4.2. The experimental results revealed that nanocrystallization greatly increased the electrochemical corrosion resistance of alloy in the normal NaCl solution (in Fig. 4.2).[23] The decreasing of grain size can also increase the stability and pitting resistance of passive film on AZ91D magnesium alloy and pure aluminum.[24,25]

4.3.1 Effect of nanocrystallization on the chemistry of passive film

Nanocrystallization can change the composition of the passive film on many metals or alloys. For stainless steel, Meng *et al.*[20] thought that nanocrystallization promotes Cr enrichment in the passive film, which means more Cr^{3+} than Fe^{2+} was involved in the formation of the passive film on the Fe–10Cr alloy. On the other hand, less Cr^{3+} than Fe^{2+} participated in the formation of the passive film on the coarse crystalline alloy. Therefore, the passive film on the NC coating has a higher corrosion resistance than that of the coarse crystalline alloy. This idea is based on electrochemical impedance spectroscopy measurements and analysis. Furthermore, Ye *et al.*[26] studied the corrosion resistance of 309 stainless steel of both NC and cast materials in the transpassive region. Through analyzing the element map of passive film on both materials by electron probe microanalyzer (EPMA), it was found that elemental Cr was distributed uniformly in the passive film on the NC coating whereas it was not uniform in that on the corresponding coarse crystalline alloy. However, the amount of Cr was not certain in the passive film.

In order to understand the effect of nanocrystallization in detail, the passive film on an Ni-based alloy has been studied. X-ray photoelectron spectroscopy (XPS) results indicated that the composition of the passive film was significantly different between the NC coating and the corresponding traditional coarse crystalline alloy. The passive film on the conventional alloy consisted of Cr, Ti and Ni oxides, whereas only Cr and Ti oxides were present in the passive film on the NC coating. There were distinctly different quantities of the elements present in the two passive films. As shown in Table 4.1,[23] more Cr exists in the passive film on the NC coating. The results testified that nanocrystallization improved the enrichment of passive elements in the passive film, which may be one of the main reasons for the high corrosion resistance of nanomaterials.

Table 4.1 XPS composition for the passive film on both materials[23]

Material	Oxide layer composition from XPS(at.%)		
	Cr_2O_3	NiO	TiO_2
Coarse crystalline alloy	62.31%	20.96%	16.73%
NC coating	79.34%	0	20.66%

Another interesting result is the appearance of elemental Ni in the passive film on the NC material. Figure 4.3 shows the EPMA element distribution maps of Cr, Ti and Ni in traditional coarse crystalline alloy and sputter-deposited NC thin film. In Fig. 4.3(a), it is clear that, around grain boundaries on the coarse crystalline alloy, Cr concentration is poor with very limited amounts showing. There is a reversed result for Ni, the concentration of which is higher at the grain boundaries. It can be seen that the small grain sizes promote uniform element distribution (in Fig. 4.3(b)).[23] There was no great difference between the distributions of all elements recorded on the NC thin film.

From these results it can be inferred that, during passivation, Ti and Cr oxides were formed first. The passive film could not form a continuous layer rapidly because of the large grain size of the coarse crystalline alloy. Therefore, elemental

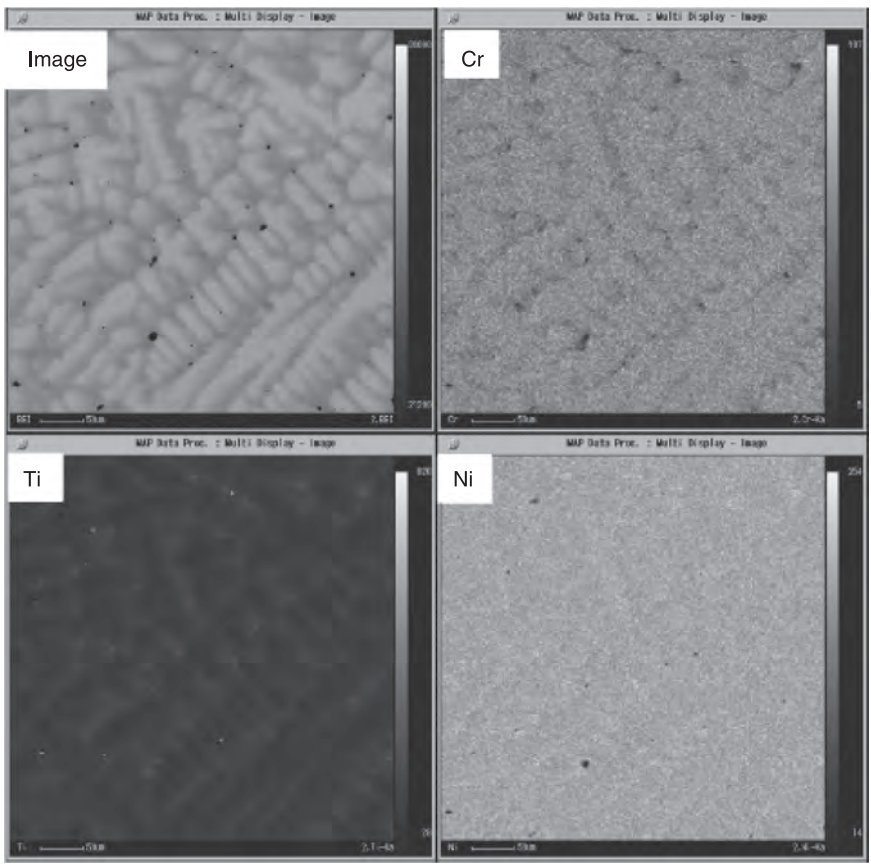

(a)

4.3 EPMA element maps of Cr, Ti and Ni element on the surface of (a) the conventional coarse crystalline Ni-based alloy and (b) the corresponding NC coating.[23]

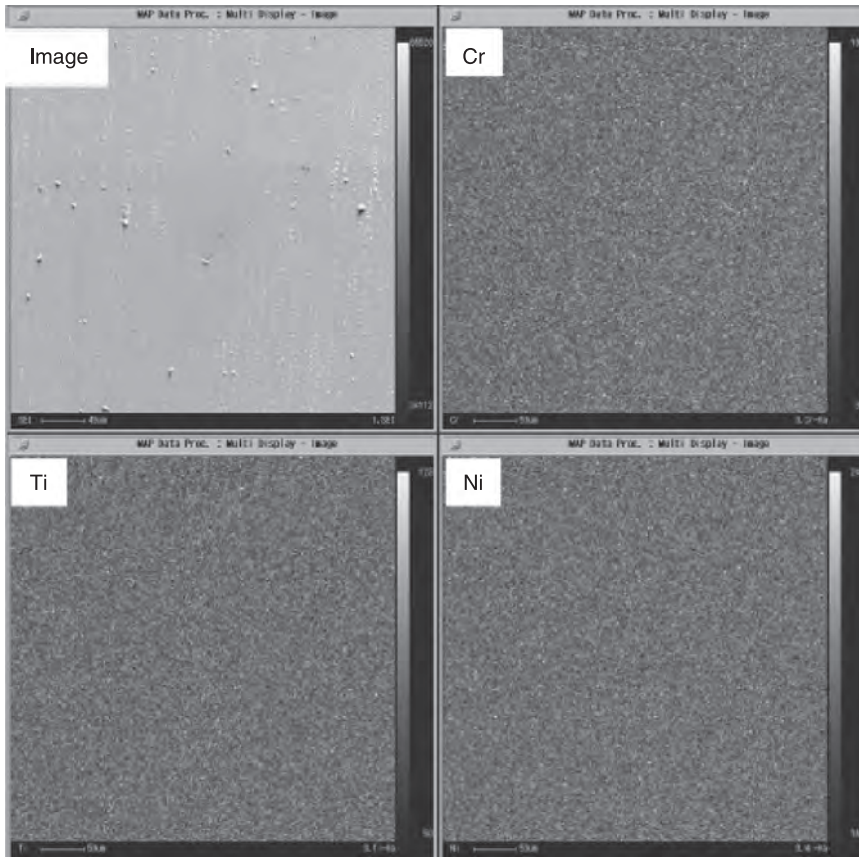

(b)

4.3 Continued.

Ni was present in the passive film. The NC material has a unique surface, which evidently influences each corrosion dynamic process, passivation being an important process among them. The small grain sizes facilitate rapid formation of the oxide layer. The small grain size should promote the diffusion of passive elements such as Cr and Ti, which increases the corresponding content. As a result, a continuous Cr and Ti oxide layer rapidly formed on the NC coating without Ni oxides. It is clear that the passive film on the NC coating without Ni oxides and with more Cr has higher resistance than that of the coarse crystalline alloy. Therefore, it can be concluded that nanocrystallization can promote the enrichment of passive elements such as Cr and Ti in the passive film.

Another influence of nanocrystallization on the composition of the passive film is the presence of Cl^- in the film. Some investigations noted that Cl^- could be incorporated into the passive film in order to change its corrosion resistance.[25,27,28]

However, the effect of nanocrystallization during the formation of the passive film is not clear at present. XPS results indicated that the passive film on the NC coating and the corresponding coarse crystalline alloy on the Ni-based superalloy consisted of mainly Cr oxides in acidic NaCl solution.[22] However, Cl^- took part in the formation of the passive film and was incorporated into the film on the coarse crystalline alloy, but it was not incorporated into the film on the NC coating (shown in Fig. 4.4).[23] This was considered to be how nanocrystallization increased the corrosion resistance.[22] According to this phenomenon, nanocrystallization can decrease the adsorption ability of Cl^- on the surface of the material, which can corrupt the Cl^- so that it is incorporated in the passive film. This idea was proven by the measurement of the potential of zero free charge (pzfc) (in Fig. 4.5).[22] The results indicated that the adsorption of Cl^- was greatly decreased on the NC coating in acidic NaCl solution.

Regarding the adsorption of Cl^- on the surface of materials, Intrui and Szklarska-Smialowska[4] theorized that the presence of a large number of defects would result in a high degree of distribution of Cl^- on the metal surface. The Cl^- concentration at each of the defects of fine-grained NC materials is greatly reduced when compared with the case of coarse-grained materials. As a result, localized enrichment of Cl^- and subsequent acidification at

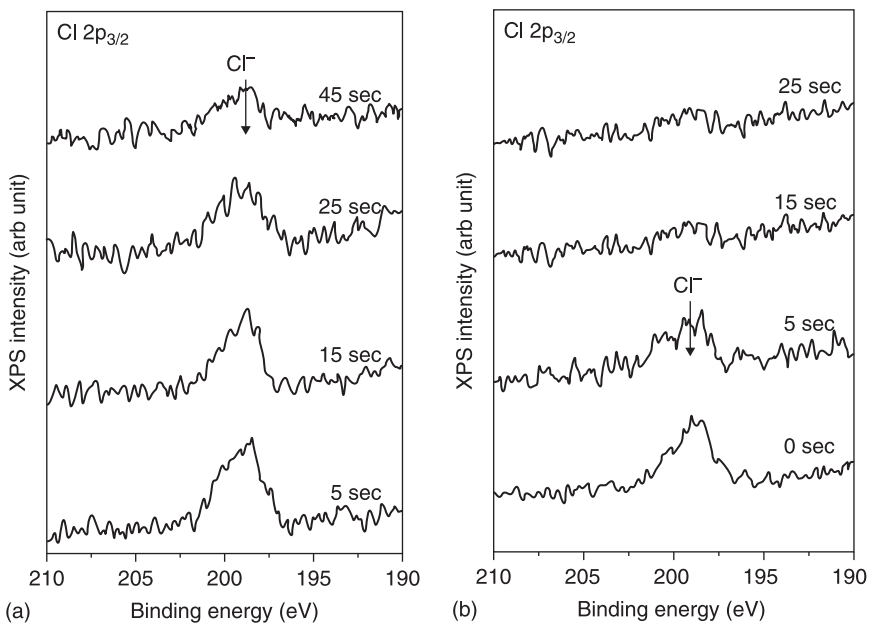

4.4 Cl 2p XPS depth profile spectra from the conventional coarse crystalline Ni-based alloy (a) and the corresponding NC coating (b) after passivation for 30 minutes at 0 V in 3.5% NaCl solution. The depth is indicated in the spectrum.[22]

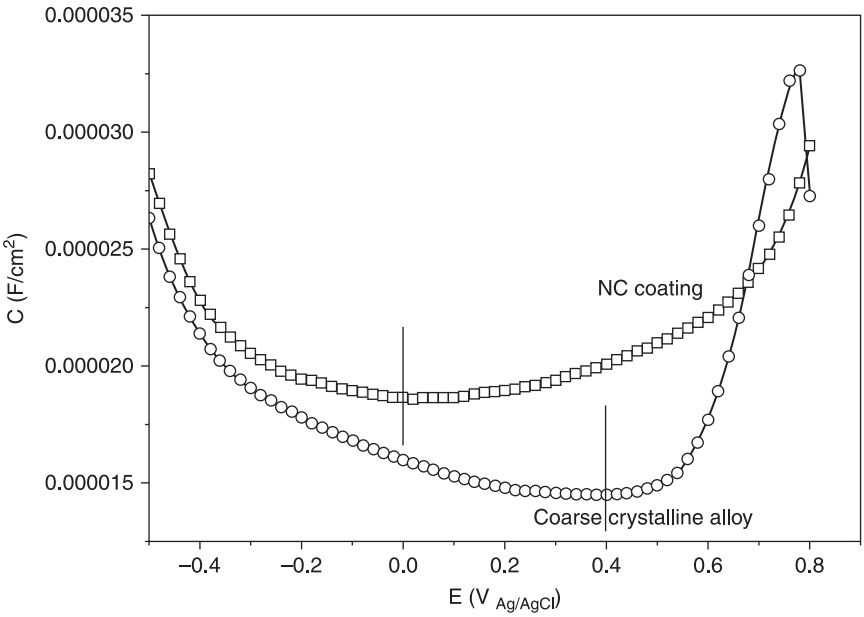

4.5 Double-layer capacities as a function of electrode potential for the conventional coarse crystalline Ni-based alloy (○) and the NC coating (□) in 0.5 M NaCl + 0.05 M H_2SO_4.[22]

each defect on the grain boundary site requires a greater driving force and therefore a more anodic potential for stable pit growth. The present authors argue that Cr easily forms bonds with Cl^- in theory. On the surface of the NC coating of the Ni-based superalloy, there are large numbers of grain boundaries with high elemental Ni. This leads to a decrease in elemental Cr compared with the coarse crystalline alloy in the same scale, which may subsequently decrease the amount of adsorbed Cl^- on the surface of the NC coating in NaCl acidic solution.

On the other hand, Zhang *et al.*[25] found that nanocrystallization changed the semiconductive properties of the passive film on pure Al, from n-type to p-type in acidic NaCl solution. It is hypothesized that Cl^- participates in the oxide film formation and changes the oxide film from n-type to p-type. It is likely that Cl^- occupies the oxygen vacancies and interstitials of the lattice of Al_2O_3. However, this presumption has not been proven in experiments.

From the above results, we can conclude that nanocrystallization can significantly influence the chemistry or composition of the passive film, which influences the corrosion resistance. It can promote the enrichment of passive elements such as Cr and Ti, and it can also decrease the adsorption of Cl^-, both of which are due to the small grain size and the unique surface of NC coatings.

4.3.2 Effect of nanocrystallization on the structure of passive film

Nanocrystallization changes the thickness of passive film. Figure 4.6[23] shows XPS Cr spectra from the passive films in 3.5% NaCl solution on an Ni-based NC coating and the corresponding coarse crystalline alloy. After 40 seconds of bombardment, using the same bombardment parameters, the Cr^{3+} peak disappeared in the passive film on the NC coating but was still present in the film on the coarse crystalline alloy. This indicates that the passive film on the NC coating was thinner than that on the coarse crystalline alloy in normal NaCl solution. This may be due to the uniform element distribution on the whole surface and the fact that the element diffusion is fast to form a compact film. Thus, the formed oxide layer of the NC coating was thinner than that of the corresponding conventional coarse crystalline alloy.

However, nanocrystallization increased the thickness of the passive film on the magnesium alloy with rare elements.[29] It is well known that the passive film on magnesium alloy is mainly the corrosion product layer on the sample, which blocks the dissolution of the material and inhibits the corrosion process. Therefore,

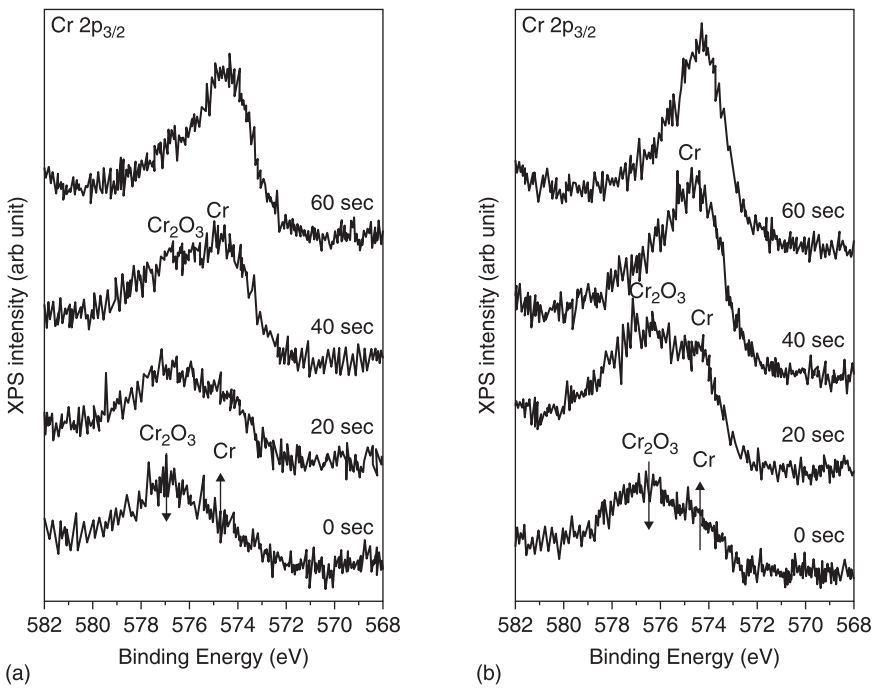

4.6 Cr 2p XPS depth profile spectra from the coarse crystalline Ni-based alloy (a) and the corresponding NC coating (b) after passivation for 30 minutes at 0 V in 3.5% NaCl solution. The depth is indicated in the spectrum.[23]

nanocrystallization promotes the dissolution of the alloy and forms more products on the sample. Finally, the film layer was much thicker than that of the coarse crystalline alloy.

Nanocrystallization also changes the compact properties of the passive film. After cathodic reduction, the variation of the current with time for each specimen was measured at a fixed potential. If the contribution of the double layer charge is neglected, the initial drop of current density should be related to the growth of a protective film on the electrode surface. The current decreases with time as follows:[30]

$$I = 10^{-(A+klgt)} \qquad [4.1]$$

where I represents current density, t is time, A is constant and k represents the slope of the double-log plot for potentiostatic polarization; $k = -1$ indicates the formation of a compact, highly protective passive film, while $k = -0.5$ indicates the presence of a porous film, growing as a result of a dissolution and a precipitation process.[31,32] It has been found that a porous passive film was present on the 309 stainless steel, and that nanocrystallization improved a compact film formation,[21] which is an interesting phenomenon.

The passive film formed on the surface of a cast Ni-based superalloy was a porous oxide layer with a large amount of defects. However, the passive film formed on the NC coating was initially a porous one. It then changed to an oxide layer with better compact properties in 3.5% NaCl solution (Fig. 4.7).[23]

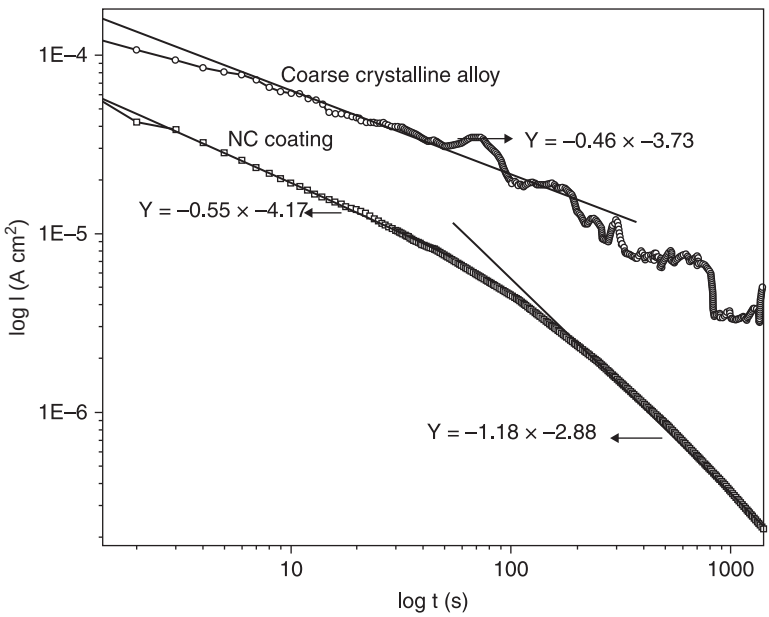

4.7 Double-log plots of current-time for the coarse crystalline Ni-based alloy (○) and the corresponding NC coating (□) in 3.5% NaCl solution.[23]

The microstructure influences not only the composition but also the initial growth of the passive film, which determines the compact properties. The initial oxide layer formation is accompanied by the gradual growth of the oxide film. Oxide growth by cation diffusion over vacancies requires the annihilation of the vacancies by the increase of either misfit or misorientation interfacial dislocations.[23,33]

Although the coarse crystalline alloy possesses grain boundaries with more dislocations, the grain boundary could inhibit the movement of dislocation at normal temperatures.[34] Thus, the annihilation of the vacancies at the interface of scale/metal would be inhibited by the grain boundary, leading to an increase in the amount of cation vacancies in the interface. As the vacancies pile to some extent, a hole or pore is formed and even the initially formed oxide layer becomes fractured. Thus, a passive film with poor compact properties will form. The large amount of Ni oxide increases the matching poor area in the oxide layer and increases the stress between the different oxides; this can have the effect of decreasing the compact properties of the passive film. On the other hand, there are numerous grain boundaries on the NC coating, which will also adversely affect the compact properties of the oxide layer, as earlier described for the coarse crystalline alloy. Nevertheless, the small grain size of the NC coating ensures rapid reformation of the oxide layer and thus repairs the passive film. Therefore, the latter passive film will have superior compact properties, which would increase the corrosion resistance of the NC coating. The poor compact properties of the passive film should influence its protective ability as a film and decrease the corrosion resistance of the material.

4.3.3 Effect of nanocrystallization on the semiconductive properties of passive film

Among the influences of nanocrystallization on the properties of a passive film, its semiconductive properties are a most important issue, which is widely discussed in the corrosion field. The influence is mainly divided into two aspects: one is the semiconductor type; the other is the carrier density and electron energy level. Nanocrystallization can lead to the reversal of the semiconductor type. The passive film on a Fe–20Cr NC coating was amorphous at a low potential and became an n-type semiconductor at a higher potential. However, the passive film on the corresponding coarse crystalline alloy was p-type.[35] For pure aluminum, in acidic (pH = 2) sodium sulfate aqueous solution, the passive films, both on the cast and on microcrystalline (MC) Al, were n-type semiconductors. In acidic (pH = 2) sodium chloride aqueous solution, the passive film on the cast Al exhibited n-type semiconductor properties, whereas the passive film on the MC Al exhibited p-type semiconductor properties. In NaF solutions, when $[F^-] \geq 0.03$ mol/l, the passive film was an n-type semiconductor on the cast Al, and a p-type semiconductor on the MC Al.[36]

Meng[35] considered that Fe had a more rapid rate of dissolution than that of Cr, i.e. [Fe]/[Cr] = 9:1. The NC coating can form a film with a faster rate of dissolution on the surface. Therefore, there should be more Fe oxides in this film, which would be an n-type semiconductor. Another theory regarding the reversal of the semiconductive properties by nanocrystallization is the incorporation of Cl^- in the passive film. Because pure Al_2O_3 is an n-type semiconductor, it is most likely that Cl^- occupies the oxygen vacancies and interstitials of the lattice of Al_2O_3 on the MC aluminum, which consequently changes the semiconductor type from n-type to p-type by providing acceptors.[25] $F^-$and Cl^- can also influence the semiconductor type of pure MC Al in NaF + NaCl aqueous solutions: when $[Cl^-]<[F^-]$, the effect of F^- is predominant and the passive film is an n-type semiconductor; when $[Cl^-]>[F^-]$, the effect of Cl^- is predominant and the passive film is a p-type semiconductor.[36] However, there is no clear evidence from experiments to validate the above ideas.

For cast Ni-based superalloy, the passive film showed n-type semiconductive properties. But p-type semiconductor behavior was observed on the passive film of the corresponding NC coating (Fig. 4.8). Experimental results indicated that Cl^- was incorporated into the passive film of the coarse crystalline alloy (in Fig. 4.4), which led to the reversal of the semiconductor type of the passive film. The reason for this could be the decrease of adsorption ability of the Cl^- by nanocrystallization, which corrupts the Cl^- so that it is incorporated in the passive film.[22]

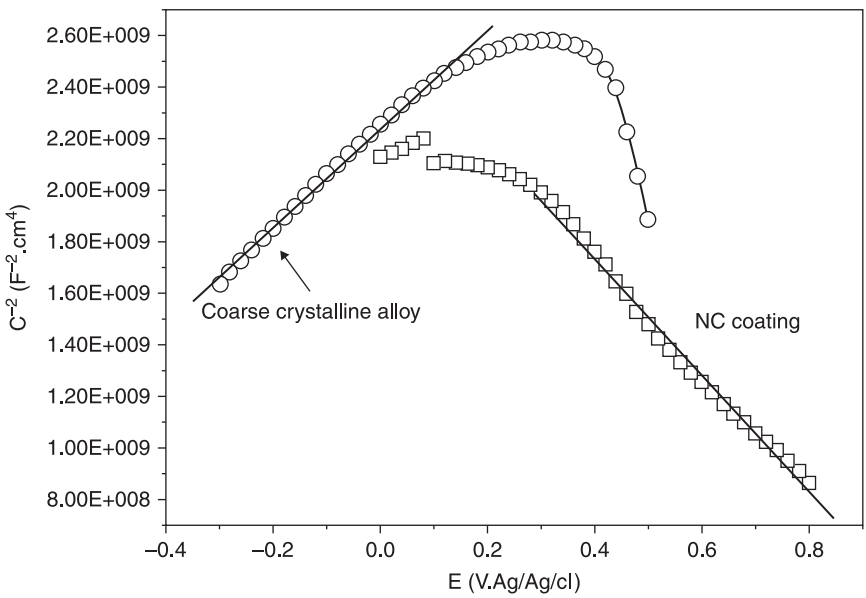

4.8 Mott–Schottky plots of the coarse crystalline Ni-based alloy (○) and the corresponding NC coating (□) in 0.5 M NaCl + 0.05 M H_2SO_4.[22]

The Cr_2O_3 without Cl^- is a p-type semiconductor with redundant cation vacancies ($V_{m.}$). However, for Cr_2O_3 with Cl^-, if the dopant of Cl^- occupies the position of O^{2-} ($Cl_o\cdot$), the replacement of Cl^- could decrease the negative charge of the original O^{2-} position, which can in turn increase the amount of anion vacancies ($V_o^{\cdot\cdot}$) and *e*:

$$Cl_{cl}^{\times} \rightarrow Cl_o\cdot + e' \qquad [4.2]$$

The increase of the amount of anion vacancies ($V_o^{\cdot\cdot}$) in the passive film makes the semiconductive properties of the passive film change from p-type to n-type. If the dopant of Cl^- locates the interstitial position of the lattice, the cation vacancies will increase and the passive film will become a p-type semiconductor.

$$Cl_{cl}^{\times} \rightarrow Cl_i^{-1} + h\cdot \qquad [4.3]$$

However, the experimental results indicate the passive film formed on coarse crystalline alloy is an n-type semiconductor. Therefore, the Cl^- incorporated into the passive film of coarse crystalline alloy should replace the O^{2-} position in the oxide. The incorporation of Cl^- into the passive film changes the film formed on the coarse crystalline alloy from p-type to n-type in acidic solution.

With regards to the effect of decreasing grain size on the adsorption of Cl^-, the present authors theorize that the natural difference of the elements leads to the above result. The electron configuration of Al is [Ne] $3s^23p^1$, which is not fit to form a chemical bond with Cl^-. Therefore, the adsorption of Cl^- depends on the surface energy of the material. Defects are primarily located at the grain boundaries; therefore decreasing the grain size increases the defects on the surface. Cl^- adsorbs onto the surface of the MC Al coating with more defects, which leads to the participation of Cl^-. However, Ni and Cr are the main constituent elements of an Ni-based superalloy and their distributions differ. The electron configurations of Ni and Cr are respectively [Ar] $3d^84s^2$ and [Ar] $3d^54s^1$. For these metals, the orbital of their outer electronic structure participates to form a chemical bond. Morrison[37] points out that Ni has a partially filled d orbital and Cr has an unfilled d orbital. Therefore, in theory, Cr forms a bond more easily with Cl^-. On the surface of the NC coating, large numbers of the grain boundaries have high levels of elemental Ni, which leads to a decrease in the levels of elemental Cr compared with the coarse crystalline alloy in the same scale. This can consequently decrease the amount of adsorbed Cl^- on the surface of the NC coating in NaCl acidic solution. The grain size has been shown to affect the adsorption of Cl^- as well as the corresponding reversal of the semiconductor type.[38] Therefore, the nature of the materials tested differs greatly, as the adsorption of Cl^- affects them significantly differently.

Nanocrystallization has been shown to decrease the carrier density of the semiconductive passive film, such as Fe–10Cr, Fe–20Cr, 309 stainless steel, 304 stainless steel, AZ91D magnesium alloy and Ni-based superalloys.[20–25,35,36] However, for pure Al, whether in solution with or without Cl^-, nanocrystallization

increased the carrier density.[25] The decrease of carrier density may be related to the formation of a more compact film compared with the conventional alloy. Li *et al.*[24] pointed out that the energy band of the product film on microcrystalline AZ91D alloy increased, suggesting that electronic transition became difficult from valence band to Fermi level, which could lead to the decrease of acceptor concentration of the product film on the MC coating. The increase of the carrier density of film on Al in the solution without Cl^- may be due to the increase in defects in the passive film on the MC coating. However, the increase of carrier density in the solution with Cl^- is likely to be due to the incorporation of Cl^- in the film on the MC coating, which increased by almost one magnitude.

According to the point defect model (PDM), the carrier diffusion coefficients (donor or acceptor) in the passive films can be calculated. The carrier diffusion coefficient is a very important parameter that can influence passivation. Li *et al.*[39] found that the donor density for the metal/film interface of NC bulk 304 stainless steel was lower than that for the metal/film interface of cast 304 stainless steel. Therefore, the lower donor density and the lower diffusion coefficient restrained the electrochemical reaction in the passive film and improved its stability, which consequently increased the protective ability of the NC bulk 304 stainless steel.

The corrosion behavior of NC Ni-based superalloy is affected by the difference in grain size.[38] Electrochemical corrosion behavior is particularly affected by grain size. The smaller grain size of the material decreases the carrier diffusion coefficient and increases the corrosion resistance. This is due to the decrease in the amount of Cl^- adsorbed on the surface, which promotes the formation of a compact passive film in acidic solution.

Another focus for research is on which type of semiconductor has more corrosion resistance. Nanocrystallization can reverse the semiconductor type of a material from p-type to n-type or from n-type to p-type. After the nanocrystallization, the corrosion resistance of passive materials appears to have been enhanced. However, according to a series of investigations, there is at present no distinct evidence to support which type has more resistance.

4.3.4 Effect of nanocrystallization on the growth of passive film

Nanocrystallization influences the morphology and growth function of the passive film. However, only a little information is available regarding the *in situ* growth mechanism of materials and no report exists, to the authors' knowledge, of *in situ* atomic force microscopy (AFM) observations of the growth process of NC structures.

Passivation of a conventional austenite stainless steel commences at local positions (Fig. 4.9(a)); these then become connected to form a surface film (Fig. 4.9(b), (c)). The passive film then propagates into a continuous layer with

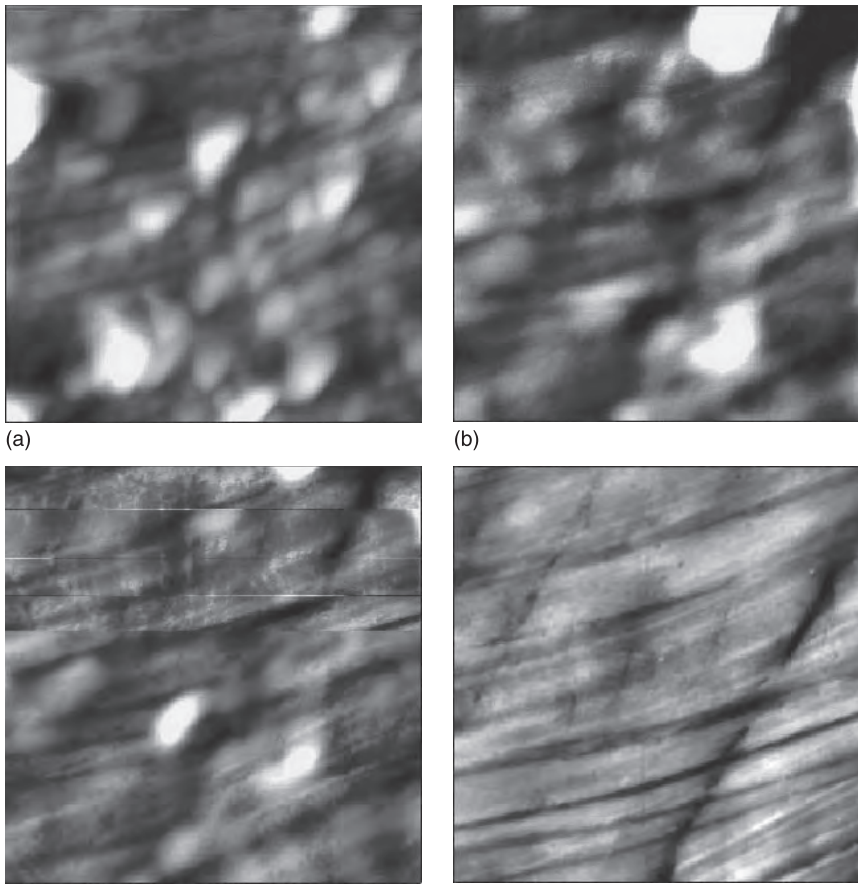

4.9 In situ AFM images of the coarse crystalline stainless steel in the initial stage under anodic polarization in 3.5% NaCl solution: (a) formation of passive particles, (b) formation of continuous passive film, (c) and (d) the growth of passive film.[40]

several scratches due to mechanical polishing (Fig. 4.9(d)). These AFM images indicate that the passive film was formed rapidly on the sample and that pitting corrosion ensued after the continuous film formed.[40]

The passive film formation on austenitic stainless steel NC coating is greatly different from that which is formed on conventional coarse crystalline stainless steel. Because a lot of small particles piled up on the surface of the coating, the oxide particles grew up in their original positions (in Fig. 10(a), 10(b)). Moreover, it was clear that the small oxide particles on the NC coating gradually grew to form a continuous passive film (in Fig. 10(c), 10(d)). The growth of the particles continued until the passive film was broken down.[40]

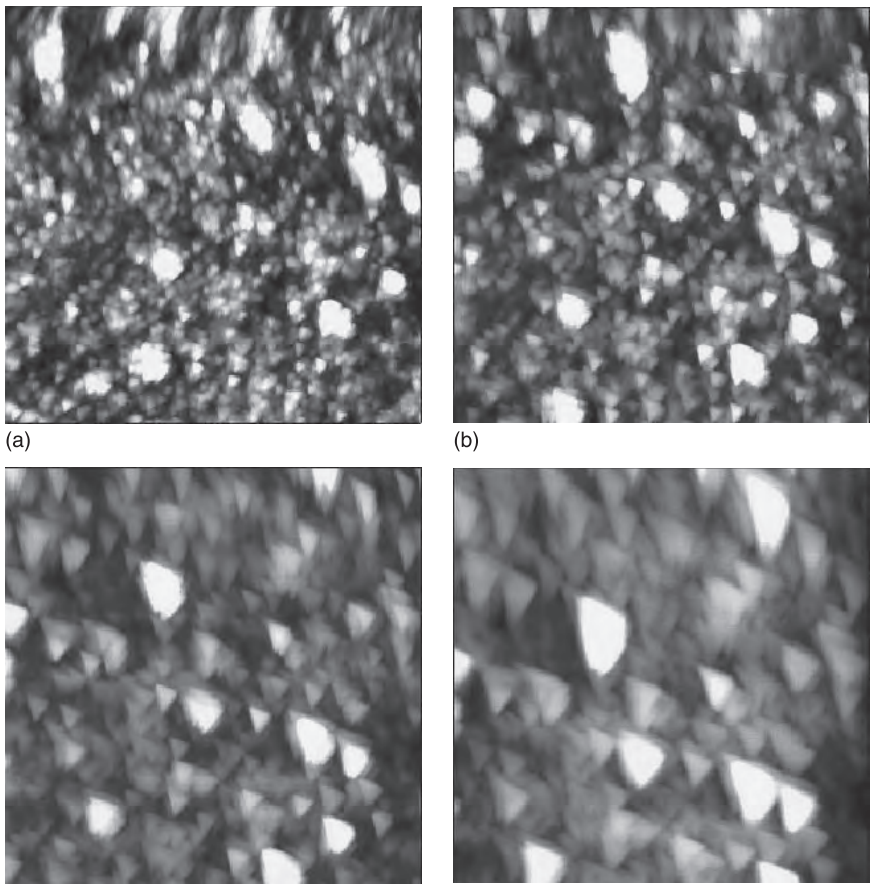

4.10 In situ AFM images of the nanocrystalline coating in the initial stage under anodic polarization in 3.5% NaCl solution: (a) the original morphology of NC coating in solution, (b), (c) and (d) the growth of passive particles under potential in solution.[40]

According to the above experimental results, it can be concluded that nanocrystallization influences passivation depending on fast element diffusion and special adsorbed abilities. The small grain size improves elemental diffusion, which changes the composition of the passive film (passive elements become enriched, for example Cr or Ti). This also helps the film form in a more compact way; it influences the morphology and growth process of the passive film. The small grain size also changes the surface condition, which influences the adsorption of the ions. Incorporating ions into the passive film can influence the semiconductive properties. All of these things will increase the corrosion resistance of the materials.

4.4 Pitting corrosion of nanocrystalline metals

The pitting corrosion resistance and sensitivity to Cl^- of metals/alloys is influenced by the structural characteristics of the passive films. Generally, passive films that possess high amounts of passive elements or uniform structures have a high pitting resistance and weak Cl^- sensitivity. The growth rate of NC passive films is usually fast and is composed of NC and amorphous crystals. The passive film possesses large numbers of grain boundary defects and surface active areas, both of which promote the dispersion of Cl^- adsorbed onto materials. As a result, compared with a coarse alloy with few active spots, the adsorption of Cl^- is weak in the local active area, which to some degree weakens the corrosion of Cl^-. Therefore, NC materials have high local corrosion resistance in containing Cl^-.

Intrui and Szklarska-Smialowska[4] found that the pitting potential of 304 stainless steel in 0.3 wt% solution was increased about 850 mV by nanocrystallization, which has been shown to decrease the Cl^- sensitivity due to a smaller grain size. Research into sputtering AZ91D magnesium alloy,[24] Fe-20Cr,[35] 309 stainless steel[26] and pure Al thin films[25] found that both passive ability and pitting corrosion resistance were promoted by nanocrystallization. However, the existence of grain boundaries in the passive film on NC materials can influence the stability of the passive film. The dissolution rate of the passive film on NC materials of Mg alloy, 309 stainless steel and other metals has been shown to be higher than that of corresponding coarse crystalline alloys, which means that the stability of the passive film decreases with nanocrystallization (see Fig. 4.11). Further research

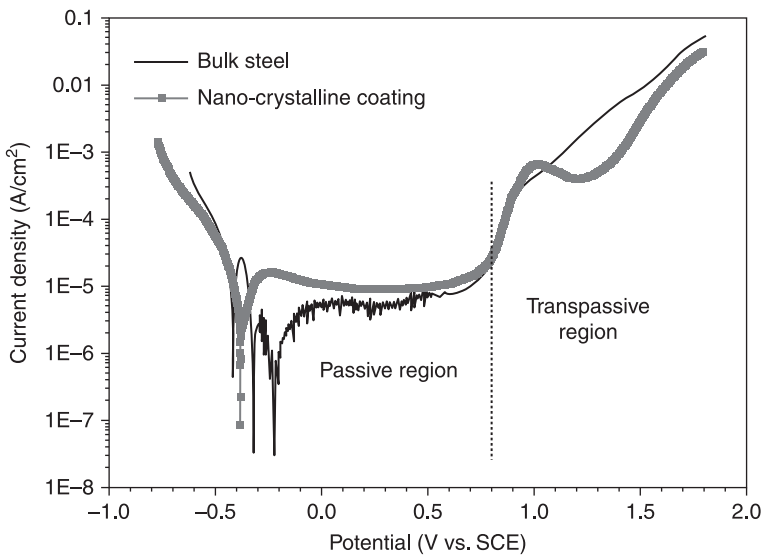

4.11 Potentiodynamic polarization plots of 309 stainless steel in 3.5% NaCl solution.[26]

indicates that an increase in the carrier density of the passive film can promote the electrochemical dissolution of the passive film, and that the large grain sizes in NC materials may lead to higher carrier density, which can in turn increase the dissolution rate.

It is interesting that some passive NC materials have worse passive abilities compared with coarse crystalline alloy. Barbucci *et al.*[41] found that NC Cu90Ni10 alloy (20 nm) made using the ball-milling technique has a lower pitting potential in 0.3% Na_2SO_4 with different amounts of Cl^-. They also theorized that the block effect of a large amount of grain boundaries inhibits the growth of passive film, and that the large amount of defects in NC materials also leads to corrosion.

4.4.1 Effect of nanocrystallization on the pit initiation process

Electrochemical noise (EN) analysis, including the power spectral density (PSD_i) and wavelet transform, indicated that the controlling pitting mechanism of a cast austenite stainless steel was a slow event of metastable pit generation and reparation; however, for the NC coating it was a fast metastable pitting mechanism (Fig. 4.12).[40] The stochastic approach was also applied to investigate the metastable pitting process of both samples (coarse crystalline alloy and NC coating), which also showed that metastable pits occurred more frequently on the NC coating than on the coarse crystalline alloy. However, there was an increased probability of stable pits developing from metastable pits.

In situ AFM observations found that an initial metastable pit was observed (in the white circle in Fig. 4.13(a)). Figure 4.13(b) shows the growth of the metastable pit, which is rapidly healed in the next picture (Fig. 4.13(c)). After this healing process there is no further change for a period of time (called stopping time), and then the metastable pits form and heal again. After several cycles of pit initiation and healing (during which the stopping time becomes progressively shorter), a stable pit appears and never repairs (Fig. 4.13(d)).[40] After this period, the stable growth of the pit controls the whole corrosion process. However, this is not observed in the image of the NC coating, the process of which seems to be faster than that of the coarse crystalline alloy.

The microstructure of the NC coating influenced the morphology of the formed oxide particles; the voids within the oxide scale are shown in different piled layers and the boundaries of these oxide particles could serve as incubation sites for metastable pits. Although the metastable pits were able to begin appearing on the NC coating, the small grain size promoted diffusion of the element to rapidly repair or heal the pits. The pitting corrosion mechanism of the NC coating was dominant because of the fast metastable pits' initiation and death; therefore the pitting corrosion resistance was higher than that of the corresponding coarse crystalline stainless steel.

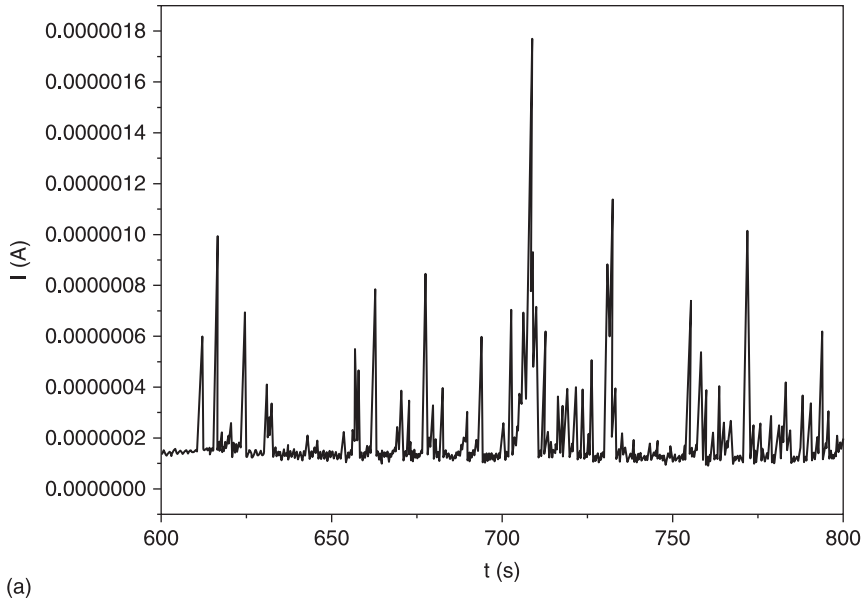

(a)

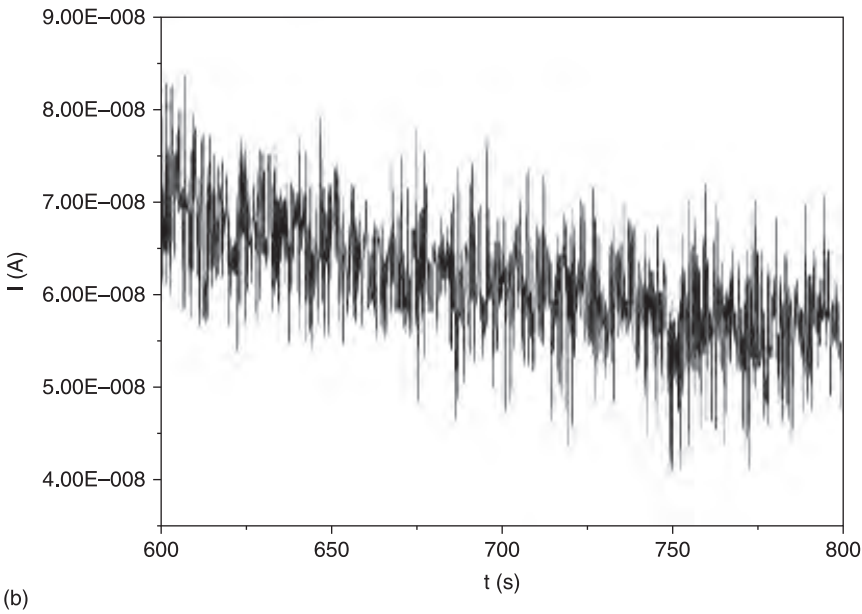

(b)

4.12 Current electrochemical noise of the coarse crystalline austenitic stainless steel (a) and the corresponding NC coating (b) under anodic polarization during 600–800 s in 3.5% NaCl solution.[40]

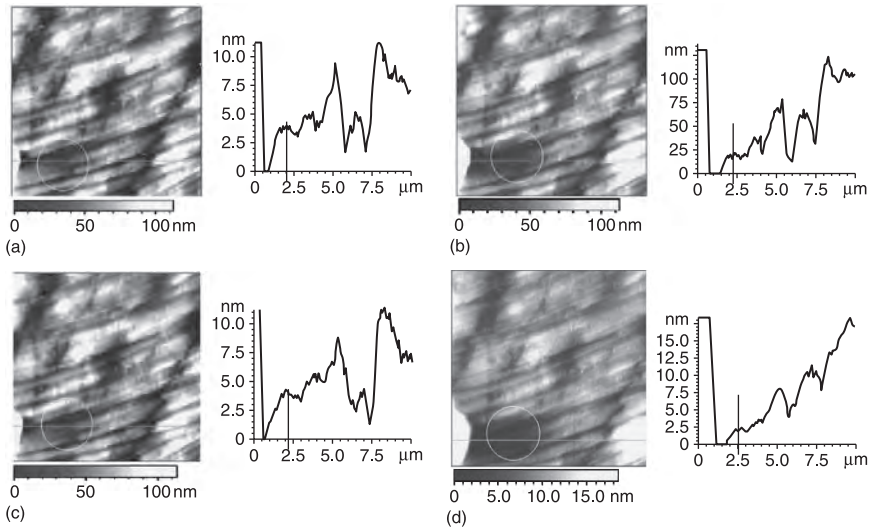

4.13 In situ AFM images of the coarse crystalline alloy in the pitting stage under anodic polarization in 3.5% NaCl solution: (a) the formation of a metastable pit, (b) the growth of the pit, (c) the reparation of the pit and (d) the growth of the pit.[40]

4.4.2 Effect of nanocrystallization on the pit growth process

Generation and reparation of metastable pits were not observed on an austenitic stainless steel NC coating, nor was the process of metastable pitting. Once the pit formed, it grew directly to a stable pit state (in Fig. 4.14) with subsequent dissolution of the sample. This observation suggests that the pits formed at the boundaries of the oxide particles.[40]

The shape of the pit on the NC coating are dish shaped.[42,43] Compared with a conventional coarse crystalline austenitic stainless steel, pit propagation on the NC coating was significantly less, which suggested that nanocrystallization decreased the rate of stable pitting nucleation and growth. Regarding the observed decrease in pit depth at the later stages, it is possible that the pit re-passivated lengthwise or the path around the pit was dissolved with growth of the pit.

According to the *in situ* observation by AFM, the oxide particles on the NC coating formed continuously; this suggested that the passivation ability of the NC coating was very strong. Generally, pitting corrosion dissolution and passivation proceeded simultaneously, but dissolution progressed at a faster rate than passivation. However, because the passivation ability of the NC coating was so significant, passivation proceeded effectively and growth

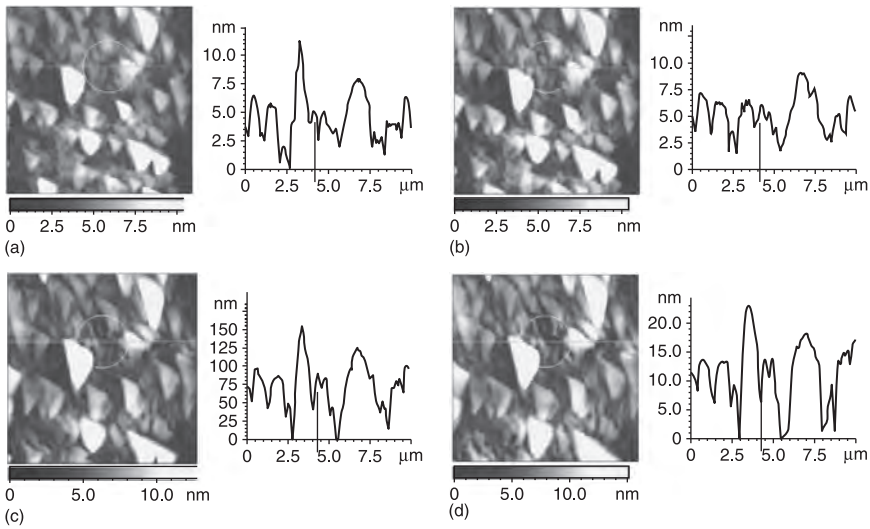

4.14 In situ AFM images of the NC coating in the pitting stage under anodic polarization in 3.5% NaCl solution: (a) the formation of a metastable pit, (b), (c) and (d) the growth of the pit.[40]

of the pit was restricted compared with the conventional coarse crystalline stainless steel.

The present authors theorize that nanocrystallization increases the unstable points on the surface of the materials, which increases the possibility of local corrosion. However, the excellent ability of element diffusion helps to heal the local corrosion points, which inhibits the growth of the local corrosion.

4.5 Effect of grain size on electrochemical corrosion behaviors

In aqueous solutions, the main failure form of metallic materials is electrochemical corrosion. It is well known that many factors can affect the corrosion rate of NC materials in aqueous solution, such as composition and structure. For a fixed composition, grain size is an important factor that affects the corrosion process. Hashimoto and coworkers[44,45] have studied the corrosion behavior of amorphous alloys with NC heterogeneous precipitation. After amorphous Cr–Zr alloys (15 nm, 17 nm and 22 nm amorphous Cr–60Zr thin films) were treated at a high temperature, precipitation of Zr was observed with different particle sizes. They found that there was a relationship between the size of the precipitates and the pitting potential. The pitting potential of amorphous Cr–67Zr alloy was highest when the size of the precipitates observed was below 20 nm. The pitting resistance

of amorphous Cr–Zr alloy deteriorated as the size increased. The precipitation of Zr phase is shown to lead to an increase in the amount of Cr in the matrix, which encourages the enrichment of Cr in the passive film. Although the corrosion resistance of Zr is poor, the length of the Zr phase is small, and the passive film, which is rich in elemental Cr, can protect the whole material. When the amount of precipitated Zr is more than 20 nm, the passive film enriched with elemental Cr cannot cover the whole surface of the material, which is the reason why the corrosion resistance of 22 nm Zr alloy decreases compared with alloys with a smaller grain size.

The other alloys studied were Cr–Nb, Al–Cr and Cr–Ti. It was found that there was a critical size of precipitates at which point the corrosion resistance changed. In the same way, Mehmood *et al.*[45] studied the corrosion behavior of different grain sizes for Al–Cr amorphous coating in 0.1 M and 0.5 M HCl solution. They found that the precipitation phase of Al enriched the Cr in the matrix and increased the corrosion resistance. However, when the grain size was larger than 20 nm, the corrosion resistance of materials decreased. El-Moneim and coworkers[46] studied how grain growth affects the corrosion behavior of NC NdFeB magnets. They found that the corrosion resistance increased with the increasing grain size of the hard magnet phase.

Li *et al.*[14] found that the corrosion behavior of low-carbon steel with an NC outer layer (grain size about 20 nm), which was produced by USSP, was affected by the grain size, as shown in Fig. 4.15. When the grain size was

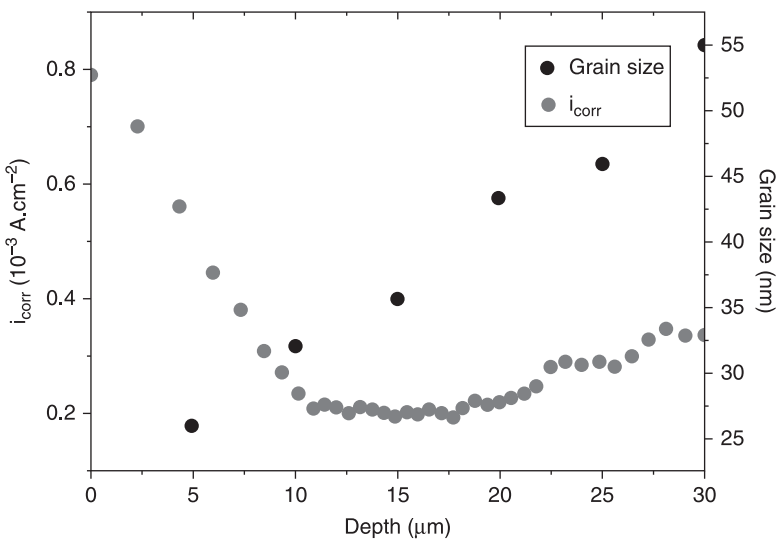

4.15 Corrosion rate and grain size vs. depth for SNC low-carbon steel in 0.05 mol/l H_2SO_4 + 0.05 mol/l Na_2SO_4 solution.[14]

>35 nm, there was no significant difference in the electrochemical behavior of the material; when the grain size was <35 nm, the corrosion rate increased in correlation with the decrease in grain size. The NC coating of low-carbon steel, produced using the magnetron sputtering technique (grain size about 40 nm), also increased the dissolution rate when compared with bulk steel with the same chemistry. Because of this acceleration of dissolution, researchers came to the conclusion that the change is due to the increase of the active ability of metals on NC coating, which accelerates the kinetics of the anodic reaction.

The grain size also significantly influences the corrosion behavior of Ni-based superalloys in acid solution. The corrosion resistance of sputtering Ni-based NC thin films increases with the decrease of grain size, as shown in Fig. 4.16. Further studies indicate that the amount of Cl^- adsorbed decreased with the decrease in grain size. This decrease of grain size promoted the formation of a more compact passive film. The smaller grain size also increased the re-passivation ability of the passive film on NC thin film. All of these results show that the corrosion resistance of NC thin film is increased when compared with the conventional coarse crystalline Ni-based alloy.

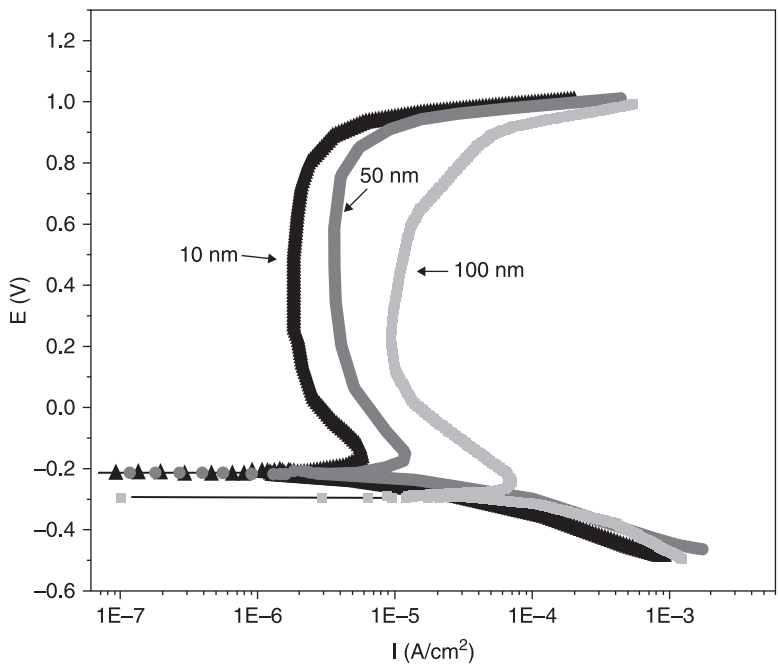

4.16 Potentiodynamic polarization plots of three grain size Ni-based super alloy NC coatings in 3.5% NaCl solution.[40]

4.6 Conclusions

Nanocrystallization of metals/alloys increases the amount of active atoms in materials, as well as increasing the reaction activities of the materials themselves. For active materials, nanocrystallization increases the corrosion rate, as well as the grain size, which greatly influences the dissolution rate; for passive materials, nanocrystallization promotes the formation ability of passive film and increases the corrosion resistance. However, from present research results, there are many unknown problems that require further research in order to be fully understood. Firstly, the influence of nanocrystallization on the corrosion behavior of metals/alloys is affected not only by the grain size, but also by the changed structure and chemicals of the metals/alloys by the nanocrystallization process. For this reason it is important that research into NC materials considers these above influences.

Secondly, although several investigations have found that there are many changed characteristics of the materials caused by nanocrystallization, the relation of these characteristics to the grain size has not yet been confirmed. For example, nanocrystallization decreases the amount of Cl^- adsorbed by materials. But there are still other questions unanswered, such as the critical grain size for this change and whether the surface adsorption energy has changed with the grain size. Nanocrystallization promotes the amount of elemental Cr in the passive film, but it is not known what the relationship of grain size is with regard to the diffusion factors of Cr in the passive film. There is also the question of whether the diffusion mechanism of elemental Cr changes with regard to the smaller grain size. There are still a series of problems which have not yet been properly understood and must wait for future research to give the answers.

4.7 References

1. Z. Liu, T. Wu, K. Dahm and F. Wang (2002), 'The effect of coating grain size on the elective oxidation behavior of Ni-Cr-Al alloy', *Scrip. Mater.*, **37**: 1151–8.
2. X. Y. Wang and D. Y. Li (2002), 'Mechanical and electrochemical behavior of nanocrystalline surface of 304 stainless steel', *Electrochim. Acta*, **47**: 3939–47.
3. S. Shriram, S. Mohan, N. G. Renganathan and R. Venkatachalam (2000), 'Electrodeposition of nanocrystalline nickel—a brief review', *Trans. IMF*, **78**(5): 194–7.
4. R. B. Intrui and Z. Szklarska-Smialowska (1992), 'Localized corrosion of nanocrystalline 304 type stainless steel film', *Corrosion*, **48**: 398–403.
5. F. H. Wang, H. Lou, S. Zhu and W. Wu (1997), 'The mechanism of scale adhesion on sputtered microcrystallized Co-Cr-Al films', *Oxid. Met.*, **48**: 39–50.
6. F. H. Wang (1996), 'The effect of nanocrystallization on the selective oxidation and adhesion of Al_2O_3 scales', *Oxid. Met.*, **48**: 215–24.
7. H. Lou, X. Sun and H. Guan (1996), 'Oxidation behavior of sputtered microcrystalline coating of superalloy KF17 at high-temperature', *Mater. Sci. Eng. A*, **207**: 121–8.
8. C. Wang, F. Jiang and F. Wang (2004), 'Corrosion inhibition of 304 stainless steel by nano-sized Ti/Si coating in an environment containing NaCl and water vapor at 400–600 C', *Oxid. Met.*, **62**: 1–13.

9. F. Wang, S. Geng and S. Zhu (2002), 'Corrosion behavior of a sputtered K38G nanocrystalline coating with a solid NaCl deposit in wet oxygen at 600 to 700°C', *Oxid. Met.*, **58**: 185–95.
10. S. Geng, F. Wang and S. Zhu (2002), 'High-temperature oxidation behavior of sputtered IN738 nanocrystalline coating', *Oxid. Met.*, **57**: 23–43.
11. Y. Shu (1999), 'Corrosion behavior of some metals and coatings under the synergistic effect of solid NaCl and water vapor at 500–700°C', PhD thesis, the Institute of Corrosion and Protection of Metals (in Chinese).
12. H. Gleiter (1989), 'Nanocrystalline materials', *Prof. Mater. Sci.*, **33**: 223–315.
13. K. Lu (1996), 'Nanocrystalline metals crystallized from amorphous solids: nanocrystallization, structure, and properties', *Mater. Sci. Eng. R*, **16**: 161–221.
14. Y. Li, F. Wang and G. Liu (2004), 'Grain size effect on the electrochemical corrosion behavior of surface nanocrystallized low-carbon steel', *Corrosion*, **60**: 891–6.
15. H. Lu, Y. Li and F. Wang (2006), 'Corrosion behavior of Cu-20Zr alloy in hydrochloric acid solution', *Corros. Sci.*, **48**: 2106–19.
16. H. Lu, Y. Li and F. Wang (2006), 'Enhancement of the electrochemical behavior for Cu-70Zr alloy by grain refinement', *Surf. Coat. Tech.*, **201**: 3393–8.
17. W. Zeiger, M. Schneider, D. Scharnwber and H. Worch (1995), 'Corrosion behavior of a nanocrystalline FeA18 alloy', *Nanostruct. Mater.*, **6**: 1013–16.
18. S. J. Thorpe, B. Ramaswami and K. T. Aust (1988), 'Corrosion and Auger studies of a Ni-based metal-metalloid glass', *J. Electrochem. Soc.*, **135**: 2162–70.
19. X. Y. Wang and D. Y. Li (2002), 'Mechanical and electrochemical behavior of nanocrystalline surface of 304 stainless steel', *Electrochim. Acta*, **47**: 3939–47.
20. G. Meng, Y. Li and F. H. Wang (2006), 'The corrosion behavior of Fe-10Cr nanocrystalline coating', *Electrochim. Acta*, **51**: 4277–84.
21. W. Ye, Y. Li and F. H. Wang (2006), 'Effects of nanocrystallization on the corrosion behavior of 309 stainless steel', *Electrochim. Acta*, **51**, 4426–32.
22. L. Liu, Y. Li and F. H. Wang (2007), 'Influence of nanocrystallization on passive behaviour of Ni-based superalloy in acidic solutions', *Electrochim. Acta*, **52**: 2392–400.
23. L. Liu, Y. Li and F. H. Wang (2007), 'Influence of micro-structure on corrosion behaviour of Ni-based superalloy in 3.5% NaCl solutions', *Electrochim. Acta*, **52**: 7193–202.
24. Y. Li, T. Zhang and F. Wang (2006), 'Effect of microcrystallization on the corrosion behaviour of AZ91D magnesium alloy', *Electrochim. Acta*, **51**: 2845–50.
25. B. Zhang, Y. Li and F. H. Wang (2007), 'Electrochemical Behavior of Microcrystalline Aluminum in acid solutions', *Corros. Sci.*, **49**: 2071–82.
26. W. Ye, Y. Li and F. H. Wang (2009), 'The improvement of the corrosion resistance of 309 stainless steel in the transpassive region by nano-crystallization', *Electrochim. Acta*, **54**: 1339–49.
27. E. McCafferty (1995), 'The electrode kinetics of pit initiation on aluminum', *Corros. Sci.*, **37**: 481–92.
28. Z. Szklarska-Smialowska (1999), 'Pitting corrosion of aluminum', *Corros. Sci.*, **41**: 1743–67.
29. H. Wang (2009), 'Electrochemical corrosion behaviors of two magnesium alloys containing rare earth elements', PhD thesis, the Institute of Metal Research, Chinese Academy of Sciences (in Chinese).
30. H. H. Hassan (2005), 'Effect of Cl^- on the corrosion behavior of steel in 0.1 M citrate', *Electrochim. Acta*, **51**: 526–71.

31. A. Gebert, U. Wolff, A. John, J. Eckert and L. Schultz (2001), 'Stability of the bulk glass-forming Mg65Y10Cu25 alloy in aqueous electrolytes', *Mater. Sci. Eng. A*, **299**: 125–35.
32. J. R. Galvele, R. M. Torresi and R. M. Carranza (1990), 'Passivity breakdown, its relation to pitting and stress–corrosion–cracking processes', *Corros. Sci.*, **31**: 563–71.
33. B. Pieraggi, B. MacDougall and R. A. Rapp (2005), 'The role of the metal/oxide interface in the growth of passive films in aqueous environments', *Corros. Sci.*, **47**: 247–56.
34. P. Zhao *et al.* (1999), *The basic acknowledge of materials science*. Harbin, China: Harbin Institute of Technology, p. 45.
35. G. Meng (2005) 'Effect of nanocrystallization on electrochemical corrosion behavior of Fe-Cr alloys', PhD thesis, the Institute of Metal Research, Chinese Academy of Sciences (in Chinese).
36. B. Zhang, Y. Li and F. H. Wang (2009), 'Electrochemical behaviour of microcrystalline aluminium in neutral fluoride-containing solutions', *Corros. Sci.*, **51**: 268–75.
37. S. R. Morrison (1977), *The Chemical Physics of Surfaces*. New York and London: Plenum Press, p. 166.
38. L. Liu, Y. Li and F. H. Wang (2008), 'Influence of grain size on the corrosion behavior of a Ni-based superalloynanocrystalline coating in NaCl acidic solution', *Electrochim. Acta*, **53**: 2453–62.
39. N. Li, Y. Li, S. Wang and F. H. Wang (2006), 'Electrochemical corrosion behavior of nanocrystalline bulk 304 stainless steel', *Electrochim. Acta*, **52**: 760–5.
40. L. Liu, Y. Li and F. H. Wang (2008), 'Pitting mechanism on an austenite stainless steel nanocrystalline coating investigated by electrochemical noise and *in situ* AFM analysis', *Electrochim. Acta*, **54**: 768–80.
41. A. Barbucci, G. Farne, P. Matteazzi, R. Riccieri and G. Cerisola (1998), 'Corrosion behavior of nanocrystalline Cu90Ni10 alloy in neutral solution containing chlorides', *Corros. Sci.*, **41**: 463–75.
42. P. C. Pistorius and G. T. Burtein (1992), 'Growth of corrosion pits on stainless steel in chloride solution containing dilute sulfate', *Corros. Sci.* **33**: 1885–97.
43. P. Ernst and R. C. Newman (2002), 'Pit growth studies in stainless steel foils – 1. Introduction and pit growth kinetics', *Corros. Sci.*, **44**: 927–41.
44. X. Y. Li, E. Akiyama, H. Habazaki, A. Kawashima, K. Asami and K. Hashimoto (1997), 'An XPS study of passive films on corrosion resistant Cr-Zr alloys prepared by sputter deposition', *Corros. Sci.*, **39**: 1365–80.
45. M. Mehmood, B. P. Zhang, E. Akiyama, H. Habazaki, A. Kawashima *et al.* (1998), 'Experimental evidence for the critical size of heterogeneity areas for pitting corrosion of Cr-Zr alloys in 6M HCl', *Corros. Sci.*, **40**: 1–17.
46. A. A. El-Moneim, A. Gebert, M. Uhlemann, O. Gutfleisch and L. Schultz (2002), 'The influence of Co and Ga additions on the corrosion behavior of nanocrystalline NdFeB magnets', *Corros. Sci.*, **44**: 1857–74.
47. H. Lu, Y. Li and F. Wang (2006), 'Improved corrosion behavior of nanocrystalline Cu-20Zr film in HCl solution', *Thin Solid Film*, **510**: 197–203.

5

Electrodeposition: the versatile technique for nanomaterials

D. SOBHA JAYAKRISHNAN, CSIR – Central Electrochemical Research Institute, India

Abstract: Electrodeposition is a well-known conventional surface modification method to improve the surface characteristics, decorative and functional, of a wide variety of materials. Now, electrodeposition is emerging as an accepted versatile technique for the preparation of nanomaterials. Work done in this direction is discussed in this chapter. The basics of electrodeposition are introduced, then the electrodeposition of nanomaterials using special techniques for reducing grain size. Methods such as pulse and pulse reverse current deposition, template-assisted deposition and use of additives and grain refiners are explained with suitable examples. Deposition of nanostructured metals, alloys, metal matrix composites, multilayers and biocompatible materials reported in the literature are discussed. Finally, there is a discussion of the improved corrosion resistance of electrodeposited nanostructured materials, quoting results reported in literature.

Key words: electrodeposition, nanomaterials, pulse and pulse reverse electrodeposition, template-assisted deposition, additives and grain refiners, nanostuctured metals and alloys, nanocomposites, multilayers, biocompatible materials, corrosion resistance of electrodeposited nanostuctured materials.

5.1 Introduction

Electrodeposition of metals and alloys is of wide interest and finds application in a number of fields such as electroplating, electrowinning and electrorefining. Many items, from domestic components to advanced technological devices, are electrodeposited to impart an appealing appearance, endow them with specific surface engineering properties and protect them from corrosion (Pletcher, 1981). The electrodeposition technique involves deposition of a metal or alloy coating over a conducting surface by means of electrolysis from a well-formulated electrolyte known as a bath (Lowenheim, 1974), which can be an aqueous solution of a simple salt or a complex salt type. The discharge of a metal depends on its position in the electrochemical series (Glasstone, 1960) and the chemistry of the solution from which deposition is done.

5.1.1 Mechanism of electrodeposition

An electrolysis cell circuit consists of an anode (the positive electrode), a cathode (the negative electrode), an electrolytic bath, a current source and an ampere/volt

meter (Raub and Muller, 1967). Reduction and oxidation occur at the cathode and anode respectively due to metal ions and electrons that can cross the electrode–electrolyte interface. The cathode is the conducting substrate on which electrodeposition is to be done; the anode can be either soluble or inert. The overall reactions taking place during electrolysis can be represented as Eq. 5.1 at the cathode, Eq. 5.2 at a soluble anode and Eq. 5.3 at an insoluble anode:

$$M^{z+} + ne^- \rightarrow M \quad [5.1]$$

$$M \rightarrow M^{z+} + ne^- \quad [5.2]$$

$$H_2O \rightarrow 2H^+ + 1/2\ O_2 \uparrow + 2\ e^- \quad [5.3]$$

In simple salt solutions, metal ions are present in bulk solution as hydrated ions; the metal ion when hydrated is represented as $M(H_2O)_x^{Z+}$, where x is the number of water molecules in the primary hydration sheath. The reactions involved in the discharge process (Raub and Muller, 1967) of ions under the influence of an electric field are the transport of hydrated ions towards the cathode surface, the alignment of water molecules in the diffusion layer, the removal of water molecules in the Helmholtz layer, discharge followed by adsorption of the ions at the cathode surface as 'adatoms', surface diffusion and the incorporation of adatoms into the crystal lattice at the growth point. A schematic representation of these steps is given in Fig. 5.1.

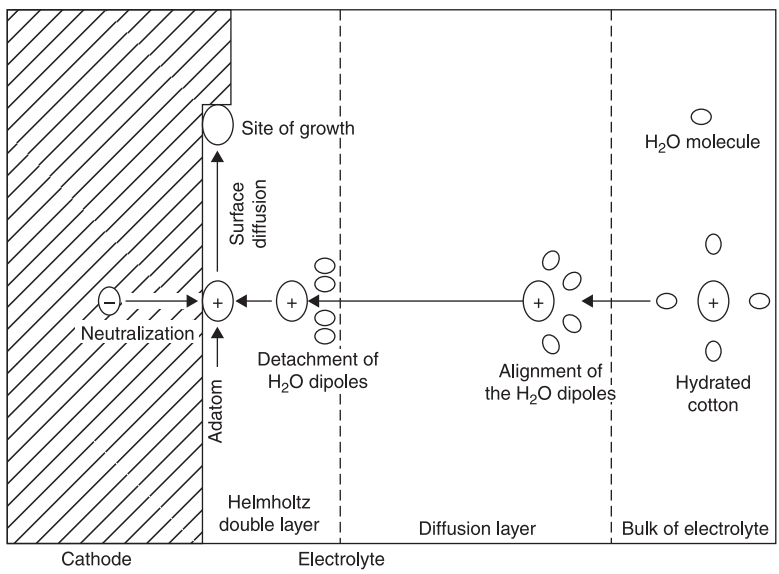

5.1 Schematic representation of steps in the cathodic deposition of metals.

The mechanism of electrodeposition from complex electrolytes is more complicated than from simple salt solutions. In complex electrolytes, discharge of metal ions must be preceded by ligand removal, analogous to hydration sheath removal in simple salt solutions (Lyons, 1954). Electrodeposition from complex electrolytes occurs with a high over-potential (Ettel, 1984) compared with simple salt solutions, resulting in deposits of refined grain size, higher throwing power due to improved secondary current distribution and favorable conditions for codeposition of metals due to closer metal deposition potentials.

5.1.2 Fundamentals of metal deposition

Faraday's laws provide the theoretical basis of electrodeposition (Antropov, 1977). The quantity of metal deposited (W) at the cathode surface can be expressed as the product of quantity of total coulombs passed (Q_c) and the electrochemical equivalent of the metal (z_c):

$$Q_c = \int I \partial t \quad [5.4]$$

$$z_c = M_w / nF \quad [5.5]$$

$$W = \int I \partial t \, M_w / nF \quad [5.6]$$

where I is the current applied over a period of time t, M_w is the molar mass of the metal that undergoes electroreduction by taking n number of electrons and F is the Faraday constant. Electrodeposition reactions that take place in the cathode/electrolyte interfacial region are heterogeneous and involve mass transfer and charge transfer steps. The rate of reduction, and hence the cathodic current, is determined by the slowest step among the sequence of steps.

5.1.3 Thermodynamics and kinetics of electrodeposition

The nucleation (Wang, 2006) on the electrode substrate is influenced by the crystal structure of the substrate, specific free surface energy, adhesion energy, lattice orientation of the electrode surface and crystallographic lattice mismatch at the nucleus–substrate interface boundary. The final size distribution of the electrodeposits strongly depends on the kinetics of nucleation and growth; nucleation is of two types, instantaneous and progressive. In instantaneous nucleation, all the nuclei form instantaneously on the electrode substrate and subsequently grow with the time of electrodeposition. In progressive nucleation, the number of nuclei that are formed is a direct function of the time of electrodeposition. These nuclei gradually grow and overlap, and therefore the progressive nucleation process exhibits zones of reduced nucleation rate around the growing stable nuclei.

5.2 Nanomaterials applied by electrodeposition

5.2.1 Nanomaterials

Nanostructured materials have gained importance due to their significantly enhanced properties (Kadirgan, 2006; Gurrappa and Binder, 2008; Ashby *et al.*, 2009; Aliofkhazraei, 2011). As a material becomes more and more finely divided it reaches a point where the physical properties that the bulk material possesses begin to differ significantly. Several new and non-equilibrium (metastable state) processing methods have been developed during the last few decades to improve the performance of existing materials. A novel method of transforming a material to a metastable state is to reduce its grain size to a few nanometers, at which the proportion of atoms in the grain boundaries is equivalent to, or higher than, those inside the grains. Materials with such small grain sizes are referred to as nanocrystalline (NC) materials (and also as nanocrystals, nanostructures, nanophase materials or nanometer-sized crystalline solids), and have much improved properties compared with those exhibited by conventional grain sized (>10 μm) polycrystalline materials. The combination of unique compositions and novel microstructures leads to the extraordinary potential of NC materials for a variety of structural and non-structural applications.

NC materials are single phase or multiphase polycrystals, the crystal size of which is of the order of a few (typically 1–100) nanometers in at least one dimension. They are normally classified into different categories depending on the number of dimensions in which the material has nanometer modulations. They can be equiaxed and are termed nanostructure crystallites (three-dimensional (3D) nanostructures), or they can have a lamellar structure and are termed layered nanostructures (two-dimensional (2D) nanostructures), or they can be filamentary (one-dimensional (1D) nanostructures). Additionally, zero-dimensional (0D) atom clusters and cluster assemblies are also considered. The length and width are much greater than the thickness in layered nanocrystals, and the length is substantially larger than the width or diameter in filamentary nanocrystals. NC materials may contain crystalline, quasi-crystalline or amorphous phases and can be metals, ceramics or composites. Of the above materials, most attention has been paid to synthesis, consolidation and characterization of the 3D nanostructured crystallites, followed by those of 2D layered nanostructures. While the former are expected to be used in applications based on their high strength, improved formability and soft magnetic properties, the latter are intended for electronic applications.

In these materials with a small grain size of a few nanometers, the fraction of atoms in the grain boundaries is comparable to that in the grains. Therefore, NC materials can be considered to consist of two structural components, i.e. small crystallites with long-range order and different crystallographic orientations constituting the crystalline component, and a network of intercrystalline regions (grain boundaries, triple junctions, etc), the structure of which differs from region to region, referred to as the interfacial component. As a result of this, NC materials

exhibit a variety of properties that are different and often considerably improved in comparison with those of conventional coarse-grained polycrystalline materials. Due to their superior characteristics of strength/hardness, enhanced diffusivity, improved ductility/toughness, reduced density, reduced elastic modulus, higher electrical resistivity, increased specific heat, higher coefficient of thermal expansion, lower thermal conductivity, increased corrosion and wear resistance and superior soft magnetic properties, nanostructured coatings offer great potential for various applications.

5.2.2 Electrodeposition of nanomaterials

Among the diverse processes available, the electrochemical method is a well-accepted technique for the synthesis of a wide range of nanostructured materials, e.g. metal nanoparticles, nanowires, nanofilms, bulk NC metals, laminated composites, multilayered coatings and nanoparticle-reinforced composite coatings. Electrodeposition of a pure metal, or codeposition of an alloy from an electrolyte, takes place on the surface of the target, which is the cathode of the electrochemical system of the coating process. This process happens by applying an external current (direct or pulsed) to the electrodeposition system. By this method, 2D and 3D nanostructures of metals, alloys and nanocomposites have been deposited successfully. 1D nanostructure crystallites can also be prepared using the electrodeposition method by utilizing the interference of one ion with the deposition of the other.

Electrodeposition techniques can yield porosity-free finished products that do not require subsequent consolidation processing (Palumbo *et al.*, 1991; Bakonyi *et al.*, 1993). Further, the process requires low initial capital investment and provides high production rates with few shape and size limitations. Electrodeposition is an important technique for the fabrication of nanostructured materials, offering control over the structure, composition and properties, and thus facilitates the preparation of novel materials with enhanced properties that cannot be obtained by other techniques. Table 5.1 lists some of the interesting applications of electrodeposited NC materials. Bicelli *et al.* (2008) provide a list of experimental methods that have been reported in the literature for the investigation of nano-electrodeposits and nano-electrodeposition systems. These methods encompass microscopy (electron microscopy and scanning-probe techniques), spectroscopy (atomic absorption, characteristic X-rays, mass, Mossbauer, photoelectron, visible), diffractometry (electrons and X-rays), calorimetry, magnetometry and mechanical measurements (bending, indentations, stress, tensile testing, wear resistance).

The electrochemical deposition of nanostructured materials is a two-step process (Natter and Hempelmann, 2003) consisting of 1) the formation of a high nuclei number and 2) the controlled growth of the deposited nuclei. These two conditions can be realized by correct choice of the chemical and physical

Table 5.1 Electrodeposited nanomaterials and their applications

Nanomaterials	Applications
Cu	Foil for printed circuit boards
Pb	Battery grids
Ni, Ni-P, Zn Ni, Co, Co P	Corrosion resistant coatings
Co-P, Ni-B_4C	Cr replacement coatings
Ni, Cu	Electronic connectors
Co, Ni or Fe on Cu	Electrical conductors
Ni-Fe	Electromagnetic shielding
Ni, Co, Ni-Fe, Co-Fe	Free-standing soft magnets
Ni-P	Electrosleeve
Ni Mo	Catalysts for hydrogen evolution
Ni, Fe, Co, Ni Fe	Armor laminates
Ni, Ni-SiC, Ni-Al_2O_3, Co, Co-P	Hard facing applications
Ni-Fe	Magnetic recording heads
Ni-MoS_2, Ni-BN	Self lubricating coatings
Ni Fe, Co Fe	Transformer core materials
Ni, Ni-SiC, Ni-P, Co, Co-P	Wear resistant coatings
Ni on polymers	Metal/polymer hybrids

process parameters. The size and the number of nuclei can be controlled by the over-potential η:

$$r = \frac{2\sigma V}{ze_0\ [\eta]} \qquad [5.7]$$

In this electrochemical version of the Kelvin equation (Budevski *et al.*, 1996), r is the critical nucleation radius, σ the specific surface energy, V the atomic volume in the crystal and z the number of elementary charges e_0. This equation reveals that the higher the over-potential, the smaller the formed nuclei, and hence, by increasing the over-potential, we get a higher current density which is responsible for a high nuclei formation rate. Over-potential is an electrochemical term which refers to the potential (voltage) difference between a half-reaction's thermodynamically determined reduction potential and the potential at which the redox event is experimentally observed.

Various electrochemical strategies have been pioneered and investigated for the fabrication of a variety of nanostructured materials (Erb *et al.*, 2002). For example, electrodeposition offers novel routes to nanosized particles via arrested and templated electrodeposition. Electrodeposition yields grain sizes in the nanometer range when the electrodeposition variables (e.g. bath composition, pH, temperature, current density, etc) are chosen such that nucleation of new grains is favored rather than growth of existing grains (Clark *et al.*, 1997). This was achieved by using high deposition rates, formation of appropriate complexes in the bath, addition of suitable surface active elements to reduce surface diffusion of adatoms and so forth.

5.3 Special techniques for grain size reduction

5.3.1 Use of pulse and pulse reverse currents

Pulse electrodeposition has proven to be one of the most effective methods in fabrication of nanostructured metal coatings. As compared with traditional direct current (DC) electrodeposition, pulse current (PC) electrodeposition offers more process controllable parameters which can be adjusted independently and can withstand much higher instantaneous current densities. Therefore, metal coatings fabricated by pulse electrodeposition possess more unique compositions and microstructures than can be obtained by DC electrodeposition. A large body of theoretical research has been carried out over the years by Cheh (1971), Chin (1983), Ibl (1980) and Yin (1996) and an overview of the effect of pulse electrodeposition on the composition and microstructure of metal coatings has been presented by Landolt and Marlot (2003). The broad selection of the appropriate bath chemistry and plating parameters like pulse current density, time on/off and duty cycle provides the flexibility to control structure, morphology (crystallite size and shape) and composition of materials. Average current density in pulse plating is given by the equation (Natter and Hempelmann, 2003):

$$I_{\text{ave}} = \frac{I_{\text{pulse}} \times t_{\text{on}}}{t_{\text{on}} + I_{\text{off}}} \qquad [5.8]$$

where t_{on}, t_{off} and I_{pulse} stand for on time, off time and pulse current density. As per the equation relating the critical nucleation radius r and over-voltage η (Eq. 5.7), by applying a high over-voltage/high current density a high nuclei formation rate can be achieved, but this can be maintained for only a few milliseconds (t_{on}) because the metal ion concentration in the vicinity of the cathode decreases drastically and therefore the process becomes diffusion controlled. But in pulse deposition the current is switched off for 20–100 ms (t_{off}). During the off time, the metal ions diffuse from the bulk electrolyte to the cathode and compensate the metal ion depletion. In this break a second effect is observed due to exchange currents: Ostwald ripening sets in and causes crystallite growth.

Based on these facts, there are several possibilities to control the crystallite size: the crystallite size can be decreased by increasing the current density for a constant t_{on}; the crystallite size can be increased for long t_{off} due to Ostwald ripening; the use of organic additives (grain refiners) enables the control of the crystallization process during the t_{off} time because these molecules are adsorbed on the electrode surface in a reversible way and hinder the surface diffusion of the adatoms; and changing the temperature influences all diffusion processes (ion diffusion in the electrolyte, surface diffusion of the nuclei) – if small crystallite sizes are desired, the deposition should be performed at lower temperatures.

Natter and Hempelmann (1996) demonstrated that, in the pulsed electrochemical deposition of NC copper, the nanostructure of the resulting material can be deliberately tuned by taking appropriate physical measures (parameters of the current pulses and temperature) and chemical measures (chemical composition of the bath, the concentration of the metal ions and the pH value). They proposed an atomistic deposition mechanism that allows the interpretation of this phenomenon as subtle interplays between nucleation, physisorption and grain growth processes. A large cathodic over-potential favors a high nucleation rate, resulting in the formation of crystallite nuclei in large quantities but small size. The necessary huge current density cannot be achieved for DC electrolysis because of ionic transport limitations in the electrolyte. But huge current densities are feasible as peak current densities in short current pulses, because in this way sufficient ionic transport takes place in the off times between two pulses provided these times are long enough and there is sufficient stirring in the electrolyte.

The effect of plating parameters on average crystallite size and hardness of three Cu–Ni alloys A, B and C prepared from a citrate bath (Ghosh *et al.*, 2000) by pulse and DC plating methods is shown in Table 5.2 (Ghosh *et al.*, 2006). The grain size was measured from a transmission electron microscopy (TEM) micrograph using comprehensive image analysis software. The crystallite size of the DC-plated NC-C alloy was larger than that of pulse-plated alloy (NC-A) deposited under the same average current density, I_{ave} = 2 A dm^{-2}. The crystallite size decreases with the increase in average current density applied during pulse plating. The microhardness was found to be higher for PC-plated alloys than for the DC-plated alloys, which, although NC, had a larger crystallite size. The hardness value increased with the decrease in grain size and the increase in Ni

Table 5.2 Effect of DC and PC plating parameters on average crystallite size and hardness of Cu–Ni

Samples	Description	Deposition conditions	Microhardness KHN_{50}	Average crystalline size (nm)
NC-A	PC 35.8 wt% Cu	f = 100 Hz, I_p = 20 A dm^{-2} I_a = 2 A dm^{-2}, RT, pH 9	452	12.7
NC-B	PC 26.0 wt% Cu	f = 50 Hz, I_p = 20 A dm^{-2} I_a = 4 A dm^{-2}, RT, pH 9	736	6.6
NC-C	DC 30.6 wt% Cu	I_a = 2 A dm^{-2}, RT, pH 9	400	27.8
D	Monel-400	—	260	15 000

Note: I_p – pulse current density, I_a – average current density, f – pulse frequency

Source: Ghosh *et al.* (2006)

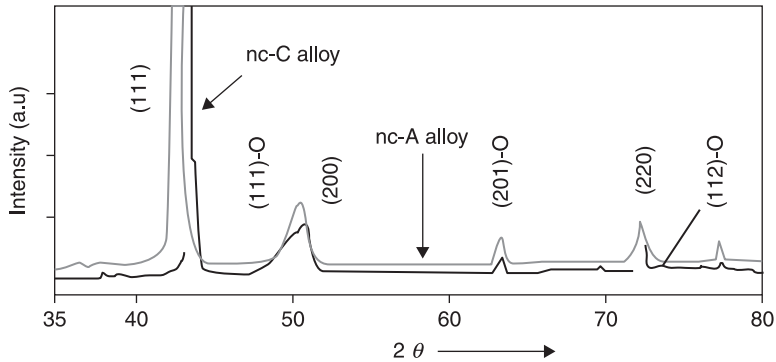

5.2 XRD pattern of pulse-plated NC-A and DC-plated NC-C alloys (Ghosh *et al.*, 2006).

content of the alloy. The observed hardness value for conventional Monel 400 (KHN_{50} = 260) was much lower than electrodeposited NC alloys. X-ray diffraction (XRD) pattern (Fig. 5.2) showed from its observed peak broadening effect that the deposited alloys were nanocrystalline in nature in both PC and DC deposition conditions (Ghosh *et al.*, 2006).

Pulse reverse current (PRC) technique enables intentional adjustment of the nanostructure (grain size, grain size distribution, microstress) which is responsible for the physical and chemical properties by introducing anodic pulses during cathodic pulsed current. The average current in the PRC technique is given by the equation:

$$I_{ave} = \frac{I_c t_c - I_a t_a}{t_a + t_c} \qquad [5.9]$$

where I_c and I_a stand for cathodic and anodic current density, t_c and t_a for cathodic and anodic time.

The PRC technique was used by Natter and Hempelmann (2003) for stabilization of nanostructured nickel crystallites by a homogeneous distribution of nickel oxide into the grain boundaries. A tartrate bath containing nickel sulfate, potassium sodium tartrate, ammonium chloride and saccharin was used with a cathodic pulse and an anodic pulse. By controlling the anodic pulse current density, the content of nickel oxide could be changed (Table 5.3). By this method, nano Ni (crystallite size 19 nm), intentionally doped with defined oxygen amounts of 956, 1805 and 6039 ppmw, was produced.

Wang *et al.* (2005) showed that a suitable electrodeposition method plays an important role in determining the microstructure, hardness and wearing behavior of composite coatings through preparation and characterization of Ni–ZrO_2 composite nanocoatings by DC, PC and PRC electrodeposition. Ni–ZrO_2 composite coatings exhibit higher hardness, less friction and better wear

Table 5.3 Process parameter used for nano nickel deposition by pulse reverse plating

$t_{on\ cathodic}$ (mS)	$I_{cathodic}$ (mA/cm^2)	$t_{on\ anodic}$ (mS)	I_{anodic} (mA/cm^2)	t_{off} (mS)	O content (ppmw)
1	1250	1	–200	48	956
1	1250	1	–500	48	1805
1	1250	1	–1000	48	6039

Source: Natter and Hempelmann (2003)

resistance than those of pure nickel coatings which were prepared under the same electrodeposition conditions. PC and PRC composite coatings exhibited lower wear weight loss than that of DC composite coatings.

5.3.2 Template-assisted deposition

Template-assisted electrodeposition is another important technique for synthesizing metallic nanomaterials with controlled shape and size. Arrays of nanostructured materials with specific arrangements can be prepared by this method (Bera *et al.*, 2004; Gurrappa and Binder, 2008). Template synthesis of nanomaterials is reported widely (Furneaux *et al.*, 1989; Martin, 1994; Hulteen and Martin, 1997; Schonenberger *et al.*, 1997; ElGiar *et al.*, 2000; Tiginyanu *et al.*, 2008; Baranov *et al.*, 2010).

Template-assisted electrodeposition processes can be broadly divided into two types: active template assisted and restrictive template based. The formation of nanostructures in active template synthesis results from the growth of nuclei that invariably nucleate at the holes and defects of the electrode substrate. The subsequent growth of these nuclei at the template yields the desired surface morphology of the nanostructures, which can therefore be synthesized by choosing an electrode with an appropriate surface. Highly oriented pyrolytic graphite (HOPG), for example, is used extensively as an electrode substrate for the electrodeposition of silver, gold, molybdenum, palladium and platinum nanostructures. Electrodeposition initiates at the step edges, dislocations and defect sites of the electrode surface. Table 5.4 presents the various active template substrates used for template-assisted electrodeposition of metallic nanostructures (Bera *et al.*, 2004).

Another method of template-assisted synthesis, mainly used for the growth of metal nanowires, involves the deposition of metal into the cylindrical pores or channels of an inert, non-conductive nanoporous electrode material. Track etch membranes, porous alumina, nanoporous conductive rubber polymers, metals, semiconductors, carbons and other solid materials have been used as templates to prepare nanometer-sized particles, fibrils, rods and tubules. The experimental set

Table 5.4 Various active template substrates used for electrodeposition of metallic nanostructures

Template substrate	Elements deposited	Size and shape of nanostructures	Reference
Highly oriented pyrolytic graphite (HOPG)	Ag	Flat island of diameter 0.29 nm	Vazquez *et al.* (1992)
		Clusters of 10 nm diameter	Potzschke *et al.* (1995)
		Disc (diameter 20–60 nm and height 1.5–5 nm)	Zoval *et al.* (1996)
	Au	Aggregate (size 500 nm and height 70 nm)	Martín *et al.* (1997)
	Mo	Nanowire of 15 nm diameter	Zach *et al.* (2000)
	Pd	Island of 200–300 nm grain size range	Gimeno *et al.* (2002)
		Two-dimensional branched island (100–160 nm)	Gimeno *et al.* (2001)
		Mesowires of grain size 50–300 nm	Favier *et al.* (2001)
	Pt	—	Zoval *et al.* (1998)
Graphite	Pd	—	Bera *et al.* (2004)
surface	Ni	Spherical particles of 20–600 nm size	Zach and Penner (2000)
Al foil with laser hole	Pd	Arrays of nanoparticles with 5 nm diameter	Bera *et al.* (2003)
Stainless-steel grain interior	Pd	Agglomerated particles (average size 70 nm)	Bera *et al.* (2004)
Carbon tape	Pd	Meso-sized particles	Bera *et al.* (2004)

Source: Bera *et al.* (2004)

up showing the electrochemical cell along with a restrictive template for electrodeposition is schematically presented in Fig. 5.3 (Bera *et al.*, 2004). Various electrode substrates used for restrictive template-based electrodeposition of metallic nanostructures are presented in Table 5.5 (Bera *et al.*, 2004).

5.3.3 Use of additives and grain refiners

Natter and Hempelmann (1996) demonstrated that the main reasons for the nanocrystal formation are over-potential phenomena (high nucleation rate) and adsorption/desorption processes of inhibiting molecules (slow grain growth). In a detailed description of the influence of organic additives like coumarin, saccharin, dimethyl aminopropyne and sodium allyl sulfonate on the microstructure of

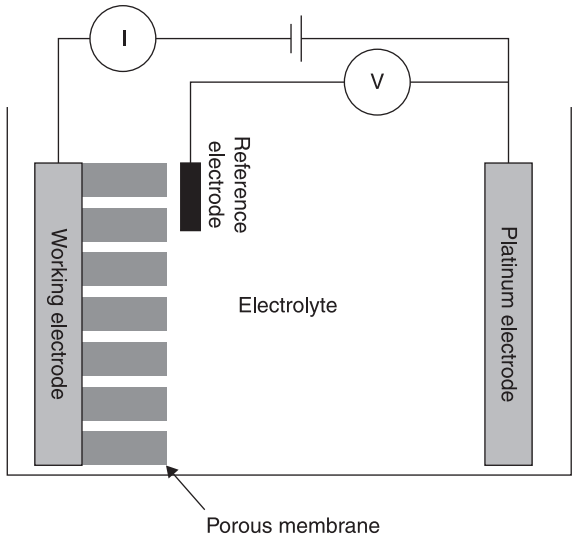

5.3 Schematic electrode arrangement for the synthesis of nanowires through restrictive template-assisted electrodeposition (Bera *et al.*, 2004).

Table 5.5 Various restrictive template substrates used for electrodeposition of metallic nanostructures

Template substrate	Deposited material	Size and shape of nanostructures	Reference
Nanoindented holes	Ni–Fe island	Diameter of 5 nm	Carrey *et al.* (2002)
Polyethylene glycol and polyvinyl pyrrolidone	Nanostructured Pd	Surface area 50 m^2g^{-1}	Tsirlina *et al.* (2002)
Semiconductor InAs quantum well	Magnetic nanowires Co nanowires	Magnetic nanowire of width 20 nm	Fasol and Runge (1997)
Mesoporous silica	Ni and Co	Dimension not reported	Aranda and García (2002)
	Pd nanowire	Nanowires with 30 nm diameter	Whitney *et al.* (1993)
	—	Diameter of 7 nm	Wang *et al.* (2003)

Source: Bera *et al.* (2004)

nickel deposits, Dennis and Fuggle (1967) discussed the inhibition of grain growth by additives. Results showing the effect of saccharin on reduction of grain size to ~ 25 and 15 nm in DC plating of nickel (Rashidi and Amadeh, 2009) and Ni–Cu alloys (Cui and Chen, 2008) are reported.

To study the effects of organic additives on the structure of gold deposited from a conventional gold(I) sulfite bath under pulse plating conditions at an average current density of 3 mA/cm^2, Natter and Hempelmann (2003) used a compound with free amino groups (butanediamine), a complex former (diammonium EDTA) and an agent with a sulfur component (saccharin). For the electrolytes free of additives, crystallite sizes in the range of 100 nm were obtained. Upon addition of a very small amount of the additive butanediamine, a strong reduction (about a factor of two) in the crystallite size was observed (Fig. 5.4). These three compounds can be classified in three groups. Butanediamine shows the best activity, whereas the minimum crystallite size that can be achieved with diammonium EDTA or saccharin is 40 and 54 nm. This behavior shows that the free electron pairs of the nitrogen atoms in butanediamine interact strongly with the gold surface and therefore the inhibiting effect is very strong. It was shown that the additives function through an adsorption process and are not occluded in the deposit.

Additives were found to be effective as grain refinement agents, grain coarsening agents and texture forming agents. A possibility to increase the cathodic overpotential is to decrease the concentration of free metal ions, which can be achieved by complex formation. For this reason a small grain size can be expected for the deposition from a bath with a strong complex former. Natter and Hempelmann (1996) focused on the effects of organic additives such as different carboxylic acids and organic amines on the nanostructure and grain size of copper deposited from an acid copper bath at average pulse current density of 1.25 A/cm^2. The

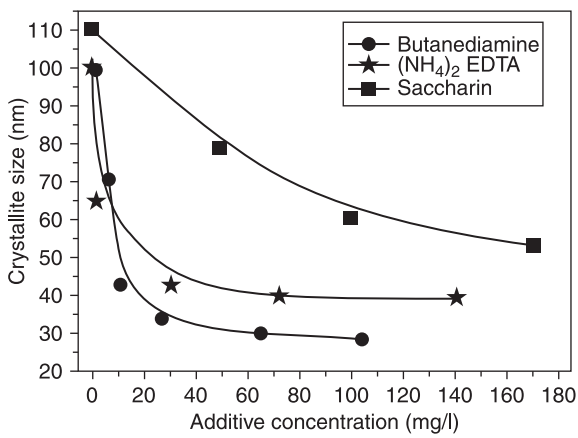

5.4 The activity of different grain refiners (butanediamine, ammonium ethylenediaminetetraacetic acid, benzosulfimide) on the nanostructure of gold deposits (Natter and Hempelmann, 2003).

interaction of citric acid and disodium EDTA with the metal surface is a reversible physisorption, whereas tartaric acid irreversibly blocks the low-energy growth sites and an oriented grain growth takes place. Malonic acid is an activator substance because it removes the water molecules from the inner Helmholtz plane and the copper ions can discharge easily. The exchange current is the main reason for the grain growth, which takes place during the off times between the pulses in such a way that larger grains grow at the expense of smaller ones, with the interface energy as the driving force. Grain growth is hardly avoidable, but it should occur only for a short off time and only at a low rate.

To limit the time of grain growth, the off time between two current pulses has to be optimized as short as possible and as long as necessary for the recovery of the bulk ion concentration in the depleted layer in the vicinity of the cathode. For NC copper deposits prepared from a citrate bath, small crystallite size (10 nm) was observed for longer off times. This is achieved because of the addition of organic inhibitor molecules, which adsorb during the off time on the freshly deposited layer and thus, if the adsorption enthalpy is sufficiently large, severely inhibit the ion exchange processes. For short off times only a small fraction of the inhibitor molecules reach the growth sites because of the slow diffusion rate of the large organic molecules. Simultaneously, these adsorbed large molecules inhibit the surface diffusion of adatoms, which represents another mechanism of grain growth. The adsorbed organic molecules also have a certain inhibiting effect on the ion deposition during the pulse, but, since the strong cathodic polarization, and thus the driving force for the electrodeposition, is very large, organic molecules adsorbed with not too large adsorption enthalpy are easily replaced. Therefore, the free enthalpy of adsorption must be large enough to disturb the ion exchange between the pulses (inhibition) but not too large to prevent desorption during the pulses (passivation).

Citric acid and disodium EDTA fulfill these requirements. Figure 5.5 shows the XRD pattern of copper deposits with increasing concentration of citric acid, which show an increasing line width and decrease in particle size from >50 to 11 nm. This is explained in terms of the inhibition of growth sites by the additive. At low concentrations, not all active sites are occupied and the growth of the copper deposit advances unlimited at active zones, resulting in larger particle sizes. For higher concentrations, the active sites are hindered by the inhibitor molecules and the copper ions are forced to occupy other areas, resulting in reduction of grain growth.

Natter and Hempelmann (2003) reported that, in alloy deposition, the best way to vary the crystallite size without a change of the alloy composition was the use of additives as grain refiners. In a Fe–Ni alloy deposition study, the variation of the crystallite size by the variation of the pulse parameter was impossible because this changed the alloy composition also. A Ni0.8Fe0.2 alloy with a crystallite size of 37 nm was obtained from a bath free of additives, but on addition of saccharin (1 g/l) the crystallite size decreased (16 nm) without a change in the alloy composition.

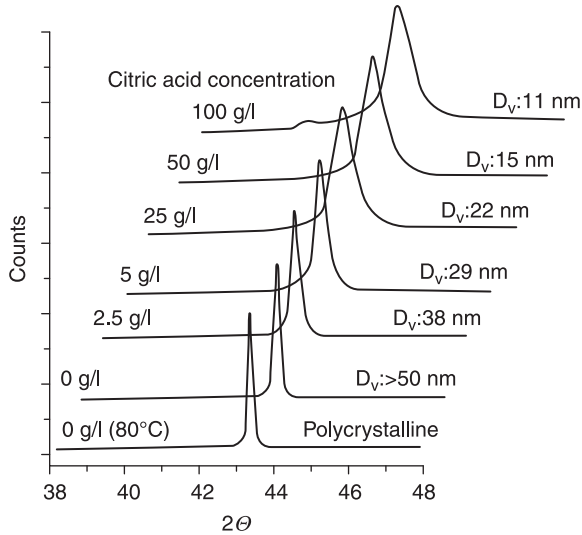

5.5 X ray diffraction patterns (111 reflection) of nanocrystalline copper deposits prepared from electrolytes with variable citric acid content (Natter and Hempelmann, 1996).

5.4 Electrodeposited nanomaterials

5.4.1 Metals such as nickel, cobalt, iron, copper, zinc and chromium

Nanocrystalline deposits of Ni (Natter *et al.*, 1998), Co (Przenioslo *et al.*, 2001a), Fe (Natter *et al.*, 2000), Cu (Natter and Hempelmann, 1996) and Cr (Przenioslo *et al.*, 2001b) with crystallite sizes between 10 and 100 nm prepared by pulse electrodeposition are reported. The grain size distribution in NC copper deposited by pulse deposition from an acid copper bath containing citric acid studied by TEM and scanning electron micrography (SEM) are shown in Fig. 5.6 and 5.7 (Natter and Hempelmann, 1996).

Electroplated nickel is a relatively soft material with hardness ~230 VHN, but coatings with NC structure exhibit higher microhardness values of 600 to 640 VHN as-plated (Hui and Richardson, 2004; Brooman, 2005). NC nickel of about 17 nm size produced by electrodeposition significantly enhances the electrocatalytic activity for hydrogen evolution due to the increased density of active surface sites (Haseeb *et al.*, 1993). Electrochemically prepared Co nanofilms exhibit three to five times greater coercivity (Hc) than polycrystalline Co (Bartlett *et al.*, 2001).

Fabrications of arrays of nickel and cobalt nanowires have been reported through electrodeposition at constant potential (Whitney *et al.*, 1993). In order to fabricate

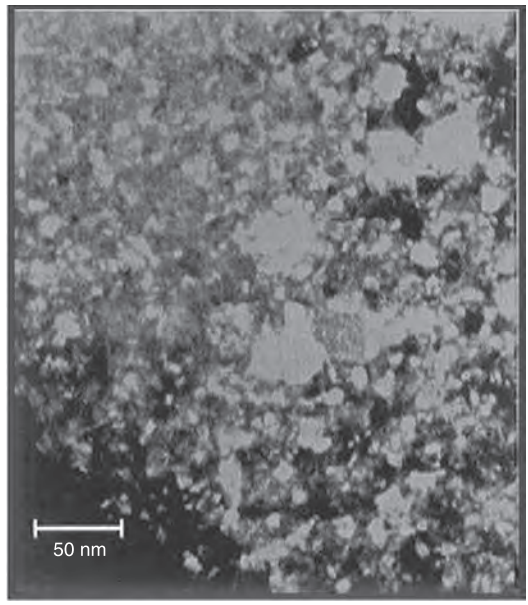

5.6 Transmission electron micrograph of NC copper; the most frequent grain size is 15 nm (Natter and Hempelmann, 1996).

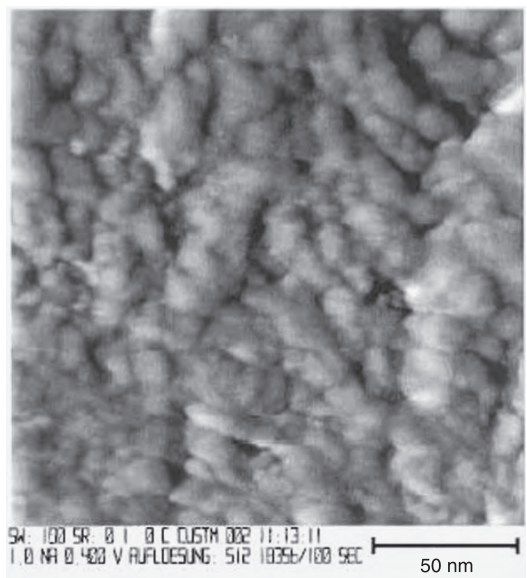

5.7 Scanning tunneling microscopy measurement of NC copper deposit (Natter and Hempelmann, 1996).

arrays of nanowires on a polycarbonate porous membrane, a copper film was first sputter-deposited to make the working electrode. The electrodeposition solution was confined to the bare side of the membrane so that deposition was initiated onto the copper film through the pores. It was observed that the electrodeposition current was directly proportional to the area of electrodeposits at any given potential under a pseudo-steady state condition. Nickel nanoparticles with a narrow size distribution have been electrodeposited on a graphite surface using the hydrogen coevolution method (Zach and Penner, 2000). The electrodeposition of metal at large over-potential invariably results in instantaneous nucleation, which is non-selective, mostly due to the formation of a large number of nuclei on defect-free terraces, as well as at defects such as step edges on the surfaces. The nuclei density is expected to be of the order of 10^9 cm^{-2}. The dependence of the number of nuclei on time was investigated by Milchev *et al.* (1974) in a wide range of voltage intervals using different glassy carbon electrodes and the data for the steady state nucleation rate interpreted on the basis of both classical and atomistic concepts of nucleation phenomena. Fe nanowires were electrodeposited into the holes of porous anodic aluminum oxide (AAO), which was prepared electrochemically (Yang *et al.*, 2000). Magnetic measurements showed that its easy magnetization direction is perpendicular to the sample plane. This type of nanowire array has potential applications in perpendicular magnetic recording.

5.4.2 Precious metals such as gold, silver and platinum group metals

The voltammetric behavior of gold nanowire arrays prepared by the electrochemical method showed a significant enhancement of the ratio between the total electrolytically exposed surface area and the surface area accessible by diffusion in comparison with macroscopic flat gold electrodes (Kunoshi *et al.*, 2000). The electrodeposition of gold on HOPG from acidic aqueous solutions was studied by Martín *et al.* (1997) using electrochemical techniques complemented with *ex situ* scanning tunneling microscopy. The kinetics of gold electrodeposition are consistent with a nucleation and 3D growth process. A model including a potential dependent energy barrier at step edges accounts for the morphology transition for gold electrodeposition on HOPG. It was shown that dendritic aggregates are produced when the gold surface is negatively charged at a potential less than the potential of zero charge. Such growth behavior results from the anisotropic corner surface diffusion caused by the varying energy barriers for the diffusion of surface atoms at step edges, as has been observed for metal deposition from vapor. Rounded kinked gold crystals are formed when the gold surface is positively charged at potential greater than the potential of zero charge. This was attributed to the leveling and lowering of barrier heights at step edges induced by chloride ion adsorption on gold aggregates.

Natter and Hempelmann (2003) investigated the deposition of NC gold samples from a proprietary gold (I) sulfite bath under pulse current conditions. The pulse current density (I_{pulse}) was optimized keeping t_{on} and t_{off} at constant value (Fig. 5.8). The smallest crystallite size of 12 nm was obtained at an I_{pulse} value of 0.5 A/cm^2 and powder formation was observed on the electrode surface at higher current densities. The effect of the t_{off} on the nanostructure of the deposits is shown in Fig. 5.9; the smallest crystallites can be found for the shortest off times, which supports the assumption of the recrystallization process of the nuclei during the off time.

Zhu *et al.* (2001) prepared silver nanorods by an electrochemical technique from an aqueous solution of $AgNO_3$ in the presence of polyethylene glycol (PEG), and found that the concentrations of $AgNO_3$ and PEG affect the formation of nanorods. Suarez *et al.* (2007) optimized a pulse reverse plating sequence of cycles consisting of several cathodic pulses and a small anodic pulse for the deposition of high conductivity nanocoatings of silver with grain size of 40–50 nm from a cyanide plating bath. Gong *et al.* (2009) showed that, by introducing ultrasonic power in a non-cyanide silver bath, (111) and (200) crystal plane orientation in the deposit significantly improved and the grain sizes decreased. The electrodeposition study of silver on the HOPG substrate (Potzschke *et al.*, 1995) using *in situ* scanning tunneling microscopy revealed that at low over-potentials the deposition process on the atomically flat terraces of HOPG was inhibited because of weak substrate deposit interaction leading to preferential silver deposition at step edges and other surface defects. Such step-edge deposition involves the preferential nucleation and subsequent growth of nanoparticles on a certain crystal surface. A potentiostatic pulse method was used (Zoval *et al.*, 1996) to electrochemically deposit silver

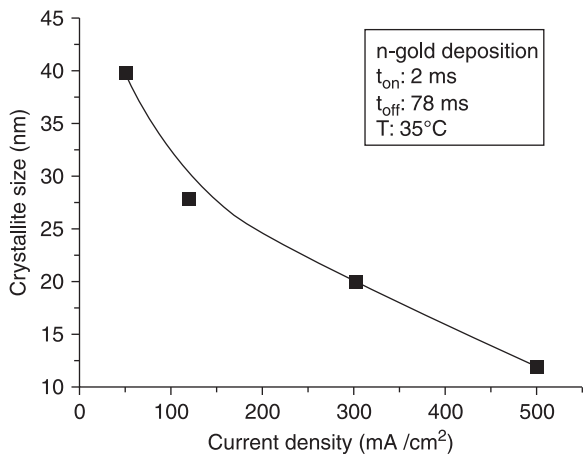

5.8 The dependence of crystallite size on the pulsed current density for gold deposited from a commercial sulfite bath (Natter and Hempelmann, 2003).

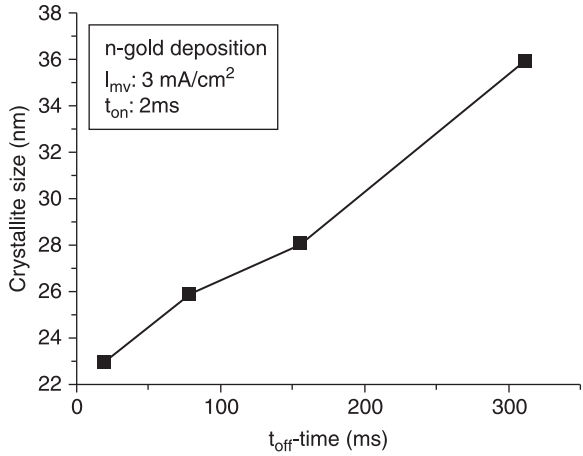

5.9 The effect of off time on the nanostructure of gold deposits (Natter and Hempelmann, 2003).

nanocrystallites on the atomically smooth graphite basal plane surface. The particles were disc shaped and well separated, with a height of 1.5–5 nm and an apparent diameter of 20–60 nm.

Electrochemically deposited nanostructured platinum metals exhibit higher catalytic performance and stability for various catalytic reactions, as well as unique magnetic properties, compared with conventional metals (Forrer *et al.*, 2000). The pulse electrodeposition method for nanostructured Pd is reported by Natter *et al.* (1996). Favier *et al.* (2001) attempted to fabricate hydrogen sensors and switches with the help of palladium nanoparticles electrodeposited onto the graphite step edges. Stable, two-dimensionally branched palladium islands, 100–160 nm in size, were electrodeposited (Gimeno *et al.*, 2001) on HOPG from an aqueous acidic palladium chloride solution with an excess of sodium perchlorate at a potential of a few millivolts above the threshold potential of the hydrogen evolution reaction. Platinum nanocrystals were deposited (Zoval *et al.*, 1998) on the basal plane of HOPG from dilute (1.0 mM) $PtCl_6^{2-}$ containing electrolytes using a pulse potentiostatic method. The deposition of platinum nanocrystals occurred via an instantaneous nucleation and diffusion limited growth mechanism which resulted in a narrow particle size distribution for mean crystallite diameters smaller than 40 Å.

Since electrodeposition occurs at the defect sites, arrays of palladium nanoparticles were synthesized by Bera *et al.* (2003) by electrodepositing them on the surface of an aluminum layer obtained from a digital video disc (DVD) that usually has a 50 μm thick aluminum layer between two polycarbonate layers. The

aluminum layer with arrays of laser holes was exposed by peeling off one polycarbonate layer, and palladium nanoparticles from a palladium chloride solution were electrodeposited on the holes. Pits in the aluminum layer were created during data recording, and palladium nanoparticles preferentially deposited into the pits, making arrays of metallic nanoparticles. Bera *et al.* (2004) reported results which strongly indicate that the surface of the active template plays an important role in shape and size distribution of metallic nanoparticles during electrodeposition.

Palladium nanoparticles deposited on a freshly cleaved graphite surface were faceted and their shape was mostly spherical. Nuclei were formed at almost all parts of the electrode surface; however, the presence of a large number of nanoparticles near the edges and boundaries indicates a preferential nucleation process. In a study on the growth of the palladium nuclei on an AISI 316 grade stainless steel electrode followed by SEM studies, it was found (Bera *et al.*, 2004) that, although nucleation occurred preferentially at the grain boundaries, extensive growth took place only for nuclei within the grain interior during electrodeposition. The probable reason for the discrepancy in deposition of palladium particles on the grain rather than on the grain boundary may be due to the presence of oxide ridges at the grain boundaries of stainless steel, where the formation of chromium oxide is easy at room temperature. The role of amorphous carbon substrate as a template for the electrodeposition of palladium showed that, although the template consists of carbon, the shape of the electrodeposited metallic particle differs from that of the cleaved graphite surface. The nuclei formed at random locations, fractal growth behavior was observed and the attachment between the deposits and carbon substrate was weak.

The synthesis of Pt metal nanowires and nanotubes electrochemically deposited through nanoporous membranes was reported by Ichikawa (2000). Palladium deposits with high specific surface areas, up to $50\,m^2\,g^{-1}$, have been synthesized by Tsirlina *et al.* (2002) from palladium chloride solutions with additions of polyethylene glycol and polyvinyl pyrrolidone. Details of the globular structure of the deposits depend on the polymer additives. A comparison with electrochemically determined true surface areas demonstrates the coalescence of nanoparticles. Wang *et al.* (2003) electrochemically synthesized thin films composed of ordered arrays of palladium nanowires using silica mesoporous channels. Mesoporous channels were deposited on a conductive glass substrate. In this method, nanowires with face-centered cubic crystal structure are continuously deposited from the conductive substrate upward until the mesoporous channels are filled.

5.4.3 Nanocrystalline alloys

To obtain hardness value comparable to hard chromium coatings, NC (15 to 20 nm grain size) electroplated Ni–Co alloys were considered, as they exhibit

microhardness values in the range of 820 to 900 VHN (Hui and Richardson, 2004; Brooman, 2005). When these were heat treated, precipitation hardening occurred and microhardness values as high as 1000 to 1150 VHN were obtained. Electrodeposition of NC cobalt alloy coatings (Prado *et al.*, 2009), as an environmental alternative to hard chrome deposits under the strategic environmental research and development program for the US Defense Department, reveals that nano CoP exhibits properties equivalent to (and in many ways better than) hard chromium-like high hardness, enhanced ductility, lower wear rates, superior corrosion resistance and no issues with hydrogen embrittlement after baking. The nano CoP process differs, however, in that it uses pulse plating technology for controlling and building fully dense, nano grain size (5 to 15 nm) deposits leading to improved material properties. As a result of Hall–Petch strengthening, NC alloys such as nano CoP display significant increases in hardness and strength. The nCoP exhibits hardness in the range of 530–600 VHN as deposited. A further increase in hardness can be obtained by annealing the deposited material through a precipitation hardening mechanism, to induce the precipitation of Co phosphides from supersaturated solid solution at elevated temperatures.

Fasol and Runge (1997) deposited magnetic permalloy (Ni–Fe) nanowires on the edge of an InAs quantum well. Carrey *et al.* (2002) used a nanoindented Al_2O_3/Al foil to preferentially electrodeposit Ni–Fe nanoparticulate arrays from an electrodeposition bath containing a solution of nickel and iron sulfate. Ni–Cu alloys had earlier been used mainly for decorative purposes; in recent times there has been a renewed interest in the electrodeposition of NC Ni–Cu alloys (Quang *et al.*, 1985; Chassaing *et al.*, 1987; Cherkaoui *et al.*, 1988; Ying, 1988; Roy *et al.*, 1994). This alloy is a component in multilayers of Cu Ni/ Cu which show giant magnetoresistance (GMR) properties and find application in magnetoresistive devices (Kazeminezhad *et al.*, 2004).

Pulse electrodeposition of nano Cu–Ni alloys was reported by Natter *et al.* (1998). NC Ni–Cu alloys having average grain size in the range 2–30 nm have been synthesized under pulse as well as DC plating conditions (Ghosh *et al.*, 2006). High-resolution electron microscopic (HREM) examination revealed that deposited NC alloys were dense in nature.

The deposition of Fe–Ni alloys is of industrial interest because these materials find applications in electronic devices (e.g. PC hard disk). The most popular alloys are Permalloy (soft magnetic properties) and Invar (very low thermal expansion). The magnetic and mechanical properties of Fe–Ni alloy can be designed by nanostructuring. Natter and Hempelmann (2003) used an electrolyte containing 40 g/l $NiSO_4$, 20 g/l $(NH_4)Cl$, 20 g/l Na citrate, 5 g/l citric acid, 1 g/l saccharin, 45 g/l boric acid and a variable content of iron (II) ammonium sulfate. The pulse parameters used were t_{on} 2 ms, t_{off} 48 ms and I_{pulse} 250 mA/cm^2. For different concentrations of iron salts, alloys (crystallite size, 16–19 nm) with iron content between 0 and 71 mol% could be obtained.

5.4.4 Nanocomposites

Electrodeposition of nanocomposite coatings refers to electrolysis in which nanosized particles are suspended in electrolyte and are embedded in the electrodeposited solid phase, imparting special properties depending on the degree and type of nanoparticle incorporation in the deposit. The insoluble powders added to the composite electrodeposition solution can be oxides, carbides or nitrides, such as SiO_2, Al_2O_3, ZrO_2, TiO_2, SiC, WC and Si_3N_4, or diamond, and can also be solid lubricant materials such as PTFE, graphite or MoS_2. The excellent performance of electrodeposited composite coatings, especially in mechanical and chemical processes, accounts for the widespread use of this technique (Ferkel *et al.*, 1997; Benea *et al.*, 2001).

Ni–SiC nanocomposite coating, which is simultaneously composed of both NC Ni matrix and dispersed inert SiC nanoparticles, has been fabricated by the ultrasonic electroplating technique in a modified Watts bath containing SiC nanoparticles by Cai *et al.* (2010). The influence of mechanical stirring and ultrasonication on the surface morphology, microstructure, anticorrosion property and electrocatalytic activity for hydrogen evolution of the obtained NC Ni–SiC nanocomposite film showed that mechanical stirring prevents the sedimentation of the inert particles suspended in solutions, while ultrasonication prevents the particles' agglomeration. In the case of only mechanical stirring to disperse the SiC nanoparticles, the composite surface was cauliflower-like, while in the case of both mechanical stirring and ultrasonication the obtained Ni–SiC composite film was much smoother and composed of particles with a mean diameter of 42.9 nm, and the SiC particles were uniformly dispersed into the Ni matrix.

Parida *et al.* (2010) reported on the use of stirring and ultrasonic agitations to resist agglomeration of ultrafine particles in a plating bath for the preparation of a homogeneous coating of nanoscale TiO_2 (~30 nm) dispersed nickel on steel substrate by DC deposition from Watts nickel solution. TiO_2 nanoparticle reinforced Ni composite coatings obtained by electrodeposition exhibit unusual photoelectrochemical characteristics, which can be used to study electronic transitions in semiconductors (Li *et al.*, 2002).

Gul *et al.* (2008) discussed the electrodeposition, increased surface hardness and wear resistance of electrodeposited Ni–Al_2O_3 and Ni–SiC nanoparticle reinforced metal matrix composite (MMC) coatings. Electrochemically layered copper nickel nanocomposites exhibit considerable enhancement in hardness in comparison with pure Ni (Simunovich *et al.*, 1994). The addition of nanometer-sized aluminum oxide particles to a Watts nickel electrolyte produced a Ni matrix composite with significantly improved hardness, according to Li *et al.* (2005). The hardness was dependent on the type of titanium dioxide added; in general, anatase nanoparticles (~12 nm diameter) gave better results than rutile microparticles (~1000 nm). Erler *et al.* (2003) produced a series of nickel nanoceramic composites, with codeposition of particles of Al_2O_3 and TiO_2 in the

nanometer range (10–30 nm) and with successful incorporation of particles up to 2 vol%. Codeposition of these ceramic nanoscaled particles during the electroplating process brings improvement in technical properties.

Preparation of nano Ni–TiN coatings by ultrasonic electrodeposition on the surface of mild steel was investigated by SEM, atomic force microscopy (AFM), high-resolution transmission electron microscopy (HRTEM) and XRD by Xia *et al.* (2010). The AFM results indicate that moderate ultrasonication led to homogeneous dispersion of TiN particles in the coatings. HRTEM and XRD results demonstrate that the average diameter of Ni grains and TiN particles were approximately 60 nm and 40 nm, respectively. The Ni–TiN nanocoatings greatly improved the microhardness of the surface.

Novel Ni-based nanostructured coatings with high temperature oxidation resistance were fabricated (Peng *et al.*, 2004) by composite electrocodeposition. The electrodeposited nanocoatings were prepared from a nickel sulfate electrolyte bath with the addition of Cr nanoparticles of average size 39 nm, or Al nanoparticles of size ~ 75 nm. The Cr or Al nanoparticles were dispersed among the NC Ni grains. The nanocomposites Ni10.9Cr at 900°C and Ni28.0Al at 1050°C exhibited superior oxidation resistance as a result of the formation of a continuous chromia or alumina scale respectively. It was proposed that the dispersion of Cr or Al nanoparticles among the NC Ni grains greatly increased the surface density of the nucleation sites for Cr_2O_3 or Al_2O_3; simultaneously, the nanostructured coatings favored rapid healing of the narrowed Cr_2O_3 or Al_2O_3 nuclei during a very short transient period, which consequently led to the suppression of NiO growth.

Nanostructures form protective oxidation scales with superior adhesion to the substrate (Gao *et al.*, 2004). The high density of grain boundaries provides fast diffusion paths, promoting selective oxidation of protective oxide scales. The fine-grained coatings and/or the fine-grained oxide scales show a fast creep rate at high temperatures, which can release the stresses accumulated in the scales, thereby reducing the scale spallation tendency. The oxides formed on NC coatings are micro-pegged onto the grain boundaries to form a complex interface that results in better scale adhesion to the metal substrate. A Ni–Cr nanocomposite with an average Cr concentration of 11 wt% was deposited onto nickel plate by simultaneous electrodeposition of Ni and Cr nanoparticles from a nickel sulfate bath (Zhang *et al.*, 2005). The nanocomposite consisted of a NC Ni matrix and dispersed Cr nanoparticles with a mean size of 33 nm. Friction and wear performance of codeposited Ni–Cr composite coatings were comparatively evaluated by sliding against Si_3N_4 ceramic balls under non-lubricated conditions by Zhao *et al.* (2009). It was found that the incorporation of Cr particles enhances the microhardness and wear resistance of Ni coatings. The wear resistance of a Ni composite coating containing Cr nanoparticles was higher than that of the Ni composite coating containing Cr microparticles.

Copper composite coatings have been investigated for their potential engineering applications resulting from the outstanding properties of wear

resistance, anticorrosion and self-lubrication achieved through incorporation of various inert particles such as SiC, SiO_2, graphite, Al_2O_3, MoS_2, TiO_2, PTFE, etc. (Buelens *et al.*, 1983; Stojak and Talbot, 2001). Morales and Podlaha (2004) studied the effect of Al_2O_3 nanopowder on copper electrodeposition. Ultrasonication during electrocodeposition efficiently reduced the agglomeration of nanoparticles and reduced the grain size of the Cu matrix (Kim *et al.*, 2010). Smaller nanoparticles were more efficiently de-agglomerated by ultrasonication, which resulted in more enhanced mechanical properties in the 50 nm Al_2O_3 nanoparticle enhanced specimens.

Yang *et al.* (2008) reported the preparation of single-walled carbon nanotube reinforced copper composite coatings by the electrochemical deposition method, and Guo *et al.* (2006) reported the pulse plating of copper–ZrB_2 composite coatings. Celis *et al.* (1977 and 1987) and Fransaer *et al.* (1992) reported the kinetics and mechanism of copper–Al_2O_3 nanocomposite deposition. Deposition conditions and properties of Cu–TiO_2 nanocomposites prepared by the electrodeposition method onto copper substrate using an acid copper plating bath containing dispersed nanosized TiO_2 were discussed by Ramalingam *et al.* (2009). The microhardness and wear resistance of the Cu–TiO_2 nanocomposite coatings were higher than for electrodeposited copper.

The impact of carbon nanomaterials on the formation and properties of electrodeposited copper composite coatings was investigated by Medeliene *et al.* (2010) and a relation found between the crystalline parameters of the existing forms of carbon nanomaterials (CNMs) and structural morphology and crystallography of the electrodeposited copper composite coatings, as well as their functional performance (hardness, roughness, resistivity). Surface roughness measurements showed a smoother profile while hardness increased and electrical resistivity was close to that of copper.

Kim *et al.* (2010) examined the effects of ultrasonication during electrodeposition on the mechanical properties of nanocomposite copper films containing inert Al_2O_3 nanoparticles (50 nm and 300 nm in diameter). Ultrasonication efficiently reduced the agglomeration of nanoparticles and reduced the grain size of the Cu matrix. Smaller nanoparticles were more efficiently de-agglomerated by ultrasonication, which resulted in more enhanced mechanical properties in the 50 nm Al_2O_3 nanoparticle enhanced specimens. Reducing the grain size by ultrasonication seems to be an important parameter in enhancing the overall mechanical properties of nanocomposites, including hardness, elastic modulus, yield stress, ultimate tensile stress and elongation.

Inframat Corporation (2003a) had demonstrated that WC/Co-Ni nanocoating could be obtained via electrocodeposition of WC/Co nanoparticles from a nickel sulfamate colloidal solution. Properties of this WC/Co–Ni nanocoating were compared with conventional electroplated hard chromium and thermal sprayed WC/Co. Benefits derived from this nanocoating include high hardness and wear resistance, low coefficient of friction, and a smooth deposited surface. A US

Army program on innovative coating technologies investigated WC nanoparticle strengthened Ta nanocoating (Inframat Corporation, 2003b) prepared via an environmentally benign electrocodeposition process for gun barrel surface applications to replace highly toxic electroplated hard chrome.

The composite coatings containing Zn and nanoparticles like carbon nanotubes, nanosized carbon paste, nanoparticles of TiO_2, silica, SiC, ceramic powders, Fe_2O_3, etc, are gaining importance due to their corrosion resistance properties (Muller *et al.*, 2003). Praveen and Venkatesha (2009) electrodeposited composite film of zinc and carbon black on mild steel using zinc electrolyte containing dispersed nanosized carbon black and the coating was non-porous with higher hardness and corrosion resistance.

5.4.5 Multilayers

Alternating layers of two different materials with different laminate thickness in the range of nanometers can be fabricated by electrochemical deposition. This technique demonstrates the capability of the relatively inexpensive process of electrodeposition for the production of advanced materials with ultrafine microstructure (Schwarzacher *et al.*, 1997). Electrodeposition of multilayers can be carried out using either a single or dual bath approach. In dual bath electrodeposition the substrate is transferred to suitable electrolytes during the deposition of each layer. A single bath is a more desirable process and compositional modulation of the layers can be achieved by pulsing the current or potential.

One of the first examples of compositionally modulated multilayer (CMM) materials synthesized by deposition of alternate layers having different compositions in a sandwich-like fashion was demonstrated by Blum (1921), when alternate Cu and Ni layers, tens of microns thick, were deposited from two different electrolytes (Podlaha *et al.*, 2006). The resulting Cu/Ni multilayer improved the tensile strength of the electrodeposit compared with elemental copper deposits. Today, CMM materials of interest include materials with not only improved mechanical properties like hardness, fracture and tensile strength (Foecke and Lashmore, 1992), but also magnetic properties (Schwarzacher and Lashmore, 1996: Kazeminezhad and Schwarzacher, 2004).

Magnetic metallic multilayers such as Fe/Cr and Co/Cu separated by non-magnetic spacer layers of a few nm thick result in a significant reduction of the electrical resistance of the multilayers under an applied magnetic field, a phenomenon known as GMR. Cobalt–copper multilayer has been thoroughly studied by Shima *et al.* (2002) and Yamada *et al.* (2002). The current in plane (CIP) magnetoresistance was measured for electrodeposited Co/Cu multilayer film with 1000 repeat bilayers, deposited from an electrolyte containing 0.005 M $CuSO_4$ and 0.5 M $CoSO_4$ by keeping the current flow parallel to the multilayers during the MR measurement. The magnetic field in this case will be perpendicular to the current flow (i.e. transverse). The decrease in resistance is

dependent on a variety of factors like the choice of electrolytes, bilayer number and layer thickness.

Multilayered Co/Cu wires produced by electrodeposition (Doyle *et al.*, 1992) with layer thickness in the range of 3 to 100 nm exhibited a GMR effect similar to that reported for sputtered multilayers. Electrodeposited Co–Ni–Cu/Cu superlattices showed (Blondel *et al.*, 1995) a previously unreported transition from GMR to anisotropic magnetoresistance (AMR) and back to GMR upon annealing. TEM investigations on Co–Ni–Cu/Cu superlattice nanowires revealed extensive twinning, while magneto transport measurements confirmed that these superlattice nanowires exhibit current perpendicular to plane (CPP) GMR. They have shown the possibility of measuring the CPP GMR as a function of temperature for samples with resistance values reaching hundreds of ohms by fabricating multilayered nanowires by electrodeposition. Blondel *et al.* (1997) deposited a wide range of artificially structured coatings such as epitaxial multilayered materials (Cu/Ni) and amorphous materials in combination with crystalline materials (NiPx/Sn) by suitably controlling the electrochemical deposition conditions.

5.4.6 Biocompatible coatings

The range of applications of nanotechnology in medicine and biomedical engineering is vast and spans areas such as implant and tissue engineering, and diagnosis and therapy. The incorporation of functionalized and modified nanostructures in various biomedical applications and recent research approaches and developments in nanobiotechnology with special emphasis on load-bearing implants and novel tissue engineered scaffolds have been reviewed by Saji *et al.* (2010).

The electrochemical method provides an important contribution to the development of nanostructured compounds and is a novel approach to the synthesis of biomedical coatings and composites. Ti alloys have been used extensively in orthopedic and dental implants (Noort, 1987) as these materials possess a number of excellent properties such as low specific weight, high corrosion resistance and biocompatibility. Coatings of Ti alloys with materials such as bioceramics and polymers have been utilized to improve biocompatibility and corrosion resistance. TiO_2 coatings on Ti alloys have been demonstrated to show promising *in vivo* corrosion behavior, acting as a chemical barrier against release of metal ions from the implant (Kurzweg *et al.*, 1998). Among the various techniques for deposition of TiO_2 films on Ti6Al4V, such as the sol-gel method, ion beam enhanced deposition, pulse laser deposition, etc, electrodeposition offers a number of advantages such as low cost of equipment, rigid control of film thickness and deposition on complicated shapes (Kern *et al.*, 2006).

While electrodepositing titania for use in biomedical implants, varying the bath compositions and deposition parameters allows control over the morphology and

porosity of the films. Karpagavalli *et al.* (2007) studied the biocompatibility and corrosion behavior of nanostructured TiO_2 film deposited on Ti6Al4V from $TiCl_4$, H_2O_2 in methanol–water by DC deposition. SEM micrographs exhibited the formation of amorphous and crystallite TiO_2 nanoparticles with mean particle size of TiO_2 in the nanometer level (~30–50 nm) on Ti6Al4V before and after being annealed at 500°C (Fig. 5.10). Rat bone cells and human aortic smooth muscle cells were grown on these substrates to study their cellular responses *in vitro*. The

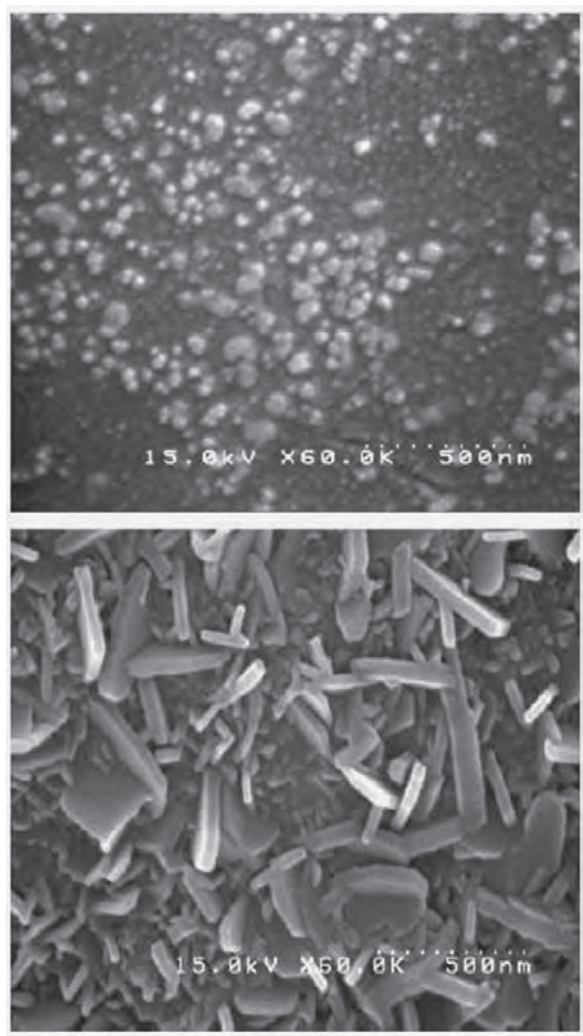

5.10 SEM micrographs of nanostructured TiO_2 deposited on Ti6Al4V (a) as deposited, (b) annealed at 500°C (Karpagavalli *et al.*, 2007).

SEM images revealed enhanced cell adhesion, cell spreading, and proliferation on nano TiO_2 coated Ti6Al4V compared with those grown on uncoated substrates for both cell lines.

Hydroxyapatite (HA) has been widely used as a biocompatible material in many areas of medicine, mainly for contact with bone tissue, because its chemical composition is similar to that of bone tissue. For biomedical applications thin films of HA were prepared over implant materials using electrophoretic deposition (Zhitomirsky and GalOr, 1997; Zhitomirsky, 2000) or electrolytic deposition (Shirkhanzadeh, 1998). Nanosized HA is currently under investigation for several applications, which are either in advanced research states or undergoing development with considerable commercial opportunities (Ferraz *et al.*, 2004) and electrodeposition is a potential method for preparation of nanostructured coatings of HA on Ti6Al4V surgical alloy substrates.

5.5 Corrosion resistance of electrodeposited nanomaterials

Saji and Thomas (2007) discussed the superior corrosion resistance behavior of NC metals studied in different environments. Masdek and Alfantazi (2010) made a survey of existing literature on corrosion behavior of electrodeposited nanostructured pure metals and their alloys as well as composites. They concluded that earlier assumptions that nanoprocessing would have a detrimental effect on the corrosion performance of materials, due to the increase in intercrystalline defects such as grain boundaries and triple junctions, have been proven wrong by the results of investigations into the corrosion resistance of nanomaterials in various corrosive environments. Some of the corrosion resistance investigations on nanostructured metals, alloys, composites and biomaterials are discussed below.

Enhanced corrosion resistance of steel coated with NC Ni over microcrystalline Ni is reported. Rofagha *et al.* (1991) investigated the corrosion behavior of NC nickel (32 nm grain size) in 2N H_2SO_4 in de-aerated media and found that the corrosion potential of NC nickel was shifted about 200 mV further to the positive than that of polycrystalline nickel. The study also showed that NC processing of nickel catalyzes hydrogen reduction processes, reduces kinetics of passivation and compromises passive film stability. Mishra and Balasubramaniam (2004) compared the corrosion behavior of NC nickel of different grain sizes (8–28 nm) in 1 mol H_2SO_4 electrolyte with that of bulk nickel. The zero current potential, passive current density and breakdown potential were found to increase with decrease in grain size. An increase in passive current density indicates the defective nature of passive film formed on NC nickel. The tendency for localized corrosion was lower in the case of NC nickel, as indicated by an increased breakdown potential. The corrosion rate of freshly exposed NC nickel was found to be lower compared with bulk nickel, indicating a higher hindrance to anodic

dissolution from the NC nickel surfaces. XRD analysis indicated that the NC nickel deposits were compressively strained, with microstrain increasing with decreasing grain size.

Youssef *et al.* (2004) compared corrosion behavior of NC zinc produced by pulse current electrodeposition with electrogalvanized steel in 0.5 N NaOH electrolyte. The estimated corrosion rate of NC zinc (90 μA/cm^2) was found to be about 60% lower than that of electrogalvanized steel; the passive film formed on the NC zinc surface seems to be the dominating factor for this. The NC structure enhances both kinetics of passivation and stability of the passive film formed. Anodic and cathodic Tafel slopes of NC zinc (~40 and 107 mV/decade) are found to be lower than those of electrogalvanized steel (~59 and 128 mV/decade), indicating higher activation energy for dissolution for NC zinc.

The corrosion behavior of NC alloys has been assessed by several techniques in various environments. Corrosion behaviors of two types of NC Cu–Ni alloys (details on alloys in Table 5.2) were compared with cast Monel-400 alloy in 3% NaCl solution and it was found that corrosion current density (i_{corr}) of NC alloys was superior to Monel-400 (Fig. 5.11 and Table 5.6). Both optical and SEM examination of the corroded surface revealed a well-defined pitting type of attack for Monel-400, unlike the homogeneous corrosion of NC alloys. Thorpe *et al.* (1988) reported an enhanced corrosion resistance of NC Fe32Ni36Cr14P12B6 compared with that of its amorphous counterpart. The authors attributed this improved corrosion resistance to the observed greater Cr enrichment of the

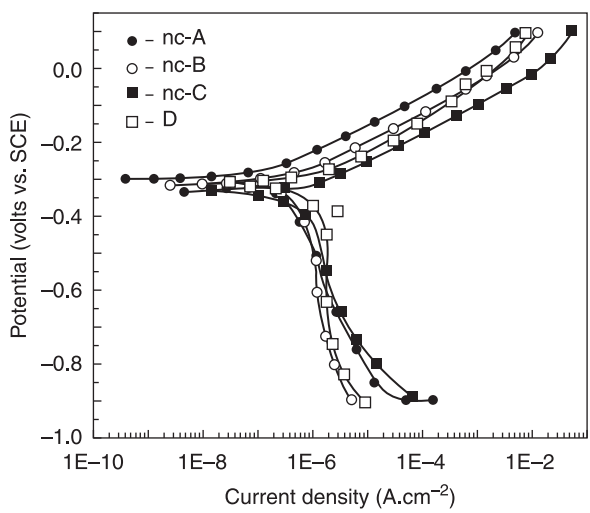

5.11 Potentiodynamic polarization plot of nanocrystalline and conventional Ni–Cu alloys in 3% NaCl solution (Ghosh *et al.*, 2006).

Table 5.6 Corrosion data for three different Ni–Cu alloys from 3% NaCl solutions

Sample	I_{corr} (μA cm^{-2})	E_{corr} observed (V vs SCE)	β_a (V/dec)	B_c (V/dec)	R_P (Ohm cm^2)
De-aerated					
NC- A	1.13×10^{-1}	–0.294	0.080	–0.180	3.75×10^4
NC- B	2.51×10^{-1}	–0.305	0.083	–0.219	2.52×10^4
NC- C	3.12×10^{-1}	–0.322	0.074	–0.194	2.13×10^4
D	8.07×10^{-1}	–0.314	0.085	–0.322	1.37×10^4
Aerated					
NC- A	1.267	–0.225	0.210	–0.154	3.62×10^3
D	2.237	–0.218	0.600	–0.126	3.1×10^3

Source: Ghosh *et al.* (2006)

electrochemical surface film via rapid interphase boundary diffusion. Bragagnolo *et al.* (1989) reported improved corrosion resistance with NC Fe72Si10B15Cr3 metallic glass wires. Zeiger *et al.* (1995) reported enhanced corrosion resistance of NC Fe 8 wt% Al in Na_2SO_4 solution. Alves *et al.* (2003) observed that NC (Ni70Mo30)90B10 alloys are less sensitive to corrosion in alkaline solutions than the coarse-grained material.

Benea *et al.* (2002) reported that the incorporation of 20 nm SiC particles during Ni deposition improves the corrosion resistance, as revealed from impedance and cathodic polarization measurements, due to the modification of the surface morphology and crystallinity of the nickel matrix. The results obtained by polarization and EIS methods showed that, when compared with the traditional polycrystalline Ni film, Ni–SiC nanocomposite film (Cai *et al.*, 2010) exhibits enhanced corrosion resistance in NaCl solutions. In corrosion tests, Ni–TiN nanocoatings showed better corrosion resistance than Ni coatings, since the presence of TiN particles diminished the interspaces and improved the compactness of the coatings (Xia *et al.*, 2010). Benea *et al.* (2000) reported, using the impedance spectroscopy method, on the improved corrosion behavior of copper and copper matrix composite coatings, with ZrO_2 particles embedded by electrodeposition from an acid copper sulfate plating bath. Ramalingam *et al.* (2009) reported that the corrosion resistance of Cu–TiO_2 nanocomposite coatings was higher than that of electrodeposited copper. Corrosion rates from immersion studies, and anodic polarization curves for pure zinc coating and composite coating samples, in 3.5% NaCl solution in Fig. 5.12 and 5.13 respectively (Praveen and Venkatesha, 2009) show the improved corrosion resistance of Zn nanosized carbon black composites compared with Zn.

Nanocrystalline alloy coatings, oxide dispersive alloy coatings and metal oxide composite coatings show superior high temperature corrosion resistance. A Ni–Cr nanocomposite with an average Cr concentration of 11 wt% deposited onto nickel

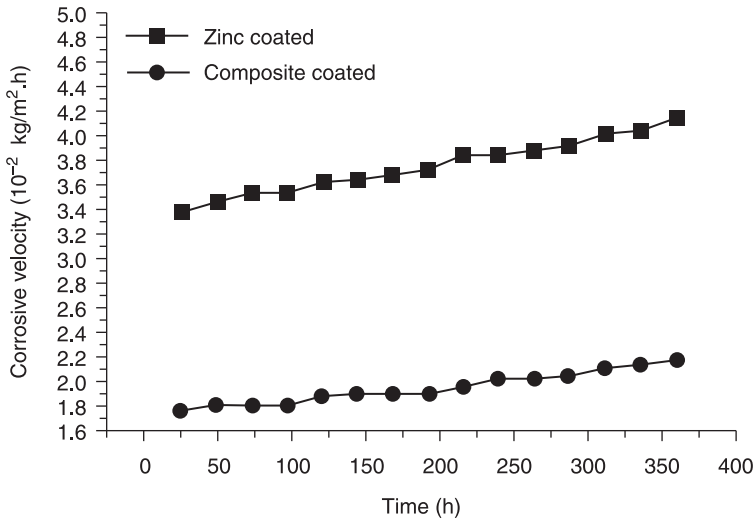

5.12 Corrosion rate with immersion time for pure zinc coating and composite coating samples in 3.5% NaCl solution (Praveen and Venkatesha, 2009).

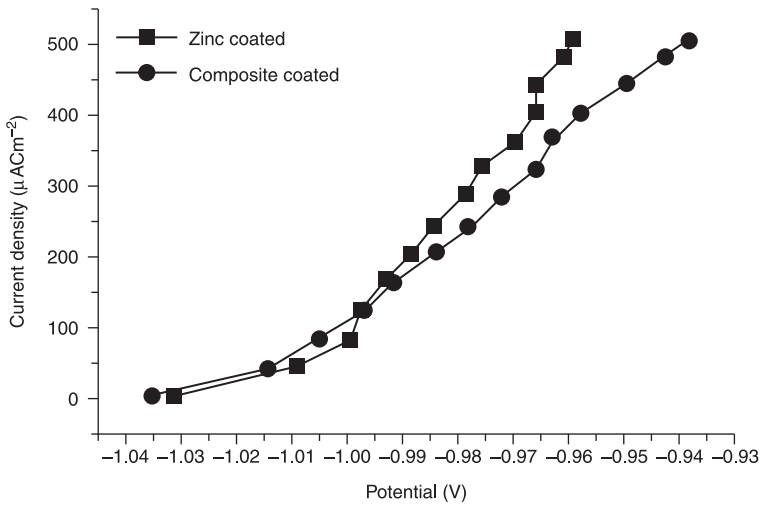

5.13 Anodic polarization curves for pure zinc coating and composite coating samples in 3.5% NaCl solution (Praveen and Venkatesha, 2009).

plate by electrodeposition of Ni and Cr nanoparticles from a nickel sulfate bath (Zhang *et al.*, 2005) showed superior hot corrosion resistance under molten Na_2SO_4–K_2SO_4–NaCl in air at 700°C. The results demonstrate that it was not primarily the Cr content but the unique structure of the nanocomposite that was responsible for its superior hot corrosion resistance. The protection mechanism lies in the fast formation of a continuous chromia scale on the nanocomposite, due to the easy nucleation of chromia on both chromium nanoparticles and abundant nickel grain boundaries, and then fast linking of the nuclei as a result of enhanced diffusion of Cr through those grain boundaries.

Corrosion behavior of uncoated and TiO_2 deposited Ti6Al4V was evaluated by Karpagavalli *et al.* (2007) in freely aerated Hank's solution at 37°C by the measurement and analysis of open circuit potential variation with time, Tafel plots and electrochemical impedance spectroscopy. The electrochemical results indicated that nano TiO_2 coated Ti6Al4V showed a better corrosion resistance (Table 5.7, Fig. 5.14) in simulated biofluid than uncoated Ti6Al4V.

Table 5.7 E_{corr} and I_{corr} and corrosion rate determined from the Tafel plots of uncoated Ti6Al4V and TiO_2 deposited Ti6Al4V in Hank's solution at 37°C

Sample	E_{corr} (mV)	I_{corr} (μA)	Corrosion rate (mpy)
Ti6Al4V	–285	0.08	0.05
TiO_2 deposited Ti6Al4V	–191	0.03	0.02

Source: Karpagavalli *et al.* (2007)

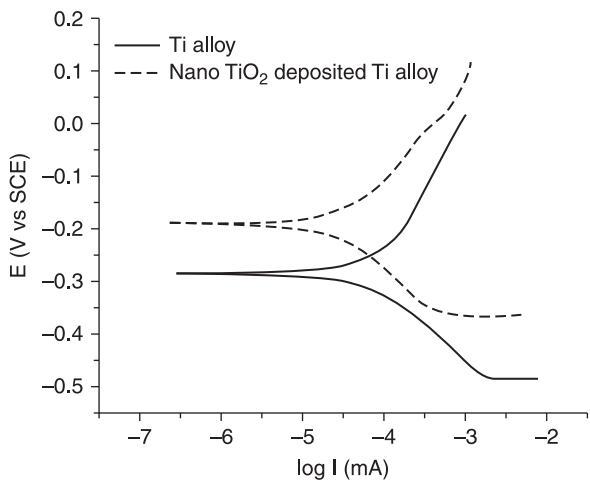

5.14 Tafel plots of TiO_2 deposited Ti6Al4V and uncoated Ti6Al4V in Hank's solution at 37°C (Karpagavalli *et al.*, 2007)

5.6 Conclusions

Electrodeposition is a versatile technique for the production of nanostructured materials with lower capital investment, higher production rates and few shape and size limitations. Electrodeposited nanomaterials such as nanostructured metals, alloys and metal matrix composites have proven successful in providing superior corrosion resistance of substrate materials compared with the corresponding microstructured materials.

5.7 Acknowledgments

Permission from the Director, CSIR Central Electrochemical Research Institute, Karaikudi, to contribute this chapter is gratefully acknowledged.

5.8 References

Aliofkhazraei V. M. (2011), *Nanocoatings: size effect in nanostructured films*. Berlin: Springer-Verlag, ISBN: 3642179657.

Alves H., Ferreira M. G. S. and Koste U. (2003), 'Corrosion behavior of nanocrystalline (Ni70Mo30)90B10 alloys in 0.8 M KOH solution', *Corros. Sci.*, **45**, 1833–45, doi:10.1016/S0010–938X(02)00243–3.

Antropov L. I. (1977), *Theoretical electrochemistry*. Moscow: Mir Publications.

Aranda P. and García J. M. (2002), 'Porous membranes for the preparation of magnetic nanostructures', *J. Magn. and Magn. Mater.*, **249**, 214–19, doi: 10.1002/chin.200319212.

Ashby M. F., Ferreira P. J. and Schodek D. L., (2009), *Nanomaterials, nanotechnologies and design: an introduction for engineers and architects.* Oxford: Butterworth-Heinemann, ISBN 9780750681490.

Bakonyi I., Toth-Kadar E., Tarnoczi T., Varga L. K., Cziraki A. *et al.* (1993), 'Structure and properties of fine grained electrodeposited nickel', *Nanostruct. Mater.*, **3**, 155–61, doi: 10.1016/0965–9773(93)90073-K.

Baranov S. A., Globa P. G., Yushchenko S. P. and Dikusar A. I. (2010), 'On the electrodeposition for manufacturing of meso and nano materials by the template synthesis method at a variable diameter of the template pores', *Surface Engineering and Applied Electrochem*, **46**(2), 87–90, doi: 10.3103/S1068375510020018.

Bartlett P. N., Birkin P. N., Ghanem M. A., Groot P. and Sawicki M. (2001), 'The electrochemical deposition of nanostructured cobalt films from lyotropic liquid crystalline media', *J. Electrochem. Soc.*, **148**, C119–23, http://dx.doi.org/10.1149/1.1342178.

Benea L., Mitoseriu O., Galland J., Wenger F. and Ponthiaux P. (2000), 'Corrosion study of copper composite coating by impedance spectroscopy method', *Mater. Corros.*, **51**, 491, doi: 10.1002/1521–4176(200007)51:7<491.

Benea L., Bonora P. L., Borello A., Martelli S., Wenger F. *et al.* (2001), 'Composite electrodeposition to obtain nanostructured coatings', *J. Electrochem. Soc.*, **148**, C461–5, http://dx.doi.org/10.1149/1.1377279.

Benea L., Bonora P. L., Borello A., Martelli S., Wenger F. *et al.* (2002), 'Preparation and investigation of nanostructured SiC–nickel layers by electrodeposition', *J. Solid State Ionics*, **151**, 89–95, doi:10.1016/S0167–2738(02)00586–6.

Bera D., Kuiry S. C., Patil S. and Seal S. (2003), 'Palladium nanoparticle arrays using template-assisted electrodeposition', *Applied Physics Letters*, **82**(18), 3089–91, doi:10.1063/1.1572465.

Bera D., Kuiry S. C. and Seal S. (2004), 'Synthesis of nanostructured materials using template-assisted electrodeposition', *Journal of the Minerals, Metals and Materials Society*, **56**(1), 49–53, doi: 10.1007/s11837–004–0273–5.

Bicelli L. P., Bozzini B., Mele C. and D'Urzo L. (2008), 'A review of nanostructural aspects of metal electrodeposition', *Int. J. Electrochem. Sci.*, **3**, 356–408.

Blondel A., Meler J., Doudin B., Ansermet J. P., Attenborough K. *et al.* (1995), 'Wire-shaped magnetic mutilayers for current perpendicular to plane magnetoresistance measurements', *J. Magn. and Magn. Mater.*, **148**, 317–18, doi:10.1016/0304–8853(95)00252–9.

Blondel A., Doudin B. and Ansermet J. P. (1997), 'Comparative study of the magnetoresistance of electrodeposited Co/Cu multilayered nanowires made by single and dual bath techniques', *J. Magn. and Magn. Mater.*, **165**, 34, doi:10.1016/S0304–8853(96)00467–2.

Blum W. (1921), 'The structure and properties of alternately deposited metals', *Trans. Am. Electrochem. Soc.*, **40**, 307–20.

Bragagnolo P., Waseda Y., Palumbo G. and Aust K. T. (1989), 'Corrosion/coating of advanced materials', *Proc. MRS Symposium*, **4**, 469–74.

Brooman E. W. (2005), 'Compliant electrodeposited and electroless nanostructured and nanocomposite coatings to replace chromium coatings', *Galvanotechnik*, **12**, 103.

Budevski E., Staikov G. and Lorenz J. W. (1996), *Electrochemical Phase Transformation and Growth*. Weinheim: VCH, p. 161.

Buelens C., Celis J. P., and Roos J. R. (1983), 'Electrochemical aspects of the codeposition of gold and copper with inert particles', *J. Appl. Electrochem.*, **13**, 541–8, doi:10.1007/BF00617528.

Cai C., Zhu X. B., Zheng G. Q., Yuan Y. N., Huang X. Q. *et al.* (2010), 'Electrodeposition and characterization of nano-structured NiSiC composite films', *Surface and Coatings Technology*, **205**(11), 3448–54, doi:10.1016/j.surfcoat.2010.12.002.

Carrey J., Bouzehouane K., George J. M., Ceneray C., Blon T. *et al.* (2002), 'Electrical characterization of noncontacts fabricated by nanoindentation and electrodeposition', *Applied Physics Letters*, **81**(4), 760–2, doi:10.1063/1.1495524.

Celis J. P. and Roos J. R. (1977), 'Kinetics of the deposition of alumina particles from copper sulfate plating baths', *J. Electrochem. Soc.*, **124**, 1508–11, http://dx.doi.org/10.1149/1.2133102.

Celis J. P., Roos J. R., Buelens C. (1987), 'A mathematical model for the electrolytic codeposition of particles with a metallic matrix', *J. Electrochem. Soc.*, **134**, 1402–8, http://dx.doi.org/10.1149/1.2100680.

Chassaing E., Quang K. V. and Wiart R. (1987), 'Mechanism of copper nickel alloy electrodeposition', *J. Appl. Electrochem.*, **17**, 1267–80, doi: 10.1007/BF01023611.

Cheh H. Y. (1971), 'The limiting rate of deposition by P. R. Plating', *J. Electrochem. Soc.*, **118**, 1132–4, http://dx.doi.org/10.1149/1.2408262.

Cherkaoui M., Chassaing E. and Quang K. V. (1988), 'Pulse plating of Ni–Cu alloys', *Surf. Coat. Technol.*, **34**, 243–52, doi:10.1016/0257–8972(88)90116–8.

Chin D. T. (1983), 'Mass transfer and current-potential relation in pulse electrolysis', *J. Electrochem. Soc.*, **130**, 1657–67, http://dx.doi.org/10.1149/1.2120058.

Clark D., Wood D. and Erb U. (1997), 'Industrial applications of electrodeposited nanocrystals', *Nanostructured Materials*, **9**(1–8), 755–8, doi:10.1016/S0965–9773(97)00163–3.

Cui X. and Chen W. (2008), 'Saccharin effects on direct current electroplating of nanocrystalline Ni–Cu alloys', *J. Electrochem. Soc.*, **155**(9), K133–9, http://dx.doi.org/10.1149/1.2948362.

Dennis J. K. and Fuggle J. J. (1967), 'Electron microscopy of electrodeposited nickel', *Electroplat. Metal Fin.*, **20**(12), 376.

Doyle D. M., Palumbo G., ElSherik A. M., Erb U. and Aust K. T. (1992), *Proc. Nanophases Nanocrystalline Structures.* California, p 51.

ElGiar E. M., Said R. A., Bridges G. E. and Thomson D. J. (2000), 'Localized electrochemical deposition of copper microstructures', *J. Electrochem. Soc.*, **147**, 586–92, http://dx.doi.org/10.1149/1.1393237.

Erb U., Aust K. T. and Palumbo G. (2002), 'Electrodeposited nanocrystalline materials', in Koch C. C. (Ed.), *Nanostructured materials processing, properties and potential applications.* Norwich, NY: William Andrew Publishing, p. 179.

Erler F., Jakob C., Romanus H., Spiess L., Wielage B. *et al.* (2003), 'Interface behavior in nickel composite coatings with nano-particles of oxide ceramic', *Electrochim. Acta*, **48**, 3063–70, doi:10.1016/S0013–4686(03)00380–3.

Ettel V. A. (1984), 'Fundamentals, practice and control in electrodeposition – an overview', in Warren I. H. (Ed.), *Application of polarization measurements in the control of metal deposition.* Amsterdam: Elsevier.

Fasol G. and Runge K. (1997), 'Selective electrodeposition of nanometer scale magnetic wires', *Applied Physics Letters*, **70**, 2467–8, doi:10.1063/1.118858.

Favier F., Walter E. C., Zach M. P., Benter T. and Penner R. M. (2001), 'Hydrogen sensors and switches from electrodeposited palladium mesowire arrays', *Science*, **293**(5538), 2227–31, doi: 10.1126/science.1063189.

Ferkel H., Muller B. and Riehemann W. (1997), 'Electrodeposition of particle-strengthened nickel films', *Mater. Sci. Eng. A*, **234–6**, 474–66, doi:10.1016/S0921–5093(97)00266–9.

Ferraz M. P., Monteiro F. J. and Manuel C. M. (2004), 'Hydroxyapatite nanoparticles: A review of preparation methodologies', *J. Appl. Biomaterials Biomechanics*, **2**, 74–80.

Foecke T. and Lashmore D. (1992), 'Mechanical behavior of compositionally modulated alloys', *Scr. Metal Mater.*, **27**, 651–6.

Forrer P., Schlottig F., Siegenthaler H. and Textor M. (2000), 'Electrochemical preparation and surface properties of gold nanowire arrays formed by the template technique', *J. Appl. Electrochem.*, **30**, 533–41, doi: 10.1023/A:1003941129560.

Fransaer J., Celis J. P. and Roos J. R. (1992), 'Analysis of the electrolytic codeposition of non-Brownian particles with metals', *J. Electrochem. Soc.*, **139**, 413–25, http://dx.doi.org/10.1149/1.2069233.

Furneaux R. C., Rigby W. K. and Davidson A. P. (1989), 'The formation of controlled porosity membranes from anodically oxidized aluminum', *Nature*, **337**, 147–9, doi: 10.1038/337147a0.

Ghosh S. K., Grover A. K., Dey G. K. and Totlani M. K. (2000), 'Nanocrystalline Ni–Cu alloy plating by pulse electrolysis', *Surf. Coat. Technol.*, **126**(1), 48–63, doi:10.1016/S0257–8972(00)00520-X.

Ghosh S. K., Dey G. K., Dusane R. O. and Grover A. K. (2006), 'Improved pitting corrosion behavior of electrodeposited nanocrystalline Ni–Cu alloys in 3.0 wt.% NaCl solution', *Journal of Alloys and Compounds*, **426**(1–2), 235–43, doi: 10.1016/j.jallcom.2005.12.094.

Gimeno Y., Creus A. H., González S., Salvarezza R. C. and Arvia A. J. (2001), 'Preparation of 100–160 nm sized branched palladium islands with enhanced electrocatalytic properties on HOPG', *Chem. Mater.*, **13**(5), 1857–64, doi: 10.1021/cm0100164.

Gimeno Y., Creus A. H., Carro P., González S., Salvarezza R. C. and Arviaet A. J. (2002), 'Electrochemical formation of palladium islands on hopg: kinetics, morphology, and growth mechanisms', *Journal of Physical Chemistry B*, **106**, 4232–44, doi: 10.1021/jp014176e.

Glasstone S. (1960), *The fundamentals of electrochemistry and electrodeposition*. Palisade, NJ: Franklin Publishing.

Gong T., Bai X. J., Xiang X., Feng S., Ling C. Y. and Zhang G. T. (2009), 'Microstructure of ultrasonic electrodepositing nano silver coatings', *Advanced Materials Research*, **413**, 79–82, doi: 10.4028/www.scientific.net/AMR.79–82.413.

Gul H., Killie F., Ashan S., Alp A. and Akbulut H. (2008), *Proc. 2nd international conference on the heat treatment and surface engineering of tools and dies*. Bled, Slovenia, p. 55.

Guo D., Zhang M., Jin Z., and S. Kang (2006), 'Pulse plating of copper-ZrB_2 composite coatings', *J. Mater. Sci. Technol.*, **22**(4), doi:10.1149/1.2133102.

Gurrappa I. and Binder L. (2008), 'Electrodeposition of nanostructured coatings and their characterization – a review', *Sci. Technol. Adv. Mater.*, **9**(043001), 1–11, doi:10.1088/1468–6996/9/4/043001.

Haseeb A., Blanpain B., Wouters G., Celis J. P. and Roos J. R. (1993), 'Electrochemical deposition: a method for the production of artificially structured materials', *Mater. Sci. Eng. A*, **168**, 137–40.

Hui W. and Richardson R. (2004), Proceedings of the 2004 AESF/EPA Conference on environmental and process excellence, p. 80.

Hulteen J. C. and Martin C. R. (1997), 'A general template based method for the preparation of nanomaterials', *J. Mater. Chem.*, **7**, 1075–87, doi: 10.1039/A700027H.

Ibl N. (1980), 'Some theoretical aspects of pulsed electrolysis', *Surf. Technol.*, **10**(2), 81–104, doi:10.1016/0376–4583(80)90056–4.

Ichikawa M. (2000), 'Novel templating fabrication of platinum group metals nanoparticles and wires in micro/meso pores', *Platinum Met. Rev.*, **44**(3), doi: 10.1002/chin.200025265.

Inframat Corporation (2003a), http://www.inframat.com/electro2.htm.

Inframat Corporation (2003b), http://www.dodsbir.net/selections/abs2003–2/armyabs032.htm.

Kadirgan F. (2006), 'Electrochemical nano-coating processes in solar energy systems', *International Journal of Photoenergy*, **2006**, 1–5, doi:10.1155/IJP/2006/84891.

Karpagavalli R., Zhou A., Chellamuthu P. and Nguyen K. (2007), 'Corrosion behavior and biocompatibility of nanostructured TiO_2 film on Ti6Al4V', *Journal of Biomedical Materials Research Part A*, **83A**, 1087–95, doi: 10.1002/jbm.a.31447.

Kazeminezhad I. and Schwarzacher W. (2004), 'Giant magnetoresistance in electrodeposited Ni–Cu/Cu multilayers and anisotropic magnetoresistance in pulse-plated NixCu1-x alloy films', *J. Solid State Electrochem.*, **8**(3), 187–9, doi: 10.1007/s10008–003–0422–8.

Kern P., Schwaller P. and Michler J. (2006), 'Electrolytic deposition of titania films as interference coatings on biomedical implants: Microstructure, chemistry and nano-mechanical properties', *Thin Solid Films*, **494**, 279–86, doi:10.1016/j.tsf.2005.09.068.

Kim M., Sun F., Lee J., Hyun Y. K. and Lee D. (2010), 'Influence of ultrasonication on the mechanical properties of Cu/Al_2O_3 nanocomposite thin films during electrocodeposition, *Surf. Coat. Tech.*, **205**(7), 2362–8, doi:10.1016/j.surfcoat.2010.09.049.

Kunoshi C. T., Correa O. V., de Lima N. B. and Ramanathan L. V. (2000), *Ultrafine Grained Mater.*, **110**, 99.

Kurzweg H., Heimann R. B., Troczynski T. and Wayman M. L. (1998), 'Development of plasma-sprayed bioceramic coatings with bond coats based on titania and zirconia', *Biomaterials*, **19**, 1507–11.

Landolt D. and Marlot A. (2003), Microstructure and composition of pulse-plated metals and alloys, *Surf. Coat. Technol.*, **169**, 8–13, doi:10.1016/S0257–8972(03)00042–2.

Li J., Jiang J., He H. and Sun Y. (2002), Synthesis, microstructure, and mechanical properties of TiO_2/Ni nanocomposite coatings, *J. Mater. Sci. Lett.*, **21**, 939–41, doi:10.1023/A:1016073606681.

Li J., Sun Y., Sun X. and Qiao J. (2005), 'Mechanical and corrosion-resistance performance of electrodeposited titania–nickel nanocomposite coatings', *Surf. Coat. Tech.*, **192** (2–3), 331–5, doi:10.1016/j.surfcoat.2004.04.082.

Lowenheim F. A. (1974), *Modern electroplating*. New York: John Wiley & Sons.

Lyons E. H. (1954), 'Electronic Configuration in Electrodeposition from Aqueous Solutions', *J. ElectroChem. Soc.*, **101**, 376–81, http://dx.doi.org/10.1149/1.2781284.

Martin C. R. (1994), 'Nanomaterials: a membrane based synthetic approach', *Science*, **266**, 1961–5, doi: 10.1126/science.266.5193.1961.

Martín H., Carro P., Creus A. H., González S., Salvarezza R. C. and Arvia A. J. (1997), 'Growth mode transition involving a potential-dependent isotropic to anisotropic surface atom diffusion change, gold electrodeposition on HOPG followed by STM', *Langmuir*, **13**, 100–10, doi: 10.1021/la960700a.

Masdek N. R. N. and Alfantazi A. (2010), 'Review of studies on corrosion of electrodeposited nanocrystalline metals and alloys', *ECS Transactions*, **28**(24), 249–60, http://dx.doi.org/10.1149/1.3496436.

Medeliene V., Juskenas R., Kurtinaitiene M., Selskiene A. and Stankevic V. (2010), 'The impact of carbon nanomaterials on the formation and properties of electrodeposited copper composite coatings', *Materials Science*, **16**(1), 35–9.

Milchev A., Stoyanov S. and Kaischew R. (1974), 'Atomistic theory of electrolytic nucleation I', *Thin Solid Films*, **22**, 255–65, doi: 10.1016/0040–6090(74)90296-X.

Mishra R. and Balasubramaniam R. (2004), 'Effect of nanocrystalline grain size on the electrochemical and corrosion behavior of nickel', *Corros. Sci.*, **46**, 3019–29, doi:10.1016/j.corsci.2004.04.007.

Morales L. A. and Podlaha E. J. (2004), 'The Effect of Al_2O_3 nanopowder on Cu electrodeposition', *J. ElectroChem. Soc.*, **151**, C478–83, http://dx.doi.org/10.1149/1.1752934.

Muller C., Sarret M. and Benballa M. (2003), 'ZnNi/SiC composites obtained from an alkaline bath', *Surf. Coat. Technol.*, **162**, 49–53, doi:10.1016/S0257–8972(02)00360–2.

Natter H. and Hempelmann R. (1996), 'Nanocrystalline copper by pulsed electrodeposition: The effects of organic additives, bath temperature, and pH', *J. Phys. Chem.*, **100**, 19525–32, doi: 10.1021/jp9617837.

Natter H., Hempelmann R. and Krajewski T. (1996), 'Nanocrystalline palladium by pulsed electrodeposition', *B. Phys. Chem.*, **100**, 55–64, doi: 10.1002/bbpc.19961000111.

Natter H., Schmelzer M. and Hempelmann R. (1998), 'Nanocrystalline nickel and nickel-copper alloys: synthesis, characterization and thermal stability', *J. Mater. Res.*, **13**, 1186–97, doi: 10.1557/JMR.1998.0169.

Natter H., Schmelzer M., Löffler M. S., Krill C. E., Fitch A. *et al.*, (2000), 'Grain growth kinetics of nanocrystalline iron studied *in situ* by synchrotron real time X-ray diffraction', *J. Phys. Chem. B*, **104**(11), 2467–76, doi: 10.1021/jp991622d.

Natter H. and Hempelmann R. (2003), 'Tailor-made nanomaterials designed by electrochemical methods', *Electrochimica Acta*, **49**, 51–61, doi: 10.1016/j.electacta.2003.04.004.

Noort R. V. (1987), 'Titanium: The implant material of today', *J. Mater. Sci. Mater. Med.*, **22**, 3801–11, doi: 10.1007/BF01133326.

Palumbo G., Doyle D. M., El-Sherik A. M., Erb U. and Aust K. T. (1991), 'Intercrystalline hydrogen transport in nanocrystalline nickel', *Scr. Metall. Mater.*, **25**, 679, doi:10.1016/0956–716X(91)90114-G.

Parida G., Chaira D. and Basu A. (2010), 'Ultra fine TiO_2 dispersed metallic coating on steel', *International Conference on Synthesis Characterization, Consolidation and Modeling of Nanomaterials.* ICON 2010, Coimbatore, India.

Peng X., Thou Z., Shang Y. and Wang F. (2004), 'On the development and the oxidation of novel Ni–Cr and Ni–Al nanocoatings by composite electrodeposition', *Materials Science Forum*, **461–4**, 409–16.

Pletcher D. (1981), *Industrial electrochemistry.* New York: Chapman & Hall.

Podlaha E. J., Li Y., Zhang J., Huang Q., Panda A. *et al.* (2006), 'Electrochemical deposition of nanostructured metals' in Gogotsi Y. (Ed.), *Nanomaterials Handbook.* Oxford: Taylor & Francis, ISBN 0849323088, 9780849323089.

Potzschke R. T., Gervasi C. A., Vinzelberg S. Staikov G. and Lorenz W. J. (1995), 'Nanoscale studies of electrodeposition on HOPG (0001)', *Electrochimica Acta*, **40**(10), 1469–74, doi:10.1016/0013–4686(95)00049-K.

Prado R. A., Facchini D., Mahalanobis N., Gonzalez F. and Palumbo G. (2009), 'Electrodeposition of nanocrystalline cobalt alloy coatings as a hard chrome alternative', DOD Corrosion Conference. https://www.corrdefense.org.

Praveen B. M. and Venkatesha T. V. (2009), 'Generation and corrosion behavior of Zn-nanosized carbon black composite coating', *Int. J. ElectroChem. Sci.*, **4**, 258–66.

Przenioslo R., Winter R., Natter H., Schmelzer M., Hempelmann R. *et al*., (2001a), 'Fractal pore distribution and magnetic microstructure of pulse electrodeposited nanocrystalline Ni and Co', *Phys. Rev. B*, **63**, 54408, doi: 10.1103/PhysRevB.63.054408.

Przenioslo R., Winter R., Natter H., Schmelzer M., Hempelmann R. *et al*., (2001b), 'Studies of the fractal microstructure of nanocrystalline and amorphous chromium obtained by electrodeposition', *J. Alloys Compounds*, **328**, 259–63, doi: 10.1016/S0925–8388(01)01306–8.

Quang K. V., Chassaing E., LeViet B., Celis J. P. and Roos J. R. (1985), 'Codeposition of nickel and copper', *Met. Finish.*, **83**(10), 25–8.

Ramalingam S., Muralidharan V. S. and Subramania M. (2009), 'Electrodeposition and characterization of Cu–TiO_2 nanocomposite coatings', *Solid State Electrochem.*, **13**, 1777–83, doi: 10.1007/s10008–009–0870-X.

Rashidi A. M. and Amadeh A. (2009), 'The effect of saccharin addition and bath temperature on the grain size of nanocrystalline nickel coatings', *Surf. Coat. Techn.*, **204**(3), 353–8, doi:10.1016/j.surfcoat.2009.07.036.

Raub E. and Muller K. (1967), *Fundamentals of metal deposition.* New York: Elsevier.

Rofagha R., Langer R., El-Sherik A. M., Erb U., Palumbo G. *et al*., (1991), 'The corrosion behavior of nanocrystalline nickel', *Scr. Metall. Mater.*, **25**, 2867–72, doi:10.1016/0956–716X(91)90171-V.

Roy S., Matlosz M. and Landolt D. (1994), 'Effect of corrosion on the composition of pulse-plated Cu–Ni alloys', *J. ElectroChem. Soc.*, **141**, 1509–17, http://dx.doi.org/10.1149/1.2054954.

Saji V. S. and Thomas J. (2007), 'Nanomaterials for corrosion control', *Current Science*, **92**(1), 51–5.

Saji V. S., Choe H. C. and Yeung K. W. K. (2010), 'Nanotechnology in biomedical applications: a review', *International Journal of Nano and Biomaterials*, **3**(2), 119–39.

Schonenberger C., VanderZande B. M. L., Fokkink G. J., Henny M., Schmid C. *et al.* (1997), 'Template synthesis of nanowires in porous polycarbonate membranes: electrochemistry and morphology', *J. Phys. Chem. B*, **101**, 5497–505, doi: 10.1021/jp963938g.

Schwarzacher W. and Lashmore D. S. (1996), 'Giant magnetoresistance in electrodeposited films', *IEEE Trans. Magn.*, **32**, 3133–53, doi: 10.1109/20.508379.

Schwarzacher W., Attenborough K., Michel A., Nabiyouni G. and Meier J. P. (1997), Electrodeposited nanostructures, *J. Magn. and Magn. Mater.*, **165**, 23–9, doi:10.1016/S0304–8853(96)00465–9.

Shima M., Riba L. S., McMichael R. D., and Moffat T. P. (2002), 'Magnetic properties of ultrathin laminated Co/Cu films prepared by electrodeposition', *J. ElectroChem. Soc.*, **149**, C439–44, http://dx.doi.org/10.1149/1.1494826.

Shirkhanzadeh M. (1998), 'Direct formation of nanophase hydroxyapatite on cathodically polarized electrodes', *J. Mater. Sci.*, **9**, 67–72.

Simunovich D., Schlesinger M. and Snyder D. D. (1994), 'Electrochemically layered copper-nickel nanocomposites with enhanced hardness', *J. ElectroChem. Soc.*, **141**, L10–11, http://dx.doi.org/10.1149/1.2054717.

Stojak J. L. and Talbot J. B. (2001), 'Effect of particles on polarization during electrocodeposition using a rotating cylinder electrode', *J. Appl. Electrochem.*, **31**, 559, doi: 10.1023/A:1017558430864.

Suarez C., Chavez E., Diez J. A., Grande H. and Guixa R. (2007), 'High conductivity silver nanocoatings on aluminium obtained from pulse plating techniques', *Trans. Inst. Metal Finish.*, **85**(1), 46–50, doi: 10.1179/174591907X162486.

Thorpe S. J., Ramaswami B. and Aust K. T. (1988), 'Corrosion and Augur studies of a nickel base metal metalloid glass', *J. ElectroChem. Soc.*, **135**, 2162–70, http://dx.doi.org/10.1149/1.2096233.

Tiginyanu I., Monaico E. and Monaico E. (2008), 'Ordered arrays of metal nanotubes in semiconductor envelope', *ElectroChem. Comm.*, **10**, 731–4, doi: 10.1016/j.elecom.2008.02.029.

Tsirlina G. A., Petrii O. A., Safonova T. Y., Papisov I. M., Vassiliev S. Y. *et al*., (2002), 'Quasitemplate synthesis of nanostructured palladium electroplates', *Electrochimica Acta*, **47**(22–3), 3749–58, doi: 10.1016/S0013–4686(02)00345–6.

Vazquez L., Creus A. H., Carro P., Ocon P., Herrasti P. *et al.* (1992), 'Scanning tunneling microscopy and scanning electron microscopy observations of the early stage of silver deposition on graphite single crystal electrodes', *J. Phys. Chem.*, **96**(25), 10454–60, doi: 10.1021/j100204a062.

Wang D., Zhou W. L., McCaughy B. F., Hampsey J. E., Ji X *et al.* (2003), 'Electrodeposition of metallic nanowire thin films using mesoporous silica templates', *Advanced Materials*, **15**, 130–3, doi: 10.1002/adma.200390025.

Wang W., Hou F. Y., Wang H. and Guo H. T. (2005) 'Fabrication and characterization of Ni–ZrO_2 composite nanocoatings by pulse electrodeposition', *Scripta Materialia*, **53**, 613–18, doi: 10.1016/j.scriptamat.2005.04.002.

Wang J. (2006), 'Electrodeposition: a simple method for the syntheses of nanomaterials'. http://www.chembio.uoguelph.ca/educmat/chm753/Third%20Class/Jingpeng.ppt.

Whitney T. M., Searson P. C., Jiang J. S. and Chien C. L. (1993), 'Fabrication and magnetic properties of arrays of metallic nanowires', *Science*, **261**(5126), 1316–19, doi: 10.1126/science.261.5126.1316.

Xia F. F., Li C., Wang F., Wu H., Wang J. D. *et al.* (2010), 'Preparation and characterization of Nano Ni–TiN coatings deposited by ultrasonic electrodeposition', *Journal of Alloys and Compounds*, **490**(1–2), 431–5, doi: 10.1016/j.jallcom.2009.10.026.

Yamada I. A., Houga T., and Ueda Y. (2002), 'Magnetism and magnetoresistance of Co/Cu multilayer films produced by pulse control electrodeposition method', *J. Magn. and Magn. Mater.*, **239**, 272–5, doi: 10.1016/S0304–8853(01)00569–8.

Yang S., Zhu H., Yu D., Jin Z., Tang S. and Du Y. (2000), 'Preparation and magnetic property of Fe nanowire array', *J. Magn. and Magn. Mater.*, **222**, 97–100, doi: 10.1016/S0304–8853(00)00541–2.

Yang Y. L., Wang Y. D., Ren Y., He C. S., Deng J. N. *et al.* (2008), 'Single-walled carbon nanotube-reinforced copper composite coatings prepared by electrodeposition under ultrasonic field', *Mater. Lett.*, **62**, 47–50, doi: 10.1016/j.matlet.2007.04.086.

Yin K. M. (1996), 'Duplex diffusion layer model for pulse with reverse plating', *Surf. Coat. Technol.*, **88**, 162–4, doi: 10.1016/S0257–8972(96)02904–0.

Ying R. Y., (1988), 'Electrodeposition of copper-nickel alloys from citrate solutions on a rotating disk electrode', *J. Electrochem. Soc.*, **135**(12), 2957–64, http://dx.doi.org/10.1149/1.2095469.

Youssef K. M. S., Koch C. C. and Fedkiw P. S. (2004), 'Improved corrosion behavior of nanocrystalline zinc produced by pulse current electrodeposition', *Corros. Sci.*, **46**, 51–64, doi: 10.1016/S0010–938X(03)00142–2.

Zach M. P. and Penner R. M. (2000), 'Nanocrystalline nickel nanoparticles', *Advanced Materials*, **12**, 878–83, doi: 10.1002/1521–4095(200006).

Zach M. P., Ng K. H. and Penner R. M. (2000), 'Molybdenum nanowires by electrodeposition', *Science*, **290**, 2120–3, doi: 10.1126/science.290.5499.2120.

Zeiger W., Schneider M., Scharnweber D. and Worch H. (1995), 'Corrosion behavior of a nanocrystalline FeA18 alloy', *Nanostruct. Mater.*, **6**, 1013–16, doi: 10.1016/0965–9773(95)00234–0.

Zhang C., Peng X., Zhao J. and Wang F. (2005), 'Hot corrosion of an electrodeposited Ni–11 wt % Cr nanocomposite under molten Na_2SO_4–K_2SO_4–NaCl', *J. ElectroChem. Soc.*, **152**(9), B321–6, http://dx.doi.org/10.1149/1.1952667.

Zhao G., Zhou Y. and Zhang H., (2009), 'Sliding wear behaviors of electrodeposited Ni composite coatings containing micrometer and nanometer Cr particles', *Transactions of Nonferrous Metals Society of China*, **19**(2), 319–23, doi: 10.1016/S1003–6326(08)60271-X.

Zhitomirsky I. and GalOr L. (1997), 'Electrophoretic deposition of hydroxyapatite', *J. Mater. Sci. Mater. Med.*, **8**, 213–19, doi: 10.1023/A:1018587623231.

Zhitomirsky I. (2000) 'Electrophoretic hydroxyapatite coatings and fibers', *Mater. Lett.*, **42**, 262–71, doi: 10.1016/S0167–577X(99)00197–4.

Zhu J. J., Liao X. H., Zhao X. N. and Chen H. Y. (2001), 'Preparation of silver nanorods by electrochemical methods', *Mater. Lett.*, **49**, 91–5, doi: 10.1016/S0167–577X(00)00349–9.

Zoval J. V., Stiger R. M., Biernacki P. R. and Penner R. M. (1996), 'Electrochemical deposition of silver nanocrystallites on the atomically smooth graphite basal plane', *J. Phys. Chem.*, **100**(2), 837–44. doi: 10.1021/jp952291h.

Zoval J. V., Lee J., Gorer S. and Penner R. M. (1998), 'Electrochemical preparation of platinum nanocrystallites with size selectivity on basal plane oriented graphite surfaces', *Journal of Physical Chemistry B*, **102**(7), 1166–75, doi: 10.1021/jp9731967.

6

Moderate temperature oxidation protection using nanocrystalline structures

R. K. SINGH RAMAN, Monash University, Australia
and P. SINGH, University of Connecticut, USA

Abstract: We hypothesised that a nanostructure can bring about dramatic improvements in the oxidation resistance of low chromium iron–chromium alloys at moderate temperatures. A nanocrystalline Fe–10wt%Cr alloy was found to undergo oxidation at a rate that was an order of magnitude lower than its microcrystalline counterpart. Importantly, the oxidation resistance of nanocrystalline Fe–10wt%Cr alloy was comparable to that of the common corrosion-resistant microcrystalline stainless steels. We outline the difficulties in processing nanocrystalline iron–chromium ferritic alloys as well as the success in circumventing them. The recently reported roles of nanocrystalline structures in oxidation resistance of a few other systems are also considered.

Key words: nanocrystalline, microcrystalline, oxidation corrosion resistance, crystalline and intercrystalline components, thermal stability.

6.1 Introduction

Single or multi-phase polycrystalline solids with grain size typically less than 100 nm are known as nanocrystalline (NC) materials.[1,2] Because of their extremely fine grain size, the NC materials are composed of a remarkably high density of interfaces (grain boundaries and triple points).[3,4] As a result, those properties that depend on the grain size and grain boundaries may be considerably different in the case of a NC metal/alloy as compared with its conventional microcrystalline (MC) counterpart. For example, NC metals and alloys exhibit increased mechanical strength, enhanced diffusivity and higher specific heat and electrical resistivity. Attempts are being made to exploit the attractive physical properties of NC metallic materials. However, several such applications will require the materials to demonstrate acceptable levels of resistance to environmental degradation. A proper understanding of environment-assisted degradation of NC metallic materials (metals/alloys) is particularly important, since grain size and grain boundaries are known to influence corrosion processes.

Oxidation/corrosion resistance of NC metals and alloys has received very limited research attention. However, NC metals and alloys have been reported to exhibit different oxidation/corrosion resistance from their MC counterparts.[5–7] It is also emphasised that, besides the interest in investigating the role of NC structures in oxidation/corrosion, another aspect is the possibility

of exploiting the enhanced grain boundary phenomena (such as diffusion) for the purpose of developing oxidation/corrosion resistant alloys with considerably less alloying content.[5] In this context, developing commercially viable materials processing routes for producing and retaining NC structures of oxidation/corrosion resistant alloys is a major challenge. Therefore, this chapter also provides a brief description of the challenges in synthesising NC metals and alloys, and the attempts at circumventing these challenges. Though ferrous systems (primarily iron and iron–chromium systems) are the major materials covered in this chapter, the reported literature on the corrosion resistance of other systems has also been reviewed.

6.2 Structure and properties of nanocrystalline metals

Though there are variations of a few orders of magnitude in their grain size, the structure and dimensions of grain boundaries in NC and MC materials have been suggested to be similar.[8–13] However, based on the thermodynamic properties of NC materials, Fecht[14] suggested the grain boundary energy to be considerably greater in the case of NC iron (produced by ball milling) as compared with the same alloy composition in the MC state. Several other researchers believe grain boundaries in the NC state to be more disordered than in conventional MC materials.[15–19] Though the 'grains' and 'grain boundaries' in the NC state have been visualised in a way which is entirely different from the traditional concept (of large grains separated by considerably thin boundaries in the case of conventional microcrystalline materials), in this chapter the terms 'grains' and 'grain boundaries' will continue to be used in the traditional sense. However, it may be important to reflect that the structure of NC materials is visualised as consisting of two components: a crystalline component (CC), which is formed by small equiaxed single crystals, and the intercrystalline component (IC),[8,20] as shown in Fig. 6.1. The IC component forms a network and surrounds the CC crystallites. The fraction of IC increases with decreasing size of crystallites and may even exceed the CC fraction (when the crystallites are of sizes below a critical size).

As described earlier, because of their remarkably fine grain size, the grain boundaries constitute a remarkably large volume fraction of NC materials. As a result, those mechanical, electrical, magnetic and chemical properties that profoundly depend on grain size and grain boundary phenomena are also remarkably different in the case of NC materials as compared with their MC counterparts. Though NC structure and grain size can influence most properties, of particular relevance to this chapter are the thermal stability and diffusion characteristics of NC materials. Readers interested in the role of NC in various other properties may refer to a few lead publications on the topic.[4,20–23]

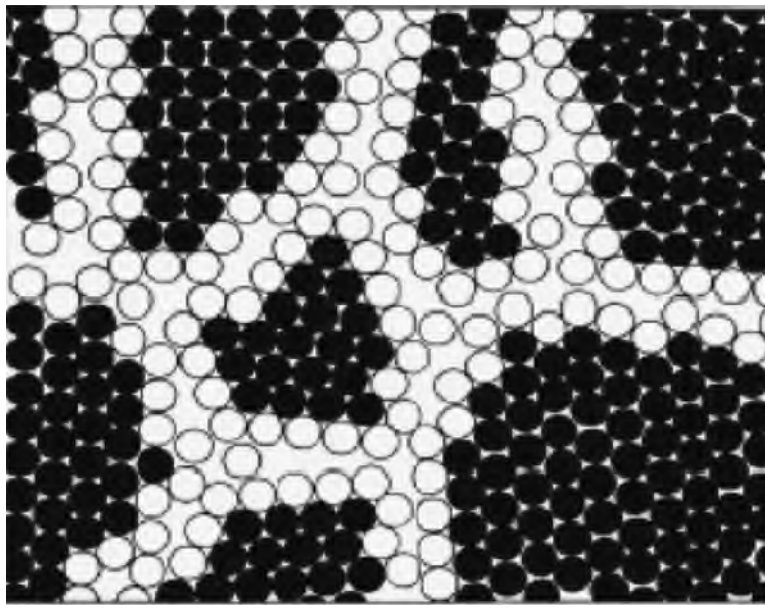

6.1 Model of a nanostructured material: filled circles represent crystalline component (CC) atoms whereas the open circles represent intercrystalline component (IC) atoms.[8,20]

6.3 Thermal stability and synthesis of nanocrystalline metals and alloys

6.3.1 General principles

Because IC constitutes a remarkably high volume fraction of NC materials (as shown in Fig. 6.1), the interfacial energy of such materials is generally considerably high. As a result, NC materials in general are exceedingly susceptible to thermally assisted grain growth,[8,20] which decreases the total energy of the system. Therefore, it is often essential to take into account their thermal instability while processing such materials. Thermal instability may also be a factor in considering any elevated temperature engineering application of NC materials (such as resistance to oxidation by high temperature gases). In fact, some of the low-melting engineering metals (i.e. Sn, Pb, Al and Mg) can undergo considerable grain growth, even at normal temperatures.[20,24] However, metals with high melting points may possess thermal stability at considerably higher temperatures. For example, iron and iron-based alloys resist grain growth up to higher temperatures, 400–600°C.[8,25–31] Similar behaviour has been reported for other metals (e.g. Co).[32]

There is some inconsistency in the literature on the temperature at which sudden grain growth may kick in. In their study on grain growth of pulse electrodeposited

NC-Fe, Natter *et al.*[29] reported a sudden grain growth at 410°C, whereas Malow and Koch[27] did not find such behaviour until a temperature range of 500 to 530°C. This inconsistency is generally attributed to the presence of different levels of impurities in the NC materials that may come inherently from the processing techniques employed in different studies.[25–27,29,33] The presence of impurities may enhance thermal stability for classical reasons such as pinning of the grain boundaries and the formation of second phase particles.[30–32]

6.3.2 Synthesis of Fe and Fe-based nanocrystalline materials

Several techniques have been employed for producing NC solids in powder and thin film forms. The techniques of inert gas condensation,[34–38] pulsed plasma deposition[24] and sputtering[36] have exclusively been used for processing thin films or small amounts of NC materials, whereas it is necessary to produce/process bulk samples for oxidation/corrosion or mechanical testing. Electrodeposition[29,39,40] and severe plastic deformation[25–27,41–57] have been recognised as the two relatively successful methods for processing NC materials in bulk quantities. Pulse electrodeposition has been employed successfully for processing NC materials in bulk,[40] most notably Ni–Fe and Ni–Co alloys.[58,59] However, synthesis of NC alloys or metals by electrodeposition often requires the use of additives for the purpose of biasing nucleation over growth of the depositing grains. These additives are believed[4] to remain in the material as impurities and may cause poor mechanical properties (such as embrittlement), typically observed in NC electrodeposits.

Among the plastic deformation techniques, advanced ball milling has produced artefact-free NC powders.[60,61] However, the ball-milled powders need to be compacted. Groza[62] has reviewed various techniques employed for compaction of different NC materials: high pressure/lower temperature compaction, *in situ* consolidation,[63] hot compaction[64] and explosive compaction.[65] However, compaction of NC Fe or Fe-based alloys may be a non-trivial task. The difficulties arise due to the restrictions on plastic deformation posed by the body centred cubic (BCC) structure causing high hardness. Such restrictions necessitate consolidation at high pressures/temperatures. For example, pure iron with an average grain size of 10 nm has a hardness of 10 GPa.[66] Plastic deformation, a necessary condition for effective compaction, requires the applied pressure to be in excess of the yield stress and approximately one-third of the hardness (i.e. 3.5 GPa). The necessary plastic flow, high densification and inter-particle bonding can be achieved by compaction/sintering at high temperatures. However, processing at excessively high temperatures will commonly lead to grain growth and loss of NC structure.

Co-author Singh Raman and his co-workers have successfully processed NC Fe–Cr alloy discs with close-to-theoretical density and without excessive grain

growth.[31] NC powder of Fe–10wt% Cr alloy was produced by ball milling, and the powder was compacted into discs by employing a suitable combination of prior thermal softening and compaction at a moderate temperature and pressure. However, it was essential to establish a suitable temperature regime for softening without causing an excessive grain growth. For this purpose, the ball-milled alloy powders were annealed at 500, 600 and 700°C in a forming gas atmosphere for different durations, and average grain size of the powder was determined by the well-established X-ray diffraction (XRD) technique[67] after various intermittent durations. Figure 6.2 shows the change in XRD patterns of Fe–10Cr alloy powder with increasing time of annealing at 600°C. As shown in Fig. 6.2, the diffraction line broadening of Bragg reflection peaks decreases as a result of the grain growth (grain size increases with the annealing time (Fig. 6.3)). This pattern was consistent also at 500 and 700°C. However, grain growth is a strong function of temperature, as suggested from the increasing intensity of the initial grain growth with temperature (Fig. 6.3).

Initial grain growth is rapid at each of the three temperatures. The as-milled and annealed powder samples were compacted into pellets under a uniaxial pressure. It was necessary to reduce the hardness of the powders before subjecting them to a pressure compaction. Based on the grain growth data shown in Fig. 6.3, a prior annealing at 600°C for 30 min was selected with a view to prior softening of the powder without any excessive grain growth. Although prior annealing at 600°C for 30 min would result in some grain growth (as suggested in Fig. 6.3), the grain size of the alloy was still found to be 42 nm, which is well within the NC range.

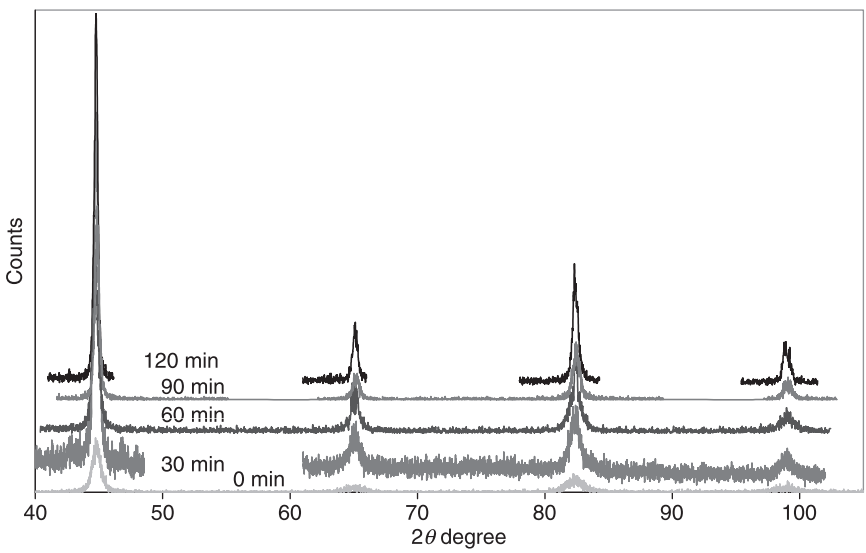

6.2 XRD profiles for ball-milled NC Fe–10Cr alloy annealed at 600°C for different times.[5]

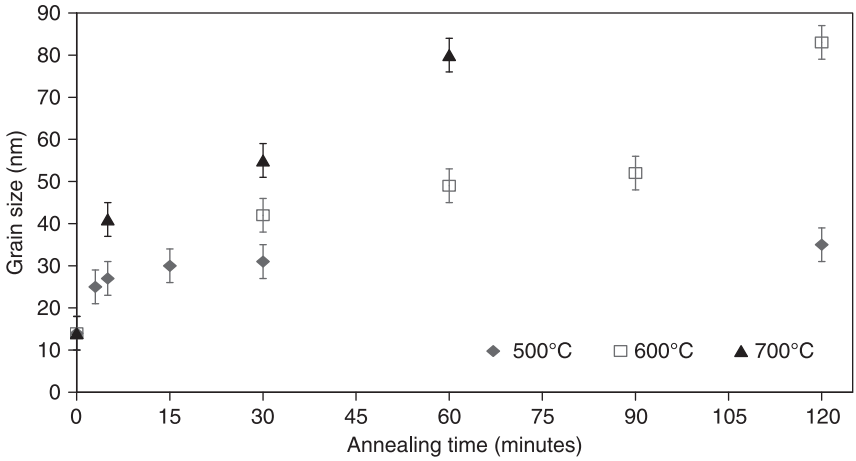

6.3 Grain growth in Fe–10Cr NC alloy at 500°C, 600°C and 700°C.[5]

Most importantly, because of the softening caused by the prior annealing it was possible to compact the powder into pellets (diameter = 12 mm, thickness = 1.5 mm) at room temperature at a pressure of 3 GPa. Compacted pellets were sintered for 1h at 600°C, which further improved the density (close to 100% of the theoretical density). Although the sintering caused some further grain growth, the grain size of the sintered pellets was determined to be 52 ± 4 nm. At each stage (compaction and sintering), the grain size was determined by diffraction line broadening (as shown in Fig. 6.2).

6.4 Degradation of nanocrystalline metals and alloys by environment

Most metals suffer corrosion as a result of their inherent thermodynamic instability in elemental form. However, the progress of corrosion is largely governed by one or a combination of the following phenomena:

1. Electrochemical non-homogeneity at the metal surface, and
2. Diffusion of elemental/ionic species: (a) in the metal substrate, and/or (b) through the layer of corrosion product or through the electrolytic environment immediately adjacent to the metal surface.

The NC structure can remarkably influence the nature and/or degree of both electrochemical non-homogeneity at the surface and diffusion in the bulk of metals. Besides, there may be other influences due to the NC structure (the degree of which will vary from metal to metal). For example, the structure (such as grain size) and associated properties (such as mechanical property) of the corrosion films developed on NC substrate may be considerably different from those on a MC substrate. Thus,

a NC structure of the metal influencing the structure of the corrosion films can also indirectly influence diffusion through the layer of corrosion film.

It is relevant to note that diffusion in the metal and through the corrosion film is the predominating phenomenon in the case of degradation of metals due to gaseous corrosion at elevated temperatures. On the other hand, electrochemical non-homogeneity will essentially have a predominating influence on electrochemical corrosion at low temperatures. Given that the grain boundaries and triple junctions (i.e. high energy areas with a much greater degree of disorder) are nearly always anodic,[7,68–71] the corrosion rate of NC materials in most simplistic terms would be expected to be considerably higher than that of MC materials of similar chemical composition, and this view is often supported in the literature.[6,7,68,69,72,73] However, the corrosion resistance of some materials is reported to be superior in NC form. Such contrast in the influence of a nanostructure may depend on the environment–material system. In the case of electrochemical corrosion of pure metals, the anodic behaviour of grain boundaries and the associated anode–cathode area ratio are the governing factors, whereas the effect of alloying elements would be the additional factor in the case of alloys.

Early fundamental studies on the role of nanostructure in electrochemical corrosion were carried out on Co,[74–76] Cu,[74,77–80] Ni,[73,81–84] and Ni-based binaries.[6,72,85,86] The extent of localised corrosion at grain boundaries is reported to decrease in the case of some NC metals (i.e. Cu and Co),[72,74,80] in comparison with their MC counterparts, which is attributed to: (a) decrease in the difference in the electrochemical potentials of grains and grain boundaries and (b) the greater anode-to-cathode area ratio in NC materials. A few studies[87–91] have been carried out to compare the electrochemical corrosion of NC and MC iron–chromium alloys.

Electrochemical corrosion resistance of a NC surface of 316 stainless steel developed by surface mechanical attrition treatment was found to be considerably inferior to the MC unmodified bulk. This behaviour is attributed to the considerable increase in the 'fast diffusion channels' for ions, i.e. grain boundaries and triple junctions in the NC material.[87] In another study, the grain refinement of stainless steels to a nanometric level is reported to improve the corrosion resistance, as suggested by the considerably extended passivation for NC in the polarisation plots.[89] The authors have attributed this behaviour to the greater chromium diffusion in the NC structure, which may be argued given the very low diffusivity (i.e. 10^{-40}–10^{-43} m^2 s^{-1}) at ambient temperatures.

6.5 Oxidation resistance of nanocrystalline metals/alloys

6.5.1 General principles

During oxidation, binary alloys with certain alloying elements (i.e. Cr, Al and Si) can form a continuous layer of chromia, alumina or silica, conferring substantial oxidation resistance. This has formed the basis of the development of common

oxidation resistant alloys such as stainless steels. Formation of a continuous layer of surface oxide is called 'external oxidation'.[92] If, on the other hand, the inward flux of oxygen exceeds the outward flux of solute during the oxidation process, isolated oxide particles form in the sub-surface. This phenomenon is called 'internal oxidation'.[92]

For external oxidation and formation of a continuous layer of chromia, alumina or silica, a critical concentration of solute is required, which can be calculated by Wagner's treatment[93] for various systems/conditions. The critical amount of a solute for such a transition depends directly on its diffusivity in the alloy, besides other factors (concentration of solute element, diffusivity in the oxide scale, temperature, etc). The extremely fine grain size and the high volume fraction of grain boundaries of NC materials[8] can cause an extraordinary increase in diffusivity, and NC structures may have beneficial effects in the development of the protective oxide layer. For example, oxidation resistance of an Fe–Al and an Fe–B–Si alloy in the NC state is reported[87,94] to be superior to that in the MC state. This behaviour is attributed to Al and Si, the well-known protective oxide film formers, being the predominantly diffusing species respectively in the two alloys, and the nanostructure facilitating their diffusion and expedited formation of protective films (of Al/Si oxide).

6.5.2 Oxidation resistance of nanocrystalline Fe–Cr alloys

In the temperature range of 300 to 400°C, chromium diffusion in a NC Fe–Cr system is reported to be about four orders of magnitude greater than in a MC Fe–Cr alloy.[5] Given the extremely fine grain size and the resulting high diffusivity in NC Fe–Cr alloys, one would expect the Cr concentration required for internal-to-external transition to become substantially lower. Singh Raman *et al.*[95] proposed a hypothesis: (a) the oxidation resistance of NC Fe–Cr alloys should be considerably superior to MC alloys of the same composition, and (b) it should be possible to attain remarkable oxidation resistance at considerably lower chromium contents of NC Fe–Cr alloys, as opposed to the considerably greater minimum chromium contents (13–15wt%) required for development and maintenance of the Cr_2O_3 layers in common stainless steels. In this context, it is noted that, though the minimum chromium content for the development of a Cr_2O_3 layer is 13% for ferritic alloys and approximately 15% for austenitic alloys, common stainless steels contain at least 18 wt% chromium in order to provide sufficient chromium in the subscale for the purpose of self-healing in the event of disruption in the initial protective layer of Cr_2O_3.

Singh Raman *et al.*[5,95] have recently reported the role of NC structures in remarkably improving oxidation resistance. In this context, it may be imperative to first have an overview of the role of grain size in development of the protective layer of oxidation resistant oxide (which is generally the inner layer of the multilayered oxide scale). As suggested earlier, for a given combination of

alloy–environment–temperature, where predominantly diffusing species can form a protective film and provide oxidation resistance, a decrease in grain size will facilitate protective film formation. Iron–chromium alloys (such as stainless steels) are the most commonly employed corrosion resistant MC materials. A common high-Cr alloy (such as 18Cr–8Ni stainless steel) forms during oxidation an inner layer of Fe/Ni oxide that eventually converts into a protective oxide, i.e. Cr_2O_3, when sufficient Cr diffuses from the alloy bulk to the oxide scale–alloy interface.[96] The kinetics of transition of Fe/Ni oxide into the protective layer of Cr_2O_3 depends on the supply of chromium by diffusion in the alloy matrix, which is governed profoundly by grain size of the alloy. As clearly demonstrated in the literature,[97] a fine grain (~17 μm or less) 18Cr alloy easily developed a uniform layer of Cr_2O_3. For the same alloy with grain sizes greater than ~40 μm, this protective layer of Cr_2O_3 was difficult to form during air-oxidation, as the inner layer of $(Fe,Cr)_3O_4$ continued to grow due to insufficient chromium supply.[98] Low-chromium Fe–Cr alloys fail to form a protective layer of Cr_2O_3.[98–101] Singh Raman *et al.*[100,101] have investigated the role of grain size (15–60 μm) in oxidation resistance of such low-Cr alloys. Grain boundary diffusion in MC low-chromium alloys is never enough for the formation of a contiguous protective layer of Cr_2O_3. In fact, the alloy suffers predominant and extensive oxidation along grain boundaries, and a decrease in grain size rather increases the grain boundary internal oxidation.

The most common and simple testing for the oxidation rates of metals and alloys at elevated temperatures is the determination of weight gain per unit surface area with time. In order to compare the influence of NC with respect to MC structures on oxidation, NC and MC Fe–10%Cr alloy powders were produced by ball milling, compacted into pellets and sintered, as described earlier (in Section 6.3.2). The pellets of both NC and MC materials were oxidised at 300 to 400°C. Typical oxidation kinetics data (Fig. 6.4) show the MC alloy to be oxidising at a considerably greater rate than the NC alloy. However, the striking features of the oxidation kinetics and oxide scale are:

1. After 3120 min of oxidation at 300°C, weight gain of the MC alloy was found to be nearly an order of magnitude greater than that of the NC alloy of the same composition. This influence was enhanced at 350°C: weight gain of the MC alloy was found to be well in excess of an order of magnitude greater.
2. Both NC and MC alloys follow parabolic kinetics in the initial period (as evidenced by the weight gain^2 vs time plots). But, during subsequent oxidation, NC Fe–10Cr alloy showed a considerable departure from the parabolic behaviour whereas MC alloy continued to follow parabolic kinetics.
3. The considerable difference in the oxidation kinetics between NC and MC alloys after the initial period is also manifest in some stark differences in colour of the oxidised samples.
4. It is interesting that the colour of the NC alloy changed considerably after the initial period in spite of no significant weight gain.

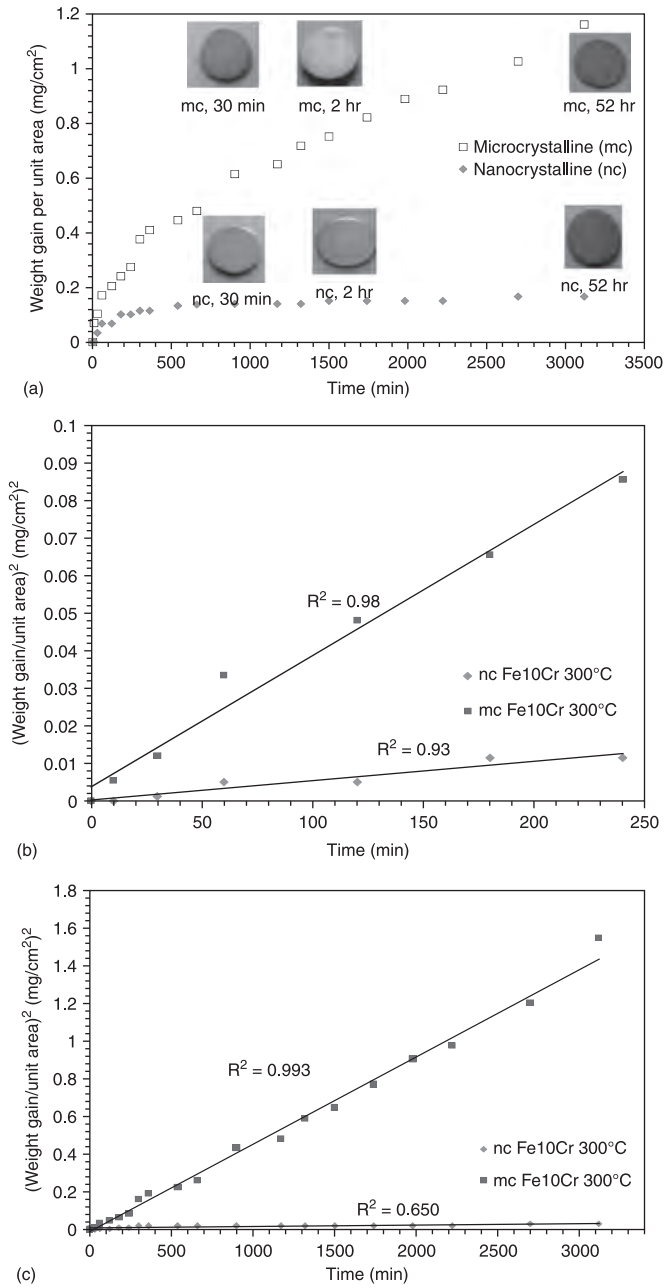

6.4 Oxidation kinetics of NC and MC Fe–10Cr alloys, oxidised at 300°C: (a) weight gain vs. time plots for 3120 min, (b) weight gain^2 with time, suggesting parabolic kinetics for MC alloy but departure from parabolic kinetics for NC alloy, and (c) weight gain^2 with time (up to 240 min), suggesting parabolic kinetics for both MC and NC alloys.[5, 95]

In this study, it has been possible to provide a concrete understanding of the remarkable difference in the oxidation kinetics. Interested readers are encouraged to refer to an elaborate description elsewhere;[5] however, brief descriptions of the oxidation kinetics and colour evolution at 300°C are provided below.

In order to investigate the reason for the considerable difference in oxidation rates (Fig. 6.4) of the NC and MC states of the same alloy composition (Fe–10%Cr alloy), oxide scales were characterised. As described earlier, the oxidation resistance of Fe–Cr alloys is associated primarily with the chemical characteristics and the Cr content of the thin inner oxide scale. Depth profiles for Cr, Fe and O were generated using secondary ion mass spectroscopy (SIMS). Thin oxide films formed over NC and MC Fe–10wt%Cr alloy during air oxidation (30 min/300°C) were characterised by SIMS depth profiling. Typical depth profiles for Cr, O and Fe for the oxidised specimens are presented respectively in Fig. 6.5(a), (b) and (c). A comparison of the Fe, O and Cr profiles for the two specimens suggests the oxide film developed on MC Fe–10Cr alloy to be considerably thicker. Fe and O profiles of the two low-Cr alloys would suggest a greater Fe and O content in the case of the outer scale of NC Fe–10Cr alloy. The greater content of Fe-rich oxide in NC Fe–10Cr alloy is attributed to a greater grain boundary oxidation in the initial stages, due to the far greater grain boundary area at the surface of a nanometric grain size material as compared with the MC alloy of the same composition.

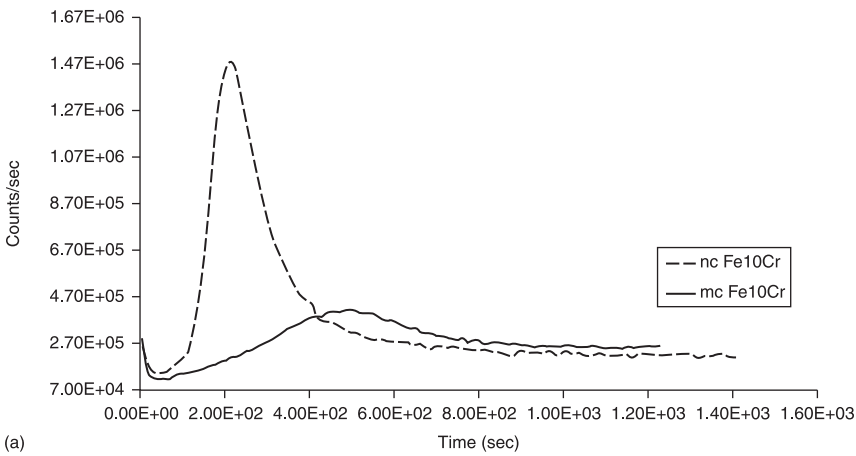

6.5 (a) SIMS depth profile for Cr in oxidised samples of Fe–10%Cr NC and MC alloys, using Cs^+ primary beam; (b) SIMS depth profile for O in oxidised samples of Fe–10%Cr NC and MC alloys, using Cs^+ primary beam; (c) SIMS depth profile for Fe in oxidised samples of Fe–10%Cr NC and MC alloys, using Cs^+ primary beam.[95]

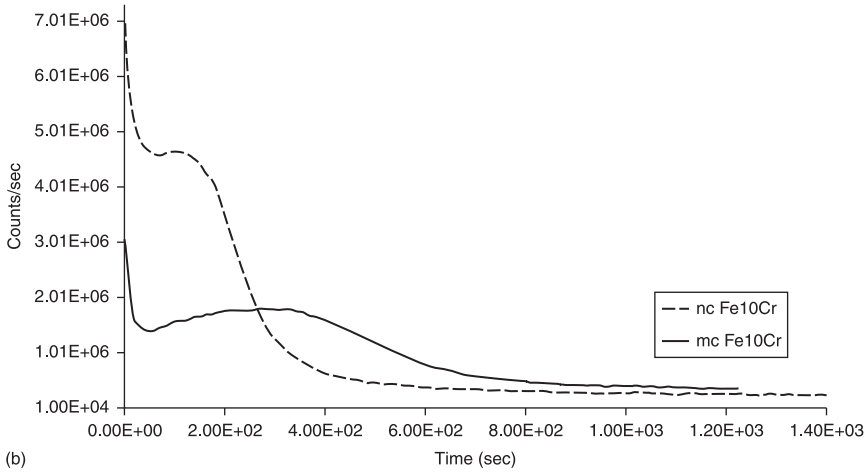

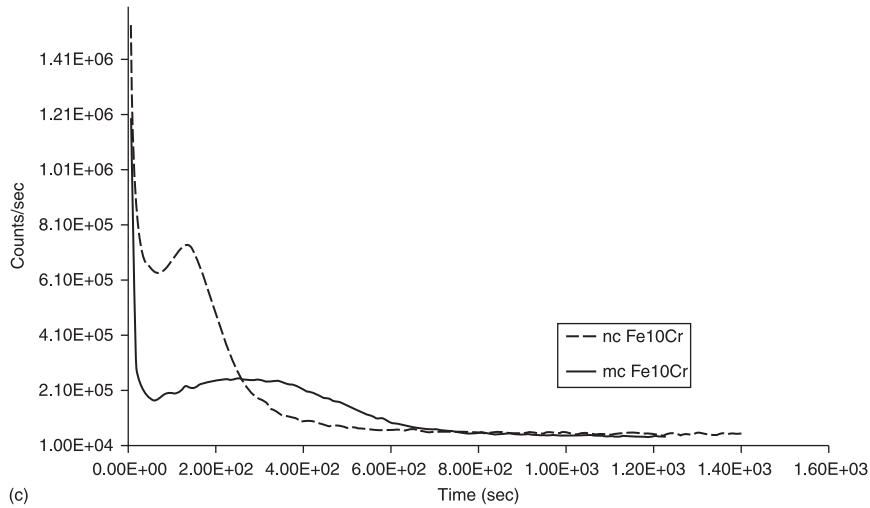

6.5 Continued.

The most notable finding of the SIMS profiles is that the highest Cr content of the inner layer of NC Fe–10Cr alloy is considerably higher (>4 times) than the highest Cr content in the inner layer of MC Fe–10Cr alloy. The remarkably higher Cr content of the inner oxide layer on NC Fe–10Cr alloy (as established in Fig. 6.5(a)) has been found to be comparable to the chromium content of the inner oxide layer that develops on a Fe–20Cr MC alloy[5] (which is well known to establish a protective layer of Cr_2O_3). Thus, it was inferred that the NC Fe–10Cr

alloy developed a protective oxide layer of Cr_2O_3, in spite of its considerably low chromium content. As the reported literature[98–101] would suggest, the inner oxide layer of MC alloys with low Cr (<12%) would at best be a mixed spinel type Fe–Cr oxide. Such low chromium alloys would fail to develop a Cr_2O_3 layer.[98] It seems that the remarkably greater oxidation rate of MC Fe–10Cr alloy (as compared with NC Fe–10Cr alloy) can be explained on the basis of the considerably higher Cr content of the inner oxide layer and possible development of the protective oxide layer of Cr_2O_3 over the latter. As a result of the considerable difference in chemical composition (chromium content) and the thickness of the oxide scales developed over the NC and MC Fe-10Cr alloys, the colour of the pellets of the two materials oxidised for over 3000 min is distinctly different.[5]

Comparison of the SIMS depth profiles for oxygen for NC and MC Fe–10Cr alloys (Fig. 6.5(b)) suggests that the oxide scale developed over NC alloy has: (i) less thickness (as a result of less effective protective scale, as discussed above), and (ii) somewhat greater overall oxygen content (on the basis of the areas under the two profiles). However, a careful comparison of the oxygen profiles with Fe and Cr profiles (Fig. 6.5(a)–(c)) would suggest that the location of the peak for O corresponds more to the peak for Fe in the NC alloy, owing to the greater grain boundary oxidation of Fe in the early stages of oxidation of the NC alloy, as discussed earlier. At the peak location for Cr the oxygen content is considerably less. So, the apparently greater oxygen content of the peak is largely associated with the greater grain boundary oxidation of Fe in the early stages. The eventual diffusion-assisted establishment of the Cr_2O_3 layer ensures that the oxidation rate of this alloy is considerably lower. On the other hand, the O, Fe and Cr profiles for the MC alloy would suggest the inner scale to be a mixed oxide of Fe and Cr, which is much less protective than the inner scale on the NC alloy, as described earlier.

For developing an understanding of how the considerably greater oxidation resistance of NC Fe–10Cr alloy (in comparison with MC Fe–10Cr alloy) compares with the resistance of an alloy with a much higher Cr content, samples of NC and MC Fe–20Cr alloys were also oxidised at 300, 350 and 400°C for durations up to 3120 min. The weight gains of these alloys at 300°C were too low to be detected by the gravimetric balance used for this study. However, it was possible to characterise the chemical composition of the thin oxide scales developed at the two temperatures. Oxidation kinetics of NC and MC Fe–20Cr alloys at 350°C[5] suggest only a little improvement in oxidation resistance due to the NC structure. However, what is most relevant to note is that the weight gains and the Cr contents of the inner oxide scale at the end of the 3120 minute oxidation of MC Fe–20Cr alloy were similar to those of the NC Fe–10Cr alloy at 350°C, suggesting the degree of oxidation resistance conferred by the NC structure at only 10% chromium to be similar to that of the alloy with twice as much chromium but a MC structure.

Fe–Cr alloys with considerably lower chromium content have demonstrated a remarkable oxidation resistance at 300 to 400°C as a result of the NC structure.[5] The NC structure enhances diffusion and thus accounts for the improved oxidation resistance. In simplistic terms, one would expect this trend to continue with increasing temperature. However, the stability of the NC structure at higher temperatures (for example, the grain growth shown in Fig. 6.3) may become an issue. Another factor will be the balance between the increasing growth rate of non-protective external oxide and the chromium supply; this aspect needs to be investigated in detail.

6.6 Conclusions

As a result of their extremely fine grain size, NC metals and alloys possess remarkably different properties. However, because such materials have poor thermal stability and are highly susceptible to grain growth, their large scale processing is a challenge. Alloys containing elements that can form protective oxide scale (namely, Cr, Si and Al) have shown superior resistance to degradation due to gaseous corrosion at moderately high temperatures. Recent studies have established that the NC structure possesses a remarkably superior resistance to oxidation of an Fe–10Cr alloy (than its MC counterpart) at moderately high temperatures (300 to 400°C). This behaviour has been convincingly attributed to the much greater diffusivity of chromium in the NC alloy and, as result, the ability of the NC alloy to develop a protective layer of chromium oxide (in spite of only 10 wt% Cr in the alloy).

6.7 Acknowledgements

The motivation for accomplishing this chapter came from experimental and theoretical work of recent years on corrosion/oxidation of NC alloys in the author Raman Singh's group. This program received funding support from Australian Research Council's Discovery Projects scheme and has benefitted immensely from a collaboration with Professor Carl Koch (North Carolina State University) for synthesis of the NC alloys, as well as from the dedicated work of past and present graduate students, Dr Rajeev Gupta and Mr B.V. Mahesh.

6.8 References

1. Siegel R. W. *NanoStructured Materials* 1994; **4**:121.
2. Suryanarayana C. and Froes F. H. *Metal. Mater. Trans. A* 1992; **23A**: 1071.
3. Schaefer H. E., Würschum R., Birringer R. and Gleiter H. *Structure and Properties of nanometer sized solids – Physical research*. To be published (reference from *Scripta Metallurgical et Materi* 1990; **24**: 1347).
4. Koch C. C., Youssef K. M., Scattergood R. O. and Murty K. L. *Advanced Eng. Mater.* 2005; **7**: 787.
5. Singh Raman R. K., Gupta R. K., and Koch C. C. *Philosophical Magazine* 2010; **90**: 3233.

6. Rofagha R., Erb U., Ostrander D., Palumbo G. and Aust K. *NanoStructured Materials* 1993; **2**: 1.
7. Kirchheim R., Huang X. Y., Cui P., Birringer R. and Gleiter H. *NanoStructured Materials* 1992; **1**: 167.
8. Gleiter H. *Progress in Materials Science* 1989; **33**: 223.
9. Siegel R. W. *NanoStructured Materials* 1991; **3**: 1.
10. Siegel R. W. *Annu. Rev. Mater. Sci.* 1991; **21**: 559.
11. Thomas G. J., Siegel R. W. and Eastman J. A. *Scripta metallurgica* 1990; **24**: 201.
12. Siegel R. W. *MRS Bull*. 1990; **15**: 60.
13. Siegel R. W. *Mater. Sci and Engineering A* 1993; **A68**: 189.
14. Fecht H. J. *NanoStructured Materials* 1992; **1**: 125.
15. Zhu X., Birringer R., Herr U. and Gleiter H. *Phys. Rev. B* 1987; **35**: 9085.
16. Haubold T., Birringer R., Lengeler B. and Gleiter H. *Phys. Lett. A* 1989; **135**: 461.
17. Mutschele T. and Kirchheim R. *Scripta Materialia* 1987; **21**: 1101.
18. Horvath J., Birringer R. and Gleiter H. *Solid State Comm*. 1987; **62**: 319.
19. Wallner G., Jorra E., Franz H., Peisl J., Birringer R. *et al. Mater. Res. Symp. Proc*. 1989; **132**: 149.
20. Gleiter H. *Acta Mater.* 2000; **48**: 1.
21. Kumar K. S., Swygenhoven H. V. and Suresh S. *Acta Mater.* 2003; **51**: 5743.
22. Suryanarayana C., Mukhopadhyay D., Patnkar S. N. and Froes F. H. *J. Mater. Res.* 1992; **7**: 2114.
23. Meyers M. A., Mishra A. and Benson D. J. *Prog. Mater. Sci*. 2006; **51**: 427.
24. Birringer R. *Mater. Sci. and Engineering* 1989; **A117**: 33.
25. Bonetti E., Bianco L. D., Pasquini L. and Sampaolesi E. *NanoStructured Materials* 1999; **12**: 685.
26. Moelle C. H. and Fecht H. J. *NanoStructured Materials* 1995; **6**: 421.
27. Malow T. R. and Koch C. C. *Acta Mater.* 1997; **45**: 2177.
28. Perez R. J., Jiang H. G., Dogan C. P. and Lavernia E. J. *Metall. Mater. Trans. A* 1998; **29A**: 2468.
29. Natter H., Schmelzer M., Loeffler M. S. and Hempelmann R. *Materials Science Forum* 2000; **343–6**: 683.
30. Perez R. J., Jiang H. G. and Lavernuia E. J. *NanoStructured Materials* 1997; **9**: 71.
31. Gupta R. K., Singh Raman R. K. and Koch C. C. *Materials Science and Engineering A* 2008; **494**: 253.
32. Song X., Zhang J., Li L., Yang K. and Liu G. *Acta Mater*. 2006; **54**: 5541.
33. Omuro K., Miura H. and Ogawa H. *Materials Science Forum* 1999; **318–20**: 701.
34. Tanimoto H., Farber P., Würschum R., Valiev R. Z. and Schaefer H. E. *NanoStructured Materials* 1999; **12**: 681.
35. Trapp S., Limbach C. T., Gonser U., Campbell S. J and Gleiter H. *Physical Review Letters* 1995; **75**: 3760.
36. Hernando A., Cebollada A., Menendez J. L. and Briones F. *Electronic transport in nanocrystalline iron: A low T magnetoresistance effect*. Vol. 262. San Diego: Elsevier, 2003; p.1.
37. Fougere G. E., Weertman J. R. and Siegel R. W. *NanoStructured Materials* 1995; **5**: 127.
38. Segers D., Petegem S. V., Loffler J. F., Swygenhoven H. V., Wagner W. *et al*., *NanoStructured Materials* 1999; **12**: 1059.
39. Natter H., Schmelzer M., Loeffler M. S., Krill C.E., Fitch A. *et al*., *Journal of Physical Chemistry B* 2000; **104**: 2467.
40. Karimpoor A. A., Erb U., Aust K. T. and Palumbo G. *Scripta Mater.* 2003; **49**: 651.

41. Malow T. R. and Koch C. C. *Metall. Mater. Trans. A* 1998; **29A**: 2285.
42. Malow T. R. and Koch C. C. *Acta Mater.* 1998; **46**: 6459.
43. Khan A. S., Zhang H. and Takacs L. *Int. J. Plasticity* 2000; **16**: 1459.
44. Chen B., Penwell D., Kruger M. B., Yue A. F. and Fultz B. *J. Appl. Phys.* 2001; **89**: 4794.
45. Fecht H. J., Hellstern E., Fu Z. and Johnson W. L. *Metall. Mater. Trans. A* 1990; **21A**: 2333.
46. Daroczi L., Beke D. L., Posgay G., Zhou G. F. and Bakker H. *NanoStructured Materials* 1993; **2**: 515.
47. Sinha P. and Collins G. S. *Hyperfine Interactions* 1994; **92**: 949.
48. Bonetti E., Bianco L. D., Fiorani D., Rinaldi D., Caciuffo R. *et al*., *Physical Review Letters* 1999; **83**: 2829.
49. Bonetti E., Scipione G., Valdre S., Enzo S., Frattini R. *et al*., *Journal of Materials Science* 1995; **30**: 2220.
50. Malow T. R., Koch C. C., Miraglia P. Q. and Murty K. L. *Mater. Sci. and Engineering* 1998; **A252**: 36.
51. Szabo S., Beke D. L., Harasztosi L., Daroczi L., Posgay G. *et al*., *NanoStructured Materials* 1997; **9**: 527.
52. Elkedim O., Cao H. S. and Fluzin P. *Materials Science Forum* 1999: 312.
53. Elkedim O., Cao H. S., Meunier C. and Gaffet E. *Materials Science Forum* 1998: 269–72.
54. Tian H. H. and Atzmon M. *Acta Mater*. 1999; **47**: 1255.
55. Sobczak E., Swilem Y., Dorozhkin N. N., Nietubyc R., Dluzewski P. *et al*., *J. Alloys Compd.* 2001; **328**: 57.
56. Cheng S., Ma E., Wang Y. M., Kecskes L. J., Youssef K. M. *et al.*, *Acta Mater.* 2005; **53**: 1521.
57. Koch C. C. *Rev. Adv. Mater. Sci*. 2003; **5**: 91.
58. Hibbard G. D. Proc. 15th Int. Symposium: Processing and Fabrication of Advanced Materials. Cincinnati: MS&T; 2006, p. 297.
59. Seo J. H., *Mater. Sci. Forum* 2005; **475–9**: 3483.
60. Youssef K. M., Scattergood R. O., Murty K. L., Horton J. A. and Koch C. C. *Appl. Phys. Lett.* 2005; **87**(091904): 1–3.
61. Youssef K. M., Scattergood R. O., Murty K. L. and Koch C. C. *Scripta Materialia* 2006; **54**: 251.
62. Groza J. R. 'Nanocrystalline Powder Consolidation Methods' in *Nanostructured Materials: Processing, Properties, and Applications*, ed. C. C. Koch. Norwich, NY: William Andrew Pub.; 2007.
63. Youssef K. M., Scattergood R. O., Murty K. L. and Koch C. C. *Applied Physics Letters* 2004: **85**.
64. Elkedim O., Cao H. S. and Guay D. *Journal of Materials Processing Technology* 2002; **121**: 383.
65. Guruswamy S., Michael R. L. Srisukhumbowornchai N., Michael K. M. and Joseph P. T. *IEEE Trans* 2000; **36**: 3219.
66. Siegel R. W. *Materials Science Forum* 1997; **235–8**: 851.
67. de Keijster T. H., Longford J. I., Mittemeijer E. J. and Vogel A. B. P., *J. Appl. Crystallography* 1982; **15**: 308.
68. Barbucci A., Farne G., Matteazzi P., Riccieri R. and Cerisola G. *Corros. Sci.* 1999; **41**: 463.
69. Aledresse A. and Alfantazi A. *J. Materials Science* 2004; **39**:1523.
70. Yamashita M., Mimaki S., Hashimoto S. and Miura H. *Philos. Mag. A* 1991; **63**: 707.
71. Mauer R., Erb U. and Gleiter H. *Mater. Sci. and Engineering* 1984; **63**: L13.

72. Kim S. H., Aust K. T., Erb U., Gonzalez F. and Palumbo G., *Scripta Mater*. 2003; **48**: 1379.
73. Rofagha R., Langer R., El-Sherik A. M., Erb U., Palumbo G. *et al*., *Scripta Metall. Mater.* 1991; **25**: 2867.
74. Jung H. and Alfantazi A. *Electrochimica Acta* 2006; **51**: 236.
75. Palumbo G., Gonzalez F., Brennenstuhl A. M., Erb U., Shmayda W. *et al*., *NanoStructured Materials* 1997; **9**: 737.
76. Wang L., Lin Y., Zeng Z., Liu W., Xue Q. *et al*., *Electrochimica Acta* 2007; **52**: 4342.
77. Vinogradov A., Mimaki T., Hashimoto S. and Valiev R. *Materials Science Forum* 1999; **312–4**: 641.
78. Thorpe S. J., Ramaswami B. and Aust K. T. *J. Electrochem. Soc.* 1988; **135**: 2162.
79. Cheng D., Tellkamp V. L., Lavernia C. J. and Lavernia E. J. *Annals of Biomedical Engineering* 2001; **29**: 803.
80. Vinogradov A., Mimaki T., Hashimoto S. and Valiev R. *Materials Science Forum* 1999; **312–14**: 641.
81. Lu L., Wang L. N., Ding B. Z. and Lu K. *Mater. Sci. and Engineering* 2000; **A286**: 125.
82. Wang S., Rofagha R., Roberge P. R. and Erb U. *Electrochem. Soc. Proc.* 1995; **95–8**: 244.
83. Tang P. T., Watanabe T., Anderson J. and Bech-Nielsen G. J. *Appl. Electrochem*. 1995; **25**: 347.
84. Liu L., Li Y. and Wang F. *Electrochimica Acta* 2007.
85. Ghosh S. K., Dey G. K., Dusane R. O. and Grover A. K. *Journal of Alloys and Compounds* 2006; **426**: 235.
86. Gonzalez F., Brennenstuhl A. M., Palumbo G. and Erb U. *Mater. Sci. Forum* 1996; **225–7**: 831.
87. Tong H. Y., Shi F. G. and Lavernia E. J. *Scripta Metall. Mater.* 1995; **32**: 511.
88. Ye W., Li Y. and Wang F. *Electrochimica Acta* 2006; **51**: 4426.
89. Meng G., Li Y. and Wang F. *Electrochimica Acta* 2006; **51**: 4277.
90. Kwok C. T., Cheng F. T., Man H. C and Ding W. H. *Materials Letters* 2006; **60**: 2419.
91. Wang X. Y. and Li D. Y. *Electrochimica Acta* 2002; **47**: 3939.
92. Kofstad P. *High Temperature Corrosion*. New York: Elsevier; 1988.
93. Wagner C. J. *Electrochem. Soc*. 1952; **369**: 103.
94. El Kedim O., Paris S., Phigni C., Bernard F., Gaffet E. *et al*., *Mater. Sci. Eng.* 2004; **A369**: 49.
95. Singh Raman R. K. and Gupta R. K. *Corrosion Science* 2009; **51**: 316.
96. Leistikow S., Wolf I. and Grabke H. J. *Werkst. Korros.* 1987; **38**: 556.
97. Shida Y., Ohtsuka N., Muriama J., Fujino N. and Fujikawa H. Proc. JIMS-3, High Temp. Corros., *Trans. Jap. Inst. Met.*, 1983; 631.
98. Singh Raman R. K. *Metallurgical and Materials Transactions A* 1995; **26A**: 1847.
99. Singh Raman R. K. *Metallurgical and Materials Transactions A* 1998; **28A**: 577.
100. Singh Raman R. K, Khanna A. S. and Gnanamoorthy J. B., *J. Mater. Sci. Letters* 1990; **9**: 353.
101. Singh Raman R. K, Gnanamoorthy J. B and Roy S. K. *Trans. Indian Inst. Metals* 1992; **46**: 391.

7

High temperature oxidation protection using nanocrystalline coatings

W. GAO and Z. LI, The University of Auckland, New Zealand and
Y. HE, University of Science and Technology Beijing, China

Abstract: This is an overview of the research work at The University of Auckland in collaboration with the University of Science and Technology Beijing on the development of nanostructured coating systems for protection of alloys from high temperature oxidation. The first section will cover the preparation of nanocrystalline metallic coatings by unbalanced magnetron sputtering and electro-spark deposition. The effect of grain size reduction on the selective oxidation of alloys, and the growth of protective oxide scales such as Al_2O_3 and Cr_2O_3 on the external surfaces at elevated temperatures, will be discussed. The second part will be focused on our recent progress on fabrication and characterization of ceramic coatings with nanostructural features; in particular, multilayered and composite oxide coatings for applications in high temperature oxidation protection.

Key words: oxidation, deposition, coating, sputtering, ceramic, nanomaterials.

7.1 Introduction

Thermodynamically, when exposed to high temperature atmospheres, most metals will be oxidized through extensive reactions with carbon, nitrogen, oxygen or sulfur. Oxidation of metallic structural components inevitably results in the regression of the load-bearing cross-section and eventually leads to premature failure of the structure. In this respect, the oxidation of metals should be prevented by every means.

Metals and alloys for high temperature applications are therefore commonly incorporated with certain alloying elements to improve their resistance to oxidation attack (Wood and Stott, 1987). The principle is that, when the concentration of these elements exceeds a critical value, selective oxidation will take place to develop an external scale exclusively composed of their oxides (Fig. 7.1). Aluminum (Al), chromium (Cr) and sometimes silicon (Si) are typical examples of this practice since their oxides, Al_2O_3, Cr_2O_3 and SiO_2, have low defect concentration and are stable at high temperatures. A scale of these oxides can be an effective barrier to the diffusion of reactants, therefore inhibiting internal oxide precipitation and significantly decreasing reaction rate (lower metal consumption) and protecting the underlying substrate from further attack as long as this scale is integral and adherent during service.

A higher content of the alloying element will then be beneficial to the establishment and maintenance of the protective oxide scale of excellent oxidation

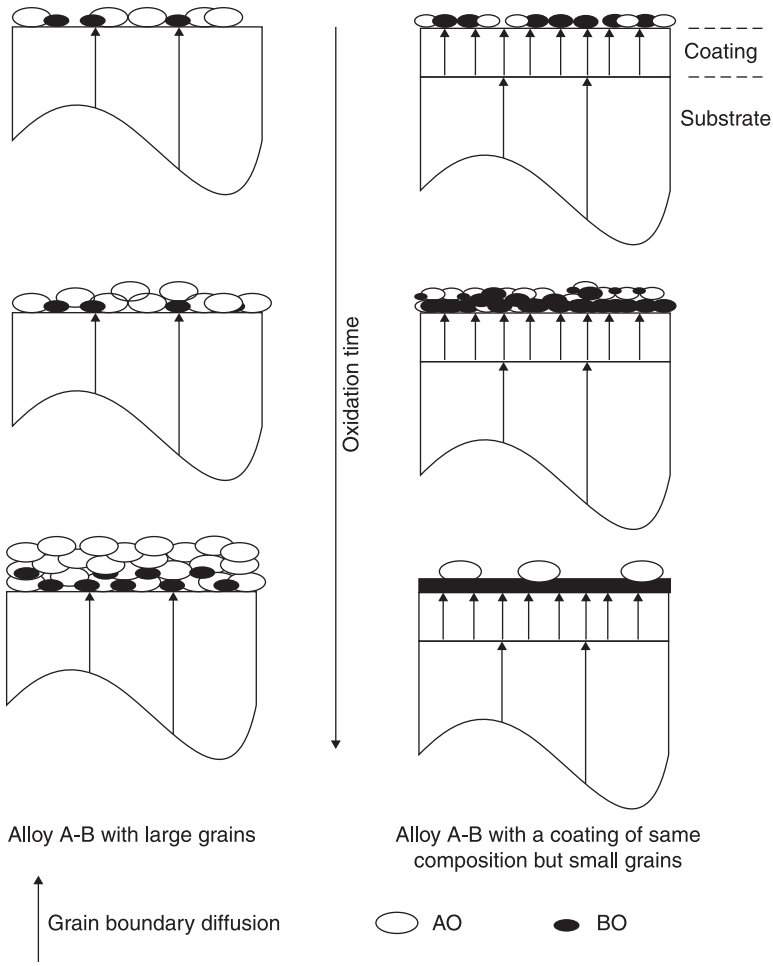

7.1 Enhanced selective oxidation of binary alloy A-B by grain size reduction.

resistance. However, it does have adverse effects on the machinability of alloys. A typical example is that Al content is normally lower than ~6wt% in order to make a balance between mechanical and environmental performance of high temperature alloys. This amount, however, cannot always ensure the re-healing of a protective Al_2O_3 scale when subjected to thermal cycling or mechanical impact.

Nanocrystalline materials often possess unique properties that are different from their large grain sized counterparts (Vollath, 2008). These materials are finding more and more applications, particularly in electronic, photonic, magnetic and biomedical fields (Gogotsi, 2006). In the 1990s it had been noticed that size reduction, i.e. microcrystallization and nanocrystallization, could promote

selective processing and enhance the high temperature oxidation resistance of many alloys (Wang and Lou, 1990; Lou *et al.*, 1992; Gao *et al.*, 2001). In this chapter, progress in research on development of oxidation resistant alloy, alloy-oxide and ceramic coatings with nanocrystal and microcrystal grains will be reviewed in brief. A vast array of literature is available on this topic, and the focus will therefore be confined to the collaborative investigation work of The University of Auckland (UOA), New Zealand, and the University of Science and Technology Beijing (USTB), China.

7.2 High temperature oxidation resistant metallic coatings

In the development of high temperature alloy systems, the application of a coating onto a metallic substrate is one of the popular approaches proposed to meet the different requirements of mechanical and oxidation performance. More importantly, this approach is cost-effective because the material in the coating (higher oxidation resistance but higher materials cost) normally is only about 0.01 to 2% of the material in the bulk.

High temperature oxidation resistant coatings can be applied onto their substrates through many chemical and physical techniques. The typical examples can be chemical vapor deposition (CVD), physical vapor deposition (PVD), cladding, electrochemical deposition, sol–gel and laser/electron beam surface treatment (Goldstein, 1997). Composition, grain size and thickness of these coatings can be modulated in a wide range through processing control so that they can meet the requirements of different working conditions. In our studies, magnetron sputtering, electro-spark deposition, sol–gel and modified pack cementation were used to produce metallic and ceramic coatings for protection of various alloys against high temperature corrosion.

7.2.1 Coating deposition

Coatings by magnetron sputtering

Unbalanced magnetron sputtering, a popular PVD technique, was used by the authors' group to deposit microcrystalline and nanocrystalline coatings with a wide range of compositions onto various alloy substrates. A distinct advantage of sputtering deposition is that the grain size, composition and structure of the coating can be easily tuned through the control of working gas pressure, power density forwarded to the target, substrate to target distance, bias applied to the substrate and target configuration (Mattox, 2010).

The correlation between argon (Ar) pressure, growth rate and grain size had been established for the deposition of Ni–Cr–Al coatings (Liu *et al.*, 1997, 1998a). It was revealed that the deposition rate increased with Ar pressure in the chamber.

The relationship between coating grain size and Ar pressure was approximately parabolic, with a maximum grain size (~600 nm) at a pressure of 15–20 mTorr. Grain size as small as ~50 nm can be obtained with a low Ar pressure of 2–5 mTorr.

Co-deposition and reactive deposition can also be readily performed with unbalanced magnetron sputtering. In our studies, co-deposition was mainly achieved by sputtering from two targets in a face-to-face configuration, or from a composite target containing separate smaller parts of different alloys or metals. The control of the composition of these coatings was mainly achieved through adjusting the densities of power forwarded to the different targets, or the constitution (ratio of surface areas) of the composite target. Reactive deposition was performed in an atmosphere containing working gas, e.g. inert argon, and reactive gas, e.g. oxygen or nitrogen. Metal-oxide or metal-nitride coatings can be produced if the pressure of the reactive gas is higher than the critical pressure for complete reactive sputtering. Our results indicated that the co-deposited FeCrNi–Al coatings normally had a uniform structural characteristic and an average grain size of ~100 nm (He *et al.*, 2000). On the other hand, the coatings of reactive deposition showed the formation of clusters of ~500 nm, each of which, however, appeared to consist of many smaller grains.

Coatings by electro-spark deposition

Electro-spark deposition (ESD) is a technique that uses the highly concentrated electrical energy stored in capacitors to initialize electro-sparks between anode and cathode. The high temperature generated by the spark results in partial melting and/or mixing of the superficial layer of the electrode and/or substrate materials (depending on the type of electrode material used). During the interval between two electro-sparks, the small amount of molten material solidifies rapidly to form a coating layer. This method was originally designed to produce hard and wear-resistant surface coatings for machine parts (Dahotre *et al.*, 1995). Because of the benefits of fast melting and solidification, it has been recently modified by the authors' group to produce oxidation resistant nanocrystalline and microcrystalline coatings with well-controlled compositions, favorable microstructures and strong metallurgical bonding to substrate (Li *et al.*, 2000). This technique has the advantage of using simple and portable equipment.

The latest version of ESD, series double-pole electro-pulse discharge (SEPD), connected both poles of the power supply to two depositing electrodes between which the substrate was located as an electrostatic induction electrode. It changed the established manner of discharging fields in traditional ESD processes and deposition took place with two pairs of electrodes, leading to significantly increased deposition efficiency (Xu *et al.*, 2002a, 2002b).

Nanocrystalline and microcrystalline alloy coatings with grain sizes of 50 to 500 nm can be established quickly on relative large surfaces. Oxide nanoparticles can be applied onto the substrate so that oxide dispersive strengthening (ODS)

alloy coatings can be produced (see Fig. 7.2) (He *et al.*, 2002). The small additions of reactive element oxides in alloys can improve the spallation resistance and reduce the growth rate of oxide scales. This technique has been proven to be very successful for the fabrication of a variety of coating systems, such as Ni–20Cr, Fe–18Cr–8Ni, Ti–Al and Fe–Cr–Ni–Al–Y_2O_3 (He *et al.*, 2000; Li *et al.*, 2001a; He *et al.*, 2002; Li *et al.*, 2003).

Mechanical action enhanced technique

Recently, a combined pack aluminizing and ball peening process was developed by the authors' group (collaborative research at USTB and UOA) to produce nanostructured aluminide intermetallic coatings on carbon steel, stainless steel and/or Ni-based superalloys at a relatively low operating temperature (440–600°C) and in a short time (15–120 min) (see Fig. 7.3) (Zhan *et al.*, 2006a,

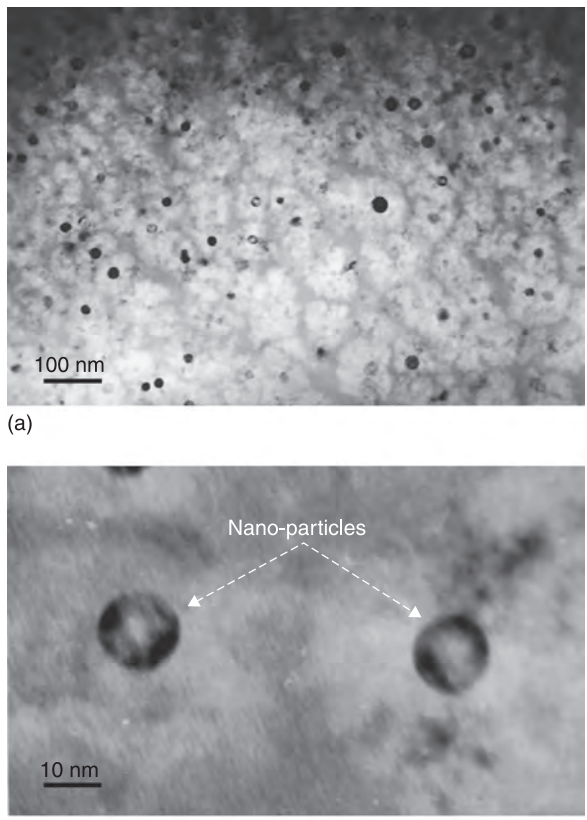

7.2 (a) Microstructure of nanosized oxide particles in the oxide dispersion coatings. (b) shows two typical oxide particles with a spherical shape at a higher magnification. The composition of these particles is very similar to $YAlO_3$, analyzed by EDS.

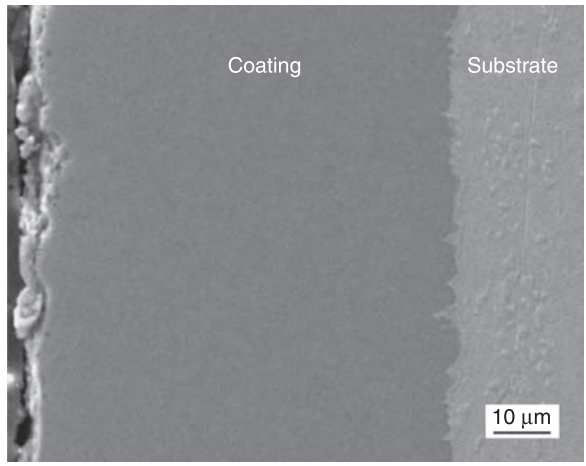

7.3 Cross-sectional morphology of a nanocrystalline Fe–Al intermetallic coating formed on carbon steel at 560°C for 90 min.

2006b, 2006c, 2006d, 2007, 2009). In this process, small alloy balls were added into a retort containing Al powder, filler and activator. The last three were used for conventional pack cementation. The retort heated in a furnace was then vibrated by a mechanical vibrator (see Fig. 7.4). The formation of aluminide coatings in this process was believed to typically occur through the following four steps:

1. Strong impact from vibrating balls led to welding of Al particles onto the substrate and an Al-rich layer was formed on the surface.
2. Random-directional ball peening also induced severe plastic deformation of the substrate and cleavage of grains, resulting in the formation of a large amount of structural defects such as dislocation lines and parallel slip bands in grains, dense dislocation walls in grain boundaries and cleavage crystals. These defects greatly accelerated atomic diffusion. Local high temperature at the impact zones also promoted atomic diffusion, leading to the nucleation aluminide phases at grain boundaries and other structural defects. An initial layer was formed on the substrate surface as a result of repeated impact of balls.
3. Grains of the aluminide phased in the initial alloy layer were refined by subsequent ball impact and another Al-layer was formed on the top.
4. Diffusion of aluminum and substrate elements took place between the newly formed Al-layer and the initial alloy layer. The inward diffusion of aluminum was hindered by the coarse grains of the substrate, while the outward diffusion of the substrate elements was enhanced along the large amount of grain boundaries and defects in the alloy layer. The continuous ball impact may cause a series of reactions, including breaking the Al-rich layer on the surface, causing a more homogeneous and dense microstructure.

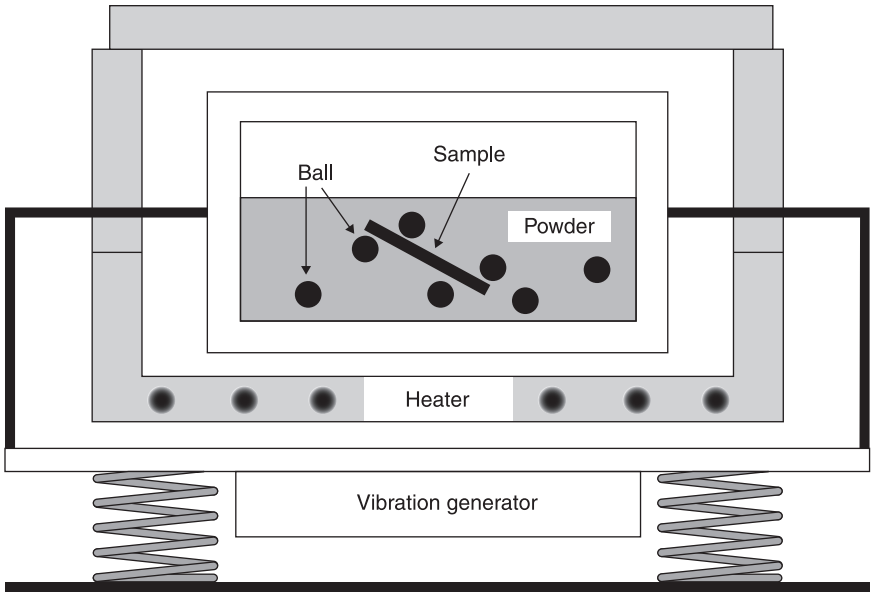

7.4 A schematic diagram of the equipment for coating fabrication with mechanical action.

It can be seen that in this process surface nanostructuring induced by ball peening and atomic diffusion were carried out simultaneously, thus eliminating grain growth in post-heat treatment. The formation of the coatings is related to plastic deformation, grain refinement, atomic diffusion and new phase nucleation and growth and is very different from conventional pack aluminizing.

Detailed transmission electron microscopy (TEM) observation with coatings formed on carbon steels revealed irregularly shaped nanocrystals of random crystallographic orientations and a wide size distribution (see Fig. 7.5). The large crystals were about 100 to 150 nm in size (region A in Fig. 7.5(a)) and the small ones were about 30 to 50 nm (region B in Fig. 7.5(a)), all with well-defined grain boundaries. Inside the large crystals, ultrafine cells could be seen as well. The formation of these nanocrystals was attributed to the plastic deformation induced by ball peening. Grain refinement was realized by dislocation reactions and brittle fracture. Dislocation walls transformed to sub-grain boundaries and large-angle grain boundaries with increasing deformation. Ultrafine equiaxed grains with random crystallographic orientations and narrow size distribution (20–35 nm) were also observed. These types of nanocrystals were not reported with other surface mechanical nanostructuring treatment. They were developed through a thermodynamics process, i.e. chemical reaction, atomic diffusion and nucleation of new phases, instead of by plastic deformation.

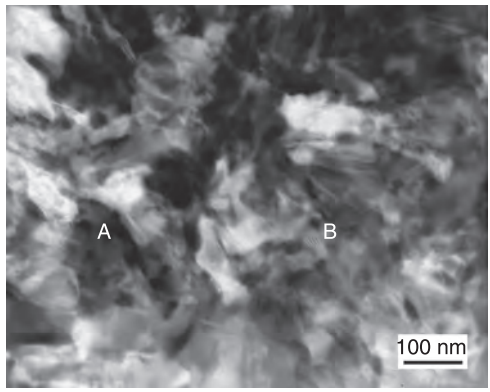

(a)

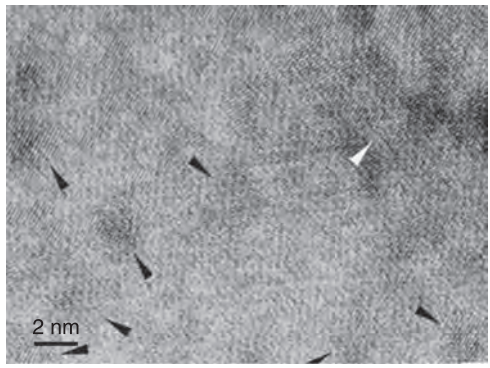

(b)

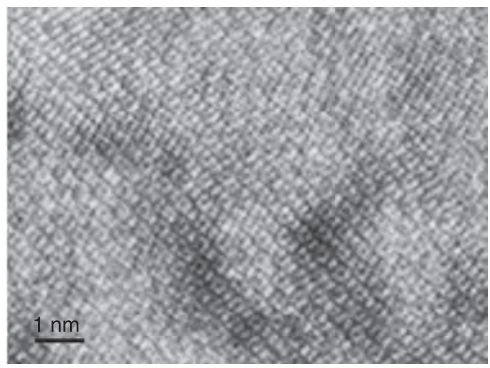

(c)

7.5 TEM characterization of nanostructured Fe-Al produced by a combined pack-aluminizing and ball peening process. (a) Shows the nanocrystallites formed in the grain boundary areas. They are exhibiting irregular shapes, random crystallographic orientations and a wide size distribution (100–150 nm in region A and 30–50 nm in region B). (b) Shows the structure of cubic shaped crystallites with different orientations. (c) A HRTEM image, indicates that the cubic cells in (b) are exhibiting square shape and parallel array with almost same orientation.

7.2.2 Selective oxidation of nanocrystalline coatings

As mentioned in the previous section, high temperature alloys mainly rely on the formation and maintenance of a protective oxide scale on their external surfaces. This can be achieved if the content of the alloying (or solute) element in the substrate is higher than a critical value. According to the classical selective oxidation theory developed by Wagner (1959), the minimum content of the solute metal, N_M, for the formation of an exclusive external oxide scale is estimated as:

$$N_M = \left(\frac{\pi g N_O D_O V_m}{3 D_M V_{ox}} \right)^{1/2} \quad [7.1]$$

where g is a constant, $N_O D_O$ is the oxygen permeability in the alloy, V_m is the molar volume of the alloy, D_M is the diffusion coefficient of the solute metal in the alloy and V_{ox} is the molar volume of the oxide.

This equation therefore indicates that an increase in the outward diffusion of the alloying element would decrease the minimum content of the desired alloy component if all other factors were unchanged. One of the most important advantages of nanocrystalline coatings compared with their large grain sized counterparts is their ability to enhance short-circuit diffusion through their much higher density of grain boundaries. Mathematical models based on simultaneous diffusion through the crystal lattice and grain boundary have been established to predict selective oxidation behavior and to describe oxidation kinetics of nanostructured alloys (Liu *et al.*, 1998a, 2000). These models showed a good agreement with the experimental results obtained by the authors and other researchers.

In Ni–20Cr–Al, a typical high temperature alloy system, >6 wt% Al, is normally required to form a protective Al_2O_3 scale (Wallwork and Hed, 1971). If the Al content is lower than this, complex oxides consisting of Cr_2O_3, $NiCr_2O_4$ and internal Al_2O_3 precipitates form, resulting in high oxide scale growth rates and poor oxidation resistance. With grain size reduction, the critical Al content can be substantially reduced. In the authors' group, Ni–20Cr–*x*Al coatings of different grain sizes and Al contents were produced by magnetron sputtering. Isothermal oxidation testing results indicated that, when the grain size of Ni–20Cr–Al coatings was at the level of ~60 nm, alloys containing ~2 wt% Al could form a complete α-Al_2O_3 scale at 1000°C in air (Liu *et al.*, 1998a). This is only one-third of the amount required in a large-grained alloy and is a direct result of enhanced Al outward diffusion through the higher density of grain boundaries in the nanocrystalline coating.

For Fe–Ni–Cr–Al alloys (310SS) of normal grain size, a scale composed of both alumina (internal) and chromia (external) was formed during oxidation when their Al content was around 5 wt%. When the coatings have a nanocrystalline

structure, an even smaller amount of Al (~3.36 wt%) could produce an alumina external scale, indicating that the selective oxidation of Al was greatly promoted by nanostructuring (Liu *et al.*, 1999a, 1999b).

Ni_3Al is a marginal Al_2O_3-forming alloy and its selective oxidation behavior depends on a number of factors such as alloy composition, oxidation temperature and microstructure. For example, NiO was formed as the main oxidation product at 900°C, while $NiAl_2O_4$ and Al_2O_3 were formed with increasing temperatures (Kuenzly and Douglass, 1974). On the other hand, the Ni_3Al + 5% Cr and Ni_3Al + 5% Cr + 0.3% Y (wt%) coatings showed very different oxidation behaviors. The oxides detected after oxidation at 900°C and 1050 to 1200°C were θ-Al_2O_3 and α-Al_2O_3, respectively. This phenomenon indicated that the selective oxidation of Al had also been promoted (Liu and Gao, 2001).

Similar effects could also be observed with coating grain size reduction through the ESD process (Xu *et al.*, 2002a, 2002b). The oxide scale formed on the uncoated Fe–18Cr–8Ni steel was composed of NiO, $FeCr_2O_4$ and a small amount of Cr_2O_3. The oxide scale on the alloy coating, on the other hand, consisted mainly of Cr_2O_3 with a small amount of Fe_3O_4 while Cr_2O_3 was the main oxide formed on the alloy coating with dispersive Y_2O_3 nanoparticles.

7.2.3 Improved oxide scale spallation resistance

An external oxide scale should be established quickly when exposed to a high temperature atmosphere. However, this is not the only requirement for a highly protective oxide scale, since most alloys for high temperature applications will be subjected to heating and cooling cycles during service. This oxide scale must be strong, tough and adherent to its substrate. A common problem for many oxide scales is that they can be protective at the initial stage but tend to crack or spall after long periods of exposure. This is particularly true when the parts experience shocks during thermal cycles. Physical failure of the originally protective oxide scale results in the growth of another oxide scale of lower protection capability from the substrate depleted of the alloying element, substantially reducing the service life of the parts.

Experimental observations showed that the oxide scales formed on nanocrystalline and microcrystalline coatings normally demonstrated a much higher resistance to cracking and spallation than those formed on a substrate alloy of coarse grains. This was supported by cyclic and long-term oxidation tests with coatings of Ni–Cr, Fe–Cr–Ni, Fe–Cr–Ni–Al, Ni–Cr–Al, FeAl, NiAl and TiAl intermetallic compounds. Failure and spallation of thermally grown oxide scale is a complex process influenced by many chemical and mechanical factors. The mechanisms behind the enhanced scale spallation resistance through nanocrystallization or microcrystallization are also complicated. The following might apply, according to our experimental results.

Firstly, grain size reduction down to nanoscale levels can promote selective oxidation of alloying elements and a complete and thin oxide scale can be

established in shorter periods and provide higher protection. For example, α-Al_2O_3 was formed on Ni–Cr–Al and Fe–Cr–Ni–Al while Cr_2O_3 was observed on Ni–Cr and Fe–Cr–Ni nanocrystalline and microcrystalline coatings. On large-grained alloys, complex scales composed of oxides of Al, Cr, Ni and Fe were formed with internal precipitates. In comparison with those scales grown on fine-grained coatings, these oxide scales were thicker and less protective and had a higher probability of premature failure.

Secondly, temperature change during heating–cooling cycles will develop severe thermal stresses in both oxide scale and substrate as a result of their different coefficients of thermal expansion (CTEs). Metals usually have a greater linear CTE than oxides. Therefore, the oxide scale will experience an average compressive stress during cooling and the metallic substrate has a tensile stress. The compressive stress accumulated has to be released through some mechanism. The most damaging way is the physical failure of scale, i.e. local detachment, crack and/or partial spallation. Alternatively, the plastic deformation of oxide scales and metal substrates could contribute to the release of the compressive stress and influence the adhesion of oxide scales to their substrates. At high temperatures, the creep rate of oxide scales or metals can be estimated as (Kofstad, 1988):

$$\varepsilon = \frac{\sigma\Omega}{d^2 kT} \cdot \left(B_1 D_V + \frac{B_2 \delta D_B}{d} \right) \qquad [7.2]$$

where σ is the applied tensile stress, Ω is the atomic volume, d is the average grain size, B_1 and B_2 are constants, D_V and D_B are the diffusion coefficients along grain boundaries and through lattice, δ is the width of grain boundaries and k is the Boltzmann constant.

It can be seen that ε is inversely proportional to d^3. Thus, a small grain size of the alloy and oxide would favor a higher creep rate. Coatings produced by magnetron sputtering and ESD are composed of nanocrystals and microcrystals. As a direct consequence, oxide scales grown from these coatings also consist of very fine oxides due to the increased heterogeneous nucleation rate. The diffusion creep rate may be much higher in the scale and coating of smaller grains than in the large-sized scale and alloy substrate. Consequently, they may release stress more effectively through plastic deformation.

In addition, the coatings produced by ESD have a metallurgical bonding to their substrates. The interface between coating and substrate is not sharp and the compositional and structural changes in this area are not abrupt. The mechanical mismatch between oxide scale and underlying coating could therefore be minimized, favoring a higher interfacial stability during thermal cycling.

Spallation of oxide scale may occur when the elastic strain energy contained within that part of the scale is equal to the energy required to form new surfaces from the underlying oxide–metal interface (Evans, 1995):

$$\lambda^2 \xi W^* \geq \lambda^2 \gamma_F$$
$$\gamma_F = \gamma_{ox} + \gamma_M - \gamma_{oxM} \quad [7.3]$$

where γ_F is the fracture energy per unit area of the interface, γ_{ox} and γ_M are the surface energies of the oxide and the metal, respectively. γ_{oxM} is the energy of the oxide–metal interface, λ is the spacing between shear cracks, and W^* is the elastic energy.

During sputtering deposition, bombardment of high-energy particles to the growing coating surface produces compressive stress in the coating. This could also introduce more structural defects into the surface. The surface energy of the coating is believed to be higher than the surface of the alloy without surface coating. The value of γ_F may therefore be increased to a higher level that can stand higher elastic energy accumulated in thermal cycling.

Thirdly, the nanocrystalline/microcrystalline structure of the coatings can increase oxide nucleation at grain boundary areas. A distinct feature of the coatings produced by magnetron sputtering is the formation of columnar grain structures. Oxides could grow inwardly along this long and vertical grain boundary and form into pegs that can strongly hold the oxide scales in place and therefore allow the oxide–metal interface to withstand high stress. This so-called 'micro-pegging' effect results in a better scale adhesion to the metal substrate (see Fig. 7.6) (Liu and Gao, 2001).

In addition, oxide scales of ridge network are commonly formed on sputtering deposited Al-containing coatings. It is believed that this ridge structure may also

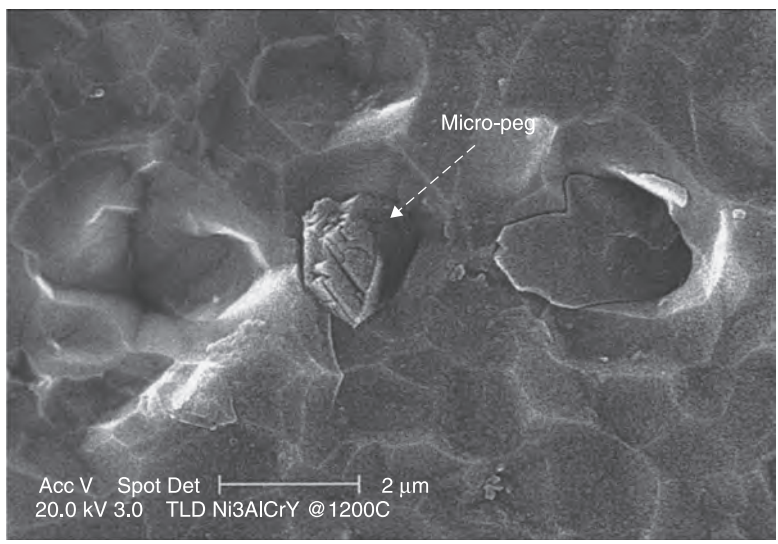

7.6 Micro-pegs and pits formed at the oxide–metal interface of the Ni_3Al +Y coating produced by magnetron sputtering (50 hours of oxidation at 1200°C in a pure oxygen atmosphere).

grow into the metallic substrate due to the inward diffusion of oxygen. The inward grown ridges, therefore, can also play a role in scale–metal contraction to further improve the scale adhesion and spallation resistance.

Finally, large voids or thermal grooves could be observed on the exposed oxide–metal interface of large grain sized alloys, such as cast FeAl, Ni_3Al and NiAl (Smialek, 1978; Hindam and Smeltzer, 1980; Taniguchi *et al.*, 1986; Grabke, 1999). In contrast with this, few voids were observed at the interface between oxide scale and nanocrystalline/microcrystalline coatings after oxidation. These voids will impair the interfacial bonding strength since the oxide–metal contact area is reduced. Growth of Al_2O_3 scales on fine-grained Ni–Al alloys, particularly on those containing rare earth elements (e.g. Y), was typically dominated by the inward diffusion of oxygen rather than outward diffusion of alloying element. This behavior favors a tighter interfacial contact between oxide scale and substrate (Liu and Gao, 2001).

7.3 Ceramic coatings for high temperature oxidation protection

Grain size reduction can significantly increase the outward diffusion of the alloying element through short circuits and therefore decrease its critical amount for selective oxidation. From Wagner's theory, it can also be seen that a decrease of the oxygen permeability in the alloy could also achieve the same goal. Another approach used in our studies is hence to inhibit oxygen diffusion by applying ceramic coatings onto alloy substrates.

Ceramics are candidates for numerous applications in high temperature corrosive environments. Oxides, such as alumina and zirconia, are the dominant ceramic compounds because of their generally refractory character and high chemical stability at elevated temperatures in the presence of an oxygen-containing atmosphere. Specifically, Al_2O_3 coatings can act as a barrier to the inward diffusion of oxygen while rare earth element oxides (e.g. ZrO_2 and Y_2O_3) may suppress the outward diffusion of metallic ions through the thermally grown oxide scale. Coatings based on these oxides have therefore been applied onto various metals and alloys through many techniques to improve high temperature oxidation resistance of the alloy substrate. These techniques typically include CVD, PVD, electrophoresis, electrochemical deposition and sol–gel.

7.3.1 Multilayered coatings

Multilayered coating systems we discuss here are composed of alternate layers of two or more different types of materials. The thickness of each sub-layer is in the range of a few nanometers to sub-micrometer level. The spacing between two layers is so small that the defect size and dislocation movement can be effectively

suppressed by the interfaces, so that the properties of these multilayered coatings are different from those of the single-layer coatings (Celis *et al.*, 1995; Levin *et al.*, 1995). These properties may include fracture strength and toughness, fatigue and impact strengths. It is believed that this laminated structure would retard inward oxygen diffusion effectively, leading to improved high temperature corrosion resistance for the underlying substrates.

In the authors' group, a technique combining electrochemical deposition and sintering has successfully produced ZrO_2/Al_2O_3 and $(ZrO_2–Y_2O_3)/(Al_2O_3–Y_2O_3)$ based multilayered composite coatings on steel substrates (Yao *et al.*, 2007a, 2007b; Gao *et al.*, 2010). The thickness of each layer was in the range of 80–500 nm and the coating was composed of grains with an average diameter of ~40 nm (see Fig. 7.7). In these coating systems, ZrO_2 or $ZrO_2–Y_2O_3$ sub-layers are to provide

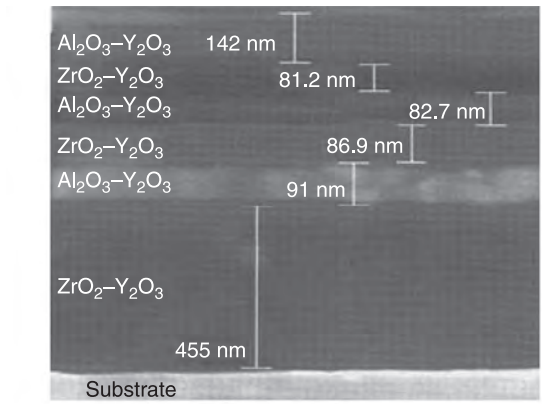

(a)

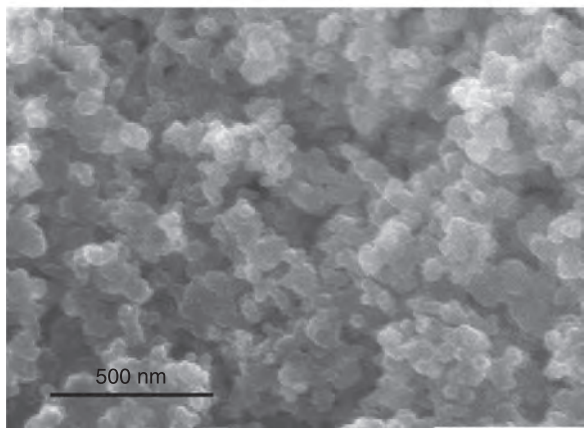

(b)

7.7 $(ZrO_2–Y_2O_3)/(Al_2O_3–Y_2O_3)$ composite coating with six sub-layers: (a) cross-section and (b) top surface.

resistance to thermal shock and enhance the adhesion between the thermally grown oxide scale and alloy substrate, since the coefficient of thermal expansion of ZrO_2–Y_2O_3 is very close to that of many alloys. The layer containing $A1_2O_3$ is to reduce ion and oxygen diffusion since it has good stoichiometry. In addition, nanosized/microsized oxide particles on the alloy surface can influence the nucleation process at the initial oxidation stage and change the mass transfer mechanism in the process of oxidation, thus promoting the selective oxidation of Cr in the alloy substrate, reducing the formation of holes at the interface and improving the adhesion of the scale to the substrate (He and Stott, 1994, 1996; Li *et al.*, 2001b).

Oxidation tests at 900°C showed that these multi-laminated coatings could provide higher oxidation resistance than the monolithic ZrO_2–Y_2O_3 or $A1_2O_3$–Y_2O_3 coatings. Further, the oxidation resistance increased with the number of laminated layers. For example, the oxide scale formed on the uncoated Fe–25Cr–9Ni–N alloy was mainly composed of Fe and Cr oxides, while $A1_2O_3$ and Cr_2O_3 were detected on the coated alloys. However, it was noticed that the oxidation mass gain for steels coated with these multilayered coatings still showed breakdown behavior after a certain time period, though the improvement in scale spallation resistance lasted a longer time. This might be related to a thermal mismatch between the sub-layers containing Al_2O_3 and ZrO_2. Thus, it is believed that, although this type of coating containing alternating nano- and micro-sub-layers of different ceramics may provide a new approach for development of high temperature coatings with both low oxidation rate and high thermal shock resistance, the process procedures and materials must be optimized to achieve better performance.

7.3.2 Composite coatings

Another strategy, therefore, is to develop composite coatings that consist of microsized oxide particles as skeleton (to establish a thick coating) and nanosized oxide particles that occupy the spaces between large particles (to inhibit oxygen diffusion through these fast routes) (see Fig. 7.8). The oxides for the large and small particles are carefully selected to achieve a) a better thermal match between coating and alloy substrate under thermal cyclic conditions, thus improved resistance to scale failure; and b) an effective barrier to inward oxygen diffusion.

In a typical procedure, nano- and microsized particles were dispersed into a sol–gel solution by high energy ball milling. Microsized particles were surrounded by the nanosized particles precipitated from the sol–gel solution, forming composite clusters (see Fig. 7.9) (Yao *et al.*, 2005). This composite structure can reduce the aggregation tendency of the nanostructured particles. This green product was then applied onto steel substrate by painting or electrophoretic deposition. Dense and uniform composite coatings (Al_2O_3–Y_2O_3, Al_2O_3–ZrO_2, ZrO_2–Y_2O_3 and Al_2O_3–ZrO_2+Y_2O_3) of various thicknesses (2–300 μm) were then successfully produced by sintering assisted by a variety of techniques, such as

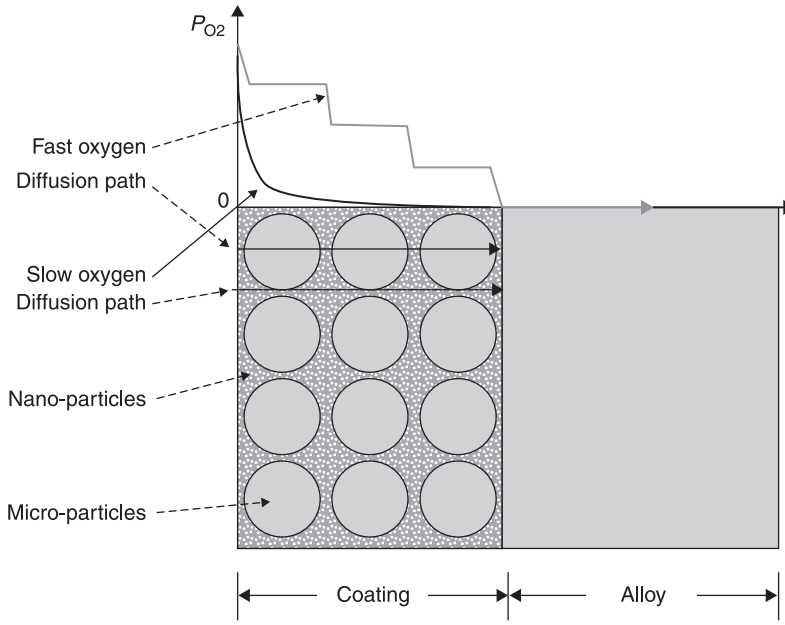

7.8 A schematic showing different oxygen diffusion paths in composite coatings.

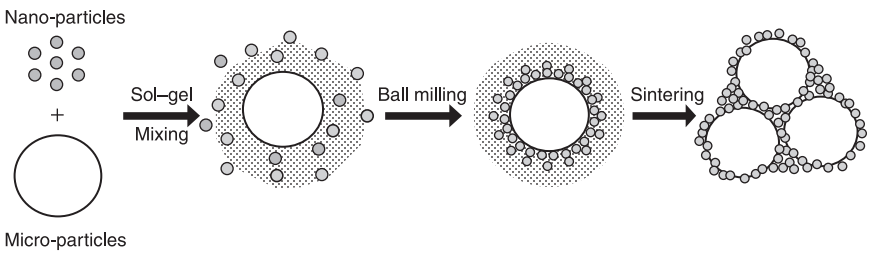

7.9 A schematic showing the formation of composite particles by high-energy ball milling of the sol–gel derived precursors.

thermal pressure filtration, centrifugal force and microwave (Yao *et al.*, 2006; He *et al.*, 2006; Yao *et al.*, 2007; Ren *et al.*, 2010) on stainless steel and Ni-based superalloys.

Oxidation test using 1Cr13 alloy coated with YPSZ-Al_2O_3 (Yttria Partially Stabilized Zirconia–Alumina) composite coatings in air at 900°C clearly showed that oxidation mass gain and oxide scale spallation decreased with an increase of the YPSZ-Al_2O_3 ratio (see Fig. 7.10). This type of coating can be applied onto

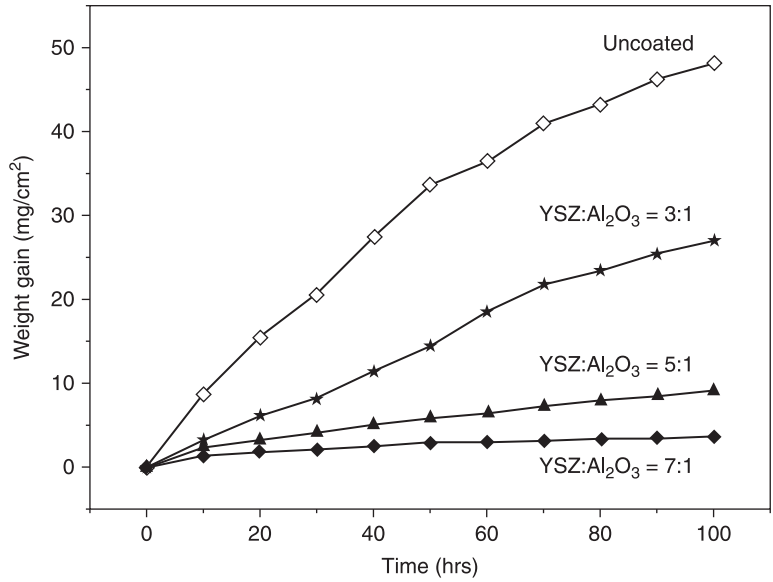

(a)

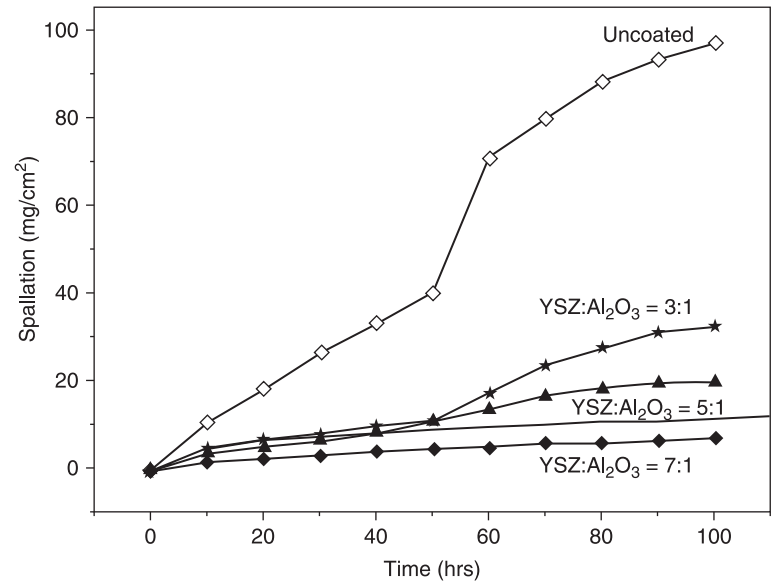

(b)

7.10 Oxidation kinetics (a) and oxide scale spallation (b) of 1Cr13 alloy coated with YPSZ–Al_2O_3 composite coatings at 900°C in air.

various alloys to improve their resistance to oxidation at high temperature if the ratio of different oxide components can be adjusted to balance the chemical, mechanical and thermal requirements. It can also be used as an ideal interlayer in the thermal barrier coating system to improve the adhesions at both the interfaces of coating/thermally-grown oxide (TGO) and TGO/MCrAlY.

7.4 Conclusions

We have demonstrated two strategies for improving the oxidation resistance of alloys exposed to high temperatures, i.e. the increase of outward diffusion of the alloying element to promote its selective oxidation and fast formation of an external protective oxide scale, and the decrease of inward oxygen diffusion through ceramic coatings of low diffusivity. Nanocrystalline and microcrystalline coatings possess superior performance in these applications. First, the nanostructured alloy coatings can provide much higher density of grain boundaries and other structural defects for short-circuit diffusion. Adhesion and spallation resistance of the thin and complete oxide scales grown on these coatings can also be significantly improved through effective stress release and mechanical holding effects endowed by fine grain oxide scales.

Ceramic coatings with a multilayered structure can effectively inhibit oxygen diffusion while those composite coatings with both micro- and nanosized oxide particles can provide an effective barrier for oxygen diffusion and concurrently minimize thermal mismatches between coating and alloy substrate by adjusting the phase ratio and microstructure. Processing techniques developed in the authors' lab are capable of producing dense, uniform and crack-free coatings of well-controlled thickness that can have wide application in the protection of high temperature structural components.

7.5 Acknowledgements

The authors thank their collaborators and group members for their invaluable contributions, particularly Drs F. Wang, Z. Liu and H. Gong.

7.6 References

Celis J., Van Acker K., Callewaert K. and Van Houtte P. (1995), 'Residual stress measurements in electrolytic copper-nickel compositionally modulated multilayers', *J. Electrochem. Soc.*, **142**, 70–4.

Dahotre N., Hampikian J. and Striglich J. (1995), *Elevated temperature coatings: science and technology*. Warrendale, PA: Minerals, Metals and Materials Society.

Evans H. (1995), 'Stress effects in high-temperature oxidation of metals', *Int. Mater. Rev.*, **40**, 1–40.

Gao J., He Y. and Wang D. (2010), 'Fabrication and high temperature oxidation resistance of ZrO_2/Al_2O_3 micro-laminated coatings on stainless steel', *Mater. Chem. Phys.*, **123**, 731–6.

Gao W., Liu Z. and Li Z. (2001), 'Nano- and microcrystal coatings and their high-temperature applications', *Adv. Mater.*, **13**, 1001–4.

Gogotsi Y. (2006), *Nanomaterials handbook*. Raton, FL: Taylor & Francis.

Goldstein A. (1997), *Handbook of nanophase materials*. New York: Marcel Dekker.

Grabke H. (1999), 'Oxidation of NiAl and FeAl', *Intermetallics*, **7**, 1153–8.

He K., Gong H., Li Z. and Gao W. (2000), 'Oxidation behavior of stainless steel-A1 coatings produced by co-sputtering and reactive sputtering', *Mater. Lett*., **46**, 53–9.

He Y. and Stott F. (1994), 'The selective oxidation of Ni-15%Cr and Ni-10%Cr alloy promoted by surface-applied thin oxide films', *Corros. Sci*., **36**, 1869–84.

He Y. and Stott F. (1996), 'The effects of thin surface-applied oxide coatings on the selective oxidation of alloys', *Corros. Sci.*, **38**, 1853–68.

He Y., Huang Z., Qi H., Wang D., Li Z. *et al*., (2000), 'Oxidation behavior of micro-crystalline Ni-20Cr-Y_2O_3 ODS alloy coatings', *Mater. Lett.*, **45**, 79–85.

He Y., Pang H., Qi H., Wang D., Li Z. *et al*., (2002), 'Micro-crystalline Fe-Cr-Ni-Al-Y_2O_3 ODS alloy coatings produced by high frequency electric-spark deposition', *Mater. Sci. Eng. A*, **334**, 179–86.

He Y., Zhang K., Li L. and Wang D. (2006), 'Nano-/micro-composite ceramic coatings prepared by thermal pressure filtration of sol–gel paints', *Int. J. Modern Phys. B*, **20**, 4649–54.

Hindam H. and Smeltzer W. (1980), 'Growth and microstructure of α-Al_2O_3 on β-NiAl', *J. Electrochem. Soc.*, **127**, 1630–5.

Kofstad P. (1988), *High temperature corrosion*. London: Elsevier.

Kuenzly J. and Douglass D. (1974), 'Oxidation mechanism of Ni_3Al containing yttrium', *Oxid. Met.*, **8**, 139–78.

Levin I., Kaplan W., Brandon D. and Layyou A. (1995), 'Effect of SiC submicrometer particle size and content on fracture-toughness of alumina-SiC nanocomposites', *J. Am. Ceram. Soc.*, **78**, 254–6.

Li Z., Gao W., Kwok P. and He Y. (2000), 'Electro-spark deposition coatings for high temperature oxidation resistance', *High Temp. Mater. Proc.*, **19**, 443–58.

Li Z., Gao W. and He Y. (2001a), 'Protection of a Ti_3Al-Nb alloy by electro-spark deposition coating', *Scripta Mater.*, **45**, 1099–105.

Li Z., Gao W. and He Y. (2001b), 'Oxidation behavior of a Ti_3Al-Nb alloy with surface thin oxide films', *Oxid. Met*., **56**, 495–516.

Li Z., Gao W., Yoshihara M. and He Y. (2003), 'Improving oxidation resistance of Ti_3Al and TiAl intermetallic compounds with electro-spark deposit coatings', *Mater. Sci. Eng. A*, **347**, 243–52.

Liu Z., Gao W., Dahm K. and Wang F. (1997), 'The effect of coating grain size on the selective oxidation behaviour of Ni-Cr-Al alloy', *Scripta Mater.*, **37**, 1551–8.

Liu Z., Gao W., Dahm K. and Wang F. (1998a), 'Oxidation behavior of sputter-deposited Ni-Cr-Al micro-crystalline coatings', *Acta Mater.*, **46**, 1691–700.

Liu Z., Gao W. and Wang F. (1998b), 'Oxidation behavior of FeAl intermetallic coatings produced by magnetron sputter deposition', *Scripta Mater.*, **39**, 1497–502.

Liu Z., Gao W. and Li M. (1999a), 'Cyclic oxidation of sputter-deposited nanocrystalline Fe-Cr-Ni-Al alloy coatings', *Oxid. Met.*, **51**, 403–19.

Liu Z., Gao W. and He Y. (1999b), 'Oxidation behaviour of nanocrystalline Fe-Ni-Cr-Al alloy coatings', *Mater. Sci. Technol.*, **15**, 1447–50.

Liu Z., Gao W. and He Y. (2000), 'Modeling of oxidation kinetics of Y-doped Fe-Cr-Al alloys', *Oxid. Met*., **53**, 341–50.

Liu Z. and Gao W. (2001), 'Oxidation behavior of cast Ni_3Al alloys and microcrystalline Ni_3Al + 5% Cr coatings with and without Y. doping', *Oxid. Met.*, **55**, 481–504.
Lou H., Wang F., Xia B. and Zhang L. (1992), 'High-temperature oxidation resistance of sputtered micro-grain superalloy K38G', *Oxid. Met.*, **38**, 299–307.
Mattox D. (2010), *Handbook of physical vapor deposition (PVD) processing* (2nd Edition). Norwich, NY: William Andrew – Elsevier Science.
Ren C., He Y. and Wang D. (2010), 'Al_2O_3/YSZ composite coatings prepared by a novel sol-gel process and their high-temperature oxidation resistance', *Oxid. Met.*, DOI 10.1007/s11085-010-9210-x.
Smialek J. (1978), 'Oxide morphology and spalling model for NiAl', *Metall. Trans. A*, **9**, 309–20.
Taniguchi S., Shibata T. and Tsuruoka H. (1986), 'Isothermal oxidation behaviour of Ni_3Al-0.1B base alloys containing Ti, Zr, or Hf additions', *Oxid. Met.*, **26**, 1–17.
Vollath D. (2008), *Nanomaterials: an introduction to synthesis, properties and application*. Weinheim: Wiley-VCH.
Wagner C. (1959), 'Reaktionstypen bei der oxydation von legierungen', *Z. Elektrochem.*, **63**, 772–90.
Wallwork G. and Hed A. (1971), 'Some limiting factors in use of alloys at high temperatures', *Oxid. Met.*, **3**, 171–84.
Wang F. and Lou H. (1990), 'Oxidation behavior and scale morphology of normal-grained CoCrAl alloy and its sputtered microcrystalline coating', *Mater. Sci. Eng. A*, **129**, 279–85.
Wood G. and Stott F. (1987), 'Oxidation of alloys', *Mater. Sci. Technol.*, **3**, 519–30.
Xu Q., He Y., Qi H., Wang D., Li Z. *et al.* (2002a), 'Oxidation behavior of micro- and nano-crystalline coatings deposited by series double-pole electro-pulse discharge', *Mater. Lett.*, **56**, 85–92.
Xu Q., He Y., Qi H., Wang D., Li Z. *et al.*, (2002b), 'Microcrystalline coatings deposited by series double-pole electro-pulse discharge and its high-temperature oxidation behavior', *Science in China E*, **45**, 477–84.
Yao M., He Y., Zhang W. and Gao W. (2005), 'Oxidation resistance of boiler steels with Al_2O_3-Y_2O_3 nano- and micro-composite coatings produced by sol–gel process', *Mater. Trans.*, **46**, 2089–92.
Yao M., He Y., Zhang Y. and Yang Q. (2006), 'Al_2O_3-Y_2O_3 Nano- and micro-composite coatings on Fe-9Cr-Mo alloy', *J Rare Earths*, **24**, 587–90.
Yao M., He Y., Wang D. and Gao W. (2007a), 'Nano/micro-laminated (ZrO_2-Y_2O_3)/(Al_2O_3-Y_2O_3) composite coatings and their oxidation resistance', *Oxid. Met.*, **68**, 1–8.
Yao M., Li F., Zhang Y. and He Y. (2007b), 'Micro-laminated (ZrO_2-Y_2O_3)/(Al_2O_3-Y_2O_3) coatings on Fe-25Cr alloy and their high temperature oxidation resistance', *Surf. Rev. Lett.*, **14**, 499–505.
Yao M., He Y. and Zhang Y. (2007c), 'Nano- and microcomposite Al_2O_3-Y_2O_3 coatings produced by sol-gel process', *J. Dispers. Sci. Technol.*, **28**, 219–22.
Zhan Z., He Y., Wang D. and Gao W. (2006a), 'Preparation of aluminide coatings at relatively low temperatures', *Trans. Nonferrous Met. Soc. China*, **16**, 647–53.
Zhan Z., He Y., Wang D. and Gao W. (2006b), 'Low-temperature processing of Fe-Al intermetallic coatings assisted by ball milling', *Intermetallics*, **14**, 75–81.
Zhan Z., He Y., Wang D. and Gao W. (2006c), 'Micro-/nano-crystal aluminized ODS coatings', *Mater. Sci. Forum.*, **522–3**, 323–30.
Zhan Z., He Y., Wang D. and Gao W. (2006d), 'Nanocrystalline iron-aluminum coatings assisted by ball peening processes', *Int. J. Nanosci.*, **5**, 775–80.

Zhan Z., He Y., Wang D. and Gao W. (2007), 'Aluminide coatings formed on Fe-13Cr steel at low temperature and its oxidation resistance', *Oxid. Met.*, **68**, 243–51.
Zhan Z., He Y., Li L., Liu H. and Dai Y. (2009), 'Low-temperature formation and oxidation resistance of ultrafine aluminide coatings on Ni-base superalloy', *Surf. Coat. Technol.*, **203**, 2337–42.

8

Nanocoatings to improve the tribocorrosion performance of materials

T. S. N. SANKARA NARAYANAN, National Metallurgical Laboratory, India

Abstract: Tribocorrosion is the degradation of materials caused by simultaneous mechanical and chemical/electrochemical interactions between surfaces in relative motion, resulting in irreversible transformation of materials or of their functions. The present chapter addresses the role of nanomaterials in tribocorrosion. It focuses on the ability of nanoparticles to provide a lubricating effect, and the usefulness of nanostructured coatings such as thermally sprayed FeCu/WC–Co and WC–Co coatings, electrodeposited Ni–Co alloy, Ni–nano SiC, electroless Ni–P–nano SiC coatings and nanostructured titanium in improving the tribocorrosion performance of materials. The limitations of using nanoparticles and nanostructured coatings under tribocorrosion conditions are also addressed.

Key words: tribocorrosion, nanoparticles, nanocrystalline coatings, free corrosion potential, fretting corrosion, microabrasion corrosion.

8.1 Introduction

8.1.1 Nanomaterials

Materials with a grain size of <100 nm are classified as nanomaterials (Gleiter, 1989, 1992; Suryanarayana, 1995; Suryanarayana and Koch, 1999, 2000; Suryanarayana, 2005). Their unique atomic structure, i.e. the presence of a large volume fraction of intercrystalline components (as much as 50% of the total crystal volume) such as grain boundaries and triple junctions, and the reduction in grain size, make them fundamentally different from more commonly known polycrystalline and amorphous materials. Nanomaterials offer unique physical and mechanical properties such as high hardness and strength, enhanced electrical resistivity, higher thermal expansion coefficient, higher heat capacity, improved tribological properties, better fatigue properties, superplasticity at low temperature, etc, compared with their glassy and/or crystalline counterparts with the same chemical composition (Gleiter, 1989, 1992; Lu, 1996; Koch *et al.*, 1999; Lu *et al.*, 2000; Koch, 2003a; Meyers *et al.*, 2006; Koch *et al.*, 2007).

Numerous methods, which include inert gas condensation, high energy ball-milling, flame pyrolysis, electron beam vapour deposition, rapid solidification, reactive sputtering, chemical vapor deposition, sol–gel technique, microemulsion, co-precipitation, hydrothermal method, spark erosion and electrodeposition, are available for the synthesis of nanocrystalline materials (Koch, 2003b;

Suryanarayana, 2001, 2004, 2005; Koch *et al.*, 2007; Suryanarayana and Prabhu, 2007; Gurrappa and Binder, 2008). Nanostructured materials find widespread applications; the most promising among them are hydrogen storage in the form of metal hydrides and microspheres that can be injected into the body and, upon illumination, help to destroy tumors (Suryanarayana, 2005).

8.1.2 Tribocorrosion

Tribocorrosion is defined as the science of surface transformations resulting from the interaction of mechanical loading and chemical/electrochemical reactions that occur between various elements of a tribosystem exposed to a corrosive environment. It combines the mechanical and chemical interactions of body, counterbody, interfacial medium and the environment, including friction, lubrication, wear and tribologically activated chemical and electrochemical reactions. Fig. 8.1 depicts the various types of contact modes and schematic representations of tribological contacts involving simultaneous mechanical and chemical effects.

Tribocorrosion leads to irreversible transformation of materials or of their functions because of the simultaneous mechanical and chemical/electrochemical interactions between surfaces in relative motion. Tribocorrosion degradation affects components in numerous industries such as mining, mineral processing, biomedical, automobile, food, nuclear, offshore, marine, oil and gas production, etc. However, it is found to be beneficial in chemical–mechanical planarization (CMP) of wafers in the electronics industry and in metal grinding or cutting in presence of aqueous emulsions. Hence, it is important to understand the interaction of mechanical wear and chemical/electrochemical processes with each other, either to prevent tribocorrosion or to use it effectively in applications such as CMP and metal grinding/cutting.

Materials that rely on a passive layer are particularly sensitive to tribocorrosion. Once the passive layer is removed, the bare metal surface will be exposed to the corrosive medium and it will be susceptible to corrosion damage. If the passive layer could not regenerate quickly, then the material would undergo significant corrosion damage. It was observed that material removal in a tribocorrosion system usually exceeds the sum of mechanical and corrosion contributions measured separately (Goodman, 1994; Meunier and Sedel, 1998).

The most common forms of tribocorrosion are corrosion wear, erosion corrosion, fretting corrosion and microabrasion corrosion. Corrosion wear can be defined as the degradation of materials due to the combined action of mechanical removal and chemical/electrochemical reactions of the corrosive medium. Erosion corrosion is associated with degradation of materials by flow-induced mechanical erosion of the material, or the protective (or passive) oxide layer on its surface by impinging liquid, abrasion by slurry, particles suspended in fast flowing liquid or gas, bubbles or droplets, cavitation, etc, and the corrosivity of the medium (Stack and Abdulrahman, 2010; Stack *et al.*, 2010a). Erosion corrosion is observed in

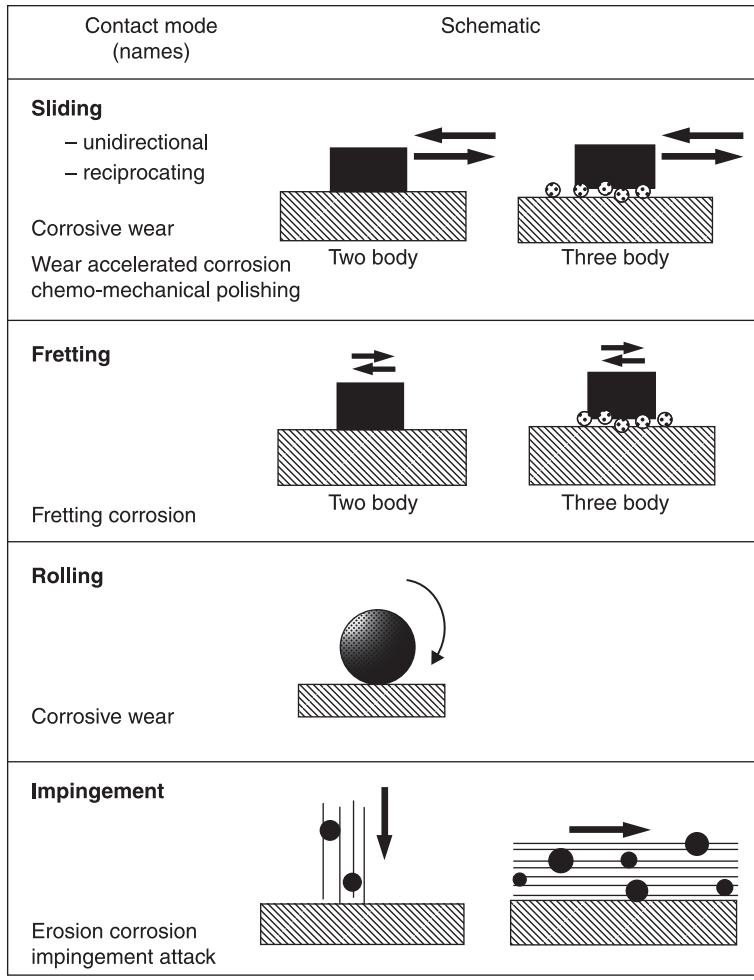

8.1 Different types of contact modes and their schematic representation for tribological contacts involving simultaneous mechanical and chemical effects (Landolt *et al.,* 2001).

pumps, impellers, propellers, valves, heat exchanger tubes and other fluid handling equipment.

Fretting corrosion is the deterioration of material that occurs at the interface of two contacting surfaces due to small oscillatory movements arising between them in the presence of a corrosive medium. Orthopedic implants, predominantly hip and knee joints, exposed to physiological medium often encounter damage due to fretting corrosion, which results in a reduction in their lifetime (Thull and

Schaldach, 1976; Brown *et al.*, 1988; Hoeppner and Chandrasekaran, 1994; Rabbe *et al.*, 1994). The modular interfaces of total joint prostheses, primarily at the fixation of implant stem and bone or cement, are subjected to micro-motion (<100 μm) that could result in fretting corrosion (Windler and Klabunde, 2001). Electrical connector contact is another area where fretting corrosion is a common form of degradation (Antler, 1985; Braunovic, 1989; Swingler *et al.*, 2000; Hannel *et al.*, 2001; Malucci, 2001; Park *et al.*, 2006a, 2006b, 2007a, 2007b, 2008; Sankara Narayanan *et al.*, 2007, 2008a, 2008b).

Microabrasion corrosion is the degradation of the material by the combined action of particle abrasion, mechanical load and corrosivity of the medium (Gee *et al.*, 2003; Stack and Mathew, 2003; Stack *et al.*, 2005). Microabrasion corrosion is commonly observed in orthopedic implants, particularly on hip joints (Sinnett-Jones *et al.*, 2005; Bello *et al.*, 2007; Sun *et al.*, 2009a, 2009b; Stack *et al.*, 2010b).

The mechanism of tribocorrosion is not thoroughly understood due to the complexity of the chemical, electrochemical, physical and mechanical processes involved (Fig. 8.2) (Landolt *et al.*, 2001; Lemaire and Le Calvar, 2001; Benea *et al.*, 2004; Celis *et al.*, 2006). During tribocorrosion, many reactions could take place at the same time and the quantity of reaction products might be very small. In addition, metastable phases might be important inside a contact, which then transform into stable reaction products outside the contact. The complex

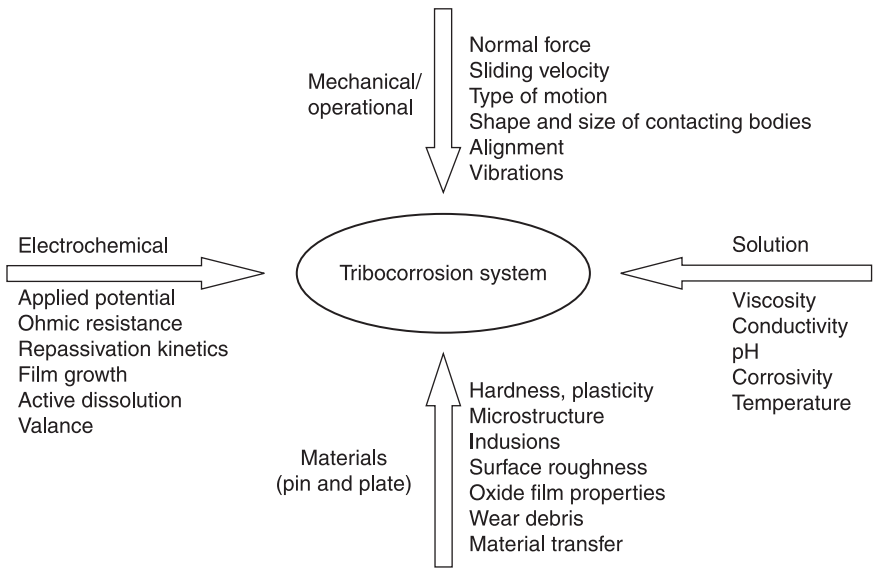

8.2 The various parameters that affect the tribocorrosion behavior of a sliding contact under electrochemical control (Landolt *et al.*, 2001).

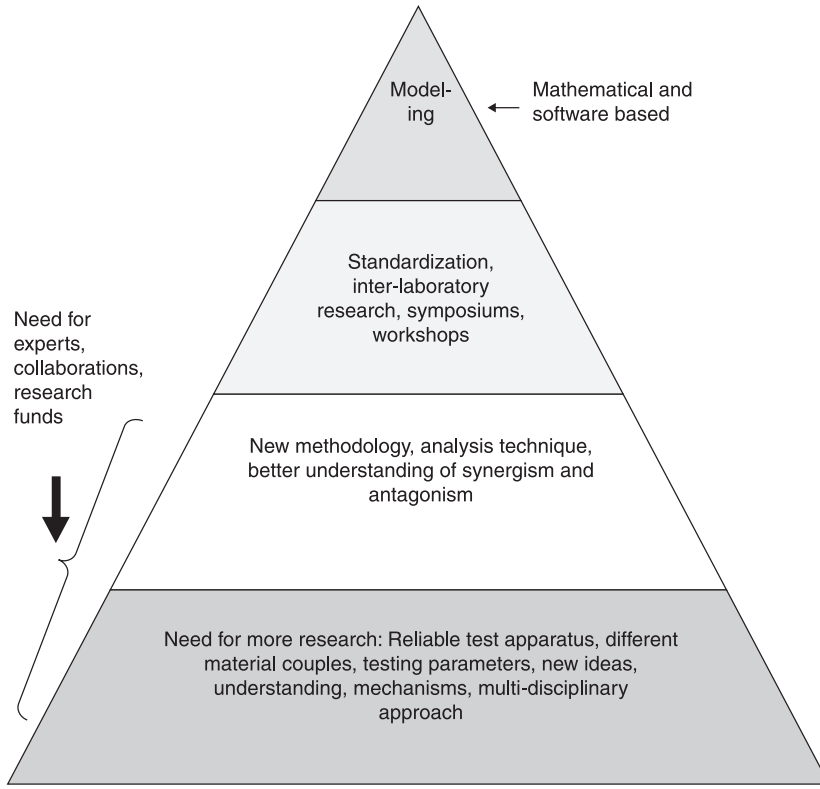

8.3 Schematic of the future perspectives of tribocorrosion research in the next decade (Mathew *et al.*, 2009).

chemical, electrochemical, physical and mechanical processes involved are not independent of each other but mostly result in a synergistic effect, which makes understanding of the mechanism of tribocorrosion difficult. Much remains to be explored in the area of tribocorrosion. The future perspectives of tribocorrosion research in the next decade are shown as a schematic in Fig. 8.3 (Mathew *et al.*, 2009).

8.2 The role of nanoparticles in tribocorrosion

8.2.1 Nanoparticles in lubricants

The use of nanoparticles as extreme pressure and anti-wear additives for liquid lubricants assumes significance. WS_2 particles (average diameter: 100 nm) have been shown to reduce the wear of self-mated steel sliding couples by a factor of approximately two for loads below 400 N and by a factor of ten above this

threshold (Rapoport *et al.*, 2003). Similarly, addition of nanosized particles such as $NiMoO_2S_2$ (Ye *et al.*, 2002), Cu (Tarasov *et al.*, 2002), ZnS (Chen and Liu, 2001), LaF_3 (Zhou *et al.*, 2001), Ni (Qiu *et al.*, 2001), CeF_3 (Qiu *et al.*, 1999) and TiO_2 (Xue *et al.*, 1997) to oil or liquid paraffin reduced the wear and friction of self-mated steel sliding systems. Ye *et al.* (2002) have reported that the maximum non-seizure load in a four steel ball test lubricated with synthetic oil was significantly increased when 13 nm $NiMoO_2S_2$ particles were added, while particles with a diameter of 3 μm micrometer had significantly smaller effects. Similarly, the addition of nanosized particles of magnesium borate (Hu *et al.*, 2002), Ni (Qiu *et al.*, 2001), CeF_3 (Qiu *et al.*, 1999) and TiO_2 (Xue *et al.*, 1997) to oil increased the maximum non-seizure load typically by a factor of two. The observed wear reducing effect was attributed to deposition of nanoparticles on the contacting surfaces (Xue *et al.*, 1997; Qiu *et al.*, 2001; Tarasov *et al.*, 2002; Hu *et al.*, 2002; Rapoport *et al.*, 2003). The deposit of nanoparticles acts as a third body reducing asperity interactions and thus increasing load bearing capacity of the rubbing pairs (Rapoport *et al.*, 2003). The nanosized particles were also found to be more efficient than micron-sized particles in reducing friction in an alumina-on-steel sliding system.

8.2.2 Effect of nanoparticles on tribocorrosion of stainless steel (SS) and Co–Cr–Mo alloy

Effect of alumina nanoparticles on the corrosion wear of 316L SS

Nanoparticles have received widespread acceptance as extreme pressure and anti-wear additives for liquid lubricants. If the nanoparticle deposits can act as a third body to help reduce asperity interactions and increase the load-bearing capacity of rubbing pairs (Rapoport *et al.*, 2003) then action of such a third-body layer on tribocorrosion behavior will be of much interest. In addition, the possibility of using aqueous suspensions of nanoparticles as an alternative to oil-in-water emulsion is worth exploring.

The effect of alumina nanoparticles (150 nm) suspended in an aqueous acetate buffer solution on the tribocorrosion behavior of an AISI 316L SS was studied by Radice and Mischler (2006). Four different types of experiments were performed. The first type of test involved a ball-on-flat (alumina ball over 316L SS flat) contact configuration (standard configuration), while in the second type of test the contact configuration was reversed (as this would avoid sedimentation of alumina particles at the interface). The third type of test involved a sequential test method in which, at the end of the first test performed using nanoparticles, the subsequent test was conducted by replacing the electrolyte with a fresh acetate buffer without nanoparticles. In the fourth type of test, a commercial oil-in-water emulsion (Castrol H4 sol. R61, 3% in H_2O)

was used instead of the alumina nanoparticles. Excepting the second type of test, all the other three test types were conducted using the standard contact configuration.

The reduction in coefficient of friction by a factor of two (see Fig. 8.4(a)) and the decrease in anodic current (see Fig. 8.4(b)) and extent of wear by one order of magnitude (see Fig. 8.5) suggest that the alumina nanoparticles provide a

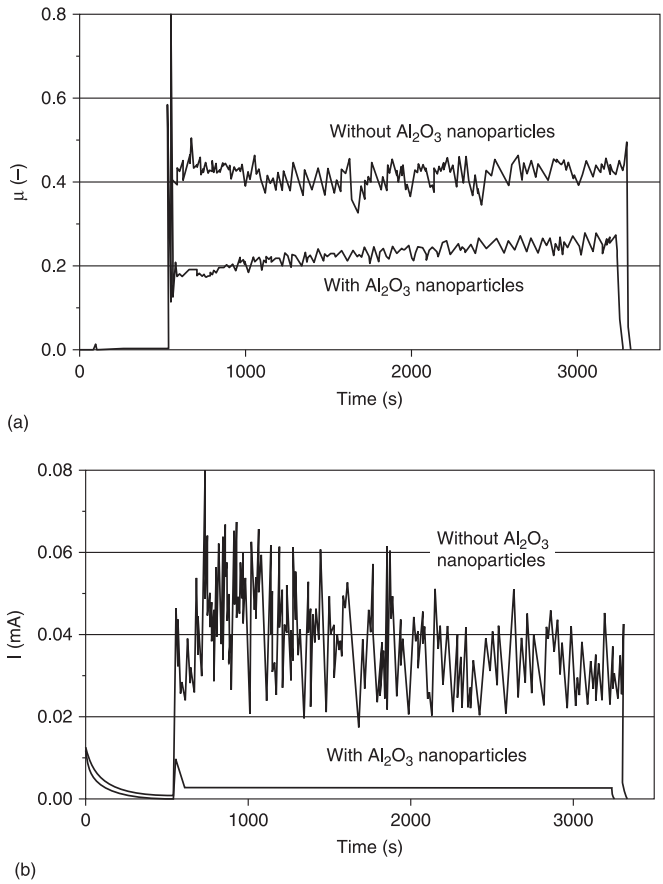

8.4 Evolution of (a) the mean coefficient of friction and (b) current of an AISI 316L SS disc (20 mm diameter and 6 mm height) after subjecting it to corrosion wear against an alumina ball (6 mm ∅) in an acetate buffer. The Al_2O_3 nanoparticles (150 nm) were added as a 20 vol.% suspension (1:1 mixture of deionized water and acetate buffer) (conditions: –0.5 V/MSE; load: 6N; frequency: 2 Hz; configuration: standard; ball-on-flat) alumina ball-on-316L flat) (Radice, 2006).

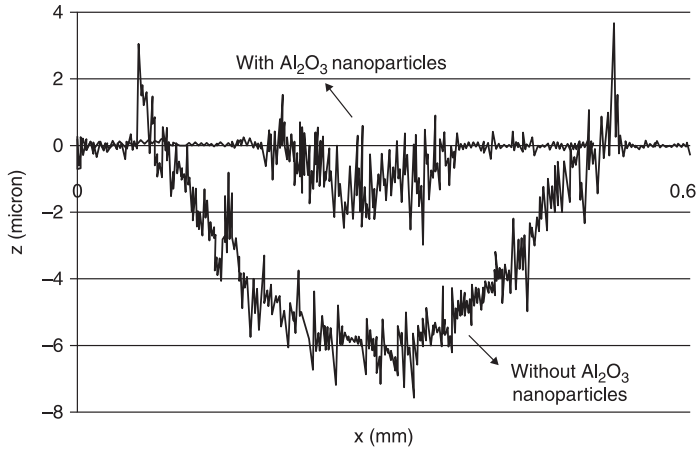

8.5 Wear profile of the AISI 316L SS disc after subjecting it to corrosion wear against an alumina ball in an acetate buffer under the same test conditions as Fig. 8.4 (Radice, 2006).

lubrication effect during the corrosion wear process. The morphology of the worn-out region indicates the presence of a layer of compacted particles that acts as a third body, protecting the 316L SS against abrasion and depassivation (at passive potential). These observations confirm the ability of alumina nanoparticles to provide a lubrication effect. However, the hard and abrasive nature of these particles has caused abrasion and flattening of the alumina ball counter body.

The mechanisms that contribute to the formation of a third-body layer during the corrosion wear process are sedimentation, adsorption due to electrostatic interactions and mechanical compaction within the contact due to rubbing. Sedimentation does not seem to be the predominant mechanism, since the possibility of its occurrence is negligible when the standard contact configuration is reversed. Particle adsorption is influenced by surface charge on the particle, which is a function of the solution chemistry, the pH and the electric potential established across the metal/liquid interface (electrode potential). The isoelectric point of Al_2O_3 particles is in the range of 8 to 9. At lower pH values, adsorption of H^+ ions on the hydrated particle surface imparts a positive surface charge and electrostatically stabilizes the nanoparticles in suspensions. The electrode potential also influences the electrostatic adhesion of suspended nanoparticles onto the metal surface. The morphological features of the wear track, however, confirm that the occurrence of particle adsorption did not help improve the tribological behavior, as evidenced by the sequential test. Hence, it is evident that formation of a layer of rather loose particles on the metal surface alone is not sufficient to prevent corrosion wear, and some mechanical loading is necessary to form a protective compact nanoparticle layer.

Attempts to remove the nanoparticle layer by wiping reveals that those formed outside the wear track could be completely removed while those formed within the wear track could only be partially removed. This indicates the contribution from mechanical compaction to the formation of the third-body layer. Hence, the observed lubricant effect of nanoparticles in suspension could be attributed to the build-up of a third body composed of multilayers of nanoparticles compacted on the metal surface, which slides against the alumina ball counter body. The contact pressure and rigidity, as well as the interaction forces between particles, are critical parameters in determining the formation and stability of the third body. It should be noted that the third-body layer cannot be permanently embedded in the metallic surface, nor does it form a type of protective coating on the metal. Rather, it was kept active by a dynamic process involving a continuous flow of nanoparticles entering the contact, getting compacted into the third body and being replaced after a certain time.

Comparison of the mean values of coefficient of friction and total wear volume of 316L SS subjected to corrosion wear against the alumina ball in an acetate buffer under varying experimental conditions reveals some interesting results (see Fig. 8.6). The alumina nanoparticle suspension and the oil emulsion showed similar lubricant effects in terms of friction and wear. This confirms the potential of nanoparticle suspensions as chemically stable and non-polluting lubricants. The performance of nanoparticle suspensions in providing a lubricating action could be further improved by optimizing the suspension (nature of particles, size, pH and concentration). The study reveals that suspensions containing nanoparticles could be effectively utilized to reduce the extent of material damage under tribocorrosion conditions.

Effect of nanosized alumina particles on the microabrasion corrosion of Co–Cr–Mo alloy

Metal-on-metal hip replacements, particularly those based on Co–Cr–Mo alloys, are considered as useful alternatives to metal-on-polymer hip replacements in providing superior wear resistance, longer service life and reduced inflammatory osteolysis (Amstutz *et al.*, 1996; Chan *et al.*, 1996; Pabinger *et al.*, 2003; St. John *et al.*, 2004; Schmalzried, 2004, 2005; Howie *et al.*, 2005; Yan *et al.*, 2007). Despite their low wear rate and longevity of survival, there are some concerns over the use of Co–Cr–Mo alloy based joints due to the unknown biological responses to the nanosized metallic wear particles and released metal ions (Jacobs *et al.*, 1998; Tipper *et al.*, 2001). Implant retrieval (Wimmer *et al.*, 2001, 2003) and laboratory simulation studies (Wang *et al.*, 1999; Catelas *et al.*, 2001) reveal that Co–Cr–Mo alloy-based implants encounter two-body sliding wear (Buscher and Fischer, 2005) and three-body abrasive wear (Yan and Dowson, 2006) as the predominant wear mechanisms. These studies indicate that the formation of sub-micron sized hard particles such as fractured

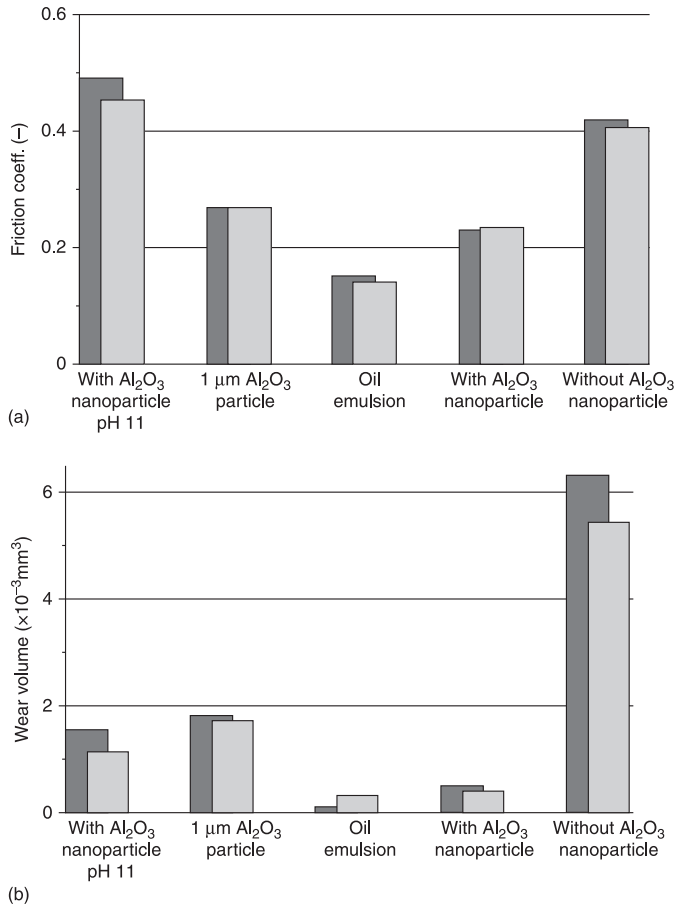

8.6 Comparison of the mean values of (a) coefficient of friction and (b) total wear volume of AISI 316 SS subjected to corrosion wear against an alumina ball in an acetate buffer – pH of the suspension was adjusted to 11; Degussa Al_2O_3 particles (1 μm) and oil emulsion (Castrol H4 sol. R61, 3% in H_2O); all other conditions as Fig. 8.4 (Radice, 2006).

carbides, bone cements, bone and metal debris could act as third bodies and induce abrasion.

It is well known that the wear rates and wear mechanisms resulting from third-body abrasive wear are influenced by abrasive size, geometry and hardness, as well as volume fraction (Kramer and Demer, 1961; Rabinowicz and Mutis, 1965; Williams and Hyncica, 1992; Zum Gahr, 1999; Stachowiak, 2000; Stachowiak and Stachowiak, 2004; Bello *et al.*, 2007). The size of the abrasive particles could influence their motion within a lubricated contact and alter the wear mechanisms

(Williams and Hyncica, 1992). The particles could roll or tumble through the gap separating the surfaces, producing relatively minor indentation type damage and wear. A lubrication film could also be developed in the gap between the surfaces in the contact. However, only a limited number of studies focus on the influence of third-body particles on the material degradation of Co–Cr–Mo alloy joints (Sinnett-Jones *et al.*, 2005; Sun *et al.*, 2009a).

The effect of nano and micron-sized abrasives on the abrasion–corrosion behaviour of cast Co–Cr–Mo alloy (ASTM F 75) against a ZrO_2 ball (25.4 mm Ø) in simulated hip joint environments such as 0.9% NaCl and 25% bovine serum (BS), was studied by Sun *et al.* (2009b). Nanosized (300 nm) and micron-sized (1 μm) Al_2O_3 particles were chosen as the abrasive particles as they were comparable in size and hardness to the wear particles found *in vivo*. Slurries containing varying volume fraction of Al_2O_3 particles were used to cause abrasion on the Co–Cr–Mo alloy. The two-dimensional surface profile of the wear scar of cast Co–Cr–Mo alloy subjected to micro-abrasion–corrosion against the ZrO_2 ball using a slurry containing 0.006 vol.% of both nano and micron-sized Al_2O_3 particles in 25% BS conforms to a hemispherical shape (see Fig. 8.7). However, the difference in the degree of wear damage induced by nano and micron-sized Al_2O_3 particles has resulted in a significant variation in the width and depth of the scar as well as the surface roughness. The increase in mechanical damage observed

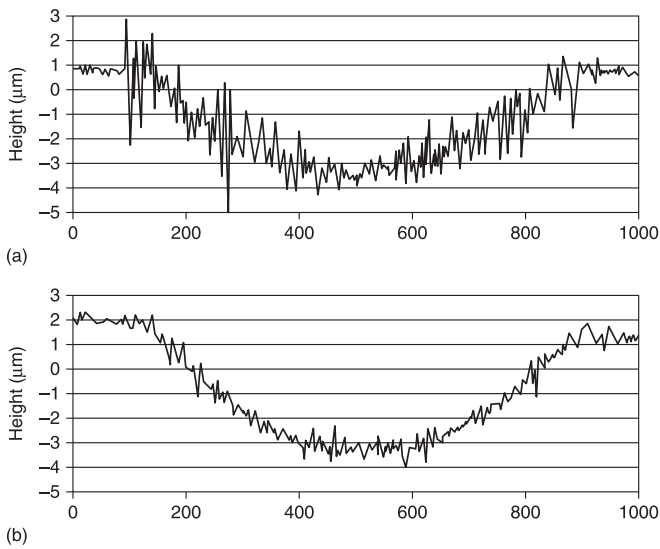

8.7 Wear scar profiles of a cast Co–Cr–Mo alloy (ASTM F 75) subjected to micro-abrasion–corrosion against a ZrO_2 ball (25.4 mm ∅) using a slurry containing Al_2O_3 particles in 25% bovine serum (BS) (a) 0.006 vol.% 1 μm Al_2O_3 particles in BS, and (b) 0.006 vol.% 300 nm Al_2O_3 particles in BS (Sun *et al.*, 2009).

in the presence of micron-sized particles is due to the increase in the effective attack angles at which the abrasive particle meets the surface and thus encourages machining or cutting wear (Williams and Hyncica, 1992). The specific wear rates and wear-induced corrosion current of Co–Cr–Mo alloy subjected to micro-abrasion–corrosion using abrasive slurries containing varying volume fractions of 1 μm Al_2O_3 particles (see Fig. 8.8) are generally higher than those obtained using 300 nm Al_2O_3 particles (see Fig. 8.9).

The morphological features of wear scars of cast Co–Cr–Mo alloy reveal grooving abrasion as the predominant wear mechanism, irrespective of whether the slurry contains micron- or nanosized Al_2O_3 particles in 0.9% NaCl and 25% BS (see Fig. 8.10). The extent of damage at the contact zone appears to be more

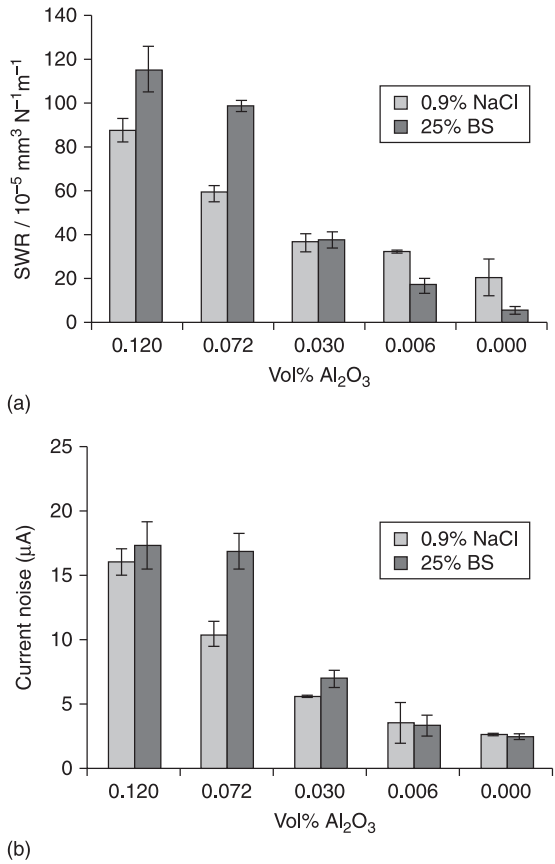

8.8 (a) Specific wear rates and (b) wear-induced corrosion current obtained for a cast Co–Cr–Mo alloy (ASTM F 75) subjected to micro-abrasion–corrosion against a ZrO_2 ball (25.4 mm ∅) using a slurry containing varying concentrations of 1 μm Al_2O_3 particles in 0.9% NaCl and 25% bovine serum (BS) (Sun *et al.*, 2009).

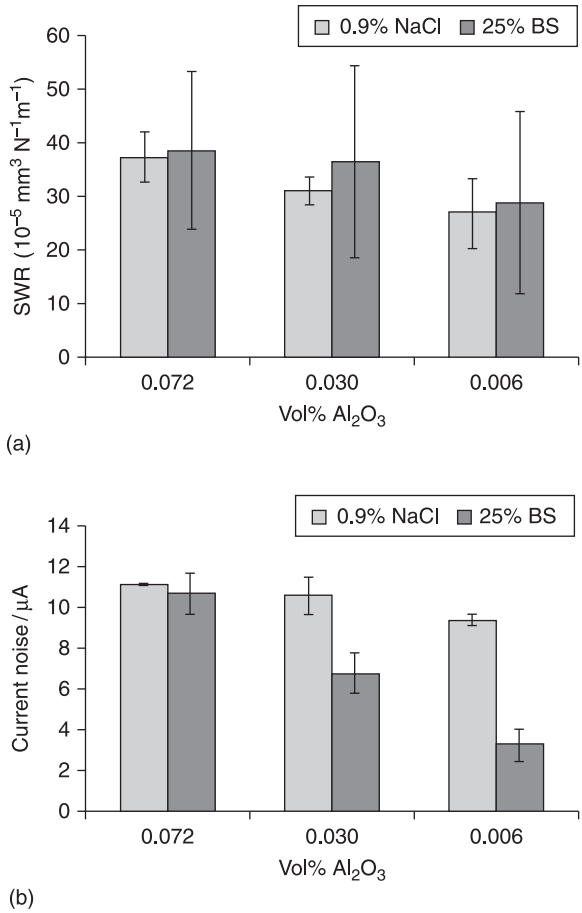

8.9 (a) Specific wear rates and (b) wear-induced corrosion current obtained for a cast Co–Cr–Mo alloy (ASTM F 75) subjected to micro-abrasion–corrosion against a ZrO_2 ball (25.4 mm ∅) using a slurry containing varying volume fractions of 300 nm Al_2O_3 particles in 0.9% NaCl and 25% bovine serum (BS) (Sun *et al.*, 2009).

severe in 0.9% NaCl than in 25% BS. This is due to the formation of conglomerates, which consist of proteinaceous material and metal debris. These conglomerates could act as rolling elements within the tribo-contact, which enhance the surface separation, provide lubrication for the contact, reduce the abrasivity of the hard particles and contribute to the polishing effect of the wear scar surface. Similar roll-ups of proteinaceous material have been reported previously (Wimmer *et al.*, 2001; Sun *et al.*, 2009a) for *in vivo* and *in vitro* studies. The nanosized Al_2O_3 particles are likely to be trapped within the conglomerates, which enables a reduction in the specific wear rate and the extent of damage at the contact zone.

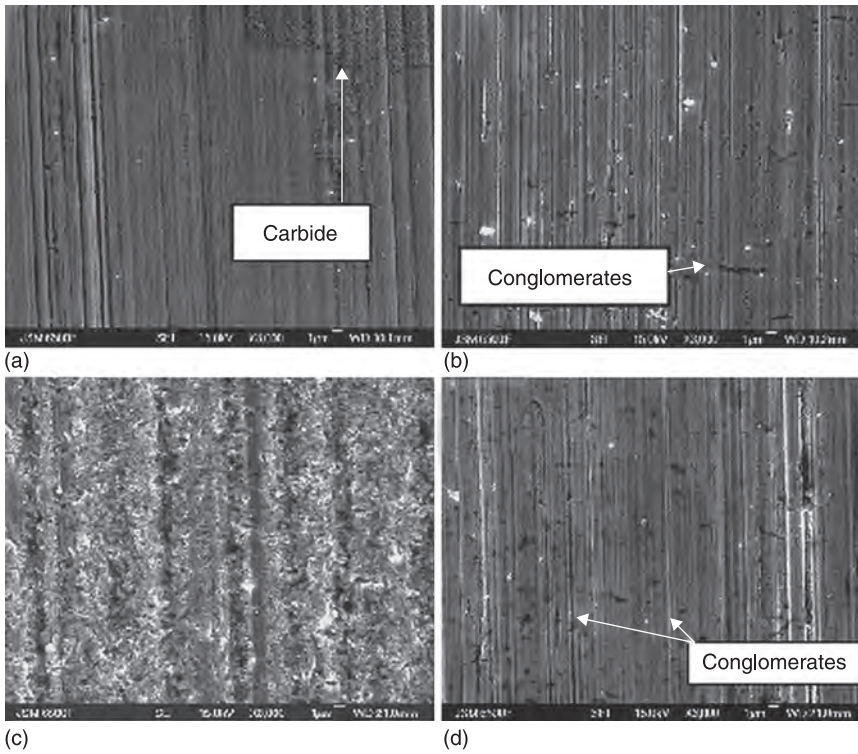

8.10 Morphological features of wear scars of cast Co–Cr–Mo alloy subjected to micro-abrasion–corrosion against a ZrO_2 ball (25.4 mm ∅) using a 0.006 vol.% alumina slurry containing 300 nm ((a) and (b)) and 1 μm Al_2O_3 particles ((c) and (d)), in 0.9% NaCl ((a) and (c)) and 25% bovine serum (BS) ((b) and (d)) (Sun *et al.*, 2009).

The results of this study indicate that nanosized Al_2O_3 particles could reduce the extent of material damage by microabrasion corrosion. In bovine serum, the formation of conglomerates traps the Al_2O_3 nanoparticles and provides a lubricating effect.

Effect of cobalt nanoparticles on the biotribocorrosion behavior of Co–Cr–Mo alloy hip prostheses

As already mentioned in Section 8.2.2, there are some concerns over the use of Co–Cr–Mo alloy based joints due to the nanosized metallic wear particles (Jacobs *et al.*, 1998; Tipper *et al.*, 2001). The size and quantum of these wear particles could influence the tribocorrosion behavior. The effect of cobalt nanoparticles (average diameter: ~28 nm) on the biotribocorrosion behavior of wrought Co–Cr–Mo alloy hip prostheses (36 mm diameter hips) was studied by Yan *et al.* (2009). BS (25%, v/v) and 0.3% NaCl (5 ml for each test) were employed as lubricants in

this study. Immersion of Co–Cr–Mo alloy hip implants in 0.3% NaCl enables the formation of a stable passive oxide layer. However, as soon as the load (300 N) is applied and the motion is started, a rapid cathodic shift in free corrosion potential (FCP) is observed, suggesting removal of the passive oxide layer (see Fig. 8.11(a)). The FCP remains in the active direction until the motion is stopped. Once the application of load and motion is removed, the FCP exhibits an anodic shift and reaches the initial steady state value, indicating repassivation of the damaged areas of the contact zone. However, addition of 50 mg of cobalt nanoparticles to 0.3% NaCl at a constant load of 300 N has resulted in a further shift in FCP towards the cathodic direction (see Fig. 8.11(a)). The extent of cathodic shift in FCP becomes much higher when a swing phase load of 300 N (2 kN 300 N) is applied to the system (see Fig. 8.11(b)). In contrast, addition of 50 mg of cobalt nanoparticles to 25% BS has caused a relatively smaller shift in FCP towards the cathodic direction than in 0.3% NaCl under constant as well as swing phase loading conditions (see Fig. 8.11(c)). The friction factor of Co–Cr–Mo alloy hip implants in 0.3% NaCl and in 25% BS is relatively higher at high swing load condition than at constant load condition. In addition, it is much lower in BS than in 0.3% NaCl under both loading conditions (see Fig. 8.12). Addition of cobalt nanoparticles increased the friction factor at both loading conditions and in both media.

The effect of varying concentrations of cobalt nanoparticles (0 mg, 1 mg, 5 mg, 10 mg, 30 mg and 50 mg added every 3 min. to the system) on the change in FCP of Co–Cr–Mo alloy hip implant obtained under a load of 300 N in different media

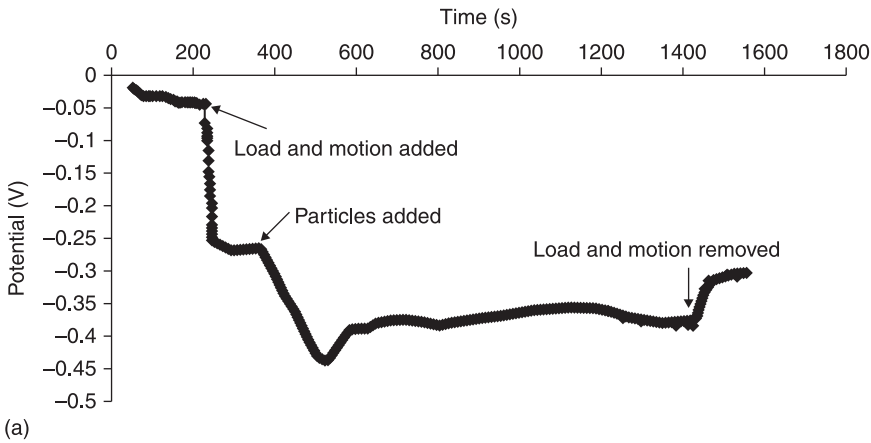

8.11 Change in FCP (V vs. Ag/AgCl) of a Co–Cr–Mo alloy hip implant measured as a function of time before and after the addition of 50 mg cobalt nanoparticles (average diameter: ~28 nm) under different loading conditions and in different media: (a) in 0.3% NaCl at 300 N; (b) in 0.3% NaCl at 2 kN 300 N; and (c) in 25% bovine serum at 300 N and 2 kN 300 N (Yan *et al.*, 2009).

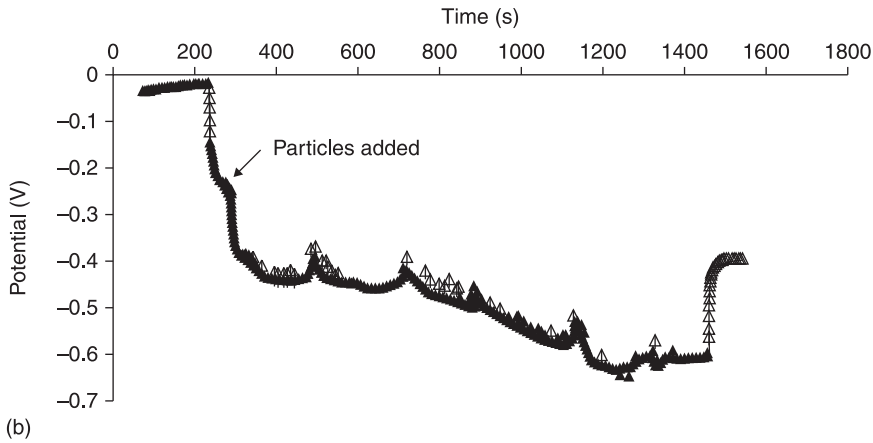

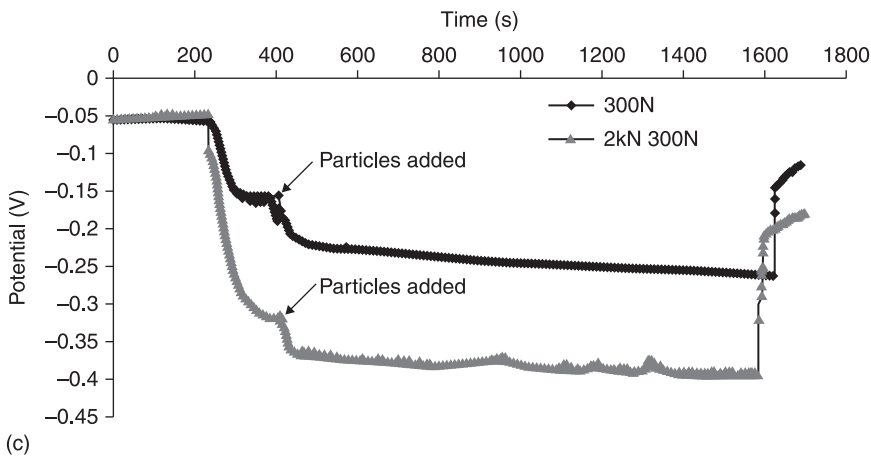

8.11 Continued.

reveals interesting results (see Fig. 8.13). A continuous cathodic shift in FCP with increase in concentration of cobalt nanoparticles is not observed. In contrast, a stabilized and slightly nobler FCP is noticed beyond 5 mg of cobalt nanoparticles, which is equivalent to the quantum of debris generated after approximately 600 000 cycles from a hip simulator (Tipper *et al.*, 2005). This observation is consistent with the bedding-in theory, which states that particles may act as rolling balls in the contact and result in less damage to the bearing surface. The study reveals that cobalt nanoparticles could act as abrasives. Their presence at the contact zone could increase the friction, cause local damage of the passive oxide film and accelerate the release of metal ions from the bearing surfaces of Co–Cr–Mo alloy hips. Abrasive wear is the predominant wear mechanism at low loads, whereas under higher loading conditions the wear mechanism is changed

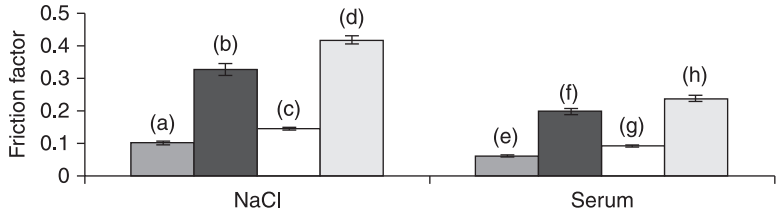

8.12 The friction factor of Co–Cr–Mo alloy hip implants obtained under different loading conditions in 0.3% NaCl ((a)–(d)) and in 25% bovine serum ((e)–(h)): at constant load of 300 N ((a) and (e)); at constant load of 300 N and with 50 mg of cobalt nanoparticles (average diameter: ~28 nm) ((b) and (f)); at swing phase load of 2 kN 300 N ((c) and (g)); and at swing phase load of 2 kN 300 N with 50 mg of cobalt nanoparticles ((d) and (h)) (Yan *et al.*, 2009)

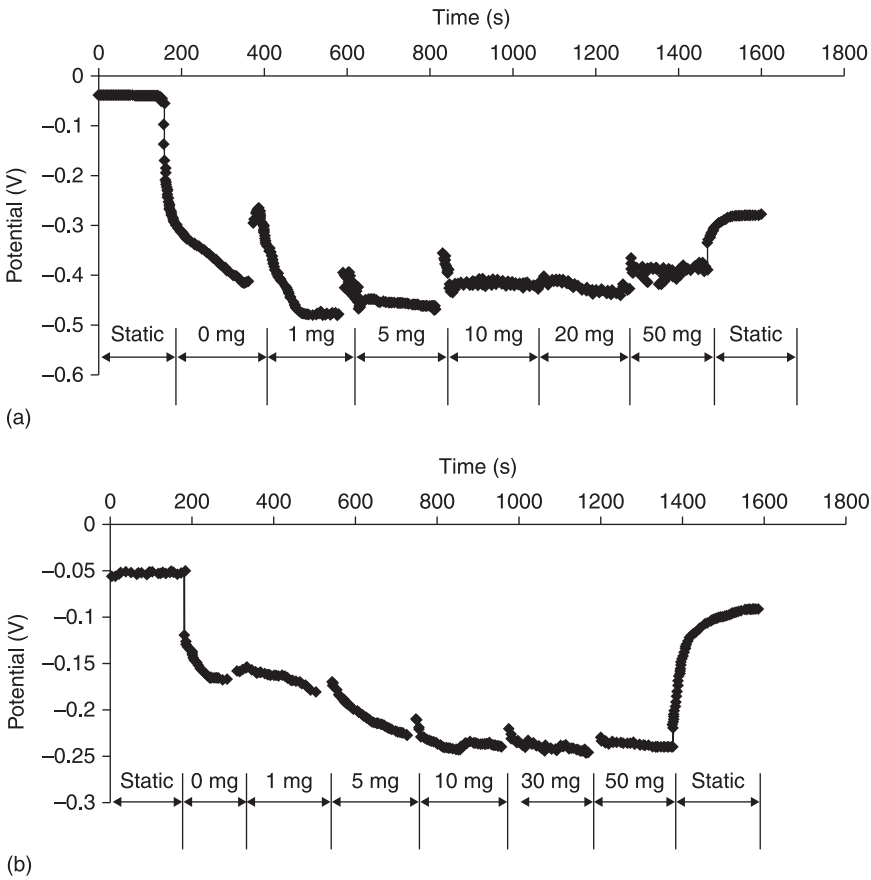

8.13 Effect of varying concentrations of cobalt nanoparticles (average diameter: ~28 nm) on the change in FCP (in V vs. Ag/AgCl) of Co–Cr–Mo alloy hip implant obtained under a constant load of 300 N in (a) 0.3% NaCl, and (b) 25% bovine serum (Yan *et al.*, 2009).

from abrasive wear to a combination of abrasive wear and adhesive wear. The effect of cobalt nanoparticles is a function of its concentration, type of mechanical motion and type of the surrounding environment.

8.3 Tribocorrosion resistance and nanocrystalline coatings

8.3.1 Effect of thermal sprayed nanostructured coatings

Nanocrystalline coatings with grain sizes in the nanometer scale exhibit novel and enhanced properties, which open up opportunities for new technological applications. Although various techniques are available for preparing nanocrystalline coatings, thermal spraying offers the unique advantages of a moderate to high rate of throughput and the ability to coat complex-shaped target materials using nanostructured feedstock powders prepared from vapor, liquid and solid materials. It will be of much interest to know how thermal sprayed nanostructured coatings would help reduce the tribocorrosion resistance of materials.

Basak *et al.* (2006) have studied the fretting corrosion behavior of thermal sprayed nanostructured FeCu/WC–Co and WC–Co coatings deposited on AISI 304 SS in Hank's solution and compared it with that of uncoated 304 SS. The change in FCP and the anodic current were measured as a function of time (see Fig. 8.14). Before the onset of fretting, the FCP of FeCu/WC–Co coated 304 SS is quite stable. With the onset of fretting, a sudden drop (cathodic shift – shift in potential in the negative direction with respect to the FCP) in FCP with a consequent increase in anodic current is observed (see Fig. 8.14(a)). Similar observations have been made earlier by other researchers (Xulin *et al.*, 1997; Galliano *et al.*, 2001; Barril *et al.*, 2005; Geringer *et al.*, 2005; Tang *et al.*, 2005; Berradja *et al.*, 2006; Azzi and Szpunar 2007; Satendra Kumar *et al.*, 2010a, 2010b, 2010c, 2010d). In fact, the drop in FCP and increase in anodic current have been observed not only during fretting but also during slurry impingement, scratching and sliding (Nevilee and McDougall, 2002; Komotori *et al.*, 2007; Lu *et al.*, 2008). It has been established that the potential of an electrode shifts in the noble direction when a passive film grows on the surface with a consequent decrease in anodic current and *vice versa* (Quan *et al.*, 2006). Hence, the sudden drop in FCP and the consequent increase in anodic current observed for FeCu/WC–Co coated 304 SS are due to the removal of the surface film induced by fretting.

During fretting, some fluctuations in the FCP of FeCu/WC–Co coated 304 SS are observed. This is due to the periodic removal (depassivation) and growth (repassivation) of the surface film in the fretted zone. Similar observations were made earlier by other researchers (Wu and Celis, 2004; Tang *et al.*, 2005; Berradja *et al.*, 2006; Quan *et al.*, 2006; Satendra Kumar *et al.*, 2010a, 2010b, 2010c, 2010d). The fluctuations in FCP observed during fretting are considered to be due to the establishment of a dynamic equilibrium between depassivation and repassivation (Tang *et al.*, 2005; Berradja *et al.*, 2006; Quan *et al.*, 2006). When

the fretting motion is stopped, the FCP of FeCu/WC–Co coated 304 SS exhibits an anodic shift (shift in potential in the noble direction with respect to the FCP), suggesting the occurrence of repassivation in the active area of the fretted zone.

A comparison of the change in FCP and anodic current measured as a function of time for uncoated, nanostructured FeCu/WC–Co and WC–Co coated 304 SS (see Fig. 8.14(a)–(c)) reveals a similar trend. However, the extent of cathodic shift in FCP with the onset of fretting, the extent of fluctuations in FCP during fretting and the extent of anodic shift in FCP after the fretting motion is stopped differ a lot in each case. The extent of cathodic shift in FCP is very high for uncoated 304 SS, which confirms the removal of the passive oxide layer with the onset of fretting. The naturally formed passive oxide layer (~4–6 nm thick) on 304 SS is not sufficiently thick to prevent damage with the onset of fretting, which results in an increase in its susceptibility to corrosion in Hank's solution. Unlike uncoated 304 SS, nanostructured WC–Co and FeCu/WC–Co coated 304 SS does not exhibit a sudden cathodic shift in FCP with the onset of fretting; rather, it is gradual. Such an observation has been made earlier for coated titanium and titanium alloys (Shenhar *et al.* 2000; Tang *et al.*, 2005; Azzi and Szpunar, 2007; Manhabosco and Muller, 2009; Satendra Kumar *et al.*, 2010b, 2010c). The absence of a sudden cathodic shift in FCP of nanostructured WC–Co and FeCu/WC–Co coated 304 SS indicates that the dense, crack-free, adherent and thick coating (~ 200 μm) is not totally removed with the onset of fretting and it effectively eliminates the generation of active sites. The progressive drop in FCP with increase in time indicates a continuous removal of the oxide layer.

Unlike uncoated 304 SS, fluctuations in FCP observed during fretting are relatively less for nanostructured WC–Co and FeCu/WC–Co coated 304 SS. In the case of uncoated 304 SS, a fresh surface is exposed to the electrolyte after every cycle and it tends to repassivate spontaneously due to its inherent nature. However, for coated 304 SS, removal of the surface layer occurs only on a limited area that limits fluctuation in FCP. During repassivation, the ability of the material to return to the steady state potential should be considered. Ideally, the potential should reach the initial steady state potential before the onset of fretting. In the present study, after the fretting motion is stopped, uncoated 304 SS tends to reach the initial steady state potential (see Fig. 8.14(b)), whereas nanostructured FeCu/WC–Co and WC–Co coated 304 SS fail to reach the initial steady state value (see Fig. 8.14(a) and 8.14(c)) in the given duration of time. Before the onset of fretting, nanostructured FeCu/WC–Co and WC–Co coated 304 SS are covered with a thick layer of coating, which imparts a more noble potential for them. However, during fretting, the continuous and permanent removal of the coated layer makes them more active. The large reduction in thickness of the coated layer due to fretting does not allow nanostructured FeCu/WC–Co and WC–Co coated 304 SS to reach the initial steady state potential in the given duration of time, after the fretting motion is stopped. The study reveals that nanostructured FeCu/WC–Co and WC–Co coatings deposited on 304 SS by thermal spraying method offer a better fretting corrosion resistance in Hank's solution.

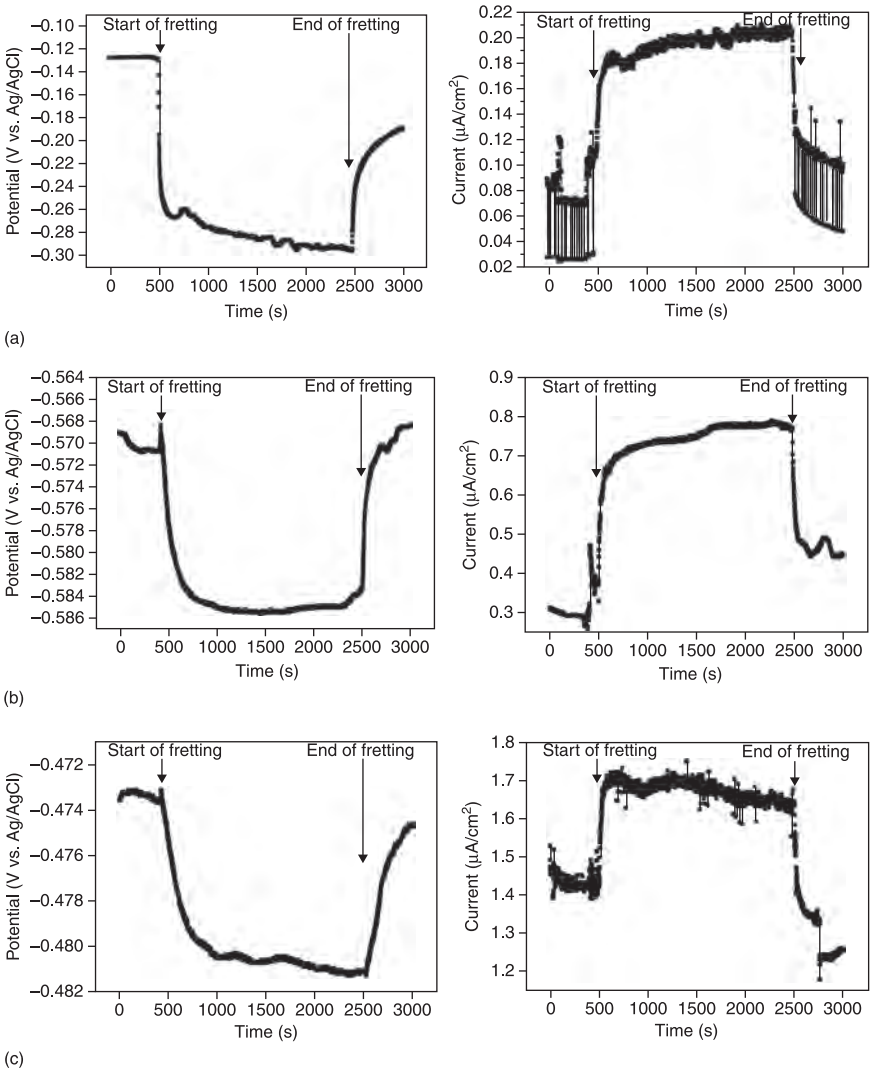

8.14 Change in free corrosion potential (FCP) and the anodic current of uncoated and thermal spray coated 304 SS, measured as a function of time (conditions: counterface material; corundum ball (10 mm ∅; hardness: 2000 HVN; R_a: < 0.02 μm); electrolyte: Hank's solution (composition in g/l: 0.185 $CaCl_2$, 0.40 KCl, 0.06 KH_2PO_4, 0.10 $MgCl_2.6H_2O$, 0.10 $MgSO_4.7H_2O$, 8.00 NaCl, 0.35 $NaHCO_3$, 0.48 Na_2HPO_4, and 1.00 D-glucose; pH 7.60; temperature: 23°C); normal load: 5 N; frequency: 5 Hz; displacement amplitude: 200 μm; number of fretting cycles: 10 000); (a) nanostructured FeCu/WC–Co coated 304 SS; (b) uncoated AISI 304 SS; and (c) nanostructured WC–Co coated 304 SS (Basak *et al.*, 2006).

8.3.2 Effect of electrodeposited nanocrystalline coatings

Effect of electrodeposited nanocrystalline Ni–Co alloy coatings on the corrosion wear of AISI 1045 carbon steel

Electrodeposition (ED) is one of the most cost-effective methods in preparing nanocrystalline coatings with high hardness and excellent corrosion and wear resistance. ED nanocrystalline Ni–Co coatings are widely used in many industrial applications. However, one of the major limitations of this type of coating is poor performance in corrosive media. Under tribocorrosion conditions, the mechanically assisted damage and poor corrosion resistance of the coating become a matter of concern regarding the performance of this type of coating. Hassani *et al.* (2009) have studied the tribocorrosion behavior of ED nanocrystalline Ni–Co coated AISI 1045 carbon steel in NaOH using a reciprocating ball-on-plate tribometer. The tribocorrosion tests were performed both at open circuit potential (OCP) and under anodic polarization conditions. In the first case, the FCP of ED nanocrystalline Ni–Co coated steels was monitored before, with the onset of, during and after sliding (see Fig. 8.15), while in

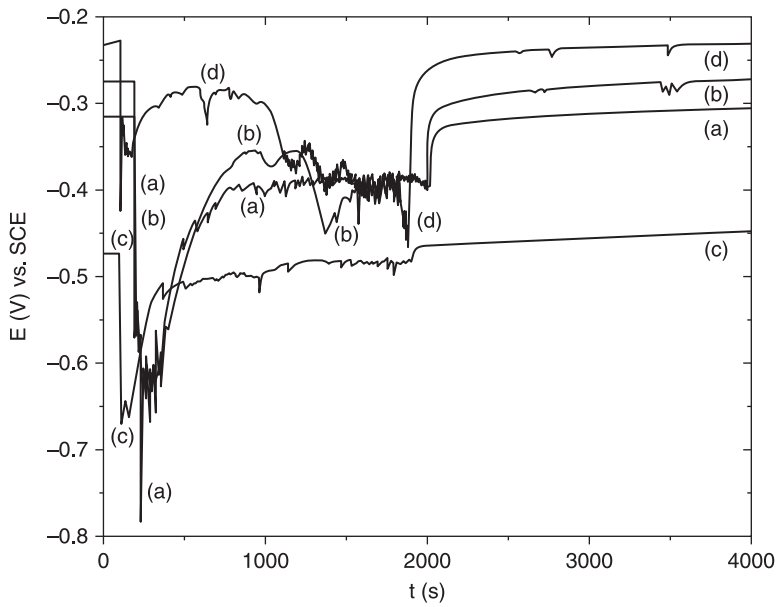

8.15 Change in free corrosion potential (FCP) of electrodeposited nanocrystalline Ni–Co alloy coatings (Watts-type bath: 250 g/l $NiSO_4.6H_2O$, 4 g/l $CoSO_4.7H_2O$, 45 g/l $NiCl_2.6H_2O$ and 30 g/l H_3BO_3; pH: 4.3; temperature: 43 °C), in NaOH measured as a function of time: (a) and (b) no additive; (c) saccharin (1 g/l); and (d) sodium lauryl sulfate (0.25 g/l); (a) prepared at 40 mA/cm^2; (b)–(d) prepared at 55 mA/cm^2 (tribocorrosion test conditions: ball-on-flat configuration; counterface: 4.75 mm ∅ alumina ball; normal load: 4.5 N; stroke length: 5 mm; frequency: 1 Hz; number of cycles: 1800) (Hassani *et al.*, 2009).

the second case, the coated steels were polarized to + 0.4 V (with respect to their OCPs) and the resultant anodic current was monitored (see Fig. 8.16).

Before the onset of sliding, the formation of a passive film upon immersion in NaOH solution results in a stable FCP (see Fig. 8.15) and decay in current density (see Fig. 8.16). With the onset of sliding, a cathodic shift in FCP and a significant increase in anodic current are observed, suggesting removal of the passive film induced by sliding and a high degree of anodic dissolution. During sliding, the continuous formation and removal of the passive film causes fluctuations in FCP and anodic current. When sliding ceases, the FCP tends to reach the initial potential (see Fig. 8.15) and the current is decreased again (see Fig. 8.16), suggesting the occurrence of repassivation in the damaged area of the wear track. The change in FCP is a function of the intrinsic corrosion potentials of the worn and unworn areas as well as the degree of repassivation of the worn-out area (Mischler, 2008). Since the intrinsic corrosion potentials of the worn and unworn areas are different, formation of a galvanic cell between them would influence the FCP (Celis *et al.*, 2006; Benea *et al.*, 2009). Similarly, the rate of repassivation would continuously change the ratio of active to passive area of the worn-out

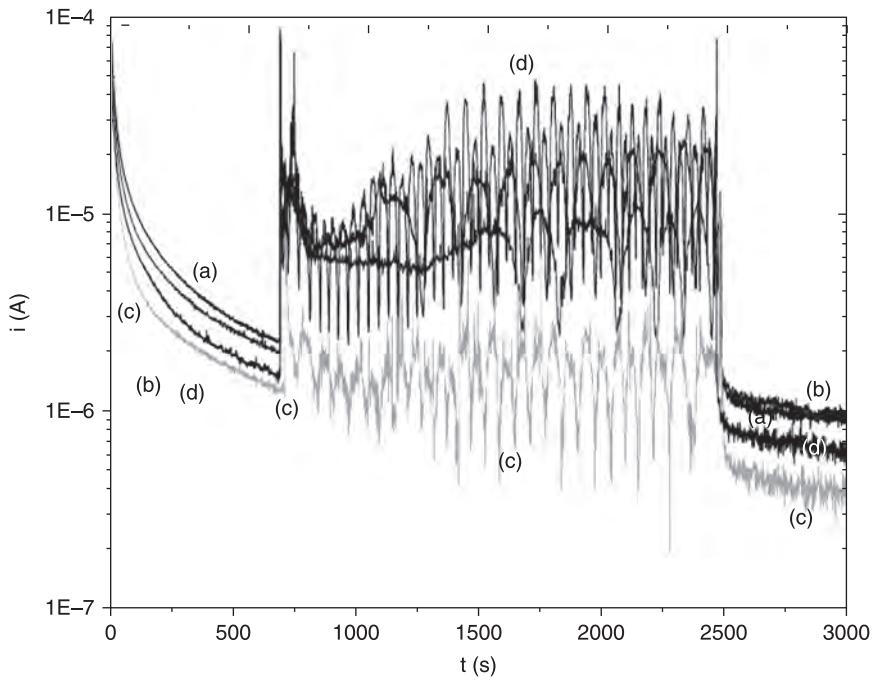

8.16 Change in anodic current of electrodeposited nanocrystalline Ni–Co alloy coatings recorded before, during and after sliding wear in NaOH under the same test conditions as Fig. 8.15: (a), (b) no additive; (c) saccharin (1 g/l); and (d) sodium lauryl sulfate (0.25 g/l); (a) prepared at 40 mA/cm^2; (b)–(d) prepared at 55 mA/cm^2 (Hassani *et al.*, 2009).

surface as a function of time and influence the FCP. The current measured during the sliding wear flows mainly through the wear track area (Mischler, 2008), thus confirming the transition of the surface area of wear track from passive to active during the sliding wear.

A comparison of the tribocorrosion behavior of all four types of coatings reveals that ED nanocrystalline Ni–Co alloy coating prepared in the presence of saccharin offers a better performance. The difference in performance could be related to their characteristic properties. ED nanocrystalline Ni–Co alloy coatings prepared in the absence of additives and in the presence of sodium lauryl sulfate exhibit a pyramidal morphology (see Fig. 8.17), a {2 0 0} texture, a grain size of 40–6 nm and a hardness of 303–30 $HV_{0.1}$. However, for coatings prepared in the presence of saccharin the pyramidal growth is inhibited, which results in a bright and smooth surface morphology (see Fig. 8.17) with {1 1 1} as the major texture component, a grain size of 22 nm and a hardness of 572 $HV_{0.1}$. The morphology of the wear track patterns of ED nanocrystalline Ni–Co alloy coatings (see Fig. 8.18) reveals that the surface far away from the wear track is not affected by the corrosion process, as no visible corrosion effect is observed in this zone. In the middle of the wear track, the worn-out area appears to be uniform without asperities.

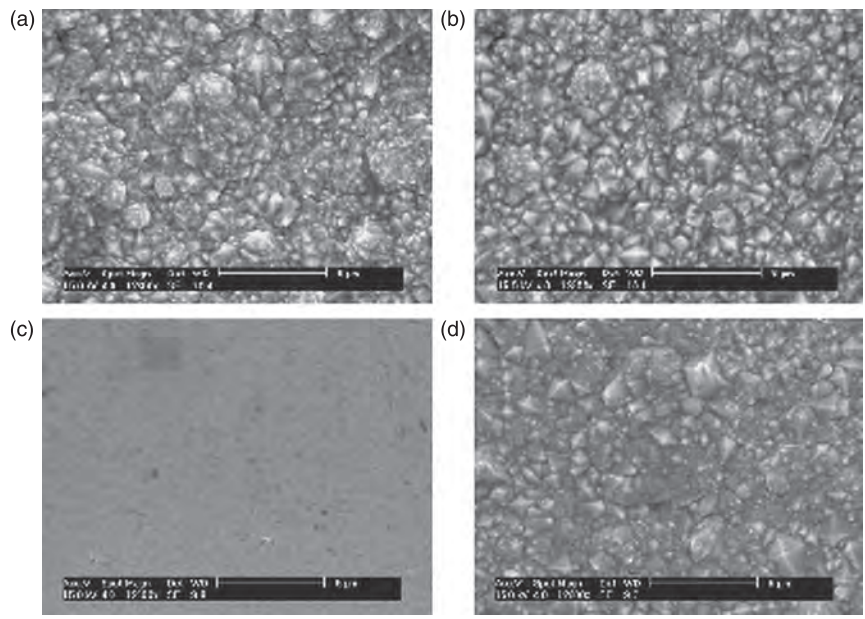

8.17 Surface morphology of electrodeposited nanocrystalline Ni–Co alloy coatings under the same test conditions as Fig. 8.15: (a), (b) no additive; (c) saccharin (1 g/l); and (d) sodium lauryl sulfate (0.25 g/l); (a) prepared at 40 mA/cm^2; (b)–(d) prepared at 55 mA/cm^2 (Hassani *et al.*, 2009).

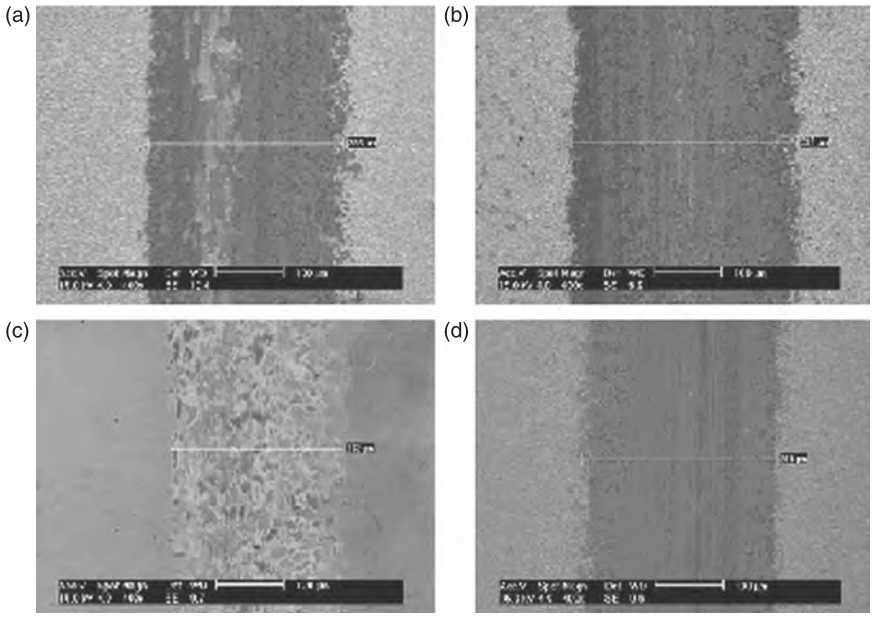

8.18 Surface morphology of the wear track of electrodeposited nanocrystalline Ni–Co alloy coatings after subjecting them to tribocorrosion tests at their respective OCPs under the same test conditions as Fig. 8.15: (a), (b) no additive; (c) saccharin (1 g/l); and (d) sodium lauryl sulfate (0.25 g/l); (a) prepared at 40 mA/cm^2; (b)–(d) prepared at 55 mA/cm^2 (Hassani *et al.*, 2009).

The formation of sliding grooves suggests that the tribocorrosion process proceeds mainly through an abrasive wear mechanism for all the four types of coatings. However, the wear track width is different for all these coatings. ED nanocrystalline Ni–Co alloy coating prepared at 55 mA/cm^2 in the presence of saccharin exhibits a smaller track width (~252 μm). The higher hardness (572 $HV_{0.1}$) and the smooth surface could have reduced the contribution of the surface to mass losses. In this case, the passive oxide layer is removed only from a smaller area and a lower amount of debris is produced in the wear track. Hence, it is evident that a high hardness and lower surface roughness are essential to achieve a better tribocorrosion performance.

Effect of electrodeposited Ni-nano SiC composite coatings on the corrosion wear of steel and stainless steel

The idea of codepositing various second-phase particles in a metal or alloy matrix, and thereby taking advantage of their desirable qualities such as hardness, wear and abrasion resistance and corrosion resistance, has led to the development of composite coatings, with a wide range of possible combinations and properties (Kerr *et al.*,

2000; Balaraju *et al.*, 2003; Low *et al.*, 2006). These coatings are obtained by codepositing various second phase particles in electro- or electroless deposited metal or alloy matrix. Almost any particle that can be held in suspension without reacting with the plating bath can be codeposited. Both micron- and nanosized particles could be codeposited with the metal matrix. Effective dispersion of particles in the plating bath is a major challenge in codeposition of nanosized particles because of their strong tendency towards agglomeration and sedimentation. The embedding mechanism of the nano and micron-sized particles could be characterized as 'intracrystalline' and 'intercrystalline', respectively (Gyftou *et al.*, 2005). The number density of the particles in the coating varies between 2.23×10^{15} and 11.18×10^{15} particles/cm^3 for nanosized particles, while it is between 30.80×10^{10} and 12.12×10^{10} particles/cm^3 for micron-sized particles (Gyftou *et al.*, 2005).

The corrosion wear behaviour of ED pure Ni and Ni-nano SiC composite coatings was studied by Benea *et al.* (2002). The FCP values, measured under static condition and before the application of load, are −198 and −260 mV vs. Ag/AgCl for ED Ni-nano SiC composite coating and for pure Ni coating, respectively. With the onset of rotation, in the absence of any applied load, a shift in FCP is observed (see Fig. 8.19(a)). For ED pure Ni, this shift occurs in the cathodic direction, whereas for ED Ni-nano SiC composite coating, an anodic shift in FCP is observed. Increase in rotation speed leads to a further shift in FCP without changing the trend. This is due to the variation in the nature of surface film formed on these coatings. With the application of a normal load of 30 N, a cathodic shift in FCP is observed for both pure Ni and Ni-nano SiC composite coatings, suggesting removal of the passive layer and activation of the surface (see Fig. 8.19(b)). Among them, the FCP is relatively noble for ED Ni-nano SiC composite coating. Increasing the rotation speed does not seem to exert a major influence on the FCP of these coatings. However, increase in load from 10 to 30 N causes a cathodic shift in FCP. Hence, it is evident that the evolution of FCP is mainly dependent on the wear parameters and the applied load (for a given rotation speed).

The difference in performance of ED pure Ni and ED Ni-nano SiC composite coatings arises from their characteristic properties. The decrease in grain size and increase in microhardness (from 148 $HV_{0.025}$ to 450 $HV_{0.025}$) enables ED Ni-nano SiC composite coating to offer a lower coefficient of friction and better tribocorrosion performance when compared with the ED pure Ni coating. Reinforcement of harder SiC particles in the ductile Ni matrix facilitates a reduction in ductility of the matrix in the contact region and causes a reduction in the extent of wear (Kato, 2010). Surface profile measurements made in the middle region of the wear scar confirm the significant decrease in surface roughness for ED Ni-nano SiC composite coating when compared with ED pure Ni coating (see Fig. 8.20). A comparison of the wear corrosion rate of pure Ni and Ni-nano SiC composite coatings (see Fig. 8.21) reveals that the nanocomposite coating offers a better performance.

The corrosion wear behaviour of ED Ni-nano SiC composite coated SS in 0.5 M K_2SO_4 was studied by Benea *et al.* (2009). The change in FCP of ED

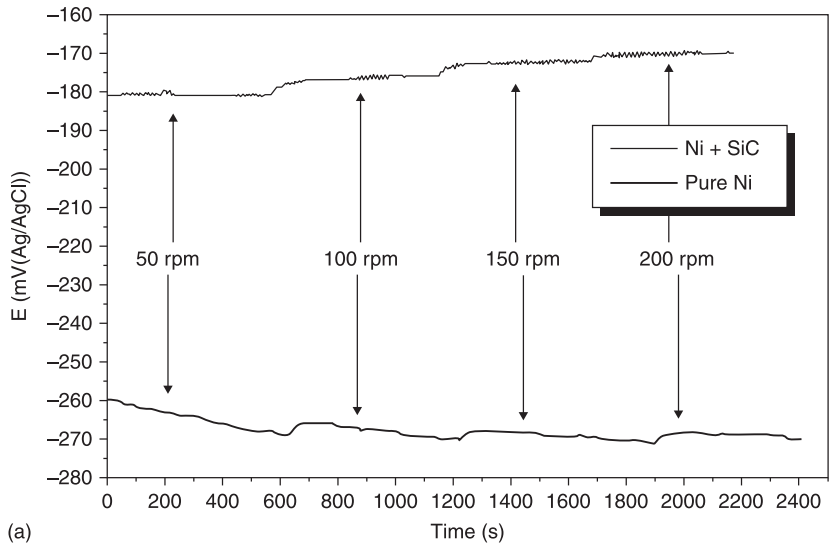

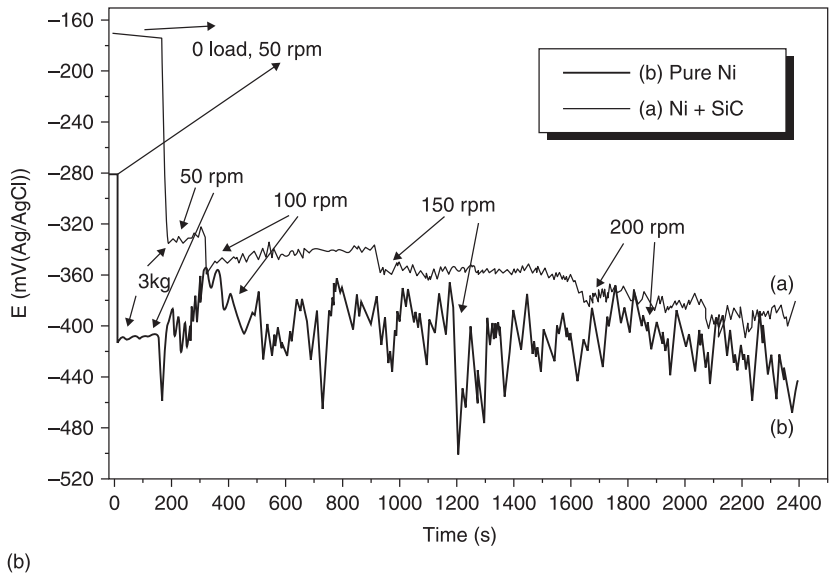

8.19 Change in free corrosion potential (FCP) as a function of time for ED pure Ni coating and ED Ni-nano SiC composite coating in 0.5 M Na_2SO_4 (pH: 5.70) at different rotation speeds of the cylinder: (a) without applied load, and (b) with a normal load of 30 N (conditions: mean diameter of SiC: 20 nm; coating thickness: 100 μm; contact configuration: rotating (0 and 250 rpm) coated steel cylinder against alumina parallelepiped) (Benea *et al.*, 2002).

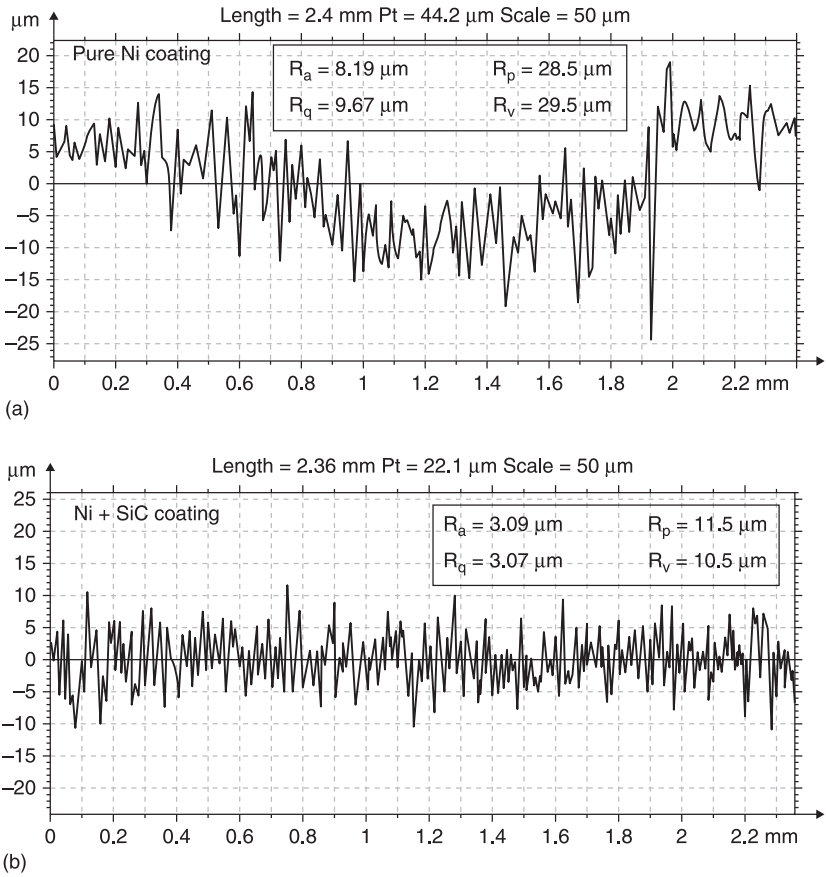

8.20 Surface profile measured at the middle of the wear scar and the corresponding roughness parameters of (a) ED pure nickel coating and (b) ED Ni-nano SiC composite coating obtained at a normal sliding load of 20 N, under the same test conditions as Fig. 8.19 (Benea *et al.*, 2002).

Ni–SiC nanostructured coatings is recorded during continuous as well as intermittent fretting tests (see Fig. 8.22). Before the onset of friction, the potential of the sample remains stable. With the onset of friction, a cathodic shift in FCP is observed, suggesting removal of the surface layer and activation of the surface at the contact zone. The FCP remains active until the friction is removed, suggesting the increase in susceptibility of the coated SS to corrosion during this period. These observations confirm the transition of the contact zone from passive to active during friction in both continuous and intermittent test conditions. When friction is stopped, the FCP exhibits an anodic shift. However, it fails to reach the initial steady state potential (i.e. potential measured before friction is applied), which suggests a delay in the repassivation kinetics (Fig. 8.22(b)). This is due to the occurrence of significant damage at the contact zone during the corrosion wear

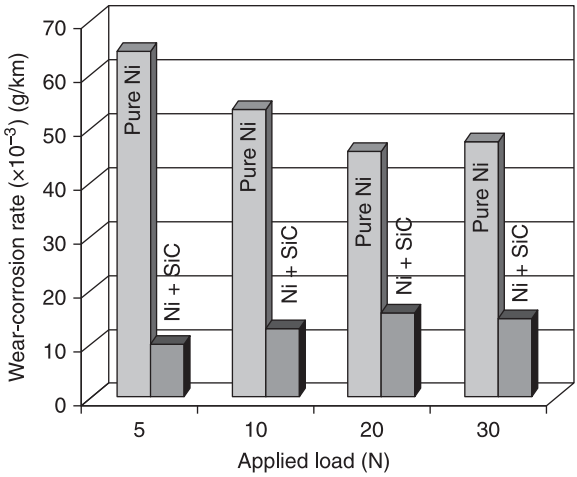

8.21 Wear corrosion rate of electrodeposited pure nickel and Ni-nano SiC nanocomposite coatings in 0.5 M Na_2SO_4 (pH: 5.70) at different applied loads under the same test conditions as Fig. 8.19 (Benea *et al.*, 2002).

process. The observed changes in FCP suggest that the depassivation–repassivation process takes place during both continuous and intermittent friction test conditions.

The tribocorrosion behavior of ED Ni–SiC nanostructured composite coatings in 0.5 M K_2SO_4 was also evaluated by polarization studies in both the absence and presence of applied load (10 and 15 N; 120 rpm) (see Fig. 8.23). In the absence of applied load, ED Ni–SiC nanostructured composite coating presents a wide passivation plateau (0.8 V) starting immediately after the zero-current potential, limited at the cathodic end by the hydrogen evolution and by the transpassive dissolution domain at the anodic end. The anodic current on the passivation plateau is in the order of 10 μA. When load is applied, there is no change in current in the region of hydrogen evolution. However, an increase in anodic current is observed in the potential range from −0.8 to −0.0 vs. mercury-mercuric sulfate electrode (SSE), which indicates dissolution of the coating. With increase in normal load, the anodic current is increased further. This potential dependent dissolution reaction appears to be due to the slow oxide growth rate compared with the frequency of mechanical depassivation caused by the friction.

The observed changes can be explained based on a concept of 'active wear track'. Under friction, the measured current I can be considered as the sum of two partial currents, I_t and I_p,

$$I = I_t + I_p \qquad [8.1]$$

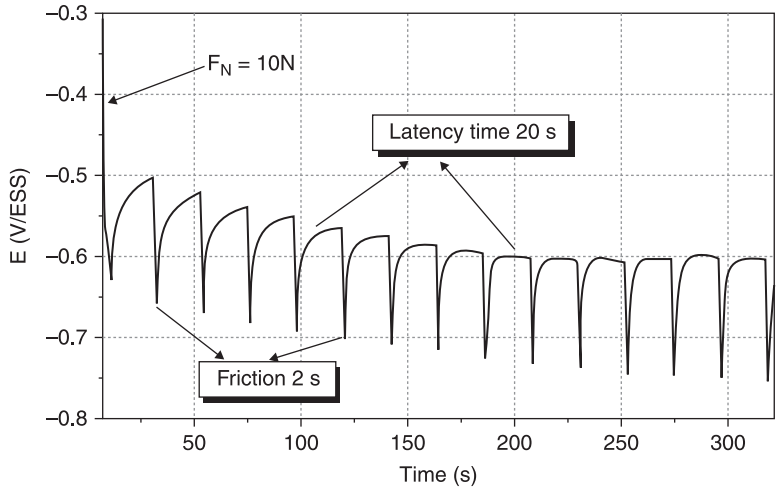

(a)

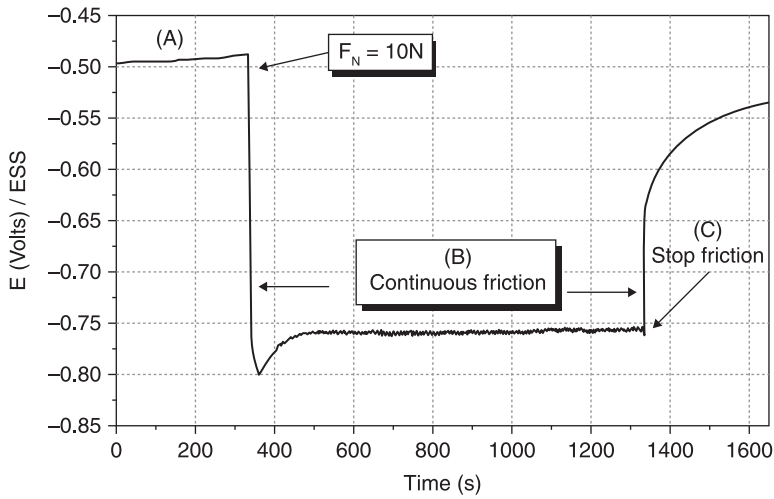

(b)

8.22 Change in free corrosion potential (FCP) of ED Ni-SiC nanostructured coatings in 0.5 M K_2SO_4 (conditions: Watts nickel bath; average diameter of SiC: 20 nm; coating thickness: 50 μm; contact configuration: pin-on-disc; disc: coated steel; pin: 7 mm ∅ cylindrical alumina pin having a lower spherical end of 100 mm radius; applied load: 5–20 N; rotation speed: 30–120 tours/min.): (a) variation in the FCP during intermittent friction test with a latency time of 20 s; and (b) variation in the FCP during continuous friction test – before loading (area A), during continuous friction (area B), and after stopping the friction (area C). (Potentials are in volts vs. mercury–mercuric sulfate electrode (SSE)) (Benea *et al.,* 2009).

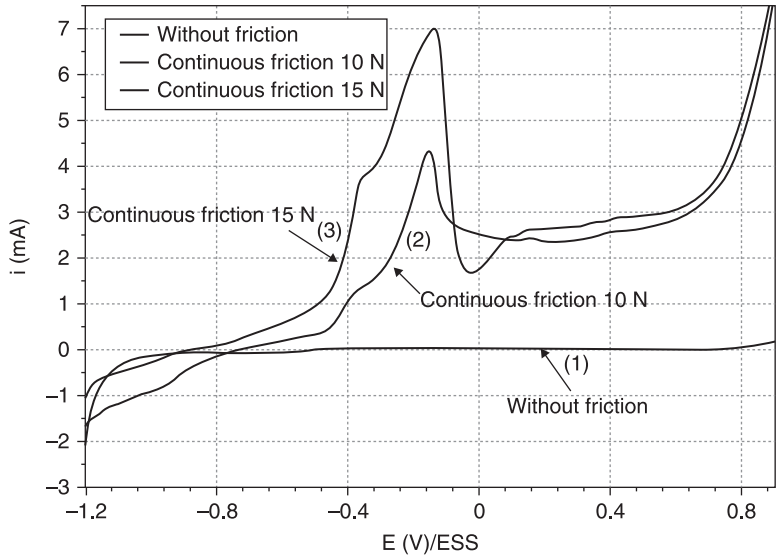

8.23 Potentiodynamic polarization curves of ED Ni–SiC nanostructured composite coating in 0.5 M K_2SO_4 recorded by direct potential scan at 0.1 V/min under the same test conditions as Fig. 8.22: Curve (1), no friction applied; Curve (2), continuous friction at 10 N; 120 rpm; Curve (3), continuous friction at 15 N, 120 rpm. (Potentials are in volts vs. mercury–mercuric sulfate electrode (SSE)) (Benea *et al.*, 2009).

where I_t is the current originating from the wear track areas where the passive film is destroyed and the surface is active, and I_p is the current linked to the surface that is not subjected to friction and remains in a passive state.

The tribocorrosion behavior of ED Ni–SiC nanocomposite coated SS in 0.5 M K_2SO_4 reveals that the coating exhibits a stable FCP under static conditions and the application of friction destroys the passive oxide film, thus making the surface active and promoting dissolution. The overall performance of nanocomposite coatings under conditions of tribocorrosion is determined by the kinetics of mechanical removal of the passive layer with the applied friction and by the kinetics of the repassivation when the friction is stopped.

The tribocorrosion behavior of ED Ni–P–SiC nanocomposite coatings having different volume fractions of nanoparticles was studied by Malfatti *et al.* (2009). These coatings were prepared by varying the bath loading of the nanosized SiC particles. For a bath loading of 10, 80 and 200 g/l, the number of SiC particles incorporated in the ED Ni–P matrix per μm^2 is 0.21, 0.84 and 1.44. These coatings are designated as NiPSiC10, NiPSiC80 and NiPSiC200, whereas the coating prepared in the absence of SiC particles is represented as NiP. All of them were heat treated at 420°C for 1 h in an inert atmosphere. The current–time transients of NiP, NiPSiC10, NiPSiC80 and NiPSiC200 coatings under

tribocorrosion conditions in 0.6 M NaCl (see Fig. 8.24) reveal a significant increase in anodic current for all the coatings, suggesting removal of the surface layer and activation of the surface at the contact zone. The anodic current is comparable for NiP and NiPSiC10 coatings, while it is much higher for NiPSiC80 and NiPSiC200 coatings. This observation suggests that increase in number density of nanosized particles in the NiP matrix beyond a threshold level causes a deleterious influence on tribocorrosion.

The microhardness of NiPSiC10, NiPSiC80 and NiPSiC100 nanocomposite coatings exhibits a linear increase with the number density of particles per unit area. In addition, lower wear rates are observed for NiPSiC80 and NiPSiC200 nanocomposite coatings compared with those of NiPSiC10 and NiP coatings. The increase in hardness of NiPSiC80 and NiPSiC200 enables them to achieve a better wear resistance. However, these coatings exhibit a poor tribocorrosion performance. Electrochemical measurements performed in 0.6 M NaCl in the absence of tribological conditions indicate that the corrosion current density is relatively higher for NiPSiC80 and NiPSiC200 than NiPSiC10 and NiP coatings. This could be due to increase in surface roughness and residual stress with increase in number density of particles per unit area. The coefficient of friction measured during tribocorrosion is relatively higher for the NiPSiC200 coating than for the NiP coating (see Fig. 8.25). This could be due to the entrapment of debris (both from the NiP matrix as well as from the SiC particle). The higher hardness of NiPSiC200 could also be a reason for the formation of cracks in the coating – the electrolyte could penetrate through these cracks and promote delamination of the coating, which would enhance entrapment of debris at the contact zone.

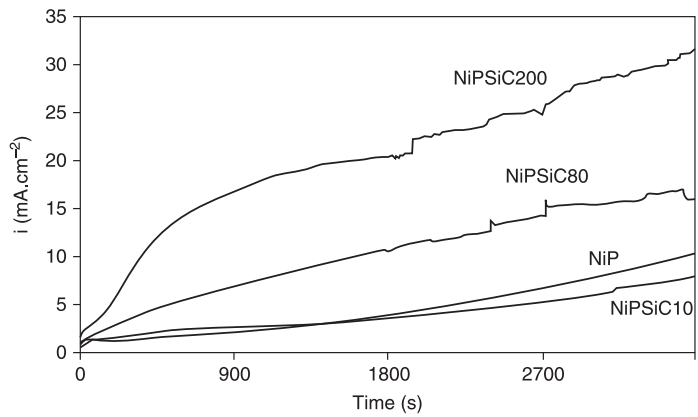

8.24 Current–time transients of NiP, NiPSiC10, NiPSiC80 and NiPSiC200 coatings under tribocorrosion conditions in 0.6 M NaCl (conditions: contact configuration: ball-on-plate; coated steel as plate and corundum ball (5 mm ∅) as counter body; load: 8 N; frequency: 2 Hz; stroke length: 1 mm; number of fretting cycles: 3500. Tests were conducted with an impressed anodic potential of + 400 mV vs. SCE) (Malfatti *et al.*, 2009).

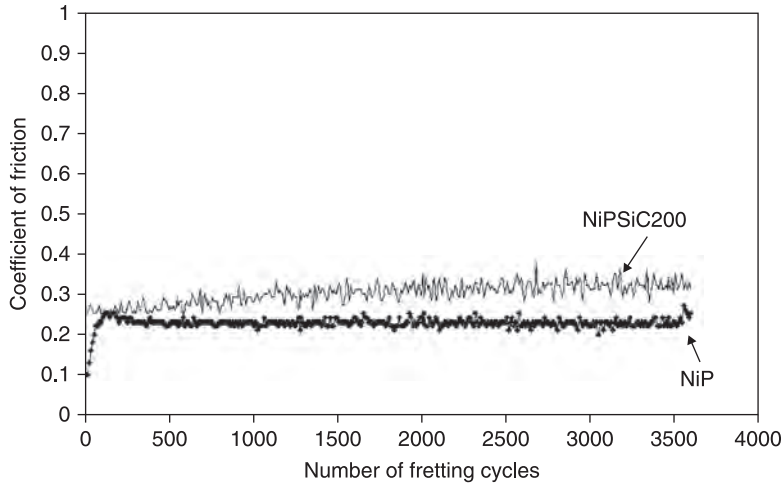

8.25 Friction coefficient of NiP and NiPSiC200 coatings during tribocorrosion in 0.6 M NaCl under the same test conditions as Fig. 8.24 (Malfatti *et al.,* 2009).

8.3.3 Effect of electroless deposited nanocomposite coating

Effect of electroless Ni-P-nano SiC composite coatings on the cavitation erosion corrosion of steel

The continuous formation and collapse of numerous bubbles at the surface of a component, created due to localized pressure changes during high-velocity fluid flow, could lead to cavitation erosion. Collapse of these bubbles is always accompanied by the emission of shockwaves and micro-jets, which will exert stress pulses on solid surfaces in the vicinity. Repetitions of shockwaves on the solid surface will eventually lead to fatigue failure, fracture and material loss (Brennen, 1995; Kwok *et al.*, 2000). Cavitation erosion is commonly observed in valves in nuclear power plants and in pumps in the petroleum industry. Cavitation erosion is essentially a mechanical process. However, in many working environments, cavitation erosion and corrosion occur simultaneously, and if corrosion does occur it will accelerate the rate of cavitation erosion damage.

Lin and He (2005) have compared the role of electroless (EL) NiP composite coatings incorporated with micron- and nanosized SiC particles on the cavitation erosion of AISI 1045 steel. The EL Ni-P-nano SiC and Ni-P-micro SiC composite coatings were prepared by dispersing nano (25–50 nm) and micron- (5 μm) sized particles in an acidic hypophosphite-reduced EL nickel plating bath maintained at 90 ± 1°C. The deposition time was 3 h and the coating thickness was 60 μm. All the coatings were subjected to post heat-treatment to achieve a better hardness and wear

resistance. The cavitation erosion corrosion of EL Ni-P-nano SiC and EL Ni-P-micro SiC composite coatings in 3.5% NaCl was determined in accordance with ASTM G 32–98. The horn frequency and amplitude were set at 20 kHz and 25 μm, respectively. The mass loss of the specimens and the macroscopic surface changes were determined at 15-minute intervals during the entire test period of 240 minutes.

Incorporation of nanosized SiC particles in the EL NiP matrix increased the hardness from 627 ± 43 to 704 ± 60 $HV_{0.05}$. However, incorporation of micron-sized SiC particles increased the hardness to 1669 $HV_{0.05}$. The cumulative mass loss versus time (see Fig. 8.26) due to cavitation erosion corrosion in 3.5% NaCl is found to be very low for EL Ni-P-nano SiC composite coating compared with its counterpart incorporating micron-sized SiC particles. The EL Ni-P-nano SiC coated specimen exhibits a smooth and uniform surface after the cavitation erosion corrosion test with no visible pits (see Fig. 8.27). The uniform distribution of the nanosized SiC particles in the EL NiP matrix (R_a: 0.95 ± 0.060 μm) inhibits the formation of pits. However, the higher surface roughness (R_a: 1.72 ± 0.051 μm) promotes bubble formation and causes detachment of the SiC particles, which results in the formation of small cavities on the surface of EL Ni-P-micro SiC coated steel (see Fig. 8.27). Hence, it is evident that incorporation of nanosized particles in EL NiP matrix could provide a better cavitation erosion corrosion resistance and inhibit the onset of erosion damage near surface defects.

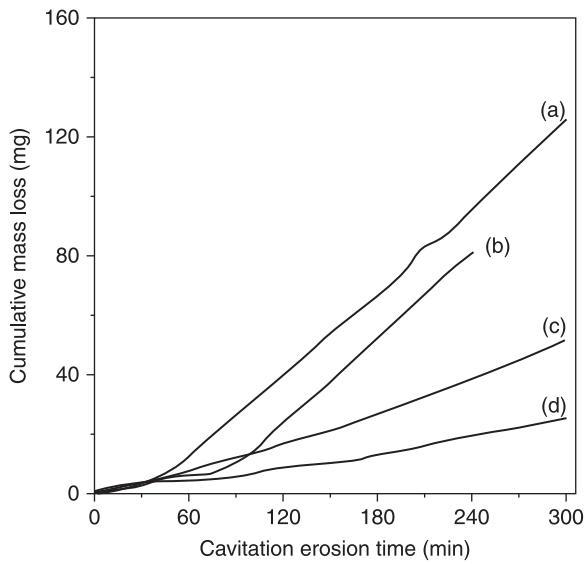

8.26 Cumulative mass loss measured as a function of cavitation erosion time in 3.5 wt% NaCl for: (a) uncoated AISI 1045 steel; (b) EL NiP coated steel; (c) EL Ni-P-micro SiC coated steel and (d) EL Ni-P-nano SiC coated steel (all the coated steels are subjected to heat treatment) (Lin *et al.*, 2006).

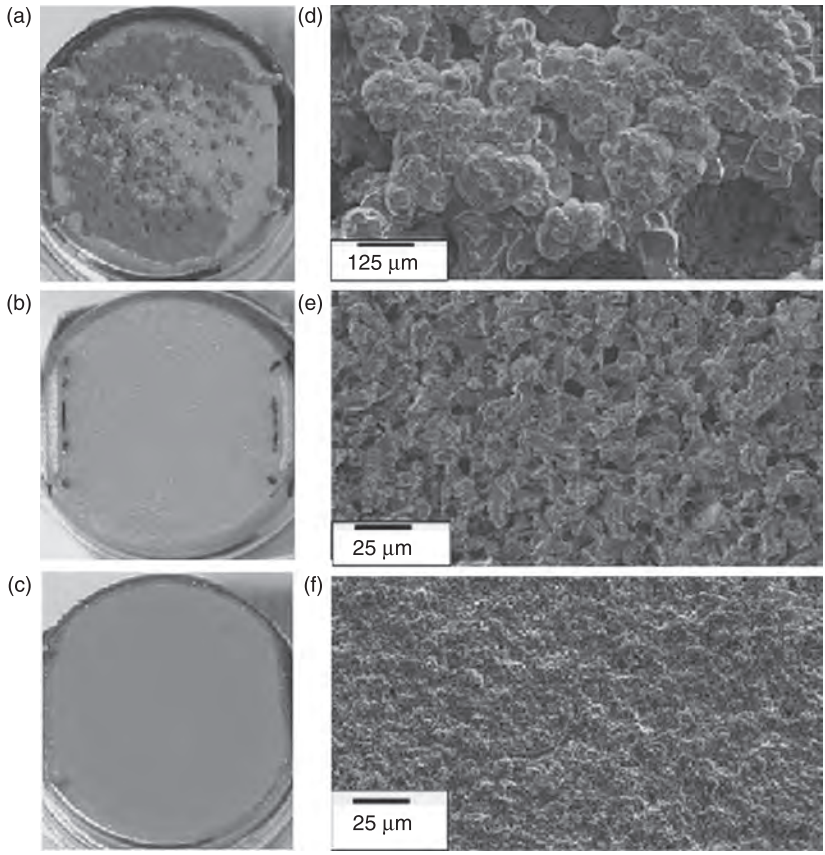

8.27 Visual appearance ((a)–(c)) and surface morphology ((d)–(f)) of EL NiP coated steel ((a) and (d)); EL Ni-P-micro SiC coated steel ((b) and (e)); and EL Ni-P-nano SiC coated steel ((c) and (f)) (all subjected to heat treatment) after 240 min of cavitation erosion in 3.5 wt% NaCl (Lin *et al.*, 2006).

8.3.4 Effect of nanostructuring on the tribocorrosion of titanium

Nanostructuring enables an improvement in hardness and tribological behavior of a variety of materials. Hence, it will be of great interest to know how nanostructuring can help to improve tribocorrosion resistance. The tribocorrosion behavior of nanostructured titanium sliding against an alumina ball in phosphate buffer solution (PBS) was studied by Faghihi *et al.* (2010). Untreated and annealed titanium were used as controls. Annealing of titanium was carried out in a tubular furnace at 800°C for 12 h in an ultra-pure argon atmosphere subsequently cooled to room temperature. Nanostructuring of titanium was

achieved using the principle of severe plastic deformation by high-pressure torsion. During this treatment, the titanium discs (12 mm Ø and 1 mm thick) were placed between anvils, compressed and deformed under an applied pressure of 6 GPa at room temperature for five complete cycles, which is equivalent to a true logarithmic strain of ~6.

The cathodic shift in FCP observed with the onset of sliding (see Fig. 8.28) suggests removal of the oxide layer. The fluctuations in FCP observed during sliding indicate continuous formation and removal of the passive oxide layer. The anodic shift in FCP after the sliding motion is stopped suggests repassivation of the damaged material surface in the wear track (Azzi and Szpunar, 2007). The change in FCP, measured as a function of time, appears to be similar for nanostructured, annealed and untreated titanium (see Fig. 8.28). However, the width and depth of the wear track clearly indicate the difference in their performance under tribocorrosion conditions. The width of the wear track for nanostructured titanium is ~473 ± 26 μm, which is much lower than ~670 ± 19 μm and ~696 ± 39 μm for untreated and annealed titanium, respectively (see Fig. 8.29). The wear depth measured at the cross-section of the wear tracks was ~10.6 ± 1.5 μm, ~18.9 ± 1.0 μm and ~21.6 ± 0.5 μm for nanostructured, untreated and annealed titanium, respectively (see Fig. 8.30). The

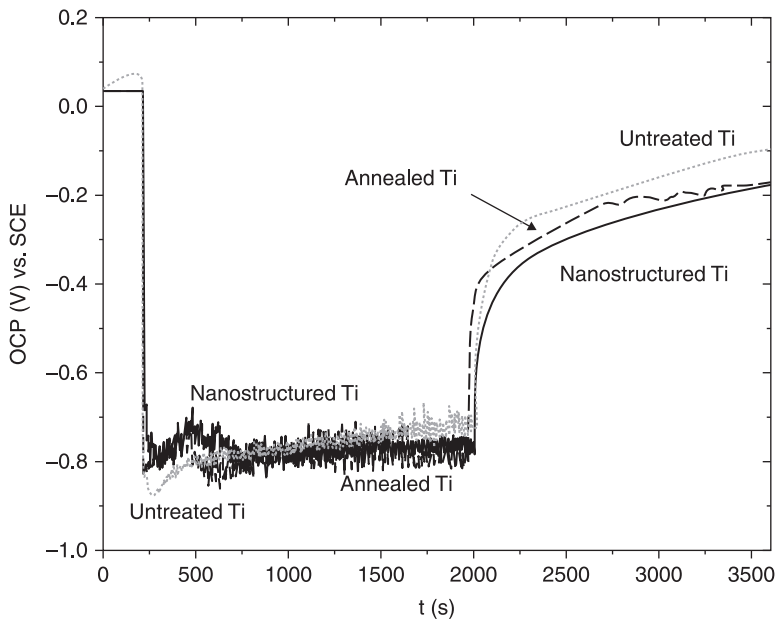

8.28 Change in free corrosion potential (FCP) of untreated, annealed and nanostructured titanium sliding against the alumina ball in phosphate buffer solution as a function of time (conditions: ball-on-plate contact configuration; counter face: 4.75 mm ∅ alumina ball; load: 5 N; stroke length: 5 mm; frequency: 1 Hz) (Faghihi *et al.*, 2010).

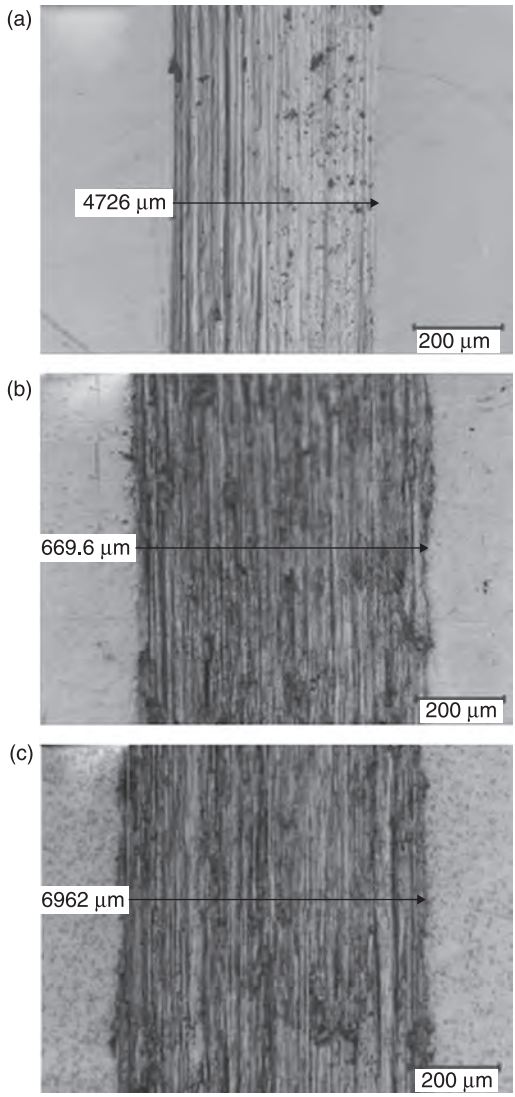

8.29 Wear tracks of (a) nanostructured, (b) untreated and (c) annealed titanium substrates after subjecting them to tribocorrosion testing in a phosphate buffer solution under the same test conditions as Fig. 8.28 (Faghihi *et al.*, 2010).

wear tracks of untreated and annealed titanium are rough. Several grooves, signs of severe plastic deformation and intergranular fracture features could be seen on the worn surfaces of these samples (see Fig. 8.31). In contrast, the extent of deformation and generation of wear debris are relatively less for nanostructured titanium, suggesting the involvement of a mild abrasion wear mechanism (see Fig. 8.31).

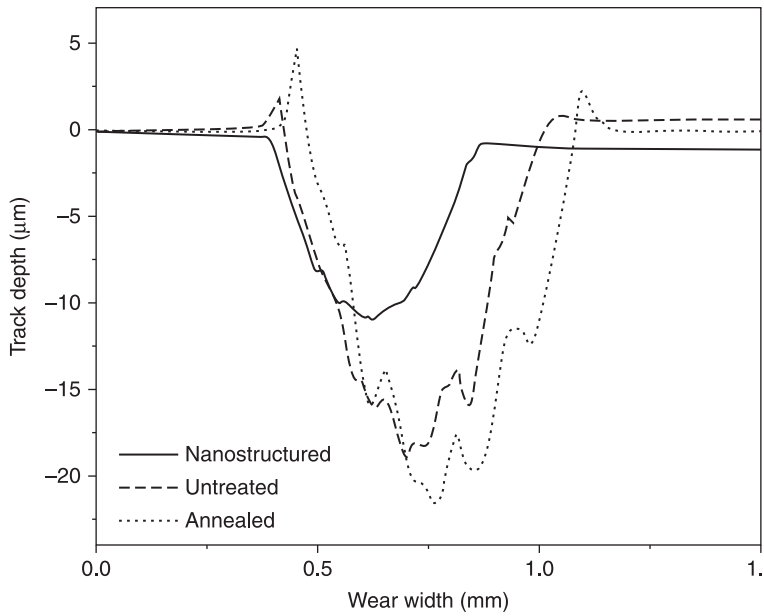

8.30 Wear depth measured at the cross-section of the wear tracks of annealed, untreated and nanostructured titanium after subjecting them to tribocorrosion testing in a phosphate buffer solution under the same test conditions as Fig. 8.28 (Faghihi *et al.*, 2010).

Nanostructured titanium has higher hardness and strength than untreated and annealed titanium. Both untreated and annealed titanium exhibit a preferred orientation of $(10^{-}10)$ and $(11^{-}20)$ before the wear test. However, after sliding against the alumina ball, their texture is changed to (0002), which could be correlated with a strain-induced transformation. In contrast, nanostructured titanium exhibits a preferred texture of (0022) both before and after the wear test. The stresses accumulated because of the change in texture at the surface could have contributed to the increase of the wear rate under application of the load. This attribute is supported by the surface and subsurface cracks observed for untreated and annealed samples within the plastically deformed regions (see Fig. 8.31) (Geiger *et al.*, 1998; Buscher *et al.*, 2004; Kim *et al.*, 2007).

The study demonstrates that nanostructured titanium obtained by high-pressure torsion offers a better tribocorrosion performance than untreated and annealed titanium. The nanostructured titanium has been shown to possess higher surface energy and hydrophilicity and a positive effect on the bone-forming cell response compared with the coarse-grained samples (Faghihi *et al.*, 2007). The excellent biological surface activity, superior bulk properties and improved tribocorrosion performance suggest nanostructured titanium as a promising alternative for the currently used materials for titanium-based medical devices.

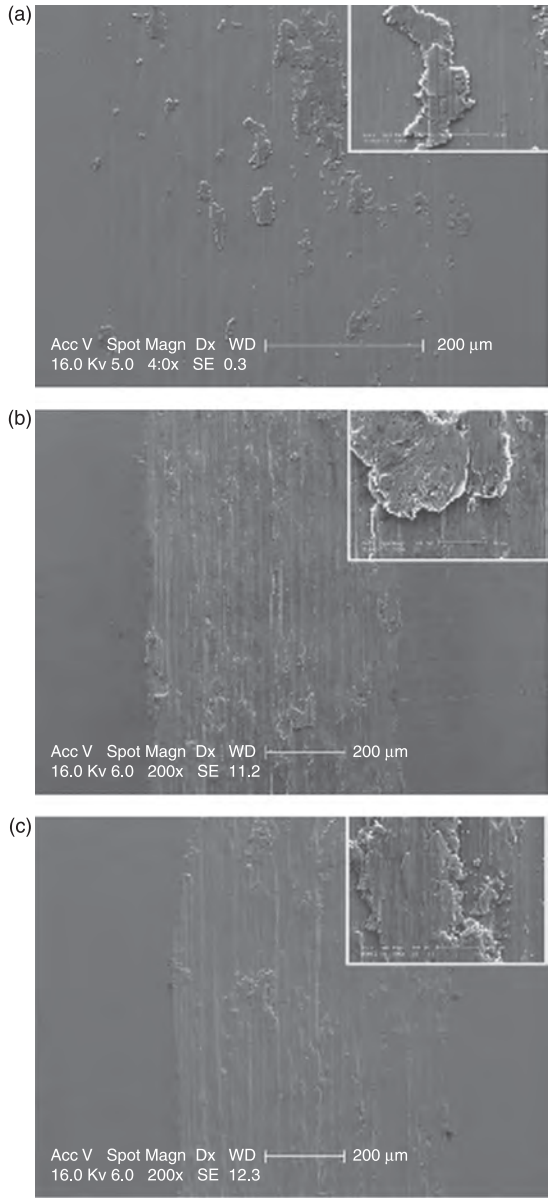

8.31 SEM analysis of worn surface morphologies of (a) nanostructured, (b) untreated and (c) annealed titanium substrates after subjecting them to tribocorrosion testing in a phosphate buffer solution under the same test conditions as Fig. 8.28 (Faghihi *et al.*, 2010).

8.4 Conclusions

The tribocorrosion behavior of materials depends on many factors: equipment design and operation, electrochemical conditions that prevail at the interface, properties of the electrolyte and surface of the contacting materials, and the nature of any tribochemically assisted surface layer. The most important aspect is that none of these factors act independently, but they are mutually dependent on each other and often exhibit a synergy.

Nanoparticles have the ability to provide a lubrication effect during the corrosion wear process. However, formation of a layer of rather loose particles on the metal surface alone is not sufficient and some mechanical loading is necessary to form a protective and compact nanoparticle layer which can act as a third body, protecting the metal surface against abrasion and depassivation (at passive potential). The contact pressure and rigidity, as well as the interaction forces between particles, are critical parameters in determining the formation and stability of this third-body layer. The ability of nanoparticle suspensions to compete with the commercially available oil-in-water emulsions in terms of friction and wear confirms their potential as a chemically stable and non-polluting lubricant in the near future.

The formation of nanosized debris at the contact zone could increase friction, cause local damage to passive oxide film and accelerate the release of metal ions during micro-abrasion–corrosion. However, the resultant effect is a function of the quantity of nanosized debris, the type of mechanical motion and the nature of the surrounding environment. Beyond a threshold level, the nanosized particles might act as rolling balls in the contact, which is consistent with the bedding-in theory. Bovine serum would enable the formation of conglomerates, which could trap the nanosized particles. These factors could effectively reduce the extent of abrasion–corrosion damage.

Nanostructured materials and coatings, in general, offer an improved performance under tribocorrosion conditions. Their overall performance is determined by the kinetics of mechanical removal of the passive layer with the applied friction, and by the kinetics of the repassivation when the friction is stopped. However, improvements in mechanical properties such as high hardness and ductility, etc, and in surface properties such as the uniform distribution of particles in the case of composite coatings, lower surface roughness, lower residual stresses, favorable textures with lower accumulation of stresses, etc, are necessary to achieve better performance.

8.5 Acknowledgments

The author thanks Dr S. Srikanth, Director, National Metallurgical Laboratory, Jamshedpur, for his keen interest and kind permission to publish this book chapter. The author expresses his sincere thanks to Professor Mischler, Professor R. J. K. Wood and Professor M. M. Stack for their kind help in providing useful materials and many helpful discussions in writing this chapter.

8.6 References

Amstutz H. C., Campbell P., McKellop H., Schmalzried T. P., Gillespie W. J. *et al.* (1996), 'Metal on metal total hip replacement workshop consensus document', *Clin. Orthop. Relat. Res.*, **329**(Suppl), S297–303.

Antler M. (1985), 'Electrical effects of fretting connector contact materials: A review', *Wear*, **106**, 5–33. (doi:10.1016/0043-1648(85)90101-2)

Azzi M. and Szpunar J. A. (2007), 'Tribo-electrochemical technique for studying tribocorrosion behavior of biomaterials', *Biomol. Eng.*, **24**, 443–6. (doi:10.1016/j.bioeng.2007.07.015)

Balaraju J. N., Sankara Narayanan T. S. N. and Seshadri S. K. (2003), 'Electroless Ni–P composite coatings', *J. Appl. Electrochem.*, **33**, 807–16. (doi: 10.1023/A:1025572410205)

Barril S., Mischler S. and Landolt D. (2005), 'Electrochemical effects on the fretting corrosion behaviour of Ti6Al4V in 0.9% sodium chloride solution', *Wear*, **259**, 282–91. (doi:10.1016/j.wear.2004.12.012)

Basak A. K., Matteazzi P., Vardavoulias M. and Celis J. P. (2006), 'Corrosion–wear behaviour of thermal sprayed nanostructured FeCu/WC-Co coatings', *Wear*, **261**, 1042–50. (doi:10.1016/j.wear.2006.03.026)

Bello J. O., Wood R. J. K. and Wharton J. A. (2007), 'Synergistic effects of micro-abrasion corrosion of UNS S30403, S31603 and S32760 stainless steels', *Wear*, **263**, 149–59. (doi:10.1016/j.wear.2006.12.044)

Benea L., Bonora P. L., Borello A. and Martelli S. (2002), 'Wear corrosion properties of nano-structured SiC–nickel composite coatings obtained by electroplating', *Wear*, **249**, 995–1003. (doi:10.1016/S0043-1648(01)00844-4)

Benea L., Ponthiaux P., Wenger F., Galland J., Hertz D. *et al.* (2004), 'Tribocorrosion of stellite 6 in sulfuric acid medium: electrochemical behaviour and wear', *Wear*, **256**, 948–53. (doi:10.1016/j.wear.2003.06.003)

Benea L., Wenger F., Ponthiaux P. and Celis J. P. (2009), 'Tribocorrosion behaviour of Ni-SiC nano-structured composite coatings obtained by electrodeposition', *Wear*, **266**, 398–405. (doi:10.1016/j.wear.2008.04.018)

Berradja A., Bratu F., Benea L., Willems G. and Celis J. P. (2006), 'Effect of sliding wear on tribocorrosion behaviour of stainless steels in a Ringer's solution', *Wear*, **261**, 987–93. (doi:10.1016/j.wear.2006.03.003)

Braunovic M. (1989), 'Fretting damage in tin-plated aluminium and copper connectors', *IEEE Trans. Comp., Hybrids, Manuf. Technol.*, **12**, 215–23. (doi: 10.1109/33.31426)

Brennen C. E. (1995), *Cavitation and Bubble Dynamics*. New York: Oxford University Press, pp. 1–30.

Brown S. A., Hughes P. J. and Merrit K. (1988), '*In vitro* studies of fretting corrosion of orthopaedic materials', *J. Ortho. Res.*, **6**, 572–9. (doi: 10.1002/jor.1100060415)

Buscher R., Gleising B., Dudzinski W. and Fischer A. (2004), 'The effects of subsurface deformation on the sliding wear behaviour of a microtextured high-nitrogen steel surface', *Wear*, **257**, 284–91. (doi:10.1016/j.wear.2003.12.013)

Buscher R. and Fischer A. (2005), 'The pathways of dynamic recrystallization in all-metal hip joints', *Wear*, **259**, 887–97. (doi:10.1016/j.wear.2005.02.036)

Catelas I., Bobyn J. D., Medley J. B., Krygier J. J., Zukor D. J. *et al.* (2001), 'Effects of digestion protocols on the isolation and characterization of metal–metal wear particles. I. Analysis of particle size and shape', *J. Biomed. Mat. Res.*, **55**, 320–9. (doi: 10.1002/1097-4636(20010605))

Celis J. P., Ponthiaux P. and Wenger F. (2006), 'Tribo-corrosion of materials: Interplay between chemical, electrochemical, and mechanical reactivity of surfaces', *Wear*, **261**, 939–46. (doi:10.1016/j.wear.2006.03.027)

Chan F. W., Bobyn J. D., Medley J. B., Krygier J. J., Yue S. (1996), 'Engineering issues and wear performance of metal on metal hip implants', *Clin. Orthop. Relat. Res.*, **333**, 96–107.

Chen S. and Liu W. (2001), 'Characterization and antiwear ability of non-coated ZnS nanoparticles and DDP-coated ZnS nanoparticles', *Mater. Res. Bull.*, **36**, 137–43. (doi:10.1016/S0025-5408(00)00477-3)

Faghihi S., Azari F., Zhilyaev A. P., Szpunar J. A., Vali H. *et al.* (2007), 'Cellular and molecular interactions between MC3T3-E1 pre-osteoblasts and nanostructured titanium produced by high-pressure torsion', *Biomaterials*, **28**, 3887–95. (doi:10.1016/j.biomaterials.2007.05.010)

Faghihi S., Li D. and Szpunar J. A. (2010), 'Tribocorrosion behaviour of nanostructured titanium substrates processed by high-pressure torsion', *Nanotechnology*, **21**, 485703. (doi: 10.1088/0957-4484/21/48/485703)

Galliano F., Galvanetto E., Mischler S. and Landolt D. (2001), 'Tribocorrosion behavior of plasma nitrided Ti-6Al-4V alloy in neutral NaCl solution', *Surf. Coat. Technol.*, **145**, 121–31. (doi:10.1016/S0257-8972(01)01309-3)

Gee M. G., Gant A., Hutchings I., Bethke R., Schiffman K. *et al.* (2003), 'Progress towards standardisation of ball cratering', *Wear*, **255**, 1–13. (doi:10.1016/S0043-1648(03)00091-7)

Geiger M., Roth S. and Becker W. (1998), 'Influence of laser-produced microstructures on the tribological behaviour of ceramics', *Surf. Coat. Technol.*, **100–1**, 17–22. (doi:10.1016/S0257-8972(97)00581-1)

Geringer J., Forest B. and Combrade P. (2005), 'Fretting-corrosion of materials used as orthopaedic implants', *Wear*, **259**, 943–51. (doi:10.1016/j.wear.2004.11.027)

Gleiter H. (1989), 'Nanocrystalline materials', *Prog. Mater. Sci.*, **33**, 223–315. (doi:10.1016/0079-6425(89)90001-7)

Gleiter H. (1992), 'Nanostructured Materials', *Adv. Mater.*, **4**, 474–81. (doi: 10.1002/adma.19920040704)

Goodman S. B. (1994), 'Compatibility of biomedical implants', in Kovacs P. and Istephanous N. S. (Eds), *Proceedings of the Electrochemical Society*, Pennington, NJ: The Electrochemical Society Inc.

Gurrappa I. and Binder L. (2008), 'Electrodeposition of nanostructured coatings and their characterization – A review', *Sci. Technol. Adv. Mater.*, **9**, 043001 (doi:10.1088/1468-6996/9/4/043001)

Gyftou P., Stroumbouli M., Pavlatou E. A., Asimidis P. and Spyrellis N. (2005), 'Tribological study of Ni matrix composite coatings containing nano and micro SiC particles', *Electrochim. Acta*, **50**, 4544–50. (doi:10.1016/j.electacta.2004.10.090)

Hannel S., Fouvry S., Kapsa P. and Vincent L. (2001), 'The fretting sliding transition as a criterion for electrical contact performance', *Wear*, **249**, 761–70. (doi:10.1016/S0043-1648(01)00685-8)

Hassani Sh., Raeissi K., Azzi M., Li D., Golozar M. A. *et al.* (2009), 'Improving the corrosion and tribocorrosion resistance of Ni–Co nanocrystalline coatings in NaOH solution', *Corros. Sci*, **51**, 2371–9. (doi:10.1016/j.corsci.2009.06.026)

Hoeppner D. W. and Chandrasekaran V. (1994), 'Fretting in orthopaedic implants: A review', *Wear*, **173**, 189–97. (doi:10.1016/0043-1648(94)90272-0)

Howie D. W., McGee M. A., Costi K. and Graves S. E. (2005), 'Metal-on-metal resurfacing versus total hip replacement-the value of a randomized clinical trial', *Orthop. Clin. N. Am.*, **36**, 195–201. (doi:10.1016/j.ocl.2004.12.001)

Hu Z. S., Lai R., Lou F., Wang L. G., Chen Z. L. *et al.* (2002), 'Preparation and tribological properties of nanometer magnesium borate as lubricating oil additive', *Wear*, **252**, 370–4. (doi:10.1016/S0043-1648(01)00862-6)

Jacobs J. J., Skipor A. K., Patterson L. M., Hallab N. J., Paprosky W. G. *et al.* (1998), 'Metal release in patients who have had a primary total hip arthroplasty. A prospective, controlled, longitudinal study', *J. Bone Jt Surg. Am.*, **80**, 1447–58.

Kato K. (2010), 'Wear in relation to friction – a review', *Wear*, **241**, 151–7. (doi:10.1016/S0043-1648(00)00382-3)

Kerr C., Barker D., Walsh F. and Archer J. (2000), 'Electrodeposition of composite coatings based on metal matrix-included particle deposits', *Trans. IMF*, **78**, 171–8.

Kim Y. S., Kim S. D. and Kim S. J. (2007), 'Effect of phase transformation on wear of high-nitrogen austenitic 18Cr-18Mn-2Mo-0.9N steel', *Mater. Sci. Eng. A*, **449**, 1075–8. (doi:10.1016/j.msea.2006.02.294)

Koch C. C., Morris D. G., Lu K. and Inoue A. (1999), 'Ductility of nanostructured materials', *Mater. Res. Soc. Bull.*, **24**, 54–8.

Koch C. C. (2003a), 'Top-down synthesis of nanostructured materials: Mechanical and thermal processing methods', *Rev. Adv. Mater. Sci.*, **5**, 91–9.

Koch C. C. (2003b), 'Optimization of strength and ductility in nanocrystalline and ultrafine grained metals', *Scripta Mater.*, **49**, 657–62. (doi:10.1016/S1359-6462(03)00394-4)

Koch C. C., Ovid'ko I. A., Seal S. and Veprek S. (2007), *Structural Nanocrystalline Materials: Fundamentals and Applications*. Cambridge: Cambridge University Press.

Komotori J., Hisamori N. and Ohomoric Y. (2007), 'The corrosion/wear mechanisms of Ti-6Al-4V alloy for different scratching rates', *Wear*, **263**, 412–18. (doi:10.1016/j.wear.2006.11.025)

Kramer I. R. and Demer L. J. (1961), 'The effect of surface removal on the plastic behaviour of aluminium single crystals', *Trans. AIME*, **221**, 780–6.

Kwok C. T., Cheng F. T. and Man H. C. (2000), 'Synergistic effect of cavitation erosion and corrosion of various engineering alloys in 3.5% NaCl solution', *Mater. Sci. Eng. A.*, **290**, 145–54. (doi:10.1016/S0921-5093(00)00899-6)

Landolt D., Mischler S. and Stemp M. (2001), 'Electrochemical methods in tribocorrosion: a critical appraisal', *Electrochim. Acta*, **46**, 3913–29. (doi:10.1016/S0013-4686(01)00679-X)

Lemaire E. and Le Calvar M. (2001), 'Evidence of tribocorrosion wear in pressurized water reactors', *Wear*, **249**, 338–44. (doi:10.1016/S0043-1648(00)00544-5)

Lin C. J. and He J. L. (2005), 'Cavitation erosion behavior of electroless nickel-plating on AISI 1045 steel', *Wear*, **259**, 154–9. (doi:10.1016/j.wear.2005.02.099)

Low C. T. J., Wills R. G. A. and Walsh F. C. (2006), 'Electrodeposition of composite coatings containing nanoparticles in a metal deposit', *Surf. Coat. Technol.*, **201**, 371–83. (doi:10.1016/j.surfcoat.2005.11.123)

Lu B. T., Luo J. L., Mohammadi F., Wang K. and Wan X. M. (2008), 'Correlation between repassivation kinetics and corrosion rate over a passive surface in flowing slurry', *Electrochim. Acta*, **53**, 7022–31. (doi:10.1016/j.electacta.2008.02.083)

Lu K. (1996), 'Nanocrystalline metals crystallized from amorphous solids: nanocrystallization, structure, and properties', *Mater. Sci. Eng. R*, **16**, 161–221. (doi:10.1016/0927-796X(95)00187-5)

Lu L., Sui M. L. and Lu K. (2000), 'Superplastic extensibility of nanocrystalline copper at room temperature', *Science* **287**, 1463–6. (doi: 10.1126/science.287.5457.1463)

Malfatti C. F., Veit H. M., Santos C. B., Metzner M., Hololeczek H. *et al.* (2009), 'Heat Treated NiP–SiC Composite Coatings: Elaboration and Tribocorrosion Behaviour in NaCl Solution', *Tribol. Lett.*, **36**, 165–73. (doi 10.1007/s11249-009-9471-1)

Malucci R. D. (2001), 'Characteristics of films developed in fretting experiments on tinplated contacts', *IEEE Trans. Comp. Packag. Technol.*, **24**, 399–407. (doi: 10.1109/6144.946486)

Manhabosco T. M. and Muller I. L. (2009), 'Tribocorrosion of Diamond-Like Carbon Deposited on Ti6Al4V', *Tribol. Lett.*, **33**, 193–7. (doi: 10.1007/s11249-009-9408-8)

Mathew M. T., Srinivasa Pai P., Pourzal R., Fischer A. and Wimmer M. A. (2009), 'Significance of Tribocorrosion in Biomedical Applications: Overview and Current Status', *Adv. Tribol.*, **2009**, 250986 (doi: 10.1155/2009/250986)

Meunier A. and Sedel L. (1998), 'Actes des journees francophones de tribologie-corrosion', in *Societe Tribologique de France*, Kapsa Ph (Ed.). Paris: SIRPE, pp. 193–200.

Meyers M. A., Mishra A. and Benson D. J. (2006), 'Mechanical properties of nanocrystalline materials', *Prog. Mater. Sci.*, **51**, 427–556. (doi:10.1016/j.pmatsci.2005.08.003)

Mischler S. (2008), 'Triboelectrochemical techniques and interpretation methods in tribocorrosion: A comparative evaluation', *Tribol. Int.*, **41**, 573–83. (doi:10.1016/j.triboint.2007.11.003)

Nevilee A. and McDougall B. A. B. (2002), 'Electrochemical assessment of erosion-corrosion of commercially pure titanium and a titanium alloy in slurry impingement', *Proc. Instn. Mech. Engrs., Part L – Materials, Design and Applications*, **216**, 31–41.

Pabinger C., Biedermann R., Stocke B., Fischer M. and Krismer M. (2003) 'Migration of metal-on-metal versus ceramic-on-polyethylene hip prostheses', *Clin. Orthop. Relat. Res.*, **412**, 103–10.

Park Y. W., Sankara Narayanan T. S. N. and Lee K. Y. (2006a), 'Effect of fretting amplitude and frequency on the fretting corrosion behaviour of tin plated contacts', *Surf. Coat. Technol.*, **201**, 2181–92. (doi:10.1016/j.surfcoat.2006.03.031)

Park Y. W., Sankara Narayanan T. S. N. and Lee K. Y. (2006b), 'Fretting wear behaviour of tin plated contacts: influence on contact resistance', *Surf. Rev. Lett.*, **13**, 635–44. (doi: 10.1142/S0218625X06008591)

Park Y. W., Sankara Narayanan T. S. N. and Lee K. Y. (2007a), 'Degradation of tin-plated connectors by fretting corrosion—evaluation of surface characteristics', *Tribol. Int.*, **40**, 548–59. (doi:10.1016/j.triboint.2006.05.008)

Park Y. W., Sankara Narayanan T. S. N. and Lee K. Y. (2007b), 'Effect of temperature on the fretting corrosion of tin-plated brass connectors', *Wear*, **262**, 320–30. (doi:10.1016/j.wear.2006.05.020)

Park Y. W., Sankara Narayanan T. S. N. and Lee K. Y. (2008), 'Fretting corrosion of tin plated contacts', *Tribol. Int.*, **41**, 616–28. (doi:10.1016/j.triboint.2007.02.002)

Qiu S., Dong J. and Chen G. (1999), 'Tribological properties of CeF_3 nanoparticles as additives in lubricating oils', *Wear*, **230**, 35–8. (doi:10.1016/S0043-1648(99)00084-8)

Qiu S., Zhou Z., Dong J. and Chen G. (2001), 'Preparation of Ni nanoparticles and evaluation of their tribological performance as potential additives in oils', *J. Tribol.*, **123**, 441–3. (doi:10.1115/1.1286152)

Quan Z., Wu P. Q., Tang L. and Celis J. P. (2006), 'Corrosion-wear monitoring of TiN coated AISI 316 stainless steel by electrochemical noise measurements', *Appl. Surf. Sci.*, **253**, 1194–7. (doi:10.1016/j.apsusc.2006.01.062)

Rabbe L. M., Rieu J., Lopez A. and Combrade P. (1994), 'Fretting deterioration of orthopaedic implant materials – Search for solutions', *Clin. Mater.*, **15**, 221–6. (doi:10.1016/0267-6605(94)90049-3)

Rabinowicz E. and Mutis A. (1965), 'Effect of abrasive particle size on wear', *Wear*, **8**, 381–0. (doi:10.1016/0043-1648(65)90169-9)

Radice S. and Mischler S. (2006) 'Effect of electrochemical and mechanical parameters on the lubrication behaviour of Al_2O_3 nanoparticles in aqueous suspensions', *Wear*, **261**, 1032–41. (doi:10.1016/j.wear.2006.03.034)

Rapoport L., Leshchinsky V., Lapsker I., Volovik Yu., Nepomnyashchy O. *et al.* (2003), 'Tribological properties of WS_2 nanoparticles under mixed lubrication', *Wear*, **255**, 785–93. (doi:10.1016/S0043-1648(03)00044-9)

St. John K. R., Zardiackas L. D. and Poggie R. A. (2004), 'Wear evaluation of cobalt-chromium alloy for use in a metal-on-metal hip prosthesis', *J. Biomed. Mater. Res. B*, 68B, 1–14. (doi: 10.1002/jbm.b.10053)

Sankara Narayanan T. S. N., Park Y. W. and Lee K. Y. (2007), 'Fretting-corrosion mapping of tin-plated copper alloy contacts', *Wear*, **262**, 228–33. (doi:10.1016/j.wear.2006.05.015)

Sankara Narayanan T. S. N., Park Y. W. and Lee K. Y. (2008a), 'Fretting corrosion of lubricated tin-plated contacts', *Ind. Lubr. Tribol.*, **60**, 233–41. (doi: 10.1108/00368790810895169)

Sankara Narayanan T. S. N., Park Y. W. and Lee K. Y. (2008b), 'Evaluation of electroless Ni-B coating under fretting conditions for electrical connector contact applications', *Surf. Rev. Lett.*, **15**, 443–52. (doi: 10.1142/S0218625X08011573)

Satendra Kumar, Sankara Narayanan T. S. N., Ganesh Sundara Raman S. and Seshadri S. K. (2010a), 'Evaluation of fretting corrosion behaviour of CP-Ti for orthopaedic implant applications', *Tribol. Intl*, **43**, 1245–52. (doi:10.1016/j.triboint.2009.12.007)

Satendra Kumar, Sankara Narayanan T. S. N., Ganesh Sundara Raman S. and Seshadri S. K. (2010b), 'Fretting corrosion behaviour of thermally oxidized CP-Ti in Ringer's solution', *Corros. Sci.*, **52**, 711–21. (doi:10.1016/j.corsci.2009.10.029)

Satendra Kumar, Sankara Narayanan T. S. N., Ganesh Sundara Raman S. and Seshadri S. K. (2010c), 'Surface modification of CP-Ti to improve the fretting-corrosion resistance: Thermal oxidation vs. anodizing', *Mater. Sci. Eng. C*, **30**, 921–7. (doi:10.1016/j.msec.2010.03.024)

Satendra Kumar, Sankara Narayanan T. S. N., Ganesh Sundara Raman S. and Seshadri S. K. (2010d), 'Fretting-corrosion mapping of CP-Ti in Ringer's solution', *Wear*, **268**, 1537–41. (doi:10.1016/j.wear.2010.01.026)

Schmalzried T. P. (2004), 'How I Choose a Bearing Surface for my Patients', *J. Arthroplasty*, **19**, 50–3. (doi:10.1016/j.arth.2004.09.001)

Schmalzried T. P. (2005), 'Metal-on-metal resurfacing arthroplasty: No way under the sun! – In Opposition', *J. Arthroplasty*, **20**, 70–1. (doi:10.1016/j.arth.2005.03.007)

Shenhar A., Gotman I., Radin S., Ducheyne P. and Gutmanas E. Y. (2000), 'Titanium nitride coatings on surgical titanium alloys produced by a powder immersion reaction assisted coating method: residual stresses and fretting behavior', *Surf. Coat. Technol.*, **126**, 210–18. (doi:10.1016/S0257-8972(00)00524-7)

Sinnett-Jones P. E., Wharton J. A. and Wood R. J. K. (2005), 'Micro-abrasion-corrosion of a CoCrMo alloy in simulated artificial hip joint environments', *Wear*, **259**, 898-909. (doi:10.1016/j.wear.2005.02.045)

Stachowiak G. B. (2000), 'Particle angularity and its relationship to abrasive and erosive wear', *Wear*, **241**, 214–19. (doi:10.1016/S0043-1648(00)00378-1)

Stachowiak G. B. and Stachowiak G. W. (2004), 'Wear mechanisms in ball-cratering tests with large abrasive particles', *Wear*, **256**, 600–7. (doi:10.1016/j.wear.2003.10.029)

Stack M. M. and Mathew M. (2003), 'Micro-abrasion transitions of metallic materials', *Wear*, **255**, 14–22. (doi:10.1016/S0043-1648(03)00204-7)

Stack M. M., Jawan, H. and Mathew M. (2005), 'On the construction of micro-abrasion maps for a steel/polymer couple in corrosive environments', *Tribol. Int.*, **38**, 848–56. (doi:10.1016/j.triboint.2005.02.013)

Stack M. M. and Abdulrahman G. H. (2010), 'Mapping erosion-corrosion of carbon steel in oil exploration conditions: Some new approaches to characterizing mechanisms and synergies', *Tribol. Int.*, **43**, 1268–77. (doi:10.1016/j.triboint.2010.01.005)

Stack M. M., Abdelrahman S. M. and Jana B. D. (2010a), 'Some perspectives on modelling the effect of temperature on the erosion–corrosion of Fe in aqueous conditions', *Tribol. Int.*, **43**, 2279–97. (doi:10.1016/j.triboint.2010.07.015)

Stack M. M., Rodling J., Mathew M. T., Jawan H., Huang W. *et al.* (2010b), 'Micro-abrasion–corrosion of a Co-Cr/UHMWPE couple in Ringer's solution: An approach to construction of mechanism and synergism maps for application to bio-implants', *Wear*, **269**, 376–82. (doi:10.1016/j.wear.2010.04.022)

Sun D., Wharton J. A., Wood R. J. K., Ma L. and Rainforth M. (2009a), 'Microabrasion-corrosion of cast CoCrMo alloy in simulated body fluids', *Trib. Int.*, **42**, 99–110. doi:10.1016/j.triboint.2008.05.005

Sun D., Wharton J. A. and Wood R. J. K. (2009b), 'Micro-abrasion–corrosion of cast CoCrMo -Effects of micron and sub-micron sized abrasives', *Wear*, **267**, 52–60. doi:10.1016/j.wear.2009.01.011

Suryanarayana C. (1995), 'Nanocrystalline Materials', *Internat. Mater. Rev.*, **40**, 41–64.

Suryanarayana C. (2001), 'Mechanical Alloying and Milling', *Prog. Mater. Sci.*, **46**, 1–184. (doi:10.1016/S0079-6425(99)00010-9)

Suryanarayana C. (2004), *Mechanical Alloying and Milling*. New York: Marcel Dekker, Inc.

Suryanarayana C. (2005), 'Recent Developments in Nanostructured Materials', *Adv. Eng. Mater.*, **7**, 983–92. (doi: 10.1002/adem.200500135)

Suryanarayana C. and Koch C. C. (1999), 'Nanostructured Materials' in *Non-Equilibrium Processing of Materials*, Suryanarayana C. (Ed.). Oxford: Elsevier Science Pub., pp. 313–46.

Suryanarayana C. and Koch C. C. (2000), 'Nanocrystalline Materials – Current Research and Future Directions', *Hyperfine Interactions*, **130**, 5–44. (doi:10.1023/a:1011026900989)

Suryanarayana C. and Prabhu B. (2007), 'Synthesis of Nanostructured Materials by Inert-Gas Condensation Methods' in *Nanostructured Materials: Processing, Properties, and Applications*, Second Edition, Koch C. C. (Ed.). Norwich: William Andrew, Inc., pp. 47–90.

Swingler J., McBride J. W. and Maul C. (2000), 'The degradation of road tested automotive connectors', *IEEE Trans. Comp. Packag. Technol.*, **23**, 157–64. (doi: 10.1109/6144.833055)

Tang B., Wu P. Q., Fan A. L., Qin L., Hu H. J. *et al.* (2005), 'Improvement of corrosion-wear resistance of Ti-6Al-4V alloy by plasma Mo-N surface modification', *Adv. Engg Mater.*, **7**, 232–8. (doi: 10.1002/adem.200400207)

Tarasov S., Kolubaev A., Belyaev S., Lerner M. and Tepper F. (2002), 'Study of friction reduction by nanocopper additives to motor oil', *Wear*, **252**, 63–9.. (doi:10.1016/S0043-1648(01)00860-2)

Thull R. and Schaldach M. (1976), *Corrosion of highly stressed orthopaedic joint replacements*. Berlin: Springer, pp. 242–56.

Tipper J. L., Firkins P. J., Besong A. A., Barbour P. S. M., Nevelos J. *et al.* (2001), 'Characterisation of wear debris from UNMWPE on zirconia ceramic, metal-on-metal and alumina ceramic-on-ceramic hip prostheses generated in a physiological anatomical hip joint simulator', *Wear*, **250**, 120–8. (doi:10.1016/S0043-1648(01)00653-6)

Tipper J. L., Ingham E., Jin Z. M. and Fisher J. (2005), 'The science of metal-on-metal articulation', *Current Orthopaedics* **19**, 280–7. (doi:10.1016/j.cuor.2005.08.002)

Wang A., Bobyn J. D., Yue S., Medley J. B. and Chan F. W. (1999), 'Residual abrasive material from surface grinding of metal–metal hip implants: a source of third-body

wear?', in *ASTM Special Technical Publication–1365*. Philadelphia: American Society for Testing and Materials, pp. 125–34.

Williams J. A. and Hyncica A. M. (1992), 'Abrasive wear in lubricated contacts', *J. Phys. D: Appl. Phys.*, **25**, A81–A90. (doi: 10.1088/0022-3727/25/1A/015)

Wimmer M. A., Loos J., Nassutt R., Heitkemper M. and Fischer A. (2001), 'The acting wear mechanisms on metal-on-metal hip joint bearings: in vitro results', *Wear*, **250**, 129–39. (doi:10.1016/S0043-1648(01)00654-8)

Wimmer M. A., Sprecher C., Hauert R., Tager G. and Fischer A. (2003), 'Tribochemical reaction on metal-on-metal hip joint bearings: a comparison between in-vitro and in-vivo results', *Wear*, **255**, 1007–14. (doi:10.1016/S0043-1648(03)00127-3)

Windler M. and Klabunde R. (2001), 'Material science, surface science, engineering, biological responses and medical applications', in *Titanium in Medicine*, Brunette D. M., Tengvall P., Textor M. and Thomsen P. (Eds). Berlin: Springer-Verlag, pp. 703–46.

Wu P. Q. and Celis J. P. (2004), 'Electrochemical noise measurements on stainless steel during corrosion–wear in sliding contacts', *Wear*, **256**, 480–90. (doi:10.1016/S0043-1648(03)00558-1)

Xue Q., Liu W. and Zhang Z. (1997), 'Friction and wear properties of a surface-modified TiO_2 nanoparticle as an additive in liquid paraffin', *Wear*, **213**, 29–32. (doi:10.1016/S0043-1648(97)00200-7)

Xulin S., Ito A., Tateishi T. and Hoshino A. (1997), 'Fretting corrosion resistance and fretting corrosion product cytocompatibility of ferritic stainless steel', *J. Biomed. Mater. Res.*, **34**, 9–14. (doi: 10.1002/(SICI)1097-4636(199701)

Yan Y., Neville A. and Dowson D. (2006), 'Biotribocorrosion—an appraisal of the time dependence of wear and corrosion interactions: II. Surface analysis', *J. Phys. D: Appl. Phys.*, **39**, 3206–12. (doi: 10.1088/0022-3727/39/15/S11)

Yan Y., Neville A. and Dowson D. (2007), 'Biotribocorrosion of CoCrMo orthopaedic implant materials—Assessing the formation and effect of the biofilm', *Tribol. Int.*, **40**, 1492–9. (doi:10.1016/j.triboint.2007.02.019)

Yan Y., Neville A., Dowson D., Williams S. and Fisher J. (2009), 'Effect of metallic nanoparticles on the biotribocorrosion behaviour of Metal-on-Metal hip prostheses', *Wear*, **267**, 683–8. (doi:10.1016/j.wear.2008.12.110)

Ye P., Jiang X., Li S. and Li S. (2002), 'Preparation of $NiMoO_2S_2$ nanoparticle and investigation of its tribological behavior as additive in lubricating oils', *Wear*, **253**, 572–5. (doi:10.1016/S0043-1648(02)00042-X)

Zhou J., Wu Z., Zhang Z., Liu W. and Dang H. (2001), 'Study on an antiwear and extreme pressure additive of surface coated LaF_3 nanoparticles in liquid paraffin', *Wear*, **249**, 333–7. (doi:10.1016/S0043-1648(00)00547-0)

Zum Gahr K. H. (1999) 'Wear by hard particles', *Trib. Int.* **31**, 587–96. (doi:10.1016/S0301-679X(98)00079-6)

9

Self-healing nanocoatings for corrosion control

M. G. S. FERREIRA, M. L. ZHELUDKEVICH, J. TEDIM and K. A. YASAKAU, University of Aveiro, Portugal

Abstract: This chapter provides an overview of nanotechnology-based self-healing coatings. Different perspectives on the self-healing concept are presented and discussed in detail, with particular relevance for different trends in terms of coating technology. The chapter starts with an introduction on the self-healing concept, followed by a short description of different self-healing coatings. The detailed discussion of anticorrosion coatings begins with systems traditionally used in corrosion protection, including corrosion conversion coatings. Then, different self-healing systems consisting of surface treatments based on silane coatings, sol–gel coatings with nanoreservoirs and conductive polymers are reviewed in detail. The type, specific applications, performance and associated protection mechanisms are critically discussed in the context of their promising utilization as corrosion protective systems in real-life applications.

Key words: self-healing, conversion coatings, silane coatings, nanoreservoirs, nanostructured coatings.

9.1 Introduction

The enormous economic impact of corrosion of metallic structures in aggressive environments is a very important issue worldwide. The most typical corrosive environments are the natural waters: atmospheric moisture containing man-generated pollutants and man-made solutions. Therefore, metallic structures operated in such environments suffer from continual and strong corrosion attack. This is especially important for transport systems, often used in a wide variety of environments that can combine different corrosive impact factors.

The application of protective coatings is the most common and cost-effective method of improving corrosion protection, and therefore the durability, of metallic structures from aircraft to household equipment. The main role of organic polymer coatings in corrosion protection is to act as a barrier against corrosive species, resisting the flow of charge, both electronic and ionic. However, defects appear in the protective films during exploitation of the coated structures, allowing corrosive agents access to the metallic surface. The action of UV radiation, temperature gradients, mechanical stresses and vibration, aligned with the impacts of aggressive technical fluids, leads to formation of micro-cracks and micro-pores in the protective coatings. Stone chipping and scratching during automatic washing of vehicles, and erosion impacts and defects appearing during aircraft operation, also result in the formation of large discontinuities in polymer layers.

The corrosion processes develop faster after disruption of the protective barrier and therefore an active 'self-healing' of defects in coatings is strongly desired in order to provide a long-term protection effect.

9.2 Concept of 'self-healing'

The term 'self-healing' can be defined as the ability of a material to recover its initial properties after destructive actions of the external environment or from the influence of internal stresses. Many terms are used in materials science, such as 'self-recovery', 'self-repair', 'autonomic-healing', 'autonomic-repairing', 'self-remedying' and others, to define this property. However, even a partial recovery of the main functionality of a material can also be considered as a self-repair ability. The same can also be applied not only to the bulk materials but to functional coatings as well. Thus, in the case of protective coatings the term 'self-healing' can be interpreted in different ways. The traditional interpretation of self-healing is based on the full recovery of the coating functionalities due to a real healing of the defect, restoring the initial coating integrity. However, the main function of anticorrosion coatings is the protection of a subjacent metallic substrate against an environmentally induced corrosion attack. Thus, it is not obligatory to recover all of the properties of the film in this case. The hindering of the corrosion activity in the defect by the coating itself employing any mechanisms can be already considered as self-healing, because the corrosion protective system recovers its main function, namely corrosion protection, after being damaged. Both of these approaches to self-healing in protective coatings will be considered in this chapter.

In nature, damage to an organism evokes a healing response. Many 'natural' materials are themselves self-healing composites (Ghosh, 2008). For example, living plants are able to refill voids in their epicuticular wax layers by wax self-assembly (Koch and Ensikat, 2008; Koch *et al.*, 2009). Human skin is also an example of a complex self-healing system which can repair defects by blood clotting (Filipovic *et al.*, 2008). Broken bones can also be self-repaired by the human body employing different mechanisms. The repair strategies of living organisms attract materials designers looking for low-weight structures with enhanced service life. These bio-inspired approaches do not completely imitate the real biological processes involved because the latter are too complex. Instead, the designers of self-healing materials try to combine traditional engineering approaches with biological self-healing mechanisms. The field of self-healing materials is currently only in the incubation stage. Many academic and industrial groups actively explore new concepts for different kinds of self-repair materials. However, the number of commercialized self-healing materials is so far small. Van der Zwaag makes a prediction of the possible industrial applications where such materials can be used in first turn because of strong social demands (van der Zwaag *et al.*, 2007):

- Structures where long-term performance (above 40 years) must be assured (engineering structures such as tunnels).

- Applications where a very high reliability is needed (nuclear and space technologies, aircraft).
- Applications where high reliability is requested and the repairs are very expensive (underground pipelines, wind farms).
- Applications where high surface quality and aesthetic aspects are important. (cars, optical systems).

In the following section the application of the self-healing approach to bulk composites and coatings is presented.

9.3 Polymer bulk composites and coatings

Before starting discussion on self-healing coatings, the general approaches for development of self-healing materials should be reviewed, as development of the self-healing coatings is very often inspired by ideas coming from bulk materials. The next section will present a short overview of different strategies on design of the self-healing polymer and composite materials. The self-healing function for the polymer-based materials can be achieved in two main ways:

- reversible cross-linking of the broken chemical bonds
- repair of the defect by the healing agent released from micro-/nanoreservoirs.

Covalently cross-linked polymer networks confer superior mechanical properties such as high modulus and high fracture resistance together with superior chemical and thermal resistance. However, the strong covalent cross-linking leads to irreversible polymer networks which have no reparability. Once a cross-link bond is broken it cannot be re-established, leading to propagation of the defect in the polymer matrix. One possibility to bring self-healing properties to the polymer networks is to employ reversible covalent and non-covalent cross-linking reactions such as hydrogen bonding, ionic forces, metal-ligand bonds, dipole–dipole interactions, Coulombic interactions, mechanical interlocking and reversible Diels–Alder reactions. However, reversible cross-linked polymers will normally only exhibit their self-healing capability under the action of external triggers such as elevated temperature or photo- and chemical activation.

Several self-healing polymer composites were recently reported. An outstanding example is an epoxy-based system able to heal cracks autonomically, as described by White *et al.* (2001). The polymer bulk material contains a microencapsulated healing agent that is released upon crack initiation. Then, the healing agent is polymerized upon contact with the embedded catalyst, bonding the crack faces and recovering the material's toughness. Dicyclopentadiene-filled microcapsules (50–200 μm) with a urea–formaldehyde shell were prepared using standard microencapsulation techniques. The polymer shell of the capsule provides a protective barrier between the catalyst and the monomer to prevent polymerization

during the preparation of the composite. However, the chemistry of this system had a significant drawback due to the probability of side reactions with the polymer matrix and air.

A new and advanced self-healing polymer system based on tin-catalysed polycondensation of phase-separated droplets containing hydroxyl end-functionalized polydimethylsiloxane and polydiethoxysiloxane was recently suggested by the same group (Cho *et al.*, 2006). The concept of phase separation of the healing agent was employed in this work, simplifying processing greatly as the healing agent was just mixed into the polymer matrix. The catalyst, di-*n*-butyltin dilaurate (DBTL) microencapsulated within a polyurethane shell, is embedded in a vinyl ester matrix and can be release when the capsules are broken by mechanical damage. The released catalyst initiates polymerization of monomers from the surrounding droplets, healing the propagating crack. This new system confers high stability in humid environments and high temperatures (> 100°C).

The work of White was rapidly followed up by other groups, and many other self-healing systems were developed, such as self-validating adhesives (Allsop *et al.*, 1998) and self-healing epoxy composites (Brown *et al.*, 2005; Yin *et al.*, 2007). The original idea of hollow spheres was extended to hollow reinforcement fibres, used in fibre-reinforced plastic, containing a liquid resin. The repair process in this case is triggered after an impact loading of the material. The hollow glass fibres, ranging in diameter from 30 to 100 μm with a hollowness of up to 65%, can be filled with uncured resin systems that bleed into a damage site upon fibre fracture. After being cured they provide a method of crack blocking and recovery of mechanical integrity.

An even more advanced approach was recently suggested, employing a self-healing system capable of the autonomous repairing of repeated damage events (Toohey *et al.*, 2007). The substrate composite delivers the healing agent to the cracks in a polymer coating via a three-dimensional microvascular network embedded in the substrate. Crack damage in the coating is repaired repeatedly, mimicking a body–skin system. However, this approach cannot be used in the case of corrosion protective coatings since a microvascular network cannot be created in a metallic substrate.

In the following section, a review of more traditional conversion coatings that can also exhibit self-healing properties against corrosion damage is presented. Then, surface treatments with silane coatings are discussed as passive and active corrosion protective systems with self-healing abilities. In addition, the positive and negative roles of different inhibitive additives for the enhancement of active corrosion protection properties of silane coatings are discussed. Sol–gel coatings with nanoreservoirs of inhibitors are reviewed as emerging technologies for the active corrosion protection of metals. The chapter ends with the application of conductive polymer coatings to corrosion protection and the concluding remarks.

9.4 Traditional conversion coatings

9.4.1 Chromate conversion coatings

Chromate conversion coatings are obtained by chemical reaction with the metal being treated, to form a complex chromate film over the entire surface. The coatings can be applied to aluminium, zinc, cadmium and magnesium. Aluminium chromate conversion coatings are amorphous in structure with a gel-like composition hydrated with water. This characteristic endows aluminium chromate conversion coatings with unique self-healing properties when scratched or abraded. Metal exposed by a scratch slowly becomes covered by a chromate protective film. Soluble chromates leach from the conversion coating areas adjacent to the scratch and precipitate on the open metal surface, thereby providing a self-healing of the defect (Kendig *et al.*, 1993).

Chromate treatments produce effective paint bonds through molecular adhesions with the film being bound to the metal, in turn offering the same type of adhesion to the organic coating. The film reduces creep corrosion, forming an effective barrier against corrosive attack through pores or scratches in the paint. With aluminium, chromate is an excellent pre-treatment for paint or adhesives since it greatly enhances the product's ability to form a bond with the substrate. It is frequently used on electrical and electronic equipment because it provides increased corrosion resistance while remaining electrically conductive. This coating is amorphous, permitting cold forming without rupture of the film. During the chromate conversion, aluminium oxide and chromic oxide are produced in accordance with the conversion reaction shown below:

$$2Al + 2Na_2CrO_4 \rightarrow Al_2O_3 + 2Na_2O + Cr_2O_3 \qquad [9.1]$$

All chromate conversion coatings use chromic acid in the form of its soluble salts. During the process, a thin, gel-like film is produced on the aluminium surface. The films produced by this process vary in colour, depending on the aluminium alloy being treated, surface conditions and the type of chromate. Chromate conversion coating leaves no measurable build-up on the component(s) and provides excellent corrosion resistance. The coating is conductive and offers in yellow iridescent to clear iridescent colouring. Electrical resistance increases with the darkness of the yellow colour.

The use of chromate conversion coatings has led to progressively greater restrictions imposed by national and international legislation (European Union directive 2002/95/EC on the Restriction of Hazardous Substances (RoHS) and European Union directive 2002/96/EC on Waste Electrical and Electronic Equipment (WEEE)) relating to concerns over health, safety and environmental protection regarding the use of these treatments. However, the aeronautical industry is a major chromates consumer until a viable alternative can be found.

A Trivalent Chromate Process (TCP) that complies with the above regulations and is free from hexavalent chromium is offered in the market and is used in some applications (Alpha Metal Finishing).

9.4.2 Phosphate conversion coatings

Phosphate coatings are made up of thin crystalline layers of phosphate compounds that adhere to the surface of the metal substrate. The phosphate crystals are porous and can be formed from zinc, manganese or iron phosphate solutions. Each of the three types provides a phosphate coating with slightly different properties, such as crystal size and coating thickness. This allows a more specialized coating to be selected for the particular application required for part of the structure. These coatings are usually applied to carbon steel, low-alloy steel and cast iron. The coating is formed by either spraying or immersing the substrate into a solution of dilute phosphoric acid combined with other chemicals that assist in the coating process. Phosphate coatings can also be applied to zinc, cadmium, aluminium, tin and galvanized steel, but are difficult to apply on material with high alloys, which are often immune to the phosphoric acid. The main components of a phosphating solution are:

- phosphoric acid (H_3PO_4)
- ions (cations) of bivalent metals: Zn^{2+}, Fe^{2+}, Mn^{2+}
- accelerator – an oxidizing reagent (nitrate, nitrite, peroxide) increasing the coating process rate and reducing the grain size of the deposit.

When a steel panel is introduced into the phosphating solution (for example zinc phosphate), a topochemical reaction takes place in which the iron dissolution is initiated at the microanodes present on the substrate by the free phosphoric acid present in the bath. Hydrogen evolution occurs at the microcathodic sites (Sankara Narayanan, 2005):

$$3Fe + 6H^{+} + 2PO_4^{3-} \rightarrow 3Fe^{2+} + 2PO_4^{3-} + 3H_2 \qquad [9.2]$$

Consumption of phosphoric acid for the reaction causes reduction of the acidity of the solution in the layer adjacent to the metal surface. Solubility of zinc phosphate in the neutralized solution is lowered, resulting in precipitation of the salt and its deposition on the substrate surface:

$$3Zn^{2+} + 2PO_4^{3-} \rightarrow Zn_3(PO_4)_2 \qquad [9.3]$$

Zinc phosphate coating is applied when increased corrosion resistance is required.

Iron phosphate coatings are applied when strong adhesion of a subsequent painting is required. In contrast to the solutions for zinc phosphate and manganese phosphate coatings, in which the metal ions are a constituent of the composition, in iron phosphate solutions iron ions are provided by the dissolving substrate.

Manganese phosphate coatings are applied when wear resistance and anti-galling properties are required. Manganese phosphate also possesses the ability to retain oil, which further improves anti-friction properties and imparts corrosion resistance to the coated parts.

Although phosphate coatings provide good adhesion and some barrier protection, when the coating becomes damaged the corrosion progresses rapidly starts on the open metal surface because low solubility phosphates do not possess enough inhibiting power compared with chromates and thus cannot provide self-healing of the damaged zone. Nevertheless, a self-healing effect can be observed when the phosphate coating includes soluble phosphates that can leach from the coating and precipitate at the defective sites, as was demonstrated by Aramaki (2003).

9.4.3 Anodizing

Anodizing is the general name applied to methods of treating metals in which the work piece is made the anode in an electrolytic cell, usually to form oxide coatings for the purpose of increasing the performance of the surface. The nature of the electrolyte, the reaction produced and operation parameters determine the structure and properties of the formed oxide film. In the case of aluminium, the anodizing process forms a layer of aluminium oxide – Al_2O_3 – or corundum, which is very hard, relatively inert and electrically insulating and can absorb dyes to colour the film. The anodic film itself grows at the aluminium/aluminium oxide interface by the continuous formation and dissolution of a layer of oxide: this is the so-called barrier layer and its thickness is a function of the process starting voltage. A porous, more structured layer forms on top of the barrier layer, making up the rest of the coating. All anodizing processes are sealed unless the film is used as a primer for paint or adhesives. The most common anodizing processes on aluminium use chromic acid, sulfuric acid or oxalic acid (Wernick *et al.*, 1987). Other acids, such as phosphoric acid and boric sulfuric acid mix, are now used in the market for anodizing in the aerospace industry.

Chromic acid anodizing (CAA) is currently used in the aerospace industry in order to treat high-strength aluminium alloys such as AA 2024-T3. However, the process uses chemicals that contain Cr (VI), which is contra-indicated from the health and environmental points of view since it is toxic and carcinogenic. The corrosion resistance is excellent relative to the thickness of the coating, which normally lies in the range of 2 to 5 μm. Sulfuric acid anodizing is the most frequently used aluminium anodizing process. It produces coatings up to 25 μm for conventional coatings and up to 100 μm for hard coatings. Conventional coatings are primarily decorative or protective. Hard coat anodizing is processed at higher voltages and current densities and is mostly used for engineering applications.

Boric sulfuric acid anodizing was developed by Boeing Company as a chromic acid anodizing replacement for non-critical fatigue parts. Paint adhesion is equal

or superior to chromic acid, and the process is more energy-efficient than chrome-based processes. However, anodic coatings made in non-chromate containing electrolytes cannot provide self-healing of defects when the coating is damaged. Therefore, the coating must be sealed by an inhibitive compound in order to enhance the corrosion protective properties of anodic films.

9.4.4 Rare earths conversion coatings

The salts of rare earth (RE) elements have been found to confer an effective corrosion inhibition effect on aluminium alloys (Bethencourt *et al.*, 1998; Twite and Bierwagen, 1998; Davo and de Damborenea, 2004). They control the cathodic reaction by precipitating metal hydroxide ($Ln(OH)_3$) at local regions, which is associated with an increase of pH due to oxygen reduction (Aballe *et al.*, 2001; Arenas *et al.*, 2001; Davo and de Damborenea, 2004). Cerium showed maximum corrosion protection efficiency compared with other RE compounds (Yasakau *et al.*, 2006). Cerium nitrate revealed superior corrosion inhibition properties in comparison with lanthanum nitrate, probably due to the lower solubility of the hydroxide. The insoluble film at the cathodic sites blocks the cathodic reduction of oxygen. As a result, the current supplied to the anodic reaction decreases and the Al dissolution is reduced. An important role in the superior efficiency of cerium can also be played by Ce^{4+}, which can be formed at high pH values in aerated chloride environments (Bilal and Muller, 1992; Aldykiewicz *et al.*, 1996). Aramaki (2003) has demonstrated that, after damage to specially designed cerate conversion coatings, Ce ions can escape the conversion layer and precipitate at the active corrosion site on zinc substrate, providing some self-healing effect. Nevertheless, cerate conversion layers mostly provide barrier protection, and when the conversion coating becomes damaged there is no significant self-healing observed due to lack of soluble cerium ions in the layer.

RE compounds can be introduced in corrosion protection systems for aluminium alloys using different strategies. The formation of a conversion coating composed of a hydrated oxide layer on top of the aluminium alloy offers an enhanced corrosion protection (Campestrini *et al.*, 2004; Palanivel *et al.*, 2005). Another approach is the use of the cerium conversion coating technique to seal the porous film of an anodized aluminium alloy (Yu and Cao, 2003). Cerium-based inhibitors can also be introduced in the thin hybrid coatings used as pre-treatment for aluminium alloys, where they have exhibited promising results (Kasten *et al.*, 2001; Voevodin *et al.*, 2001a; Zheludkevich *et al.*, 2005a). The introduction of cerium compounds can, however, decrease the stability of the hybrid matrix by decreasing the barrier properties. The introduction of zirconia nanoparticles doped with cerium ions into a hybrid sol–gel matrix was found to successfully avoid the negative effect of the cerium cations on the film and to provide a prolonged release of cerium inhibitor in places of localized corrosion (Zheludkevich *et al.*, 2005a, 2005b). Although many works have

been dedicated to the investigation of corrosion inhibition using RE-based inhibitors, there are still numerous contradictions and ambiguities concerning the mechanism of this inhibition.

9.5 Sol–gel silane coatings

9.5.1 Inorganic and hybrid sol–gel coatings with passive protection

Sol–gel derived coatings have been used for decades on many metals, including stainless steel, iron, aluminium, copper, nickel and others, in many different applications such as electric insulation, mechanical resistance, water repellency, adhesion promotion, oxidation resistance and corrosion resistance (Guglielmi, 1997). Historically, the first type of sol–gel coatings were inorganic oxide sol–gel derived films. Inorganic sol–gel coatings based mostly on zirconate, silica and ceria were developed and investigated in many works for corrosion protection of different metallic substrates (Izumi *et al.*, 1989; Atik *et al.*, 1994; Di Maggio *et al.*, 1997; Vasconcelos *et al.*, 2000; Fedrizzi *et al.*, 2001; Khobaib *et al.*, 2001; Feil *et al.*, 2009; Andreatta *et al.*, 2010). Particular studies show that the corrosion protection conferred by zirconia sol–gel films applied on steel substrates is similar to the commercially available tricationic phosphate pre-treatment (Vasconcelos *et al.*, 2000). In contrast to zirconia layers, silica films deposited on stainless steel are not as good, though the increase of firing temperature during the coating preparation increases the corrosion protection of silica films (Atik *et al.*, 1994; Vasconcelos *et al.*, 2000). Khobaib *et al.* showed that silica sol–gel pre-treated AA2024 substrate coated with a polyurethane layer provided an acceptable corrosion protection level similar to the conventional chromate system. However, results of corrosion tests for scribed panels clearly demonstrate the superior performance of the chromate pre-treatment over the inorganic sol–gel based coating systems, which is related to the latter's lack of active corrosion protection (Khobaib *et al.*, 2001).

One of the major disadvantages of inorganic sol–gel coatings is the formation of cracks during the drying process. Crackability becomes a more severe problem when coating thickness exceeds critical values and therefore dense, crack-free coatings can only be obtained with low thickness, below several hundreds of nanometres. Local breakdown of sol–gel coatings at cracks causes pitting corrosion of aluminium and stainless steel after contact with corrosive species (Guglielmi, 1997). Sometimes the thermal treatment of the sol–gel films may be critical. Sol–gel derived inorganic coatings prepared using low temperature drying can offer better barrier properties against wet corrosion than fired sol–gel films. However, the barrier properties of these coatings are insufficient to achieve good protection against corrosive species due to formation of non-compact coatings with high volumes of micropores.

Cracks may be produced during the curing process due to shrinkage and thermal expansion mismatches between the metal and inorganic layers. In order to minimize the effects of thermal mismatch, inorganic sol–gel films may be mixed with different inorganic oxides such as zirconia that have higher thermal expansion coefficients (Boysen *et al.*, 1999). The application of multi-layer films or the introduction of fillers may partially solve drying problems, although the problems with thermal expansion mismatch persist.

In spite of the disadvantages, inorganic sol–gel coatings provide a good adhesion layer to the metallic substrate (Thim *et al.*, 2000; Fedrizzi *et al.*, 2001). The advantage of sol–gel coatings is the formation of strong Van der Waals bonds between the hydrolysed silane molecules and the metallic surface. These bonds can be transformed to stable covalent Me-O-Si bonds during the film drying stage (Metroke *et al.*, 2001). In humid environments, a cleaned surface of metal contains many hydroxyl groups. Upon contact with a sol–gel solution, hydrolysed siloxane molecules are attracted to the metal surface by van der Waals and electrostatic forces. During curing of the sol–gel film, stable covalent bonds are formed between the metal surface and silane molecules during the water condensation reaction as shown in Fig. 9.1(a). Schmidt *et al.* estimated the thermodynamic possibility of Si-O-Al bonds formation in sol–gel film/aluminium substrate systems. Thermodynamic calculations show that the alumina/silica mixed compounds altogether have a lower Gibbs energy than the boehmite, which is produced during the first stage of oxidation of aluminium in the presence of moisture (Schmidt *et al.*, 2003). The enthalpy of interaction between Al-OH and HO-Si groups is −462 kJ/mol and is sufficiently lower than for the reaction of Al-OH and Al-OH groups, being −48 kJ/mol, leading to the formation of a more stable alumina/sol–gel film interface.

Hybrid sol–gel films, in contrast to pure inorganic films, combine the properties of organic polymeric material with the properties of ceramic. The inorganic components mostly contribute to the increase of scratch resistance, durability and adhesion to the metal substrate. The organic component increases density,

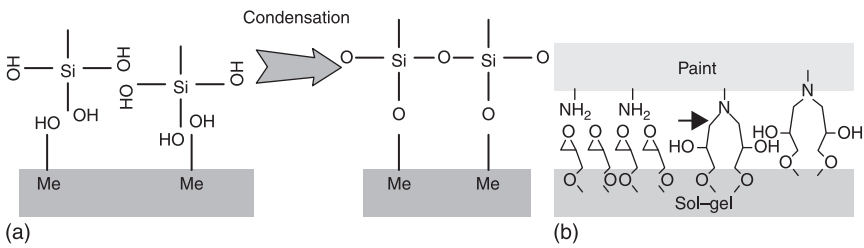

9.1 (a) Schematic representation of the formation of covalent bonds between a metallic (Me) substrate and silica based sol–gel film; (b) formation of chemical bonds between epoxy groups of a sol–gel film and amino groups of a paint.

flexibility and functional compatibility with organic paint systems. Hybrid coatings can be prepared over a continuous compositional range from almost inorganic to almost organic (Thim *et al.*, 2000; Mackenzie *et al.*, 2003). The properties of these coatings can be changed, adjusting many parameters to form an optimum coating. An advantage of the organically modified sol–gel systems is the possibility to prepare thick, crack-free coatings (Ono *et al.*, 2004). The mechanical properties and adhesion to specific organic paint systems can be significantly improved in comparison to sol–gel materials based on non-functional organosilanes (Boysen *et al.*, 1999; Mackenzie *et al.*, 1998; Joshua Du *et al.*, 2001; Hofacker *et al.*, 2002). The enhanced adhesion is attributed to the presence of functional groups in sol–gel coatings that can chemically react with the functional groups of organic paints, therefore greatly increasing the adhesion between the two systems (Fig. 9.1(b)).

Sol–gel hybrid materials can be classified into two major classes (Schubert *et al.*, 1995; Judeinstein and Sanchez, 1996). Class I of hybrid materials or coatings is based on the physical mixing of organic and inorganic phases without covalent bonds between inorganic and organic components (Fig. 9.2(a)). Van der Waals, ionic and hydrogen bonding interactions are the only forces that arise between the components. The synthesis of such hybrid materials can be performed by simple mixing of inorganic sol with organic matrix (Haas, 2000; Mayer *et al.*, 2000; Ono *et al.*, 2004). The produced composites have different valuable mechanical properties, in particular increased hardness when the organic polymer matrix is impregnated with inorganic oxide nano and micro-particles. However, such materials cannot provide adequate barrier protection because of porosity and loss of chemical bonds.

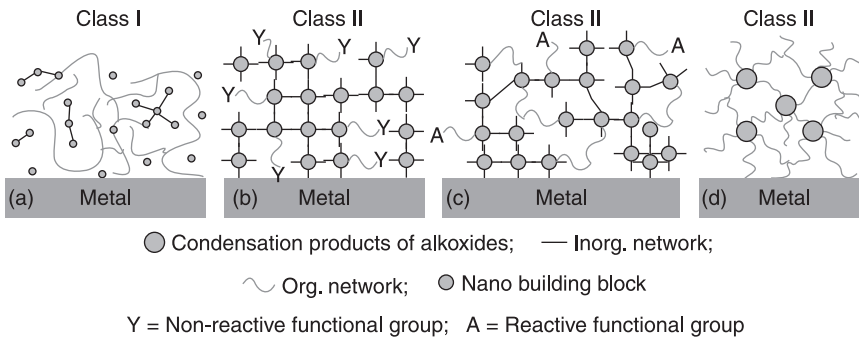

9.2 (a) Class I hybrid material (no covalent bonds are formed between inorganic and organic phases). Class II hybrid materials: (b) hybrid network with added functionality (Y) linked by inorganic bonds; (c) hybrid network linked by inorganic and organic bonds via A groups; (d) organic–inorganic network made of nano building blocks linked through organic bonds.

Class II hybrid materials are made of precursors with covalent or complex bonded organic groups. The commonly used sol–gel precursors are organoalkoxysilanes and metal alkoxides. Such materials can be classified into two groups based on the type of the organoalkoxysilane organic part, namely *non-functional* organoalkoxysilanes and *organofunctional* alkoxysilanes (Mackenzie *et al.*, 1998; Joshua Du *et al.*, 2001; Hofacker *et al.*, 2002).

The first group, presented in Fig. 9.2(b), shows an example of the sol–gel network formed by organomodified alkoxides $(RO)_n$-E-Y and metal alkoxides $E(OR')_m$ linked by oxygen bridges (where E = Si for organomodified alkoxides and E = Zr, Ti, Ce for metal alkoxides). The specific functionality group (Y) does not react and is retained inside the hybrid material. In this example metal alkoxides are optionally added for the purpose of inorganic network formation. Methyl groups are commonly used as the organic part for preparation of the hybrids with non-functional component (Rubio *et al.*, 2000; Conde *et al.*, 2003; Sheffer *et al.*, 2003).

In the second case (Fig. 9.2(c)), the inorganic network is formed via condensation reaction of alkoxy groups of alkoxides, whereas the organic network is formed through the polymerization reaction of functional groups 'A' present in the organomodified precursor $(RO)_n$-Si-A.

The third case (Fig. 9.2(d)) shows the organic–inorganic network formed by connecting the inorganic nanoparticles, which are also called 'nano building blocks', through the organic functional groups.

Nanostructured class II sol–gels can be obtained through the preliminary controlled hydrolysis of inorganic precursors such as zirconia, titania, etc, alkoxides that are mixed with pre-hydrolysed organomodified silane solution. The obtained sol–gel coatings have well-defined nanostructural properties due to the presence of inorganic zirconia or titania nanoparticles. Such coatings demonstrate enhanced corrosion protection and mechanical properties compared with sol–gel films prepared using only inorganic or organosilane parts. The size of inorganic oxide nanoparticles can be varied depending on the hydrolysis conditions. Another type of nanostructured coatings comprises inorganic clusters of silicates or silsesquioxanes. Such clusters can have cubic cage geometry with silicon atoms situated in corners. Silsesquioxanes can be prepared by the sol–gel process of organofunctional silanes and then used as building units for hybrid sol–gel materials.

Organofunctional silane compounds usually contain epoxy (Atik *et al.*, 1997; Hoebbel *et al.*, 1998; Chou *et al.*, 2001, 2003; Parkhill *et al.*, 2001; Metroke *et al.*, 2002a; Conde *et al.*, 2003; Ono *et al.*, 2004; Voevodin *et al.*, 2005), acrylic and alkyd (Smarsly *et al.*, 2003), allyl (Joshua Du *et al.*, 2001), phenyl (Sheffer *et al.*, 2003), amino (Ni *et al.*, 2000) or vinyl functional groups (Joshua Du *et al.*, 2001; Liu *et al.*, 2005; Hu *et al.*, 2007). Some of the organofunctional groups used (epoxy, vinyl, methacrylic, etc) can be additionally polymerized for the formation of an organic network as shown in Fig. 9.2(c) and (d). Organofunctional groups, in addition to chemical reactivity, are used to achieve tailored compatibility

of the sol–gel pre-treatments to organic paint systems and to alter hydrophobicity of the coatings (Mayrand *et al.*, 1998; Joshua Du *et al.*, 2001; Sheffer *et al.*, 2003). The amino and epoxy groups are especially suitable for reacting with the epoxy-based organic coatings to provide an excellent binding of organic coatings to the sol–gel pre-treatments (Fig. 9.1(b)) (Joshua Du *et al.*, 2001; Mayrand *et al.*, 1998).

Hybrid sol–gel systems are well known not only for their tailored surface properties or mechanical properties. Such materials have been thoroughly investigated as corrosion protective coatings for many metallic substrates such as steel and stainless steel substrates (Atik *et al.*, 1997; Mayrand *et al.*, 1998; Menning *et al.*, 1998; Chou *et al.*, 2001, 2003; Ono *et al.*, 2004), copper and copper-containing alloys (Pilz *et al.*, 1997; Bescher and Mackenzie, 2003; Li *et al.*, 2009; Rao *et al.*, 2011), aluminium (Chen *et al.*, 1998; Parkhill *et al.*, 2001) and aluminium alloys (Metroke *et al.*, 2002a, 2005; Conde *et al.*, 2003; Ono *et al.*, 2004). In general, the presence of organomodified silanes in hybrid coatings enhances the protection properties of coatings applied on different substrates like steel (Menning *et al.*, 1998), stainless steel (Gallardo *et al.*, 2003), electrogalvanized steel (Mayrand *et al.*, 1998) and aluminium (Sheffer *et al.*, 2003). However, the protection properties also depend on the type of organic groups. In the case of phenyl functionalized silanes, the corrosion protection of aluminium alloys is better because of the higher hydrophobicity of phenyl groups (Parkhill *et al.*, 2001). On the other hand, sol–gel coatings containing amino groups, which have hydrophilic characteristics, increase protection and possess especially strong bonding properties to both electrogalvanized steel and epoxy coatings (Mayrand *et al.*, 1998).

Sol–gel coatings containing epoxy groups exhibit increased corrosion protection of AA2024 substrates due to the additional polymerization of epoxy groups that leads to enhanced flexibility and elimination of cracks in the coatings (Parkhill *et al.*, 2001; Voevodin *et al.*, 2001b, 2001c). The barrier properties of the sol–gel coatings can be further increased if cross-linking agents like superacids and different amines are used in the sol–gel process (Metroke *et al.*, 2002b). However, a better effect is achieved when using amino silanes as cross-linked agents due to the formation of inorganic bonds between the silanol groups after condensation and polymerization of epoxy and amino groups (Metroke *et al.*, 2002b; Khramov *et al.*, 2003). The methacrylate-containing hybrid sol–gel coatings on stainless steel and aluminium substrates also provide enhanced corrosion protection by forming a uniform, defect-free and relatively dense physical barrier against corrosion species (Chou *et al.*, 2001, 2003; Ono *et al.*, 2004). Increasing the metacrylate component concentration tends to promote the formation of thicker films on aluminium alloy and stainless steel (Chou *et al.*, 2001; Ono *et al.*, 2004). Nevertheless, too high a concentration of organics impairs the corrosion protection and adhesion of the sol–gel coatings to the metallic substrate.

The addition of organic functional groups and/or organic polymers to sol–gel coatings increases coating thickness, flexibility and metal resistance to corrosion. Nonetheless, a high content of organic groups can decrease mechanical properties such as scratch or wear resistance while increasing the adhesion and minimizing cracking of the coating (Atanacio *et al.*, 2005). In some cases both mechanical and corrosion resistance of the sol–gel coatings is appreciated. Such properties of hybrid sol–gel coatings can be adjusted by introducing inorganic nano and micro-particles (Chen *et al.*, 1998; Malzbender *et al.*, 2002; Conde *et al.*, 2003; Gallardo *et al.*, 2003; Palanivel *et al.*, 2003; Montemor *et al.*, 2006a).

Usually, the addition of nanoparticles does not destroy the coating properties. Corrosion protection and mechanical properties become enhanced due to stabilization of the interface between the nanoparticles and coating matrix (Chen *et al.*, 1998; Malzbender *et al.*, 2002) or due to the higher hydrophobicity of the coating with nanoparticles (Conde *et al.*, 2003). Particles with diameter in the nano range are commonly used as reinforcements for hybrid sol–gel coatings. However, when the diameter of the particles is higher than 500 nm the suspensions become unstable, which hinders the preparation of uniform sol–gel films. The addition of very small amounts (around 15 ppm) of 1 micron silica particles in a bis-silane based sol–gel network increases corrosion protection and mechanical properties of the coatings, whereas higher amounts have an adverse effect (Palanivel *et al.*, 2003; Montemor *et al.*, 2006a). In the case of glass micro-particles (around 3 microns), additional cracking may occur when particle size exceeds the coating thickness (Gallardo *et al.*, 2003). The cracking usually happens in the neck between the particle and coating matrix, which results in development of corrosion activity near the defects. Therefore, a compromise between the sol–gel coating thickness and particle size is needed to improve the coating corrosion resistance.

9.5.2 Hybrid sol–gel coatings with incorporated inhibitors

Hybrid sol–gel coatings provide a dense barrier against corrosive species with good surface adherence to both metal substrate and organic paints. However, the coating alone is not sufficient to protect a metal substrate from corrosion. In many cases, the coatings contain micro-pores, cracks and areas of low cross-linking density which provide a path for diffusion of corrosive species such as water, oxygen and chloride ions to the coating/metal interface. Some sol–gel coatings present a ‘self-healing’ effect and partial recovery of the corrosion protective properties, but this effect is much lower than in the case of the chromate pre-treatments. Therefore, sol–gel coatings can provide an adequate protection of the metal substrate only when they are free of mechanical defects, which is hardly achievable in industrial applications. The incorporation of corrosion inhibitors inside the sol–gel coatings can partially enhance active corrosion protection and prolong coating lifetime.

The incorporation of an inhibitor into the sol–gel matrix can be performed in different ways (Osborne *et al.*, 2001). The simplest mechanism is based on inhibitor trapping by the sol–gel matrix as demonstrated in Fig. 9.3(a). In this case, no chemical interaction occurs between the inhibitive molecules and the sol–gel network. The release of inhibitor is governed by its diffusion when water penetrates the sol–gel matrix. When corrosion starts, the inhibitor becomes available at the active corrosion place and restricts the corrosion process. The second mechanism implies chemical integration of the inhibitor in the sol–gel matrix through bonding with inorganic and organic functional groups, which can occur for organic and organometallic inhibitors (Fig. 9.3(b)). Another possible mechanism includes interactions of inhibitors with organic functional groups or inorganic network of the sol–gel matrix (Fig. 9.3(c)). The interactions occur between the organic inhibitor and functional groups like phenyl, vinyl, etc, present in the sol–gel matrix and through the formation of complexes with metal oxides, such as Ti, Zr and Ce, having unsaturated coordination. Consequently, the inhibitor molecules become immobilized, which can be used to control the release of inhibitor from the sol–gel matrix.

Inorganic inhibitors

Incorporation of inorganic or organic corrosion inhibitors into the hybrid films can significantly improve the corrosion protection of metallic substrates. Different kinds of inorganic inhibitors such as cerium salts, vanadates, molybdates, permanganates and phosphates have been incorporated in sol–gel coatings with the aim of increasing the corrosion protection of metallic substrates. The results of many works show that the incorporation of cerium (III) dopants into sol–gel coatings generally enhances corrosion protection for many substrates, like aluminium alloys (Joshua Du *et al.*, 2001; Kasten *et al.*, 2001; Voevodin *et al.*, 2001a; Cabral *et al.*, 2006; Trabelsi *et al.*, 2007; Moutarlier *et al.*, 2008; Rosero-Navarro *et al.*, 2008; Yasakau *et al.*, 2008), magnesium alloys (Barranco *et al.*, 2010; Montemor and Ferreira, 2007a, 2007b), galvanized steel (Trabelsi *et al.*,

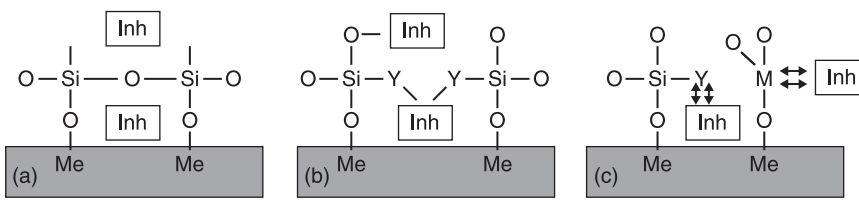

9.3 Schematic representation of inhibitor incorporation in the sol–gel matrix: (a) no interaction between inhibitor and matrix; (b) integration of inhibitor within the organic–inorganic matrix; and (c) interaction of inhibitor with organic functional groups or inorganic constituents.

2005, 2006; Montemor *et al.*, 2006b), zinc (Aramaki, 2002; Garcia-Heras *et al.*, 2004) and stainless steel substrates (Pepe *et al.*, 2006). Since cerium-based compounds provide good corrosion protection and are much less toxic than chromates, they have been one of the main candidates as environmentally friendly corrosion inhibitors.

Sol–gel films with cerium nitrate increase the corrosion resistance of AA2024 as evaluated by impedance spectroscopy and the scanning vibrating electrode technique (SVET) (Yasakau *et al.*, 2008). However, the addition of soluble cerium salts like cerium acetates, oxalates and nitrates in sol–gels is not always beneficial. The obtained coatings can have low barrier properties and fast release of inhibitor (Joshua Du *et al.*, 2001; Moutarlier *et al.*, 2008) and usually fail salt spray tests. Studies made by Garcia-Heras *et al.* show that the critical concentration of the cerium inhibitor introduced into the silica based sol–gel matrix is in the 0.2–0.6 range (wt% of Ce^{3+}). A higher concentration could lead to formation of defects in the network of the sol–gel film (Garcia-Heras *et al.*, 2004). When the efficiency of Ce^{3+} and Ce^{4+} salts in sol–gel coatings is compared, the Ce^{4+} salts show better corrosion protection (Pepe *et al.*, 2006), which is related to the formation of a more stable protective layer made of cerium (IV) oxide-hydroxides (Yasakau *et al.*, 2006).

Sol–gel coatings with other inorganic inhibitors such as $NaVO_3$, Na_2MoO_4 or $KMnO_4$ show weak corrosion protection due to low matrix stability and high solubility of the inorganic compounds (Joshua Du *et al.*, 2001; Voevodin *et al.*, 2001a; Moutarlier *et al.*, 2008). Glow discharge optical emission spectroscopy (GDOES) measurements performed by Moutarlier *et al.* proved fast release of $KMnO_4$, Na_2MoO_4 and cerium salts from the coating during immersion in corrosive electrolyte (Moutarlier *et al.*, 2008). The results of microstructural investigation performed prior to corrosion tests identified significant degradation of the sol–gel coatings with incorporated Na_2MoO_4 and $KMnO_4$ inhibitors. The additives led to formation of particles and aggregates in the coating which increased the porosity and lowered the protection of the coating. The positive effect of the addition of molybdate compounds as corrosion inhibitors to the sol–gel coatings can be achieved when molybdate is added in the 'bound' form after reaction with cycloaliphatic amine forming the compound $(R–NH^{3+})_2MoO_4$ in contrast to the 'free' ionic form (MoO_4^{2-}). The bound form of the inhibitor prevents its undesirable interaction with the sol–gel matrix and increases the matrix stability (Mascia *et al.*, 2006). Release studies also demonstrate that when molybdate is added in 'bound' form the release becomes slowed down.

Inhibitors with high solubility cannot provide long-term active corrosion protection of the coated alloy because of the very fast release of inhibitor from the coating. Moreover, the osmotic pressure can cause the formation of blisters and delamination of the coating during immersion, which can significantly affect the coating integrity and the corrosion protection. Therefore, inhibitive compounds with low solubility might be preferable candidates for incorporation into the sol–gel coatings. Strontium aluminium polyphosphate (SAPP) has been recently

reported by Raps *et al.* as one of the potential inhibitive compounds for corrosion protection of AA2024 (Raps *et al.*, 2009). The addition of SAPP to different sol–gel coatings applied to AA2024 increases the barrier protection and provides active corrosion protection by stabilizing the intermediate oxide resistance. Neutral salt spray tests after 336 h according to ASTM B117 presented in Fig. 9.4 clearly demonstrate the worst performance of uninhibited sol–gel (Fig. 9.4(a)) compared with the sol–gel with impregnated SAPP particles (Fig. 9.4(b)).

Organic inhibitors

Apart from inorganic compounds, organic inhibitors can also be incorporated into the sol–gel matrix following the scheme presented in Fig. 9.3 where inhibitors can be trapped by the sol–gel matrix or when they interact with the sol–gel matrix. Many studies show an improvement of corrosion protection of sol–gel coated metallic substrates such as 2024 aluminium alloy (Voevodin *et al.*, 2003; Khramov *et al.*, 2004, 2005; Palanivel *et al.*, 2005; Quinet *et al.*, 2007; Yasakau *et al.*, 2008), aluminium (Sheffer *et al.*, 2004), magnesium alloys (Supplit *et al.*, 2007; Shi *et al.*, 2009; Galio *et al.*, 2010), copper (Tan *et al.*, 2008) when inhibitors are present in the sol–gel matrix. Examples of promising inhibitors incorporated in the sol–gel matrix are presented below.

In general, the addition of inhibitors to sol–gel systems provides additional corrosion protection of metal. Khramov *et al.* studied the corrosion protection properties of hybrid sol–gel films deposited on aluminium alloy with different incorporated organic inhibitors such as mercaptobenzothiazole and mercaptobenzimidazole, mercaptobenzimidazolesulfonate and thiosalicylic acid (Khramov *et al.*, 2004, 2005). Corrosion protection studied by localized methods of analysis such as SVET shows low ionic currents at the sites with artificial defects, which is attributed to active corrosion protection. An improvement of the corrosion protection has been also noticed for bis-silane films containing

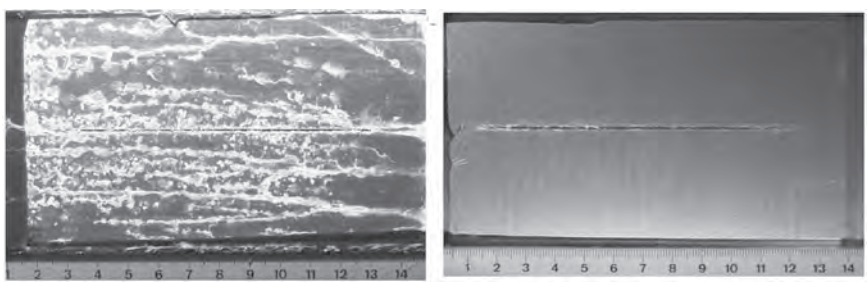

(a) (b)

9.4 Photographs of AA2024 unclad samples coated with: (a) undoped sol–gel; (b) sol–gel with SAPP inhibitor after 336 h in neutral salt spray test according to ASTM B117 (Raps *et al.*, 2009).

tolyltriazole and benzotriazole inhibitors (Palanivel *et al.*, 2005). Among the tested sol–gel coatings with 0.5 wt% of certain organic inhibitors (aminopiperazine, aminopiperidine and combinations of tetraethyl dimethylenediphosphonate and mercaptobenzothiazole), only the coating with aminopiperazine showed sufficiently high corrosion protection of 2024 aluminium alloy (Voevodin *et al.*, 2003).

The corrosion protection of magnesium alloys can be enhanced using sol–gel coatings with incorporated inhibitors. Among different inorganic and organic inhibitors, 2-methyl piperidine (Shi *et al.*, 2009), triethylphosphate, 1,2,4-triazole (Supplit *et al.*, 2007) and 8-hydroxyquinoline (8HQ) (Galio *et al.*, 2010) have been reported to extend the corrosion protection of AZ31 magnesium alloy when incorporated into the sol–gel coatings. The increase of corrosion protection in the case of the 8HQ inhibitor was associated with the formation of insoluble complexes of 8HQ with metals (Galio *et al.*, 2010).

In spite of the higher protective efficiency of sol–gel coatings with incorporated inhibitors, elevated concentrations of organic compounds can negatively affect the sol–gel matrix stability. The influence of adding the organic compound tetrachloro-*p*-benzoquinone (chloranil) into a hybrid organosiloxane/zirconia sol–gel matrix has been investigated in order to improve corrosion protection of aluminium alloy (Quinet *et al.*, 2007). Adding a high content of chloranil leads to a disorganization of the sol–gel matrix and consequently to lower corrosion protection. Such disorganization could occur because of low solubility of the organic compound in the sol–gel. Thus, the crystallized compound can create defects and voids in the sol–gel matrix, which negatively influences the barrier properties of the sol–gel coating. In contrast to that, the incorporation of lower concentrations of chloranil has resulted in homogeneous structures, increasing the protective properties of the sol–gel coatings.

9.5.3 Self-healing by intelligent release of organic corrosion inhibitors

The incorporation of organic compounds into sol–gel systems does not always provide an additional corrosion inhibition compared with undoped sol–gel coatings. Such effects can be related to a low release of organic compounds from the sol–gel system due to the electrostatic interactions between the organic compounds and the sol–gel components. However, a proper trigger can affect the inhibitor/sol–gel interactions and therefore provide the release of inhibitor. In several cases the release of organic molecular species from the hybrid sol–gel matrix can be described by the pH-dependent triggered release mechanism, which often implies protonation or de-protonation of the nitrogen atom in functional groups (Vreugdenhil and Woods, 2005). When the ζ-potential of the sol–gel matrix becomes comparable with the charge of the organic molecule, the inhibitor is ‘pushed’ out of the coating. Such triggering of the desorption processes can

provide an 'intelligent' release of the corrosion inhibitor only in places of local pH changes originating from localized corrosion processes. The corrosion studies show that some ionizable inhibitors (mercaptobenzimidazolesulfonate and thiosalicylic acid) show far weaker effects than those of non-ionizable inhibitors (mercaptobenzothiazole and mercaptobenzimidazole), since the first are too strongly attached to the sol–gel matrix and thus cannot be released during corrosion (Khramov *et al.*, 2005).

A controlled release of inhibitor can also be achieved when there are interactions between the functional groups of the sol–gel matrix and the inhibitor, as schematically shown in Fig. 9.3(c). An additional inhibition effect was revealed when phenylphosphonic acid was introduced into a hybrid sol–gel film containing phenyl groups (Sheffer *et al.*, 2004). The inhibitor becomes entrapped inside the sol–gel matrix due to specific π–π interactions between the phenyl rings. Sol–gel coatings with phenylphosphonic acid deposited on aluminium substrates demonstrate enhanced corrosion protection attributed to the prolonged release of phosphonate ions.

The incorporation of organic inhibitors can also lead to the destruction of the protective properties of the sol–gel coatings. This effect has been demonstrated by Yasakau *et al.* (2008), who performed a corrosion study on AA2024 samples coated with sol–gel films containing additives of benzotriazole (BTA). The impedance measurements demonstrated a rapid decrease of barrier properties of the sol–gel coatings with the BTA inhibitor, which caused significant corrosion damage. This effect was attributed to the chemical interaction of BTA with the components of the sol–gel system, which caused modification of the sol–gel network and rapid corrosion progress. On the contrary, the incorporation of 8HQ in the sol–gel system increases the corrosion performance of the coated AA2024 (Yasakau *et al.*, 2008).

The presented approaches may be used to design a successful corrosion protection system with performance levels close to those of chromate-based systems. Nevertheless, there are some important issues to take into consideration when using a direct inhibitor addition approach. First of all, the solubility of the inhibitor in the corrosive environment must be taken into account. Highly soluble inhibitors may cause an excessive coating blistering due to the action of osmotic pressure. Moreover, the higher solubility increases leaching of the inhibitor from the coating. Another important problem appears when a corrosion inhibitor chemically interacts with the components of the coating formulation, leading to deactivation of the inhibitor and/or reduction of its mobility, weakening the barrier properties of the coating. A negative example of inhibitor interaction with sol–gel matrix is presented in Fig. 9.5. BTA addition causes the formation of inhomogeneities within the sol–gel matrix which become sites for significant corrosion attack (Fig. 9.5(a) and (b)). When soluble inorganic salts like sodium molybdate are introduced (Moutarlier *et al.*, 2008), particles more than 10 micron form due to a crystallization process which affects the matrix barrier protection (Fig. 9.5(c)).

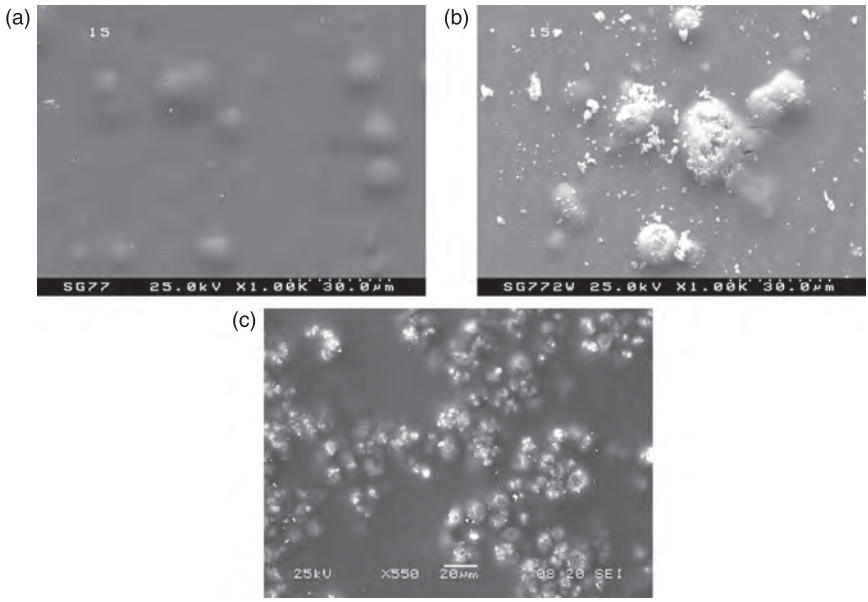

9.5 Sol–gel coating with benzotriazole inhibitor (a) before and (b) after corrosion; (c) Sol–gel coating with sodium molybdate before corrosion (Moutarlier *et al.*, 2008).

Summarizing the information presented above, it can be seen that the direct addition of inhibitors to sol–gel coatings confers additional corrosion protection, and in some cases active protection and self-healing effects. On the other hand, the addition of inhibitors is associated with a number of problems. Therefore, other strategies of inhibitor addition might be used that isolate an inhibitor from the coating components and provide a controlled release of inhibitor on demand.

9.6 Sol–gel coatings with nanoreservoirs

Direct addition of corrosion inhibitors to the sol–gel coating matrix can provide an additional active corrosion protection effect on the one hand, but at the same time can negatively influence adhesion and barrier properties. Moreover, the active inhibitors can often be deactivated as a result of chemical interactions with the ingredients of the coating formulation. Therefore, immobilization of the active inhibiting species inside special particulate carriers or reservoir layers can provide an efficient solution aiming at prevention of the negative effects originating from the undesirable coating/inhibitor interactions (Ghosh, 2008).

Recent developments in surface science and technology show new and more attractive concepts of self-healing coatings. These approaches are based on the

integration of nanoscale containers (carriers) loaded with active inhibiting compounds, or layered reservoirs, into the existing structures of conventional coating systems. These self-healing protective coatings should provide fast release of the inhibitors on demand within a short time after changes in the coating integrity or in the environment aggressiveness. The nanocontainers or reservoir-layers are introduced to the passive barrier coating system keeping the active species in a 'trapped' form. By definition, a nanocontainer (or nanoreservoir) is a nanosized volume filled with an active substance confined in a porous core and/or a protective shell.

The immobilization of active inhibiting species reduces the probability of excessive and uncontrollable inhibitor leaching or pigment-induced osmotic blistering. These problems are typical for coatings containing inhibitor salts if they are too soluble or prepared with too small a particle size. The immobilization approach also allows creation of 'smart' delivery systems which are able to release corrosion inhibitors in a controllable way, only on demand from the action of different corrosion-relevant triggers such as local change of pH or the presence of corrosive anions. When the local environment changes, or if a corrosion process starts in the coating defect, the containers respond to this signal and release the immobilized active material (Shchukin *et al.*, 2006).

The delivery of inhibitors can be based on different possible release mechanisms that depend upon the encapsulation approaches. The simplest example is uncontrollable leakage of active ingredients from a polymer capsule ruptured under mechanical stresses. This approach was used by Yang and Van Ooij when triazole inhibitor was encapsulated using plasma polymerization to produce PP-perfluorohexane and PP-pyrrole layers employing RF plasma discharge (Yang and Van Ooij, 2004). The release of the inhibitor from such a capsule is possible only when it is mechanically ruptured.

Another relatively simple approach involves a desorption-based mechanism. This type of delivery can be classified as a prolonged release, but it is not a controlled release; uncontrollable leaching is usually difficult to avoid in such cases. However, under certain circumstances the kinetics of the desorption processes are dependent on the conditions in the surrounding environment, such as pH or ionic strength. In this way a certain control of the leaching can be achieved. The release on demand can be accomplished via application of trigger-responsive polymer shells or pre-layers such as polyelectrolytes sensitive to pH. Another mechanism of triggered release of inhibiting species can be based on the ion-exchange reaction when inhibiting anions are displaced by corrosive anions. The previously mentioned examples of release mechanisms are relevant for autonomous self-healing processes. In the case of induced self-healing, an external action should be applied to provoke the release of an active agent.

In this section the main approaches to inhibitor encapsulation and immobilization on different carriers and inside reservoir layers will be overviewed in terms of their applicability to self-healing sol–gel based anticorrosion coatings. Different

techniques that can be used for the development and study of different levels of inhibitor immobilization are discussed. Most of the immobilization approaches are also widely exploited in other areas where delivery of active agent on demand is pursued. Medicine, cosmetics and fertilizers are among the most typical examples.

9.6.1 Types of nanoreservoir

Layer reservoirs

Active self-healing functionality can be added to hybrid sol–gel based coatings introducing an additional functional layer that acts as an inhibitor container. Different approaches can be used to create such a layer between a metallic substrate and a hybrid coating or atop the coating. Inorganic porous reservoir pre-layers were recently reported as functional elements of sol–gel based active protective coatings. The advantage of this approach is the availability of corrosion inhibitor in large quantities in the vicinity of the metal surface. A novel approach aimed at developing a nanoporous reservoir for storing corrosion inhibitors on the metal/coating interface has been proposed by Lamaka *et al.* (2006, 2007). A porous titania layer on the surface of AA2024 aluminium alloy was developed, controllably hydrolysing titanium alkoxide in the presence of a template agent. The titania particles were self-assembled in a porous network on the AA2024 aluminium alloy matrix replicating the microstructure of the native porous aluminium oxide. Then, the metallic substrate covered with TiO_2 was immersed in a corrosion inhibitor solution (BTA) and finally over-coated with a hybrid sol–gel film. In this case, the inhibitor container is a three-dimensional oxide nanostructured porous layer with a large effective surface area available for inhibitor adsorption. This complex system shows enhanced corrosion protection in comparison with a simple one-layer sol–gel film. Moreover, the bi-layer coating demonstrates well-defined self-healing ability leading to effective long-term active corrosion protection.

The anticorrosion performance of these coatings assessed by electrochemical impedance spectroscopy shows that the lower impedance was obtained when BTA was directly added to the sol–gel matrix, whereas the best performance was achieved with inhibitor-doped TiO_x coated with a hybrid film. In terms of active corrosion protection, there is a periodic decrease/increase of impedance associated with the breakdown followed by the self-healing of the intermediate oxide layer. SVET was employed to study the self-healing ability of bi-layer systems at the micro level. The measurements of local corrosion current evolution in the zones of artificial defects have demonstrated well-defined corrosion activity on the surface of AA2024 coated with sol–gel film only, while no corrosion activity was revealed even after 24 hours on the alloy treated with a bi-layer system. The reported results show that the adsorbed inhibitor is leached out from the porous

pre-treatment layer to the defect, healing it. The developed surface, formed by the self-assembled layer, also offers good adhesion between the oxide and the sol–gel film due to the high contact area between the two phases. Moreover, the employment of this reservoir approach avoids the negative effects of the inhibitor on the stability of the sol–gel coating.

Rosero-Navarro *et al.* (2010) have recently suggested a multi-layer sol–gel hybrid inorganic/organic coating system with a structure composed of an intermediate cerium-containing layer deposited between two undoped hybrid layers. The obtained results have shown the migration of the cerium ions into the defects towards the substrate providing additional active corrosion protection. The combination of the physical barrier (blank hybrid sol–gel) and the active protection (Ce-containing interlayer) enables an effective protective system for aluminium alloys.

Biopolymer chitosan can also be used as a 'green' candidate for reservoir layers. The application of natural polymer materials as reservoirs for environmentally friendly corrosion inhibitors constitutes an attractive and relatively unexplored approach to the development of 'green' self-healing coatings. Chitosan is one such interesting candidate due to its good film-forming properties, superior adhesion to metallic surfaces and many organic polymers. Another important feature of chitosan is its high ability to form complexes with potential corrosion inhibitors in a reversible manner. Cerium (III) was employed as the corrosion inhibitor for aluminium 2024 alloy in the work of Zheludkevich *et al.* (2011). Scanning electron microscopy (SEM) and energy dispersive spectrometry (EDS) in Fig. 9.6 clearly demonstrate preferential immobilization of Ce ions in the biopolymer layer. The superior corrosion protection performance with well-defined active inhibition of the electrochemical reactions in the artificial

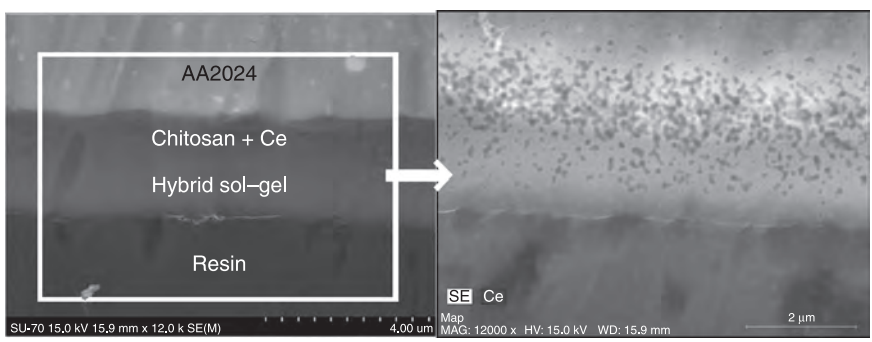

(a) (b)

9.6 (a) SEM cross-section of bi-layer coatings with Ce-containing chitosan; and (b) EDS map of the same zone indicating distribution of Ce cations (Zheludkevich *et al.*, 2011).

defects was demonstrated in the case of sol–gel coatings with an inhibitor-loaded chitosan pre-layer.

The reservoir layers described above provide an efficient way to store corrosion inhibitor, preventing its interaction with sol–gel matrix. However, the release of corrosion inhibitors stored in such reservoirs is uncontrollable. Polyelectrolyte reservoir films can be applied in order to achieve release of corrosion inhibiting species on demand, as suggested by Lamaka *et al.* (2008). The reservoirs are composed of layers of oppositely charged polyelectrolyte molecules deposited on AA2024 aluminium alloy coated with hybrid sol–gel film. The container is prepared via layer-by-layer sequential spray-coating deposition of water solutions of poly(ethyleneimine) (PEI), poly(sodium styrenesulfonate) (PSS) and 8HQ. The active corrosion protection of AA2024 alloy coated with such a bi-layer system is demonstrated by EIS and SVET.

The obtained results demonstrate that inhibitor-containing polyelectrolyte films remarkably improve the long-term protection performance, providing additional 'smart' anticorrosion properties based on the delivery of inhibiting species 'on demand'. The triggered delivery of inhibitor is possible since the configuration of the polyelectrolyte molecules depends on the presence of H^+ ions, making the polyelectrolyte film sensitive to the pH of the surrounding solution (Grigoriev *et al.*, 2009). The acceleration of the inhibitor release is observed in the alkaline region. PEI/PSS polyelectrolyte complex consists of strong polyanion (PSS) and weak polycation (PEI). This structure of polyelectrolyte multi-layers provides the possibility of complex dissolution and inhibitor release at an alkaline pH, starting at a pH of around 8. Therefore, the developed reservoir system provides inhibitor storage at neutral pH, and fast release on demand in the alkaline region resulting from the cathodic activities.

Nanocontainers

Another strategy is based on the use of nanocarriers as storage/delivery systems that can be directly incorporated in the hybrid sol–gel matrix. In this section different strategies for the creation of nanocontainers of corrosion inhibitors will be reviewed as well as their performance in self-healing hybrid sol–gel coatings. One of the simplest ways is to use *oxide nanoparticles* as carriers for corrosion inhibitors. The oxide nanoparticles are potential reinforcements for the polymer coatings (Chen *et al.*, 1998; Malzbender and de With, 2002; Conde *et al.*, 2003; Gallardo *et al.*, 2003). Incorporation of the nanoparticles into hybrid sol–gel formulations leads to an additional improvement of the barrier properties due to an enhanced thickness and a low crackability of such composites (Malzbender and de With, 2002; Zheludkevich *et al.*, 2006). Moreover, an additional active corrosion protection and a self-healing ability can be achieved when the oxide nanoparticles are doped with a corrosion inhibitor. A major challenge in the formation of thin layers with the incorporation of nano-oxides is to avoid the

formation of particle agglomerates (Brusciotti *et al.*, 2010). Agglomeration affects the film uniformity and might create preferential paths for corrosion attack. If this issue is avoided, the barrier properties of thin sol–gel films are improved by the addition of oxide nanodispersed particles (Rosero-Navarro *et al.*, 2008).

Zheludkevich *et al.* (2005a, 2005b) have suggested the immobilization of cerium (III) cations on amorphous zirconia nanoparticles via controllable hydrolysis of tetrapropoxyzirconium (TPOZ) in the presence of $Ce(NO_3)_3$. The resulting sol mixed with a siloxane-based hybrid sol–gel formulation leads to a nanocomposite coating containing oxide nanocontainers of cerium ions. The large surface area of the carriers resulting from the small diameters of the nanoparticles provides sufficient loading capacity. The prolonged release of inhibitor from the surface of oxide nanoparticles confers an enhanced long-term corrosion protection on AA2024 aluminium alloy. Moreover, the use of oxide nanocarriers prevents the negative effects of cerium ions on the hydrolytic stability of hybrid sol–gel coatings (Zheludkevich *et al.*, 2005b). This idea was followed by other researchers when boehmite nanoparticles were synthesized and introduced to the hybrid sol–gel coating as nanocontainers of corrosion inhibitor (Pirhady Tavandashti and Sanjabi, 2010).

The inhibiting ions can also be immobilized on the surface of commercially available nanoparticles by a simple adsorption in an inhibitor-containing solution. Silica- and ceria-based nanocarriers obtained by this method provide additional active corrosion protection to an organosilane coating applied to galvanized steel (Montemor and Ferreira, 2007c). The nanoparticles themselves can also confer an inhibiting action in some cases. For example, ceria nanoparticles show a well-defined active anticorrosion effect. However, the structure and nanosize of such particles is a key factor. The large and crystalline particles of ceria are extremely insoluble and unable to release any inhibiting species. In the work of Schem *et al.* (2009), small 5 nm size amorphous ceria nanoparticles were introduced to hybrid organic–inorganic sol–gel matrices employed as coatings for an AA2024-T3 aluminium alloy. Electrochemical studies indicate a generally beneficial effect of incorporation of ceria nanoparticles, although the performance of the coated alloy depends on the nanoparticle content.

Another possible method for using the nanoparticle surface as an inhibitor carrier is to adsorb the inorganic corrosion inhibiting anions onto the particle surface by an ion-exchange mechanism (Pippard, 1983). However, this approach can also lead to an undesirable release of the inhibitor initiated by the presence of harmless ions in the surrounding environment. Organic corrosion inhibitors can also be immobilized on the surface of nanoparticles. Chemical anchoring of an organic inhibitor to aluminium oxyhydroxide nanoparticles through carboxylic bonds was employed in protective coatings for aluminium, copper, nickel, brass and bronze substrates (Cook, 2005). High specific surface area of the oxyhydroxide nanocarrier (at least 100 $m^2 \cdot g^{-1}$) allows a higher quantity of corrosion inhibitor to be delivered into the damaged part of the coating. Hydroxide ions generated from the corrosion of these metals trigger the release of corrosion inhibitors from the

particles at pH 9. Thus, the release of the inhibitor is started only by the corrosion process, preventing undesirable leakage of the inhibitor from an intact coating during exploitation.

Various strategies are suggested to increase the loading of oxide nanocontainers by increasing the surface area or forming hollow oxide nanocontainers (Kartsonakis *et al.*, 2010). One of the examples is shown in Fig. 9.7. Cerium molybdate *hollow nanospheres* were suggested as possible nanocontainers for 8HQ or with 1-H-benzotriazole-4-sulfonic acid (1-BSA) as corrosion inhibitors (Kartsonakis *et al.*, 2010). These nanospheres were synthesized using a three-step process: first, polystyrene (PS) nanospheres were produced using emulsion polymerization; second, the PS spheres were coated via the sol–gel method to form a cerium molybdate layer; finally, the nanocontainers were made by calcination of cerium molybdate coated PS nanospheres. The calcined nanospheres were loaded with 8HQ or with 1-BSA. The loading of 8HQ achieved 5.22% w/w and that of 1-BSA was 16.43%. Electrochemical measurements have demonstrated that inhibitor is released from the nanocontainers, suppressing the corrosion activities on steel and AA2024 surfaces.

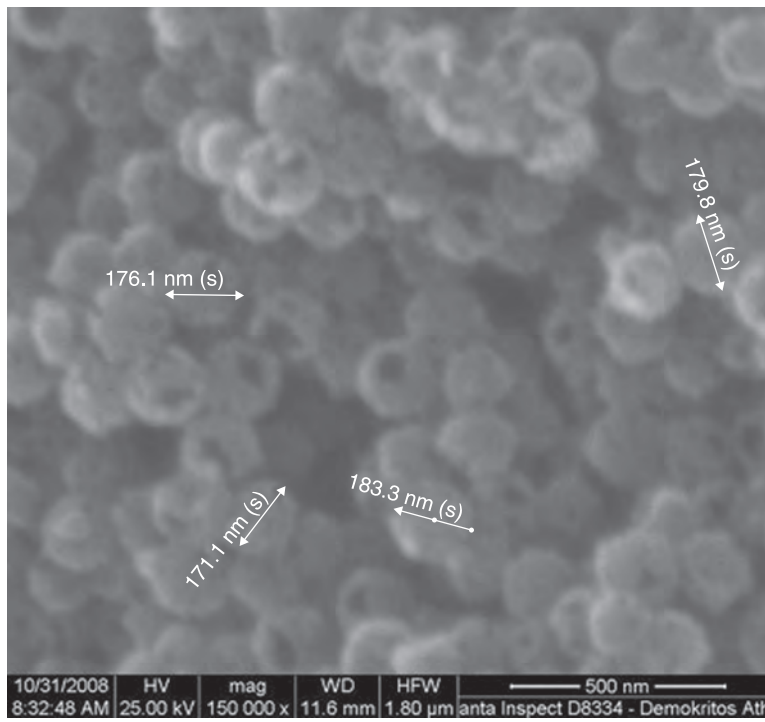

9.7 SEM images of cerium titanium oxide hollow nanospheres with diameter around 170–180 nm (Kartsonakis and Kordas, 2010).

Mesoporous nanoparticles can also be considered as potential nanocontainers. Borisova *et al.* (2011) have suggested the synthesis of monodisperse, mesoporous silica nanoparticles loaded with 1H-benzotriazole and embedded in a hybrid sol–gel coating. The developed nanoparticles exhibit high surface area (~1000 $m^2 \cdot g^{-1}$), narrow pore size distribution (d ~3 nm), and large pore volume (~1 $ml \cdot g^{-1}$). This confers high uptake and storage of the corrosion inhibitor in the mesoporous nanocarriers. The homogeneously distributed BTA-loaded mesoporous silica nanocontainers in the hybrid film improve the corrosion resistance of the aluminium alloy AA2024 as demonstrated by SVET experiments. These results, as well as the controlled pH-dependent release of BTA from the mesoporous silica nanocontainers, suggest an inhibitor release triggered by the corrosion process.

Even higher loading capacity can be achieved when porous fillers with hollow cellular structure are loaded with organic and/or inorganic inhibitors (Schmidt, 2002). The hollow cellular structure material may be represented by zeolite or halloysite nanotubes. Zeolite particles are attractive carriers also because the cations in their structure are rather loosely held and can readily be exchanged for the inhibiting cations in the contact solution (Eckler and Ferrara, 1988).

Halloysite was found to be a viable and inexpensive nanoscale container ($4 per kg with the supply of 50 000 tons per year) for the encapsulation of active molecules. Halloysite is defined as a two-layered aluminosilicate, chemically similar to kaolin, which has predominantly hollow tubular structure in the submicron range. The neighbouring alumina and silica layers create a packing disorder which causes them to curve. As for the most natural materials, the size of halloysite particles varies within 1 to 15 μm of length and 10 to 150 nm of inner diameter depending on the deposits. Halloysite nanotubes are capable of entrapping a range of active agents (within the inner lumen, as well as within void spaces in the multi-layered aluminosilicate shell) followed by their retention and release. Both hydrophobic and hydrophilic agents can be embedded after an appropriate pre-treatment of the halloysite (Luca and Thompson, 2000). Cheap halloysite nanotubes as prospective nanocontainers for anticorrosion coatings with active corrosion protection were recently demonstrated (Fix *et al.*, 2009). Halloysite nanotubes were loaded with BTA or 8HQ and then incorporated into a hybrid sol–gel coating. The results of corrosion tests demonstrated superior corrosion protection performance of halloysite-containing hybrid sol–gel films compared with that of blank coatings.

The halloysite nanotubes can provide a significant loading of corrosion inhibitor. However, the release of the inhibitor from the nanocontainers can be very fast. Large quantities of the inhibitor can be released during the preparation of a sol–gel coating and therefore several strategies were considered in order to decrease the rate of inhibitor release from the halloysites and preferably to confer release on demand. Abdullayev and Lvov have tried to seal the nanotube openings with stoppers (Abdullayev and Lvov, 2010). To create tube end stoppers, BTA-loaded halloysites were exposed to a solution containing Cu(II) ions, leading to

the formation of insoluble complexes at the openings of the halloysites. Controllable release of benzotriazole was achieved, and the release time may be varied from ten to hundreds of hours. To prevent undesirable leakage of the loaded inhibitor from the halloysite interior, the outer surface can be modified by a deposition of several alternating polyelectrolyte multi-layers of PAH and PSS, as shown in Fig. 9.8. Another function of the polyelectrolyte shell is to provide the release of the encapsulated inhibitor in a manner controlled by pH changes in the environment surrounding the halloysite nanotube (Shchukin *et al.*, 2008), which will prevent a spontaneous leakage of the inhibitor and perform its release triggered by the pH changes directly in the corrosion zone.

The possibility of creating a smart self-healing anticorrosion coating based on layer-by-layer assembled nanocontainers was recently demonstrated by Zheludkevich *et al.* (Shchukin *et al.*, 2006, 2007; Zheludkevich *et al.* 2007). Silica nanoparticles were used as a template and BTA as an organic corrosion inhibitor. The layer-by-layer deposition procedure was employed involving both large polyelectrolyte molecules and small BTA molecules. The initial SiO_2 nanoparticles are negatively charged and so deposition of the positive PEI was performed in the first stage. Then, deposition of the negative PSS layer occurred. Deposition of the third inhibitor layer was accomplished in acidic media (pH = 3) from a 10 mg ml^{-1} solution of BTA. The latter two deposition steps (PSS and BTA) were repeated once to ensure a high inhibitor loading in the final layer-by-layer structure. The optimal number of PSS/BTA bi-layers that should be deposited onto silica nanoparticles is two (Shchukin *et al.*, 2007). One bi-layer is not sufficient for the self-healing effect of the final protective coating, while three or more bi-layers drastically increase aggregation of the nanocontainers during assembly and coating deposition.

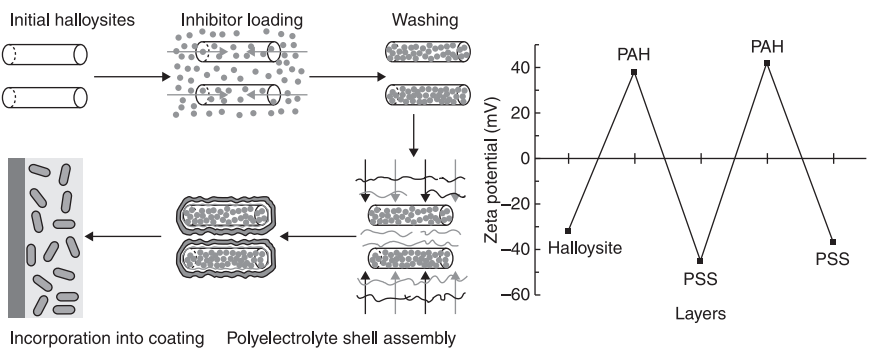

9.8 Schematic illustration of the fabrication of 2-mercaptobenzothiazole-loaded halloysite/polyelectrolyte nanocontainers. Right: zeta potential data for sequential deposition of PAH and PSS polyelectrolytes on halloysite nanotubes, pH 7.5 (Shchukin *et al.*, 2008).

The samples coated with the hybrid film doped with layer-by-layer nanocontainers demonstrated sufficiently enhanced performance in corrosion tests in comparison to an undoped sol–gel film or a film doped directly with free non-immobilized BTA. It was demonstrated that local corrosion activity triggers the release of a portion of BTA from the nanocontainers, hindering the corrosion process in the defective area. Such a 'smart' self-healing effect can be originated from the active feedback between the coating and the localized corrosion processes.

The most probable mechanism is based on the local change of pH in the damaged area due to the corrosion processes. When the corrosion processes start, the pH value is changed in the neighbouring area, which opens the polyelectrolyte shells of the nanocontainers in a local area with the following release of BTA. Then, the released inhibitor suppresses the corrosion activity and the pH value recovers, closing the polyelectrolyte shell of nanocontainers and terminating further release of the inhibitor, as schematically shown in Fig. 9.9 (Zheludkevich *et al.*, 2007).

A quite simple approach to inhibitor entrapment is based on *complexation* of organic molecules by cyclodextrin (Khramov *et al.*, 2004, 2005). In the beginning, this concept was suggested for controllable drug delivery systems (Uekama *et al.*, 1998). Cyclodextrins are known complexation agents that can act as hosts forming

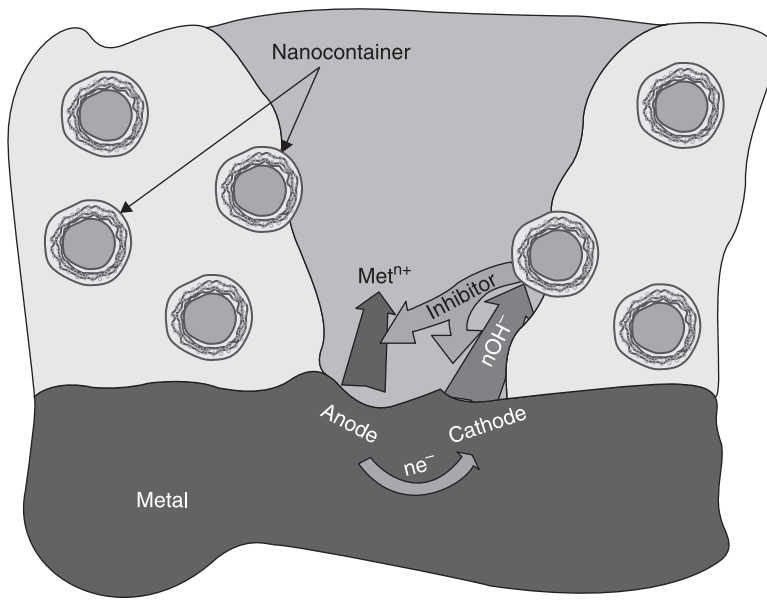

9.9 Scheme of the controllable release of the inhibitor from LbL nanocontainers and the 'smart self-healing' process (Zheludkevich *et al.*, 2007).

inclusion complexes with various organic guest molecules that fit, into the size of the cyclodextrin cavity. Organic aromatic and heterocyclic compounds are usually the main candidates for the inclusion complexation reaction (Rekharsky and Inoue, 1998). Several organic heterocyclic compounds are known inhibitors for various metallic substrates and so the cyclodextrins can be effectively used for immobilization of these species. Two organic corrosion inhibitors, mercaptobenzothiazole (MBT) and mercaptobenzimidazole (MBI), were selected by Khramov *et al.* (2004) to be added to a hybrid sol–gel used for corrosion protection of AA2024 aluminium alloy. MBT and MBI were introduced to the sol–gel formulations as inclusion host/guest complexes with β-cyclodextrin. The hybrid films doped with corrosion inhibitors provided superior corrosion protection when compared with the undoped ones. Moreover, the coatings doped with inhibitors in entrapped form outperformed those made by a simple addition, as the complexation equilibrium resulted in the slowed release of the inhibitor and its continuing delivery to the corrosion sites followed by self-healing of corrosion defects. However, complexation with cyclodextrin confers only a prolonged release of the inhibitor without delivery on demand as a response to any corrosion-relevant external stimuli.

A promising class of containers is based on the ion-exchange release mechanism. The kinetics of inhibitor delivery in such cases are tightly controlled by the concentration of cations or anions present in the corrosive environment. Inhibiting inorganic cations can be incorporated as exchangeable ions associated with *cation-exchange solids* (Bohm *et al.*, 2001; Buchheit *et al.*, 2002; McMurray *et al.*, 2003). The advantage of this approach is that the cation exchange pigment is completely insoluble, avoiding osmotic blistering (Bohm *et al.*, 2001). Bentonite clays are a form of montmorillonite and exhibit intrinsic cation exchange properties. They are constituted by stacked negatively charged aluminosilicate layers. The negative charge of these layers is compensated by the cations intercalated between the aluminosilicate sheets. The interaction between the sheets and the exchangeable cations is purely electrostatic. Therefore, the principal exchangeable cations (sodium (I) and calcium (II)) can be easily exchanged in the laboratory by passing a suspension of bentonite through a cation exchange column or by repeatedly washing the bentonite with a solution containing the desired cation. Calcium (II) and cerium (III) cation-exchanged bentonite can be used as containers of respective inhibiting cations.

An even more interesting case is represented by *anion-exchange nanocontainers*, which are used to immobilize anionic inhibitors (Leggat *et al.*, 2002; Buchheit *et al.*, 2003; Wang *et al.*, 2004). The release of inhibitor anions can be triggered in this case by aggressive corrosive ions present in the surrounding environment. Layered double hydroxide (LDH) is a host/guest structure and can be used as an effective anion exchanger. Structurally, LDHs consist of stacks of mixed-metal hydroxides positively charged, stabilized by anions and solvent molecules situated between the positive layers. The anion exchange pigment can play a double role,

absorbing the harmful chlorides and releasing the inhibiting ions in response. Furthermore, the release of inhibitors can also be indirectly triggered by pH changes: at very high pH the inhibitors can be exchanged with hydroxyl anions, whereas at very low pH the LDHs dissolve, releasing the entrapped inhibitors. The 'trap' function alone can already provide additional anticorrosion effects in filiform corrosion tests when non-inhibited pigments with carbonates and sulfates are used in organic coatings (McMurray and Williams, 2004). Absorption of chlorides from an aggressive electrolyte in the vicinity of a defect decreases the aggressiveness of the corrosive medium decreasing the rate of the corrosion processes. The use of additional inhibiting LDH nanocontainers can confirm the active feedback conferring a self-healing ability.

LDHs can be prepared by different methods, including by co-precipitation or ion exchange, constituting a versatile structure to allocate different inorganic and organic anions such as vanadates (VO_x) (Tedim *et al.*, 2010; Zheludkevich *et al.*, 2010), phosphates (H_xPO_4) (Tedim *et al.*, 2010), 2-mercaptobenzothiazolate and quinaldate (Poznyak *et al.*, 2009), ethyl xanthate, oxalate and BTA (Williams and McMurray, 2004). X-ray diffraction showed that these materials are crystalline, and the peak positions at low 2Θ angles allowed correlation between the gallery height and size and orientation of different anions. In addition, EDS analysis qualitatively indicated that the intercalation of corrosion inhibitors had been successful. Fig. 9.10 shows SEM and transmission electron microscopy (TEM) of LDHs intercalated with vanadates (LDH-VO_x).

More recently, the combination of LDHs with different intercalating anions was suggested to achieve an enhancement of the corrosion protection of AA2024 substrates (Tedim *et al.*, 2010). The combination of different nanoreservoir/inhibitor systems could be a way of overcoming some technical obstacles, like the low loading of inhibitors in the protective coatings or the negative effect of a high

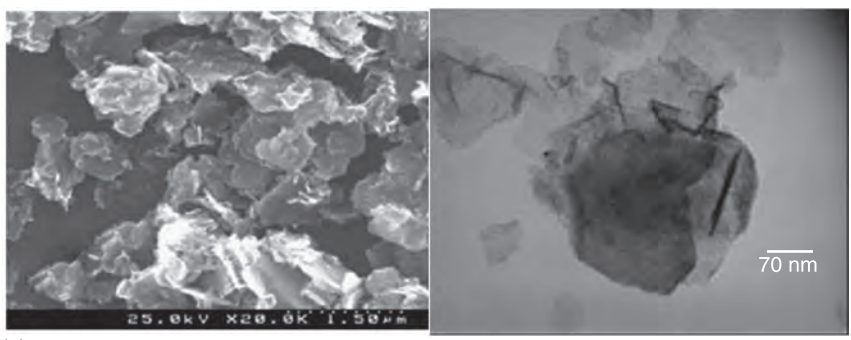

(a) (b)

9.10 (a) SEM and (b) TEM images of LDH-VOx. (b) Reprinted with permission from Zheludkevich *et al.*, 2010; Tedim *et al.*, 2010.

concentration of nanocontainers on the coating barrier properties. The anions used in this study were VO_x, $H_xPO_4^-$ and MBT. For bare AA2024 substrates immersed in NaCl solution, synergistic anticorrosion activity was observed when LDH-VO_x and LDH-H_xPO_4 or LDH-VO_x and LDH-MBT were combined. This effect can be attributed to the increase of stability of the native oxide film. Similar studies were also performed for painted AA2024 substrates. The coating consisted of a sol–gel pre-treatment followed by a water-based epoxy primer and an epoxy-based top coat. LDH nanocontainers were added to both pre-treatment and primer. The results showed that a positive effect was obtained when LDH-MBT was added to the sol–gel and LDH-VO_x was present in the primer, contributing to an enhancement of both intermediate oxide film and coating stability.

9.7 Conductive polymer coatings

In previous sections, different prospective coating systems for corrosion protection of metallic substrates were presented. The main function of a coating is to act as a barrier, delaying the ingress of oxygen, water and electrolyte species. Other functionalities can then be added to sustain the protection of underlying substrates when the barrier fails, including microcapsules capable of restoring coating integrity upon mechanical impact, dispersion of corrosion inhibitors in the coating matrix or the incorporation of nanocontainer/corrosion inhibitors for their controlled release. All the coatings presented so far are *insulating* in nature, not capable of conducting charge.

Here, the application of *conducting polymers* to corrosion protection, and specifically the electrically conducting polymers of conjugated type, will be described. A reader outside the corrosion field may look at the utilization of conductive polymers as coating as a paradox, since the main coating function is to impede the contact between metal and electrolyte species, and the use of systems whose properties are based upon the conduction of charge carriers apparently conflicts with that purpose. In fact, there are many examples in the literature showing that a careful selection of polymer is required and that the conditions under which it will protect the active metal substrate are very specific, otherwise leading to disastrous results. There are two main points that should be highlighted at this stage. The first is the considerable number of published works reporting apparently conflicting results. The second, probably a consequence of the first, is the open discussion on the corrosion protecting mechanisms associated with conjugated polymers and different active metals.

Conducting polymer is a broad concept referring to polymers with the ability to conduct charge and can be classified according to the associated type of conductivity. When conductivity arises from ionic mobility only, the polymers are termed *ion-conducting polymers*. One representative system is poly(ethylene) oxide (PEO) and its interaction with salts (Doscher *et al.*, 1951). In the case of polymeric systems with redox active species, electronic conductivity exists and

the designation *electrically conducting polymers (ECPs)* is applied. Depending on the mechanism of electron transfer, ECPs can be divided into two sub-groups: *redox* and *conjugated* polymers. For redox polymers like polyvinylferrocene (PVF) (Daum and Murray, 1981) the mechanism of electron transfer is by electron hopping (Doblhofer *et al.*, 1982; Mortimer and Anson, 1982). In conjugated polymers the mobility of charge carriers is different. The structure is characterized by an extended π-conjugated system which, upon doping, leads to the creation of charge carriers with the ability to move in the delocalized π-systems. As a result, conjugated polymers exhibit higher conductivity than redox polymers. Examples of conjugated polymers include polyacetylene, polypyrrole (PPy) and polythiophene (PTh) (Fig. 9.11).

PPy and PTh are characterized by the existence of non-degenerate ground states, arising from differences in energy of the two mesomeric forms, namely aromatic and quinoid. In the undoped (reduced) form, the band gap is high enough to prevent electrons moving freely and the structure of the polymer is aromatic. On doping (oxidation), there is a loss of electron and the valence band is no longer fully occupied; in this state the polymer adopts a quinoid structure, with the formation of intermediate electronic states in the band gap thereby becoming conductive (Brédas *et al.*, 1984). There are different types of doping that generate mobile charge carriers in conjugated polymers: (i) redox doping, (ii) doping without dopant ions and (iii) non-redox doping (McDiarmid, 2001). Redox doping is perhaps the most common and can occur by charge transfer (chemical and electrochemical) doping. The example of conductivity previously highlighted for PPy and PTh is of *p*-type doping (removal of electrons). One example of non-redox doping is by acid–base chemistry, observed for polymers possessing strong basic atoms within the π-backbone; in this case the conductivity arises from protonation and not from changes in the number of electrons. The most representative example of acid–base doping is polyaniline (PANi), although it may also be doped by redox processes (Chiang and MacDiarmid, 1986; McDiarmid *et al.*, 1987) (Fig. 9.12). One of the most important applications of conducting polymers in doping states is corrosion protection.

The corrosion behaviour of steel substrate coated with PANi was firstly reported by DeBerry (1985), although an earlier work by Mengoli and colleagues (1981) already refers to polymerization of PANi on iron. Since then, the majority of reported studies in this field involve the application of PPy, PTh and PANi, and

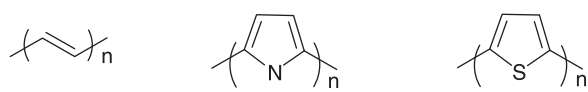

(a) (b) (c)

9.11 Structures of (a) trans-polyacetylene, (b) polypyrrole and (c) polythiophene.

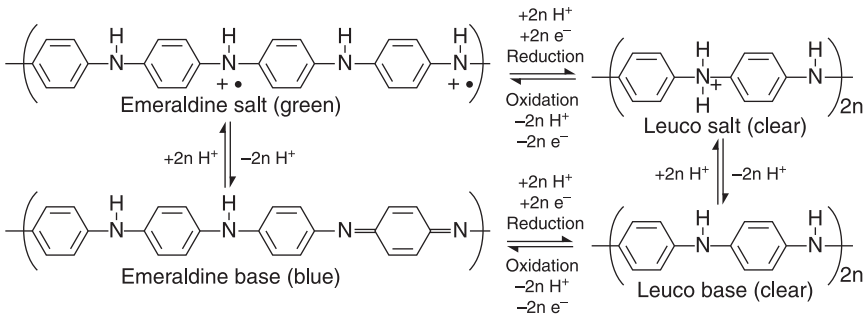

9.12 Proton and electron transfer in PANi. The most oxidized form (pernigraniline) is not shown (Tallman *et al.*, 2002).

the most studied metallic substrates by far are iron and corresponding alloys. There are several important reviews available in the literature listing the most relevant works in this field and shedding some light on different corrosion mechanisms, namely the works by Tallman *et al.* (2002) and Spinks *et al.* (2002), and more recently by Lacaze *et al.* (2010).

Conducting polymers exhibit unique characteristics that can be used in the context of corrosion protection. The reduction potential of conducting polymers like PPy, PTh and PANi is positive with respect to some of the most active metals like iron, zinc, aluminium and magnesium (Table 9.1). This fact can anticipate anodic protection as a relevant protection mechanism. Another point is that doping

Table 9.1 Reduction potentials of different redox couples

Redox couple	Reduction potential (vs. SHE at pH 7)
Mg/Mg^{2+}	–2.36
Al/Al_2O_3	–1.96
Zn/Zn^{2+}	–0.76
Fe/Fe^{2+}	–0.62
H_2/H_2O	–0.41
H_2O/O_2	+0.82
CrO_4^{2-}/Cr_2O_3	+0.42
Polypyrrole	–0.1 to +0.3[a]
Polyaniline	+0.4 to +1.0[a]
Polythiophene	+0.8 to +1.2[a]

Source: Tallman *et al.*, 2002.

requires charge compensation by ions from/to the electrolyte. In the case of PPy and PTh, doping is electronic (redox) while in PANi it may be protonic and/or electronic. The incorporation of ionic species opens different possibilities for corrosion protection, namely the incorporation of corrosion inhibitors, whose release can be triggered by changes in either the electrochemical potential or pH (in the case of PANi).

Conducting polymers can be prepared by chemical or electrochemical techniques. Electrochemical synthesis provides easier routes when compared with chemical synthesis and allows control over film formation, especially relevant if polymers are required as thin films deposited on the surface of metallic substrates. However, electrochemically synthesized polymers are usually more porous, a feature that requires consideration when a barrier effect is necessary. Another important aspect in the corrosion field is that the application of potential/current necessary to promote electropolymerization may accelerate dissolution (corrosion) of the metal. In some cases, an oxide pre-layer is deposited between the metal and the polymer to promote adhesion and hinder metal dissolution during the electropolymerization process (Tallman *et al.*, 2002; Spinks *et al.*, 2002). Alternatively, the application of layered coatings based on different conducting polymers can be a strategy to overcome the problem of metal dissolution. In the work of Lacroix *et al.* (2000), a layer of PPy was firstly deposited on zinc and mild steel in neutral conditions, followed by deposition of PANi in an acidic medium, because the direct deposition of PANi on those metallic substrates was not possible in an acidic medium, causing dissolution of the metal.

An alternative to *in situ* chemical and electrochemical polymerization is the utilization of processable pre-formed polymers. However, ICPs are usually insoluble and not fusible. To overcome these difficulties, processable ICPs can be obtained by proper functionalization of the heterocycle monomers or colloidal dispersions of conducting polymers used (Spinks *et al.*, 2002).

Earlier in this chapter, protective coatings used in corrosion protection were demonstrated to have two main functions: to provide a physical barrier against the ingress of aggressive species and confer corrosion inhibition when the barrier fails. Indeed, conducting polymers processed as coatings can display a barrier effect (Wessling, 1994; Wey *et al.*, 1995; McAndrew *et al.*, 1996) and, since their building block units are heterocyclic compounds, also some sort of active corrosion protection can be expected (Sathiyanarayanan *et al.*, 1992). Nevertheless, the mechanisms according to which conducting polymers can inhibit corrosion processes are more complex than simple barrier/corrosion inhibition mechanisms. When conducting polymers are electrodeposited on metal substrates they also carry ions and water (solvent) molecules from solution, showing too high a porosity to work as a proper barrier. The porosity of electrodeposited polymers can be decreased by controlling the conditions of electrodeposition (Van Schaftinghen *et al.*, 2006). Moreover, to decrease the amount of water within the polymer matrix, heat treatments can be applied, as evidenced in the work of

Hermelin *et al.* (2008). PPy films electrodeposited on zinc substrate from aqueous solution in the presence of diisopropylsalicylate and salicylate showed an improvement of the barrier effect after dehydration at 180°C in air, which was attributed to the cross-linking of PPy chains by O_2.

Another property that can also be controlled is the permeability of the polymeric matrix to aggressive ions such as chlorides. The type of electrolyte used in the polymerization stage can restrict the movement of ions within the deposited coating. If the electrolyte used in the polymerization stage is constituted by small ions, one may expect that, in doping/dedoping processes, anions and/or cations participate in the charge compensation process. On the other hand, if one of the electrolyte ions is large, its mobility within the coating will be limited, thereby favouring the counter ion to be the main player in the charge compensation process. The use of large anions like polystyrene sulfonate or sodium dodecylsulfate during the electropolymerization of PPy promotes cation mobility and decreases the permeability of chloride anions (Hien *et al.*, 2005).

A relevant aspect for coating protection is adhesion to the metal, and in the case of conducting polymers it is greatly dependent on the doping state of the polymer (oxidized polymers exhibit greater adhesion than in the reduced state). The use of oxidized polymers deposited on active metals such as iron, aluminium and zinc can thus lead to additional protection mechanisms compared with insulating coatings. The oxidized polymer/metal system can show more positive corrosion potentials than the bare metal (Wessling, 1994; Talo *et al.*, 1997) and can also displace the electrochemical interface from the metal–solution interface to the coating–solution interface, as long as the polymer barrier is free of defects, the permeability to solution species is low and the polymer remains in oxidizing states. In this case, the cathodic reaction can occur at the polymer–solution interface, if the redox potential of O_2/H_2O is more positive than for conducting polymers (in the case of PANi, PPy and PEDOT this is true). The occurrence of cathodic reaction at the polymer–solution interface was demonstrated in the work of Michalik and Rohwerder (2005). Additionally, the generation of OH^- at the polymer/solution interface and not at the metal/polymer interface reduces the cathodic disbondment of the coating.

Another mechanism associated with the coating of an active metal with a conducting polymer in the oxidized state is the so-called ennobling mechanism (Spinks *et al.*, 2002). This is a form of anodic protection according to which the oxidized polymer will set the underlying metal in its passive state. To achieve passivation, several parameters come into play, namely the type of metal, pH of solution and nature of the anions close to the metal interface. This mechanism has been accepted for ferrous substrates coated with PANi in acidic media (Lu *et al.*, 1995; Ahmad and McDiarmid, 1996; Cook *et al.*, 2004), with protonated PANi being able to provide high current density for passivation of defects above the Flade potential. This effect has also been demonstrated for PPy-coated iron and steel (Michalik and Rohwerder, 2005), but not for polymethylthiophene-coated

substrates (Rammelt *et al.*, 2003). The main difference between PANi/PPy and polymethylthiophene is that the former polymers are oxidized in contact with O_2 whereas the latter is not, and to attain a passivated state the conducting polymer is required to be capable of re-oxidizing (Wessling, 1997). The ennobling protection has some limitations: the size of defect to be passivated and the current density required to passivate it limit the ennobling effect to small defects; the type of anions in contact with the defect will also influence the Flade potential, the range of potential on which the metal is in a passivated state and the current density necessary for passivation. Besides, different phenomena can disrupt protection by this mechanism, including cathodic delamination (increase in the defect area) and slow re-oxidation of the conducting polymer (Lacaze *et al.*, 2010). Within the restricted conditions mentioned, ennobling can be envisaged as a self-healing process of small defects inflicted on the coating (Ahmad and McDiarmid, 1996).

In the aforementioned protection mechanisms, it is possible to infer that barrier effect, displacement of interface and ennobling effect greatly depend on specific conditions that in real-life systems cannot be controlled. One interesting possibility associated with the application of conducting polymers in oxidizing states is to use corrosion inhibitors as dopant ions. Therefore, when damages occur in the polymer, or aggressive species simply diffuse through the coating to the metal–polymer interface, a galvanic coupling is established between the oxidized polymer and the metal, thereby leading to polymer reduction and release of the inhibiting ions. This process is termed self-healing, triggered by electrochemical potential variations, and the concept is identical to that of nanocontainers dispersed on coating matrices that release inhibitors on demand (Zheludkevich, 2008). At this point, it is also relevant to note that self-healing by dopant ions does not restrict and can be used in conjugation with some of the corrosion mechanisms presented before.

The self-healing effect provided by dopant ions has been observed in the work of Dominis *et al.* (2003) for emeraldine salt primers loaded with different corrosion inhibitors. Also, in the work of Kinlen *et al.* (2002), PANi formulations with phosphonic acid derivatives as dopant anions showed better corrosion protection performances than formulations with sulfonic acids and derivatives. Kendig *et al.* (2003) also reported the development of 'smart' coatings based on conducting polymers doped with different corrosion inhibitors, showing that the release of inhibitors was triggered by the electrochemical activity at defects. In the work of Paliwoda-Porebska *et al.* (2005, 2006) the cathodic delamination rate in iron coated with PPy doped with phosphomolybdates was found to decrease in comparison with PPy doped with molybdates.

In a more recent work, Michalik and Rohwerder (2005) studied the self-healing effect in defected PPy conducting coatings deposited on gold, using the scanning Kelvin probe technique. They concluded that, in thick (1 μm) PPy films doped with tosylate anions, the transport of small cations is fast and responsible for polymer reduction and delamination. According to this study, the cationic transport

follows a percolation mechanism and to achieve good protection extended percolation networks must be avoided. In other words, polymer conductivity does not need to be very high, just enough to maintain satisfactory conductivity.

In spite of the variety of corrosion protection mechanisms, the application of pure conducting polymers in 'real life' conditions is somewhat limited. The incorporation of water, high porosity and low adhesion in undoped states, and in general the specific conditions under which the polymer can protect the metal *vs.* the broad range of environmental conditions that can be found in exposure sites, contribute to the lower performance of conducting polymers with respect to currently used 'insulating' polymeric coatings. There are, however, some strategies that can be used to improve the performance of conducting polymers. Tan and Blackwood (2003) prepared multi-layered coatings based on PANi and PPy, which were found to be better for corrosion protection of stainless steel than single PANi coatings. Very recently, Kowalski *et al.* (2010) prepared a PPy bi-layer system with differentiated permeselectivity towards ions (Fig. 9.13). In the inner layer the dopant anions are $PMo_{12}O_{40}^{3-}$ and HPO_4^{2-}, conferring (active) corrosion protection to the underlying carbon steel substrate, whereas the outer layer is doped with dodecylsulfate anions. In this way, the large anions from the outer layer limit the movement of anions from solution to the metal substrate (e.g. Cl–) and the movement of smaller inhibiting anions in the opposite direction. The outer layer works as a barrier, whilst the inner works as a reservoir for corrosion inhibitors to be provided to the metallic substrate. The resulting coating was found to induce self-healing of artificially introduced defects.

The works of Rajagopalan and Iroh (2001) and of Iroh *et al.* (2003) showed that composites of PANi with PPy have decreased porosity and improved corrosion protection. Other works suggest that blends of conducting polymers with non-conducting polymers such as poly(methyl methacrylate) (Silva *et al.*, 2005) or

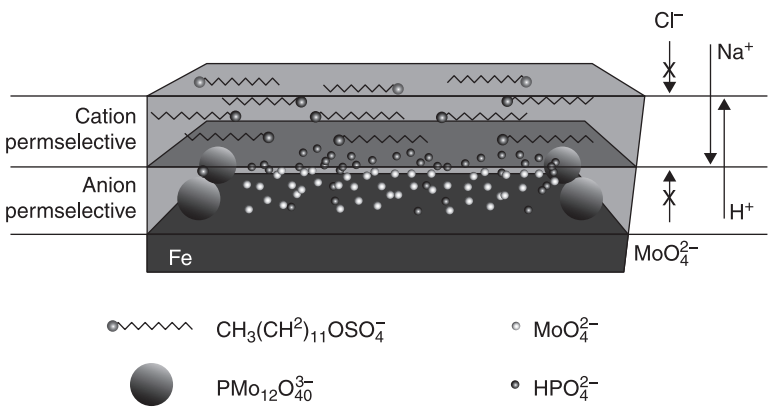

9.13 Scheme of a bi-layered PPy coating on steel (Kowalski *et al.*, 2010).

polyacrylic (Rout *et al.*, 2003) improve the corrosion protection of different metal alloys. Conducting polymers have also been used as pigments in coating formulations (Wessling, 1998; Sathiyanarayanan *et al.*, 2005; Azim *et al.*, 2006), with evidence of improved corrosion protection.

More recently, there has been work devoted to the development of clay conducting polymer composites to increase corrosion protection. The incorporation of inorganic nanoclays like montmorillonite enhances corrosion protection of steel and aluminium when compared with pristine polymers (Zaarei *et al.*, 2008) (Fig. 9.14). Yeh *et al.* (2001) reported the preparation of PANi/montmorillonite and PPy/montmorillonite (Yeh *et al.*, 2003) composite clays with monomers being firstly intercalated in the clays, followed by one-step oxidative polymerization. Improved corrosion protection was found in both cases with respect to pristine polymers. Moreover, in the work with PANi (Yeh *et al.*, 2001), permeability to O_2 was also measured and found to decrease in the presence of clay. In other work by the same group (Chang *et al*., 2006; Yeh *et al.*, 2007) PANi and derivatives doped with dodecylbenzene sulfonic acid by emulsion polymerization in the presence of Na^+-montmorillonite and organo-montmorillonite clays were prepared. Corrosion studies performed for nanocomposites with low loadings of Na^+-montmorillonite showed improvement of anticorrosion performance with respect to emeraldine base form of 'bare' PANi, attributed to an increase of the barrier effect, and also decreased the permeability of O_2 and H_2O in the nanocomposite.

In addition to the improvement of barrier effect that clay materials can impart to conducting polymers, the interface of polymer/solution or polymer/air can also be tuned to hinder the ingress of species. One strategy to change the wettability of conducting polymers' surface is by grafting of different groups or use of dopant anions; the other is to create a rough surface (Bai *et al.*, 2008). Xu *et al.* (2005) recently used the fact that conducting polymers in oxidized states incorporate dopant ions, which can influence the wettability of the polymer. Then, depending

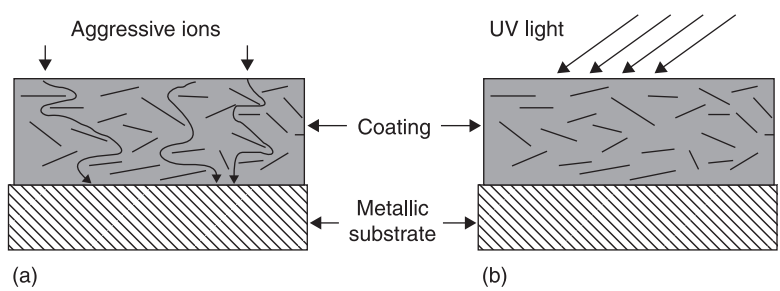

9.14 Advantages of incorporation of clays in conducting polymers: (a) lengthening of diffusion path and (b) shielding of UV radiation (Zaarei *et al.*, 2008).

on the doping state of the polymer, wettability can be controlled by the electrical potential. In this work PPy was electropolymerized on gold-coated glass substrate in the presence of $FeCl_3$, doped with perfluorooctanesulfonate anions. The obtained film was porous on different scales (pores of 10–50 μm, with the walls of pores showing small pores of 1–4 μm, with assemblies of PPy under-micron sized particles surrounding the small pores). This porous structure on different scales was the basis for achieving superhydrophobicity/superhydrophilicity, with the structure being superhydrophobic in the doping state and superhydrophilic in the undoped state. Another strategy to generate rough surfaces is by control via electrochemical methods. Liu *et al.* (2003) reported the growth of polyaniline nanowires on the surface of platinum using a programmed constant-current method, designed to control nucleation and growth rates.

9.8 Conclusions

This chapter highlights the state of the art of self-healing materials for application in corrosion protection and control. Different methodologies of self-healing have been presented, including the classical self-healing of materials that mimics the biological processes occurring in living organisms, as well as the self-healing of coatings applicable to the specific case of reduction of the corrosion rate of active metals. In general, the application of the first strategy would allow recovery of the structural properties of coatings or bulk materials after mechanical damage and loss of integrity. However, when corrosion protection of metallic substrates is required and the protecting coating has completely lost its integrity, leaving some metal parts unprotected, unstoppable corrosion processes can occur on the metal surface, resulting in significant metal degradation, even after recovery of coating integrity. The second self-healing approach employs protective systems that include 'active' additives capable of reducing the corrosion rate of metals, even when the protective system loses mechanical integrity.

Various systems corresponding to the described self-healing approaches have been presented. These systems include polymeric composites with organic polymerizable agents, inorganic conversion layers with passive and active corrosion protective properties, silane-based coatings with incorporated inhibitive additives or nanocontainers with inhibitors and conductive polymeric coatings. In spite of the variety of corrosion protective mechanisms, all the materials fulfil the same main purpose, namely the prevention, or at least hampering, of corrosion activity. Nevertheless, the utilization of only one type of self-healing approach may not be enough to achieve the highest protection efficiency necessary for real-life conditions. The combination of different protection mechanisms will provide superior protection abilities of such multi-level systems. Multi-level systems may comprise different protection mechanisms, including: 'nanotraps' that can consume corrosive species diffusing from outside the coating; water displacement capsules that will respond to coating damage and prevent water

electrolyte reaching the metal surface; capsules with polymerizing agent that can be additionally used to recover the coating integrity; nanocontainers with inhibitors incorporated in the coating that will provide active corrosion protection of the underlying metallic substrate. Finally, with extensive development of nanotechnology, materials exhibiting self-healing ability will be optimized and consequently implemented in different areas of industry.

9.9 References

Aballe A., Bethencourt M., Botana F. J. and Marcos M. (2001), 'CeCl$_3$ and LaCl$_3$ binary solutions as environment-friendly corrosion inhibitors of AA5083 Al–Mg alloy in NaCl solutions', *J. Alloys Compd.*, **323**, 855–8.

Abdullayev E. and Lvov Y. (2010), 'Clay nanotubes for corrosion inhibitor encapsulation: release control with end stoppers', *J. Mater. Chem.*, **20**, 6681–7.

Ahmad N. and McDiarmid A. G. (1996), 'Inhibition of corrosion of steels with the exploitation of conducting polymers', *Synth. Met.*, **78**, 103–10.

Aldykiewicz A. J., Davenport A. J. and Isaacs H. S. (1996), 'Studies of the formation of cerium-rich protective films using x-ray absorption near-edge spectroscopy and rotating disk electrode methods', *J. Electrochem. Soc.*, **143**, 147–54.

Allsop N. A., Bowditch M. R., Glass N. F. C., Harris A. E. and O'Gara P. M. (1998), 'Thermal analysis in the development of self validating adhesives', *Thermochim. Acta.*, **315**, 67–75.

Alpha Metal Finishing, Chromate Conversion. Available from: http://www.alphametal.com/services/chromate-conversion [Accessed 27 May 2011].

Andreatta F., Paussa L., Aldighieri P., Lanzutti A., Ondratschek D. *et al.* (2010), 'Water-based ZrO$_2$ pretreatment for AA2024 aluminum alloy', *Surf. Interface Anal.*, **42**, 293–8.

Aramaki K. (2002), 'Self-healing mechanism of an organosiloxane polymer film containing sodium silicate and cerium(III) nitrate for corrosion of scratched zinc surface in 0.5 M NaCl', *Corros. Sci.*, **44**, 1621–32.

Aramaki K. (2003), 'Self-healing mechanism of a protective film prepared on a Ce(NO3)3-pretreated zinc electrode by modification with Zn(NO3)2 and Na3PO4', *Corros. Sci.*, **45**, 1085–1101.

Arenas M. A., Bethencourt M., Botana F. J., de Damborenea J. J. and Marcos M. (2001), 'Inhibition of 5083 aluminium alloy and galvanised steel by lanthanide salts', *Corros. Sci.*, **43**, 157–70.

Atanacio A. J., Latella B. A., Barbé C. J. and Swain M. V. (2005), 'Mechanical properties and adhesion characteristics of hybrid sol-gel thin films', *Surf. Coat. Technol.*, **192**, 354–64.

Atik M., Lima Neto P., Avaca L. A., Aegerter M. A. and Zarzycki J. (1994), 'Protection of 316L stainless steel against corrosion by SiO2 coatings', *J. Mater. Sci. Lett.*, **13**, 1081–15.

Atik M., Luna F. P., Messaddeq S. H. and Aegerter M. A. (1997), 'Ormocer (ZrO2;-PMMA) Films for Stainless Steel Corrosion Protection', *J. Sol-Gel Sci. Technol.*, **8**, 517–22.

Azim S. S., Sathiyanarayanan S. and Venkatachari G. (2006), 'Anticorrosive properties of PANI–ATMP polymer containing organic coating', *Prog. Org. Coatings*, **56**, 154–8.

Bai H., Li C. and Shi G. (2008), 'Electrochemical Fabrication of Superhydrophobic Surfaces on Metal and Semiconductor Substrates', *J. Adhes. Sci. Technol.*, **22**, 1819–39.

Barranco V., Carmona N., Galván J. C., Grobelny M., Kwiatkowski L. and Villegas, M. A. (2010), 'Electrochemical study of tailored sol-gel thin films as pre-treatment prior to organic coating for AZ91 magnesium alloy', *Prog. Org. Coat.*, **68**, 347–55.

Bescher E. and Mackenzie J. D. (2003), 'Sol-Gel Coatings for the Protection of Brass and Bronze', *J. Sol-Gel Sci. Technol.*, **26**, 1223–6.

Bethencourt M., Botana F. J., Calvino J. J., Marcos M. and Rodriguez-Chacon M. A. (1998), 'Lanthanide compounds as environmentally friendly corrosion inhibitors for aluminum alloys: a review', *Corros. Sci.*, **40**, 1803–19.

Bilal B. A. and Muller E. (1992), 'Thermodynamic study of cerium(4+)/cerium(3+) redox reaction in aqueous solutions at elevated temperatures 1. Reduction potential and hydrolysis equilibria of cerium(4+) in perchloric acid solutions', *Z. Naturforsch., A: Phys. Sci.*, **47**, 974–84.

Bohm S., McMurray H. N., Powell S. M. and Worsley D. A. (2001), 'Novel environment friendly corrosion inhibitor pigments based on naturally occurring clay minerals', *Mater. Corros.*, **52**, 896–903.

Borisova D., Möhwald H. and Shchukin D. G. (2011), 'Mesoporous Silica Nanoparticles for Active Corrosion Protection', *ACS Nano*, **5**, 1939–46.

Boysen W., Frattini A., Pellegri N. and de Sanctis O. (1999), 'Protective coatings on copper prepared by sol-gel for industrial applications', *Surf. Coat. Technol.*, **122**, 14–17.

Brédas J. L., Scott J. C., Yakushi K. and Street G. B. (1984), 'Polarons and bipolarons in polypyrrole: Evolution of the band structure and optical spectrum upon doing', *Phys. Rev. B*, **30**, 1023–5.

Brown E. N., White S. R. and Sottos N. R. (2005), 'Retardation and repair of fatigue cracks in a microcapsule toughened epoxy composite—Part II: In situ self-healing', *Compos. Sci. Technol.*, **65**, 2474–80.

Brusciotti F., Batan A., De Graeve I., Wenkin M., Biessemans M. *et al.* (2010), 'Characterization of thin water-based silane pre-treatments on aluminium with the incorporation of nanodispersed CeO_2 particles', *Surf. Coat. Tech.*, **205**, 603–13.

Buchheit R. G., Mamidipally S. B., Schmutz P. and Guan H. (2002), 'Active Corrosion Protection in Ce-Modified Hydrotalcite Conversion Coatings', *Corrosion*, **58**, 3–14.

Buchheit R. G., Guan H., Mahajanam S. and Wong F. (2003), 'Active corrosion protection and corrosion sensing in chromate-free organic coatings', *Prog. Org. Coat.*, **47**, 174–82.

Cabral A. M., Trabelsi W., Serra R., Montemor M. F., Zheludkevich M. L. *et al.* (2006), 'The corrosion resistance of hot dip galvanised steel and AA2024-T3 pre-treated with bis-[triethoxysilylpropyl] tetrasulfide solutions doped with Ce(NO3)3', *Corros. Sci*, **48**, 3740–58.

Campestrini P., Terryn H., Hovestad A. and de Wit J. H. W. (2004), 'Formation of a cerium-based conversion coating on AA2024: relationship with the microstructure', *Surf. Coat. Technol.*, **176**, 365–81.

Chang K.-C., Lai M.-C., Peng C.-W., Chen Y.-T., Yeh J.-M. *et al.* (2006), 'Comparative studies on the corrosion protection effect of DBSA-doped polyaniline prepared from in situ emulsion polymerization in the presence of hydrophilic Na^+-MMT and organophilic organo-MMT clay platelets', *Electrochim. Acta*, **51**, 5645–53.

Chen Y., Jin L. and Xie Y. (1998), 'Sol-Gel Processing of Organic-Inorganic Nanocomposite Protective Coatings', *J. Sol-Gel Sci. Technol.*, **13**, 735–8.

Chiang J.-C. and MacDiarmid A. G. (1986), 'Polyaniline: Protonic acid doping of the emeraldine form to the metallic regime', *Synth. Met.*, **13**, 193–205.

Cho B. S. H., Andersson H. M., White S. R., Sottos N. R. and Braun P. V. (2006), 'Polydimethylsiloxane-Based Self-Healing Materials', *Adv. Mater.*, **18**, 997–1000.

Chou T. P., Chandrasekaran C., Limmer S. J., Seraji S., Wu Y. *et al.* (2001), 'Organic-inorganic hybrid coatings for corrosion protection', *J. Non-Cryst. Solids*, **290**, 153–62.
Chou T. P., Chandrasekaran C. and Cao G. Z. (2003), 'Sol-Gel-Derived Hybrid Coatings for Corrosion Protection', *J. Sol-Gel Sci. Technol.*, **26**, 321–7.
Conde A., Durán A. and de Damborenea J. J. (2003), 'Polymeric sol–gel coatings as protective layers of aluminium alloys', *Prog. Org. Coat.*, **46**, 288–96.
Cook A., Gabriel A. and Laycock N. (2004), 'On the Mechanism of Corrosion Protection of Mild Steel with Polyaniline', *J. Electrochem. Soc.*, **151**, B529–B535.
Cook R. L. (TDA Research, Inc., Wheat Ridge, CO) (2005). *Releasable corrosion inhibitor compositions*. US patent application 6933046, 2005-Aug-23.
Daum P. and Murray R. W. (1981), 'Charge-transfer diffusion rates and activity relationships during oxidation and reduction of plasma-polymerized vinylferrocene films', *J. Phys. Chem.*, **85**, 389–96.
Davo B. and de Damborenea J. J. (2004), 'Use of rare earth salts as electrochemical corrosion inhibitors for an Al–Li–Cu (8090) alloy in 3.56% NaCl', *Electrochim. Acta*, **49**, 4957–65.
DeBerry D. W. (1985), 'Modification of the electrochemical and corrosion behavior of stainless steels with an electroactive coating', *J. Electrochem. Soc.*, **132**, 1022–6.
Di Maggio R., Rossi S., Fedrizzi L. and Scardi P. (1997), 'ZrO2-CeO2 films as protective coatings against dry and wet corrosion of metallic alloys', *Surf. Coat. Technol.*, **89**, 292–8.
Doblhofer K., Durr W. and Jauch M. (1982), 'Electrochemical redox response of iron (II)/(III) ions implanted in permeable, polymeric electrode coatings', *Electrochim. Acta*, **27**, 677–82.
Dominis A. J., Spinks G. M. and Wallace G. G. (2003), 'Comparison of polyaniline primers prepared with different dopants for corrosion protection of steel', *Prog. Org. Coat.*, **48**, 43–9.
Doscher T. M., Myers G. C. and Atkins D. C. (1951), 'The behavior of nonionic surface active agents in salt solutions', *J. Colloid Sci.*, **6**, 223–35.
Eckler E. P. and Ferrara L. M. (International Minerals & Chemical Corp.) (1988). *Anti-corrosive protective coatings*. US patent application 4738720, 1988-April-19.
Fedrizzi L., Rodriguez F. J., Rossi S., Deflorian F. and Di Maggio R. (2001), 'The use of electrochemical techniques to study the corrosion behaviour of organic coatings on steel pretreated with sol-gel zirconia films', *Electrochim. Acta*, **46**, 3715–24.
Feil F., Fürbeth W. and Schütze M. (2009), 'Purely inorganic coatings based on nanoparticles for magnesium alloys', *Electrochim. Acta*, **54**, 2478–86.
Filipovic N., Kojic M. and Tsuda A. (2008), 'Modelling thrombosis using dissipative particle dynamics method', *Phil. Trans. Royal*, **366**, 3265–79.
Fix D., Andreeva D. V., Lvov Y. M., Shchukin D. G. and Möhwald H. (2009), 'Application of Inhibitor-Loaded Halloysite Nanotubes in Active Anti-Corrosive Coatings', *Adv. Funct. Mater.*, **19**, 1720–7.
Galio A. F., Lamaka S. V., Zheludkevich M. L., Dick L. F. P., Müller I. L. *et al.* (2010), 'Inhibitor-doped sol-gel coatings for corrosion protection of magnesium alloy AZ31', *Surf. Coat. Technol.*, **204**, 1479–86.
Gallardo J., Durán A., Garcia I., Celis J. P., Arenas M. A. *et al.* (2003), 'Effect of Sintering Temperature on the Corrosion and Wear Behavior of Protective SiO2-Based Sol-Gel Coatings', *J. Sol-Gel Sci. Technol.*, **27**, 175–83.
Garcia-Heras M., Jimenez-Morales A., Casal B., Galvan J. C., Radzki S. *et al.* (2004), 'Preparation and electrochemical study of cerium-silica sol-gel thin films', *J. Alloys Compd.*, **380**, 219–24.

Ghosh S. K. (2008), *Self-healing materials*, Weinheim, Wiley-VCH.
Grigoriev D. O., Köhler K., Skorb E., Shchukin D. G. and Möhwald H. (2009), 'Polyelectrolyte complexes as a "smart" depot for self-healing anticorrosion coatings', *Soft Matter*, **5**, 1426–32.
Guglielmi M. (1997), 'Sol-gel coatings on metals', *J. Sol-Gel Sci. Technol.*, **8**, 443–9.
Haas K. H. (2000), 'Hybrid Inorganic–Organic Polymers Based on Organically Modified Si-Alkoxides', *Adv. Eng. Mater.*, **2**, 571–82.
Hermelin E., Petitjean J., Lacroix J.-C., Chane-Ching K. I., Tanguy J. *et al.* (2008), 'Ultrafast electrosynthesis of high hydrophobic polypyrrole coatings on a Zinc electrode: Applications to the protection against Corrosion', *Chem. Mater.*, **20**, 4447–56.
Hien N. T. L., Garcia B., Pailleret A. and Deslouis C. (2005), 'Role of doping ions in the corrosion protection of iron by polypyrrole films', *Electrochim. Acta*, **50**, 1747–55.
Hoebbel D., Nacken M. and Schmidt H. (1998), 'A NMR Study on the Hydrolysis, Condensation and Epoxide Ring-Opening Reaction in Sols and Gels of the System Glycidoxypropyltrimethoxysilane-Water-Titaniumtetraethoxide', *J. Sol-Gel Sci. Technol.*, **12**, 169–79.
Hofacker S., Mechtel M., Mager M. and Kraus H. (2002), 'Sol-gel: a new tool for coatings chemistry', *Prog. Org. Coat.*, **45**, 159–64.
Hu J.-M., Liu L., Zhang J.-Q. and Cao, C.-N. (2007), 'Electrodeposition of silane films on aluminum alloys for corrosion protection', *Prog. Org. Coat.*, **58**, 265–71.
Iroh J. O., Zhua Y., Shah K., Levine K., Rajagopalan R. *et al.* (2003), 'Electrochemical synthesis: a novel technique for processing multi-functional coatings', *Prog. Org. Coatings*, **47**, 365–75.
Izumi K., Murakami M., Deguchi T., Morita A., Tohge N. and Minami T. (1989), 'Zirconia Coating on Stainless Steel Sheets from Organozirconium Compounds', *J. Am. Ceram. Soc.*, **72**, 1465–8.
Joshua Du Y., Damron M., Tang G., Zheng H., Chu C. J. *et al.* (2001), 'Inorganic/organic hybrid coatings for aircraft aluminum alloy substrates', *Prog. Org. Coat.*, **41**, 226–32.
Judeinstein P. and Sanchez C. (1996), 'Hybrid Organic-Inorganic Materials: A Land of Multidisciplinarity', *J. Mater. Chem.*, **6**, 511–25.
Kartsonakis I. A. and Kordas G. (2010), 'Synthesis and Characterization of Cerium Molybdate Nanocontainers and their Inhibitor Complexes', *J. Am. Ceram. Soc.*, **93**, 65–73.
Kasten L. S., Grant J. T., Grebasch N., Voevodin N. N., Arnold F. E. *et al.* (2001), 'An XPS Study of Cerium Dopants in Sol–gel Coatings for Aluminum 2024-T3', *Surf. Coat. Technol.*, **140**, 11–15.
Kendig M. W., Davenport A. J. and Isaacs H. S. (1993), 'The mechanism of corrosion inhibition by chromate conversion coatings from x-ray absorption near edge spectroscopy (Xanes)', *Corros. Sci.*, **34**, 41–9.
Kendig M., Hon M. and Warren L. (2003), ' "Smart" corrosion inhibiting coatings', *Prog. Org. Coat.*, **47**, 183–9.
Khobaib M., Reynolds L. B. and Donley M. S. (2001), 'A comparative evaluation of corrosion protection of sol-gel based coatings systems', *Surf. Coat. Technol.*, **140**, 16–23.
Khramov A. N., Balbyshev V. N., Voevodin N. N. and Donley M. S. (2003), 'Nanostructured sol-gel derived conversion coatings based on epoxy- and amino-silanes', *Prog. Org. Coat.*, **47**, 207–13.
Khramov A. N., Voevodin N. N., Balbyshev V. N. and Donley M. S. (2004), 'Hybrid organo-ceramic corrosion protection coatings with encapsulated organic corrosion inhibitors', *Thin Solid Films*, **447–8**, 549–57.

Khramov A. N., Voevodin N. N., Balbyshev V. N. and Mantz R. A. (2005), 'Sol-gel-derived corrosion-protective coatings with controllable release of incorporated organic corrosion inhibitors', *Thin Solid Films*, **483**, 191–6.

Kinlen P. J., Ding Y. and Silverman D. C. (2002), 'Corrosion protection of mild steel using sulfonic and phosphonic acid-doped polyanilines', *Corrosion*, **58**, 490.

Koch K. and Ensikat H. J. (2008), 'The hydrophobic coatings of plant surfaces: epicuticular wax crystals and their morphologies, crystallinity and molecular self-assembly', *Micron*, **39**, 759–72.

Koch K., Bhushan B., Ensikat H. J. and Barthlott W. (2009), 'Self-healing of voids in the wax coating on plant surfaces', *Philos. Transact. A Math. Phys. Eng. Sci.*, **367**, 1673–88.

Kowalski D., Ueda M. and Ohtsuka T. (2010), 'Self-healing ion-permselective conducting polymer coating', *J. Mater. Chem.*, **20**, 7630–3.

Lacaze P. C., Ghilane J., Randriamahazaka H. and Lacroix J.-C. (2010), 'Electroactive Conducting Polymers for the Protection of Metals against Corrosion: from Micro- to Nanostructured Films', in Eftekhari A., *Nanostructured conductive polymers*, John Wiley & Sons.

Lacroix J.-C., Camalet J. L., Aeiyach S., Chane-Ching K. I., Petitjean J. *et al.* (2000), 'Aniline electropolymerization on mild steel and zinc in a two-step process', *J. Electroanal. Chem.*, **481**, 76–81.

Lamaka S. V., Zheludkevich M. L., Yasakau K. A., Montemor M. F., Cecílio P. *et al.* (2006), 'TiOx self-assembled networks prepared by templating approach as nanostructured reservoirs for self-healing anticorrosion pre-treatments', *Electrochem. Commun.*, **8**, 421–8.

Lamaka S. V., Zheludkevich M. L., Yasakau K. A., Serra R., Poznyak S. K., *et al.* (2007), 'Nanoporous titania interlayer as reservoir of corrosion inhibitors for coatings with self-healing ability', *Prog. Org. Coat.*, **58**, 127–35.

Lamaka S. V., Shchukin D. G., Andreeva D. V., Zheludkevich M. L., Möhwald H. *et al.* (2008), 'Sol-Gel/Polyelectrolyte Active Corrosion Protection System', *Adv. Funct. Mater.*, **18**, 3137–47.

Leggat R. B., Zhang W., Buchheit R. G. and Taylor S. R. (2002), 'Performance of Hydrotalcite Conversion Treatments on AA2024-T3 When Used in a Coating System', *Corrosion*, **58**, 322–8.

Li Y.-S., Lu W., Wang Y. and Tran T. (2009), 'Studies of (3-mercaptopropyl)trimethoxylsilane and bis(trimethoxysilyl)ethane sol-gel coating on copper and aluminum', *Spectrochim. Acta, Part A*, **73**, 922–8.

Liu J., Lin Y., Liang L., Voigt J. A., Huber D. L. *et al.* (2003), 'Templateless assembly of molecularly aligned conductive polymer nanowires: a new approach for oriented nanostructures', *Chem. Eur. J.*, **9**, 604–11.

Liu Y., Sun D., You H. and Chung, J. S. (2005), 'Corrosion resistance properties of organic-inorganic hybrid coatings on 2024 aluminum alloy', *Appl. Surf. Sci.*, **246**, 82–9.

Lu W.-K., Elsenbaumer R. L. and Wessling B. (1995), 'Corrosion Protection Of Mild Steel By Coatings Containing Polyaniline', *Synt. Met.*, **71**, 2163–6.

Luca V. and Thomson S. (2000), 'Intercalation and polymerisation of aniline within a tubular aluminosilicate', *J. Mater. Chem.*, **10**, 2121–6.

MacDiarmid A. G., Chiang J.-C., Richter A. F. and Epstein A. J. (1987), 'Polyaniline: a new concept in conducting polymers', *Synth. Met.*, **18**, 285–90.

MacDiarmid A. G. (2001), 'Synthetic Metals: A Novel Role for Organic Polymers (Nobel Lecture)', *Angew. Chem. Int. Ed.*, **40**, 2581–90.

Mackenzie J. D. and Bescher E. P. (1998), 'Structures, Properties and Potential Applications of Ormosils', *J. Sol-Gel Sci. Technol.*, **13**, 371–7.

Mackenzie J. D. and Bescher E. (2003), 'Some Factors Governing the Coating of Organic Polymers by Sol-Gel Derived Hybrid Materials', *J. Sol-Gel Sci. Technol.*, **27**, 7–14.

Malzbender J. and de With G. (2002), 'Modification of the Mechanical Properties of a Sol-Gel Coating Using Silica Filler Nanoparticles', *Adv. Eng. Mater.*, **4**, 296–300.

Mascia L., Prezzi L., Wilcox G. D. and Lavorgna M. (2006), 'Molybdate doping of networks in epoxy-silica hybrids: Domain structuring and corrosion inhibition', *Prog. Org. Coat.*, **56**, 13–22.

Mayer C. R., Cabuil V., Lalot T. and Thouvenot R. (2000), 'Magnetic Nanoparticles Trapped in pH 7 Hydrogels as a Tool to Characterize the Properties of the Polymeric Network', *Adv. Mater.*, **12**, 417–20.

Mayrand M., Quinson J. F., Roche A., Roisne V. and Guyon H. (1998), 'Heteropolysiloxane Coatings on Electrogalvanized Steel: Elaboration and Characterization', *J. Sol-Gel Sci. Technol.*, **12**, 49–57.

McAndrew T. P, Miller S. A., Gilicinski A. G. and Robeson L. M. (1996), *Polym. Mater. Sci. Eng.*, **74**, 204–6.

McMurray H. N., Williams D., Williams G. and Worsley D. (2003), 'Inhibitor pretreatment synergies demonstrated using a scanning Kelvin probe technique', *Corros. Eng. Sci. Techn.*, **38**, 112–18.

McMurray H. N. and Williams G. (2004), 'Inhibition of Filiform Corrosion on Organic-Coated Aluminum Alloy by Hydrotalcite-Like Anion-Exchange Pigments', *Corrosion*, **60**, 219–28.

Mengoli G., Munari M., Bianco P. and Musiani M. (1981), 'Anodic synthesis of polyaniline coatings onto fe sheets', *J. Appl. Polym. Sci.*, **26**, 4247–57.

Menning M., Schelle C., Durán A., Damborenea J. J., Guglielmi M. *et al.* (1998), 'Investigation of Glass-Like Sol-Gel Coatings for Corrosion Protection of Stainless Steel Against Liquid and Gaseous Attack', *J. Sol-Gel Sci. Technol.*, **13**, 717–22.

Metroke T. L., Parkhill R. L. and Knobbe E. T. (2001), 'Passivation of metal alloys using sol-gel-derived materials – a review', *Prog. Org. Coat.*, **41**, 233–8.

Metroke T. L., Kachurina O. and Knobbe E. T. (2002a), 'Spectroscopic and corrosion resistance characterization of GLYMO-TEOS Ormosil coatings for aluminum alloy corrosion inhibition', *Prog. Org. Coat.*, **44**, 295–305.

Metroke T. L., Kachurina O. and Knobbe E. T. (2002b), 'Spectroscopic and corrosion resistance characterization of amine and super acid-cured hybrid organic-inorganic thin films on 2024-T3 aluminum alloy', *Prog. Org. Coat.*, **44**, 185–99.

Michalik A. and Rohwerder M. (2005), 'Conducting polymers for corrosion protection: a critical view', *Z. Phys. Chemie*, **219**, 1547–60.

Montemor M. F., Cabral A. M., Zheludkevich M. L. and Ferreira M. G. S. (2006a), 'The corrosion resistance of hot dip galvanized steel pretreated with bis-functional silanes modified with microsilica', *Surf. Coat. Technol.*, **200**, 2875–85.

Montemor M. F., Trabelsi W., Zheludkevich M. and Ferreira M. G. S. (2006b), 'Modification of bis-silane solutions with rare-earth cations for improved corrosion protection of galvanized steel substrates', *Prog. Org. Coat.*, **57**, 67–77.

Montemor M. F. and Ferreira M. G. S. (2007a), 'Electrochemical study of modified bis-[triethoxysilylpropyl] tetrasulfide silane films applied on the AZ31 Mg alloy', *Electrochim. Acta*, **52**, 7486–95.

Montemor M. F. and Ferreira M. G. S. (2007b), 'Analytical and microscopic characterisation of modified bis-[triethoxysilylpropyl] tetrasulfide silane films on magnesium AZ31 substrates', *Prog. Org. Coat.*, **60**, 228–37.

Montemor M. F. and Ferreira M. G. S. (2007c), 'Cerium Salt Activated Nanoparticles as Fillers For Silane Films: Evaluation of The Corrosion Inhibition Performance On Galvanised Steel Substrates', *Electrochim. Acta*., **52**, 6976–87.

Mortimer R. J. and Anson F. C. (1982), 'Apparent diffusion coefficients and electron propagation mechanisms in viologen polyelectrolyte coatings containing multiply charged anions', *J. Electroanal. Chem.*, **138**, 325–41.

Moutarlier V., Neveu B. and Gigandet M. P. (2008), 'Evolution of corrosion protection for sol-gel coatings doped with inorganic inhibitors', *Surf. Coat. Technol.*, **202**, 2052–8.

Ni H., Simonsick W. J., Skaja A. D., Williams J. P. and Soucek M. D. (2000), 'Polyurea/polysiloxane ceramer coatings', *Prog. Org. Coat.*, **38**, 97–110.

Ono S., Tsuge H., Nishi Y. and Hirano S.-i. (2004), 'Improvement of Corrosion Resistance of Metals by an Environmentally Friendly Silica Coating Method', *J. Sol-Gel Sci. Technol.*, **29**, 147–53.

Osborne J. H., Blohowiak K. Y., Taylor S. R., Hunter C., Bierwagen G. *et al.* (2001), 'Testing and evaluation of nonchromated coating systems for aerospace applications', *Prog. Org. Coat.*, **41**, 217–25.

Palanivel V., Zhu D. and van Ooij W. J. (2003), 'Nanoparticle-filled silane films as chromate replacements for aluminum alloys', *Prog. Org. Coat.*, **47**, 384–92.

Palanivel V., Huang Y. and Ooij W. J. (2005), 'Effects of Addition of Corrosion Inhibitors to Silane Films on the Performance of AA2024-T3 in a 0.5 M NaCl Solution', *Prog. Org. Coat.*, **53**, 153–68.

Paliwoda-Porebska G., Stratmann M., Rohwerder M., Potje-Kamloth K., Lu Y. *et al.* (2005), 'On the development of polypyrrole coatings with self-healing properties for iron corrosion protection', *Cor. Sci.*, **47**, 3216–33.

Paliwoda-Porebska G., Rohwerder M., Stratmann M., Rammelt U., Duc L. M. *et al.* (2006). 'Release mechanism of electrodeposited polypyrrole doped with corrosion inhibitor anions', *J. Solid State Electrochem.*, **10**, 730–6.

Parkhill R. L., Knobbe E. T. and Donley M. S. (2001), 'Application and evaluation of environmentally compliant spray-coated ormosil films as corrosion resistant treatments for aluminum 2024-T3', *Prog. Org. Coat.*, **41**, 261–5.

Pepe A., Aparicio M., Durán A. and Ceré S. (2006), 'Cerium hybrid silica coatings on stainless steel AISI 304 substrate', *J. Sol-Gel Sci. Technol.*, **39**, 131–8.

Pilz M. and Römich H. (1997), 'Sol-gel derived coating for outdoor bronze conservation', *J. Sol-Gel Sci. Technol.*, **8**, 1071–5.

Pippard D. A. (The British Petroleum Company Limited) (1983). *Corrosion inhibitors, method of producing them and protective coatings containing them.* US patent application 4405493. 1983–Sept-20.

Pirhady Tavandashti N. and Sanjabi S. (2010), 'Corrosion study of hybrid sol–gel coatings containing boehmite nanoparticles loaded with cerium nitrate corrosion inhibitor', *Prog. Org. Coat.*, **69**, 384–91.

Poznyak S. K., Tedim J., Rodrigues L. M., Salak A. N., Zheludkevich M. L. *et al.* (2009), 'Novel Inorganic Host Layered Double Hydroxides Intercalated with Guest Organic Inhibitors for Anticorrosion Applications', *ACS Appl. Mater. Inter.*, **1**, 2353–62.

Quinet M., Neveu B., Moutarlier V., Audebert P. and Ricq, L. (2007), 'Corrosion protection of sol-gel coatings doped with an organic corrosion inhibitor: Chloranil', *Prog. Org. Coat.*, **58**, 46–53.

Rajagopalan R. and Iroh J. O. (2001), 'Development of polyaniline-polypyrrole composite coatings on steel by aqueous electrochemical process', *Electrochim. Acta*, **46**, 2443–55.

Rammelt U., Nguyen P. T. and Plieth W. (2003), 'Corrosion protection by ultrathin films of conducting polymers', *Electrochim. Acta*, **48**, 1257–62.

Rao A. V., Latthe S. S., Mahadik S. A. and Kappenstein C. (2011), 'Mechanically stable and corrosion resistant superhydrophobic sol-gel coatings on copper substrate', *Appl. Surf. Sci.*, **257**, 5772–6.

Raps D., Hack T., Wehr J., Zheludkevich M. L., Bastos A. C. *et al.* (2009), 'Electrochemical study of inhibitor-containing organic-inorganic hybrid coatings on AA2024', *Corros. Sci*, **51**, 1012–21.

Rekharsky M. V. and Inoue Y. (1998), 'Complexation Thermodynamics of Cyclodextrins', *Chem. Rev.*, **98**, 1875–917.

Rohwerder M. and Michalik A. (2007), 'Conducting polymers for corrosion protection: What makes the difference between failure and success?', *Electrochim. Acta*, **53**, 1300–13.

Rosero-Navarro N. C., Pellice S. A., Durán A. and Aparicio M. (2008), 'Effects of Ce-containing sol-gel coatings reinforced with SiO2 nanoparticles on the protection of AA2024', *Corros. Sci.*, **50**, 1283–91.

Rosero-Navarro N. C., Paussa L., Andreatta F., Castro Y., Durán A. *et al.* (2010), 'Optimization of hybrid sol–gel coatings by combination of layers with complementary properties for corrosion protection of AA2024', *Prog. Org. Coat.*, **69**, 167–74.

Rout T. K., Jha G., Singh A. K., Bandyopadhyay N. and Mohanty O. N. (2003), 'Development of conducting polyaniline coating: a novel approach to superior corrosion resistance', *Surf. Coat. Technol.*, **167**, 16–24.

Rubio F., Rubio J. and Oteo J. L. (2000), 'Effect of TiO2 on the Pore Structure of SiO2-PDMS Ormosils', *J. Sol-Gel Sci. Technol.*, **18**, 105–13.

Sankara Narayanan T. S. N. (2005), 'Surface Pretreatment by Phosphate Conversion Coatings. A Review', *Rev. Adv. Mater. Sci.*, **9**, 130–77.

Sathiyanarayanan S., Dhawan S. K., Trivedi D. C. and Balakrishnan K. (1992), 'Soluble conducting poly ethoxy aniline as an inhibitor for iron in HCl', *Corros. Sci.*, **33**, 1831–41.

Sathiyanarayanan S., Muthukrishnan S., Venkatachari G. and Trivedi D. C. (2005), 'Corrosion protection of steel by polyaniline (PANI) pigmented paint coating', *Prog. Org. Coat.*, **53**, 297–301.

Schem M., Schmidt T., Gerwann J., Wittmar M., Veith M. *et al.* (2009), 'CeO2-filled sol–gel coatings for corrosion protection of AA2024-T3 aluminium alloy', *Corros. Sci.*, **51**, 2304–15.

Schmidt C., (DaimlerChrysler AG) (2002). *Anti-corrosive coating including a filler with a hollow cellular structure*. US patent application 6383271, 2002-May-7.

Schmidt H., Langenfeld S. and Naß R. (1997), 'A new corrosion protection coating system for pressure-cast aluminium automotive parts', *Mater. Des.*, 18, 309–13.

Schubert U., Huesing N. and Lorenz A. (1995), 'Hybrid Inorganic-Organic Materials by Sol-Gel Processing of Organofunctional Metal Alkoxides', *Chem. Mater.*, **7**, 2010–27.

Shchukin D. G., Zheludkevich M. and Möhwald H. (2006), 'Feedback active coatings based on incorporated nanocontainers', *J. Mater. Chem.*, **16**, 4561–6.

Shchukin D. G., Zheludkevich M., Yasakau K., Lamaka S., Ferreira M. G. S. *et al.* (2006), 'LbL Nanocontainers for Self-Healing Corrosion Protection', *Adv. Mater.*, **18**, 1672–8.

Shchukin D. G., Möhwald H., Ferreira M. G. S. and Zheludkevich M. L. (MPG Max Planck Ges Zur Foerder) (2007). *Corrosion Inhibiting Pigment Comprising Nanoreservoirs of Corrosion Inhibitor*, DE patent application EP1832629, Publication date: 2007-Sep-12.

Shchukin D. G., Lamaka S. V., Yasakau K. A., Zheludkevich M. L., Möhwald H. *et al.* (2008), 'Active Anticorrosion Coatings with Halloysite Nanocontainers', *J. Phys. Chem. C*, **112**, 958–64.

Sheffer M., Groysman A. and Mandler D. (2003), 'Electrodeposition of sol-gel films on Al for corrosion protection', *Corros. Sci.*, **45**, 2893–904.

Sheffer M., Groysman A., Starosvetsky D., Savchenko N. and Mandler D. (2004), 'Anion embedded sol-gel films on Al for corrosion protection', *Corros. Sci.*, **46**, 2975–85.

Shi H., Liu F. and Han E.-h. (2009), 'Corrosion protection of AZ91D magnesium alloy with sol-gel coating containing 2-methyl piperidine', *Progress in Organic Coatings*, **66**, 183–91.

Silva J. E. P., Torresi S. I. C. and Torresi R. M. (2005), 'Polyaniline acrylic coatings for corrosion inhibition: the role played by counter-ions', *Corros. Sci.*, **47**, 811–22.

Smarsly B., Garnweitner G., Assink R. and Brinker C. J. (2003), 'Preparation and characterization of mesostructured polymer-functionalized sol-gel-derived thin films', *Prog. Org. Coat.*, **47**, 393–400.

Spinks G. M., Dominis A. J., Wallace G. G. and Tallman D. E. (2002), 'Electroactive conducting polymers for corrosion control-Part 2 Ferrous metals', *J. Solid State Electrochem.*, **6**, 85–100.

Supplit, R., Koch, T. and Schubert, U. (2007), 'Evaluation of the anti-corrosive effect of acid pickling and sol-gel coating on magnesium AZ31 alloy', *Corros. Sci.*, **49**, 3015–23.

Tallman D. E., Spinks G., Dominis A. and Wallace G. G. (2002), 'Electroactive conducting polymers for corrosion control -Part 1 General introduction and a review of non-ferrous metals', *J. Solid State Electrochem.*, **6**, 73–84.

Talo A., Passiniemi P., Forsen O. and Ylasaari S. (1997), 'Polyaniline/epoxy coatings with good anti-corrosion properties', *Synth. Met.*, **85**, 1333–4.

Tan A. L. K. and Soutar A. M. (2008), 'Hybrid sol-gel coatings for corrosion protection of copper', *Thin Solid Films*, **516**, 5706–9.

Tan C. K. and Blackwood D. J. (2003), 'Corrosion protection by multi-layered conducting polymer coatings', *Corros. Sci.*, **45**, 545–57.

Tedim J., Poznyak S. K., Kuznetsova A., Raps D., Hack T. *et al.* (2010), 'Enhancement of Active Corrosion Protection via Combination of Inhibitor-Loaded Nanocontainers', *ACS Appl. Mater. Inter.*, **2**, 1528–35.

Thim G. P., Oliveira M. A. S., Oliveira E. D. A. and Melo F. C. L. (2000), 'Sol-gel silica film preparation from aqueous solutions for corrosion protection', *J. Non-Cryst. Solids*, **273**, 124–8.

Toohey, K. S., Sottos N. R., Lewis J. A., Moore J. S. and White S. R. (2007), 'Self-healing materials with microvascular networks', *Nat. Mater.*, **6**, 581–5.

Trabelsi W., Cecílio P., Ferreira M. G. S. and Montemor M. F. (2005), 'Electrochemical assessment of the self-healing properties of Ce-doped silane solutions for the pre-treatment of galvanised steel substrates', *Prog. Org. Coat.*, **54**, 276–84.

Trabelsi W., Triki E., Dhouibi L., Ferreira M. G. S., Zheludkevich M. L. *et al.* (2006), 'The use of pre-treatments based on doped silane solutions for improved corrosion resistance of galvanised steel substrates', *Surf. Coat. Technol.*, **200**, 4240–50.

Trabelsi W., Cecílio P., Ferreira M. G. S., Yasakau K., Zheludkevich M. L. *et al.* (2007), 'Surface evaluation and electrochemical behaviour of doped silane pre-treatments on galvanised steel substrates', *Prog. Org. Coat*, **59**, 214–23.

Twite R. L. and Bierwagen G. P. (1998), 'Review of Alternatives to Chromate for Corrosion Protection of Aluminum Aerospace Alloys', *Progress in Organic Coatings*, **33**, 91–100.

Uekama K., Hirayama F. and Irie T. (1998), 'Cyclodextrin Drug Carrier Systems', *Chem. Rev.*, **98**, 2045–76.

van der Zwaag S., Schmets A. J. M. and van der Zaken G. (2007), *Self-healing materials: an alternative approach to 20 centuries of materials*, Dordrecht, Springer.

Van Schaftinghen T., Deslouis C., Hubin A. and Terryn H. (2006), 'Influence of the surface pre-treatment prior to the film synthesis on the corrosion protection of iron with polypyrrole films', *Electrochim. Acta*, **51**, 1695–703.

Vasconcelos D. C. L., Carvalho J. A. N., Mantel M. and Vasconcelos W. L. (2000), 'Corrosion resistance of stainless steel coated with sol-gel silica', *J. Non-Cryst. Solids*, **273**, 135–9.

Voevodin N. N., Grebasch N. T., Soto W. S., Arnold F. E. and Donley M. S. (2001a), 'Potentiodynamic evaluation of sol-gel coatings with inorganic inhibitors', *Surf. Coat. Technol.*, **140**, 24–8.

Voevodin N. N., Grebasch N. T., Soto W. S., Kasten L. S., Grant J. T. *et al.* (2001b), 'An organically modified zirconate film as a corrosion-resistant treatment for aluminum 2024-T3', *Prog. Org. Coat.*, **41**, 287–93.

Voevodin N., Jeffcoate C., Simon L., Khobaib M. and Donley M. (2001c), 'Characterization of pitting corrosion in bare and sol-gel coated aluminum 2024-T3 alloy', *Surf. Coat. Technol.*, **140**, 29–34.

Voevodin N. N., Balbyshev V. N., Khobaib M. and Donley M. S. (2003), 'Nanostructured coatings approach for corrosion protection', *Prog. Org. Coat.*, **47**, 416–23.

Voevodin N. N., Balbyshev V. N. and Donley M. S. (2005), 'Investigation of corrosion protection performance of sol-gel coatings on AA2024-T3', *Prog. Org. Coat.*, **52**, 28–33.

Vreugdenhil A. J. and Woods M. E. (2005), 'Triggered release of molecular additives from epoxy-amine sol-gel coatings', *Prog. Org. Coat.*, **53**, 119–25.

Wang H., Presuel F. and Kelly R. G. (2004), 'Computational Modeling of Inhibitor Release and Transport from Multifunctional Organic Coatings', *Electrochim. Acta*, **49**, 239–55.

Wernick S., Pinner R. and Sheasby P. G. (1987), *The Surface Treatment and Finishing of Aluminum and its Alloys*, Teddington, Middlesex, England, Finishing Publications Ltd.

Wessling B. (1994), 'Passivation of metals by coating with polyaniline: Corrosion potential shift and morphological changes', *Adv. Mater.*, **6**, 226–8.

Wessling B. (1997), 'Scientific and Commercial Breakthrough for Organic Metals', *Synth. Met.*, **85**, 1313–18.

Wessling B. (1998), 'Dispersion as the link between basic research and commercial applications of conductive polymers (polyaniline)', *Synth. Met.*, **93**, 143–54.

Wey Y., Wang J., Jia X., Yeh J.-M. and Spellane P. (1995), *Polym. Mater. Sci. Eng.*, **72**, 563–4.

White S. R., Sottos N. R., Geubelle P. H., Moore J. S., Kessler M. R. *et al.* (2001), 'Autonomic Healing of Polymer Composites', *Nature*, **409**, 794–7.

Williams G. and McMurray H. N. (2004), 'Inhibition of Filiform Corrosion on Polymer Coated AA2024-T3 by Hydrotalcite-Like Pigments Incorporating Organic Anions', *Electrochem. Solid. St.*, **7**, B13–B15.

Xu L., Chen W., Mulchandani A. and Yan Y. (2005), 'Reversible Conversion of Conducting Polymer Films from Superhydrophobic to Superhydrophilic', *Angew. Chem. Int. Ed.*, **44**, 6009–12.

Yang H. and Van Ooij W. J. (2004), 'Plasma-treated triazole as a novel organic slow-release paint pigment for corrosion control of AA2024-T3', *Prog. Org. Coat.*, **50**, 149–61.

Yasakau K. A., Zheludkevich M. L., Lamaka S. V. and Ferreira M. G. S. (2006), 'Mechanism of Corrosion Inhibition of AA2024 by Rare-Earth Compounds', *J. Phys. Chem. B*, **110**, 5515–28.

Yasakau K. A., Zheludkevich M. L., Karavai O. V. and Ferreira M. G. S. (2008), 'Influence of inhibitor addition on the corrosion protection performance of sol-gel coatings on AA2024', *Prog. Org. Coat.*, **63**, 352–61.

Yeh J.-M., Liou S.-J., Lai C.-Y., Wu P.-C. and Tsai T.-Y. (2001), 'Enhancement of Corrosion Protection Effect in Polyaniline via the Formation of Polyaniline-Clay Nanocomposite Materials', *Chem. Mater.*, **13**, 1131–6.

Yeh J.-M., Chin C.-P. and Chang S. (2003), 'Enhanced Corrosion Protection Coatings Prepared from Soluble Electronically Conductive Polypyrrole-Clay Nanocomposite Materials', *J. Appl. Polym. Sci.*, **88**, 3264–72.

Yeh J.-M., Kuo T.-H., Huang H.-J., Chang K.-C., Chang M.-Y. *et al.* (2007), 'Preparation and characterization of poly(o-methoxyaniline)/Na^+–MMT clay nanocomposite via emulsion polymerization: Electrochemical studies of corrosion protection', *Eur. Poly. J.*, **43**, 1624–34.

Yin T., Rong M. Z., Zhang M. Q. and Yang G. C. (2007), 'Self-healing epoxy composites – Preparation and effect of the healant consisting of microencapsulated epoxy and latent curing agent', *Compos. Sci. Technol.*, **67**, 201–12.

Yu X. and Cao C. (2003), 'Electrochemical study of the corrosion behavior of Ce sealing of anodized 2024 aluminum alloy', *Thin Solid Films*, **423**, 252–6.

Zaarei D., Sarabi A. A., Sharif F. and Kassiriha S. M. (2008), 'Structure, properties and corrosion resistivity of polymeric nanocomposite coatings based on layered silicates', *J. Coat. Technol. Res.*, **5**, 241–9.

Zheludkevich M. L., Serra R., Montemor M. F., Yasakau K. A., Salvado I. M. M. *et al.* (2005a), 'Nanostructured sol-gel coatings doped with cerium nitrate as pre-treatments for AA2024-T3 – Corrosion protection performance', *Electrochim. Acta*, **51**, 208–17.

Zheludkevich M. L., Serra R., Montemor M. F. and Ferreira M. G. S. (2005b), 'Oxide nanoparticle reservoirs for storage and prolonged release of the corrosion inhibitors', *Electrochem. Commun.*, **7**, 836–40.

Zheludkevich M., Serra R., Montemor F., Salvado I. and Ferreira M. (2006), 'Corrosion protective properties of nanostructured sol–gel hybrid coatings to AA2024-T3', *Surf. Coat. Tech.*, **200**, 3084–94.

Zheludkevich M. L., Shchukin D. G., Yasakau K. A., Möhwald H. and Ferreira M. G. S. (2007), 'Anticorrosion coatings with self-healing effect based on nanocontainers loaded with corrosion inhibitor', *Chem. Mater.*, 19, 402–11.

Zheludkevich M. L. (2008), 'Self-healing anticorrosion coatings', in Ghosh S. K., *Self-healing materials*, Wiley-VCH, 101–40.

Zheludkevich M. L., Poznyak S. K., Rodrigues L. M., Raps D., Hack T. *et al.* (2010), 'Active protection coatings with layered double hydroxide nanocontainers of corrosion inhibitor', *Corros. Sci.*, **52**, 602–11.

Zheludkevich M. L., Tedim J., Freire C. S. R., Fernandes S. C. M., Kallip S. *et al.* (2011), 'Self-healing protective coatings with "green" chitosan based pre-layer reservoir of corrosion inhibitor', *J. Mater. Chem.*, **21**, 4805–12.

10

The use of nanoreservoirs in corrosion protection coatings

D. G. SHCHUKIN and D. O. GRIGORIEV,
Max-Planck Institute of Colloids and Interfaces, Germany

Abstract: The heavy economic impact of corrosion necessitates continuous efforts to improve the protective performance of anticorrosion coatings. The restrictions on the use of chromium (VI) compounds in corrosion protection due to their negative health and environmental impact have intensified the problem. One of the most promising alternatives is based on the achievements accomplished during the last two decades in nanotechnology. The following chapter provides a brief review of conventional corrosion protection solutions in comparison with this new approach, which is based on the incorporation of nano- and microcontainers into the coating matrix. Different types of nanocontainers, their specific features and advantages and the main triggers which cause the containers to open are discussed and first practical proofs of concept are demonstrated.

Key words: nanocontainer(s), self-healing, controlled release, LbL assembly, polyelectrolyte.

10.1 Introduction

10.1.1 Corrosion

The total annual worldwide detriment directly resulting from metal corrosion is tremendous. Even in developed countries the material losses and performance failure costs connected with corrosion are estimated to be 3 to 4% of GDP (Koch *et al.*, 2002; McCafferty, 2010). Preventing and slowing corrosion is therefore one of the most challenging problems facing modern industrial society.

A broad spectrum of approaches for preventing and controlling corrosion is employed today. The choice of approach depends on the specific industry branch and corresponding material(s) under protection. The most frequently used methods are: the application of different organic, ceramic and metallic protective coatings; the use of corrosion-resistant materials such as alloys (Bendall, 1995; Institute of Materials, 2002; Ahluwalia and Uhlenkamp, 2008); polymers (Pacitti, 1964; Pritchard, 1995; Schweitzer, 2000) and composites (Bogner, 2005; Gupta and Gupta, 2005; McConnell, 2005); utilization of diverse corrosion inhibitors (Sastri, 1998; Raja and Sethuraman, 2008; Saji, 2010; Zhao *et al.*, 2010) and cathodic (von Baeckmann *et al.*, 1997) or anodic (Roberge, 2000) protection. Each of these mainstream approaches to corrosion protection can be further subdivided into manifold specific special solutions determined by the particular

requirements for protection efficiency, the conditions in which protective performance has to be achieved and many other factors. In this chapter we will focus predominantly on one approach to corrosion protection that utilizes various protective coatings. Other approaches are mentioned here only briefly and so, for further information on these, the authors would like to re-direct the attention of readers to the additional sources cited.

10.1.2 Protective coatings

Contemporary protective coatings have, as a rule, a quite complex structure, which is, in turn, closely related to the underlying substrate and to the specific demands on the corrosion resistance. However, it is possible to point out some common elements present in the vast majority of protective coatings. A typical protective coating is a layered system consisting of (i) a pre-treatment layer or conversion layer; (ii) a primer layer and (iii) a top-coat layer (Fig. 10.1). Quite often, a layer of electrochemically more active metal (Zn, Cd, etc) is deposited on the top of a metal or alloy substrate to provide additional cathodic protection (Brock *et al.*, 2009).

Chromate and other conversion coatings

Until recently, the protective coatings for metal substrates contained a conversion layer fabricated using hexavalent chromium compounds (Osborne, 2001; Osborne *et al.*, 2001; Kendig and Buchheit, 2003). Due to the strong oxidative effect of chromate anion on the metal under protection, a tight solid layer of $Cr_2O_3 \cdot nH_2O$ is formed on the substrate surface (Xia and McCreery, 1998; Sinko, 2001). This conversion layer not only has excellent barrier properties, but also confers upon the coating a self-healing ability. The latter results from excessive chromate ions incorporated into the conversion layer which only loosely bond with it. Upon coating damage, chromates released at the affected site react with the metal

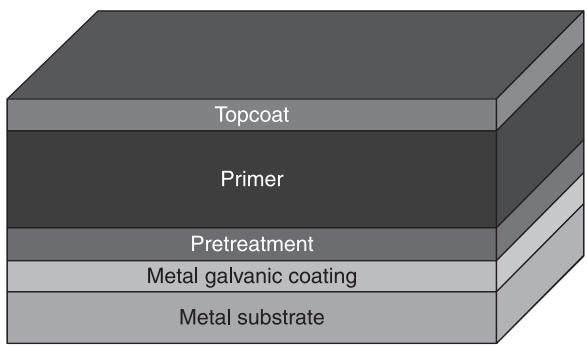

10.1 Typical layered structure of a conventional protective coating.

surface, causing both cathodic and anodic passivation (Chidambara *et al.*, 2003; Kendig and Buchheit, 2003). Moreover, excellent long-term protection is provided by the gradual release of chromates embedded into the conversion matrix and their subsequent migration to defects through aqueous medium adjacent to the surface (Zhao *et al.*, 1998; Xia *et al.*, 2000; Zhao *et al.*, 2001). Chromate conversion coatings prepared by chemical treatment are quite thin and therefore not able to store the necessary amounts of chromates (Berger *et al.*, 2007) to provide sustained corrosion protection of the substrates. A prolonged protective effect can be achieved via the addition of chromate anticorrosive pigments such as $CaCrO_4$, $SrCrO_4$ or $BaCrO_4$ into the primer layers (Scholes *et al.*, 2006) above (Le Bozec *et al.*, 2001; Carlton, 2003; Prosek and Thierry, 2004; Gao *et al.*, 2006).

Unfortunately, the strong oxidizing ability of chromates is also responsible for their extremely high environmental toxicity and can cause various life-threatening illnesses in humans, such as cancer or mutagenic damage (Twite and Bierwagen, 1998). For these reasons, the use of chromates has been banned in many corrosion protection applications since the beginning of the twenty-first century (Directive 2000/53/EC).

Currently, almost all main industry branches have ceased the utilization of chromates for corrosion protection and are searching intensively for more environmentally friendly substitutes. Various solutions have been proposed, such as compounds of several transition metals in a high oxidation state used for chemical conversion coatings, including titanium (Tsai *et al.*, 2010), vanadium (Zou *et al.*, 2011), zirconium and niobium (Ardelean *et al.*, 2008), manganese (Hughes *et al.*, 2006; Zhao *et al.*, 2006), cobalt (Hughes *et al.*, 2004), molybdenum (Magalhaes *et al.*, 2004), tungsten and silicon (Li *et al.*, 2007), cerium (Kobayashi and Fujiwara, 2006; Lin and Li, 2006; Hosseini *et al.*, 2007; O'Keefe *et al.*, 2007; Ardelean *et al.*, 2008) and other rare earth metals (Yang *et al.*, 2009; Kong *et al.*, 2010). Other proposed solutions include electrochemical chromate-free oxidation treatment (anodizing) (Knudsen *et al.*, 2004; Niu *et al.*, 2006; Alanazi *et al.*, 2010); diverse organic–inorganic pre-treatments (Hansal *et al.*, 2006; Liu *et al.*, 2006) and the application of organic inhibitors directly onto the metal substrate surface (Hernandez-Alvarado *et al.*, 2009). Dufek and Buttry (2008) present other numerous attempts to find appropriate alternatives to chromates.

A fully equivalent substitution for chromates has, to date, still not been found, however, and most of the comparative studies of chromate-free corrosion protection solutions have led unfortunately, but undoubtedly, to the conclusion that chromates provide outstandingly better corrosion resistance than any other coatings yet known. In some industry branches, due to the very high requirements for corrosion protection performance (for instance in aircraft), the use of chromates has been temporarily allowed (Velterop, 2003) whilst experts continue their intense efforts to develop a method of corrosion protection technology which is equivalent to or even better than the use of chromium compounds.

Barrier (passive) protection with organic coatings

In chromate-free coating systems, the contributions of primer and topcoat layers to the protective efficiency of the whole coating increase due to the relatively low efficiency of the chromate-substitute layer. Conventionally these layers (especially the topcoat) should facilitate good barrier properties leading to the safe isolation of the metal substrate from corrosive environmental factors and from charge transfer occurring as a consequence of the electrochemical corrosion processes. A huge variety of organic paint systems were developed for this purpose in a wide range of industries for some decades (Khanna, 2008). Organic coatings provide a physical barrier preventing access to corrosives and can eliminate corrosion as long as the coating integrity is free of defects. These organic layers are, however, not robust enough to withstand various damages, firstly due to mechanical factors (scratches, stone chipping, etc) appearing during the service life of the organic protective system (Weldon, 2009). Once damaged, the organic coating can no longer effectively resist the penetration of corrosives into the damaged area and is therefore unable to prevent the development of corrosion.

Active organic coatings with inhibitors

In terms of nanotechnology-based alternatives, a straightforward and seemingly self-evident solution is to create 'active' anticorrosion functionality in the coating matrix by the direct introduction of corrosion-preventing or corrosion-slowing agents, e.g. corrosion inhibitors in the pre-treatment, primer or topcoat layers of the protective coating system (Brooman, 2002a, 2002b, 2002c). However, numerous complications can occur due to the specific physicochemical properties of the anticorrosive agents and their interactions with the other components of the coating system. These interactions can lead to a significant reduction in the protective performance of the coating or even to its failure. Highly efficient inhibitors can only be attained if their solubility in the closest proximity to the damaged site lies within certain 'proper' limits. Very low solubility leads to lack of inhibitor in the damaged environment and consequently to weak feedback activity. Where solubility is too high, the substrate can only be protected for a relatively short time, after which the inhibitor will be rapidly leached out from the coating.

Another drawback caused by high solubility is osmotic pressure, which leads to blistering and finally even to delamination of the coating from the active surface of the substrate (Fig. 10.2). The osmotic pressure can also stimulate water to be transported through the coating, which acts as a semi-permeable membrane, causing the destruction of the passive coating matrix (Shchukin and Möhwald, 2007). Moreover, the possible chemical interaction of inhibitors with the passive matrix leads to significant shortcomings in the stability and barrier properties of the whole coating system (Raps *et al.*, 2009). The intensity of interaction and therefore the rate of release of the active load are dependent on the structural,

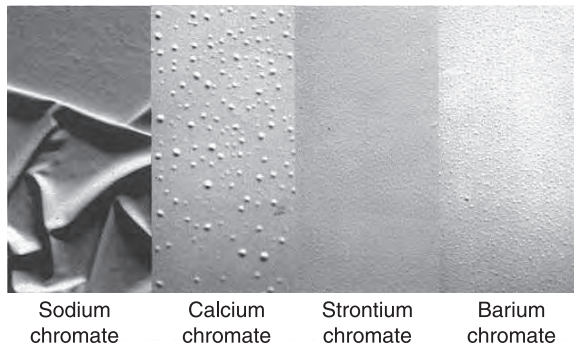

10.2 Blistering and delamination of organic coatings caused by osmotic pressure driven water permeation. Corrosion inhibitor pigment solubility increases from right to left (Sinko, 2001).

chemical and acidic/alkaline properties of the passive matrix. Additionally, an inhibitor freely dispersed inside the active matrix is often subjected to spontaneous leakage from the surface, leading to a depletion of the inhibitor during aging (Vreugdenhil and Woods, 2005).

10.2 Nanocontainers in coatings

The standard anticorrosion coatings developed so far passively prevent the interaction of corrosive species with the metal. Thick coatings are required and the 'cut-edge' problem remains. The next generation of protective coatings should be much thinner (thus reducing CO_2 emission and the quantity of raw components per $1\,m^2$ of the substrate) and possess the ability to self-heal or repair themselves in the scratched (damaged) areas. Achieving this will require the development of components to be included in the coatings which react to external or internal impact (pH, humidity changes or distortion of the coating integrity, etc) and, if possible, which are able to combine their self-healing property with another function (e.g., detection, controlled reflection, self-cleaning).

These requirements and many of the abovementioned problems found in former generations of active coatings, which were directly doped with inhibitors or other active agents, can be avoided or surmounted by the extension of the 'passive' host/'active' guest engineering concept. This concept involves the integration of micro- or nanoscale containers (carriers) loaded with the active components into the matrix of 'classical' coatings (Shchukin and Möhwald, 2007; Hughes *et al.*, 2010).

The key idea behind this approach is to create nanocontainers for the loading of active agents with shells possessing controlled permeability specific to several triggers and then to introduce them into the coating matrix (Fig. 10.3). Being uniformly distributed in the passive matrix, these nanocontainers will keep the

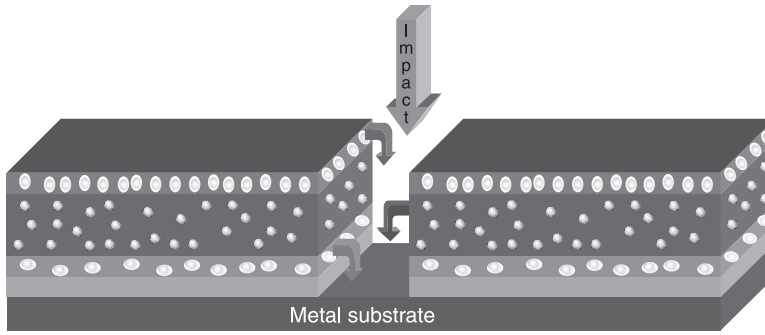

10.3 Schematic illustration of working principle of novel multifunctional self-healing coatings based on the embedded nano/microcontainers with active agents.

active material in a 'trapped' state, thus avoiding the undesirable interaction between the active component and the matrix which leads to spontaneous leakage. When the local environment undergoes changes, or if the active surface is affected by an outer impact, the nanocontainers respond to this stimulus and release encapsulated active material.

The use of different types of micro- and nanocontainers for encapsulation, controlled delivery and the release of active materials is becoming increasingly popular. The containers can have an inorganic, organic or composite origin and can be applied for the encapsulation of drugs, vitamins, quantum dots, bactericides, oils, biopolymers, corrosion inhibitors, low molecular weight compounds and many other active molecules. For example, micron-sized capsules with a layer-by-layer (LbL) assembled polyelectrolyte shell are used for the encapsulation and release of drugs, DNA, dendrimers and enzymes (Sukhorukov and Möhwald, 2007) and inorganic halloysite nanotubes were demonstrated to be suitable for the loading of ferments and inorganic nanoparticles (Veerabadran *et al.*, 2007).

The following triggers prompt the opening and closing of the container shell/stopper: local pH changes, temperature changes, electromagnetic irradiation, mechanical pressure (also ultrasonic treatment), humidity, electric (electrochemical) potential, ionic strength and dielectric permeability of the solvent. For opening by electromagnetic irradiation, the container shell would require sensitive components such as metal (silver) nanoparticles; for IR light (Javier *et al.*, 2008), dyes for visible light (Tao *et al.*, 2004); and semiconductors (TiO_2 particles) for UV light (Shchukin and Sviridov, 2006). Mechanical impact requires a certain level of rigidity or brittleness of the shell because the elastic shell can undergo deformation under pressure, but not rupture (Fery and Weinkamer, 2007); containers with a diameter of <100 nm are hardly destroyed with reasonable mechanical force because they tend to escape from the force direction. Other triggers for capsule opening were demonstrated for hydrogels, including temperature, electric potential

and high ionic strength, and for polyelectrolyte capsules, including temperature, high ionic strength and dielectric permeability of the solvent (Antipov and Sukhorukov, 2004). These triggers are usually involved in feedback active systems of a specific functionality, e.g. coatings with electrochemically reversible permeability (Koehler *et al.*, 2005).

10.2.1 Nanocontainers based on layered double hydroxides (LDHs)

Hydrophobic layers (Mitchon and White, 2006) of surfactant molecules on the surface have recently been proposed as corrosion inhibitors, but they suffer two drawbacks: (i) that the layers have limited stability and (ii) molecule-sized defects which allow water to reach the underlying surface. These problems need resolving before the surfactant can be incorporated in an inorganic host matrix, a thin film of which has previously been strongly bonded to metal surfaces such as aluminum. Layered double hydroxides (LDHs) are one such potential inorganic host. They can be expressed by the general formula $(M^{2+}_{1-x}M^{3+}_{x}(OH)_2)A^{n-}_{x/n}\cdot mH_2O$, where the cations M^{2+}(Mg^{2+}, Zn^{2+}, Fe^{2+}, Co^{2+}, Cu^{2+} and others) and M^{3+} (Al^{3+}, Cr^{3+}, Fe^{3+}, Ga^{3+} and others) occupy the octahedral holes in a brucite-like layer, and the anion A^{n-} is located in the hydrated interlayer galleries (Williams and O'Hare, 2006). The ability to vary the composition of the matrix over a wide range allows even materials with a wide variety of properties to be prepared. The LDHs have been applied as catalysts and catalyst supports (Albertazzi *et al.*, 2004), polymer stabilizers (Sorrentino *et al.*, 2005) and traps of anionic pollutants (Palmer *et al.*, 2009).

The application of hydrotalcite-like compounds in corrosion science has covered different aspects. In some studies, the LDHs have been produced *in situ*, on the top of metallic substrates as protective films (Buchheit *et al.*, 2002). Hydrotalcite-based conversion films have demonstrated good corrosion protection and some research groups have been trying to improve the interaction between these conversion films and organic coatings (Leggat *et al.*, 2002). An alternative method is to use these anionic clays as containers for corrosion inhibitors and incorporate them into the organic coatings. In this case, the aims are two-fold: not only to release the species that impart active protection, but also to trap the corrosive agents (Cl^-, SO_4^{2-}). Several works (Mahajanarn and Buchheit, 2008 and Williams and McMurray, 2004) can be found on this topic.

A class of materials with emerging importance within the LDH family are LDHs loaded with organic anions (Theng, 1974). Two short studies on these materials are available. Williams and McMurray prepared LDHs with different organic species (benzotriazole, ethyl xantate, and oxalate) by rehydration of commercial hydrotalcite (Mg_6Al_2 $(OH)_{16}\cdot CO_3\cdot 4H_2O$). The resulting layered systems were inserted into a poly(vinylbutyral) coating, prepared by a bar cast on the top of AA2024-T3.

In another report, Kendig and Hon (2005) prepared LDHs intercalated with 2,5-dimercapto-1,3,4-thiadiazolate in a similar way and studied the inhibiting properties of this anion with respect to the oxygen reduction reaction on copper. In another recently developed possibility, Zheludkevich *et al.* (2010) used Zn–Al and Mg–Al LDHs loaded with quinaldate and 2-mercaptobenzothiazolate. The anions were synthesized via anion-exchange reaction. Spectrophotometric measurements demonstrated that the release of organic anions from these LDHs into the bulk solution is triggered by the presence of chloride anions, proving the anion-exchange nature of this process. A significant reduction of the corrosion rate was observed when the LDH nanopigments were present in the corrosive media. The mechanism by which the inhibiting anions can be released from the LDHs underlines the versatility of their environmentally friendly structures and their potential application as nanocontainers in self-healing coatings.

10.2.2 Polymer-based nanocontainers

Healable polymeric systems may, for example, contain encapsulated monomers and polymerization catalysts or latent functionalities, which are able to participate in thermally reversible (Cho *et al.*, 2006), covalent bond-forming reactions (Adzima *et al.*, 2008). It has also been shown that non-covalent interactions, specifically hydrogen bonds (Fouquey *et al.*, 1990), may be used to promote healing within a supramolecular polymer blend (albeit in the presence of a plasticizing solvent). In the latter system, it is proposed that fracture propagates via the dissociation of the weak supramolecular interactions rather than by scission of the covalent bonds, so that re-assembly of the supramolecular network restores the original physical properties of the material.

Two types of polystyrene microcapsules with aqueous interior and sizes of 6 and 26 μm, respectively, were formed according to the chemistry of the stabilizing surfactants and their concentrations. The electrodeposition of microcapsules onto the metal coating carried out in the next step was only satisfactory when their size was essentially smaller than the coating thickness (60 μm), stabilizing their integrity. A similar method of producing a composite metal coating with organic liquid-containing microcapsules by electroplating of the metal substrate was chosen in order to achieve the sustained release of a liquid lubricant, lowering the friction between repeatedly contacting surfaces (self-lubricating coating) (Liqun *et al.*, 2004). Microcapsules with liquid organosilica resin as the core and polyvinyl alcohol as the shell material were prepared via o/w emulsification using an alkyl polyoxyethylene polyether type surfactant as a stabilizer. The subsequent electroplating from the mixture of electrolyte solution and capsule dispersion finishes the formation of composite capsule-contained metal coating. When the samples were subjected to a scratch or wear test, surface wetting in the immediate vicinity of the damage site was observed, confirming the release of liquid from the broken microcapsules and the ability of the coating to provide self-lubrication.

For effective performance of self-healing composite coatings, the ability to recover cracks generated during the service of a polymer is essential and may be attained by the incorporation of microcontainers with encapsulated liquid sealant. Urea–formaldehyde microcapsules filled with drying linseed oil were used for the healing of cracks in an epoxy coating (Suryanarayana *et al.*, 2008). Since the outer shell surface of the microcapsules was very rough, a good binding with the coating matrix was provided. The encapsulated linseed oil is released by the coating crack and fills the crack in a coating matrix. Finally, oxidation of the linseed oil by atmospheric oxygen leads to the formation of continuous film inside the crack.

Significant progress in the preparation of protective composite coatings with incorporated organic micro- and nanocontainers was achieved in the past decade by the group of White *et al.* (2001). In their most well-known paper they showed the first working prototype of polymeric materials with the ability to 'autonomically heal cracks' occurring in their bulk structure. The proposed self-healing material contained microcapsules (50–200 μm) with poly(urea–formaldehyde) shells filled with the healing agent – dicyclopentadiene monomer. These capsules were then mixed with epoxy resin and Ru-based Grubbs' catalyst in order to prepare a self-healing epoxy specimen. A developing crack ruptures the embedded microcapsules and releases healing agent into the crack channel due to capillary forces. Polymerization of the healing agent was triggered by a catalyst bonding the crack faces with a healing efficiency of about 60%. The proposed self-repairing approach had, however, some essential drawbacks for application in protective self-healing coatings: (i) the concentration of Grubbs' catalyst has to be quite high and thus increases the price of coating, especially in the case of large surfaces to be protected; (ii) the relatively large size of the capsules (50–200 μm) inhibits their application to coatings with thickness less than 0.5 mm because of integrity failure. Reducing the microcapsule size without reducing the self-healing efficiency requires a much higher concentration in the coating matrix. Samples with smaller microcapsules must have very good adhesion to the epoxy matrix to ensure capsule rupture under stress. Much smaller capsules (nanocapsules) filled with dicyclopentadiene as a self-healing agent were synthesized very recently using ultrasonic treatment for the preparation of initial o/w emulsions. Up to 2 v/v% of these capsules can be dispersed in an epoxy matrix, leading to a slight decrease in the tensile strength accompanied by a significant increase in fracture toughness.

Deposition of a multilayer polyelectrolyte shell directly onto the liquid oil core was performed by Grigoriev *et al.* (2008). Obtained microcontainers which were stable in aqueous dispersion for a long time quickly ruptured at the interface due to action of capillary forces. The observed fragility of these containers restricts their range of applications, especially for embedding into hard and through polymeric coatings. On the other hand, the slow curing of organic coating formulations containing solvents with similar surface values (interface tension) can lead to the containers' survival and make them potential carriers for the loading of lubricants.

Another example, below, demonstrates once more how productive the emulsion route can be in the fabrication of micro- and nanocontainers for anticorrosion coatings. Organosiloxanes form covalent bonds with the surface of a metal substrate bearing hydroxyl groups and give it coupling (in the case of usual siloxanes) or water-repelling (for long-chain terminated siloxanes) functionality (Mittal, 1992). Moreover, organosiloxanes with multiple SiOR moieties can undergo a lateral polycondensation reaction at the substrate surface, forming a two-dimensional network with excellent protective abilities against corrosion (Mittal, 1992).

These properties of organosiloxanes were taken into account by Latnikova *et al.* (2010), who have proposed encapsulating a mixture of emulsified organosiloxanes and incorporating them into a coating matrix. Micro- and nanocontainers with core-shell morphology and polyurethane/polyurea shells were successfully synthesized by emulsion interfacial polyaddition and then embedded in the corrosion protective coatings on the epoxy basis. A comparative study of their protective efficiency showed a much better performance for the coatings with organosiloxane-loaded containers.

Inhibitor-loaded emulsion droplets included in epoxy coatings essentially decelerated release behavior compared with the behavior of a free dispersed inhibitor. A combination of both types of inhibitor incorporation methods was suggested to provide the immediate, as well as the sustained, release of the active material. Polycondensation/precipitation in an emulsion system was utilized for preparation of a core-shell inhibitor- or sealant-loaded microcontainer (Kumar *et al.*, 2006). The growing molecular weight of formaldehyde–urea prepolymers led to the gradual decrease of their solubility (increase of hydrophobicity) and finally resulted in their interfacial precipitation on the surfaces of emulsion droplet yielding microcontainers. Due to the good oil solubility of the inhibitors, either camphor or alkylammonium salt of (2-benzothiazolylthio)succinic acid, they could be dissolved in the droplets of oil phase prior to the encapsulation, making preparation of the containers a quite simple two-step procedure.

10.2.3 Nanocontainers based on inorganic materials modified by layer-by-layer assembly of polyelectrolytes

The strategy of a preparation of nanocontainers based on a mesoporous oxide core was presented in Skorb *et al.* (2009). The fabrication of a polyelectrolyte shell around the container can be achieved using a LbL assembly of oppositely charged species, thereby preventing the spontaneous release of loaded corrosion inhibitor. The thickness precision at the deposition of subsequently adsorbed polyelectrolyte layers is about 2 nm. Polyelectrolyte nanocontainers completely replicate the shape of the templating colloids. The polyelectrolyte shell lends controlled release properties to the nanocontainers. The opening of the shell can only be induced by changing the surrounding pH value to the acidic or alkaline region (Sukhorukov

et al., 2000), while in neutral pH the polyelectrolyte shell remains intact, preventing undesirable leakage of the entrapped inhibitor.

Deposition of polyelectrolyte multilayers via LbL onto emulsion droplets can also be applied to the droplets of Pickering emulsions as initial templates which finally yield microcontainers with significantly improved stability (Li and Stöver, 2010). Similar containers were used by Haase *et al.* (2010) for loading of corrosion inhibitor 8-hydroxyquinoline (8HQ) in their interior. Interestingly, in this case the active agent 8HQ simultaneously also played the role of hydrophobizing agent for silica nanoparticles forming the container shells. Given the amphoteric character of 8HQ, its charge and solubility increase when exposed to low and high pH values (< 4 and > 9), leading, therefore, to enhanced electrostatic repulsion between molecules on the particle's surface and, finally, to the distribution of particulate shells around Pickering emulsion droplets. This, in turn, causes the breakup of containers and the release of the encapsulated inhibitor.

Halloysite is an economically viable naturally occurring material that can be mined as a raw mineral (Lvov *et al.*, 2002). As for most natural materials, the size of halloysite particles varies within 1–15 μm of length and 10–100 nm of inner diameter depending on the deposits. Embedding of the corrosion inhibitor (for example, benzotriazole) inside the inner volume of the halloysite G nanotubes was performed according to the adapted procedure described by Price *et al.* (2001). To attain controlled release properties in the halloysite nanotubes, the surfaces of the nanotubes could be modified by LbL deposition of polyelectrolyte bilayers (Lvov *et al.*, 2008).

10.2.4 Anticorrosion efficiency of nanocontainer-based coatings

The next step in the anticorrosion self-healing coating formation is the incorporation of the containers into the coating. Their feedback ability to respond actively to the various external impacts has to be used to anneal defects, e.g. to construct a self-repairing coating. It has been shown that there are conceptual solutions, but there are still many technical and economic issues to be resolved before a practical solution is arrived at. The stimuli have thus far been predominantly of mechanical and chemical nature, but in future researchers may begin to use others, such as friction or biological impact. Feedback loops are ubiquitous in nature and technology and are mostly used, not to remove a stimulus, but to keep it at a defined level, e.g. concentration, pH, potential. Attempting to mimic these, however, is a more demanding task which should be tackled in the future. There is nevertheless much potential for the construction of these more sophisticated regulatory loops, e.g. maintaining a fixed humidity, potential or enzyme concentration. There is a high demand for such feedback active systems in the most urgent areas of society, energy, health and raw materials, and we look forward to interesting solutions in these areas in the future.

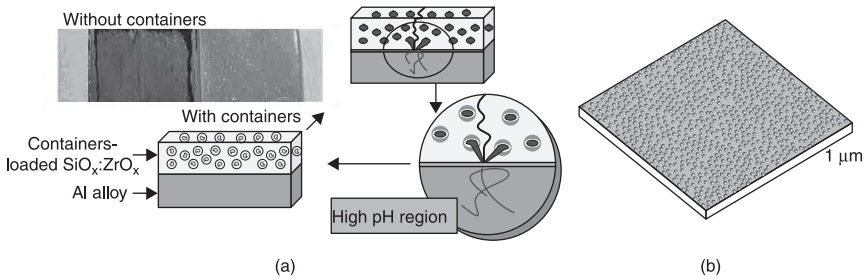

10.4 (a) Schematic of the self-healing effect of anticorrosion coatings; and (b) atomic force microscopy (AFM) images of container-loaded SiO_x:ZrO_x film (Skorb *et al.*, 2009).

It is important to achieve a uniform distribution of the containers (Fig. 10.4) because any agglomeration in the coating will result in the formation of additional defects, thus reducing the barrier properties of the coating. This distribution can be achieved either by ultrasonic agitation of the nanocontainer/paint formulation or by vigorous stirring. The electrochemical impedance spectroscopy data and optical photographs of the samples with and without nanocontainers in 0.1 M NaCl solution have shown that the highest protection was provided by the container loaded with sol-gel film. The effect of very low corrosion in the case of containers loaded with film could be explained through their additional and very important self-healing ability.

SVET (scanning vibrating electrode technique) permits the mapping of the current density in an electrolyte close to the substrate surface. The electrode vibrates and indicates the current flow in the electrolyte due to the corrosion processes occurring on the substrate surface. The measured current density vectors permit mapping of both the magnitude and direction of current flow immediately above the substrate surface. This current density map can be overlaid onto an optical micrograph of the substrate captured by a video microscope (Fig. 10.5). This capability permits the correlation of anodic and cathodic current processes with visual features on the substrate surface. The SVET is capable of providing detailed spatially resolved information not readily obtainable by other techniques. The SVET maps and corresponding optical images 12 h after the start of the corrosion test are presented in Fig. 10.5. The bare metals alloy exhibited several regions of anodic activity, reflecting sites of localized corrosion (Fig. 10.5(a)). Figure 10.5(b) shows that, for the alloy panel coated with individual sol-gel film, one peak of corrosion activity is visible; consequently this results in a higher protection ability of the alloy. Figure 10.5(c) illustrates that nanocontainer-doped sol-gel film exhibits very high anticorrosion ability, which is visible from the practical absence of anodic activity. Thus, it is visible from SVET measurements that, during the corrosion process, the corrosion centers appear in all samples. The highest corrosion occurs in the case of bare Al alloy (Fig. 10.5(a)). Second place

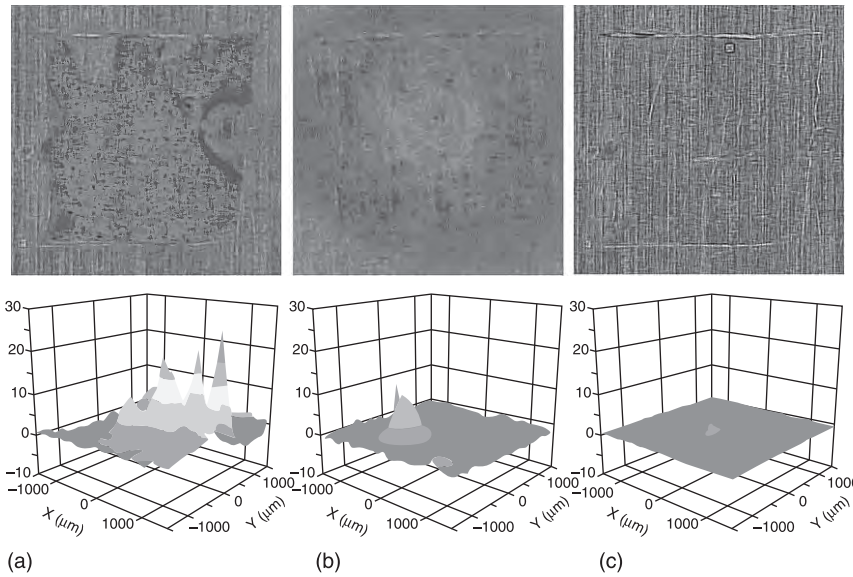

10.5 Scanning vibrating electrode measurements of the ionic currents above the surface and the corresponding optical images of (a) unmodified aluminum alloy; (b) aluminum alloy coated with SiO_x:ZrO_x film; (c) aluminum alloy coated with container-loaded SiO_x:ZrO_x film (the inhibitor of corrosion incorporated into containers). Scale units: μA cm^2, spatial resolution 150 μm. Solution: 0.1 M NaCl. Time of scanning was 12 h (Skorb *et al.*, 2009).

in the range of protection ability is the sol-gel coating (Fig. 10.5(b)). The highest protection was provided by the container loaded with sol–gel film (Fig. 10.5(c)). The effect of very low corrosion in the case of the SiOx:ZrOx film could be explained through the additional and very important ability of the SiOx:ZrOx film to self-heal.

10.3 Conclusions

The concept of using anticorrosion coatings which implement micro- or nanocontainers filled with inhibitor into the coating matrix has been successfully proven by numerous examples which show good protection performance of these coatings on the laboratory scale. The most important feature of the new generation of coatings is their self-healing ability: if the coating becomes damaged, the containers adjacent to the impact area will be activated under the influence of several environmental factors, releasing the encapsulated active substances at the damage site and thus terminating the propagation of the corrosion. The major advantage of this ‘smart’ solution is that the inhibitor will only be released at the

site where the corrosion arises and only in the quantity needed to stop it. This allows a prolonged active protection mechanism as well as a significantly increased coating sustainability. Once corrosion has been stopped, the triggering effect is usually relinquished and rate of inhibitor release reduces to zero. The contingent reproducibility between the active and passive states of the container ensures the low consumption of active agents.

Further up-scaling and transfer of this approach to the technology level does, however, involve some restrictions dictated by the industrial requirements for the coating. The high ratio between the size of the container and the coating thickness can result in the loss of physical integrity of the coating matrix and, therefore, to the failure of its barrier properties. This limits the maximum size of the containers and their content in the coating formulation. The other essential issue is the very complex chemical interplay between the materials of the substrate, the containers, the coating matrix and the inhibitor chosen for the substrate protection. Any chemical interactions leading to the deactivation of the inhibitor or to change in the structure of the coating matrix should be avoided. The compositions of all elements of the protective system have to provide good physicochemical compatibility expressed in terms of such properties as dispersibility and colloidal stability of the initial fluid coating formulation, adhesion between the containers and the matrix as well as between the matrix and the substrate in the cured state. Following this line of industrial demands, the large micrometric containers with polymeric shells are, for example, suitable for coating formulations as organic solvents which yield relatively thick coatings after curing. By contrast, submicrometer or nanoscale containers with mesoporous ceramic core (scaffold) could be appropriate for water-borne coatings with moderate or low thickness. More detailed fitting is internally determined by specific requirements to the particular anticorrosion solution, i.e. by all elements of the protective system in use.

10.4 References

Adzima J., Aguirre H., Kloxin C. J., Scott T. F. and Bowman C. N. (2008), 'Rheological and Chemical Analysis of Reverse Gelation in a Covalently Cross-Linked Diels–Alder Polymer Network', *Macromolecules*, **41**, 9112–17.

Ahluwalia H. and Uhlenkamp B. J. (2008), 'The Importance of Quality in Corrosion-Resistant Alloys in Biopharmaceutical Manufacturing', *Pharmaceut. Tech.*, **3**. Available from: http://pharmtech.findpharma.com/pharmtech/Peer-Reviewed+Research/The-Importance-of-Quality-in-Corrosion-Resistant-A/ArticleStandard/Article/detail/500410 [Accessed 5 February 2011].

Alanazi N. M., Leyland A., Yerokhin A. L. and Matthews A. (2010), 'Substitution of hexavalent chromate conversion treatment with a plasma electrolytic oxidation process to improve the corrosion properties of ion vapour deposited AlMg coatings', *Surf. Coat. Tech.*, **205**, 1750–6.

Albertazzi S., Basile F. and Vaccari A. (2004), 'Catalytic properties of Hydrotalcite-type anionic clays', in Wypych F. and Satyanarayana K. G., *Clay Surfaces: Fundamentals and Applications*. Amsterdam: Elsevier, 496–546.

Antipov A. A. and Sukhorukov G. B. (2004), 'Polyelectrolyte multilayer capsules as vehicles with tunable permeability', *Adv. Colloid Interface Sci.*, **111**, 49–61.

Ardelean H., Frateur I. and Marcus P. (2008), 'Corrosion protection of magnesium alloys by cerium, zirconium and niobium-based conversion coatings', *Corros. Sci.*, **50**, 1907–18.

Available from: http://www.bmu.de/files/pdfs/allgemein/application/pdf/vehiclesdir.pdf [Accessed 1 January 2011].

Baeckmann W. von, Schwenk W. and Prinz W. (Eds) (1997), *Handbook of Cathodic Corrosion Protection: Theory and Practice of Electrochemical Protection Processes*, Houston: Gulf Publishing.

Bendall K. C. (1995), 'Corrosion resistant alloys – an industry-wide overview of applications', *Anti-Corros. Methods M*, **42**, 12–15.

Berger R., Bexell U., Grehk T. M. and Hornstrom S. E. (2007), 'A comparative study of the corrosion protective properties of chromium and chromium free passivation methods', *Surf. Coat. Tech.*, **202**, 391–7.

Bogner B. (2005), 'Composites for chemical resistance and infrastructure applications', *Reinf. Plast.*, **49**, 30–4.

Brock T., Groteklaes M. and Mischke P. (2009), *Lehrbuch der Lacktechnologie*, 3te Auflage. Hannover: Vincentz Verlag.

Brooman E. W. (2002a), 'Modifying organic coatings to provide corrosion resistance – Part I: Background and general principles', *Met. Finish*, **100**, 48–53.

Brooman E. W. (2002b), 'Modifying organic coatings to provide corrosion resistance: Part II – inorganic additives and inhibitors', *Met. Finish*, **100**, 42–53.

Brooman E. W. (2002c), 'Modifying organic coatings to provide corrosion resistance – Part III: organic additives and conducting polymers', *Met. Finish*, **100**, 104–10.

Buchheit R. G., Mamidipally S. B., Schmutz P. and Guan H. (2002), 'Active Corrosion Protection in Ce-Modified Hydrotalcite Conversion Coatings', *Corrosion*, **58**, 3–14.

Carlton G. N. (2003), 'Hexavalent chromium exposures during full-aircraft corrosion control', *AIHA J.*, **64**, 668–72.

Chidambara D., Vasquez M. J., Halada G. P. and Clayton C. R. (2003), 'Studies on the repassivation behavior of aluminum and aluminum alloy exposed to chromate solutions', *Surf. Interface Anal.*, **35**, 226–30.

Cho S. H Andersson H. M., White S. R., Sottos N. R. and Braun P. V. (2006), 'Polydimethylsiloxane-Based Self-Healing Materials', *Adv. Mater.*, **18**, 997–1000.

Directive 2000/53/EC of the European Parliament and the council of 18.09.2000 on end-life vehicles. *Official J. of Eur. Comm.*, L269/34–L269/42.

Dufek E. J. and Buttry D. A. (2008), 'Inhibition of O_2 reduction on AA2024-T3 using a Zr(IV)-Octadecyl phosphonate coating system', *Electrochem. Solid St.*, **11**, C9–C12.

Fery A. and Weinkamer R. (2007), 'Mechanical properties of micro- and nanocapsules: Single-capsule measurements', *Polymer*, **48**, 7221–35.

Fouquey C., Lehn J.-M. and Levelut A.-M. (1990), 'Molecular Recognition Directed Self-Assembly of Supramolecular Liquid Crystalline Polymers from Complementary Chiral Components', *Adv. Mater.*, **2**, 254–7.

Gao Y., Ana U. and Wilcox G. D. (2006), 'Corrosion inhibitor doped protein films for protection of metallic surfaces: appraisal and extension of previous investigations by Brenner, Riddell and Seegmiller', *T. I. Met. Finish*, **84**, 141–8.

Grigoriev D. O., Bukreeva T., Möhwald H. and Shchukin D. G. (2008), 'New Method for Fabrication of Loaded Micro- and Nanocontainers: Emulsion Encapsulation by Polyelectrolyte Layer-by-Layer Deposition on the Liquid Core', *Langmuir*, **24**, 999–1004.

Gupta M. C. and Gupta A. P. (2005), *Polymer Composite*. New Delhi: New Age International. (P) Limited.

Haase M. F., Grigoriev D., Möhwald H., Tiersch B. and Shchukin D. G. (2010), 'Encapsulation of Amphoteric Substances in a pH-Sensitive Pickering Emulsion', *J. Phys. Chem. C*, **114**, 17304–10.

Hansal W. E. G., Hansal S., Polzler M., Kornherr A., Zifferer G. *et al.* (2006), 'Investigation of polysiloxane coatings as corrosion inhibitors of zinc surfaces', *Surf. Coat. Tech.*, **200**, 3056–63.

Hernandez-Alvarado L. A., Hernandez L. S., Miranda J. M. and Dominguez O. (2009), 'The protection of galvanised steel using a chromate-free organic inhibitor', *Anti-Corros. Method M*, **56**, 114–20.

Hosseini M., Ashassi-Sorkhabi H. and Ghiasvand H. (2007), 'Corrosion protection of electro-galvanized steel by green conversion coatings', *J. Rare Earth*, **25**, 537–43.

Hughes A. E., Gorman J., Harvey T. G., McCulloch D. and Toh S. K. (2004), 'SEM and RBS characterization of a cobaltbased conversion coating process on AA2024-T3 and ALA7075-T6', *Surf. Interface Anal.*, **36**, 1585–91.

Hughes A. E., Gorman J. D., Harvey T. G., Galassi A. and McAdam G. (2006), 'Development of permanganate-based coatings on aluminum alloy 2024-T3', *Corrosion*, **62**, 773–80.

Hughes A. E., Cole I. S., Muster T. H. and Varley R. J. (2010), 'Designing green, self-healing coatings for metal protection', *NPG Asia Mater.*, **2**, 142–51.

Institute of Materials (2002), *Corrosion Resistant Alloys for Oil and Gas Production: Guidance on General Requirements and Test Methods for H2S Service*, 2nd Edition. Leeds: Maney Publishing.

Javier M., de Pino P., Bedard M. F., Ho D., Skirtach A. G. *et al.* (2008), 'Photoactivated Release of Cargo from the Cavity of Polyelectrolyte Capsules to the Cytosol of Cells', *Langmuir*, **24**, 12 517–20.

Kendig M. H. and Hon M. (2005), 'A Hydrotalcite-Like Pigment Containing an Organic Anion Corrosion Inhibitor', *Electrochem Solid-State Lett.*, **8**, B10–B11.

Kendig M. W. and Buchheit R. G. (2003), 'Corrosion inhibition of aluminum and aluminum alloys by soluble chromates, chromate coatings and chromate-free coatings', *Corrosion*, **59**, 379–400.

Khanna A. S. (2008), *High-performance organic coatings*. Cambridge: Woodhead.

Knudsen O. O., Tanem B. S., Bjorgum A., Mardalen J. and Hallenstvet M. (2004), 'Anodising as pre-treatment before organic coating of extruded and cast aluminium alloys', *Corros. Sci.*, **46**, 2081–95.

Kobayashi Y. and Fujiwara Y. (2006), 'Corrosion protection of cerium conversion coating modified with a self-assembled layer of phosphoric acid mono-n-alkyl ester', *Electrochem. Solid St.*, **9**, B15–B18.

Koch G. H., B. Brongers M. P. H., Thompson N. G., Virmani Y. P. and Payer J. H. (2002), 'Corrosion Costs and Preventative Strategies in the United States', *Suppl. Mater. Perform.*, **42**, 2–11.

Koehler K., Shchukin D. G., Möhwald H. and Sukhorukov G. B. (2005), 'Thermal Behavior of Polyelectrolyte Multilayer Microcapsules. 1. The Effect of Odd and Even Layer Number', *J. Phys. Chem. B*, **109**, 18250–9.

Kong G., Liu R. B., Lu J. T., Che C. S. and Zhong Z. (2010), 'Study on Growth mechanism of lantanium salt conversion coating on galvanized steel', *Acta Metall. Sin.*, **46**, 487–93.

Kumar A., Stephenson L. D. and Murray J. N. (2006), 'Self-healing coatings for steel', *Prog. Org. Coat.*, **55**, 244–53.

Latnikova A., Grigoriev D. O., Hartmann J., Möhwald H. and Shchukin D. G. (2011), *Soft Matter*, **7**, 369–72.

Le Bozec N., Nazarov A., Persson D., Thierry D., Isaacs H. S. *et al.* (2001), 'The role of chromate in preventing undermining coatings on hot dip galvanised steel surfaces', *Elec. Soc. S*, 81–90.

Leggat R. B., Taylor S. A. and Taylor S. R. (2002), 'Adhesion of epoxy to hydrotalcite conversion coatings: II.Surface modification with ionic surfactants', *Colloids Surf. A*, **210**, 83–94.

Li J. and Stöver H. D. H. (2010), 'Pickering Emulsion Templated Layer-by-Layer Assembly for Making Microcapsules', *Langmuir*, **26**, 15 554–60.

Li Z., Dai C., Liu Y. and Zhu J. (2007), 'Study of silicate and tungstate composite conversion coatings on magnesium alloy', *Electroplating & Pollution Control*, 16–19.

Lin C. S. and Li W. J. (2006), 'Corrosion resistance of cerium-conversion coated AZ31 magnesium alloys in cerium nitrate solutions', *Mater. Trans.*, **47**, 1020–5.

Liqun Z., Wei Z., Feng L. and He Y. (2004), 'Electrodeposition of composite copper/liquid-containing microcapsule coatings', *J. Mater. Sci.*, **39**, 495–9.

Liu J. R., Guo Y. N. and Huang W. D. (2006), 'Study on the corrosion resistance of phytic acid conversion coating for magnesium alloys', *Surf. Coat. Tech.*, **201**, 1536–41.

Lvov Y., Price R., Gaber B. and Ichinose I. (2002), 'Thin film nanofabrication via layer-by-layer adsorption of tubule halloysite, spherical silica, proteins and polycations', *Colloids Surf. A*, **198**, 375–82.

Lvov Y., Shchukin D., Möhwald H. and Price P. (2008), 'Halloysite Clay Nanotubes for Controlled Release of Protective Agents', *ACS Nano.*, **2**, 814–20.

Magalhaes A. A. O., Margarit I. C. P. and Mattos O. R. (2004), 'Molybdate conversion coatings on zinc surfaces', *J. Electroanal. Chem.*, **572**, 433–40.

Mahajanarn P. V. and Buchheit R. G. (2008), 'Characterization of inhibitor release from Zn-Al-[V10O28]6-hydrotalcite pigments and corrosion protection from hydrotalcite-pigmented epoxy coatings', *Corrosion*, **64**, 230–40.

McCafferty E. (2010), *Introduction to Corrosion Science*. New York: Springer.

McConnell V. P. (2005), 'Resurgence in corrosion-resistant composites', *Reinf. Plast.*, **49**, 20–5.

Mitchon L. N. and White J. M. (2006), 'Growth and Analysis of Octadecylsiloxane Monolayers on Al_2O_3 (0001)', *Langmuir*, **22**, 6549–54.

Mittal K. L. (1992), *Silanes and other Coupling Agents*. Utrecht: VSP.

Niu L. Y., Jiang Z. H., Li G. Y., Gu C. D. and Lian J. S. (2006), 'A study and application of zinc phosphate coating on AZ91D magnesium alloy', *Surf. Coat. Tech.*, **200**, 3021–6.

O'Keefe M. J., Geng S. and Joshi S. (2007), 'Cerium-based conversion coatings as alternatives to hex chrome', *Metal Finishing*, **105**, 25–8.

Osborne J. H. (2001), 'Observations on chromate conversion coatings from a sol-gel perspective', *Prog. Organic Coatings*, **41**, 280–6.

Osborne J. H., Blohowiak K. Y., Taylor S. R., Hunter C., Bierwagen G. P. *et al.* (2001), 'Testing and evaluation of non-chromated coating systems for aerospace applications', *Prog. Organic Coatings*, **41**, 217–25.

Pacitti J. (1964), 'Plastics for corrosion-resistance applications', *Anti-Corros. Methods M*, **11**, 18–24.

Palmer S. J., Frost R. L. and Nguyen T. (2009), 'Hydrotalcites and their role in coordination of anions in Bayer liquors: Anion binding in layered double hydroxides', *Coord. Chem. Rev.*, **253**, 250–67.

Price R., Gaber B. and Lvov Y. (2001), '*In vitro* release characteristics of tetracycline HCl, khellin and nicotinamide adenine dinucleotide from halloysite; a cylindrical mineral', *J. Microencapsulation*, **18**, 713–22.

Pritchard G. (1995), *Anti-Corrosion Polymers: PEEK, PEKK and other Polyaryls*. Toronto: ChemTec Publishing.

Prosek T. and Thierry D. (2004), 'A model for the release of chromate from organic coatings', *Prog. Organic Coatings*, **49**, 209–17.

Raja P. B. and Sethuraman M. G. (2008), 'Natural products as corrosion inhibitor for metals in corrosive media – A review', *Mater. Lett.*, **62**, 113–16a.

Raps D., Hack T., Wehr J., Zheludkevich M. L., Bastos A. C. *et al.* (2009), 'Electrochemical study of inhibitor-containing organic–inorganic hybrid coatings on AA2024', *Corros. Sci.*, **51**, 1012–21.

Roberge P. R. (2000), *Handbook of Corrosion Engineering*. New York: McGraw–Hill.

Saji V. S. (2010), 'A Review on Recent Patents in Corrosion Inhibitors', *Recent Patents on Corrosion Science*, **2**, 6–12.

Sastri V. S. (1998), *Corrosion Inhibitors. Principles and Applications*. New York: Wiley.

Scholes F. H., Furman S. A., Hughes A. E., Nikpour T., Wright N. *et al.* (2006), 'Chromate leaching from inhibited primers Part I. Characterisation of leaching', *Prog. Organic Coatings*, **56**, 23–32.

Schweitzer P. A. (2000), *Mechanical and Corrosion-Resistant Properties of Plastics and Elastomers*. New York: Marcel Dekker.

Shchukin D. G and Sviridov D. V. (2006), 'Photocatalytic processes in spatially confined micro- and nanoreactors', *J. Photochem. Photobiol. C*, **7**, 23–39.

Shchukin D. G. and Möhwald H. (2007), 'Self-Repairing Coatings Containing Active Nanoreservoirs', *Small*, **3**, 926–43.

Sinko J. (2001), 'Challenges of chromate inhibitor pigments replacement in organic coatings', *Prog. Organic Coatings*, **42**, 267–82.

Skorb E. V., Fix D., Andreeva D. V., Möhwald H. and Shchukin D. G. (2009), 'Surface-Modified Mesoporous SiO_2 Containers for Corrosion Protection', *Adv. Funct. Mater.*, **19**, 2373–9.

Sorrentino A., Gorrasi G., Tortora M., Vittoria V., Constantino U. *et al.* (2005), 'Incorporation of Mg–Al hydrotalcite into a biodegradable Poly(3-caprolactone) by high energy ball milling', *Polymer*, **46**, 1601–8.

Sukhorukov G. B., Donath E., Moya S., Susha A. S., Voigt A. *et al.* (2000), 'Microencapsulation by means of step-wise adsorption of Polyelectrolytes', *J. Microencapsulation*, **17**, 177–85.

Sukhorukov G. B. and Möhwald H. (2007), 'Multifunctional cargo systems for biotechnology', *Trends Biotechnol.*, **25**, 93–8.

Suryanarayana C., Chowdoji Rao K. and Kumar D. (2008), 'Preparation and characterization of microcapsules containing linseed oil and its use in self-healing coatings', *Prog. Org. Coat.*, **63**, 72–8.

Tao X., Li J. B. and Möhwald H. (2004) 'Self-Assembly, Optical Behavior and Permeability of a Novel Capsule Based on an Azo Dye and Polyelectrolytes', *Chem–Eur. J.*, **10**, 3397–403.

Theng B. K. G. (1974), *The Chemistry of Clay-Organic Reactions*. New York: Wiley.

Tsai Y. T., Hou K. H., Bai C. Y., Lee J. L. and Ger M. D. (2010), 'The influence on immersion time of titanium conversion coatings on electrogalvanized steel', *Thin Solid Films*, **518**, 7541–4.

Twite R. L. and Bierwagen G. P. (1998), 'Review of alternatives to chromate for corrosion protection of aluminum aerospace alloys', *Prog. Organic Coatings*, **33**, 91–100.

Veerabadran N. G., Price R. R. and Lvov Y. M. (2007), 'Clay nanotubes for encapsulation and sustained release of drugs', *NANO*, **2**, 115–20.

Velterop L. (2003), 'Phosphoric sulphuric acid anodising: An alternative for chromic acid anodising in aerospace applications?', *ATB Metallurgie*, **43**, 284–9.

Vreugdenhil A. J. and Woods M. E. (2005), 'Triggered Release of Molecular Additives from Epoxy-Amine Sol-gel Coatings', *Prog. Org. Coatings*, **53**, 119–25.

Weldon D. G. (2009), *Failure analysis of paints and coatings*. Chichester: Wiley.

White S. R., Sottos N. R., Geubelle P. H., Moore J. S., Kessler M. R. *et al.* (2001), 'Autonomic healing of polymer composites', *Nature*, **409**, 794–7.

Williams G. and McMurray H. N. (2004), 'Inhibition of Filiform Corrosion on Polymer Coated AA2024-T3 by Hydrotalcite-Like Pigments Incorporating Organic Anions', *Electrochem. Solid-State Lett.*, **7**, B13–B15.

Williams G. R. and O'Hare D. (2006), 'Towards understanding, control and application of layered double hydroxide chemistry', *J. Mater. Chem.*, **16**, 3065–74.

Xia L. and McCreery R. L. (1998), 'Chemistry of a chromate conversion coating on aluminum alloy AA2024-T3 probed by vibrational spectroscopy', *J. Electrochem. Soc.*, **145**, 3083–9.

Xia L., Akiyama E., Frankel G. and McCreery R. (2000), 'Storage and release of soluble hexavalent chromium from chromate conversion coatings – Equilibrium aspects of Cr-VI concentration', *J. Electrochem. Soc.*, **147**, 2556–62.

Yang X., Wang G., Dong G., Gong F. and Zhang M. (2009), 'Rare earth conversion coating on Mg-8.5Li alloys', *J. Alloy Compd*, **487**, 64–8.

Zhao J., Frankel G. and McCreery R. L. (1998), 'Corrosion protection of untreated AA-2024-T3 in chloride solution by a chromate conversion coating monitored with Raman spectroscopy', *J. Electrochem. Soc.*, **145**, 2258–64.

Zhao J., Xia L., Sehgal A., Lu D., McCreery R. L. and Frankel G. S. (2001), 'Effects of chromate and chromate conversion coatings on corrosion of aluminum alloy 2024-T3', *Surf. Coat. Tech.*, **140**, 51–7.

Zhao M., Wu S. S., Luo J. R., Fukuda Y. and Nakae H. (2006), 'A chromium-free conversion coating of magnesium alloy by a phosphate-permanganate solution', *Surf. Coat. Tech.*, **200**, 5407–12.

Zhao X. D., Yang J. and Fan X. (2010), 'Review on research and Progress of Corrosion Inhibitors', *Applied Mechanics and Materials*, **44–7**, 4063–6.

Zheludkevich M. L., Poznyak S. K., Rodrigues L. M., Raps D., Hack T. *et al.* (2010), 'Active protection coatings with layered double hydroxide nanocontainers of corrosion inhibitor', *Corr. Sci.*, **52**, 602–11.

Zou Z. L., Li N., Li D. Y., Liu H. P. and Mu S. L. (2011), 'A vanadium-based conversion coating as chromate replacement for electrogalvanized steel substrates', *J. Alloy Compd*, **509**, 503–7.

11

Nanoparticle-based corrosion inhibitors and self-assembled monolayers

S. RAJENDRAN, RVS School of Engineering and Technology, Dindigul, India

Abstract: Nanomaterials such as polyelectrolytes, layered clays, sol–gel encapsulants and surface-modified nanoparticles can function as carriers of corrosion inhibitors. Carried in this way, the inhibitors can be released on demand, triggered by change in pH, ion exchange and change in oxidation state. This chapter gives an outline of such carriers with an emphasis on the surface-modified nanoparticle/nanostructure of boehmites. Subsequently, the chapter provides a detailed account of self-assembled nanofilms on various surfaces such as nickel oxide, copper oxide and iron oxide and their effect on corrosion resistance.

Key words: corrosion inhibitors, functionalized nanoparticles, self-assembled monolayers, surface-modified nanoparticles, nanofilms, release-on-demand inhibitors.

11.1 Introduction

11.1.1 Corrosion inhibitors

Corrosion is a natural, spontaneous and thermodynamically favoured process. There are several methods by which corrosion can be controlled; one such method is the use of corrosion inhibitors. Corrosion inhibitors are chemical compounds which, when added in small quantities, reduce or completely prevent the corrosion process. They may be anodic, cathodic or mixed type depending upon whether they control the anodic reaction, the cathodic reaction or both anodic and cathodic reactions. A good inhibitor is expected to have the following characteristics:[1]

- Water solubility (but not too much).
- Hydrophobicity (to displace water from metal surface).
- Reactivity with metal or high adsorption strength.
- A good delivery mechanism.

Environmental, health and safety concerns are driving the elimination of chromium and other toxic heavy metal based corrosion inhibitors from various applications. Chromates were widely used in corrosion inhibition in various liquid applications, in conversion coatings and in paints. The inhibitors used as substitutes for chromates are facing many challenges, such as:

- Inorganic non-chromate replacements are less effective and more soluble than chromates; their utility in higher concentration leads to flushing and osmotic blistering.
- For organic corrosion inhibitors, low specific gravity is a problem. Reactivity of functional groups of organics with resins can affect resin cure and can trap the inhibitor.

It is highly desirable, therefore, to develop chrome-free corrosion inhibitors and pigments with the substrate versatility necessary to meet this need without sacrificing performance. Organic molecules offer the best chance for discovery of novel, effective and low toxicity inhibitors. Quantitative structure–activity relationships for organic inhibitors are being developed to guide the inhibitor design.[1] At present, organic inhibitors are widely used in liquid applications (boilers, re-circulating cooling lines, etc) but not in coatings.

11.1.2 Nanotechnology

Nanotechnology is one of the hottest fields, draws attention from all over the world and has the potential to outdate most of the technology existing today. Nanotechnology refers to a wide range of scientific or technological phenomena that focus on the properties at the nanometre scale (around 0.1–100 nm). It is the science of developing materials by controlling individual atoms and molecules to create devices that are thousands of times smaller than current technologies permit in order to impart to them special electrical and chemical properties. Nanomaterials are important due to their unique properties that may lead to new and exciting applications, including corrosion control.[2]

Some of the unique properties of nanomaterials are listed below:

- Nanoparticles are smaller than the wavelength of visible light.
- Forces such as van der Waals, electron resistance and magnetic forces play more dominant roles than do gravitational forces or inertia.
- Very high surface-to-volume ratio, i.e. large fractions of surface atoms, and thus surface properties dominate bulk properties.
- Nanoparticles improve many of the desired properties such as chemical, heat resistance, reduction in weight and opacity.
- Nanoparticle-based corrosion inhibitors have better corrosion protection efficiency than the ordinary ones.

11.1.3 Corrosion inhibition and nanoparticles

Surface chemistry research is an interdisciplinary area on the frontiers of physical chemistry and nanoscience. Residual unbalanced forces exist on the surface of a solid. As a result of these residual forces, the surface of a solid has a tendency to attract and retain molecules of other species with which it is brought into contact.

Nanoparticles can be better inhibitors, because, as the size of the particle decreases, the surface area for a given mass and hence the number of active centres increases. This ultimately leads to efficient physisorption/chemisorption of nanosized inhibitors on corroding metal surfaces. Hence better corrosion inhibition efficiency can be realized when nanoparticles are used as corrosion inhibitors.

11.2 Surface-modified nanoparticles as corrosion inhibitors

To increase the longevity of the corrosion inhibitors it is necessary to hold the corrosion inhibitors in a non-leachable form until the onset of metal corrosion triggers the release of the corrosion inhibitor. One approach would be to incorporate into the corrosion-inhibiting material a labile bond that can be disrupted by products released from the corrosion process. For most coated metals in air/water vapour environments, the galvanic corrosion cell consists of the oxidation of the metal (anode) and reduction of oxygen (in the presence of water) to form hydroxide anions (cathode). Thus, the design of carriers that protect the reactive groups of the corrosion inhibitors while the coating is curing before releasing the corrosion inhibitors in the presence of hydroxyl groups would be an attractive corrosion-inhibiting system.

Surface-modified nanoparticles are good candidates for corrosion-inhibiting additives. Nanoparticles have high surface areas (high loadings of organic corrosion inhibitors) and novel surface chemistries (enhanced chemical reactivity) and offer multiple property enhancements without trade-offs. However, there are also some practical limitations to the use of nanoparticles as corrosion inhibitors. These include cost (paints are a commodity product), accessible surface chemistry (one needs to tether the corrosion inhibitor to the nanoparticle surface) and a release mechanism.

A material known as boehmite (AlOOH) fulfils the needs of a carrier for organic corrosion inhibitors (see Section 11.6 for different types of carriers). Commercially available boehmite is available for $2 to $3 per pound and has a high surface area (250 fm^2/g). Furthermore, commercial boehmite can easily be converted from its delivered form (30–50 micron agglomerates) to individual (40–70 nm) nanoparticle crystallites in water. Nanoparticle boehmite also has a rich and readily accessible surface chemistry.[3] Finally, the bond between a carboxylate and the boehmite particle surface is cleavable by hydroxide anions. Thus, boehmite particles that are surface-modified with carboxylic acids can serve as on-demand releasable carriers for corrosion inhibitors if the inhibitor is bound to the boehmite surface through a pH-cleavable carboxylate bond.[4] Recent modelling studies have found that the pH dependence of the inhibitor release is a critical factor in optimizing the effectiveness and service life of a functional coating.[5] This type of corrosion-inhibiting mechanism prevents premature depletion of the inhibitor reservoir of the coating.

11.3 Cerium-activated nanoparticles as corrosion inhibitors

The use of silane formulations for the pre-treatment of metallic substrates prior to painting has been increasing during recent years and some commercial formulations are available in the market of pre-painted galvanized steels. These formulations are very attractive because they present environmental friendliness, enhance adhesion to different paint systems due to the possibility of surface chemistry tailoring and provide a barrier layer that delays the corrosion processes. The modification of hybrid silane films or hybrid sol–gel coatings with different additives in order to introduce corrosion inhibition properties in their bulk has been reported in recent literature.[6–11] The modification of sol–gel coatings with organic inhibitors demonstrated positive effects on their protective performance.[6] Environmentally compliant inhibitors like $Ce(NO)_3$, $NaVO_3$ and Na_2MoO_4 were incorporated into a Zr-epoxy sol–gel.[7] The corrosion behaviour of aluminium substrates treated with sol–gel systems containing cerium ions demonstrates that cerium can inhibit the corrosion processes.[8] Literature[9] also reports that hybrid silica sol–gel coatings containing Ce^{3+} ions behave as conversion coatings on metallic zinc substrates. The anticorrosive performance of the Ce^{3+} ions entrapped in the hybrid silica sol–gel network occurs by means of the inhibitor effect and the self-repairing mechanism (probably associated with $Ce(OH)_3$ precipitation).[9]

The electrochemical behaviour of galvanized steel substrates pre-treated with bis-(triethoxysilylpropy1) tetrasulfide silane (BTESPT) solutions modified with SiO_2 or CeO_2 nanoparticles activated with cerium ions has been investigated. The electrochemical behaviour of the pre-treated substrates was evaluated via electrochemical impedance spectroscopy in order to assess the role of the nanoparticles in the silane film resistance and capacitance. The ability of the Ce-activated nanoparticles to mitigate corrosion activity at the microscale level in artificially induced defects was studied via scanning vibrating electrode technique (SVET). Complementary studies were performed using potentiodynamic polarization. The results show that the presence of nanoparticles reinforces the barrier properties of the silane films and that a synergy seems to be created between the activated nanoparticles and the cerium ions, reducing the corrosion activity. The addition of CeO_2 nanoparticles was more effective than the addition of SiO_2 nanoparticles.[12]

A new approach for the formation of 'smart' self-healing anticorrosion coatings based on silica nanoparticles layer by layer-coated with *polyelectrolyte* molecules, acting as nanoreservoirs for corrosion inhibitors, incorporated in the hybrid sol–gel protective coatings, is proposed in literature.[10] These nanoreservoirs improve corrosion protection of coated aluminium substrates and provide effective storage of the inhibitor and prolonged release 'on demand' to the damaged areas, conferring active corrosion protection with self-healing ability. The next section outlines different such nanostructure/nanoparticle carriers of corrosion inhibitors.

11.4 Functionalized nanoparticles and nanostructures as carriers

Nanostructured carriers improve the efficiency of corrosion inhibitors/biocides. The advantages are:

- Nanoparticles and nanostructures can serve as excellent carriers for inhibitors.
- Organic inhibitor, inorganic inhibitor and mixed inhibitor carriers are possible.
- Controlled and triggered release of inhibitors can be built in.

Figure 11.1 schematically represents different nanostructured carriers. As an example, noteworthy properties of nanostructured boehmite[1] to function as effective carriers are:

- Pores are accessible to water without organic burnout.
- Surface area of 260 m^2/g.
- Tunable hydrophobicity.
- Nanoporous carriers can be prepared without corrosion inhibitors and then be filled with inhibitors later.
- 'Burned-out' nanostructures can also be filled with corrosion inhibitors.
- Release rate controlled by pore size and pore hydrophobicity.

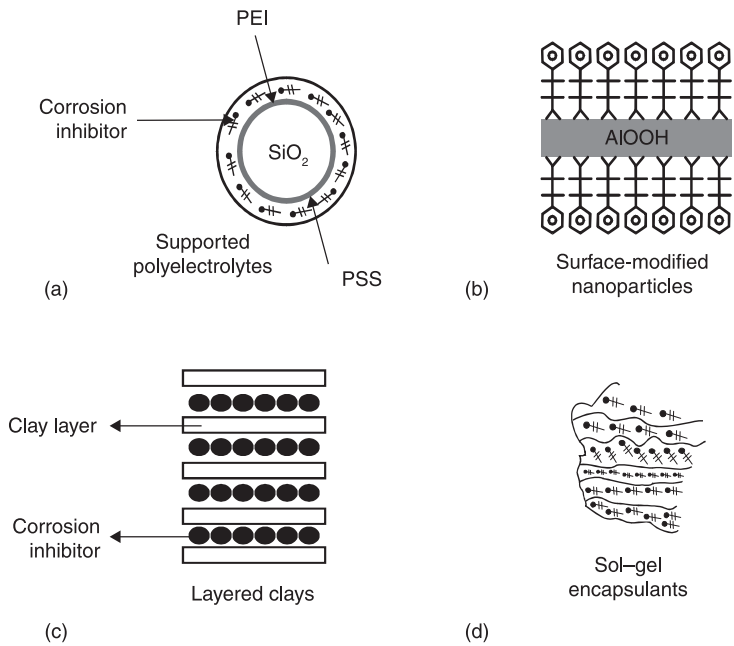

11.1 Types of nanostructured carriers: (a) supported polyelectrolytes; (b) surface-modified nanoparticles; (c) layered clays; (d) sol–gel encapsulants; (e) boehmite nanoparticle carriers; (f) nanostructured boehmite carriers.

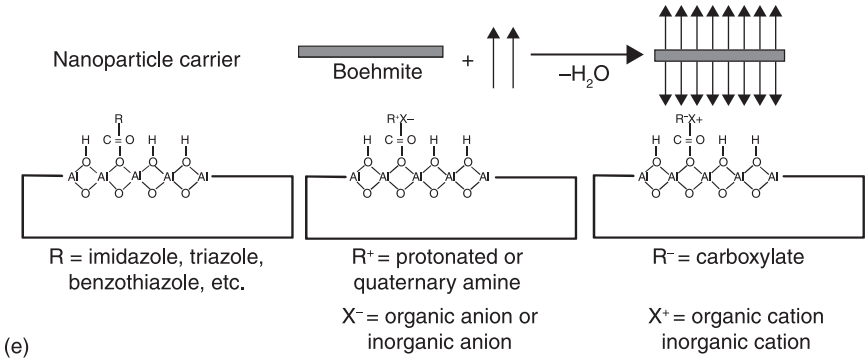

(e)

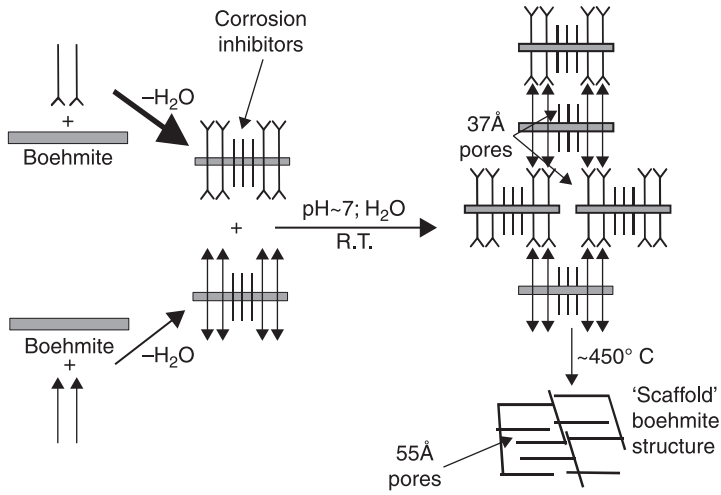

(f)

11.1 Continued.

Carboxyl groups can be anchored on boehmite particles (Fig. 11.1(e)) and they may be released on demand by change in pH, especially by hydroxide anions generated during the corrosion process. The anchored inhibitors can also be released by change in pore size which can be achieved by variation in temperature (Fig. 11.1(f)). Thus, the inhibitors remain in the coating until needed and when corrosion occurs they release, migrate to the metal surface and arrest corrosion (Fig. 11.2). Current inhibitors are selected to be slightly soluble in water, and slowly but continually leach out of the coating. In contrast, the new corrosion inhibitor additives are released only when needed to arrest corrosion. This smart release-on-demand mechanism extends the life of the coating, since the inhibitors are not being continually lost.[13]

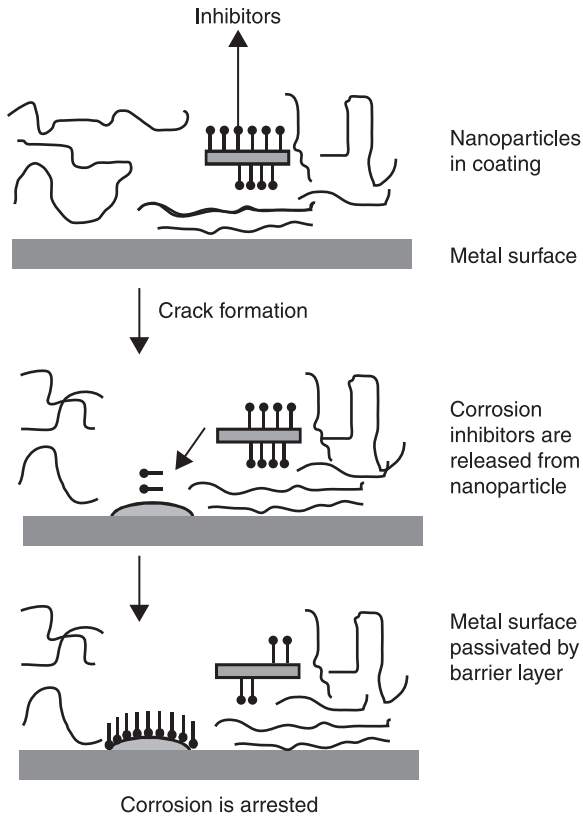

11.2 Corrosion arrested by release of corrosion inhibitor.

11.5 Nanoparticle-based biocides

Marine microbiological corrosion is responsible for considerable damage to all devices and vessels immersed in seawater, and this poses serious economic problems to maritime activities.[14–16] Employing effective antifouling marine paints containing booster biocides at non-toxic levels is one approach to solving the issue of fouling.[17–19] Copper and its oxides are common biocides in a large number of commercial antifouling marine paints. Commercially available antifouling coatings have cuprous oxide (Cu_2O) as the primary biocide, which typically varies from 20% to 76% copper content;[20] however, recent reports have shown that 26% of sampling locations/year in the UK exceeded the concentration of current Environmental Quality Standard (5 µg/l)[21] for copper,[22] and marine microalgae were able to take up copper very quickly in natural coastal seawater.[23]

Besides Cu, other metals such as zinc and silver exhibit antifungal and antibacterial properties and have been widely utilized in advanced coating

technologies.[24–28] Furthermore, silver has a remarkably low toxicity compared with other heavy metal ions,[29,30] which makes it possible to manufacture more environmentally friendly antimicrobial paint additives than copper. Recent studies proved that the biocidal activity of the common biocides increased significantly with the decrease in particle size.[31–35] Nanosilver particles have low toxicity, which makes them an environmentally friendly antimicrobial paint additive.

Similarly to the inhibitors, biocides also can be released on demand using nanostructured carriers. The leaching rate of biocides should not be too fast, which would result in rapid and premature depletion of the antifouling activity of marine coatings and an unnecessarily high concentration in the sea. However, the release rate should not be too slow, since this would undoubtedly result in fouling.[36] In order to deal with both issues, the application of core–shell nano/microstructured materials was investigated, since the shells offer protection to the cores and introduce new properties to the hybrid structures.[37–39] Up to the present time there have only been a few reports exploring marine corrosion protection based on core–shell structures employing biocides and corrosion inhibitors;[40–42] however, there are still challenges, such as the stability of core–shell particles, uniform dispersity in a matrix and control of the release rate. Ke *et al.* have successfully prepared monodispersed Ag/SiO_2 core–shell nanoparticles with a facile pathway.[43] Ag/SiO_2 core–shell nanoparticles within the size of 60 nm were applied to marine antimicrobial corrosion coatings.

Transmission electron microscopy and X-ray diffraction results indicated that the silver was completely covered by silica, and that its crystal form was not affected after being coated by silica. The effects of Ag/SiO_2 nanoparticles in the microbial corrosion of acrylic-coated steel were studied by means of electrochemical noise analysis (ENA). ENA results reveal that 1 wt% Ag/SiO_2 nanoparticles exhibit better antimicrobial corrosion activity than conventional 40 wt% Cu_2O biocides. Inductively coupled plasma optical emission spectrometry (ICP) showed very low numbers of Ag ions leaching from the matrix resin, whereas there was a much higher volume of copper ions leaching from the resin in the same period. It was concluded that Ag/SiO_2 core–shell nanoparticles could enhance long-term corrosion protection in comparison with the copper biocides. This composite has a great potential use in environmentally friendly antimicrobial coatings.[44]

11.6 Self-assembled nanofilms as corrosion inhibitors

Self-assembled monolayers (SAMs) are a powerful, simple and highly flexible means of functionalizing a solid surface. SAMs can be spontaneously formed by the immersion of an appropriate substrate into a solution of reactive molecules in an organic solvent. A SAM is composed of a large number of molecules with an active head group that chemisorbs onto a substrate, a tail group that interacts with the free surface of the film and a spacer (backbone) chain group that connects the

head and tail groups.[45,46] SAMs are versatile and have many potential applications in a number of areas such as non-wetting surfaces, lubrication, corrosion inhibition, biocompatible surfaces, monolayer lithography, etc.[45–47]

Typical SAMs, such as alkanethiols reacted with gold and alkylsilanes reacted with silica, have been studied extensively, as demonstrated by numerous reports in the literature.[45] Studies of the properties of n-alkanoic acids reacted with oxidized aluminium[48, 49] and alkyl phosphonic acids with tantalum oxide[47,50] surfaces can also be found in the literature. However, although some information is available in the literature on the behaviour of phosphonic acid SAMs,[51–57] which are one of the important classes of self-assembling organic molecules on a range of metal oxide surfaces, there is not much information reported on phosphonate SAMs on Cu in the public domain.[58–61] SAMs can be formed on various surfaces such as nickel oxide, copper oxide, iron oxide, etc.

11.6.1 Self-assembling on nickel surfaces

Nickel is a key component in the electronics industry, where it is utilized in diodes, wires and switches and as an important alloying constituent in many biomaterials.[62–69] In spite of the spontaneous formation of a nickel oxide layer under ambient conditions,[70–72] the use of nickel can cause corrosion-related issues. In electronic applications, the corrosion of the surface leads to reduced performance and device lifetime.[66,73–75] In biomedical applications, corrosion leads to Ni ion release into the body and nickel toxicity.[63,73,76,77] Therefore, forming an organic thin film on nickel oxide may serve as an effective barrier to corrosion. This is in large part due to the flexibility that SAMs offer:[78–85] they form structurally well-defined films on the solid surface and they can be deposited by a number of easy techniques such as immersing the substrate in solution, aerosol spraying and vapour deposition. Currently, immersion coating is the most popular and widely studied method for monolayer formation.[86–89]

SAMs of alkylphosphonic acids (butylphosphonic acid, octylphosphonic acid, undecylphosphonic acid and octadecylphosphonic acid) on native nickel oxide allow substrates to be functionalized easily. Monolayer formation has been investigated by diffuse reflectance Fourier transform infrared spectroscopy, non-contact mode atomic force microscopy, contact angle measurements and matrix-assisted laser desorption ionization mass spectrometry. Cyclic voltammetry and electrochemical impedance spectroscopy studies showed that the monolayer increased surface resistance to oxidation.[90]

11.6.2 Self-assembling on copper surfaces

Formation of SAMs on Cu substrates has attracted attention for both fundamental and applied research, e.g. corrosion inhibition[91–95] of Cu used in microelectronic device fabrication.[96] Cu is destined to replace Al alloy as the principal very-large

or ultra-large scale integration (VLSI/ULSI) interconnection material due to its lower electrical and thermal resistivity and greater resistance to electromigration. Despite these advantages, one of the major barriers to using it as an interconnection material is its susceptibility to corrosion. The efficiency, power output and steady-state operation of micro/nanoelectromechanical (MEMS/NEMS) devices can be critically influenced by adhesion, friction and wear.[97–102] The necessity for an ultra-thin lubricant film to minimize adhesion, friction and wear between the surfaces is thus clear. One of the lubricant systems used for this purpose is that of SAMs.

SAM films have been formed on oxidized Cu substrates by reaction with 1H,1H,2H,2H-perfluorodecylphosphonic acid (PFDP), octadecylphosphonic acid (ODP), decylphosphonic acid (DP) and octylphosphonic acid (OP). The presence of alkylphosphonate molecules, PFDP, ODP, DP and OP, on Cu was confirmed by contact angle measurement (CAM) and X-ray photoelectron spectroscopy (XPS). The PFDP/Cu and ODP/Cu SAMs were found to be very hydrophobic, having water sessile drop static contact angles of more than 140°, while DP/Cu and OP/Cu have contact angles of 119° and 76°, respectively. PFDP/Cu, ODP/Cu, DP/Cu and OP/Cu SAMs were studied by friction force microscopy, a derivative of atomic force microscopy (AFM), to better understand their micro/nanotribological properties. PFDP/Cu, ODP/Cu and DP/Cu had comparable adhesive force, which was much lower than that for unmodified Cu. ODP/Cu had the lowest friction coefficient, followed by PFDP/Cu, DP/Cu and OP/Cu, while unmodified Cu had the highest.

XPS data gave some indication that a bidentate bond forms between the alkylphosphonate molecules and the oxidized Cu surface. Such hydrophobic phosphonate SAMs could be useful as corrosion inhibitors in micro/nanoelectronic devices and/or as promoters for anti-wetting, low adhesion surfaces.[103] The proposed type of bonding for SAM of a phosphonic acid molecule (OP) is illustrated in Fig. 11.3. It appears that chemisorption of phosphonates on oxidized Cu relies on the hydroxylation of the oxide layer and that the phosphonate undergoes a condensation reaction with surface-bound copper-hydroxyl (–Cu–OH) species to form copper-phosphonate and H_2O as a byproduct: $R–PO–(OH)_2+ -Cu–OH \rightarrow R – (OH)OP–O–Cu -+H_2O$.

The advantages of copper have rapidly established it as one of the main materials for wire bonding as an alternative to gold in microelectronic packaging.[104,105] Wire bonding is the commonly used method to connect the chip to the outside world in microelectronic packaging.[106] Reduced cost, enhanced device speed and improved reliability of a monometallic system are the primary drivers of the emergence of Cu–Cu processes.[106] Ho *et al.* carried out extensive studies on copper wire bonding to copper bond pads.[105] Copper wire bonding is normally formed by a copper ball onto a copper-based bond pad in the microelectronic package. Copper bond pad oxidizes readily and the oxide continues to grow in thickness. As oxidation of copper bond pad is the main issue, this is being looked into when it is still at the wafer stage.[105] During soldering, it

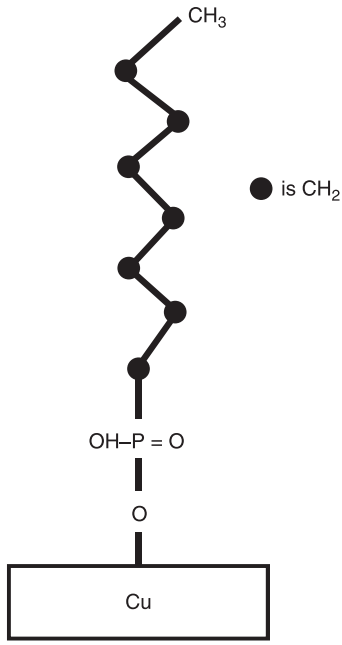

11.3 Schematic illustration of the proposed type of bonding for SAM of n-octylphosphonic acid (OP).

is a common practice to use a flux to remove any oxide layers or other contaminants from the surfaces of the metals to be joined.[107] Most fluxes consist of organic or inorganic acids, which, at the high temperature of the soldering process, chemically remove the oxides, exposing the clean, reactive metal surface. The flux residue contains ionic contaminants such as copper and tin ions and unused acidic components, which, if left on the circuit board, can cause corrosion of joints and electrical shorting due to electromigration.[107–109]

Laibinis and Whitesides reported that alkanethiols adsorbed on a copper surface form densely packed SAMs, which were found to be effective inhibitors of copper corrosion in air.[109] Feng *et al.* reported the corrosion protection of self-assembled alkanethiol monolayer on copper in a 0.5 M NaCl solution.[110] Aramaki and co-workers reported that the maximum efficiency of the SAM of octadecanethiol for protection of corrosion of copper in 0.5 M Na_2SO_4 solution was 80.3%.[111] Quan *et al.* studied the protection ability of the SAMs of Schiff bases on copper surfaces.[112,113]

SAM protects the copper bond pad surface until it is removed by the ultrasonic energy during wire bonding. The mechanism of formation of the ball bond involves the removal of the SAM by the ultrasonic energy in the first step and then the formation of welded interface in between the deformed ball and the bond pad.[105] Liu and Hutt studied SAM of octadecanethiol as preservative to enable

fluxless soldering of copper substrates.[107] Preservation of copper surfaces to enable fluxless soldering involves the etching of the copper surface in the first step to remove the native oxide, followed by the application of an organic monolayer that acts as a barrier to the diffusion of oxygen, enabling the material to be stored in air for a longer period. During the soldering process, the coating is displaced by the temperature rise and by the molten solder, revealing an oxide-free active surface that can be protected from re-oxidation by the use of an inert atmosphere.[107]

5-Methoxy-2-(octadecylthio)benzimidazole (MOTBI) monolayer was self-assembled on a fresh copper surface obtained after etching with nitric acid at ambient temperature. The optimum conditions for formation of SAM were methanol as solvent, 10 mM concentration of the organic molecule and an immersion period of 24 hours. The MOTBI SAM on the copper surface was characterized by CAM, XPS and reflection absorption Fourier transform infrared (FTIR) spectroscopy, and it is inferred that chemisorption of MOTBI on copper surface is through nitrogen. The corrosion protection ability of MOTBI SAM was evaluated in aqueous NaCl solution using impedance, electrochemical quartz crystal nanobalance, potentiodynamic polarization and weight-loss studies. While bare copper showed a charge-transfer resistance (R_{ct}) value of 1.89 kΩcm^2 in 0.20 M NaCl aqueous environment, the R_{ct} value for a SAM-covered copper surface is 123.4 kΩcm^2. The MOTBI SAM on copper afforded a corrosion inhibition efficiency of 98–99% in NaCl solution in both the concentration range and temperature range studies. The SAM functions as a cathodic inhibitor. Quantum chemical calculations showed that MOTBI has relatively small ΔE between highest occupied molecular orbital (HOMO) and lowest occupied molecular orbital (LUMO) and large negative charge in its benzimidazole ring, which facilitate the formation of a polymeric [Cu^+-MOTBI] complex on the copper surface.[114]

SAMs are utilized to prevent the electromigration and surface scattering of copper atoms while minimizing the resistance of the interconnect lines.[115] Electromigration and surface diffusion are prevented because the organic layer is covalently bound to the metal atoms in the metal interface. Additionally, the organic molecules in the organic layer are relatively large and will help hold the metal atoms in place, because it is virtually impossible for metal atoms to migrate when covalently bound to large organic molecules.

11.6.3 Self-assembling on iron and carbon steel surfaces

The self-assembling process has been investigated to improve the corrosion inhibition of iron.[116,117] Iron is a widely used metal with extensive industrial applications, and the study of its corrosion inhibition has attracted much attention.[118,119] The first work to use self-assembled films on iron for corrosion protection was self-assembling alkanethiols.[120] But the application of thiol compounds is limited because of their toxicity.[121] Felhosi *et al.*[121] studied the

formation of self-assembled films of alkane monophosphonic acids on iron surface and explained its mechanism of corrosion protection.

SAM films formed by gold nanoparticles on an iron surface have been proven to confer corrosion-inhibiting properties on the iron substrate in 0.5 M H_2SO_4 solutions. The SAMs formed by gold nanoparticles protected with sodium oleate conferred better corrosion protection on the iron substrate than the sodium oleate only. In addition, it was found that the gold nanoparticles could influence the nickel electroless plating films on the iron substrate. The structure and composition of the plating films were tested by electron probe microanalyser (EPMA). The mechanisms of the formation of the films and the nickel electroless plating reaction have been discussed.[122]

As an example of SAMs, corrosion inhibition by self-assembled films formed by adipic acid (AA) molecules on carbon steel surfaces is discussed below.[123] SAMs of AA were formed on iron oxide/carbon steel surfaces by the immersion coating method. The metal was immersed in an aqueous solution containing 60 ppm of Cl^- (to initiate the corrosion process and the formation of iron oxide) in the absence and presence of adipic acid. The formation, uniformity, ordering and bonding of the monolayers accomplished by the immersion method have been evaluated by FTIR and AFM. The electrochemical properties of the unmodified and modified carbon steel surfaces were characterized by polarization study and EIS analysis to test the ability of the monolayer to reduce the corrosion of the surface.

Well-ordered SAMs of adipic acid were formed on the iron oxide/carbon steel surface by the immersion method. This leads to ordered, robust monolayers bound to the surface in a tetradentate manner, since adipic acid is a dicarboxylic acid. Carbon steel was immersed in an aqueous solution containing 60 ppm of Cl^- and 50 ppm of adipic acid for 5 minutes, and was then taken out and rinsed in distilled water and heated in a hot air oven. The adipic acid monolayer on the iron oxide/carbon steel surface can withstand rinsing with water, concentrated acid and base exposure. Additionally, these monolayers are stable over the course of at least 1 week.

Fourier transform infrared (FTIR) and atomic force microscopy (AFM) results

The presence of two peaks (2811 and 2726 cm^{-1}) in the region of 2700 to 3000 cm^{-1}, corresponding to ν CH_2 sym and ν CH_2 unsym, indicated that the self-assembled monolayer film formed on metal surface (modified substrate) is stable, well ordered and strongly bound to the surface. The shifting of ν C = O and ν OH of the two carboxyl groups of adipic acid (1715 to 1597 cm^{-1}; 3417 to 3414 cm^{-1} respectively) confirmed that adipic acid molecules are bound to the surface in a tetra dentate manner.

The root mean square (RMS) roughness values of the film formed on the surface after immersion in various test solutions are given in Table 11.1. The

Table 11.1 The RMS roughness values of the films (SAMs) formed on iron oxide/metal surface immersed in various test solutions

Test solution	RMS roughness (nm)
Cl^- (60 ppm)	12.0558
Cl^- (60 ppm) + AA (50 ppm)	11.8833

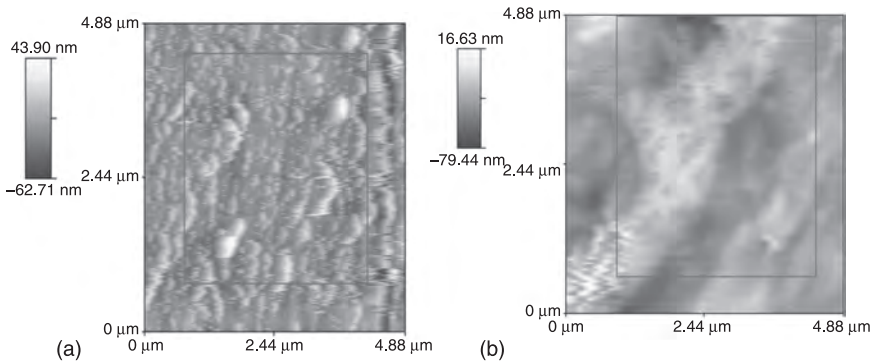

11.4 AFM topography images of carbon steel immersed in various test solutions: (a) 60 ppm Cl^- ; (b) 60 ppm Cl^- + 50 ppm adipic acid.

comparison of the RMS roughness of the unmodified substrate with the modified samples is an indicator of the film's uniformity. The RMS roughness parameter is a measure of the deviations in surface from the mean plane within the sampling area.[124] Modified surfaces with a RMS roughness similar to the control surface are considered to be films of monolayer thickness that follow the contours of the surface, while modified surfaces that have much larger RMS roughness than the control are multilayer or non-uniform films.[125,126] It is seen from Table 11.1 and Fig. 11.4 that control and modified surfaces have similar RMS roughness of 12 nm. Hence it is concluded that adipic acid molecules self-assembled on the surface forming a monolayer.

Electrochemical studies

The potentiodynamic polarization curves of carbon steel immersed in an aqueous solution containing 60 ppm of Cl^- in the absence and presence of adipic acid are shown in Fig. 11.5. The corresponding corrosion parameters are given in Table 11.2. Increase in linear polarization resistance (LPR) and decrease in corrosion current in the presence of adipic acid indicate the corrosion protection nature of SAMs of adipic acid. EIS of carbon steel immersed in an aqueous solution containing 60 ppm of Cl^- in the absence and presence of 50 ppm of adipic

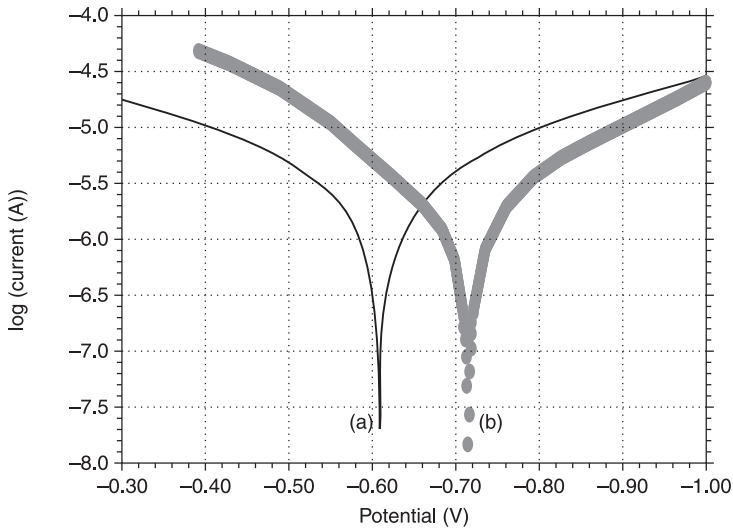

11.5 Polarization curves of carbon steel immersed in various test solutions: (a) 60 ppm Cl^- (Nyquist); (b) 60 ppm Cl^- + 50 ppm adipic acid.

Table 11.2 Corrosion parameters of carbon steel immersed in an aqueous solution containing 60 ppm of Cl^-

AA (ppm)	E_{corr} (mV vs SCE)	b_c (mV/decade)	b_a (mV/decade)	LPR (ohm cm^2)	I_{corr} (A/cm^2)
0	–609	183	189	23319.1	1.735×10^{-6}
50	–715	166	157	26664.4	1.315×10^{-6}

Table 11.3 Impedance parameters of carbon steel immersed in an aqueous solution containing 60 ppm of Cl^-

AA (ppm)	Nyquist Plot		Bode Plot
	R_t (ohm cm^2)	C_{dl} (F/cm^2)	log (Z) (ohm)
0	1225	4.1632×10^{-9}	3.119
50	2249	2.2677×10^{-9}	3.493

acid is shown in Fig. 11.6. The corrosion parameters are given in Table 11.3. In the presence of 50 ppm of adipic acid, charge transfer resistance value (R_t) and impedance increase while double layer capacitance value (C_{dl}) decreases. It is concluded from this study that SAMs of adipic acid molecules have a corrosion-preventive nature. The results indicated that adipic acid monolayers adsorbed on

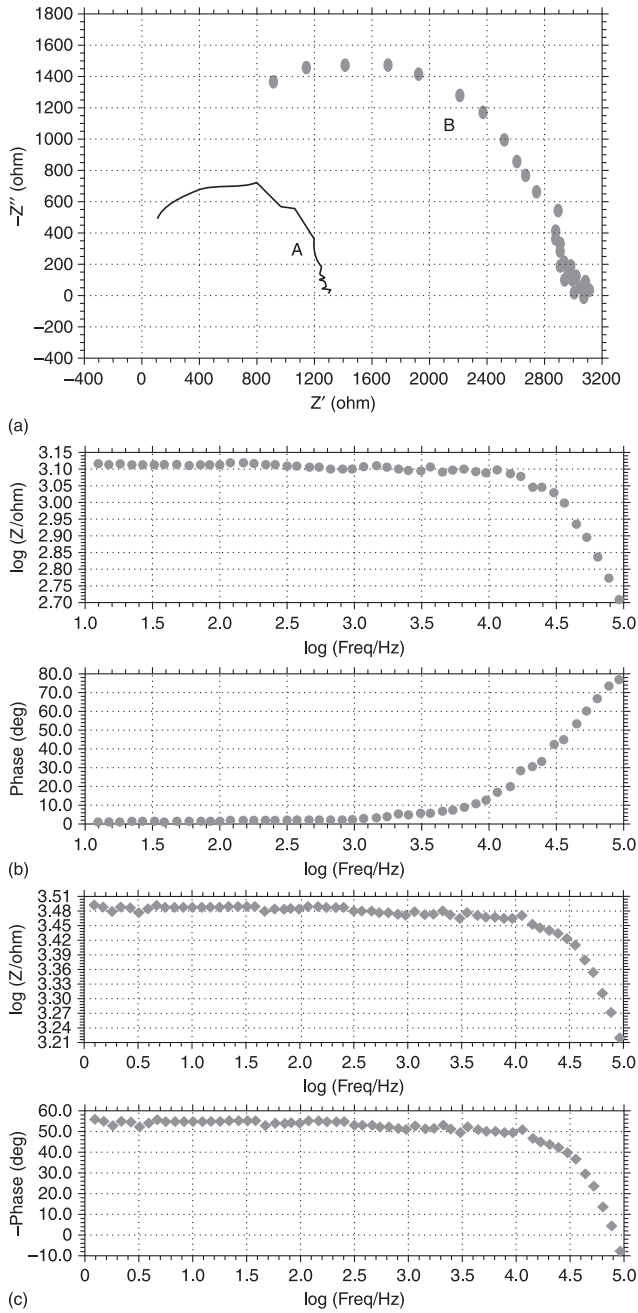

11.6 Electrochemical impedance spectra of carbon steel immersed in various test solutions: (a) A = 60 ppm Cl^- (Nyquist); B = 60 ppm Cl^- + 50 ppm adipic acid (Nyquist); (b) 60 ppm Cl^- (Bode); (c) 60 ppm Cl^- + 50 ppm adipic acid (Bode).

iron oxide can reduce electrochemical activity on the surface, often the first step in corrosion.

Monolayer formation on the iron oxide surface is a significant advance in surface modification of iron oxide and can be used as a building block for future application in corrosion barriers and electronics.

11.7 Conclusions

Nanostructured materials are good carriers for organic corrosion inhibitors, which can be smartly released on demand, thereby improving the longevity of the corrosion-protected structures. Self-assembled monolayers formed on a metal oxide/metal have potential application in corrosion inhibition as they react spontaneously on the metal surface and form compact and stable films, which are noted for their hydrophobicity.

11.8 References

1. R. L. Cook and J. Elliot, Army Corrosion Summit, Clearwater Beach FL, February 2–5, 2009 TDA Research Inc., Wheat Ridge, CO 80033 http://www.tda.com.
2. V. S. Saji and J. Thomas, *Current Science*, **92** (2007), 51.
3. R. L. Cook, B. J. Elliott, S. DeVito-Luebben, A. W. Myers and B. M. Smith, 'Surface modified particles by multi-step Michael-type addition and process for the preparation thereof', United States Patent 6,887,517, 2005.
4. R. L. Cook, 'Releasable corrosion inhibitor compositions', United States Patent 6,933,046, 2005.
5. H. Wang, F. Presuel and R. G. Kelly, 'Computational modelling of inhibitor release and transport from multifunctional organic coatings', *Electrochimica Acta*, **49** (2004), 239.
6. N. N. Voevodin, V. N. Balbyshev, M. Khobaib and M. S. Donley, *Prog. Org. Coat.*, **47** (2003), 416.
7. L. S. Kasten, J. T. Grant, N. Grebasch, N. Voevodin, F. E. Arnold *et al.*, *Surf. Coat. Technol.*, **140** (2001), 11.
8. A. Pepe, M. Aparicio, S. Cere and A. Duran, *J. Non-Cryst. Solids*, **348** (2004), 162.
9. M. Garcia-Heras, A. Jimenez-Morales, B. Casal, J. C. Galvan, S. Radzki *et al.*, *J. Alloys Compd.*, **380** (2004), 219.
10. D. G. Shchukin, M. Zheludkevich, K. Yasakau, S. Lamaka, M. G. S. Ferreira *et al.*, *Adv. Mater.*, **18** (2006), 1672.
11. V. Palanivel, Y. Huang and W. J. van Ooij, *Prog. Org. Coat.*, **53** (2005), 153.
12. M. F. Montemor and M. G. S. Ferreira, *Electrochimica Acta*, **52** (2007), 6976.
13. J. Elliott and R. Cook, Tri-Service corrosion conference, 2007, Department of Defense, USA, pp 1–7.
14. R. L. Townsin, *Biofouling*, **19** (2003), 9.
15. S. Kiil, C. E. Weinell, M. S. Pedersen and K. Dam-Johanssen, *Ind. Eng. Chem. Res.*, **40** (2001), 3906.
16. J. D. Adkins, A. E. Mera, M. A. Roe-Short, G. T. Pawlikowski and R. F. Brady, *Prog. Org. Coat.*, **29** (1996), 1.
17. I. Omae, *Chem. Rev.*, **103** (2003), 3431.
18. D. M. Yebra, S. Kiil and K. D. Johansen, *Prog. Org. Coat.*, **50** (2004), 75.

19. O. Iguerb, C. Poleunis, F. Mazeas, C. Compere and P. Bertrand, *Langmuir*, **24** (2008), 12272.
20. K. Schiff, D. Diehl and A. Valkirs, *Mar. Pollut. Bull.*, **48** (2004), 371.
21. N. Voulvoulis, M. D. Scrimshaw and J. N. Lester, *Appl. Organomet. Chem.*, **13** (1999), 135.
22. P. Matthiessen, J. Reed and M. Johnson, *Mar. Pollut. Bull.*, **38** (1999), 908.
23. M. T. S. D. Vasconcelos and M. F. C. Leal, *Environ. Sci. Technol.*, **35** (2001), 508.
24. E. L. Mann, A. Nathan, W. M. James and W. C. Sallie, *Limnol. Oceanogr.*, **47** (2002), 976.
25. S. V. Avery, N. G. Howlett and S. A. Radice, *Appl. Environ. Microbiol.*, **62** (1996), 3960.
26. Z. M. Antonietta, Z. Stefania, P. Rebecca and B. J. Riccardo, *Inorg. Biochem.*, **35** (1996), 291.
27. P. K. Stoimenov, R. L. Klinger, G. L. Marchin and K. J. Klabunde, *Langmuir,* **18** (2002), 6679.
28. Y. Yoichi, Y. Hiroshi, K. Chikara and I. Kei, *Prog. Org. Coat.*, **42** (2001), 150.
29. M. Kawashita, S. Toda, H. M. Kim, T. Kokubo and N. Masuda, *J. Biomed. Mater. Res.*, **66** (2003), 266.
30. M. S. A. S. Shah, T. Kalagara, S. Singh and S. Manorama, *Chem. Mater.*, **20** (2008), 2455.
31. N. C. Cady, J. L. Behnke and A. D. Strickland, *Advanced Functional Materials*, 21:n/a. doi:10:1002/adfm. 201100123.
32. H. L. Karlsson, P. Cronholm, J. Gustafsson and L. Moller, *Chem. Res. Toxicol.*, **61**(9) (2008), 1726.
33. K. Midander, P. Cronholm, H. L. Karlsson, K. Elihn, L. Moller, C. *et al.*, *Small*, **5** (2009), 389.
34. A. B. Smetana, K. J. Klabunde, G. R. Marchin and C. M. Sorensen, *Langmuir*, **24** (2008), 7457.
35. S. Pal, Y. K. Tak and J. M. Song, *Appl. Environ. Microbiol.*, **73** (2007), 1712.
36. L. Shtykova, C. Fant, P. Handa *et al.*, *Prog. Org. Coat.*, **64** (2009), 20.
37. O. G. Tovmachenko, C. Graf, D. J. Heuvel *et al.*, *Adv. Mater.*, **18** (2006), 91.
38. H. Sakai, T. Kanda, H. Shibata *et al.*, *J. Am. Chem. Soc.*, **128** (2006), 4944.
39. R. T. Tom, A. S. Nair, N. Singh *et al.*, *Langmuir*, **19** (2003), 3439.
40. S. R. White, N. R. Sottos, P. H. Geubelle *et al.*, *Nature*, **409** (2001), 794.
41. S. H. Cho, H. M. Andersson, S. R. White *et al.*, *Adv. Mater*. **18** (2006), 997.
42. D. G. Shchukin, S. V. Lamaka, K. A. Yasakau *et al.*, *J. Phys. Chem. C*, **112** (2008), 958.
43. X. Ke, J. X. Wang, X. L. Kang and J. F. Chen, *Mater. Lett.*, **63** (2009), 31.
44. Y. Le, P. Hou, J. Wang and J.-F. Chen, *Materials Chemistry and Physics*, **120** (2010), 351.
45. A. Ulman, *An Introduction to Ultrathin Organic Films: From Langmuir Blodgett to Self-Assembly*. San Diego, CA: Academic, 1991.
46. A. Ulman, *Chem. Rev.*, **96** (1996), 1533.
47. D. Brovelli, G. Hahner, L. Ruiz, R. Hofer, M. Textor *et al.*, *Langmuir*, **15** (1999), 4324.
48. D. L. Allara and R. G. Nuzzo, *Langmuir*, **1** (1985), 45.
49. D. L. Allara and R. G. Nuzzo, *Langmuir*, **1** (1985), 52.
50. M. Textor, L. Ruiz, R. Hofer, A. Rossi, K. Feldmann *et al.*, *Langmuir*, **16** (2000), 3257.
51. M. J. Pellerite, T. D. Dunbar, L. D. Boardman and E. J. Wood, *J. Phys. Chem. B*, **107** (2003), 11726.

52. I. L. Liakos, R. C. Newman, E. McAlpine and M. R. Alexander, *Surf. Interface Anal.*, **36** (2004), 347.
53. E. Hoque, J. A. DeRose, P. Hoffmann, H. J. Mathieu, B. Bhushan and M. Cichomski, *J. Chem. Phys.*, **124** (2006), 174710.
54. E. Hoque, J. A. DeRose, G. Kulik, P. Hoffmann, H. J. Mathieu and B. Bhushan, *J. Phys. Chem. B*, **110** (2006), 10855.
55. E. Hoque, J. A. DeRose, P. Hoffmann, B. Bhushan and H. J. Mathieu, *J. Phys. Chem. C*, **111** (2007), 3956.
56. T. W. Kelley, L. D. Boardman, T. D. Dunbar, D. V. Muyres, M. J. Pellerite *et al.*, *J. Phys. Chem. B*, **107** (2003), 5877.
57. B. Adolphi, E. Jahne, G. Busch and X. Cai, *Anal. Bioanal. Chem.*, **379** (2004), 646.
58. T. Keszthelyi, Z. Paszti, T. Rigo, O. Hakkel, J. Telegdi, L. *et al.*, *J. Phys. Chem. B*, **110** (2006), 8707.
59. M. M. Antonijevic and M. B. Petrovic, *Int. J. Electrochem. Sci.*, **3** (2008), 1.
60. W. Guo, S. Chen, and H. Ma, *J. Serb. Chem. Soc.*, **2** (2006), 167.
61. G. John and V. Alsten, *Langmuir*, **15** (1999), 7605.
62. P. Baraldi and G. Davolio, *Mater. Chem. Phys.*, **21** (1989), 143.
63. S. A. Shabalovskaya, *Bio-Med. Mater. Eng.*, **12** (2002), 69.
64. H. H. Huang, *J. Biomed. Mater. Res. Part A*, **74A** (2005), 629.
65. C. C. Shih, S. J. Lin, Y. L. Chen, Y. Y. Su, S. T. Lai *et al.*, *J. Biomed. Mater. Res.*, **52** (2000), 395.
66. Z. Mekhalif, J. Delhalle, J. J. Pireaux, S. Noel, F. Houze and L. Boyer, *Surf. Coat. Technol.*, **100–1** (1998), 463.
67. N. Shevchenko, M. T. Pham and M. F. Maitz, *Appl. Surf. Sci.*, **235** (2004), 126.
68. M. D. Irwin, D. B. Buchholz, A. W. Hains, R. P. H. Chang and T. J. Marks, *Proc. Natl. Acad. Sci. U. S. A.* (2008), 1.
69. M. W. Xu, S. J. Bao, and H. L. Li, J. *Solid State Electrochem.*, **11** (2006), 372.
70. R. J. Mckay, *Ind. Eng. Chem.*, **15** (1923), 555.
71. L. C. Flowers and J. B. Kelley, *Ind. Eng. Chem.*, **42** (1950), 719.
72. R. J. McKay, *Ind. Eng. Chem.*, **28** (1936), 1391.
73. B. Clarke, W. Carroll, Y. Rochev, M. Hynes, D. Bradley and D. Plumley, *J. Biomed. Mater. Res. Part A*, **79A** (2006), 61.
74. H. C. Lee, S. H. Son, K.-Y. Hwang and C.-H. Lee, *Ind. Eng. Chem. Res.*, **45** (2006), 3412.
75. Y. Lee, G. M. Morales and L. Yu Angew, *Chem. Int. Ed.*, **44** (2005), 2.
76. S. D. Plant, D. M. Grant and L. Leach, *Biomaterials*, **26** (2005), 5359.
77. V. C. Dinca, S. Soare, A. Barbalat, C. Z. Dinu, A. Moldovan *et al.*, *Appl. Surf. Sci.*, **252** (2006), 4619.
78. F. S. Damos, R. C. S. Luz and L. T. Kubota, *Langmuir*, **21** (2005), 602.
79. H. O. Finklea, in: R. A. Meyers (Ed.), *Self-Assembled Monolayers on Electrodes*. Morgantown: John Wiley & Sons Ltd, 2004, p. 1.
80. M. S. Wang, L. B. Palmer, J. D. Schwartz and A. Razatos, *Langmuir*, **20** (2004), 7753.
81. J. G. V. Alsten, *Langmuir*, **15** (1999), 7605.
82. F. Frederix, K. Bonroy, W. Laureyn, G. Reekmans, A. Campitelli *et al.*, *Langmuir*, **19** (2003), 4351.
83. G. K. Jennings, C. M. Jeffrey, T.-H. Yong and P. E. Laibinis, *Langmuir*, **14** (1998), 6130.
84. W. S. Dillmore, M. N. Yousaf and M. Mrksich, *Langmuir*, **20** (2004), 7223.
85. D. H. Lee, D. Kim, T. Oh and K. Cho, *Langmuir*, **20** (2004), 8124.

86. B. R. A. Neves, M. E. Salmon, P. E. Russell and J. E. B. Troughton, *Langmuir*, **17** (2001), 8193.
87. A. Raman, M. Dubey, I. Gouzman and E. S. Gawalt, *Langmuir*, **22** (2006), 6469.
88. A. Raman and E. S. Gawalt, *Langmuir*, **23** (2007), 2284.
89. M. M. Sung, K. Sung, C. G. Kim, S. S. Lee and Y. Kim, *J. Phys. Chem.*, **B104** (2000), 2273.
90. R. Quinones, A. Raman and E. S. Gawalt, *Thin solid films*, **516** (2008), 8774.
91. C. M. Whelan, M. Kinsella, H. M. Ho and K. Maex, *J. Electrochem. Soc.*, **151** (2004), B33–B38.
92. Y. S. Tan, M. P. Srinivasan, S. O. Pehkonen and S. Y. M. Chooi, *J. Vac. Sci. Technol. A*, **22** (2004), 1917.
93. R. Tremont, H. De Jesus-Cardona, J. Garcia-Orozco, R. J. Castro and C. R. Cabrerea, *J. Appl. Electrochem.*, **30** (2000), 737.
94. A. M. Skolnik, W. C. Hughes and B. H. Augustine, *Chem. Educator*, **5** (2000), 8.
95. P. E. Laibinis and G. M. Whitesides, *J. Am. Chem. Soc.*, **114** (1992), 9022.
96. J. W. Rose, *Power Energy: Proc. Inst. Mech. Eng. Part A*, **215** (2002), 115.
97. B. Bhushan, *Springer Handbook of Nanotechnology* (2nd ed.). Heidelberg: Springer-Verlag, 2007.
98. N. S. Tambe and B. Bhushan, *Nanotechnology*, **16** (2005), 1549.
99. B. Bhushan, *Tribology Issues and Opportunities in MEMS*. Dordrecht: Kluwer Academic Publishers, 1998.
100. B. Bhushan, *J. Vac. Sci. Technol. B*, **21** (2003), 2262.
101. B. Bhushan and H. Liu, *Nanotechnology*, **15** (2004), 1785.
102. B. Bhushan, *Nanotribology and Nanomechanics – An Introduction*. Heidelberg: Springer-Verlag, 2005.
103. E. Hoque, J. A. Derose, B. Bhushan and K. W. Hipps, *Ultramicroscopy*, **109** (2009), 1015.
104. Minges, L. Merrill, *Electronic Materials Handbook, Vol. 1: Packaging*. Materials Park, OH: ASM International, 1989.
105. H. M. Ho, W. Lam, S. Stoukatch, P. Ratchev, C. J. Vath III and E. Beyne, *Microelectron. Reliab.*, **43** (2003), 913.
106. C. M. Whelan, M. Kinsella, L. Carbonell, H. M. Ho and K. Maex, *Microelectron. Eng.*, **70** (2003), 551.
107. C. Liu and D. A. Hutt, *IEEE Trans. Compon. Packag. Technol.*, **29** (2006), 512.
108. C. T. Wang, S. H. Chen, H. Y. Ma, L. Hua and N. X. Wang, *J. Serb. Chem. Soc.*, **67** (2002), 685.
109. P. E. Laibinis and G. M. Whitesides, *J. Am. Chem. Soc.*, **114** (1992), 9022.
110. Y. Q. Feng, W. K. Teo, K. S. Siow, Z. Q. Gao, K. L. Tan *et al*. *J. Electrochem. Soc.*, **144** (1997), 55.
111. Y. Yamamoto, H. Nishihara and K. Aramaki, *J. Electrochem. Soc.*, **140** (1993), 436.
112. Z. Quan, X. Wu, S. Chen, S. Zhao and H. Ma, *Corrosion*, **57** (2001), 195.
113. Z. Quan, S. Chen, X. Cui and Y. Li, *Corrosion*, **58** (2002), 248.
114. B. V. Appa Rao, M. Y. Iqbal and B. Sreedhar, *Electrochmica Acta*, **55** (2010), 620.
115. D. H. Gracias, U. S. Patent, 6,858,527, February 22, 2005.
116. B. H. Sohn, J. M. Choi, S. Yoo and S. H. Yun, *J. Am. Chem. Soc.*, **125** (2003), 6368.
117. C. Wang, S. Chen, H. Ma and C. S. Qi, *J. Appl. Electrochem.*, **33** (2003), 179.
118. G. Lendvay-Gyorik, L. Meszaros, G. Meszaros and B. Lengyel, *Corros. Sci.*, **42** (2000), 79.
119. K. F. Khaled and N. Hackerman, *Electrochim. Acta*, **48** (2003), 2715.

120. K. Nozawa, H. Nishihara and K. Aramaki, *Corros. Sci.*, **39** (1997), 1625.
121. I. Felhosi, J. Teleddi, G. Palinkas and E. Kalman, *Electrochim. Acta*, **47** (2002), 2335.
122. H. Ma, S, Chem, G. Liu, J. Xu and M. Zhou, *Applied Surface Science*, **252** (2006), 4327.
123. S. Rajendran, V. Sribarathi, A. Krishnaveni, M. Manivannan, J. Jeyasundari *et al.*, Zastita Matesijala 52(2011) 163.
124. J. J. Workman, M. Koch and D. J. Veltkamp, *Anal. Chem.*, **75** (2003), 2859.
125. R. Quinones, A. Raman and E. S. Gawalt, *Surf. Interface Anal.*, **39** (2007), 593.
126. A. Faucheux, A. C. Gouget-Laemmel, C. D. Villeneuve, R. Boukherroub, F. Ozanam *et al.*, *Langmuir*, **22** (2006), 153.

12

Sol–gel nanocoatings for corrosion protection

S. S. PATHAK and A. S. KHANNA,
Indian Institute of Technology Bombay, India

Abstract: Recent research on combating corrosion and oxidation of metals has been focused on nanotechnological principles. Sol–gel coating is one outcome of nanotechnology able to tailor both the corrosion protection properties of bulk coatings and the metal oxide/polymer interface chemistry. Organic–inorganic hybrid coatings are of special interest because they combine properties of organic polymers (hydrophobicity, flexibility and functional compatibility with organic paint systems) with those of inorganic ceramics (scratch resistance, durability and adhesion to the metal substrate). Several sol–gel coatings are commercially available for a variety of engineering metallic substrates and for a wide range of applications in mild to severe corrosive environments. Sol–gel coatings are desirable for their environmental friendliness, high performance, compatibility with existing coating application technologies and for the on-demand simplicity of tailoring coating properties.

Key words: sol–gel coating, silane, corrosion resistant coating, nanocoating, environmentally friendly coating.

12.1 Introduction

Metals and alloys are widely used engineering materials and can be found in manufacturing, construction, transportation, medical and other applications. Corrosion deteriorates material integrity and aesthetic value, and impacts economic assets and the environment if left unmonitored and uncontrolled. In the most common usage of the word, corrosion means the loss of an electron of metal to a reaction with either water or oxygen in its surroundings. The nature of corrosion depends on the alloyed elements, metallurgical processing parameters and severity of the environment. Corrosion or corrosion-causing events generally start from the surface of metals. Atoms or molecules at the surface of a metal/alloy are exposed to a different environment from those in the body of the metal/alloy and thus have different free energies, electronic states, reactivities, mobilities and structures. There are many conventional technologies available to mitigate the corrosion, which either enhance the inherent corrosion resistance and performance of the metal/alloy itself (e.g. better alloy composition and metal processing parameters), reduce the corrosiveness of the operating environment or modify the interface between the metal/alloy and its surroundings (e.g. corrosion inhibitors, coatings and surface treatment). These countermeasures can be used individually or synergistically in the practices of managing corrosion.

There are many corrosion-resistant coating systems available on the market today, but none have been completely successful in preventing corrosion; there has always been a question mark over the reliability of some critical features of the coatings, such as adhesion to the substrate, precise control over surface morphology and uniformity, and resistance to water permeation. For over a decade scientists and researchers in the fields of corrosion and coatings have turned to nanotechnology in a constant effort to be more precise in explaining the natural phenomena of corrosion at the molecular or nano level (10^{-9} meter). This has become an imperative because it offers a never-before-seen glimpse into interactions on a biological cell level. The application of nanotechnology has produced numerous invaluable materials and coatings to prevent or minimize corrosion degradation.

This chapter reviews the nanotechnological approaches to corrosion protection of metal through sol–gel based coatings. Critical features of sol–gel coatings are discussed along with examples of coating systems for a variety of engineering metals and alloys.

12.2 Nanotechnology in coatings

Nanotechnology has been employed to (i) enhance the natural corrosion resistance and performance of the metal/alloy itself, by achieving a desired finely crystalline microstructure (e.g. nanocrystallization) or by modifying its chemical composition at the nanometric scale (e.g. formation of copper nanoparticles at the steel grain boundaries), and (ii) develop coatings and inhibitors with tailored properties. The schematic in Fig. 12.1 briefly summarizes the use of nanotechnology in managing corrosion. Production of high performance steel with a fine-grain structure and/or self-organization of strengthening nanophases (carbides, nitrides, carbonitrides,

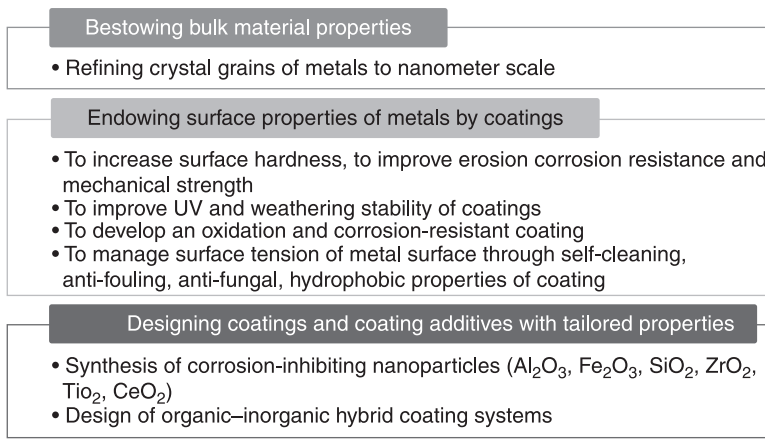

12.1 Domains where nanotechnology principles are used in enhancing natural corrosion resistance of metals or surface modification of metals.

intermetallides) is a critical example of a nanotechnological approach in making corrosion-resistant alloys.[1] Nanoscience has also been engaged to reduce the impact of corrosive environments through the alteration of the metal/corrosive electrolyte interface using metallic coatings and non-metallic coatings (e.g. formation of nanocomposite coatings on steel). Significant advancement in the corrosion protection of metals has been reported through the co-deposition of nanocomposite coatings (e.g. Ni–SiC nanocomposite coatings on steel, Ni–Al_2O_3 nanocomposite coatings on mild steel and application of ZrO_2 and TiO_2-nanoparticle sol–gel coatings).[2–4] The incorporation of nanosized particles (e.g. polyaniline/ferrite, ZnO, Fe_2O_3, halloysite clay and other nanoparticles) into conventional polymer coatings significantly enhances the anti-corrosive performance of such coatings on various substrates like steel, aluminum, copper and magnesium.[5]

There are now many nano-based coating formulations currently in use or under research and development. Sol–gel derived nanocoatings are one of the most fascinating because of their demonstrated or anticipated unique properties compared with conventional materials. Sol–gel coatings have been found to have controllable synthesis, homogeneity of matrix and easily tailored properties (e.g. resistance to corrosion, high-temperature oxidation, hydrophobicity, UV resistance, scratch resistance and anti-fouling). At this stage, we have covered broad examples of nanotechnology-based corrosion protection approaches effective in improving the natural corrosion resistance of alloys as well as in developing surface coatings (e.g. nanoparticle-doped polymer coatings, sol–gel coatings).

Before going into details, it is necessary to understand the physical dimensions of nanoscience or nanotechnology. There are two broad definitions:[6]

- In solid-state material systems, interest in physical size in nanoscience starts where normally invariant structural and physical properties start changing with size. When material is at nanoscale, macroscopic materials characteristics (e.g. dielectric constant and specific thermodynamic state functions) are no longer valid. This often occurs while the material system contains a sufficiently large number of atoms or molecules so that a first principles atomic scale model of the system is infeasible.
- A nanomaterial is one with at least characteristic size between 1 and 100 nm. There are indeed characteristics of materials and materials systems that, when extended or scaled to the nanolevel, lead to improved properties as conceptually simple (or scalable) extensions of properties from larger-sized systems.

It has been established that both of these definitions will apply to coatings with components of nanometer size. Nanostuctured materials are of a scale to which our normal understanding of material properties no longer applies. Murday[7] proposed that there are three reasons why nanostructured materials behave somewhat differently from other materials: (i) large surface-to-volume or

interface-to-volume ratios, (ii) size effects and (iii) quantum effects. These factors (changes in the energy level due to quantum effect and grain size at the nanometer scale) are considered to have significant effects on corrosion and the reactivity of nanostructured materials. Today we have the ability to make uniform nanoscale coating components and include them in a coating system of complex hierarchical structures, one that permits a new level of control over the physical and chemical properties of macroscale coating. The sol–gel based coating process has great potential to produce coatings with special properties and create new types of functional systems that can take best advantage of the size-adjustable properties of their nanosized components. There are several types of corrosion-resistant sol–gel coatings in uses ranging from decorative to high-performance engineering applications. The reasons behind the widespread exploitation of sol–gel coatings are summarized as follows:

- Sol–gel coatings can be produced with compositions that are not obtainable by other means.
- Sol–gel enables integrated multilayering at a lower cost than vacuum techniques.
- Sol–gel can be easily combined with other methods of coating synthesis and coating application processes to put down coatings on substrates from sol–gel solution.
- Sol–gel coatings are environmentally friendly and can be synthesized and applied at low temperature (close to room temperature).
- Sol–gel processes can be used to form nanostructured films (typically 200 nm to 10 μm in overall thickness) that are more resistant than metals to oxidation, corrosion erosion and wear.

12.3 Sol–gel coatings: historical perspective and chemistry

12.3.1 History of sol–gel coating development

Coatings are one of the most important and the most commercially available products utilizing sol–gel processes. Sol–gel processing produces coating materials with better purity and homogeneity compared with conventional high-temperature processes. The sol–gel process creates an oxide network by progressive condensation reactions of molecular precursors in a liquid medium;[8] it is a chemical synthesis technique that was initially used for the preparation of glasses and ceramics. Roy *et al.*[9–11] first discovered the method of synthesizing ceramic oxides (a popular silicate powder) by the sol–gel method. In 1971 Chiola *et al.*[12] synthesized low-bulk density silica by hydrolyzing tetraethoxysilane (TEOS) in the presence of cationic surfactants. Sol–gel technology in the coating world attracted more attention (in the mid-1980s) when Schmidt *et al.*[13–15] synthesized organic–inorganic hybrid materials using a sol–gel process.

12.3.2 Sol–gel chemistry: precursors and reactions

Precursors

The traditional precursors for sol–gel reactions have been metal alkoxides. In most of the sol–gel coating formulations, metal alkoxides/organofunctional metal alkoxides are used either alone or in combination with a conventional polymer capable of participating in sol–gel reactions. Sol–gel reactions start with a solution of monomeric metal or metalloid alkoxide precursors $M(OR)_n$ in an alcohol or other low-molecular-weight organic solvent. Here, M refers to a network-forming element such as Si, Ti, Zr, etc, and R is typically an organic moiety.[16–17]

Reactions

A sol–gel process is a two-step inorganic polymerization that involves hydrolysis and condensation reaction of metal alkoxides (Fig. 12.2 and 12.3). In the first step, polymerization starts by hydrolysis at the metal–alkoxy linkage yielding alcohol and new reactants, hydroxylated metal centers (M-OH). In the second step, condensation or three-dimensional propagation occurs when hydroxylated species condense to form oxypolymers (M-O-M). Polycondensation involves alkoxylation, oxolation or olation, a reaction that creates oxygen bridges and releases water or alcohol species.

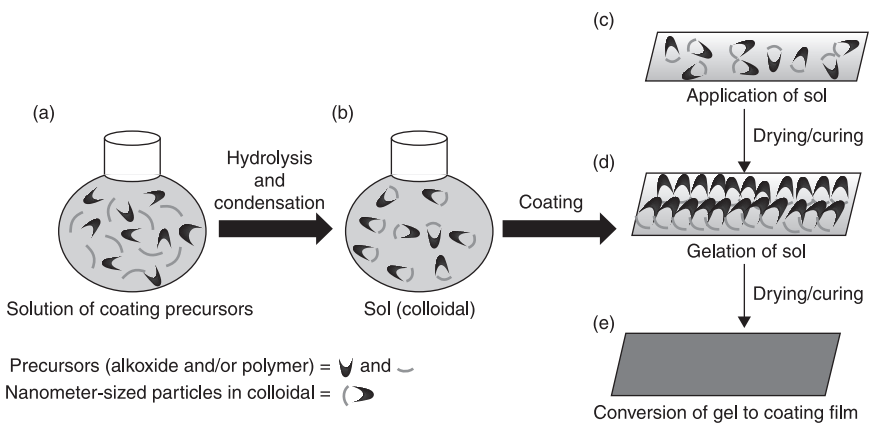

12.2 Various stages of sol–gel coating preparation and application to substrate: preparation of solution of coating precursors (a), formation of sol through hydrolysis of precursors followed by progressive condensation reactions (b), application of sol on the metal substrate (c), gelation of sol on substrate which results in the formation of a three-dimensional network throughout the liquid medium (d) and conversion of gel into solid coating film after drying/curing (e).

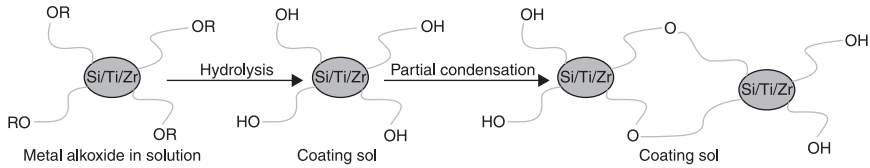

12.3 Schematics of sol–gel reactions indicating hydrolysis of silicon (Si), titanium (Ti) and zirconium (Zr) alkoxides followed by condensation of hydrolyzed moieties during coating sol formulation.

Step I: $M(OR)_n + xH_2O \rightarrow [M(OR)_{n-x}(OH)_x] + {}_xR\text{-}OH$ . . . . . .(Hydrolysis)

Step II: $M\text{-}OH + RO\text{-}M \rightarrow M\text{-}O\text{-}M + ROH$ . . . . . (Condensation)

$M\text{-}OH + HO\text{-}M \rightarrow M\text{-}O\text{-}M + HOH$ . . . . . (Condensation)

12.3.3 From sol (coating solution) to gel (coated film)

Nanoparticles of any solid dispersed in any liquid in such a way that the solid phase does not spontaneously precipitate or settle out are considered a sol. A sol can become a gel when the solid nanoparticles dispersed in it can join together to form a network of particles that spans the liquid. This requires that the solid nanoparticles in the liquid stick together. As the sol becomes a gel, its viscosity approaches infinity and finally becomes immobile. This transition from sol to gel is called gelation. The point in time when the particle network extends across the entire volume of the liquid, causing it to immobilize, is called the gel point.

Coating (sol) formulation and its conversion to coating film (after gelation) on substrate follows the same principle of sol to gel transition discussed above. If a sol of coating precursors is allowed to start to gel on the substrate, a coating film on the substrate can be formed from the gel. It is important to apply the sol on the substrate before gelation starts, which will also facilitate better adhesion of the coating to the substrate. Figure 12.4 shows a schematic of the sol–gel process of coating formulation and deposition on metal substrates.

12.3.4 Factors to be considered during sol–gel coating formulations

Formulation of a coating, in general, is one of the most influential factors on its end performance. Along with coating recipes, the rate of hydrolysis and condensation reactions also have significant impact on the stability and pot life of sol (coating solution) and coating properties. By controlling the reaction conditions, these reactions may lead to a variety of coating structures with desirable properties. The rates of hydrolysis and condensation reactions are

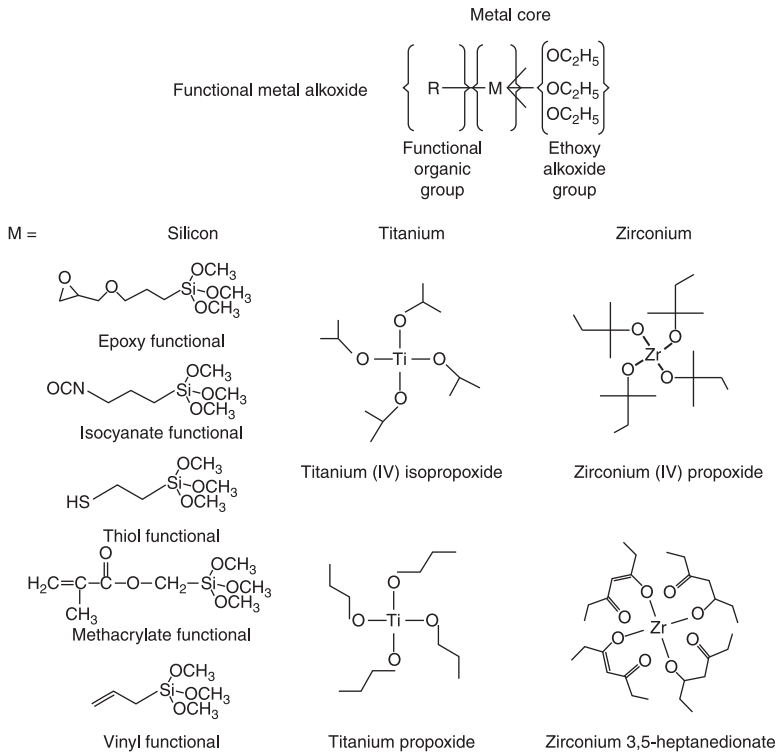

12.4 Organic–inorganic hybrids (functional metal alkoxide) conventionally used in sol–gel coatings.

considered to be affected by the nature of the ligand (e.g. Si, Ti, Zr, etc), pH, nature of the solvent, temperature, reaction time, catalysts and agitation of the sol.

12.3.5 Types of sol–gel coatings

Inorganic sol–gel coatings

Inorganic sol–gel coatings consist of only metal/oxygen (Si-O, Zr-O, Ti-O) networks and are widely used for enhancement of the oxidation and corrosion stability of metals such as stainless steel, aluminum and copper. Various sol–gel thin films of SiO_2, ZrO_2, SiO_2/TiO_2, ZrO_2/Y_2O_3 and Al_2O_3 have been produced for corrosion protection of metals.[18] For example, aluminum oxide (Al_2O_3) sol–gel film can be prepared from solutions of hydrolyzed aluminum-tri-sec-butoxide in methoxyethanol on steel. While all of these coatings showed promising corrosion resistance, unfortunately poor interfacial adhesion, shrinkage and oxidation of the substrate remained a problem. These coatings also often fail if the film is thicker than about 1 μm because of the damaging shrinkage strains during drying and densification.

Inorganic–organic hybrid based sol–gel coatings

Conventional organic coatings tend to age within 2 to 3 years and need to be stripped and repainted. It has been well observed that siloxanes suffer from adhesion loss during service and organic polymers suffer from susceptibility to weathering and UV radiation. Covalent insertion of hard inorganic microdomains, such as alkylsiloxane fragments, inside an organic polymeric network leads to attractive materials with good thermal and photostability, resistance to weathering and good adhesive properties.

Organic–inorganic hybrid coatings can be defined as coatings combining the properties of both organic and inorganic coatings in a domain of nanometric scale. The development of organic–inorganic materials was made possible by the sol–gel process. There are two different groups of organic–inorganic coating materials. In group I, hybrids with weak interactions (hydrogen, van der Waals or ionic bonds) between the organic and inorganic parts are considered; in group II, the organic and inorganic parts linked by strong bonds (covalent and iono-covalent bonds). The chemical structure of the hybrid (group I or group II) determines the critical properties, i.e. the mechanical and tribological properties, of these materials. The range of coatings currently used for corrosion protection belongs to two main classes: (i) silicon-containing compounds (i.e. alkylalkoxysilanes as pre-polymers or oligomeric siloxanes), and (ii) organic polymers. Some examples of organic–inorganic hybrids are shown in Fig. 12.4.

12.4 Critical features of sol–gel coatings for corrosion protection

12.4.1 Corrosion resistance

Metals and their alloys, such as iron, aluminum, copper and magnesium, have a natural tendency to form a thin layer of oxide/hydroxide on their surface. Oxide/hydroxide layers provide sufficient corrosion resistance to the metal in dry ambient conditions. Under continued exposure to moisture, these layers become thick but more porous, which makes them (oxide/hydroxide layers) no longer protective for the metal beneath. Rust formation on iron, white oxide formation on aluminum and magnesium, and tarnishing of copper are examples of corrosion.[19] Coating is one of the most frequently used methods to barricade the metal from moisture and other corrosive environmental factors.

The primary role of coatings in corrosion protection is to retard or prevent the diffusion of corrosive solution to the metal beneath the coating. Sol–gel coatings have the ability to undergo chemical reaction with natural oxide/hydroxide films on the metal substrate (Fig. 12.5 and Table 12.1) and passivate the metal surface. The hydroxyl group of hydrolyzed metal alkoxides (M(OH)x (OR)n-x or M-OH; M = Si, Ti, Zr) in coating sol forms a covalent bond with the hydroxyl group of natural oxide/hydroxide layers on the metal surface. The chemical

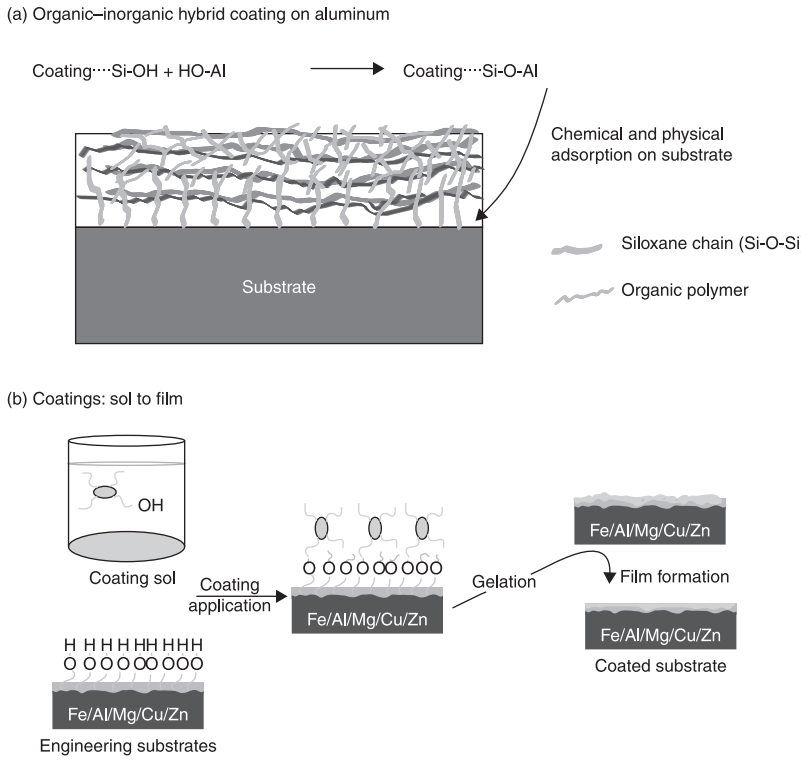

12.5 (a) Schematics of chemical bond formation between hydroxyl group on metal (iron, steel, aluminum, magnesium, copper, zinc, etc), surface and hydroxyl group (formed after hydrolysis of metal alkoxides in sol) and coating deposition on substrate; and (b) the list of processes taking place during conversion of coating solution (sol) to coating on metal surface (coating film).

Table 12.1 Metal oxides and their reaction with Si, Ti, and Zr based sol

Substrate	Anodic reaction	Natural surface oxide/ corrosion product	Reaction with substrate sol
Iron/Steel	$Fe \rightarrow Fe^{++} + 2e^-$	$Fe(OH)_2$	Fe-O-Si-, Fe-O-Ti-, Fe-O-P-Si-, Fe-O-Zr-
Aluminum	$Al \rightarrow Al^{+3} + 3e^-$	$Al(OH)_3$	Al-O-Si-, Al-O-Ti-
Magnesium	$Mg \rightarrow Mg^{+2} + 2e^-$	$Mg(OH)_2$	Mg-O-Si-, Mg-O-P-Si-
Zinc	$Zn \rightarrow Zn^{+2} + 2e^-$	$Zn(OH)_2$	Zn-O-Si-, Fe-O-Ti-, Fe-O-P-Si-
Copper	$Cu \rightarrow Cu^{+2} + 2e^-$	$Cu(OH)_2$	Cu-O-Si-, Cu-S-Si-

bonding of a sol–gel coating with a metal surface also results in better adhesion of sol–gel film to the substrate. As we know, better adhesion to the substrate is the primary requisite for proper functioning and durability of corrosion-resistant coatings. Other important features which make organic–inorganic hybrid coatings

more promising than conventional coatings are the precise control over coating thickness, homogeneity and nanostructure, hydrophobicity, scratch and abrasion resistance, and weathering stability. These properties thus have great impact on the long-term corrosion resistance of hybrid coatings. Before going into further discussion on the corrosion resistance offered by organic–inorganic hybrid coatings, we will also briefly discuss the hydrophobicity and scratch resistance stability of these coatings, with some critical examples.

12.4.2 Water repellence

Water is considered one of the key causes of corrosion and coating degradation. It also facilitates the interaction between chlorides and dissolved contaminants to the metal surface and coatings. The most effective approach to limit the effect of water on a metal surface is to lower the surface energy, and consequently the wettability, of the metal surface through water-repellent coatings. According to traditional theory, hydrophobicity shields surfaces from moisture and inhibits the electrochemical reaction of corrosion; it has already been proved that metals covered with superhydrophobic coatings exhibit better anti-corrosion properties than those covered with non-hydrophobic coatings.[20–21] The formation of a low-energy coating layer on a metal surface inhibits the penetration and interaction of water, together with contaminants, to the metal substrate. Hence, control of surface wettability yields enormously high economic and environmental benefits by preventing corrosion of metallic structures, especially in the chemical and microelectronics industries.

The hydrophobic nature of corrosion-resistant sol–gel coatings has not been sufficiently investigated, in spite of the potential technological interest. Performance of hydrophobic coatings depends upon coating stability, on the segmental reorganization whenever the coating comes in contact with water, on the molecular chains' segregation and their orientation at the polymer–air interphase, and on the polymeric network structure which controls surface and interface properties. An interesting study by Tiwari *et al.*[22] reveals that polysiloxane improves the moisture sensitivity of polyimide coatings, and that the effectiveness of polysiloxane in controlling moisture sensitivity of coatings depends on the size of the polysiloxane spheres in the coating matrix. It was proposed that moisture absorption in the polyimide coatings could be minimized by reducing the size of the polysiloxane spheres down to nanometer scale so that the maximum surface area could be achieved for the dispersed polysiloxane domain as compared with the continuous polyimide matrix. Organic–inorganic hybrid coatings have been found to impart more hydrophobic character than the inorganic sol–gel derived coatings. The presence of organic groups on metal alkoxides renders these coatings hydrophobic, making them impermeable to ions, moisture and other hydrophilic species as compared with pristine metal alkoxide based sol–gel coatings.

Sol–gel based superhydrophobic coatings exhibit extreme water repellence, with water droplets rolling off at high contact angles. Different approaches have

been described up to now in the literature for the synthesis of superhydrophobic coatings. Recently, Rao *et al.*[18] obtained a superhydrophobic coating surface on copper using methyltriethoxysilane via a sol–gel process. The coating showed the static water contact angle to be as high as 155° and the water sliding angle as low as 7°. A low sliding angle renders the surface 'non-sticky', a property that is crucial for the fabrication of water-repellent and self-cleaning surfaces. This coating not only provides improved adhesion but also acts as a barrier protection layer for minimizing the permeability of corrosive species. Some attempts have already been made to incorporate fluorsilane (3,3,3-trifluoropropyl-trimethoxysilane) in an epoxysilane–aminosilane (epoxy: 3-glycidyloxypropyl) trimethoxysilane; amine: 3-aminopropyl-methyldiethoxysilane) coating formulation to develop a hydrophobic coating.[23]

12.4.3 Scratch resistance

Excellent mechanical stability of coatings is crucial for durability, aesthetic value and protective properties. Coatings undergo various types of mechanical stresses such as wear, scratch, impact and bending during service. Two major groups of coating failure may occur during a scratch test: coating cracking and delamination. Coating cracking is mainly caused by tensile in-plane stress, while delamination is usually caused by in-plane compressive stress.[24] The scratch behavior is influenced by a combination of hardness, viscoelasticity and toughness of the coatings. To achieve optimum mechanical stability, the coating composition, microstructure and processing parameters need to be adjusted for different types of substrates under different functional constraints. The properties of sol–gel coatings can be easily modified through chemical formulation and hybridization with organic or inorganic compounds.

Belon *et al.*[25] analyzed the friction and wear properties of hybrid sol–gel coatings based on conventional epoxy resin (hydrogenated diglycidyl ether bisphenol A) mixed with an epoxy trimethoxysilane precursor such as trialkoxysilane ((3-glycidyloxypropyl)trimethoxysilane (GPMS)) or (2-(3,4-epoxycyclohexyl) ethyl)trimethoxysilane (TRIMO) in the presence of a photoacid generator (derivative of diaryliodonium salt). They reported that both the coating thickness and the addition of the hybrid monomer (silanes) tend to improve the stiffness of the pure epoxy resin; however, these two parameters also induce an increase in the dynamic friction value.

Organic–inorganic hybrid coatings based on organosilanes exhibit sufficient hardness and flexibility, adhesion and scratch resistance. The properties of organosilane coatings can be further improved by incorporating alumina, cerium oxide or zirconium oxide sol in organosilane sol during the sol–gel process. Phani *et al.*[26] developed sol–gel coatings consisting of a silica matrix embedded with nanocomposites of Al_2O_3–CeO_2 as wear, scratch resistance and corrosion resistance components for magnesium alloy substrates. Al_2O_3 and CeO_2 sol were obtained from aluminum nitrate and cerium nitrate in a pure isoproponal solvent.

Kiruthika *et al.*[27] reported the formation of hybrid coatings, derived from 3-glycidoxypropyltrimethoxysilane, zirconium-n-propoxide and methacrylic acid (MAA) based sol coatings, on mild steel.

Bautista *et al.*[28] attempted to understand how the chemical structure of the organic–inorganic hybrid influences the scratch behavior of the coatings. Three different coatings were prepared, systems with methacryloxypropyltrimethoxysilane (MAPTMS) alone or in combination with tetraethyl orthosilicate (TEOS) and 1,6-hexanedioldiacrylate (HDDA). It was found that the scratch resistances of the coatings are influenced by the presence of opened or closed polyhedral structures of the inorganic oligomer (MAPTMS and TEOS) part of the coating. The decreasing order of scratch resistance of the coatings was found to be in the following order: MAPTMS (open polyhedral structure) < MAPTMS + TEOS (open polyhedral structure) and MAPTMS + HDDA (open polyhedral structure) < methacryl POSS (closed polyhedral oligomeric silsesquioxane). The opened inorganic polyhedral decreases stiffness without loss in mechanical properties, while the presence of the closed polyhedral makes the chemical structure very tensioned. Another approach to making corrosion and scratch-resistant sol–gel coatings is the simple addition of nanoparticles (alumina, iron oxide).

12.5 Corrosion-resistant sol–gel coatings

Industry is turning towards the utilization of more and more organic–inorganic hybrid based sol–gel coatings rather than using inorganic sol–gel coatings. Organic–inorganic hybrid coatings work on the principles of (i) formation of a chemical bond between the coating and metal through hydroxyl group condensation (between a hydroxyl from natural oxide/hydroxide film on metal and a hydroxyl group formed after hydrolysis of metal alkoxide) and (ii) the creation of a three-dimensional organic–inorganic network which imparts UV and weathering resistance, and hardness with flexibility. These coatings have been found to have better adhesion than their organic and inorganic counterparts. We will restrict our discussion to organic–inorganic hybrid coatings used for most common engineering materials, such as steel, aluminum, magnesium, copper and zinc. Silane-based organic–inorganic hybrid coatings have been used for corrosion protection either alone or in combination with TiO_2, ZrO_2, Al_2O_3, CeO_2, Fe_2O_3 sol or nanoparticles.

12.5.1 Sol–gel coatings for iron and steel

Corrosion of iron or steel (anodic reaction: $Fe \rightarrow Fe^{2+} + 2e^-$ and cathodic reaction: $4Fe^{2+} + O_2 + 10H_2O \rightarrow 4Fe(OH)_3 + 8H^+$) leads to formation of surface hydroxides. The main constituents of oxides formed during atmospheric corrosion of steels are γ-FeOOH (lepidocrocite), α-FeOOH (goethite), β-FeOOH (akaganite) and δ-FeOOH (feroxyhite).[29] These hydroxyl groups in rust have a tendency to react with hydroxyl groups of hydrolyzed metal alkoxide from sol–gel coatings.

Sol–gel coatings have also been used for protecting steel due to the presence of sufficient numbers of hydroxyl groups on the steel surface. Pepe *et al.*[30] developed a tetraorthosilicate (TEOS) and methyltriethoxysilane (MTES) hybrid coating for corrosion protection of carbon steel. Chou *et al.*[31] formulated a sol–gel coating for stainless steel 304 using tetraethylorthosilicate and 3-ethylacrylicoxypropyltrimethoxy silane in acid-catalyzed reactions. Coatings acted as a physical barrier to the migration of corrosive electrolyte.

It was also found that corrosion resistance of coating with a fresh sol is better than with an aged sol. Seok *et al.*[32] investigated the protective capability of a 3-glycidyloxypropyltrimethoxysilane nanosized boehmite (AlOOH) based corrosion resistance coating for galvanized steel. Zirconia–polymethylmethacrylate hybrid (17 vol.% of polymethylmethacrylate) sol–gel coatings[33] have been found to improve the corrosion resistance of stainless steel in de-aerated H_2SO_4 (0.5 mol l^{-1}). These coatings improved the lifetime of the stainless steel by a factor of 30.

Pepe *et al.*[34] studied hybrid silica coatings containing Zn particles for low-alloy steel and galvanized metal plates. Thick, adherent and crack-free corrosion-resistant coatings containing 10% Zn particles were prepared by dip coating on carbon steel and Al/Zn coated carbon steel substrates. Yeh *et al.*[35] synthesized 3-(trimethoxysilyl)propylmethacrylate based anticorrosion coating for cold-rolled steel. The electrochemical measurement suggests that hybrid sol–gel coatings with low silica loading (e.g. 5 wt%) on cold-rolled steel (CRS) coupons were much superior in anticorrosion efficiency to those of neat PMMA based coatings. The increase of adhesion strength of sol–gel coatings on CRS coupons was attributed to the formation of Fe-O-Si covalent bonds at the interface of the coating and CRS system based on the FTIR–RAS (reflection absorption spectroscopy) studies. Lopez *et al.*[36] prepared a two-layer (inner layer: TEOS–MTES and top layer: TEOS + 3-methacryloxypropyl trimethoxysilane + 2-hydroxyethyl methacrylate) sol–gel coatings for a biocompatible AISI 316L stainless alloy used in prosthetic devices. It was observed that these coatings are stable (not damaged) in pH conditions similar to body fluid and seem to restrict the passage of potentially toxic ions to the body fluid. In another study, polysiloxane hybrid films, derived from co-polycondensation of TEOS and 3-methacryloxy propyltrimethoxysilane (MPTS), were deposited on 316 L stainless steel substrates. It was found that the film had a polysiloxane network with excellent thermal stability (410°C), corrosion resistance (TEOS/MPTS ratio of 2) and adhesion.[37]

12.5.2 Sol–gel coatings for aluminum and its alloys

When an aluminum surface is exposed to the atmosphere, it forms a natural white coloured oxide ($Al(OH)_3$) film, which is responsible for its corrosion resistance. Although this oxide film makes the aluminum surface stainless, it cannot protect the aluminum substrate under severe corrosion conditions, and therefore aluminum

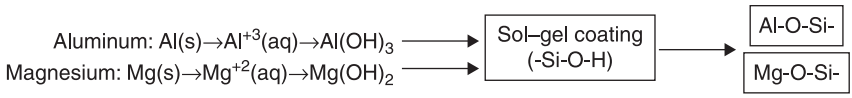

12.6 Silane based coating interaction with aluminum and magnesium.

requires protective coatings.[38] Aluminum hydroxide on an aluminum surface reacts with the hydroxyl moieties of sol–gel coatings and forms a covalent linkage between the aluminum surface and the coating (Fig. 12.6). Various silane-based sol–gel coatings have been developed for aluminum and its alloys.[39–49] It was observed that corrosion resistance of the coating is affected by formulation parameters and curing conditions such as hydrolysis water ratio, silane content, acidic or basic nature of catalyst, curing mechanism and solvent dilution.

Various types of sol–gel coatings based on SiO_2, ZrO_2, CeO_2, organofunctional metal alkoxide or combinations of these oxides have been developed to protect metallic substrates from general and localized corrosion. The protection mechanism of sol–gel coatings is based on the barrier properties. The long-term anti-corrosive properties of sol–gel film can be improved by the introduction of particles with corrosion inhibition features. In recent decades, organic inhibitors such as benzotriazole, tolytriazole or hydroxyquinoline, and inorganic inhibitors like cerium, chromium (III), molybdenum and manganese compounds, have been incorporated into sol–gel films.

Andreatta *et al.*[50] developed several ZrO_2 based pre-treatments for aluminum alloy. Feng *et al.*[51] examined the corrosion resistance of tetra-*n*-propoxyzirconium (TPOZ), with a partly hydrolysable precursor of glycidoxypropyltrimethoxysilane (GPTMS) (GPTMS/TPOZ ratio of 2.7) based sol–gel coatings on 1050 aluminum alloy. It was found that these coatings exhibit good adhesion to the etched and de-smutted alloy substrate and also significantly improve the pitting potential of the coated alloy.

Liu *et al.*[52] prepared a TEOS modified sol–gel coating using vinyltrimethoxy-silane (VMS), 3-(methacryloxy)propyltrimethoxysilane (MPMS) and 3-glycidoxypropyltrimethoxysilane (GPTMS) on a pre-treated 2024 aluminum alloy surface by dip coating. The corrosion resistance of the coated aluminum alloy and the effect of TEOS content on the corrosion resistance were evaluated by potentiodynamic polarization studies and salt spray test. Corrosion currents of VMS coating and MPMS coating were 300 times lower than those of bare samples. The anticorrosion ability of the VMS coating was strongest and decreased in the order of VMS > MPMS > GPTMS. The corrosion current of hybrid coatings was smallest when TEOS content reached 15–20%. It was found that VMS coatings have the strongest ability to resist salt spray corrosion. When cured at elevated temperatures (80°C), all of the hybrid coatings studied passed wet adhesion testing. However, water sensitivity remained for most of the room temperature cured hybrid coatings.

Pathak *et al.* developed hexamethoxymethylmelamine (HMMM)[53] and aminosilane[54] cured GPTMS and methyltrimethoxysilane (MTMS) based

waterborne organic–inorganic hybrid coatings for aluminum alloy. GPTMS–MTMS sol–gel solution was prepared by hydrolysis and condensation of GPTMS and MTMS (molar ratios 3:1). Results showed that the HMMM cured coatings were uniform, transparent and crack free. Corrosion resistance and hydrophobicity of the coating system with 20H–30H (20–30 wt% HMMM of total resin) of HMMM were found to be excellent. UV-VIS spectroscopy and UV weathering suggest that these coatings are stable in sunlight. The gloss retention for 25H coating was found to be about 83.32% without any visible pit or corrosion product. Aminosilane cross-linked coatings showed good thermal stability up to 390°C and hydrophobicity (water contact angle in the range of 59–78°) with excellent corrosion resistance. It was observed that the increase of GPTMS concentration and the number of N-H groups in aminosilane influence the corrosion resistance and hydrophobicity of coatings.

Zandi-Zand *et al.*[55] developed a hybrid coating on 1050 aluminum by hydrolysis and condensation of GPTMS and tetramethoxysilane in the presence of an acidic catalyst and bisphenol. Zandi-Zand *et al.*[56] studied the effect of aging of 3-glycidoxypropyltrimethoxysilane sol on corrosion resistance of coating and observed that fresh sol has better corrosion resistance than the aged sols. Khramov *et al.*[57] developed a set of amino silane conversion coatings by a self-assembled nanophase particle (SNAP) coating process. SNAP solution was prepared by a drop-wise addition of a mixture of silane such as tetramethoxysilane and 3-glycidoxypropyltrimethoxysilane (1:3 ratio) and an amine based epoxy ring opener such as (i) diethylenetriamine (DETA), (ii) aminopropyltrimethoxysilane, (iii) 3-(2-aminoethyl)aminopropyltrimethoxysilane or (iv) 3-(trimethoxysilyl) propyldiethylenetriamine to 0.05 M acetic acid with constant stirring for 1 hour and applied on aluminum by dip coating.

Metroke *et al.*[58] studied the effect of alkyl chain length of organosilane on corrosion resistance of coating on 2024-T3 aluminum alloy. Coatings were prepared using 0-16.6 vol.% alkyl-modified silane X_n-Si $(OR)_{4-n}$, where X = methyl, dimethyl, n-propyl, n-butyl, n-hexyl, n-octyl or i-octyl. Results showed that the corrosion resistance of coatings increases with organosilane concentration and alkyl chain length, likely due to blockage of corrosive electrolyte from substrate by alkyl groups and thereby increasing the water repellence of the coating.

Sol–gel processes incorporate corrosion inhibitors, nanoparticles and pigments in hydrolysis and condensation steps of coating synthesis, to further improve the performance or add specific properties to the coatings. Rosero-Navarro *et al.*[59] developed a cerium (III) doped sol–gel coating based on 3-methacryloxypropyl trimethoxysilane – tetraethoxysilane and colloidal SiO_2 for corrosion protection of AA2024. It was found that cerium provokes a porous structure that diminishes the barrier properties of the layers with respect to those without cerium. A self-healing sol–gel coating for anticorrosive protection of AA2024 was developed by Wang *et al.*[60] The coating was based on a cerium-doped (for the self-healing

effect) methacrylate–silica organic–inorganic hybrid, which showed excellent anticorrosive and self-healing properties.

Zheludkevich *et al.*[61] incorporated cerium nitrate as corrosion inhibitor in a zirconia nanoparticle doped sol–gel coating consisting of tetraethylorthosilicate and 3-glycidoxypropyltrimethoxysilane. Cerium nitrate, as corrosion inhibitor, was doped into the coating matrix or into the hydrolyzed tetra-*n*-propoxyzirconium (zirconiaoxide nanoparticles). It was observed that the zirconia particles present in the sol–gel coating appear to act as nanoreservoirs, providing a prolonged release of cerium ions.

Zheludkevich *et al.*[62] investigated corrosion resistance of the coating prepared by copolymerization of 3-glycidoxypropyltrimethoxysilane, tetraethylorthosilicate and tetra-*n*-propoxyzirconium on an AA2024-T3 substrate. It was observed that amorphous ZrO_2 nanoparticles (size 40–200 nm) were formed in the coating. The presence of ZrO_2 nanoparticles seems to have a pore-blocking effect in the coatings with a higher particle content. Girardi *et al.*[63] synthesized a chemically and thermally stable acrylate-based hybrid material, embedding the zirconium oxocluster $Zr_4O_4(OMc)_{12}$, where OMc = $CH_2C(CH_3)C(O)O$, for aluminum alloys. It was observed that the zirconium oxoclusters strongly interact with the acrylate matrix and a Zr-PMMM coating shows better corrosion resistance but higher water uptake than a pure PMMA coating. In a more recent attempt, various research groups around the world are working on development of a layered double hydroxide (also known as a hydrotalcite-like compound) doped sol–gel coating. It is an environmentally friendly and inexpensive option for corrosion inhibition.

12.5.3 Sol–gel coatings for magnesium and its alloys

Magnesium offers a high potential for use as a lightweight structural material and as an electromagnetic shield for electronics. However, it is the most active metal used in engineering applications and corrodes so readily in some environments that magnesium alloys serve as sacrificial anodes on structures such as ship hulls and steel pipes. Magnesium dissolves with the formation of hydrogen gas and magnesium hydroxide (Fig. 12.7), which is highly insensitive to the oxygen concentration. To improve the corrosion resistance of Mg alloys, different coating methodologies have been adopted, and sol–gel coatings are one such. Alkoxysilane-based coatings lead to the formation of self-assembled films in which the dominant feature is the presence of a very stable silicon and oxygen rich network.

Khramov *et al.*[64] synthesized hybrid organic–inorganic coatings with phosphonate functionalities and evaluated them as prospective surface treatments for magnesium materials. These coatings have been processed using a sol–gel method by hydrolysis and condensation of a mixture of diethylphosphonatoethyltriethoxysilane and tetraethoxysilane with variable molar ratios. Corrosion studies confirmed that the coating decreased the corrosion resistance of magnesium by two orders of

magnitude. Potentially, both functionalities of diethylphosphonatoethyltriethoxysilane, trialkoxysilane or trialkoxyphosphonate ester fragments are hydrolyzable. It is observed that the phosphonate groups of diethylphosphonatoethyltriethoxysilane have more affinity for the magnesium than silane head groups, and therefore the phosphonate groups react with magnesium and form P-O-Mg bonds. In addition, phosphate-based coatings perform better than pure silica coatings.

Pathak *et al.* synthesized waterborne sol–gel coatings for magnesium based on waterborne polyester[43]/polyurethane,[66] 3-glycidoxypropyltrimethoxysilane and methyltrimethoxysilane and HMMM. The coating solutions were prepared by the addition of 30 wt% of HMMM and 1 wt% of p-TSA to a mixture of polyester resin and primary sol (MTMS:GPTMS = 1:2 mol. ratios). The coatings were designated as SiPU XX_1YY_1 or SiAlk XX_1YY_1, where Si stands for organosilane in coatings, PU stands for polyurethane resin in coatings, Alk stands for alkyd resin in coatings, XX_1 stands for wt% of organosilane in coatings and YY_1 stands for wt% of polyurethane/alkyd resin in coatings. For example, SiPU 4060 stands for coating composed of 40 wt% organosilane (MTMS and GPTMS in 1:2 molar ratios) and 60 wt% of polyurethane resin; 1 wt% of p-TSA was also added for fast curing and catalyzing the sol–gel reaction. The pH of the coating solution was adjusted to make it suitable for magnesium substrate.

Scanning electron microscopy (SEM) and atomic force microscopy (AFM) confirm the continuous and crack-free coating on the magnesium substrate. The water contact angle of coatings was found to be in the range of 63–71°. It was evaluated that the coatings efficiently protected magnesium from corrosion in 3.5 wt% NaCl solutions. Figure 12.7(a–c) shows the Nyquist impedance plots of bare magnesium (Fig. 12.7(a)), SiAlk (Fig. 12.7(b)) and SiPU (Fig. 12.7(c)) coated magnesium after 30 minutes' immersion in 3.5 % NaCl. It is apparent that the diameter of the capacitive loop increased with increase in organosilane concentration in the coatings, which may be attributed to the resistance of the coatings to corrosion. This can be explained by the formation of a dense siloxane network (-Si-O-Si-) in the coating matrix which acts as a geometric barrier to the migration of water and chloride ions.

Barranco *et al.*[67] optimized the corrosion resistance of four sol–gel coating systems (inorganic, hybrid organic–inorganic, containing zirconium ions and containing cerium ions) on AZ91 magnesium alloy. The sol–gel coatings were evaluated as autonomous protective coatings as well as a pre-treatment prior to an acrylic topcoat. The coating obtained from tetramethoxysilane (TMOS) and diethoxydimethylsilane (DEDMS) as precursors and doped with Ce^{3+} was especially effective as pre-treatment for a final acrylic coating. The role of Zr^{4+} ions as active dopant of sol–gel coatings, is influenced by their coordination with chemical species present in the sol; that is, the further tendency to form other links than from Si-O-Zr in the coating network (e.g. zirconium hydroxides and/or oxides). Such new species/compounds could diminish the protective properties of the Zr-doped coating.

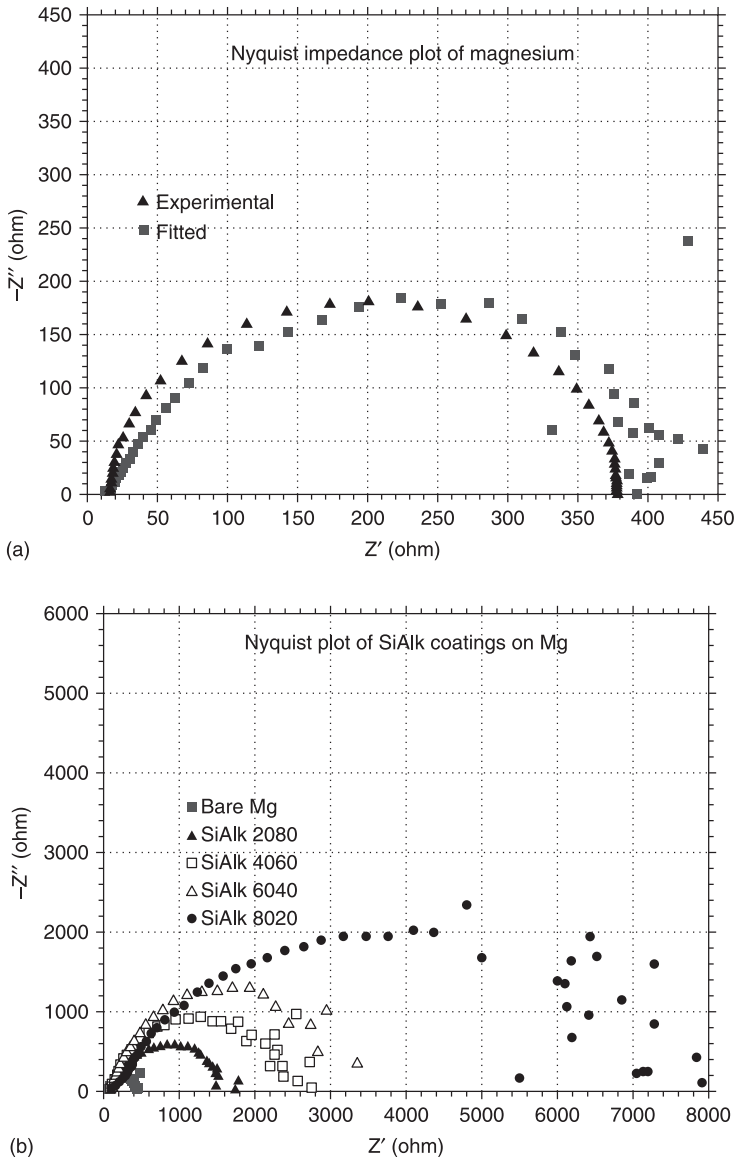

12.7 Comparative resistance of bare magnesium substrate (a), organosilane–alkyd coating, SiAlk (b), and organosilane–polyurethane coating, SiPU, (c) in 3.5% NaCl solutions; coating composition: 30 wt% of HMMM and 1 wt% of p-TSA to the mixture of polyester resin and primary sol (MTMS:GPTMS = 1:2 mol. ratios); coatings designation: SiPU XX_1YY_1 or SiAlk XX_1YY_1, where Si stands for organosilane in coating, PU stands for polyurethane resin in coating, Alk stands for alkyd resin in coating, XX_1 stands for wt% of organosilane in coating and YY_1 stands for wt% of polyurethane/alkyd resin in coating.

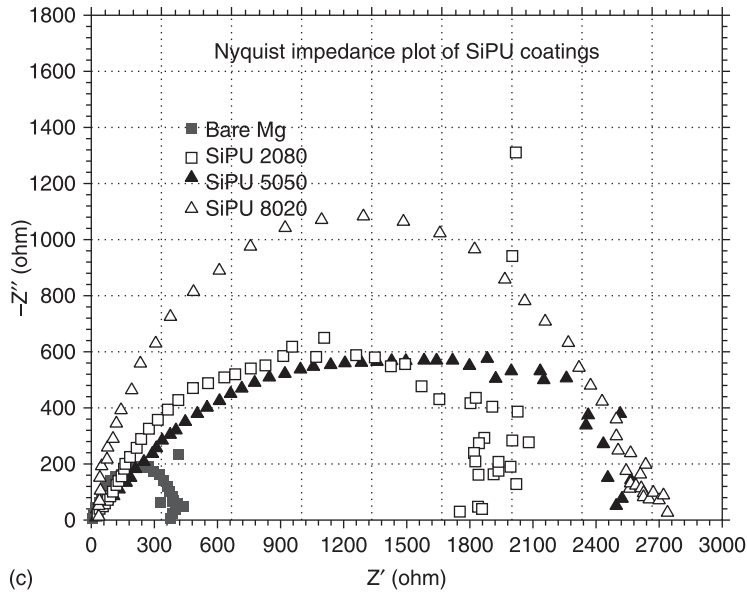

12.7 Continued.

Wang *et al.*[68] developed a scratch-resistant anticorrosion sol–gel coating for AZ31 magnesium alloy by incorporating polyaniline/silica in sol–gel film. They found that the coating has a 'self-repairing' mechanism which results from the incorporation of polyaniline in the coating. Lopez *et al.*[69] exploited the feasibility of tetraethoxysilane-based coatings on ZE41 magnesium alloy for corrosion protection.

12.5.4 Sol–gel coatings for copper

Copper is an extensively used metal in the chemical and microelectronic industries due to its high thermal and electrical conductivities, beautiful appearance and low chemical reactivity. However, copper is not stable in wet environments and undergoes oxygen reduction by forming hydroxides. At pH values below 7, the corrosion (least corrosion in pH range of 8–10) of copper becomes significant, especially below pH 5, where the formation of stable surface oxides is not possible.[38] Organothiols-based self-assembly has been widely investigated for a corrosion resistance layer on copper.[70–71] A lot of work is currently focused on the development of alkoxysilane and thiol functional alkoxysilane sol–gel coatings.

Kuan *et al.*[72] developed a thermal-cured sol–gel coating for use as a corrosion-resistant coating on copper using 3-glycidoxypropyltrimethoxysilane. It was

found that the corrosion resistance is enhanced by the addition of 3-mercaptopropyltrimethoxysilane (TPTMS), which improves adhesion of coatings to the substrate. Bescher and Mackenzie[73] studied the GPTMS and MTMS derived organic–inorganic hybrid coatings on copper and bronze surfaces. SEM images of the coated substrate showed almost no corrosion products appearing on the surfaces even after 2 years of exposure to high sulfur/humidity conditions. The GPTMS + MTMS coatings have good compatibility with a fluoropolymer coating as a topcoat, which overall improves the corrosion resistance, hydrophobicity and outdoor stability of the fluoropolymer. Li *et al.*[74] synthesized the trimethoxypropylsilane (TMPS) and bis(trimethoxysilyl)ethane (BTMSE) based organic–inorganic hybrid coating for copper by a dip coating method. Reflection and absorption infrared spectroscopy (RAIR) of coated copper substrate suggested that silanol condensation occurs in the coating films on Al and a covalent linkage exists between the TMPS film and the copper surface. The TMPS-based coating appeared to have a better affinity to Cu than to Al.

12.6 Organosilane and conventional organic polymer derived sol–gel coatings

The use of organic polymers in the manufacture of the sol–gel coatings has been considered as a consistent and continuous development of innovative sol–gel coating technology, which is characterized by the combination of novel (alkoxide or functional alkoxide-based coating) and conventional (coating based on conventional organic polymer) methods of coating formulation.[75–76] The reaction of functional alkoxide with a conventional organic polymer, as shown in Fig. 12.6, not only improves overall performance of the organic polymeric coating but also makes the organic–inorganic hybrid coating cost-effective for end users. In this section, organic–inorganic hybrid coatings prepared using conventional polymers are discussed.

12.6.1 Polyester and alkyd-based sol–gel coatings

Polyester offers flexible and scratch-resistant surfaces, but they are prone to chalking on weathering. Modification of polyesters with organosilane improves chalking and corrosion resistance, gloss retention, hardness and flexibility of the coatings. Frings *et al.*[77] developed two coating systems by sol–gel processes using a polyester–tetraethoxysilane (TEOS) and polyester–epoxy–TEOS for coil coating on pre-finish construction steel and aluminum. Two types of polyesters, namely hydroxyl-terminated and carboxyl-terminated, were used in this study. It was reported that the interaction between the organic and inorganic parts occurs via the hydroxyl end groups of polyester and the hydroxyl groups on the silanols. The influence of TEOS on the hardness of the coatings was determined and it was found that Konig hardness and T_g increase with increasing TEOS content in the

coating. The polyester–TEOS system shows an increase in hardness with increasing silica content. The acidic and basic nature of the system plays an important role in the hydrolysis of the system.

Pathak *et al.* modified the waterborne polyester,[43–44] waterborne alkyd[42] and waterborne polyurethane coating systems with an alkoxysilane such as methyltrimethoxysilane and 3-glycidoxypropyltrimethoxysilane to produce an organic–inorganic hybrid coating with improved performance for application on AA6011 aluminum alloy. Organosilane-modified waterborne polyester coatings (SiE)[44] were synthesized and applied on aluminum alloy substrates at an average coating thickness of $5 \pm 0.6\,\mu m$. The corrosion current of the SiE-coated substrate decreased by two orders of magnitude compared with the bare substrate. A significant decrease in the corrosion current was investigated for SiE coatings ($4.6–13.1 \times 10^{-7}$A), which was higher than for the polyester coating (7.8×10^{-6}A). SiE coatings were thermally stable up to 300°C with the water contact angle in the range of $64 \pm 3°$ to $73 \pm 2°$. These data indicate that the incorporation of organosilane into the polyester increased the electrical resistance of the coatings and water repellence, resulting in better corrosion protection. Thus, coatings act as barriers that restrict the diffusion of corrosive species such as water, oxygen and chloride ions towards the coating/metal interface due to the formation of a highly protective aluminum–oxygen–silicone interface at the aluminum substrate, as also indicated by FT IR study. Coatings exhibited excellent adhesion to the substrate. The pencil hardness (ASTM D 1522) of the SiE coating increased from 3H to 6H with increasing organosilane composition in the coating. This might be due to the replacement of the soft organic polymeric matrix by a hard siloxane (Si-O-Si) matrix in coatings.

Organosilane-incorporated alkyd coatings (SiAlk)[42] were developed to improve the chalking, fading, hardness and corrosion resistance of alkyd coatings. Organosilane incorporation in alkyd improved the corrosion resistance by one order of magnitude compared with a pure alkyd coating on aluminum alloy. Accelerated weathering of the coated specimen was carried out to simulate outdoor weathering using a combination of UV light and condensation (ASTM-G53). Visual examination of the exposed specimen showed that there were no white pits of corrosion product, cracking or loss of adhesion. The highest gloss retention of coating observed was 92% for 10 wt% alkyd incorporated, followed by 60 and 90 wt% alkyd coatings with gloss retention of 84% and 61%, respectively. However, yellowing of the 90 wt% alkyd incorporated coating was observed. Therefore, organosilane incorporation in alkyd improves the gloss retention and water repellence (from 64 ± 2 to 82 ± 3) of alkyd coating by water contact angle of 10°.

Easton *et al.*[78] modified the waterborne alkyd with silicon intermediates to improve weathering resistance in paints for exterior application. Organosilane incorporation in alkyds became the first choice in systems for protecting metal surfaces on bridges, railways and towers. Today they compete with other coating types, including two-pack polyurethane coating, which perform extremely well.

12.6.2 Polyurethane-based sol–gel coatings

Polyurethane coating has poor mechanical properties, thermal stability and corrosion resistance. Organosilane incorporation in polyurethane coatings (SiPU) was developed to enhance corrosion resistance, thermal stability and hardness of the polyurethane coatings.[45] Like SiAlk (alkyd-based sol–gel coatings) and SiE (polyester-based sol–gel coatings), decrease in corrosion current was observed for SiPU coatings compared with the bare aluminum. Improvement in corrosion resistance is attributed to the formation of an aluminum–oxygen–silicon interface which acts as a geometric blocking layer against the migration of chloride ions and water towards the substrate. SiPU coatings (58 ± 2°) show better water repellence than polyurethane coating (48 ± 4°). The pencil hardness of the polyurethane coating was found to be 2H, while it was enhanced from 3H to 6H with increasing silane concentration in SiPU coatings. Furthermore, the presence of siloxane (Si-O-Si) moieties in SiPU coatings made them flexible and resilient enough to sustain the mechanical stresses during service. Coatings were found thermally stable up to 206°C and the degradation of SiPU coatings was delayed by silane incorporation.

Chen *et al.*[79] prepared polyester/silica hybrid resins and polyester/silica/polyurethane hybrids via *in situ* sol–gel process and found that the extent of interaction among polyester, polyurethane and silica increases with the number of ethoxy groups in silica. Yang *et al.*[80] synthesized waterborne polyurethane–silica (0 to 50 wt%) based organic–inorganic hybrid coatings and observed that these coatings have much better thermal stability and mechanical properties than pure waterborne polyurethane resin, which is likely due to the effective interaction between silica particles and urethane polymer chains. Prabu and Alagar.[81] studied the thermal and morphological properties of a silicone–polyurethane–epoxy resin system and found the formation of inter-cross-linked networks. Jeon *et al.*[82] prepared water-dispersible polyurethane-based organic–inorganic hybrid compound through a sol–gel process. Like previous cases, it was observed that increasing the silica content improved the mechanical properties, heat stability and water resistance of the organic–inorganic hybrid material due to chemical network formation between PU and silica.

There has been continued interest in nanotechnology because it has demonstrated the achievement of unique properties compared with conventional techniques. The nanotechnology-based materials offer new solutions with the issue of corrosion degradation of metal by introducing coatings that provide corrosion resistance. Corrosion resistance of a coating is considered to be influenced by its adhesion to a metal substrate and other coating layers (if any), its hydrophobic nature and its ability to resist hygrothermal and mechanical stresses during service life.

12.7 Industrial applications of sol–gel coatings

Sol–gel coating does not need any introduction today. Sol–gel coatings have the potential to fulfil each and every expectation of the end user in terms of cost

effectiveness, environmental friendliness and unique functional properties. The cost is the most important driving force behind the growth of sol–gel coatings. Sol–gel coatings can be prepared by simple, non-vacuum processes with only a small capital investment.

Today sol–gel based coatings are being used in every sector of engineering application, such as aerospace, electronics, ships, building, decorative, etc. However, we are still in the initial stages of development and industrialization of sol–gel coatings. We face numerous problems with conventional coating adhesion and delamination during service of coated metal. Sol–gel coatings offer better adhesion to the substrate, but delamination of these coatings remains a problem. It is an open challenge for us to develop new coatings and coating precursors and establish formulation protocols for achieving better control over coating properties and the wide industrial use of sol–gel coatings.

12.8 Conclusions

Sol–gel coatings utilize the principle of nanotechnology in offering corrosion protection to metal substrates as well as their own stability under UV weathering and mechanical stresses. Using the sol–gel approach, corrosion-resistant coatings can be developed for most engineering materials for a variety of service conditions. Sol–gel coatings have the potential to lead the twenty-first-century high-performance coating market.

12.9 Acknowledgement

One of the authors would like to thank Shruti Pathak and Ishaan Pathak for their moral support during manuscript preparation.

12.10 References

1. S. V. Kolpakov, V. A. Parshin and A. N. Chekhovoi, 'Nanotechnology in the Metallurgy of Steel', in *Steel in Translation*, **37** (8) (2007), 716–21.
2. M. Lekka, N. Kouloumbi, M. Gajo and P.L. Bonora, *Electrochimica Acta*, **50** (23) (2005), 4551–6.
3. Q. Feng, T. Li and H. Teng, *Surface and Coatings Technol.*, **202** (17) (2008), 4137–44.
4. X. Shi, *Recent Patents on Engineering 2010*, **4** (1).
5. G. X. Shen, Y. C. Chen and C. J. Lin, *Thin Solid Films*, **489** (2005), 130–6.
6. D. R. Baer, P. E. Burrows and A. A. El-Azab, *Progress in Organic Coatings*, **47** (2003), 342–56.
7. J. S. Murday, 'The coming revolution—science and technology of nanoscale structures', *Adv. Mater. Process. Technol. Inform. Anal. Center*, **6** (2002), 5–10.
8. C. J. Brinker and G. W. Scherer, *Sol-gel Science: The Physics and Chemistry of Sol-gel Processing*, 1990. Boston: Harcourt Brace Jovanovich Academic Press.
9. R. Roy, *J. Am. Ceram. Soc.*, **39** (4) (1956), 145.
10. R. Roy and E. F. Osborn, *Am. Miner.*, **39** (1954), 853.

11. R. Roy, *Science*, **238** (1987), 1664.
12. J. E. Ritsko and C. D. Vanderpool, US Patent 3, 556,725 (1971).
13. H. Schmidt, *J. Non-Cryst. Solids*, **73** (1985), 681.
14. H. Schmidt and G. Philipp, *J. Non-Cryst. Solids*, **63** (1984), 283.
15. H. Schmidt, H. Scholze and H. Kaiser, *J. Non-Cryst. Solids*, **63** (1984).
16. C. J. Brinker and G. W Scherer, *Sol-Gel Science*, 1990. San Diego: Academic Press.
17. J. D. Wright and N. A. J. M. Sommerdijk, *Sol-gel Materials: chemistry and application*, 2001. Amsterdam: Gordon and Breach Science Publishing.
18. A. Rao, S. Latthe, S. Mahadik and C. Kappenstein, *Applied Surface Science*, **257** (2011), 5772–6.
19. L. L. Shreir, R. A. Jarman and G. T. Burstein, *Corrosion* (3rd edn), 2001. Oxford: Butterworth–Heinemann.
20. T. Liu, S. G. Chen, S. Cheng, J. T. Tian, X. T. Chang *et al.*, *Electrochim. Acta*, **52** (2007), 8003–7.
21. P. Wang, D. Zhang, R. Qiu and B. Hou, *Corrosion Science*, **53** (2011), 2080–6.
22. A. Tiwari, R. Sugamoto and L.H. Hihara, *Progress in Organic Coatings*, **57** (2006), 259–72.
23. P. Cardiano, S. Schiavo and P. Piraino, *Journal of Non-Crystalline Solids*, **356** (2010), 917–26.
24. Z. Chen and L.Wu, 'Scratch resistance of protective sol-gel coatings on polymeric substrates', *Tribology and Interface Engineering Series*, **55** (2008), 325–53.
25. C. Belon, M. Schmitt, S. Bistac, C. Croutxé-Barghorn and A. Chemtob, *Applied Surface Science*, **257** (2011), 6618–25.
26. A. R. Phani, F. J. Gammel and T. Hack, *Surf. Coat. Technol.*, **201** (2006), 3299–306.
27. P. Kiruthika, R. Subasri, A. Jyothirmayi, K. Sarvani and N. Y. Hebalkar, *Surface & Coatings Technology*, **204** (2010), 1270–6.
28. Y. Bautista, M. P. Gómez, C. Ribes and V. Sanz, *Progress in Organic Coatings*, **70** (2011), 358–64.
29. D. N. Singh, S. Yadav and J. K. Saha, *Corros. Sci.*, **50** (2008), 93.
30. P. Pepe, P. Galliano, M. Aparicio, A. Durán and S. Ceré, *Surf. Coat. Technol.*, **200** (2006), 3486.
31. T. Chou, C. Chandrasekhar, S. Limmer, S. Seraji, Y. Wu *et al.*, *J. Non-Cryst. Solids*, **290** (2001) 153.
32. S. I. Seok, J. H. Kim, K. H. Choi and Y. Y. Hwang, *Surf. Coat. Technol.*, **201** (2006), 3775.
33. S. H. Messaddeq, S. H. Pulcinelli, C. V. Santilli, A. C. Guastaldi and Y. J. Messaddeq, *Non-Cryst. Solids.*, **247**, 164.
34. A. Pepe, M. Aparicio, S. Ceré and A. Durán, *Materials Letters*, **59** (2005), 3937.
35. J. M. Yeh, C. J. Weng, W. J. Liao and Y. W. Mau, *Surf. Coat. Technol.*, **201** (2006), 1788.
36. D. A. López, N. C. Rosero-Navarro, J. Ballarre, A. Durán, M. Aparicio *et al. Surf. Coat. Tech.*, **202** (2008), 2194.
37. V. H. V. Sarmento, M. G. Schiavetto, P. Hammer, A. V. Benedetti, C. S. Fugivara *et al.*, *Surf. Coat. Technol.*, **204** (2010) 2689–701.
38. C. Vargel, *Corrosion of Aluminum*, 2004. Amsterdam: Elsevier.
39. S. S. Pathak and A. S. Khanna, 'Waterborne coatings for corrosion protection', in A. S. Khanna (Ed.), *High performance organic coatings: selection, application and evaluation*, 2008. Cambridge: Woodhead.
40. S. Pathak and A. Khanna, 'Organic–Inorganic Hybrid as Functional Coating', in T. Xu and C. Wu (Eds), *Advances in Solid Hybrid Membranes and Materials*, 2011. Trivandrum: Research Signpost.

41. S. S. Pathak, A. S. Khanna and T. J. M. Sinha, Paint and Coating Expo (PACE 2007). Dallas.
42. S. S. Pathak and A. S. Khanna, The Waterborne Symposium – Advances in Sustainable Coatings Technology 2008. New Orleans.
43. S. S. Pathak and A. S. Khanna, Paint and Coating Expo (PACE 2008). Los Angeles.
44. S. S. Pathak and A. S. Khanna, *Prog. Org. Coat.*, **65** (2009), 288.
45. S. S. Pathak, A. Sharma and A. S. Khanna, *Prog. Org. Coat.*, **65** (2009), 206–16.
46. A. Tiwari, J. Zhu and L. H. Hihara, *Surface and Coatings Technology*, **202** (2008), 4620–35.
47. A. Tiwari and L. H. Hihara, *Polymer Degradation and Stability*, **94** (2009), 1754–71.
48. A. Tiwari and L. H. Hihara, *Progress in Organic Coatings*, **69** (2010), 16–25.
49. A. Tiwari and L. H. Hihara, 'Novel Silicone Ceramer Coatings for Aluminum Protection', in A. S. H. Makhlouf (Ed.) *High Performance Coatings for Automotive and Aerospace Applications*, 2010. Hauppauge: Nova Science Publishers, Inc.
50. F. Andreatta, L. Paussa, P. Aldighieri, A. Lanzutti, D. Raps *et al.*, *Progress in Organic Coatings*, **69** (2010), 133–42.
51. Z. Feng, Y. Liu, G. E. Thompson and P. Skeldon, *Electrochimica Acta*, **55** (10) (2010), 3518–27.
52. Y. Liu, D. Sun, H. You and J. S. Chung, *Appl. Surf. Sci.*, **246** (2005), 82.
53. S. S. Pathak, A. S. Khanna and T. J. M. Sinha, *Prog. Org. Coat.*, **60** (2007), 211.
54. S. S. Pathak and A. S. Khanna, *Prog. Org. Coat.*, **62** (2008), 409.
55. Z. Zandi-Zand, A. Ershad-Langroudi and A. Rahimi, *Progress in Organic Coatings*, **53** (2005), 286.
56. Z. Zandi-Zand, A. Ershad-Langroudi and A. Rahimi, *Journal of Non-Crystalline Solids*, **351** (2005), 1307–11.
57. A. N. Khramov, V. N. Balbyshev, N. N. Voevodin and M. S. Donley, *Prog. Org. Coat.*, **47** (2003), 207.
58. T. L. Metroke, J. S. Gandhi and A. Apblett, *Prog. Org. Coat.*, **50** (2004), 231.
59. N. C. Rosero-Navarro, S. A. Pellice, A. Durán and M. Aparicio, *Corros. Sci.*, **50** (2008), 1283.
60. H. Wang and R. Akid, *Corros. Sci.*, **50** (2008), 1142.
61. M. L. Zheludkevich, R. Serra, M. F. Montemor, I. M. Miranda Salvado and M. G. S. Ferreira, *Surf. Coat. Technol.*, **200** (2006), 3084.
62. M. L. Zheludkevich, R. Serra, M. F. Montemor, K. A. Yasakau, I. M. M. Salvado *et al.*, *Electrochimica Acta*, **51** (2005), 208.
63. F. Girardi, F. Graziolaa, P. Aldighieri, L. Fedrizzi, S. Gross *et al.*, *Prog. Org. Coat.*, **62** (2008), 376.
64. A. N. Khramov, V. N. Balbyshev, L. S. Kasten and R. A. Mantz, *Thin Solid Film*, **514** (2006), 174–81.
65. S. S. Pathak and A. S. Khanna, Paint and Coating Expo (PACE 2008). Los Angeles.
66. S. S. Pathak, PhD Thesis 2009. IIT Bombay.
67. V. Barranco, N. Carmona, J. C. Galván, M. Grobelny, L. Kwiatkowski *et al.*, *Progress in Organic Coatings*, **68** (2010), 347–55.
68. H. Wang, R. Akid and M. Gobara, *Corrosion Science*, **52** (2010), 2565.
69. A. J. López, J. Rams and A. Ureña, *Surface and Coatings Technology*, **205** (2011), 4183–91.
70. J. Mathiyarasu, S. S. Pathak and V. Yegnaraman, *Corrosion Reviews*, **24** (5–6) (2006), 307–21.

71. S. S. Pathak, V. Yegnaraman, J. Mathiyrasu, M. Maji and A. S. Khanna, *Indian J. of Coating Technology*, **14** (2007), 5–15.
72. A. L. Kuan Tan and A. M. Soutar, *Thin Solid Film*, **516** (2008), 5706.
73. E. Bescher and J. D. Mackenzie, *J. Sol-Gel Sci. Technol.*, **26** (2003), 1223.
74. Y. S. Li., T. Tran., Y. Xu and N. E. Vecchio, *Spectrochemica Acta Part A: Molecular and Biomolecular Spectroscopy*, **65** (2006), 779.
75. K. H. Kaesler, 'Polysiloxane coatings for corrosion protection', in A. S. Khanna (Ed.), *High performance organic coatings: selection, application and evaluation*, 2008. Cambridge: Woodhead, p. 229.
76. U. Wienhold and U. Westerwelle, *Eur. Coat. J.*, **7** (2006), 41.
77. S. Frings, H. A. Meinem, C. F. V. Nostrum and R. V. Linde, *Prog. Org. Coat.*, **33** (1998), 351.
78. T. Easton and S. Poultney, *J. Coat. Technol. Res.*, **4** (2007), 187.
79. Y. C. Chen, S. X. Zhou, H. H. Yang and L. M. Wu, *J. Sol-Gel Sci. Technol.*, **37** (2006), 39.
80. Y. H. Yang, F. J. Liu, Y. P. Liu and W. T. Liao, *J. Colloid. Interf. Sci.*, **302** (2006), 123.
81. A. A. Prabu and M. Alagar, *J. Macromol. Sci. Pure Appl. Chem.*, **42A**, 175.
82. H. T. Jeon, M. K. Jang, B. K. Kim and K. H. Kim, *Colloid Surf. A: Physicochem. Eng. Aspects*, **302** (2007).

13

Polymer nanocomposites in corrosion control

C.-J. WENG, C.-H. CHANG and J.-M. YEH, Chung Yuan Christian University, Taiwan

Abstract: Polymer/clay nanocomposites (PCN) are now of great interest to polymer scientists, physicists and material scientists because of the unique properties produced by combining these components at the nanoscale level. Measuring the corrosion protection effects of PCNs as coatings is crucial to gaining a fundamental understanding of the anticorrosion mechanism of these materials. Measurement of the anticorrosive properties of PCN is also helpful in establishing the gas barrier properties of polymer/clay interactions and their structure–property relationship in nanocomposites. This is because anticorrosive performance is strongly influenced by the nanoscale structure and interfacial characteristics. In this chapter, recent advances in PCN anticorrosive coatings are discussed.

Key words: anticorrosion, organophilic clay, polymer/clay nanocomposites, electroactive polymer/clay nanocomposites, gas barrier.

13.1 Introduction

Every year, industry pays a massive and rising cost for its corrosion problems. Research and development into new materials, processes and initiatives to combat this loss is increasing, and new findings are constantly coming to light which can help to beat corrosion problems throughout industry. Oxidation corrosion is simply the process of the metal returning to its natural oxidized, or passivated, state. The force associated with this phenomenon is referred to as the oxidation potential. Some metals, such as iron, have very high oxidation potentials, which is why natural organisms use iron to oxygenate blood and why iron rusts so quickly. Sodium has such a high oxidation potential that it bursts into flame at room temperatures. Other metals, such as chromium, have very low oxidation potentials, which is why chromium rusts so slowly, if at all. In this chapter, we will discuss the prevention of corrosion of metal substrate using organic–inorganic hybrid technology.

13.1.1 Measures of corrosion prevention

Material selection

Metals and alloys: The most common method for preventing corrosion is the selection of the proper metal or alloy for a particular corrosive service (Tiwari *et al.*, 2010; Custodio *et al.*, 2010).

Metal purification: The corrosion resistance of a pure metal is usually better than that of one containing impurities or small amounts of other elements. However, pure metals are usually expensive and are relatively soft and weak. In general, pure metals are used in relatively few, special cases (Tiwari *et al.*, 2001; Custodio *et al.*, 2010).

Non-metallics: This category involves integral or solid non-metallic construction (mainly self-supporting) and sheet linings or coverings of substantial thickness (different from paint coatings). The five general classes of non-metallics are (1) rubbers (natural and synthetic), (2) plastics, (3) ceramics, (4) carbon and graphite, and (5) wood (Worspop and Kingsburf, 1950; Tiwari *et al.*, 2001; Custodio *et al.*, 2010; Zelinka and Stone, 2011).

Changing medium: Altering the environment provides a versatile means for reducing corrosion. Typical changes in the medium that are often employed include (1) lowering the temperature, (2) decreasing the velocity, (3) removing oxygen or oxidizers and (4) changing the concentration. In many cases, these changes can significantly reduce corrosion, but they must be performed with care (Welder and Partridge, 1954; Tiwari *et al.*, 2001; Custodio *et al.*, 2010).

Inhibitors: An inhibitor is a substance that, when added in small concentrations to an environment, decreases the corrosion rate. In a sense, an inhibitor can be considered a retarding catalyst. There are numerous inhibitor types and compositions. Most inhibitors have been developed by empirical experimentation and many are proprietary in nature; thus their composition is not disclosed. Inhibition is not completely understood for these reasons, but it is possible to classify inhibitors according to their mechanism and composition (Tiwari *et al.*, 2001; Custodio *et al.*, 2010; Rosenfeld, 1981).

Cathodic and anodic protection

Cathodic protection: Cathodic protection was employed before electrochemistry had been developed. Humphrey Davy used cathodic protection on British naval ships in 1824. The principles of cathodic protection may be explained by considering the corrosion of a typical metal in an acid environment. Electrochemical reactions include the dissolution of the metal and the evolution of hydrogen gas:

$$M \rightarrow M^{n+} + ne \qquad [13.1]$$

$$2H^{+} + 2e \rightarrow H_2 \qquad [13.2]$$

Anodic protection: In contrast to cathodic protection, anodic protection is relatively new; it was first suggested by Edeleanu in 1954. This technique was developed using electrode kinetics principles and is somewhat difficult to describe without introducing advanced concepts of electrochemical theory. Simply, anodic protection is based on the formation of a protective film on metals by externally applied anodic currents (Locke and Sudbury, 1960; Acello and Greene, 1962).

Coatings

Metallic and other inorganic coatings: Relatively thin coatings of metallic and inorganic materials can provide a satisfactory barrier between a metal and its environment. The chief function of such coatings (aside from sacrificial coatings such as zinc) is to provide an effective barrier. Metal coatings are applied by electrodeposition, flame spraying, cladding, hot dipping and vapor deposition. Inorganics are applied or formed by spraying, diffusion or chemical conversion. Spraying is usually followed by baking or firing at elevated temperatures. Metal coatings usually exhibit some formability, whereas the inorganics are brittle. In both cases a complete barrier must be provided. Porosity or other defects can result in an accelerated localized attack on the base metal because of the two-metal effects (Moore and McCafferty, 1981; Draper, 1982; McCafferty *et al.*, 1982).

Organic coatings: These involve a relatively thin barrier between the substrate material and the environment. Paints, varnishes, lacquers and similar coatings protect more metal per ton than any other method for combating corrosion. Exterior surfaces are most common, but inner coatings or linings are also widely utilized. Approximately $2 billion per year is spent in the United States on organic coatings. Myriad types and products are involved, and some are accompanied by outlandish claims. Substantial knowledge of this complex field is therefore required for successful performance. The best procedure for those who are inexperienced is to consult a reputable producer of organic coatings. As a general rule, these coatings should not be used where the environment would rapidly attack the substrate material (Garrett, 1964). Aside from proper application, the three main factors to consider for organic coatings, listed in order of importance, are (1) surface preparation, (2) selection of primer or priming coat and (3) selection of top coat or coats. Polymeric (or organic) coatings have been employed to protect metals against corrosion for a long time. The primary effect of a polymeric coating is to function as a physical barrier against aggressive species such as O_2 and H^+.

13.1.2 Polymer nanocomposite coatings

Chromium-containing compounds (CC) have generally been used as effective anticorrosive coatings in the past decades. However, due to the environmental and health concerns, CCs may need to be replaced by alternative materials that would not pose biological and ecological hazards. Thus, research has focused on the development of novel polymeric coating materials that contain effective anticorrosive agents. Organic or polymeric coatings on metallic substrates provide an effective barrier between the metal and its environment and/or inhibit corrosion through the presence of chemicals. These coatings generally function as a physical barrier against aggressive species such as O_2 and H^+ that cause decomposition.

Examples of representative polymers include epoxy resins (MacQueen and Granata, 1996; Dang *et al.*, 2002), polyurethanes (Moijca *et al.*, 2001) and polyesters (Deflorian *et al.*, 1996; Malshe and Sangaj, 2006). Moreover, conjugated polymers

such as polyaniline (Wessling and Posdorfer, 1999; Tan and Blackwood, 2003), polypyrrole (Krstajic *et al.*, 1997; Iroh and Su, 2000) and polythiophene (Kousik *et al.*, 2001) have also been employed as advanced anticorrosive coatings due to their redox catalytic properties, forming metal oxide passivation layers on metallic substrates. Conversely, not all neat polymeric coatings are permanently impenetrable, because small defects in the coatings can lead to gateways that allow corrosive species to attack the metallic substrate; thus, localized corrosion can occur.

As a second line of defense against corrosion, various nanoscale inorganic additives have been incorporated into various polymer matrices to generate a series of organic–inorganic hybrid anticorrosive coatings. Recently, nanoclays such as clay have attracted intensive research interest for the preparation of polymer/clay nanocomposites (PCNs) because their nanostructure displays high in-plane strength and stiffness. Typically, the chemical structure of montmorillonite (MMT) consists of two fused silica tetrahedral sheets that sandwich an edge-shared octahedral sheet of either magnesium or aluminum hydroxide. The Na^{+} and Ca^{+2} residing in the interlayer regions can be replaced by organic cations such as alkylammonium ions, by a cationic exchange reaction, to render the hydrophilic clay organophilic.

The historical development of PCNs can be traced back to the work on PCNs reported by Toyota's research group (Usuki *et al.*, 1993). According to many recently published works, the dispersion of clay was found to boost the thermal stability (Lan *et al.*, 1994), mechanical strength (Tyan *et al.*, 1999), molecular barrier (Asif *et al.*, 2011) and flame-retardant (Gilman *et al.*, 2000) properties of polymers. Recently, PCN materials used as enhanced anticorrosion coatings have been reported by Yeh's group (Yeh *et al.*, 2001 2002, 2002, 2003, 2003, 2004a, b, c, d, e, 2005, 2006, 2007; Yu *et al.*, 2004a, b, c; Chang *et al.*, 2007, 2008; Lai *et al.*, 2007; Huang *et al.*, 2011). For example, conjugated polymers (e.g. polyaniline, polypyrrole and poly(3-hexylthiophene)), thermoplastic polymers (e.g. poly(methylmethacrylate), polystyrene, poly (styrene-co-acrylonitrile) polysulfone), thermosetting polymers (e.g. polyimide and epoxy) and electroactive polymers (e.g. electroactive polyimide and epoxy) had all been blended with organo-modified clay or raw Na^{+}-MMT clay through different preparative routes, such as *in situ* polymerization or solution dispersion, to make a series of novel advanced anticorrosion coatings based on a series of electrochemical corrosion parameter measurements of corrosion potential, polarization resistance and corrosion current at room temperature.

In this chapter, we present PCN materials (including conjugated polymers, non-conjugated polymers and electroactive polymers) as model coatings to demonstrate the advanced anticorrosive properties of clay-based polymeric coatings by performing a series of electrochemical corrosion measurements.

13.2 Structure of clay

Clay minerals are an example of a wider class of compounds known as layered materials, which may be defined as 'crystalline material wherein the atoms in the

layers are cross-linked by chemical bonds, while the atoms of adjacent layers interact by physical forces' (Schoonheydt *et al.*, 1999). Both clay sheets and interlayer space have widths in the nanometer range. The predominant naturally occurring cationic clay minerals have alumino-silicate sheets that carry a negative charge, which means that the interlayer guest species must be positively charged (cationic) (Grim, 1962). Clays are generally classified by structure as allophane, kaolinite, halloysite, smectite, illite, chlorite, vermiculite, attapulgite–palygorskite–sepiolite and mixed layered minerals (Grim, 1968). PCNs are mainly based on smectite clays because of their swelling properties, which result from their capacity to host water and organic molecules between silicate layers, high cation exchange capacities, high aspect ratio and large surface area (Theng, 1979; Pinnavaia, 1983).

The surface area of a mineral when measured using an adsorption method depends on access to the internal surfaces, so that the N_2 Brunauer–Emmett–Teller (BET) method generally returns the external area, which is typically 15–50 $m^2\ g^{-1}$ for smectite clays (Grim, 1962, 1968). The internal surface area is better calculated and is about 620 $m^2\ g^{-1}$ (Helmy *et al.*, 1999; Chen and Evans, 2004).

Smectite clays consist of units in the form of 'sheets' or 'platelets', made up of two silica tetrahedral layers with a central alumina or magnesia octahedral layer. Hydrated exchangeable cations are found in the spaces between lattices, as shown in Fig. 13.1 (Paul and Robeson, 2008). The layers are held together by van der Waals and electrostatic forces, and the absence of primary chemical bonds allows the intercalation of water or polar organic molecules, causing the lattice to expand in the *c* direction (Grim, 1968).

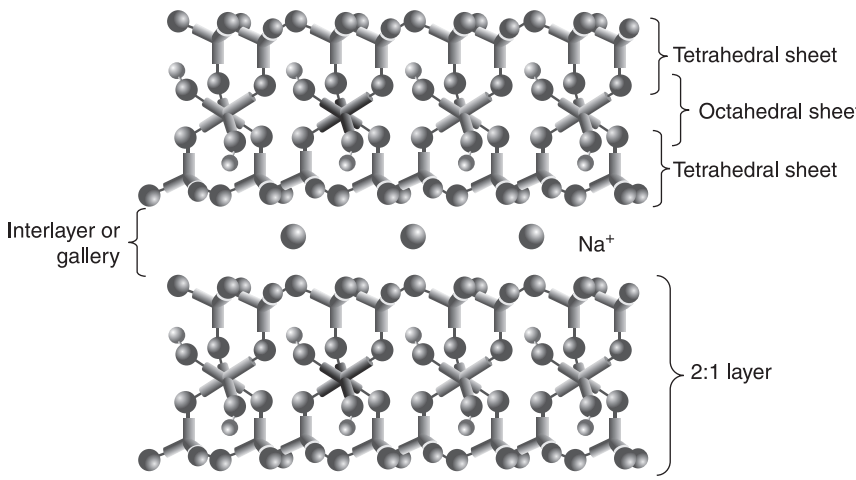

13.1 Structure of sodium montmorillonite (Paul and Robeson, 2008).

MMT and hectorite are commonly used in nanocomposites. They belong to the dioctahedral and trioctahedral groups (two and three aluminum-centered octahedrons in the unit cell respectively) and have ideal chemical formulae of $Al_2Si_4O_{10}(OH)_2 \cdot yH_2O$ and $Mg_3Si_4O_{10}(OH)_2 \cdot yH_2O$ respectively (Grim, 1968). Some Al^{3+} cations in MMT are substituted by Mg^{2+}, and similarly some Mg^{2+} cations in hectorite are substituted by Li^+. These substitutions cause charge deficiency and are balanced by external cations present in the galleries, such as Na^+, producing chemical formulae $Mx/n^{n+} \cdot yH_2O[Al_{4.0-x}Mg_x(Si_{8.0})O_{20}(OH)_4]$ and $M^{n+}_{x/n} \cdot yH_2O[Mg_{6.0-x}Li_x(Si_{8.0})O_{20}(OH,F)_4]$ (Paul and Robeson, 2008).

Natural MMT is hydrophilic and is generally considered unsuitable for hosting non-polar organic molecules without prior treatment. Interlayer cations can be exchanged with organic cations to obtain organophilic MMT, producing an 'organoclay', which has an expanded interlayer spacing and more readily produces a PCN by intercalation and/or exfoliation. Traditional modification agents behave as surfactants, such as alkyl and quaternary ammonium halides (e.g. dimethyl di (hydrogenated tallow) quaternary ammonium chloride), mainly following the Toyota research group, who used a solution of 12-aminolauric acid in concentrated hydrochloric acid as the modifier for MMT to reinforce nylon 6. Similarly, modification is necessary for hectorite to make it organophilic.

13.3 Polymer/clay nanocomposite (PCN) structures

Nanocomposites can, in principle, be formed from clay and organoclay in a number of ways, including various *in situ* polymerization (Fukushima and Inagaki, 1987; Kojima *et al.*, 1993; Biasci *et al.*, 1994; Huang *et al.*, 2000; Zhou *et al.*, 2001; Albrecht *et al.*, 2003; Kiersnowski and Piglowski, 2004), solution (Ray and Okamoto, 2003; Hussain and Hojjati, 2006) and latex (Goldberg *et al.*, 2002; Takahashi *et al.*, 2006) methods. However, the greatest interest has involved melt processing (Masenelli-Varlot *et al.*, 2000; Kim *et al.*, 2005; Vermogen *et al.*, 2005; Morgan *et al.*, 2007; Picard *et al.*, 2007) because this is generally considered more economical and more flexible for formulation and involves compounding and fabrication facilities commonly used in commercial practice. For most purposes, complete exfoliation of the clay platelets, i.e. platelets separated from one another and dispersed individually in the polymer matrix, is the desired goal of the formation process. However, this ideal morphology is frequently not achieved and varying degrees of dispersion are more common.

While far from a completely accurate or descriptive nomenclature, the literature commonly refers to three types of morphology: immiscible (conventional or microcomposite), intercalated and exfoliated. These are illustrated schematically in Fig. 13.2 along with example transmission electron microscopic (TEM) images and the expected wide-angle X-ray scans (LeBaron *et al.*, 1999; Pinnavaia and Beall, 2000; Yariv and Cross, 2002; Hussain and Hojjati, 2006; Mai and Yu, 2006; Anbarasan *et al.*, 2011).

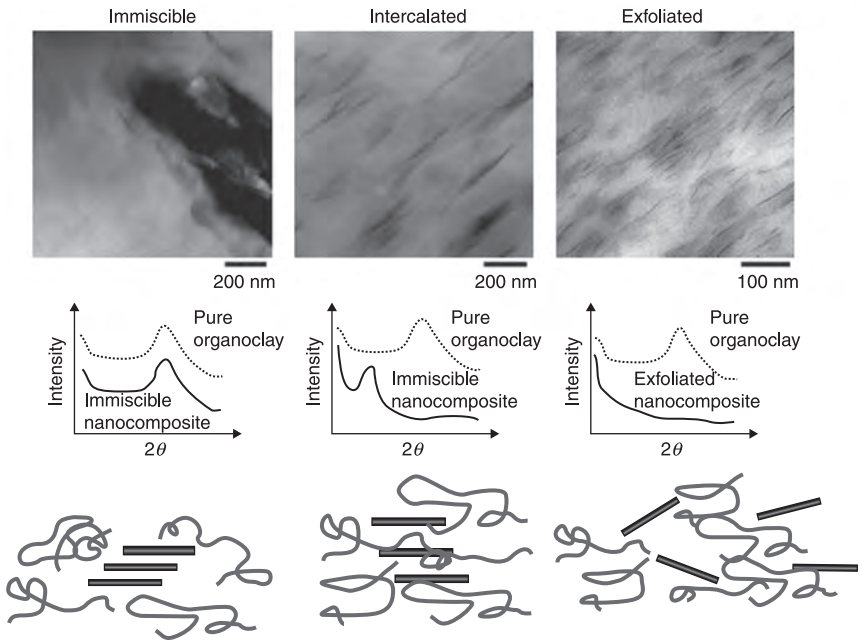

13.2 Illustration of different states of dispersion of organoclays in polymers with corresponding WAXS and TEM results (Paul and Robeson, 2008).

For the case called 'immiscible' in Fig. 13.2, the organoclay platelets exist in particles comprised of tactoids or aggregates of tactoids more or less as they were in the organoclay powder, i.e. no separation of platelets. Thus, the wide-angle X-ray scan of the polymer composite is expected to look essentially the same as that obtained for the organoclay powder; there is no shifting of the X-ray *d*-spacing. Generally, such scans are made over a low range of angles, 2θ, such that any peaks from a crystalline polymer matrix are not seen, since they occur at higher angles. For a completely exfoliated organoclay, no wide angle X-ray peak is expected for the nanocomposite since there is no regular spacing of the platelets and the distances between platelets would, in any case, be larger than wide angle X-ray scattering can detect.

13.4 Methods for synthesizing PCN

Intercalation of polymers in layered hosts, such as clay, has proven to be a successful approach to synthesize PCN materials. The preparative methods are divided into three main groups according to the starting materials and processing techniques.

Intercalation of polymer or pre-polymer from solution (Fig. 13.3(a)) (Aranda and Ruiz-Hitzky, 1992; Yano *et al.*, 1993; Jimenez *et al.*, 1997; Jeon *et al.*, 1998;

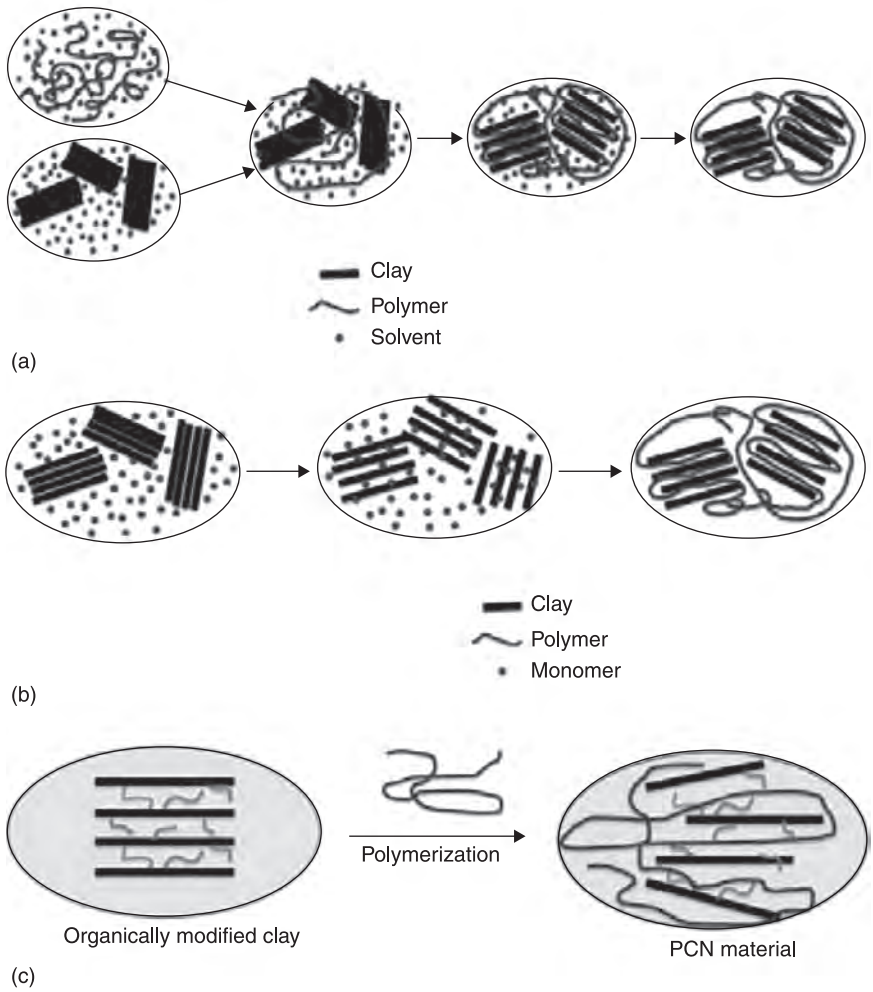

13.3 (a) Schematic representation of a PCN material obtained by intercalation of polymer from solution; (b) schematic representation of a PCN material obtained by in-situ polymerization; and (c) schematic representation of a PCN material obtained by direct melt intercalation.

Tseng *et al.*, 2001; Xu *et al.*, 2001): This is based on a solvent system in which the polymer or pre-polymer is soluble and the clay is swellable. The layered silicate is first swollen in a solvent such as water, chloroform or toluene. When the polymer and clay solutions are mixed, the polymer chains intercalate and displace the solvent within the interlayer of the clay. Upon solvent removal, the intercalated structure remains, resulting in PCN materials.

In situ *intercalative polymerization method* (Fig. 13.3(b)) (Kojima *et al.*, 1993; Usuki *et al.*, 1993; Okamoto *et al.*, 2000, 2001; Biswas and Sinha-Ray, 2001; Leu

et al., 2002; Kim *et al.*, 2003). In this method, the clay is swollen within the liquid monomer or a monomer solution so that polymer formation can occur between the intercalated sheets. Polymerization can be initiated either by heat or by radiation, by the diffusion of a suitable initiator or by an organic initiator or catalyst fixed through cation exchange inside the interlayer before the swelling step.

Melt intercalation method (Fig. 13.3(c)) (Vaia *et al.*, 1993, 1995; Vaia and Giannelis, 1997a, 1997b; Huang *et al.*, 2000; Wang *et al.*, 2001; Chisholm *et al.*, 2002; Fornes *et al.*, 2002; Usuki *et al.*, 2002). This method involves (statically or under shear) a mixture of the polymer and organically modified clay above the softening point of the polymer. This method has advantages over either *in situ* intercalative polymerization or polymer solution intercalation. First, this method is environmentally benign due to the absence of organic solvents. Second, it is compatible with current industrial process such as extrusion and injection molding. The melt intercalation method allows the use of polymers that were previously not suitable for *in situ* polymerization or solution intercalation.

13.5 Anticorrosive properties

In a non-conjugated polymer system, Yeh *et al.* (2002) reported a series of PCN materials that consisted of poly(methylmethacrylate) (PMMA) and layered MMT clay that were prepared by effectively dispersing the inorganic nanolayers of MMT clay in an organic PMMA matrix via *in situ* thermal polymerization. Organic methylmethacrylate monomers were first intercalated into the interlayer regions of organophilic clay hosts, followed by a typical free-radical polymerization. The as-synthesized PCN materials were characterized by infrared spectroscopy, wide-angle powder XRD (Fig. 13.4) and TEM (Fig. 13.5).

Figure 13.4 shows the wide-angle powder XRD patterns of organophilic clay and a series of PCN materials. For CLMA1 (1 wt% clay dispersed into PMMA matrix), there is a lack of any diffraction peak in 2θ = 2–10° as opposed to the diffraction peak at 2θ = 4.85° (d-spacing = 1.82 nm) for organophilic clay, indicating the possibility of having exfoliated organophilic clay dispersed in a PMMA matrix. When the amount of organoclay increased to 5 wt%, there was a small peak appearing at 2θ = 2.8°, corresponding to a d-spacing of 3.15 nm. This implied that there was a small amount of organoclay that could not be exfoliated in the PMMA and existed in the form of an intercalated layer structure. For CLMA10 (10 wt% clay dispersed into PMMA matrix), the interlayer distance of organoclay nanolayers could not be further increased and displayed a d-spacing of organophilic clay in the organic PMMA matrix, indicating that a large amount of organoclay existed in an intercalated layer structure.

In Fig. 13.5, the TEM of PCN materials with 5 wt% clay loading (CLMA5) reveals that the nanocomposite displays a mixed nanomorphology. Individual silicate layers, along with two and three-layer stacks, are found to be exfoliated in the PMMA matrix. In addition, some larger intercalated tactoids can also be

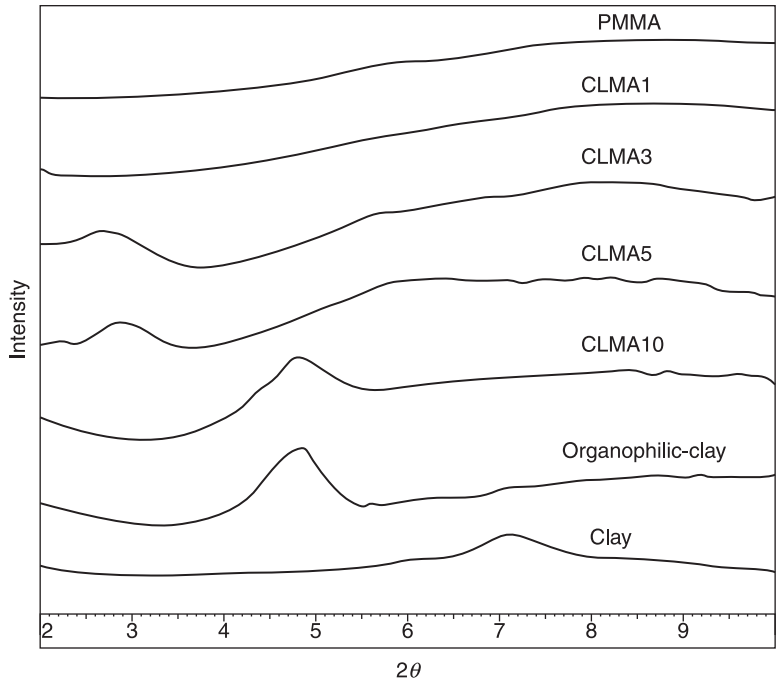

13.4 Wide-angle powder X-ray diffraction patterns of organophilic clay, PMMA and a series of PCN materials.

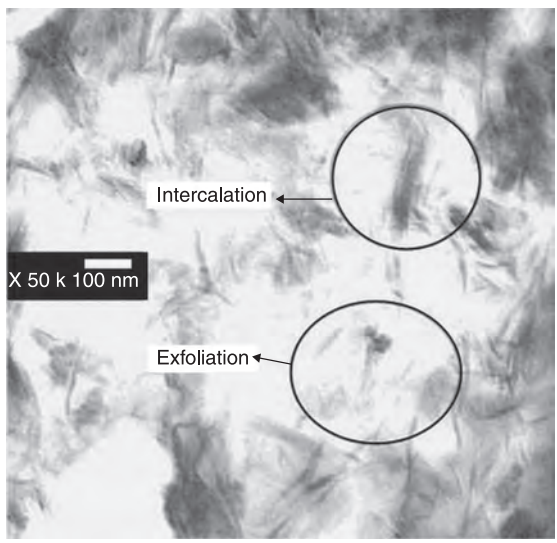

13.5 Transmission electron microscopy of PMMA/clay (5 wt%) nanocomposite.

identified. PCN coatings with 1 wt% clay loading (CLMA1) on cold-rolled steel (CRS) showed superior anticorrosion properties compared with those of bulk PMMA based on a series of electrochemical measurements of corrosion potential (E_{corr}), polarization resistance (R_p), corrosion current density (I_{corr}) and impedance spectroscopy in 3.5 wt% aqueous NaCl electrolyte (Table 13.1 and Fig. 13.6 and 13.7).

Table 13.1 Relationships of the composition of PMMA–MMT clay nanocomposite materials with the E_{corr}, R_p, i_{corr}, and R_{corr} measured using electrochemical methods

Compound code	Feed composition (wt%)		Inorganic content found in product (wt%)	Electrochemical corrosion measurement				
	PMMA	MMT		E_{corr} (mV)	R_p (KΩ cm^2)	I_{corr} (nA/cm^2)	R_{corr} (MPY)	Thickness (μm)
Bare	—	—	—	–604	2.7	1.9×10^4	36.7	—
PMMA	100	0	0	–485	3.2×10^2	1.2×10^2	2.3×10^{-1}	110
CLMA1	99	1	1.2	–379	9.2×10^2	4.5×10^1	8.0×10^{-2}	112
CLMA3	97	3	3.5	–278	6.4×10^3	9.4	1.8×10^{-2}	121
CLMA5	95	5	6.9	–78	7.5×10^3	5.7	1.1×10^{-2}	113
CLMA10	90	10	18.1	–19	1.8×10^4	2.3	4.4×10^{-3}	117
CLMA-N10	90	10	22.1	—	—	—	—	—

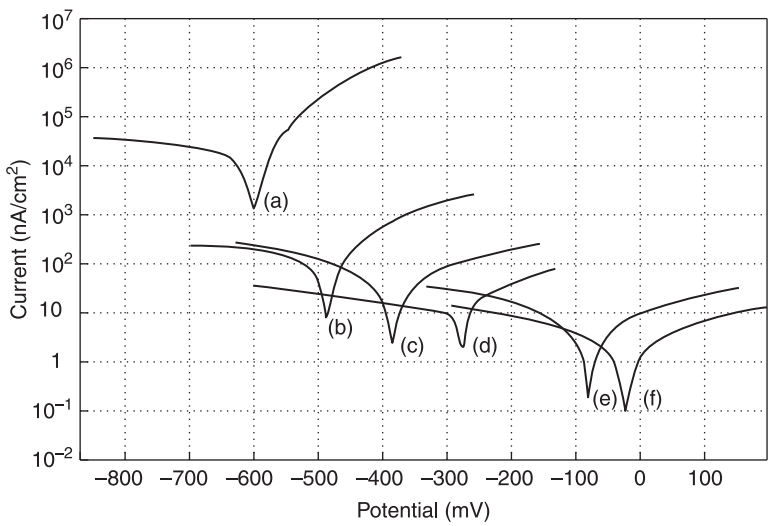

13.6 Tafel plots for (a) uncoated, (b) PMMA-coated, (c) CLMA1-coated, (d) CLMA3-coated, (e) CLMA5-coated and (f) CLMA10-coated CRS measured in 3.5 wt% NaCl aqueous solution.

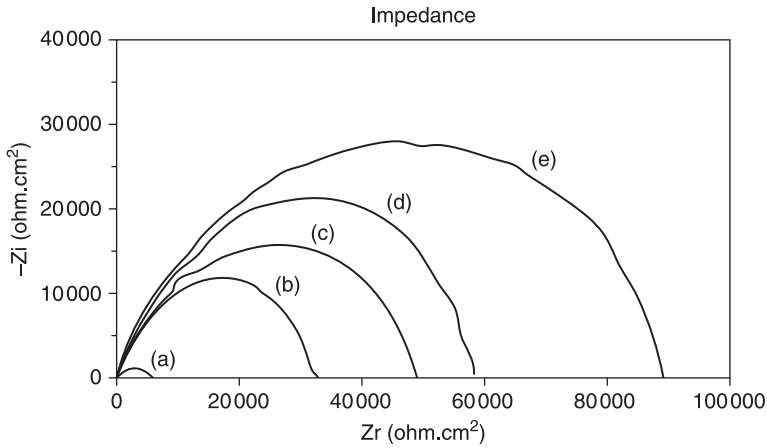

13.7 Nyquist plots of five CRS samples in 3.5 wt% NaCl aqueous solution: (a) PMMA coated, (b) CLMA1-coated, (c) CLMA3-coated, (d) CLMA5-coated and (e) CLMA10-coated.

The molecular weights of PMMA extracted from PCN materials and bulk PMMA were determined by gel permeation chromatography (GPC) with tetrahydrofuran as an eluant. Effects of the material composition on the gas and water permeability, optical clarity and thermal stability of PMMA and PCN materials, in the form of both free-standing films and fine powders, were also studied by molecular permeability analysis, ultraviolet–visible transmission spectra, differential scanning calorimetry and thermogravimetric analysis, respectively.

Anticorrosive performance of sample-coated CRS coupons can be examined from the values of corrosion potential (E_{corr}), polarization resistance (R_p), corrosion current (i_{corr}) and corrosion rate (R_{corr}), as listed in Table 13.1. The CRS coupon coated with PMMA shows a higher E_{corr} value than the uncoated CRS. However, it exhibits a lower E_{corr} value than the specimen coated with PCN materials. Such an E_{corr} value implies that the CLMA1-coated (1 wt% clay dispersed into PMMA matrix) CRS is more noble toward the electrochemical corrosion compared with the PMMA. The CLMA1-coated CRS shows a polarization resistance (R_p) value of 9.2×10^2 kΩ/cm^2 in 3.5 wt%NaCl, which is about two orders of magnitude greater than the uncoated CRS (Table 13.1). Corrosion current information can be obtained by the Tafel extrapolation method, where large cathodic and anodic polarizations provide the cathodic and anodic polarization curves for the respective corrosion processes.

The Tafel plots for PCN are shown in Fig. 13.6. Electrochemical corrosion current values of PCN materials as coatings on CRS were found to decrease gradually with a further increase in clay loading. Electrochemical impedance

spectroscopy (EIS) was also used to examine the activity difference between the CRS surface after PMMA and PCN materials treatment.

Figure 13.7 shows the Nyquist plots of the PCN. The charge-transfer resistances of samples (a), (b), (c), (d) and (e), as determined by the intersection of the low-frequency end of the semicircle arc with the real axis, are 5000, 32 000, 49 000, 58 000 and 89 000 $\Omega \cdot cm^2$, respectively. The results clearly demonstrate that the sample with the highest clay loading has the greatest anticorrosive performance.

According to the gas and water permeability analysis above, a free-standing film of PCN materials at low clay loading (e.g. 3 wt%) shows about 57% and 28% reduction of H_2O and O_2 permeability, respectively, as shown in Fig. 13.8. Furthermore, it should be noted that a further increase of clay loading results in a slightly further enhanced molecular barrier property in bulk PCN materials. The enhanced corrosion protection effect of PCN compared with bulk PMMA might have resulted from dispersing clay in the PMMA matrix to increase the tortuosity of oxygen gas and water vapor diffusion pathways.

In a conjugated polymer system, Yeh *et al.* (2001) investigated a series of nanocomposite materials consisting of an emeraldine base of polyaniline and MMT clay that were prepared by effectively dispersing the inorganic nanolayers of MMT clay in an organic polyaniline matrix (CLAN) via *in situ* polymerization. Organic aniline monomers were first intercalated into the interlayer regions of organophilic clay hosts and followed by a one-step oxidative polymerization. The as-synthesized polyaniline/clay lamellar nanocomposite materials were characterized by infrared spectroscopy, wide-angle powder XRD and TEM.

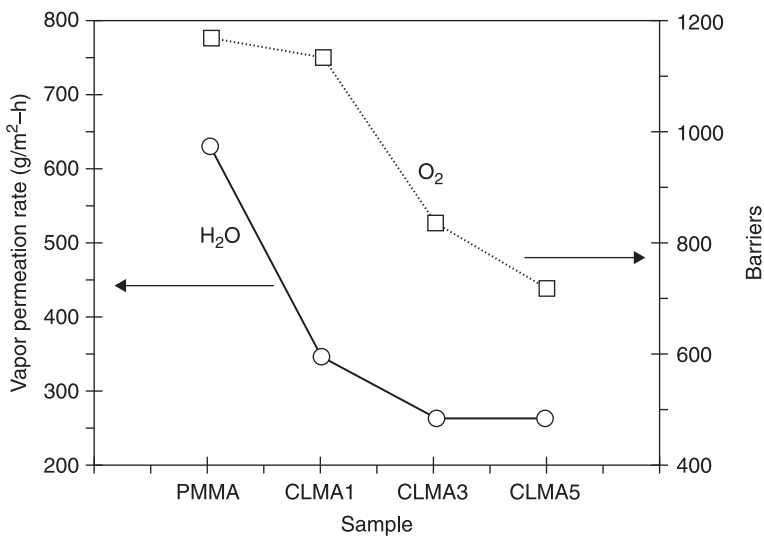

13.8 Permeability of H_2O and O_2 as a function of the MMT clay content in the PMMA/clay nanocomposite materials.

Wide-angle powder XRD patterns of organophilic clay and a series of PCN materials (Fig. 13.9) showed that there is a lack of any diffraction peak in 2θ = 2–10° as opposed to the diffraction peak at 2θ = 3.9° (d-spacing = 2.26 nm) for organophilic clay, indicating the possibility of having exfoliated silicate nanolayers of organophilic clay dispersed in a polyaniline matrix that was correspondent to TEM image (Fig. 13.10). Polyaniline–clay nanocomposites in the form of coatings with low clay loading (e.g. CLAN075; 0.75 wt% clay dispersed into polyaniline matrix) on CRS showed superior corrosion protection compared with those of conventional polyaniline based on a series of electrochemical measurements in 3.5 wt-% aqueous NaCl electrolyte (Fig. 13.11).

The molecular weights of polyaniline extracted from polyaniline/clay nanocomposite materials and bulk polyaniline were determined by gel permeation chromatography (GPC). The effects of material composition on the gas barrier properties (Fig. 13.12), thermal stability and mechanical strength of polyaniline and polyaniline/clay nanocomposite materials, in the form of both fine powders and free-standing films, were also studied by gas permeability measurements, differential scanning calorimetry, thermogravimetric analysis and dynamic mechanical analysis.

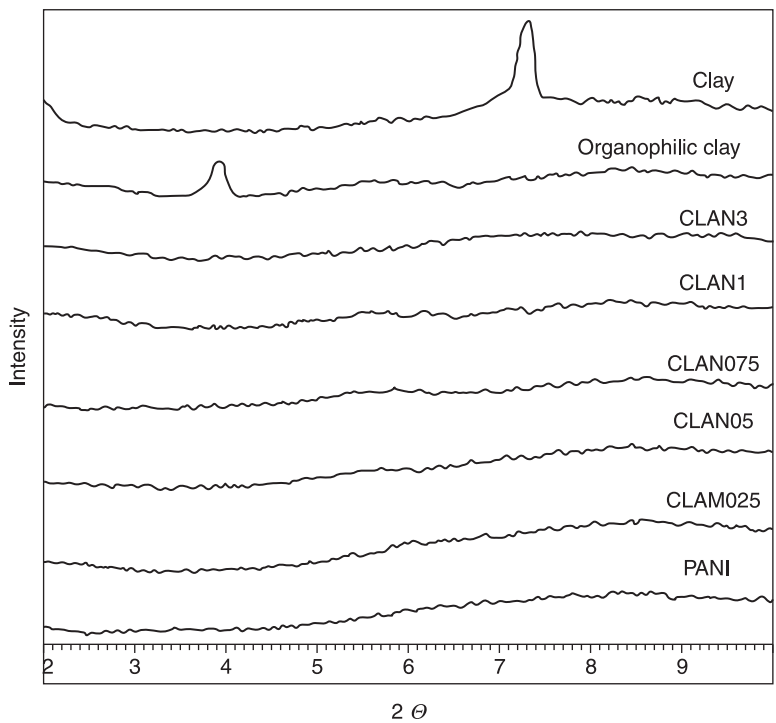

13.9 Wide-angle powder X-ray diffraction patterns of organophilic clay, polyaniline and a series of polyaniline/clay nanocomposite materials.

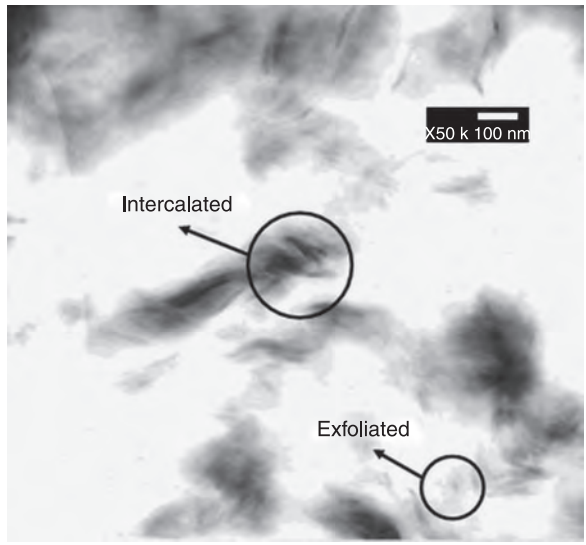

13.10 TEM of PCN03: with exfoliated single, double and triple layers and a multilayer tactoid.

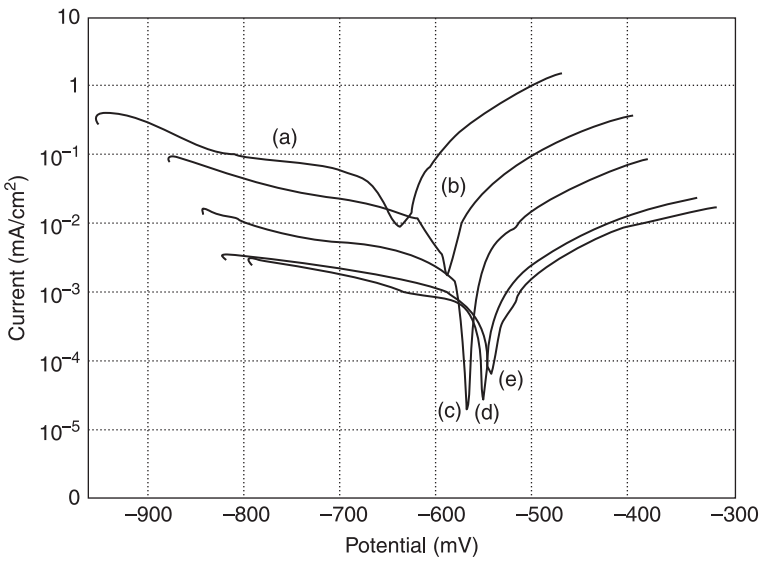

13.11 Tafel plots for (a) uncoated, (b) PANI-coated, (c) CLAN025-coated, (d) CLAN05-coated and (e) CLAN075-coated CRS measured in 3.5 wt% NaCl aqueous solution.

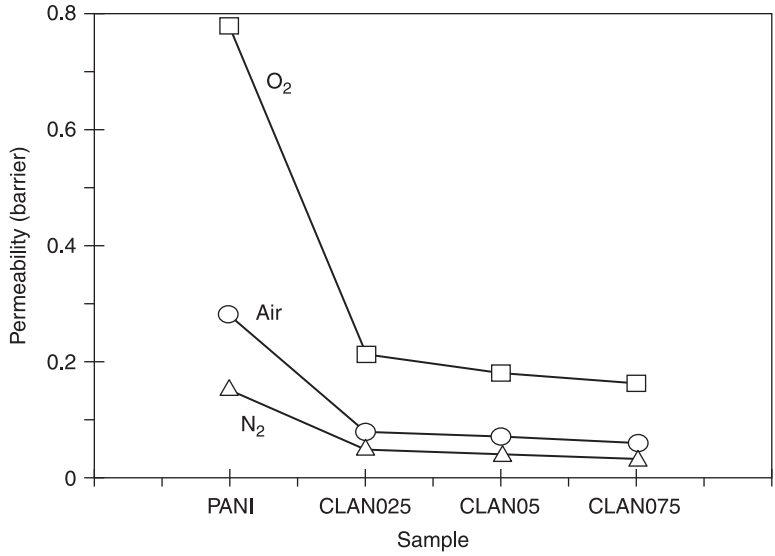

13.12 Permeability of O_2, N_2 and air as a function of the MMT clay content in the polyaniline/clay nanocomposite materials.

In an electroactive polymer system, Huang *et al.* (2011) attempted to prepare advanced PCN anticorrosive coating materials with the synergistic effects of redox catalytic capability and gas barrier properties by incorporation of well-dispersed organophilic clay platelets into amine-capped aniline trimer (ACAT)-based electroactive polyimide (EPI) matrix through chemical imidization (see Fig. 13.13).

The corrosion protection properties of electroactive polyimide/clay nanocomposite (EPCN) coatings were investigated by a series of electrochemical measurements in 3.5 wt% NaCl electrolyte. Gas barrier properties and redox behavior (i.e. electroactivity) of EPCN materials, in the form of membrane and coating, was identified by the studies of gas permeability analysis (GPA) and electrochemical cyclic voltammetry (CV), respectively.

It should be noted that the EPCN coating was found to confer advanced corrosion protection effects on a CRS electrode when compared with a neat non-electroactive polyimide (NEPI) coating, based on a series of electrochemical corrosion measurements in 3.5 wt% NaCl electrolyte. This enhanced corrosion protection may be for two possible reasons: (1) redox catalytic capabilities (i.e. electroactivity) of ACAT units existing in the electroactive PCN may induce formation of passive metal oxide layers on a CRS electrode, as evidenced by scanning electron microscopy (SEM) and electron spectroscopy for chemical analysis (ESCA) studies; (2) well-dispersed layered organophilic clay platelets embedded in the EPCN matrix are acting as an effective oxygen barrier because

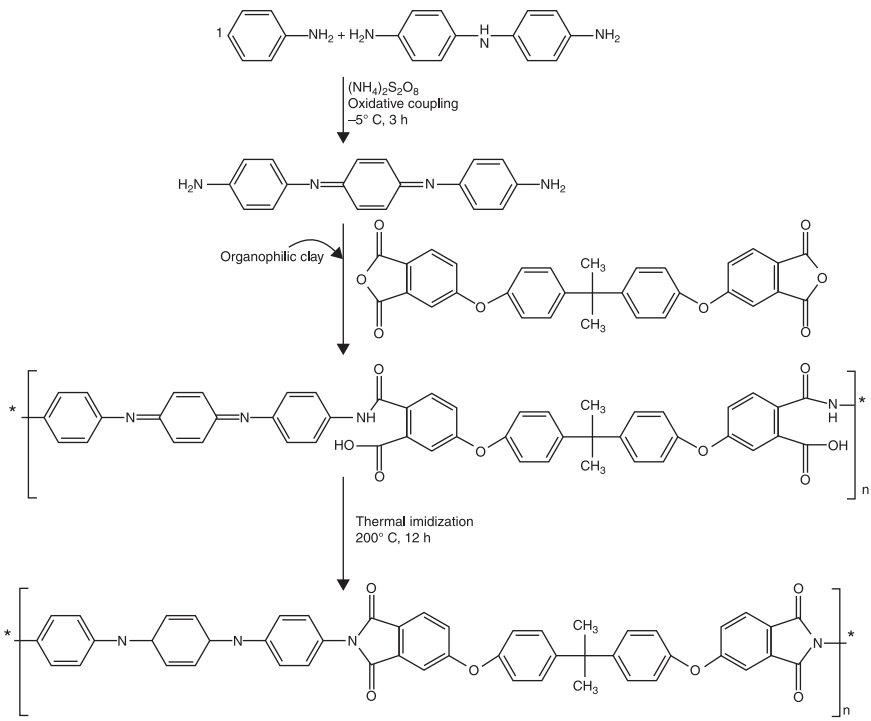

13.13 Schematic representation of the synthesis of ACAT and electroactive polyimide/clay nanocomposite (EPCN).

their high aspect ratio creates more tortuous O_2 and H_2O diffusion pathways, as evidenced by GPA.

The interlayer spacing of MMT clay (2θ = ~6.8°, *d*-spacing = 6.5 nm) increased after surface treatment with an intercalating agent to 9.6 nm (2θ = ~4.6°), as shown in Fig. 13.14. This result confirms the expansion of silicate layers in organophilic MMT clay. At the same time, there are no obvious diffraction peaks for EPCN01 (1 wt% clay dispersed in an EPI matrix) or EPCN03 in 2θ = 2~10°, whereas a diffraction peak appeared at 2θ = ~4.6° (*d*-spacing = 9.6 nm) for organophilic MMT clay, indicating the possibility of having exfoliated and intercalated silicate nanolayers of organophilic clay dispersed in the EPI matrix. In Fig. 13.15, TEM micrographs of EPCN materials, (a) 1 wt% (EPCN01) and (b) 3 wt% (EPCN03) loading, also show that the nanocomposites have a combinational morphology, including both exfoliated and intercalated nanolayered structures simultaneously in the polymer matrix.

This redox behavior of EPI and EPCN can also be further identified by an electrochemical cyclic voltammetry (CV) approach, as shown in Fig. 13.16. The electrochemical CV studies have indicated that EPCN03, in the form of a coating,

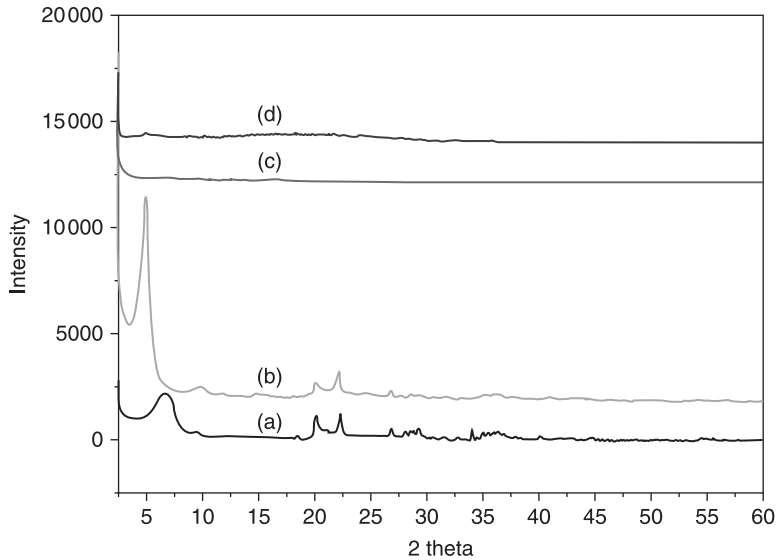

13.14 Wide-angle powder X-ray diffraction patterns of (a) MMT, (b) organophilic/MMT clay, (c) EPCN01 and (d) EPCN03 materials.

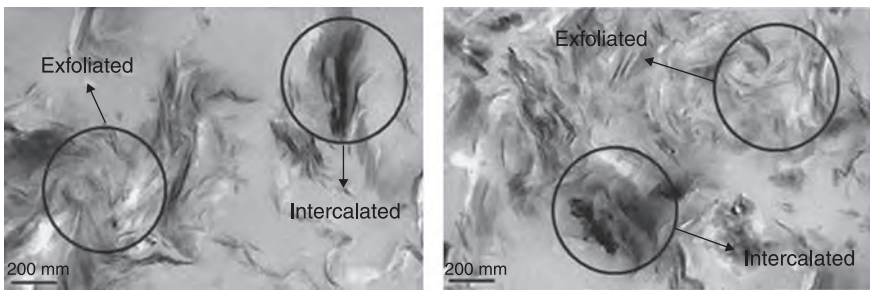

13.15 TEM micrographs of (a) EPCN01 and (b) EPCN03 materials.

showed a single oxidation peak similar to that of neat EPI. However, the CV curve of NEPI was found to exhibit zero redox current, indicating that feeding a conjugated diamine of ACAT may also incorporate electroactivity into the as-prepared EPI. Moreover, thoroughly dispersing clay platelets in the EPI matrix causes little sacrifice in electroactivity.

However, the electrochemical corrosion currents and corrosion potentials of EPCN materials as coatings on CRS were found to decrease gradually with further increases in clay loading (Fig. 13.17).

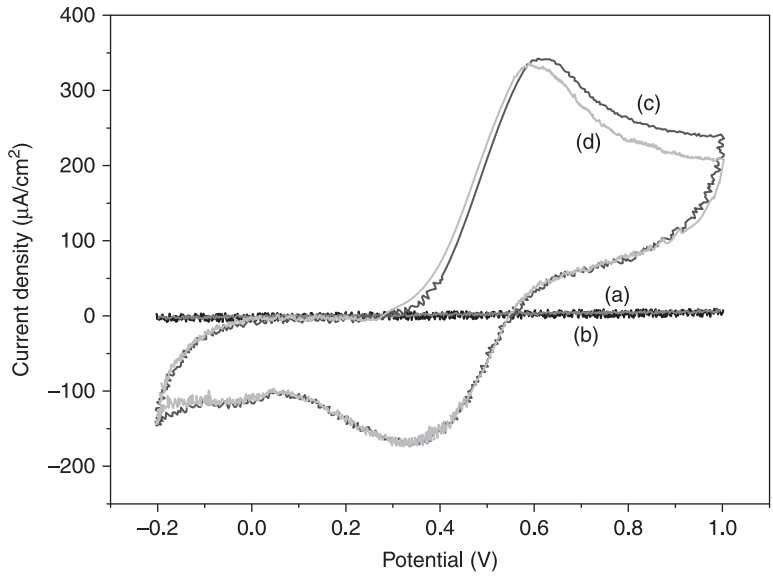

13.16 Cyclic voltammetry of polyimide shown as (a) ITO, (b) NEPI, (c) EPI and (d) EPCN03 measured in aqueous H_2SO_4 (1.0 M) with scan rate of 50 mV/s.

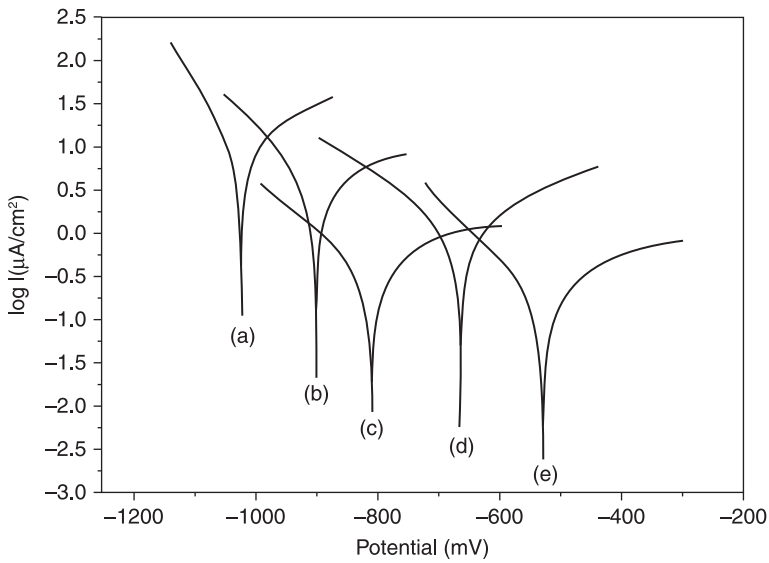

13.17 Tafel plots for (a) bare, (b) NEPI, (c) EPI, (d) EPCN01 and (e) EPCN03 measured in 3.5 wt% aqueous NaCl solution.

The mechanism of enhanced corrosion protection of EPCN coatings was found to be associated with the formation of passivating protective metal oxide layers, induced from the redox catalytic properties of ACAT elements available in as-prepared EPCN coatings, as shown in Fig. 13.18 (a), which was similar to that of PANI coatings reported in the previous literature (Wessling, 1996; Li *et al.*, 1997; Talo *et al.*, 1997; Spinks *et al.*, 2002). An enhanced corrosion protection effect of EPCN coatings compared with neat EPI may result from thoroughly dispersing organophilic clay platelets in the EPI matrix to increase the tortuosity of corrosive O_2 and H_2O diffusion pathways (Fig. 13.18(b)).

Visual observation of passivation oxide layers revealed the deposition of a grayish oxide layer film over the CRS surface (Wessling, 1994, 1996) under an EPCN coating on a CRS electrode. SEM image studies revealed that oxide layers were formed at the interface of an EPCN (i.e. EPCN03) coating and a CRS surface (Fig. 13.19(b)). However, the bare CRS surface was smooth and clear; we could not observe the passive metal oxide layer on the bare CRS surface (Fig. 13.19(a)).

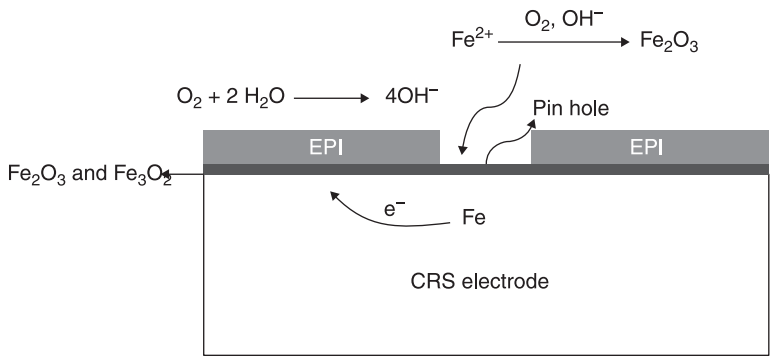

(a)

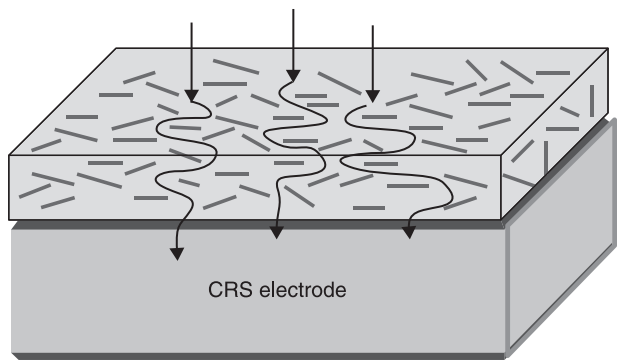

(b)

13.18 Schematic diagrams of (a) mechanism of CRS passivation by EPCN coatings and (b) diffusion pathway of oxygen gas in the EPCN.

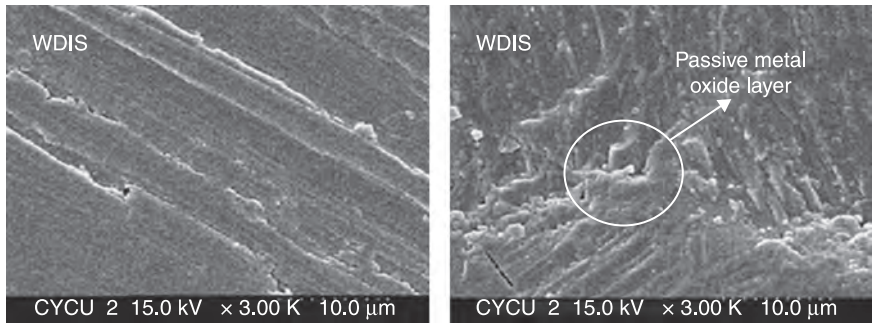

13.19 SEM surface image of (a) polished CRS and (b) CRS induced by EPCN03.

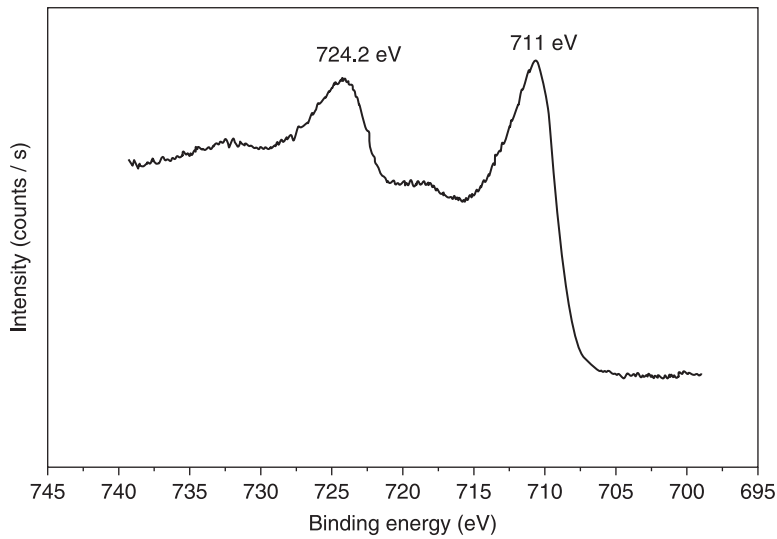

13.20 ESCA Fe 2p core level spectra of EPI.

In addition to the SEM observations, the chemical nature of the passivating oxide layers can also be identified by ESCA investigation. The typical binding energy plots versus intensity for iron oxide layers are shown in Fig. 13.20. Fe 2p spectra of FeO and Fe_3O_4 are very similar and it is hard to distinguish one from the other. Fe $2p_{1/2}$ and Fe $2p_{3/2}$ binding energies were found at approximately 724.2 and 711.0 eV, indicating that the passive oxide layer is predominately composed of Fe_2O_3, above a very thin Fe_3O_4 layer (Lu *et al.*, 1995).

13.6 Conclusions

Smectite clays can be effective reinforcing agents in the synthesis of PCN that display superior properties, even at low clay content (<3 wt%). PCN show enhanced physical properties even with a small amount of added clay, because the nanoscale dimensions of the clay particles yield a large contact area between the polymer matrices and the filler. The structure of clays, with layers of high aspect ratio, also imparts an excellent barrier that exhibits low gas permeability and enhanced anticorrosive properties. Anticorrosive properties of non-conjugated, conjugated and electroactive polymer nanocomposites with clay have been discussed above. The as-prepared PCN, in the form of coatings, showed advanced protection against corrosion on CRS coupons compared with bulk polymers, based on a series of standard electrochemical corrosion measurements including corrosion potential, polarization resistance, corrosion current and impedance spectroscopy.

The enhanced corrosion protection effect of PCN compared with bulk polymers is believed to have resulted from dispersing silicate nanolayers of clay in the polymer matrix to increase the tortuosity of diffusion pathways for H_2O and O_2 molecules, and is further evidenced by the O_2 and H_2O permeability studies on the free-standing film of as-prepared PCN.

It is noteworthy that the investigations of the corrosion protection efficiency of conjugated and electroactive polymer–layered silicate nanocomposite coatings were divided into two separate phases. Firstly, neat conjugated polymer or electroactive polymeric coatings significantly enhanced corrosion protection on CRS electrodes compared with non-conjugated polymeric coatings, and this might be attributed to the redox catalytic property of electroactive aniline trimers in the formation of passive layers of metal oxides. Secondly, the advanced anticorrosive properties of conjugated polymer coatings were revealed by the introduction of layered silicate into the matrix to form conjugated polymer–layered silicate nanocomposite materials.

13.7 References

Acello S. J. and Greene N. D. (1962), *Corrosion*, **18**, 286t–290t.

Albrecht M., Ehrler S. and Muhlebach A. (2003), 'Nanocomposites from Layered Silicates: Graft Polymerization with Intercalated Ammonium Peroxides.' *Macromol Rapid Commun*, **24**, 382–7.

Anbarasan R., Arvind P. and Dhanalakshmi V. (2011), 'Synthesis and Characterization of Polymethacrylamide–Clay Nanocomposites.' *J Appl Polym Sci*, **121**, 563–73.

Aranda P. and Ruiz-Hitzky E. (1992), 'Poly(ethylene oxide)-silicate Intercalation Materials.' *Chem Mater*, **4**, 1395–403.

Asif A., Rao V. L. and Ninan K. N. (2011), 'Preparation, Characterization, Thermo-mechanical, and Barrier Properties of Exfoliated Thermoplastic Toughened Epoxy Clay Ternary Nanocomposites.' *Polym. Adv. Technol*, **22**, 437–47.

Biasci L., Aglietto M., Ruggeri G. and Ciardelli F. (1994), 'Functionalization of Montmorillonite by methylmethacrylate Polymers Containing Side-chain Ammonium Cations.' *Polymer*, **35**, 3296–309.

Biswas M. and Sinha-Ray S. (2001), 'Recent Progress in Synthesis and Evaluation of Polymer-Montmorillonite Nanocomposites.' *Adv. Polym. Sci*, **155**, 167–221.

Chang K. C., Lai M. C., Peng C. W., Chen Y. T., Yeh J. M. *et al.* (2006), 'Comparative Studies on the Corrosion Protection Effect of DBSA-doped Polyaniline Prepared from *in situ* Emulsion Polymerization in the Presence of Hydrophilic Na^+- MMT and Organophilic Organo-MMT Clay Platelets.' *Electrochim. Acta*, **51**, 5645–53.

Chang K. C., Jang G. W., Peng C. W., Lin C. Y., Shieh J. C. *et al.* (2007), 'Comparative Electrochemical Studies at Different Operational Temperatures for the Effect of Nanoclay Platelets on the Anticorrosion Efficiency of DBSA-doped Polyaniline/Na^+–MMT Clay Nanocomposite Coatings.' *Electrochim. Acta*, **52**, 5191–200.

Chang K. C., Chen S. T., Lin H. F., Lin C. L., Huang H. H. *et al.* (2008), 'Effect of Clay on the Corrosion Protection Efficiency of PMMA/Na^+-MMT Clay Nanocomposite Coatings Evaluated by Electrochemical Measurements.' *Eur. Polym. J*, **44**, 13–23.

Chen B. and Evans J. R. G. (2004), 'Preferential Intercalation in Polymer-Clay Nanocomposites.' *J Phys. Chem B*, **108**, 14986.

Chisholm B. J., Moore R. B., Barber G., Khouri F., Hempstead A. *et al.* (2002), 'Nanocomposites Derived from Sulfonated Poly(butylene–terephthalate).' *Macromolecules*, **35**, 5508–16.

Custodio J. V., Agostinho S. M. L. and Simões A. M. P. (2010), 'Electrochemistry and Surface Analysis of The Effect of Benzotriazole on The Cut Edge Corrosion of Galvanized steel.' *Electrochim. Acta*, **55**, 5523–31.

Dang W., Kubouchi M., Yamamoto S., Sembokuya H. and Tsuda K. (2002), 'An approach to chemical recycling of epoxy resin cured with amine using nitric acid.' *Polymer*, **43**, 2953–8.

Deflorian F., Fedrizzi L. and Bonora P. L. (1996), 'Influence of the photo-oxidative degradation on the water barrier and corrosion protection properties of polyester paints.' *Corros Sci*, **38**, 1697–708.

Draper C. W. (1982), *J. Met.*, **34**, 24.

Fornes T. D., Yoon P. J., Hunter D. L., Keskkula H. and Paul D. R. (2002), 'Effect of Organoclay Structure on Nylon-6 Nanocomposite Morphology and Properties.' *Polymer*, **43**, 5915–33.

Fukushima Y. and Inagaki S. (1987), 'Synthesis of an Intercalated Compound of Montmorillonite and 6-polyamide.' *J Inclusion Phenom*, **5**, 473–82.

Garrett R. M. (1964), *Mater Prot*, **3**, 8.

Gilman J. W., Jackson C. L., Morgan A. B., Hayyis R., Jr, Manias E. *et al.* (2000), 'Flammability Properties of Polymer-Layered-Silicate Nanocomposites and Polypropylene and Polystyrene Nanocomposites.' *Chem Mater*, **12**, 1866–73.

Goldberg H. A., Feeney C. A., Karim D. P. and Farrell M. (2002), *Rubber World*, **226**, 1–17.

Grim R. E. (1968), *Clay Mineralogy*, 2nd edn. New York: McGraw-Hill.

Grim R. E. (1962), *Applied Clay Mineralogy*. New York: McGraw-Hill.

Helmy A. K., Ferreiro E. A. and S. Bussetti G. D. (1999), 'Surface Area Evaluation of Montmorillonite.' *J Colloid Interface Sci*, **210**, 167–71.

Huang H.-Y., Huang T. C., Yeh T.-C., Tsai C.-Y., Lai C. L. *et al.* (2011), 'Advanced Anticorrosive Materials Prepared from Amine-capped Aniline Trimer-based Electroactive Polyimide-clay Nanocomposite Materials with Synergistic Effects of Redox Catalytic Capability and Gas Barrier Properties.' *Polymer*, **52**, 2391–400.

Huang X., Lewis S., Brittain W. J. and Vaia R. A. (2000), 'Synthesis of Polycarbonate-Layered Silicate Nanocomposites via Cyclic Oligomers.' *Macromolecules*, **33**, 2000–4.

Hussain F. and Hojjati M. (2006), 'Review Article: Polymer-Matrix Nanocomposites, Processing, Manufacturing and Application: An Overview.' *J Compos Mater*, **40**, 1511–65.

Iroh J. O. and Su W. (2000), 'Corrosion Performance of Polypyrrole Coating Applied to Low Carbon Steel by an Electrochemical Process.' *Electrochim Acta*, **46**, 15–24.

Jeon H. G., Jung H. T., Lee S. W. and Hudson S. D. (1998), 'Morphology of Polymer/silicate Nanocomposites, High Density Polyethylene, and a Nitrile Copolymer High Density Polyethylene and a Nitrile Copolymer.' *Polym Bull*, **41**, 107–13.

Jimenez G., Ogata N., Kawai H. and Ogihara T. (1997), 'Structure and Thermal/mechanical Properties of Poly (ε-caprolactone)/clay Blend.' *J Appl Polym Sci*, **64**, 2211–20.

Kiersnowski A. and Piglowski J. (2004), 'Polymer-layered Silicate Nanocomposites Based on Poly(ε-caprolactone).' *Eur Polym J*, **40**, 1199–207.

Kim J. W., Liu F., Choi H. J., Hong S. H. and Joo J. (2003), 'Intercalated Polypyrrole/Na^+-montmorillonite Nanocomposite via an Inverted Emulsion Pathway Method.' *Polymer*, **44**, 289–93.

Kim Y. and White J. L. (2005), 'Formation of Polymer Nanocomposites with Various Organoclays.' *J Appl Polym Sci*, **96**, 1888–96.

Kojima Y., Usuki A., Kawasumi M., Okada A., Kurauchi T. *et al*., (1993), 'One-pot Synthesis of Nylon 6-clay Hybrid.' *J Polym Sci Part A Polym Chem*, **31**, 1755–8.

Kousik G., Pitchumani S. and Renganathan N. G. (2001), 'Investigation of the Corrosion Resistance Characteristics of Pigments in Alkyd Coatings on Steel.' *Prog Org Coat*, **43**, 286–91.

Krstajic N. V., Grgur B. N., Jovanovic S. M. and Vojnovic M. V. (1997), 'Corrosion Protection of Mild Steel by Polypyrrole Coatings in Acid Sulfate Solutions.' *Electrochim Acta*, **42**, 1685–91.

Lai M. C., Chang K. C., Yeh J. M., Liou S. J., Hsieh M. F. *et al*., (2007), 'Advanced Environmentally Friendly Anticorrosive Materials Prepared from Water-based Polyacrylate/Na^+-MMT Clay Nanocomposite Latexes.' *Eur Polym J*, **43**, 4219–28.

Lan T., Kaviratna P. D. and Pinnavaia T. (1994), 'On the Nature of Polyimide-Clay Hybrid Composites.' *J Chem Mater*, **6**, 573–5.

LeBaron P. C., Wang Z. and Pinnavaia T. J. (1999), 'Polymer-layered Silicate Nanocomposites: An Overview.' *Appl Clay Sci*, **15**, 11–29.

Leu C. M., Wu Z. W. and Wei K. H. (2002), 'Synthesis and Properties of Covalently Bonded Layered Silicates/Polyimide (BTDA-ODA) Nanocomposites.' *Chem Mater*, **14**, 3016–21.

Li P., Tan T. C. and Lee J. Y. (1997), 'Corrosion Protection of Mild Steel by Electroactive Polyaniline Coatings.' *Synth Met*, **88**, 237–42.

Locke C. E. and Sudbury J. D. (1960), *Chem Eng Prog* **56**, 50.

Lu W. K., Elsenbaumer R. L. and Wessling B. (1995), 'Corrosion Protection of Mild Steel by Coatings Containing Polyaniline.' *Synth Met*, **71**, 2163–6.

MacQueen R. C. and Granata R. D. (1996), 'A positron annihilation lifetime spectroscopic study of the corrosion protective properties of epoxy coatings.' *Prog Org Coat*, **28**, 97–112.

Mai Y. and Yu Z. (eds) (2006), *Polymer nanocomposites.* Cambridge: Woodhead.

Malshe V. C. and Sangaj N. S. (2006), 'Effect of introduction of structural defects on protective ability of polyesters.' *Prog Org Coat*, **57**, 37–43.

Masenelli-Varlot K., Vigier G., Vermogen A., Gauthier C., Cavaille J. Y. (2007), 'Quantitative Structural Characterization of Polymer/Clay Nanocomposites and Discussion of an "Ideal" Microstructure Leading to the Highest Mechanical Reinforcement.' *J Polym Sci Part B Polym Phys*, **45**, 1243–51.

McCafferty E., Moore P. G. and Pease G. T. (1982), 'Effect of Laser Surface Melting on the Electrochemical Behavior of an Al 1% Mn Alloy.' *J Electrochem Soc.*, **129**, 9–17.

Moijca J., García E., Rodriguez F. J. and Genescá (2001), 'Evaluation of the protection against corrosion of a thick polyurethane film by electrochemical noise.' *Prog Org Coat*, **42**, 218–25.

Moore P. G. and McCafferty E. (1981), 'Passivation of Fe/Cr Alloys Prepared by Laser-Surface Alloying.' *J Electrochem Soc*, **128**, 1391–3.

Morgan A. B. (2006), 'Flame Retarded Polymer Layered Silicate Nanocomposites: A Review of Commercial and Open Literature Systems.' *Polym Adv Technol*, **17**, 206–17.

Okamoto M., Morita S., Taguchi H., Kim Y. H., Kotaka T. *et al*., (2000), 'Synthesis and Structure of Smectic Clay/poly(methylmethacrylate) and Clay/polystyrene Nanocomposites via *in situ* Intercalative Polymerization.' *Polymer*, **41**, 3887–90.

Okamoto M., Morita S. and Kotaka T. (2001), 'Dispersed Structure and Ionic Conductivity of Smectic Clay/polymer Nanocomposites.' *Polymer*, **42**, 2685–8.

Paul D. R. and Robeson L. M. (2008), 'Polymer Nanotechnology: Nanocomposites.' *Polymer*, **49**, 3187–204.

Picard E., Vermogen A., Gerard J. F. and Espuche E. (2007), 'Barrier Properties of Nylon 6-montmorillonite Nanocomposite Membranes Prepared by Melt Blending: Influence of the Clay Content and Dispersion State: Consequences on Modelling.' *J Membr Sci*, **292**, 133–44.

Pinnavaia T. J. (1983), 'Intercalated Clay Catalysts.' *Science*, **220**, 365.

Pinnavaia T. J. and Beall G.W. (eds) (2000), *Polymer–clay Nanocomposites.* New York: John Wiley and Sons.

Potter D. I., Ahmed M. and Lamond S. (1983), *J Met*, **17**.

Ray S. S. and Okamoto M. (2003), 'Polymer/layered Silicate Nanocomposites: a Review from Preparation to Processing.' *Prog Polym Sci*, **28**, 1539–641.

Rosenfeld I. L. (1981), *Corrosion*, **37**, 371.

Schoonheydt R A, Pinnavaia T. J. and Gangas G. L. N. (1999), 'Pillared Clays and Pillared Layered Solids.' *Pure Appl Chem*, **71**, 2367.

Spinks G. M., Dominis A. J., Wallace G. G. and Tallman D. E. (2002), 'Electroactive Conducting Polymers for Corrosion Control Part 2 – Ferrous Metals.' *J Solid State Electrochem*, **6**, 85–100.

Takahashi S., Goldberg H. A., Feeney C. A., Karim D. P., Farrell M. *et al.* (2006), 'Gas Barrier Properties of Butyl Rubber/vermiculite Nanocomposite Coatings.' *Polymer*, **47**, 3083–93.

Talo A., Passiniemi P., Forsen O. and Ylasaari S. (1997), 'Polyaniline/Epoxy Coatings with Good Anti-Corrosion Properties.' *Synth Met*, **85**, 1333–4.

Tan C. K. and Blackwood D. J. (2003), 'Corrosion protection by multilayered conducting polymer coatings.' *CorrosSci*, **45**, 545–57.

Theng B. K. G. (1979), *Formation and Properties of Clay-polymer Complexes*. Amsterdam: Elsevier Scientific Publishing.

Tiwari A. and Hihara L. H. (2010), 'High Performance Reaction-induced Quasi-ceramic Silicone Conversion Coating for Corrosion Protection of Aluminium Alloys.' *Prog Org Coat*, **69**, 16–25.

Tseng C. R., Wu J. Y., Lee H. Y. and Chang F. C. (2001), 'Preparation and Crystallization Behavior of Syndiotactic Polystyrene–clay Nanocomposites.' *Polymer*, **42**, 10063–70.

Tyan H. L., Liu Y. C. and Wei K. H. (1999), 'Thermally and Mechanically Enhanced Clay/Polyimide Nanocomposite via Reactive Organoclay.' *Chem Mater*, **11**, 1942–7.

Usuki A., Kawasumi M., Kojima Y., Okada A., Kurauchi T. *et al*., (1993), *J Mater Res*, **8**, 1174.

Usuki A., Tukigase A. and Kato M. (2002), 'Preparation and Properties of EPDM–clay Hybrids.' *Polymer*, **43**, 2185–9.

Vaia R. A., Ishii H. and Giannelis E. P. (1993), 'Synthesis and Properties of Two-dimensional Nanostructures by Direct Intercalation of Polymer Melts in Layered Silicates.' *Chem Mater*, **5**, 1694–6.

Vaia R. A., Vasudevan S., Krawiec W., Scanlon L. G. and Giannelis E. P. (1995), 'New Polymer Electrolyte Nanocomposites: Melt Intercalation of Poly(ethylene oxide) in Mica-type Silicates.' *Adv Mater*, **7**, 154–6.

Vaia R. A. and Giannelis E. P. (1997a), 'Lattice Model of Polymer Melt Intercalation in Organically Modified Layered Silicates.' *Macromolecules*, **30**, 7990–9.

Vaia R. A. and Giannelis E. P. (1997b), 'Polymer Melt Intercalation in Organically Modified Layered Silicates: Model Predictions and Experiment.' *Macromolecules*, **30**, 8000–9.

Vermogen A., Masenelli-Varlot K., Segue la R., Duchet-Rumeau J., Boucard S. *et al*., (2005), 'Evaluation of the Structure and Dispersion in Polymer-Layered Silicate Nanocomposites.' *Macromolecules*, **38**, 9661–9.

Wang K. H., Choi M. H., Koo C. M., Choi Y. S. and Chung I. J. (2001), 'Synthesis and Characterization of Maleated Polyethylene/clay Nanocomposites.' *Polymer*, **42**, 9819–26.

Welder B. Q. and Partridge E. P. (1954), 'Practical Performance of Water-conditioning Gadgets.' *Ind Eng Chem*, **46**, 954–60.

Wessling B. (1994), 'Passivation of Metals by Coating with Polyaniline: Corrosion Potential Shift and Morphological Changes.' *Adv Mater*, **6**, 226–8.

Wessling B. (1996), 'Corrosion Prevention with an Organic Metal (polyaniline): Surface Ennobling, Passivation, Corrosion Test Results.' *Mater Corros*, **47**, 439–45.

Wessling B. and Posdorfer J. (1999), 'Corrosion prevention with an organic metal (polyaniline): corrosion test results.' *Electrochim Acta*, **44**, 2139–47.

Worspop F. E. and Kingsburf A. (1950), *Chem Eng Min Rev*, 173.

Xu R., Manias E., Snyder A. J. and Runt J. (2001), 'New Biomedical Poly(urethaneurea)-Layered Silicate Nanocomposites.' *Macromolecules*, **34**, 337–9.

Yano K., Usuki A., Okada A., Kurauchi T. and Kamigaito O. (1993), 'Synthesis and Properties of Polyimide–clay Hybrid.' *J Polym Sci Part A Polym Chem*, **31**, 2493–8.

Yariv S. and Cross H. (eds) (2002), *Organo-clay complexes and interactions*. New York: Marcel Dekker.

Yeh J. M. and Chin C. P. (2003), 'Structure and Properties of Poly(o-methoxyaniline)–clay Nanocomposite Materials.' *J Appl Polym Sci*, **88**, 1072–80.

Yeh J. M., Chen C. L., Chen Y. C., Ma C. Y., Huang H. Y. *et al*., (2004a), 'Enhanced Corrosion Prevention Effect of Polysulfone–clay Nanocomposite Materials Prepared by Solution Dispersion.' *J Appl Polym Sci*, **92**, 631–7.

Yeh J. M., Chen C. L., Chen Y. C., Ma C. Y., Lee K. R. *et al.* (2002), 'Enhancement of Corrosion Protection Effect of Poly(o-ethoxyaniline) via the Formation of Poly(o-ethoxyaniline)–clay Nanocomposite Materials.' *Polymer*, **43**, 2729–36.

Yeh J. M., Chen C. L., Kuo T. H., Su W. F., Huang H. Y. *et al.* (2004b), 'Preparation and Properties of (BATB–ODPA) Polyimide-clay Nanocomposite Materials.' *J Appl Polym Sci*, **92**, 1072–9.

Yeh J. M., Chin C. P. and Chang S. (2003), 'Enhanced Corrosion Protection Coatings Prepared from Soluble Electronically Conductive Polypyrrole-clay Nanocomposite Materials.' *J Appl Polym Sci*, **88**, 3264–72.

Yeh J. M., Hsieh C. F., Jaw J. H., Kuo T. H., Huang H. Y. *et al.* (2005), 'Organo-soluble Polyimide (ODA–BSAA)/montmorillonite Nanocomposite Materials Prepared by Solution Dispersion Technique.' *J Appl Polym Sci*, **95**, 1082–90.

Yeh J. M., Huang H. Y., Chen C. L., Su W. F. and Yu Y. H. (2006), 'Siloxane-modified Epoxy Resin-clay Nanocomposite Coatings with Advanced Anticorrosive Properties Prepared by a Solution Dispersion Approach.' *Surf Coat Technol*, **200**, 2753–63.

Yeh J. M., Kuo T. H., Huang H. J., Chang K. C., Chang M. Y. *et al*., (2007), 'Preparation and Characterization of Poly(o-methoxyaniline)/Na^+–MMT Clay Nanocomposite via Emulsion Polymerization: Electrochemical Studies of Corrosion Protection.' *Eur Polym J*, **43**, 1624–34.

Yeh J. M., Liou S. J., Lai C. Y., Wu P. C. and Tsai T. Y. (2001), 'Enhancement of Corrosion Protection Effect in Polyaniline via the Formation of Polyaniline-Clay Nanocomposite Materials.' *Chem Mater*, **13**, 1131–6.

Yeh J. M., Liou S. J., Lai M. C., Chang Y. W., Huang C. Y. *et al.* (2004c), 'Comparative Studies of the Properties of Poly(methylmethacrylate)–clay Nanocomposite Materials Prepared by *in situ* Emulsion Polymerization and Solution Dispersion.' *J Appl Polym Sc*, **94**, 1936–46.

Yeh J. M., Liou S. J., Lin C. G., Chang Y. P., Yu Y. H. *et al*., (2004d), 'Effective Enhancement of Anticorrosive Properties of Polystyrene by Polystyrene–clay Nanocomposite Materials.' *J Appl Polym Sci*, **92**, 1970–6.

Yeh J. M., Liou S. J., Lin C. Y., Cheng C. Y., Chang Y. W. *et al*., (2002), 'Anticorrosively Enhanced PMMA-Clay Nanocomposite Materials with Quaternary Alkylphosphonium Salt as an Intercalating Agent.' *Chem Mater*, **14**, 154–61.

Yeh J. M., Liou S. J., Lu H. J. and Huang H. Y. (2004), 'Enhancement of Corrosion Protection Effect of Poly(styrene-co-acrylonitrile) by the Incorporation of Nanolayers of Montmorillonite Clay into Copolymer Matrix.' *J Appl Polym Sci*, **92**, 2269–77.

Yu Y. H., Jen C. C., Huang H. Y., Wu P. C., Huang C. C. *et al*., (2004a), 'Preparation and Properties of Heterocyclically Conjugated Poly(3-hexylthiophene)/clay Nanocomposite Materials.' *J Appl Polym Sci*, **91**, 3438–46.

Yu Y. H., Yeh J. M., Liou S. J. and Chang Y. P. (2004b), 'Organo-soluble Polyimide (TBAPP–OPDA)/clay Nanocomposite Materials with Advanced Anticorrosive Properties Prepared from Solution Dispersion Technique.' *Acta Mater*, **52**, 475–86.

Yu Y. H., Yeh J. M., Liou S. J., Chen C. L., Liaw D. J. *et al*. (2004), 'Preparation and Properties of Polyimide–clay Nanocomposite Materials for Anticorrosion Application.' *J Appl Polym Sc*, **92**, 3573–82.

Zelinka S. L. and Stone D. S. (2011), 'Corrosion of Metals in Wood: Comparing The Results of a Rapid Test Method with Long-term Exposure Tests Across Six Wood Treatments.' *Corros Sci*, **53**, 1708–14.

Zhou Q., Fan X., Xia C., Mays J. and Advincula R. (2001), 'Living Anionic Surface Initiated Polymerization (SIP) of Styrene from Clay Surfaces.' *Chem Mater*, **13**, 2465–7.

14

Nanocoatings for corrosion protection of aerospace alloys

R. ASMATULU, Wichita State University, USA

Abstract: As the result of environmental conditions, corrosion usually takes place and degrades the surface of aluminum alloys used in aerospace manufacturing. Commonly used methods of decreasing corrosion rates to improve the lifetime of these alloys include protective coatings, passivations and anodic and cathodic fortification. In addition, new protection methods incorporating nanotechnology-associated approaches have been recently developed. These include surface treatments, nanocomposite thin-film coatings, layer-by-layer coatings, self-cleaning coatings, sol–gel coatings, ceramic coatings, nanoscale alloy coatings and top-layer coatings. Compared with conventional coating materials, nanotechnology-associated coatings significantly increase the corrosion protection of aluminum alloys. In this paper, some of the nanoscale studies involving protective coatings are analyzed and the results evaluated.

Key words: corrosion, protective coatings, passivation, anodic and cathodic fortification, nanocomposite, layer-by-layer coating, sol–gel coating.

14.1 Introduction

14.1.1 Background

Most early airplane skins were made primarily of aluminum alloys, which are lightweight and very good conductors of electricity, in addition to having a high strength compared with other materials.[1] When today's commercial and military aircraft were designed in the 1960s and 1970s, practical lifetimes of 30 to 40 years were anticipated. With increasing aircraft costs and decreasing budgets, many of these aircraft are still in service, and even higher demands have been placed on their extended service lifetimes. As a result, an ever-increasing obstacle to the flightworthiness of aircraft is corrosion, in addition to several billion dollars of repair, maintenance and other costs to air forces and commercial airlines.[2]

Aluminum alloys, the primary metals used in industry, owe their excellent corrosion resistance to a barrier oxide film (20–200 nm) that is bonded strongly to their surfaces. Even if these alloys are damaged, the oxide film quickly reforms in most situations.[1] However, due to the wide variety of environments under which aircraft must operate, urban industrial pollutants, high humidity, hot deserts and marine locations may all combine to accelerate corrosion and jeopardize the structural integrity of aircraft parts.[2] To address this problem, routine inspection

and repair, and periodic restoration of the protective treatment that inhibits corrosion, have been practiced to extend the functional life of aircraft.

Corrosion is the destructive and unwanted attack of a corrosive environment on metals and alloys, and decreases the lifetime of materials used in aircraft and spacecraft manufacturing.[1] As a result of the degradation of metal surfaces, materials can lose their mechanical, other physical, chemical and physicochemical properties and appearance.[2–8] Metal surface corrosion accounts for approximately 4% of an industrialized nation's gross national product (GNP) spent on its prevention, replacement of corroded parts, maintenance and environmental protection. This translates to nearly $300 billion direct and indirect costs to the US economy per year at 2003 prices.[8]

For more than a century, a number of different aluminum alloys have been commonly used in the aircraft industry.[1] These substrates mainly contain several alloying elements, such as copper, chromium, iron, nickel, cobalt, magnesium, manganese, silicon, titanium and zinc. It is known that these metals and alloys can be dissolved as oxides or other compounds in an aqueous medium due to the chemical or electrochemical reactions between their metal surfaces and the environment (solution). The rate of the dissolution from anode to cathode phases at the metal surfaces can be influenced by the electrical conductivity of electrolytic solutions. Thus, anodic and cathodic electron transfer reactions readily exist with bulk electrolytes in water and, hence, produce corrosive products and ions.[1–3] It is known that pure water has poor electrical conductivity, which in turn lowers the corrosion rate of materials; however, natural environmental solutions (e.g. sea water, acid rains, emissions or pollutants, chemical products and industrial waste) are highly corrosive and the environment's temperature, humidity, UV light and pressure continuously vary depending on time and the type of process involved.[2,3]

14.1.2 Aerospace alloys

Currently there are a number of aerospace alloys, including Al- and Mg-, Ni-, Co- and Ti-based alloys. In aluminum-based alloys, Al is the predominate metal in the system along with alloying elements such as copper, zinc, manganese, silicon and magnesium. Two main classifications of Al-based alloys are cast and wrought alloys, both of which are subdivided into heat-treatable and non-heat-treatable categories.[1] More than 80% of Al alloys are produced by the wrought process in the form of rolled sheets and foils because of their higher strength and lower density. The following Al alloys are commonly used in aircraft and other aerospace applications (helicopters and spacecraft): 7075, 6061, 6063, 2024 and 5052. Among these, the 7075 Al alloy is most preferred by the aircraft industry. The composition of this specific Al alloy is 5.1–6.1% zinc, 2.1–2.9% magnesium, 1.2–2.0% copper and less than 0.5% of silicon, iron, manganese, titanium, chromium and other trace metals.[9] Aluminum alloys are widely used in aircraft

fuselages and other engineering structures and compounds in which light weight and corrosion resistance are highly desired.

In addition to Al-based alloys, specially designed alloys make it possible for the aircraft industry to produce high-strength parts for jet engines and airframes where high pressure, temperature and vibration are greatly considered during their design and manufacturing.[9] Stainless steel, titanium, nickel, copper and their alloys are the major components of aerospace alloys utilized for engine blocks, providing high strength and/or the ability to perform at extremely high temperatures. The ratio of engine power to weight, airframe strength and many other factors drastically affect jet performance. Also, these alloys are designed to be strong, resistant to corrosion and able to maintain their integrity at any temperature.

Initially, little or no attention was paid to corrosion and corrosion control of commercial and military airplanes. As the age of an aircraft exceeds 20 years of service life, corrosion becomes a major concern, thus bringing corrosion prevention and control issues to the forefront of design and manufacturing. For several years now, corrosion of military aircraft and other equipment has been an ongoing problem. Data provided by the US military indicate that corrosion is potentially the number one cost, which totals approximately $20 billion annually.[10]

14.1.3 Aerospace alloy corrosion

The structural integrity of aging aircraft structures can be directly related to corrosion. As the service life of aircraft increases, eventually there will be a growing probability of corrosion formation, along with other forms of damage such as fatigue cracks, stress–corrosion cracking and other local or global damage.[11] In addition, aging aircraft can accumulate residual structural stresses in their structures, or on the rivets and around rivet holes, decreasing the mechanical properties of Al alloys and reducing the lifetimes of these highly expensive pieces of equipment.[12]

Usually, the surfaces of Al and Al alloys keep their apparent shine in a low humidity environment because of the protective oxide layer on the surface, which can be up to several hundred nanometers thick.[13] At higher humidity and temperatures, galvanic, pitting and intergranular corrosion, hydrogen embrittlement and selective leaching can take place, mainly on the surface of Al alloys if there is sufficient electrical conductivity between the environment and the metal surface.[14] Other types of corrosion can also take place on Al alloys, but these may be negligible compared with other types of corrosion forming on aircraft alloys.

Galvanic corrosion is an electrochemical process in which one of two metals preferentially corrodes in an electrolyte aqueous solution at the joint.[13] During aircraft manufacturing, Al or Mg alloys are usually in contact with highly corrosion-resistant carbon or stainless steel where galvanic corrosion can take

place, which accelerates the corrosion formation on Al or Mg alloys.[15] Riveted areas are highly vulnerable to galvanic corrosion if the rivets and alloys are of dissimilar materials. A number of procedures can prevent galvanic corrosion:[16] spraying a protective coating between dissimilar metals, insulating the electrical conductivity; balancing the anode and cathode areas; aeration of salty sea water; reducing electrolytes and electrical contacts; lowering the range of individual potential difference; removing microorganisms and dust accumulation; changing the microstructure (grain size reduction); forming a passive oxide layer; applying an impressed current; neutralizing the pH values of the solution; and reducing the content of humidity, temperature, UV light and oxygen.[9]

Pitting corrosion is a localized corrosion by which small cavities or holes are formed on the surface of metals. This is one of the more dangerous corrosions because of its limited detection and the persistence of pitting formations.[1] These small holes and cavities can lead to a catastrophic failure of the engineering systems. Surface oxide layers and other corrosion products often cover the surfaces of the pits and make them entirely invisible.[14] Aluminum pit corrosion is randomly localized in the passive region of the protective oxide layer. Based on pitting conditions, the pit width, length and shape can change over time. In an open environment, pitting corrosion is mostly initiated in the weak areas of the materials by chlorine (Cl^-) ions, fluorine (F^-) ions and oxygen, which are abundant elements on earth.[17] Pits prorogate into aluminum and Al alloys according to the following reactions:[18]

$$Al = Al_3^+ + 3e^- \quad [14.1]$$

$$Al_3^+ + 3H_2O = Al(OH)_3 + 3H^+ \quad [14.2]$$

Additionally, hydrogen evolution and oxygen reduction can take place at the intermetallic cathodes:

$$2H^+ + 2e^- = H_2 \quad [14.3]$$

$$O_2 + 2H_2O + 4e^- = 4OH^- \quad [14.4]$$

When a pit begins to form through an anodic reaction, the pH of the environment inside the pit is reduced, according to Reaction [14.2]. In order to balance the positive charges produced in Reactions [14.1] and [14.2], chlorine ions migrate into the pit sites, resulting in HCl formation and hence pitting. During the reduction reaction, local alkalinization around the cathodic particles can occur. These cathodic particles already exist in the system. Since aluminum oxide layers are usually not stable in such an environment, Al around the cathodic particles dissolves, thus creating alkaline pits on the surface.[17] Pure aluminum metal usually has lower electrode potential than its alloys, so connecting these two can accelerate galvanic corrosion as well. Most Al alloys have excellent resistance to atmospheric corrosion, and usually the requirements for additional protection are minimal in that short period.[9]

Intergranular corrosion is another type of localized corrosion, whereby the grain boundaries (or crystallites) of metals are selectively dissolved and visible boundary lines are created.[19] Grain boundaries are the precipitated and segregated sites of the metals, which makes them physically and chemically different from the remaining matrix. Here, the bulk grains are not usually attacked by the corrosion species and the depth of corrosion is often shallow.[1] Al alloys are very rich in corrosion-resistant elements such as titanium, chromium, copper and nickel, and these alloying elements can be depleted in the grain boundaries. The depleted zones on the grain boundaries are electrochemically active, and this activity is based on the alloy composition and thermo-mechanical processing.[17] These zones can also exhibit local galvanic coupling, resulting in galvanic corrosion of the Al alloys. Usually, Al-based alloys are sensitive to intergranular corrosion and can be weakened over time.

Hydrogen embrittlement is a process whereby hydrogen atoms are introduced into metals and alloys. This can seriously reduce the ductility of the materials, resulting in catastrophic brittle failures at a stress well below the yield stress of the materials.[20] In this process, hydrogen atoms dissolve into metals and increase their hardness exponentially.[9] Although hydrogen embrittlement does not affect all metals and alloys, the most vulnerable materials include high-strength steels and aluminum and titanium alloys. The main sources of hydrogen come from a hydrogen-contaminated environment, electrolysis, storage tanks, by-products of general corrosion reactions and other cathodic reactions.[14] The production of atomic hydrogen is as follows in this single-step reaction:[11]

$$H_2O + e^- = OH^- + H \qquad [14.5]$$

A hydrogen atom-rich solution provides an aggressive environment for Al alloys. Many Al alloy-based aging aircraft have corrosion damage during their service life because of corrosion-induced hydrogen embrittlement mechanisms.[21–23] More specifically, hydrogen atoms cause lattice defects (e.g. vacancies, dislocations, grain boundaries) and distortions on Al alloys and make them extremely brittle. The Aloha Airlines accident in 1988 is considered to have had this type of mechanism failure as well as other environmentally induced cracking.[11]

Selective leaching (or de-alloying) is the leaching process of a less noble metal from alloys in a suitable condition. This is a localized corrosion process. The most common elements typically undergoing selective removal include zinc, aluminum, nickel, iron, chromium and cobalt. What remains is a mechanically weak, porous structure with very low ductility.[24] Aluminum metal can preferentially dissolve from an Al alloy in a de-aluminification process. Severe marine environments and acidity accelerate the Al depletion process from the alloys. Selective leaching can be prevented by oxygen removal from the solution, cathodic protection, selection of alloying elements and grain-size reduction.[25]

In addition to these corrosions, others may also take place on aerospace alloys, including bacterial corrosion, uniform corrosion, hot temperature corrosion,

exfoliation (lamellar or layer) corrosion, deposit corrosion, crevice corrosion and fretting corrosion.[1,9,13] This deterioration, along with residual stress and fatigue, can accelerate the aging process of aircraft alloys and reduce the aircraft's overall mechanical performance. This has been an unsolved engineering problem for several decades and needs to be addressed.

14.1.4 Protective coatings

Protective coatings are frequently utilized for the purpose of protecting composite and metal and alloy surfaces against environmental attack. For the Al alloy surface, three layers of the protective coatings, such as chromate conversion coating, primer coating and a top layer coating are generally employed. Figure 14.1 shows the protective coatings on an aircraft Al alloy with approximate thicknesses.[1] Chromate conversion coatings have a good atmospheric corrosion resistance and are commonly used by the aircraft industry. Primer coating is a preparatory coating on the metal surface prior to the top coating to ensure better adhesion, higher durability and additional protection against corrosion. Finally, a polymeric top layer coat consisting of polyurethane, polyamide, polyester, resin or epoxy is applied to protect the remaining layers and substrates against chemicals, oxygen and light. The top layer is also used as a foundation for coloring and design, as these extra elements have a strong tendency to react with alloy surfaces.[20]

Polymeric coatings undergo physical, chemical and physicochemical deterioration as a result of environmental interactions. These degradations can develop in the form of swelling by radiation (solar UV light, electron beams, x-ray, β-ray and γ-ray), water absorption (causing a reduction in hardness and stiffness), dissolution, cross-linking, oxidation and color changes due to heat, acid rain, oxidative environments (O_2 and O_3) and other factors.[7] Additionally, at elevated temperatures some gas species may evolve from the coatings, thus reducing the strength, molecular weight (MW), gloss, density and glass transition temperature (*Tg*), and thereby increasing the porosity and surface roughness of the polymeric coatings. The combined effects of degradation can also take place on organic materials. Finally, the degradation process alters mechanical, electrical,

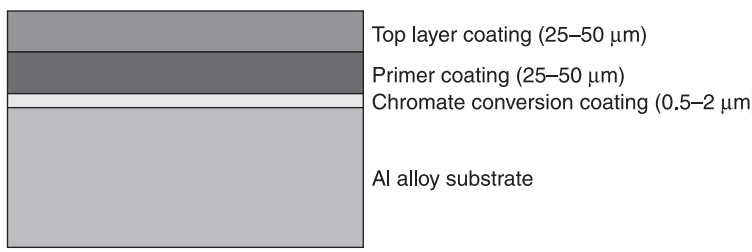

14.1 Three layers of protective coatings for Al alloys of aircraft.

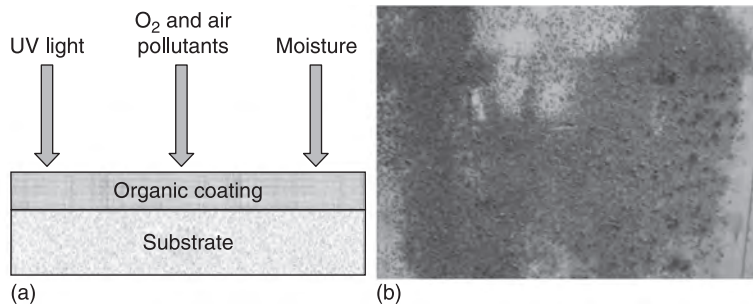

14.2 (a) Atmospheric influences on organic coating and (b) corrosion formations on a substrate coated with an epoxy-based polymeric substance.

thermal and optical properties, as well as other chemical and physicochemical properties of the materials.[2] Figure 14.2 shows the major atmospheric influences on an organic coating and corrosion formations on a substrate.[6]

Comparing all environmental conditions, the most destructive damage on a polymeric coating is the result of UV light over a long period of time. The sun emits high-intensity UV light, which causes the formation of free radicals on polymer surfaces.[2] These radicals are simply groups of atoms/molecules with an excess number of electrons that want to pair with other electrons in the polymer structure. Therefore, this process breaks the covalent bonds of polymer molecules into small molecules and initiates cross-linking reactions (extra polymerization) or oxidation.[7] During a long period of UV light exposure, these polymers can be overly cured at wavelength ranges of 300 nm to 400 nm, which in turn causes shrinkage/expansion and hence increases the internal stresses and brittleness of the polymers.[6] Because of the long-term UV exposure, synthetic and naturally occurring polymeric coatings cannot defend against environmental attack. Especially at higher levels of cross-linking, polymeric materials can degrade, eventually causing crack propagation on the protective coatings. Therefore, composites, metals and alloys under the coatings can be degraded or dissolved as oxides or other compounds.[6]

Surface treatment methods are currently used to prevent corrosion and enhance adhesion between metals and coating materials. For these purposes, chromate-, zinc- and phosphate-based materials are employed to increase the corrosion resistance of surfaces as well as enhance coating quality.[20] However, some of these materials are unacceptable from an ecological and human health point of view, and an alternative system must be considered to reduce these concerns.[1] Recently, several research programs have focused on low-toxicity materials that could replace currently used materials. These new surface treatments should improve corrosion protection and also provide good adhesion between metal and paint surfaces.[2–8]

Several recent studies on nanostructured materials (nanocomposites, nanoscale thin-film coatings, nanoparticles, nanograins, diamond-like coatings, sol–gel, etc) have also been conducted to analyze the possible corrosion-mitigating effects of such materials.[9] The motivation for this work comes from the fact that, in comparison to bulk materials, nanoscale materials may have unique physical, chemical and physicochemical properties that allow improved corrosion protection. It is known that such nanoparticles in a low dosage create a high surface area in order to allow their uniform dispersion into matrix materials; therefore, the efficiency of nanocomposites can be significantly high in terms of material properties.

14.2 Nanotechnology-associated approaches

Nanotechnology-associated coatings include nanoscale conversion coatings, nanoscale ceramic coatings, sol–gel coatings, nanocomposite coatings, thermal-barrier coatings, ceramic coatings, layer-by-layer (LBL) coatings, nanoscale self-cleaning coatings and nanoscale alloy coatings. These coatings have many applications in commercial and military aircraft to improve durability, reliability and performance of components, as well as to improve surface quality and produce corrosion-resistant coatings for combating galvanic, pitting, hydrogen embrittlement, fretting, leaching and hot corrosion.[1]

14.2.1 Nanoscale conversion coatings

Conversion coatings or surface passivations have been employed on the surfaces of metals and alloys for more than a century.[20] Conversion coatings involve (but are not limited to) molybdenum, zirconium, chromium, aluminum, vanadium, phosphate, potassium, cerium, nickel and zinc-rich layers to increase the polarization resistance of the surface and hence decrease current and potential corrosion rates.[2,8,9,26,27] However, hexavalent chromium conversion coatings have several environmental concerns, and in the near future the use of such materials will possibly be banned by the aircraft industry worldwide.[2] Wet and dry chemical processes can be applied to conversion coatings on a number of different metals with thicknesses between 20 nm and 20 μm.[1] Recently, new research programs have focused on molybdenum, zirconium and phosphate coatings, since these are more environmentally friendly for the aircraft industry.[8] In our recent studies, a thin layer of molybdenum coating was applied on Al alloys, and then a nanocomposite coating was applied on the overall surface (Fig. 14.3).[2] Polymeric nanocomposite coatings will be discussed in Section 14.2.3.

14.2.2 Sol–gel coatings

Sol–gel is a wet-chemical process that involves the formation of an inorganic colloidal suspension (sol) and gelation of the sol in a continuous liquid phase (gel)

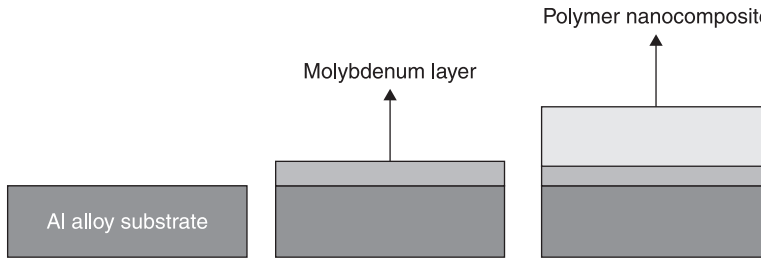

14.3 Design of corrosion conversion coating on Al alloy substrate.

to form a three-dimensional network structure. The precursors for synthesizing colloidal sols consist of organometallic compounds surrounded by reactive functional groups. Metal alkoxides, such as alkoxysilanes (tetramethoxysilane and tetraethoxysilane), aluminates, titanates, zirconates and borates, are the most used in a sol–gel process.[28] Sol–gels can be in the form of films, particles, fibers, aerogels and dense materials at micro- and nanoscale following a heat treatment. Sol–gel products are initially amorphous, so the crystalline sol–gel products can be achieved using appropriate heat treatments.

The range of applications of sol–gel-derived products in the aerospace industry continuously expands because of their resulting strength, density and chemical inertness.[28] One of the largest aircraft applications is thin-film coating on various alloy surfaces, which can be produced by spin-coating, spray-coating, roll-casting, electrophoresis and dipping. One of the main reasons for employing sol–gel coating is to replace the highly toxic chromium conversion coatings on Al alloys.[29] Generally, surface treatments using the sol–gel process improve corrosion resistance because of the formation of an oxide layer on the surface of the alloys. This protective film acts as a barrier against oxygen diffusion into the metal surface.[30]

14.2.3 Polymeric nanocomposite coatings

Nanocomposite coatings are formed by mixing two or more dissimilar materials at nanoscale to improve the physical, chemical and physicochemical properties of the new materials. The properties of nanocomposite coatings depend on several factors, including the individual components, dispersion, morphology and shape, surface functionalization, interfacial intentions and processing techniques.[31] Nanocomposite coating is one of the fastest growing areas of nanotechnology research. New nanocomposite coatings are continuously being developed with novel properties that are absent in the constituent materials. These materials offer a number of new applications in the following areas: aerospace, electronics, biomedical implants, automotive, marine, non-linear optics, mechanically reinforced lightweight materials, sensors, batteries, bioceramics, energy conversion and many others.[32]

The contact angle is an equilibrium angle where the liquid–vapor interface meets the solid surface. Usually, the concept is illustrated with a small liquid droplet resting on a flat horizontal solid surface, which can identify the surface hydrophobicity (tendency to repel water) and surface hydrophilicity (strong affinity for water) of the materials.[6] At lower contact-angle values, it is believed that coatings can absorb more water molecules and increase the corrosion and degradation rates of the materials.[33] The contact-angle method is often used in characterizing the surface properties of nanocomposite materials.[34,35]

A variety of research has been performed on polymeric nanocomposite thin-film coatings for corrosion mitigation because of their distinctive thermal stability and mechanical and molecular barrier properties.[2] These include organic (silica gel, para-aminobenzoic acid, benzophenones, etc) and inorganic (clay, silica, zirconia, titania and carbon nanotubes, graphene, carbon black, etc) nanoparticulates incorporated into polymeric matrixes (epoxy resin, polyimide, polystyrene, nylon, poly(methyl methacrylate), etc) at very low volume fractions of 0.5% to 5%.[3–7] In a nanocomposite fabrication, polymers and nanoparticles are generally synthesized by using a solution, melt interaction and/or *in situ* polymerization. Nanostructured films formed by a process involving an air nozzle spray, brush and electrostatic self-assembly (ESA) result in highly ordered and densely packed layers that can function as a barrier to underlying substrates.[8] For example, corrosion test results obtained on poly(o-ethoxyaniline)/clay nanocomposites showed that the corrosion potential (E_{corr}), corrosion current (I_{corr}) and corrosion rate (R_{corr}) exponentially decreased, while polarization resistance (R_p) significantly increased as a function of the nanoclay contents.[36–38]

The latest study was conducted on the corrosion protection of Al alloys using carbon nanotubes (CNT) and graphene-based nanocomposite coatings.[3,5,6] Nanocomposite coatings were prepared by dispersing multiwall carbon nanotubes (MWCNTs) and graphene platelets in an epoxy primer. Inclusions were mixed with the solvent reducer and sonicated for 30 minutes to ensure good dispersion. The epoxy primer was shaken on a pneumatic paint shaker and then transferred to a hot plate. The inclusions/solvent mixtures were slowly added drop-wise to the epoxy primer and the resulting solution was stirred on a hot plate for 24 hours at room temperature. After 24 hours, a curing agent was added to the mixture and stirred for 15 minutes to produce the uncured nanocomposite coating. Mixtures of 0.25%, 0.5%, 1% and 2% MWCNT or graphene were prepared, and corresponding test samples were painted at different thicknesses. Figure 14.4 shows the SEM images of the MWCNT mixtures in the epoxy primer. These images clearly show that the MWCNTs were well dispersed in the epoxy primer.[5] The nanocomposite coatings on the Al alloy substrates were then exposed to both UV chamber and salt fog chambers at different testing conditions.

Figure 14.5 shows the contact-angle values of a one-millimeter-thick coating on Al substrates with various MWCNT under various UV exposure times. As can

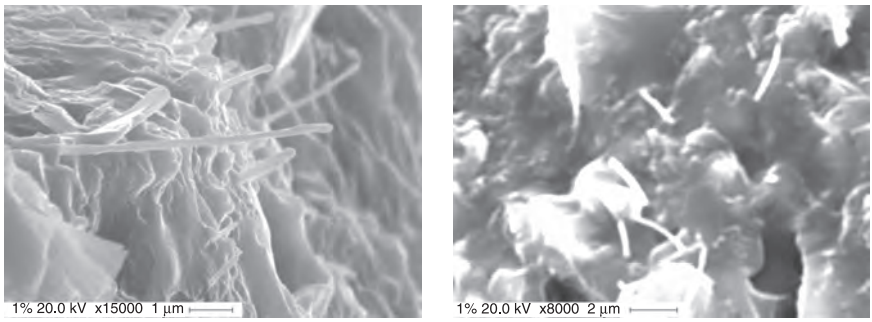

14.4 SEM images of MWCNTs dispersed into epoxy primer used for aircraft coating.

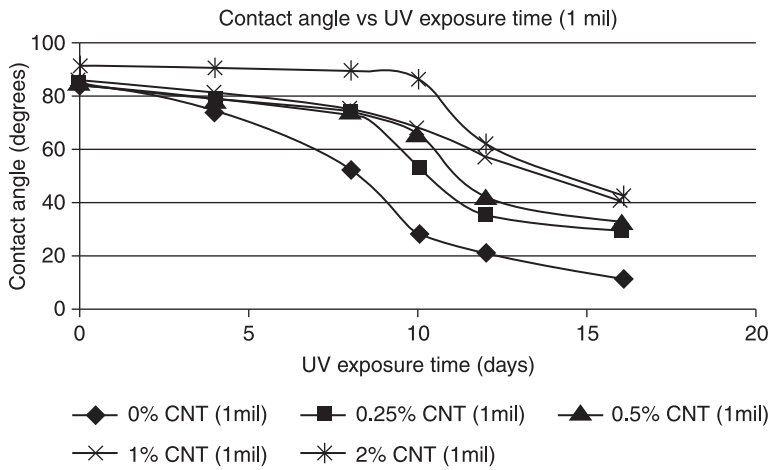

14.5 Change in contact-angle values with UV exposure time for 1-millimeter-thick coatings at different percentages of MWCNTs.

be seen, at day 0 of UV exposure, the average contact-angle values of 0%, 0.25%, 0.5%, 1% and 2% MWCNT nanocomposite coatings are between 84° and 91°; however, after 16 days of UV exposure, the contact-angle values are gradually reduced to 11°, 30°, 33°, 40° and 43°, respectively.[6] This may be attributed to the absorption and blockage of UV light by the inclusions, as well as the prevention of crack formations on the nanocomposite surfaces.[39] The data also indicate that the surface hydrophobic properties of the coatings were improved by adding carbon nanotubes, which increased the coating resistance to UV light and corrosion species.

In order to determine the degradation levels of coatings at nanoscale, atomic force microscopy (AFM) studies were conducted on the coated samples. Figure 14.6 shows the AFM surface images of 1-millimeter nanocomposite coatings at 0 day and 16 days of UV exposure.[6] These images clearly prove that the surface morphology of coated samples is entirely changed after UV exposure. At 0 day of UV exposure, the surface looks smooth and shiny, whereby a higher contact angle is achieved, while at 16 days of UV exposure, the surface smoothness and glossiness seem reduced or completely disappeared, by which a lower contact angle or hydrophilic surface has formed. This may be due to the fact that the radicalized polymer chains under UV light interact with oxygen and hydroxyl species, resulting in rougher and hydrophilic surfaces.[33]

Most aircraft skins are made of aluminum alloys that have protective organic coatings; however, these coatings experience UV degradation. This primarily occurs as a result of the weak protective coatings/paints on the surface of Al alloys. This route accelerates the aging process and fatigue cracks, and reduces the overall mechanical properties of the aircraft. The new coating systems with a

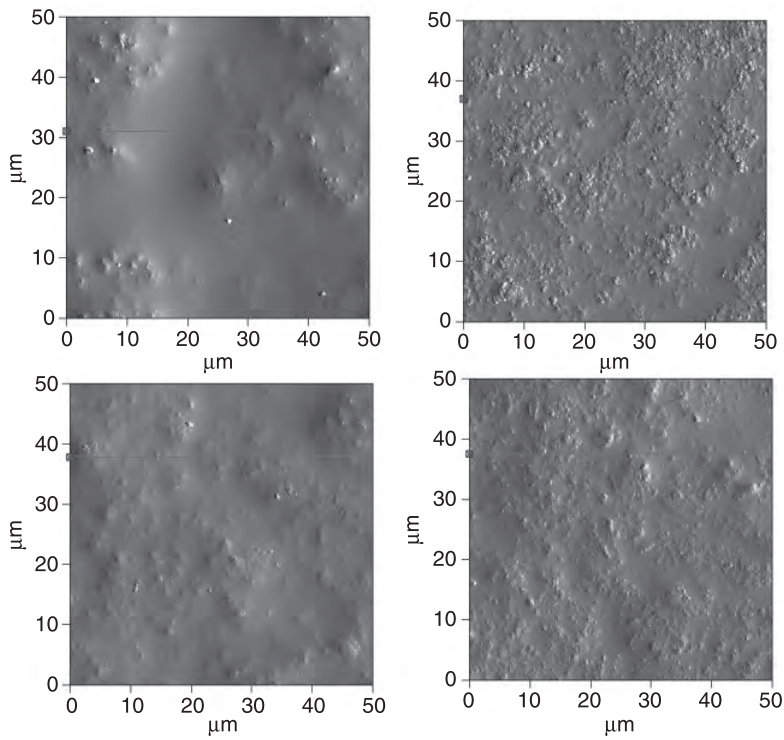

14.6 AFM surface images of coatings with carbon nanotubes before (left) and after 16 days of UV exposures (right).

higher contact angle and UV resistance values will open up new possibilities for extending the lifetime of aircraft.[6]

Polyurethane top coatings are favorable coating materials that have a wide variety of osmotic barrier, chemical, thermal, hydrolytic and oxidative stability properties, which may be advantageous for preventing the corrosion of aircraft alloys. Although some coating materials (i.e. epoxy and acrylic bases) are readily available and inexpensive in the market, their protection capabilities are limited in severe environmental conditions.[2] For this reason, urethane top coatings are preferred for protecting not only initial organic layers (or nanocomposite layers) but also material surfaces against corrosion attack.[8] Recently, fluorinated polyurethanes that have the lowest known surface energy (6 mN/m) were developed to drastically decrease the permeability of the films against corrosive ions and molecules, moisture, temperature and UV radiation. It has been reported that interfacial coating and surface treatment (plasma and chemical etching) techniques can significantly improve the adhesion between protective layers and material surfaces and, hence, increase corrosion resistance.[40] Nanocomposite urethane top coatings can also be sprayed on nanostructured surfaces to further increase the strength of the coatings used by the aircraft industry.[33]

14.2.4 Layer-by-layer coatings

Layer-by-layer (LBL) nanofilms have demonstrated value in many specific applications of coatings.[41] These films can be fabricated on glass, metals and alloys, ceramics, polymers and their compounds using a dipping technique to modify the performance (e.g. corrosion, biological, optical, electrical, tribological, thermal, magnetic and electrostatic) of the materials and also to protect the surface from environmental effects.[40,42] LBL films can be applied easily to clean surfaces. For instance, a negatively charged substrate that is dipped into a solution containing cationic polyelectrolytes (e.g. poly(diallyldimethylammonium chloride)-PDDA), which are attracted to the anionic surface, self-assembles into a single layer of molecules.[42] The resulting physical, chemical and physicochemical properties indicate that the molecular order of such individual bilayers is nearly perfect, in much the same way that the electrical charge on a free-conducting surface distributes itself uniformly over the surface in order to minimize the total system energy.[40] Subsequent anionic (e.g., polystyrene-119) and cationic monolayers are added in bilayer pairs, by alternately dipping the substrate into those positively and negatively charged solutions, to produce a multilayer nanostructured film.[42]

LBL coating provides a simple barrier against corrosive species in the same way as a conventional organic coating. A recent study revealed that the nanoclay-based LBL coatings exhibit very high corrosion protection on aluminum and Al alloys because of the molecular nature of the LBL system. The anticorrosion behavior of the LBL coating is based on the following mechanisms:[43] (i) the pH

buffer formed by the polybase and polyacid complex suppresses pH changes during corrosion; (ii) the coating regenerates and eliminates defects of the polymer chains in a swollen network; (iii) polyelectrolyte layers form a carrier for the inhibitor; and (iv) the polyelectrolyte system presents a corrosion-resistant barrier between the surface and the environment. Although LBL films are extremely light in weight and highly effective for corrosion pretention, they are very vulnerable to external forces. As soon as the films are ruptured, they no longer protect the surfaces of aircraft skins.

By modifying the surfaces or choosing appropriate polyelectrolytes, both superhydrophobic (contact angle $\theta > 150°$)[44,45] and superhydrophilic ($\theta < 5°$ in less than 0.5 sec)[46] surfaces can be created. In nature, there are many superhydrophobic surfaces, such as the sacred lotus leaf, taro leaf, grass leaf and water strider's legs. The superhydrophobicity of these materials is mostly related to the hierarchical roughness, voids, channels and hydrophobic structure of the surfaces.[45] Thus, superhydrophobic surfaces may be used for self-cleaning purposes on Al alloy surfaces, which in turn reduces corrosion rates.

14.2.5 Nanoscale ceramic coatings

Ceramic coatings can provide high-performance oxide layers on metals and alloys to solve the problems of corrosion, wear, heat, insulation and friction.[1] Some ceramic coatings include thermal spray coating, plasma spray coating, sputter coating, dry-film lubricants and other wet chemical and electrochemical coatings.[47–49] The thickness of ceramic films can range from 50 nm to several micron meters, depending on the application and coating processes. Recently, new nanoscale ceramic coatings such as Si_3N_4,[50] silicon carbide,[51] a diamond-like coating,[52] boron nitride[53] and cerium oxide[47] have been considered in metal and alloy coatings to produce promising high-temperature structural materials due to their excellent thermo-mechanical properties.

Ceramic coatings have various advantages: they increase the lifetime of parts, prevent corrosion, reduce heat on high-temperature components, reduce friction, stop thermal and acidic corrosion and improve the appearance of surfaces.[9] Although ceramic coatings have several advantages, they have some disadvantages as well: they are extremely brittle and hard to repair; de-bonding can occur during the expansion and shrinkage; corrosion easily forms at the cracks; they are heavier than organic coatings; and the coating involves additional equipment, supplies and labor.[48]

14.2.6 Nanoscale thermal barrier coatings

Thermal barrier coatings (TBCs) are high-temperature coating systems for metallic surfaces such as on gas turbines, power stations and transportation vehicles and aero-engine parts operating at elevated temperatures. These coatings serve to protect those parts exposed to high temperatures, while limiting the thermal exposure of

structural components, thus extending the lifetime of the parts and reducing oxidation, hot corrosion and erosion, and thermal fatigue.[47] TBCs consist of two layers on the surface of alloys: a metallic bond coating (or MCrAlY coatings, where M = Co, Ni or Co/Ni) and an oxide ceramic coating. The first layer (bond) is used to bind the oxide to the material surface, while the second layer (zirconia-stabilized yttria) is used to protect the material's surface against hot environmental conditions.[48]

It is reported that when compared with the conventionally used TBCs, by using a thermal barrier coating as the top layer (or interfacial layer), corrosion and erosion resistance (high surface hardness and wear resistance) of the material surface can be improved significantly.[47] Nanoscale porous coatings are used to insulate hot sections of metallic compounds from the hot gas stream of the gas turbine engines of aircraft. Air spray and electron beam physical vapor deposition techniques are employed to coat such protective layers.[30] It has also been found that nanoporosity formed on the coating materials can lead to increased corrosion resistance by dissipating excess heat.[54]

14.2.7 Nanoscale alloy coatings

Super-hard alloy coatings have been developed recently to increase the surface performance of aluminum and its alloys, steel and other components.[55,56] These coatings consist of boron, iron, carbon, cobalt, nickel, zinc and other compounds. The alloy coating can be applied on the surface using twin-wire arc spraying, sputter coating and other physical and chemical techniques. These coatings provide protection against wear, erosion, abrasion and corrosion in a harsh environment because of their smaller grain size and structure, interfacial incarnations and greater hardness (Vickers hardness).[1] A recent study showed that the corrosion resistance of electrodeposited Zn–Ni alloy coating (~15% Ni) could be seven times better than that of a pure zinc coating against corrosion attack.[8] Similar corrosion resistance was also seen on FeCrTiN alloy samples due to the higher corrosion resistance of Cr.[8]

14.3 Conclusions

Recently, nanotechnology-associated multifunctional coating systems have been developed for aircraft applications to provide corrosion protection, sense corrosion and mechanical damage of Al alloys, achieve optimal adhesion using environmentally friendlier materials, detect color changes and improve fatigue resistance of aircraft alloys. The coatings include nanoscale conversion, ceramic, sol–gel, thermal barrier, polymeric nanocomposite, nanoscale alloy, layer-by-layer and nanocomposite top layers. These coatings are usually lightweight, high-strength and thermally stable nanomaterials that can be used in various parts of aircraft. The recent progress on nanotechnology-associated coatings will make aircraft alloys more efficient, more economical and safer and will extend aircraft service life.

14.4 Acknowledgment

The author gratefully acknowledges Wichita State University for supporting this work.

14.5 References

1. Roberge, P. R. *Corrosion Engineering, Principals and Practice*, McGraw-Hill, 2008.
2. Asmatulu, R., Claus, R. O., Mecham, J. B., and Corcoran, S. G. 'Improving the Corrosion Resistance of Aluminum Alloys Using Polymeric Nanocomposite Coatings,' *Materials Science*, Vol. 43, 2007, pp. 415–22.
3. Asmatulu, R. and Revuri, S. 'Synthesis and Characterization of Nanocomposite Coatings for the Prevention of Metal Surfaces,' SAMPE, Fall Technical Conference 2008, Memphis, TN, 8–11 September, 2008, pp. 1–13.
4. Asmatulu, R., Claus, R., Mecham, J. B. and Corcoran, S. 'Corrosion Protection of Surfaces by Nanocomposite and Urethane Top Coatings,' *Smart Structures and Materials, Proceedings of SPIE*, Vol. 5761, 2005, pp. 40–51.
5. Asmatulu, R., Hille, C. and Misak, H. 'Corrosion Protection of Unclad 2024-T3 Aluminum Surface with Both Chromium Conversion and MWCNT Nanocomposite Coatings,' *SAMPE Fall Technical Conference*, Wichita, Kansas, 2009.
6. Asmatulu, R. 'UV Degradation Prevention on Fiber-Reinforced Composite Blades,' Final Technical Report, Department of Energy (#DE, FG36–08GO88149), 2010.
7. Asmatulu, R., Claus, R. O. and Tuzcu, I. 'Adhesion Failures of Thin Film Coatings by Internal and External Stresses at Interfaces,' *Proceedings of 5th International Congress on Thermal Stresses and Related Topics*, TS2003, 8–11 June, 2003, MA-6–3–1.
8. Asmatulu, R. and Claus, R. O. 'Corrosion Protection of Materials Surfaces by Applying Nanotechnology Associated Studies,' *Materials Research Society Symposium Proceedings* (MRS 2004 Spring Meeting, Boston) Vol. 788, pp. L11.44.1–L11.44.6.
9. Davis, J. R. 'Aluminum and Aluminum Alloys—ASM Specialty Handbook,' ASM International, 1993.
10. http://corrosion-doctors.org/Aircraft/Introduction.htm, accessed 25 July, 2010.
11. Kamoutsi, H., Haidemenopoulos, G. N., Bontozoglou, V., and Pantelakis, S. 'Corrosion-Induced Hydrogen Embrittlement in Aluminum Alloy 2024,' *Corrosion Science*, Vol. 48, 2006, pp. 1209–24.
12. Aloha Airlines, Flight 243, NTSB Report Number AAR-89–03, Washington, DC, adopted on 14 June, 1989.
13. Revie, R. W. and Henry, U. H. *Corrosion and Corrosion Control—An Introduction to Corrosion Science and Engineering*, 4th Edition, Wiley-Interscience, 2008.
14. Ahmad, Z. 'Principles of Corrosion Engineering and Corrosion Control,' IChemE, 2006.
15. Mansfeld, F. and Kenkel, J. V. 'Galvanic Corrosion of Al Alloys—III. The Effect of Area Ratio,' *Corrosion Science*, Vol. 15, 1975, pp. 239–50.
16. http://en.wikipedia.org/wiki/Galvanic_corrosion, accessed 25 July, 2010.
17. Svenningsen, G. 'Corrosion of Aluminum Alloys,' Department of Materials Technology, 7491 Trondheim, Norway.
18. Nisancioglu, K. 'Corrosion of Aluminum Alloys,' *Proceedings of ICAA3*, NTH and SINTEF, Trondheim, Vol. 3, 1992, pp. 239–59.

19. Thompson, G. E. 'The Role of Alloying Elements on the Surface Treatment and Finishing of Aluminum,' *Materials Science Forum*, Vol. 519–21, 2006, pp. 615–20.
20. Schweitzer, P. *Fundamentals of Corrosion: Mechanisms, Causes and Prevention Methods*, CRC Press, 2009.
21. Young, G. A., and Scully, J. R. 'The Effect of Test Temperature, Temper and Alloyed Copper on the Hydrogen Controlled Crack Growth Rate of an Al–Zn–Mg–(Cu) Alloy,' *Metallic Materials* Vol. A 33, 2002, pp. 101–15.
22. Speidel, M. O. 'Hydrogen Embrittlement and Stress Corrosion Cracking of Aluminum Alloys', In R. Gibala and R. F. Heheman (Eds.), *Hydrogen Embrittlement and Stress Corrosion Cracking*, ASM, Materials Park, OH, 1992, pp. 271–96.
23. Azofeifa, D. E., Clark, N., Amador, A. and Saenz, A. 'Determination of Hydrogen Absorption in Pd Coated Al Thin Films,' *Thin Solid Films*, Vol. 300, 1997, pp. 295–8.
24. http://en.wikipedia.org/wiki/Selective_leaching, accessed 20 July, 2010.
25. Bardal, E. *Corrosion and Protection*, Springer, 2004.
26. Guan, H. and Buchheit, R. G. 'Corrosion Protection of Aluminum Alloy 2024-T3 by Vanadate Conversion Coatings,' *Corrosion*, Vol. 60, 2004, pp. 284–96.
27. Fahrenholtz, W. G., O'Keefe, M. J., Zhou, H. and Grant, J. T. 'Characterization of Cerium-Based Conversion Coatings for Corrosion Protection of Aluminum Alloys,' *Surface and Coating Technology*, Vol. 155, 2002, pp. 208–13.
28. Sakka, S. *Handbook of Sol-Gel Science and Technology: Processing, Characterization and Application*, Kluwer Academic Publisher, 2005.
29. Feng, Z., Liu, Y., Thompson, G. E. and Skeldon, P. 'Crack-Free Sol-Gel Coatings for Protection of AA1050 Aluminium Alloy,' *Surface and Interface Analysis*, Vol. 42, 2009, pp. 306–10.
30. Hamdy, A. S. 'Advanced Nano-Particles Anti-Corrosion Ceria Based Sol Gel Coatings for Aluminum Alloys,' *Materials Letters*, Vol. 60, 2006, pp. 2633–7.
31. Ochsner, A., Ahmed, W. and Ali, N. *Nanocomposite Coatings and Nanocomposite Materials*, Trans Tech Publications, 2009.
32. Cavaleiro, A. and de Hosson, J. T. M. *Nanostructured Coatings*, Springer, 2006.
33. Erbil, Y. H. *Surface Chemistry of Solid And Liquid Interface*, Blackwell Publishing, 2006.
34. Asmatulu, R., Mahmud, G. A., Zhang, B. and Ahmed, I. 'Effects of UV Light on Water Contact Angles of Nanocomposite Coatings,' SAMPE Fall Technical Conference, Salt Lake City, UT, 11–14 October, 2010, 11 pages.
35. Asmatulu, R. and Mahmud, G. A. 'Prevention of Surface Crack Formations on Polymeric Coatings using Carbon Nanotubes,' ASME International Mechanical Engineering Congress and Exposition, Vancouver, Canada – 12–18 November, 2010, 7 pages.
35. Funakawa, S., Yamamuro, Y., Luo, H. and Sugino, T. 'Field Emission Characteristics of Boron Nitride Nanofilms Deposited on Substrate with Various Work Functions,' *Diamond and Related Materials*, Vol. 13, 2004, pp. 994–8.
36. Yeh, J. M., Chen, C. L., Chen, Y. C., Ma, C. Y., Lee, K. R. *et al.* 'Enhancement of Corrosion Protection Effect of Poly (*o*-ethoxyaniline) via the Formation of Poly (*o*-ethoxyaniline)-Clay Nanocomposite Materials,' *Polymer*, Vol. 43, No. 9, 2002, pp. 2729–36.
37. Chen, C., Khobaib, M. and Curliss, D. 'Epoxy Layered-Silicate Nanocomposites,' *Progress in Organic Coatings*, Vol. 47, No. 3–4, 2003, pp. 376–83.
38. Zaarei, D., Sarabi, A. A., Sharif, F. and Kassiriha, S. M. 'Structure, Properties and Corrosion Resistivity of Polymeric Nanocomposite Coatings Based on Layered Silicates,' *Journal of Coating Technology and Research*, Vol. 5, 2008, pp 1935–3804.

39. Mahmud, G. A. 'Increasing the Coating Resistance Against UV Degradation and Corrosion Using Nanocomposite Coating,' MS Thesis, Wichita State University, 2009.
40. Dahotre, N. B., and Nayak, S. 'Nanocoatings for Engine Applications,' *Surface and Coating Technology*, Vol. 194, 2005, pp. 58–67.
40. Gogotsi, Y. *Nanomaterials Handbook*, CRC Press, 2006.
41. Lichter, J. A., and Rubner, M. F. 'Polyelectrolyte Multilayers with Intrinsic Antimicrobial Functionality: The Importance of Mobile Polycations,' *Langmuir*, Vol. 25, No. 13, 2009, pp. 7686–94.
42. Asmatulu, R., Geist, B., Spillman, W. B., and Claus, R. O. 'Dielectric Constant and Breakdown Field Studies of Electrostatic Self-Assembled Materials,' *Smart Materials and Structures*, Vol. 14, 2005, pp. 1493–500.
43. Andreeva, D. V., Skorb, E. V. and Shchukin, D. G. 'Layer-by-Layer Polyelectrolyte/Inhibitor Nanostructures for Metal Corrosion Protection,' *ACS Applied Materials and Interface Sciences*, Vol. 2, No. 7, 2010, pp. 1954–62.
44. Zhai, L., Cebeci, F. C., Cohen, R. E., and Rubner, M. F. 'Stable Superhydrophobic Coatings from Polyelectrolyte Multilayers,' *Nano Letters*, Vol. 4, No. 7, 2004, pp. 1349–53.
45. Ceylan, M., Asmatulu, R., Khan, W. and Nuraje, N. 'Superhydrophobic Behavior of Electrospun Micro and Nanofibers,' SAMPE Fall Technical Conference, Wichita, 19–22 October, 2009, 8 pp.
46. Cebeci, F. C., Wu, Z., Zhai, L., Cohen, R. E. and Rubner, M. F. 'Nanoporosity-Driven Superhydrophilicity: A Means to Create Multifunctional Antifogging Coatings,' *Langmuir*, Vol. 22, 2006, pp. 2856–62.
47. Sculz, U., Lin, H.-T., Salem, J. and Zhu, D. 'Advanced Ceramic Coating and Interfaces II,' *Ceramic Engineering Science Proceedings*, Wiley, Vol. 28, 2008.
48. Lin, H.-T., Zhu, D., Ohji, T. and Wereszczat, A. 'Advanced ceramic coating and interfaces III,' *Ceramic Engineering Science Proceedings*, Wiley, Vol. 29, 2008.
49. Wang, K., Kim, Y. J., Hayashi, Y., Lee, C. G., and Koo, B. H. 'Ceramic Coatings on 6061 Al Alloys by Plasma Electrolytic Oxidation Under Different AC Voltages,' *Journal of Ceramic Processing Research*, Vol. 10, No. 4, 2009, pp. 562–6.
50. Gao, L. and Li, J. 'Preparation of h-BN Nanofilm Coated α-Si3N4 Composite Particles by a Chemical Route,' *Journal of Materials Chemistry*, Vol. 13, 2003, pp. 628–30.
51. Kusunose, T., Choa, Y. H., Sekino, T. and Niihara, K. 'Mechanical Properties of Si3N4/BN Composites by Chemical,' *Ceramic Society of Japan*, Vol. 2, 1998, pp. 475–9.
52. Wang, X., Qian, G. and Jin, Z. 'Preparation of SiC/BN Nanocomposite Powders by Chemical Processing,' *Materials Letter*, Vol. 58, 2004, pp. 1419–23.
53. Ni, W., Cheng, Y. T., Weiner, A. M. and Perry, T. A. 'Tribological Behavior of Diamond-Like-Carbon (DLC) Coatings Against Aluminum Alloys at Elevated Temperatures,' *Surface and Coatings Technology*, Vol. 201, 2006, pp. 3229–34.
54. http://www.inframat.com/SPS.htm, accessed 27 July, 2010.
55. Meacham, B. 'Nanocomposite Steel Alloy Coating Technology Provides Protection from Wear, Abrasion and Erosion,' The NanoSteel Company, Inc., February 2008.
56. McCrea, J. 'Nanostructured Zn-Based Electrodeposits for Cd-Replacement on High-Strength Steel Fasteners,' Project Number WP-1616, Integran Technologies Inc., ASETS Defense, Tempe, AZ, 28 February, 2008.

15

Nanoscience and biomaterial corrosion control

M. BOBBY KANNAN, James Cook University, Australia
and V. S. SAJI, Korea University, South Korea

Abstract: There is enormous interest in nanostructured biomaterials as they can stimulate tissue–biomaterial interaction more effectively. Research is focused on developing advanced nanostructured biomaterials. The major strategies include fabrication of nanocomposites, surface nanostructuring and nanostructured coatings. A potential issue of concern in terms of biocompatibility is the corrosion resistance of the modified biomaterials. This chapter presents the current trends in this area with emphasis on load-bearing orthopaedic and dental implants. A detailed account on the general and the localized corrosion of conventional metallic implants is provided. Novel fabrication strategies of nanostructured hydroxyapatite-based coatings and their roles as barrier coatings are presented. Impacts of nanoscale surface modifications on the corrosion resistance of permanent implants and novel bioresorbable implants based on magnesium alloys are highlighted.

Key words: nanocomposites, surface nanostructuring, nanostructured coatings, biocompatibility, orthopaedic and dental implants, bioresorbable.

15.1 Introduction

Metallic, ceramic, polymeric and composite biomaterials have been used extensively as orthopaedic and dental implants. Metals (stainless steels, cobalt–chromium alloys, titanium alloys), ceramics (alumina, bioglass, hydroxyapatite), polymers (ultra-high molecular weight polyethylene, polymethylmethacrylate) and their composites are widely employed in bone repairs and joint replacements. Commercially pure titanium (CP-Ti) and their alloys, cobalt–chromium (Co–Cr) cast alloys, hydroxyapatites (HA) and bioglass are the commonly used dental implant materials. Biodegradable (resorbable) scaffolds are attractive for less load-bearing applications and help to eliminate additional surgery required to remove the implant after serving its function. The series of complex post-implantation interactions at the tissue–implant interface is critical in determining the implant success. The surface topography (micro or nanostructured) of the implant can have significant impact on these cellular interactions. Other determining factors include surface chemistry changes and mechanical properties of the implants during service (Williams, 1987; Park and Bronzino, 2003).

Corrosion resistance is one of the most basic criteria in selecting metallic materials for use in surgical implant applications. In general, titanium and its alloys are immune to film breakdown under physiological conditions, whereas

cobalt-based alloys and stainless steels suffer film breakdown under certain conditions. However, all these metallic materials exposed to body fluid (which contains salts, enzymes and proteins) release ions into the surrounding tissue at a very slow rate. In fact, corrosion products are responsible for limiting the biocompatibility of metallic materials since they can potentially produce undesirable reactions in tissues. In addition, orthopaedic and dental implants are exposed to mechanical loading during their service and the synergetic effect of corrosion and mechanical loading could lead to failure of implants.

15.2 General and localized corrosion in orthopaedics and dental implants

Titanium and its alloys are known as being the most suitable metallic biomaterials. They are used in orthopaedic applications due to their excellent mechanical properties. More importantly, they form a very stable oxide layer in body fluid and hence possess exceptional biocompatibility as compared with other metal implant materials. However, these materials undergo failure due to surface reactions and mechanical loading. Passive corrosion or accelerating processes such as wear have led to the release of titanium and the other alloying elements into the surrounding tissues. This section discusses the corrosion issues in titanium and its alloys, cobalt-based alloys, stainless steels and nickel–titanium alloys.

Azevedo investigated the failure of a pure titanium reconstruction plate used for osteosynthesis. Fracture surface analysis revealed intense secondary intergranular cracking, as shown in Fig. 15.1. A selective attack of the β-precipitates on the surface of the implant was observed. The author suggested that the premature fracture of the plate was caused by a corrosion-fatigue mechanism associated with selective attack of β-phase in the region of high stress concentration (Azevedo, 2003).

As stated earlier, the passive layer of titanium alloys can potentially break down by mechanical process such as wear. However, titanium has the ability to repassivate after film breakdown. Khan *et al*. investigated the ability of various titanium alloys (Ti–6Al–4V, Ti–6Al–7Nb and Ti–13Nb–13Zr) to repassivate in phosphate buffered saline (PBS), bovine albumin solutions (in PBS) and 10% foetal calf serum (in PBS) at different pH values and at different albumin concentrations. They found that an increase in the pH had a greater effect on the corrosion behaviour of Ti–6Al–4V and Ti–6Al–7Nb than on Ti–13Nb–13Zr in PBS. Further, they found that the addition of protein to the PBS reduced the influence of pH on the corrosion behaviour of all the alloys. They also reported that proteins in the environment appear to interact with the repassivation process at the surface of these alloys and influence the resulting surface properties (Khan *et al.*, 1999).

Pitting corrosion is a localized form of corrosion by which pits are produced in the materials. This form of corrosion in load-bearing implants could lead

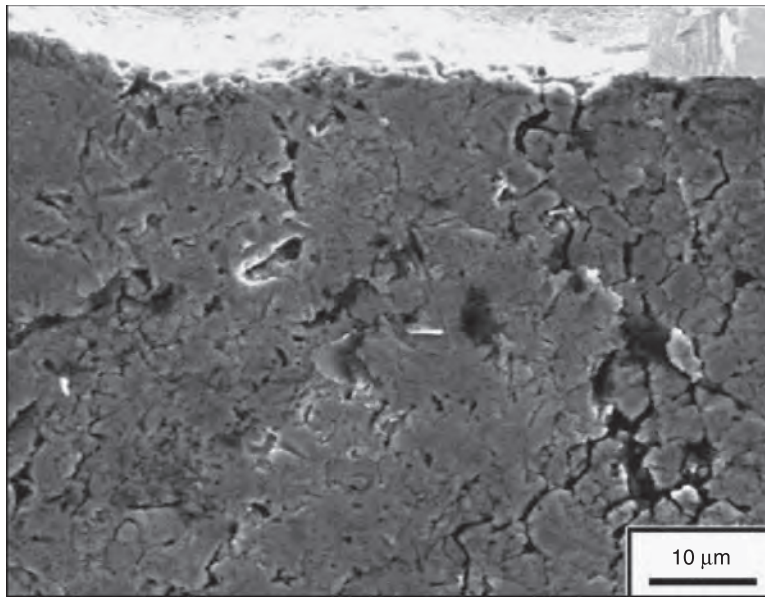

15.1 Failure analysis of a commercially pure titanium plate used for osteosynthesis, showing localized intergranular cracking found on the plate notch surface near the fracture origin (Azevedo, 2003).

to catastrophic failure. Olmedo *et al.* evaluated the biological effect of pitting corrosion of titanium. Their histological study of titanium implants subjected to pitting corrosion showed insufficient bone–implant contact. In fact, the contact was only present in the areas with no pitting and/or surface alterations. They also found that the corrosion products contained titanium around the blood vessels and areas of bone marrow in the metal–tissue interface (Olmedo *et al.*, 2008).

Dissimilar/similar metal joints are used in implant applications. In such situations, it is critical to know the galvanic corrosion effect of dissimilar metals; equally, in the case of weld joints the localized corrosion behaviour of weld/heat affected zones has to be evaluated. Reclaru *et al.* studied the corrosion behaviour of combinations of materials used in orthopaedic implants, i.e. welded stainless steel, to understand the risk of starting localized corrosion such as pitting, crevice or intergranular corrosion from a galvanic couple. They observed that sensitized samples (weld joint produced by tungsten inert gas welding) exhibited some localized intergranular corrosion, as shown in Fig. 15.2, at a small distance along the welded stainless steel (Reclaru *et al.*, 2001).

Kumar and Narayanan studied the corrosion behaviour of Ti–15Mo alloy in 0.15 M NaCl solution containing varying concentrations of fluoride ions for dental

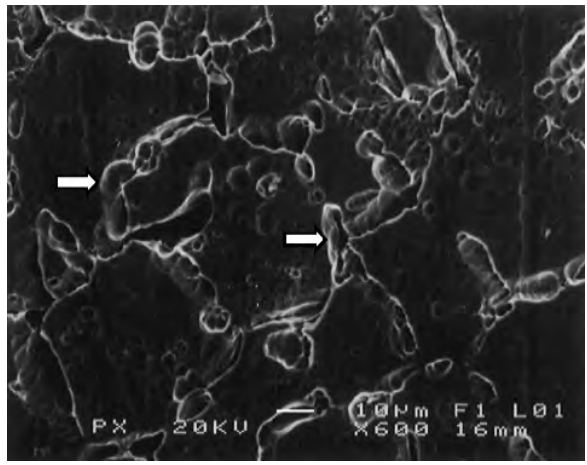

15.2 Intergranular corrosion at the interface weld of stainless steel (Reclaru *et al.*, 2001).

applications. Their study revealed that there is a strong dependence of the corrosion resistance of Ti–15Mo alloy on the concentration of fluoride ions in the electrolyte medium. They found that an increase in fluoride ion concentration increases the corrosion current density and also the passive current density of the alloy (Kumar and Narayanan, 2008). Mareci *et al.* studied the corrosion behaviour of Ti–Ta alloys (different concentrations of Ta) and Ti–6Al–7Nb alloy in fluoridated acidified saliva. They reported a decrease in corrosion resistance and less protective passive oxide films for all titanium alloys (Mareci *et al.*, 2009). Recently, Sivakumar *et al.* studied the fretting corrosion behaviour of Ti–6Al–4V alloy in artificial saliva containing different concentrations of fluoride ions. They observed cathodic shift in free corrosion potential with the onset of fretting, which indicated damage of the passive film. After the fretting motion was ceased, an instantaneous repassivation of Ti–6Al–4V alloy was observed only in artificial saliva. The negative influence of fluoride ions on passive film formation hinders instantaneous repassivation of the damaged areas of the fretted zone (Sivakumar *et al.*, 2011).

The effect of fluoride and chloride ions on the corrosion behaviour of nickel–titanium orthodontic wires was studied by Li *et al.* Their study indicated that Ni–Ti alloy was primarily susceptible to localized corrosion when exposed to a solution containing chloride ions and general corrosion in fluoride ioncontaining solution. A synergistic detrimental effect was observed on Ni–Ti alloy when exposed to solution containing fluoride and chloride ions (Fig. 15.3) (Li *et al.*, 2007). Yan *et al.* reported that organic species (proteins) enhance corrosion-related damage in Co–Cr–Mo alloy and 316L stainless steel. They also observed

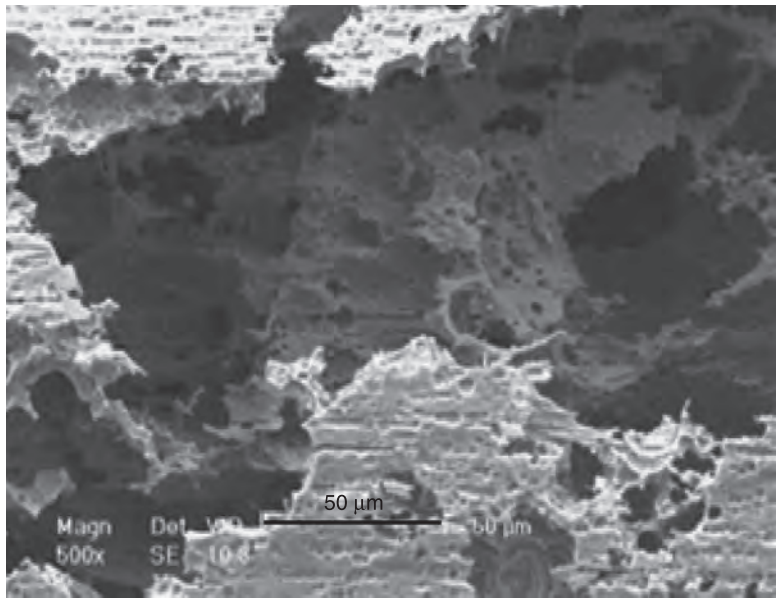

15.3 Corrosion attack on nickel–titanium wire in a solution containing chloride and fluoride (Li *et al.*, 2007).

that the constituents of bovine serum have a great influence on their corrosion behaviour. In static conditions, the authors observed passive film breakdown. However, in tribological contacts, the biofilm formed effectively reduced friction. Interestingly, the authors found that Co–Cr–Mo reactions at the surface in the contact zone formed a very complex nanostructured layer which comprised wear debris and biofilm. Moreover, they suggest that the reaction products and the process also changed the nature of the passive film formation and the film reduced the material loss (Yan *et al.*, 2007).

Stainless steels are the most commonly used biomaterial in orthopaedic implant applications. However, these materials have issues such as passivity breakdown, wear and fatigue failures. Azar *et al.* reported that shot peening treatments on 316L stainless steel increase the breakdown potential and decrease the corrosion current density as compared with untreated material in Ringer's solution (Azar *et al.*, 2010). The correlation between the microstructure and fatigue crack initiation of an austenitic stainless steel biomaterial was investigated by Giordani *et al.* It was observed that the crack initiation was caused by particle rupture rather than by separation of the particle/matrix interface. The authors suggested that coarse Z-phase precipitates and non-metallic inclusions are detrimental to the fatigue properties of the steel, and the microstructural constituents accelerate the initiation of fatigue and corrosion fatigue cracks (Giordani *et al.*, 2004).

Unfortunately, the metallic biomaterials do not sufficiently replicate the surface of the replaced bone and, as a consequence, failures of implants do occur due to insufficient bonding with adjacent bone. Hence, surface treatments are often required for better biocompatibility and osteointegration. Bioceramic coatings are widely used on medical metallic implants to modify the surface so that the implants possess the bulk properties of the substrate, i.e. the good mechanical performances of metals and the bioactive properties of bioceramics.

15.3 Nanostructured biomaterials

In recent years, biomaterials engineered at the nanometre scale have gained recognition due to their various potential advantages over conventional (micrometre scale) biomaterials. Nanostructured biomaterials are expected to interact more effectively with the biological molecules in the human body, as most of these molecules are also at the nanometre scale. Many studies have demonstrated that implants having nanotopography/nanostructure stimulate more positive cellular response than conventional materials through controlled cell growth, protein deposition, increased osteoblast adhesion and proliferation (Karlsson *et al.*, 2003; Jager *et al.*, 2007; Richert *et al.*, 2008; Saji *et al.*, 2010). The increased surface area and finer surface roughness at the nanometre scale are expected to yield better biological response of osteogenic cells and effective tissue–implant mechanical interlocking. The superior hardness and strength of nanomaterials in comparison with their microstructured counterparts are attractive in making highly wear-resistant implants. Even though the majority of the implants currently in clinical use are micrometre-scale surface roughened, it is expected that in the near future nanostructured implants will be extensively used.

The major current approaches to making nanostructured biomaterials fall under the following headings (Saji *et al.*, 2010):

- Nanoscale surface modifications altering topography.
- Nanomaterialistically manipulating the surface chemistry.
- Nanoceramic coatings.
- Nanocomposites.

There are no comprehensive standards or literature available on the corrosion behaviour of such nanostructured implants. Figure 15.4 schematically represents a few likely outcomes. The following sections discuss the effects of these modifications on the corrosion resistance of orthopaedic and dental implants. More specifically, Section 15.4 discusses the effect of nanoscale surface modifications on the corrosion behaviour of titanium based alloys. Section 15.5 discusses nanoceramic coatings with emphasis on HA coatings. Current approaches in making nanostructured coatings and nanocomposites for Mg based resorbable implants are presented in Section 15.6.

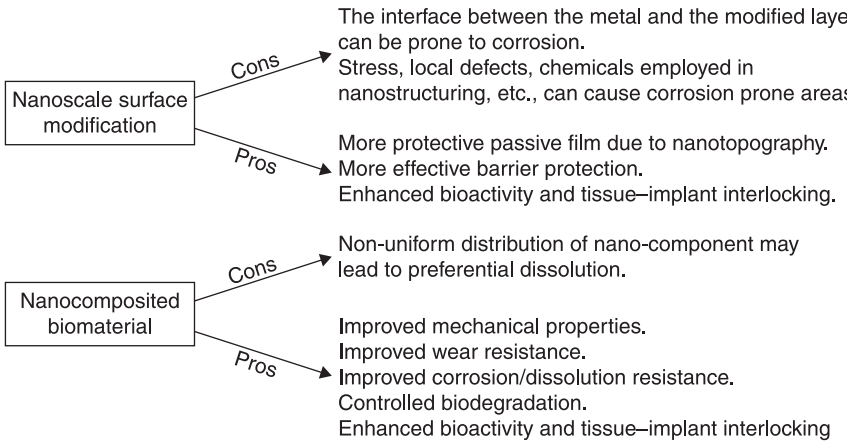

Nanostructured coatings (wear-resistant or bioactive coatings) in general improve the corrosion resistance. There exists considerable debate on nanotoxicity.

15.4 A diagram highlighting the expected pros and cons of modified biomaterials.

15.4 Nanoscale surface modifications and corrosion resistance

Significant progress has been made in the production of implants with suitable surface nanotopography (created by nanograins, pores, tubes, particles, ridges or valleys). There are diverse physical and chemical approaches investigated so far to create nanopatterning on implant surfaces, especially on titanium implants (Mendonca *et al.*, 2008). Typically applied chemical/physical approaches include acid etching, anodization, self-assembled monolayers, sputter coating, ion beam deposition, lithographic techniques, etc. In this direction, a few novel approaches such as a nanotubular oxide layer (Kubota *et al.*, 2004; Oh *et al.*, 2005; Macak *et al.*, 2007), nanoscale rod array (Liu *et al.*, 2008) and nanonodular self-assembly (Ogawa *et al.*, 2008) have been reported. Among them, nanotubular oxide layer formation through controlled anodization in a fluoride containing electrolytes is particularly promising for implant applications (Oh *et al.*, 2005). Self-ordered nanotubular layer formation can be achieved on different valve metals by optimized anodization; the method is economic and simple (Macak *et al.*, 2007).

Reported works concerning corrosion resistance of implants after nanoscale surface modifications are scanty. Depending upon the type of the implant material and the nature of modification, corrosion resistance of modified implants can be superior or inferior. For example, a thick anodized porous oxide layer improves

the general corrosion resistance of titanium alloys (Jakubowics, 2008). It has been shown that pulsed plasma electrolytic boriding can improve the corrosion resistance of titanium alloys (Aliev and Saboor, 2007). By suitable adjustment of the pulse frequency and duty cycle, the size and porosity of nanocrystalline borides (10 μm thickness layer) can be controlled and thereby superior corrosion resistance can be achieved. The overall corrosion resistance of such modified implants is determined by various parameters such as thickness of the modified layer, the interface between the implant and the modified layer, thickness of the barrier oxide layer on the implant after modification, permeability of the corrosive species through the modified layer, etc. Due to the complexity of the process, such modifications can lead to an inferior corrosion resistance. As an example, a brief discussion on the corrosion behaviour of titanium alloys after nanotubular oxide layer modification is provided below.

Recent studies have demonstrated that the corrosion resistance of titanium alloys after nanotubular oxide layer modification was inferior to that of the unmodified alloy (Saji *et al.*, 2009; Saji and Choe, 2009). Potentiodynamic polarization studies carried out at open circuit potential in Ringer's solution (9 g/l NaCl, 0.42 g/l KCl, 0.48 g/l $CaCl_2$ and 0.2 g/l $NaHCO_3$) at 37 ± 1°C showed that the corrosion current density (i_{corr} by Tafel extrapolation) of a nanotubular oxide layer coated Ti–13Nb–13Zr alloy was notably higher (18.9 μA.cm^{-2}) than that recorded for the bare alloy (1.77 μA.cm^{-2}). High i_{corr} indicates a lower corrosion resistance. The corresponding E_{corr} values were −870.58 mV_{SCE} and −608.69 mV_{SCE} for the nanotubular alloy and the bare alloy (Saji and Choe, 2009). The authors explored the interface (nanotubular oxide/barrier oxide) morphology (using focused ion beam miller/transmission electron microscopy) and suggested that the region is prone to earlier corrosion initiation. As a means to reduce the high dissolution current, various heat treatment conditions were investigated for the modified alloy. It was found that a low-temperature heat treatment (at 150°C) had noteworthy constructive impact on the corrosion behaviour and reduced the i_{corr} value considerably (2.04 μA.cm^{-2}). The corresponding potentiostatic plots recorded at 300 mV_{SCE} (a maximum potential analogous to a mouth environment) is shown in Fig. 15.5. The figure clearly demonstrates the variation of the current density with time for the three cases showing the effect of heat treatment (Saji and Choe, 2009). Being a complex phenomenon, such surface topography changes can have significant impact on the interfacial electrochemical behaviour. It is lucky that corrosion resistance can be improved and optimized by suitably controlling the modification parameters or by a post-modification strategy. It has been shown that a nanoporous anodized surface has more desirable corrosion resistance and surface passivation than an analogous nanotubular surface (Saji *et al.*, 2009). Detailed studies to evaluate the corrosion resistance of nanostructured biomaterials are crucial before any clinical application.

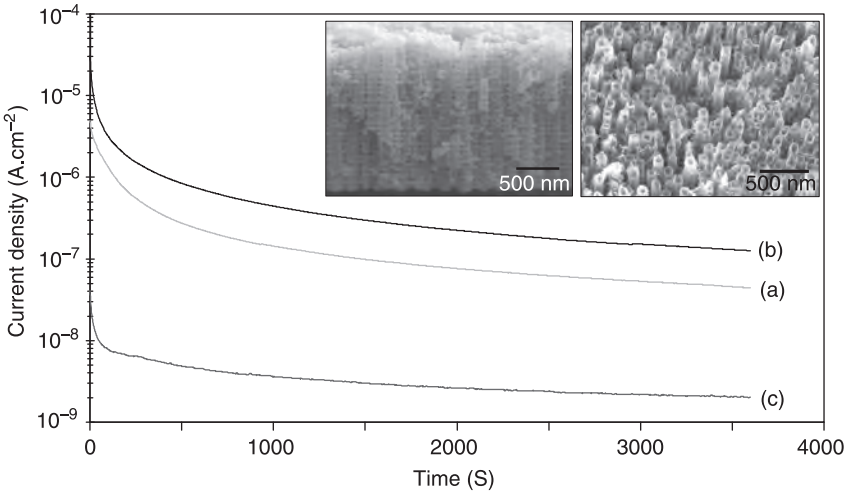

15.5 Potentiostatic polarization plots recorded at 300 mV for (a) bare titanium alloy, (b) nanotubular alloy and (c) nanotubular alloy after heat treatment at 150°C. The inset shows the lateral and surface appearances of the nanotubes formed on the alloy (Saji and Choe, 2009).

15.5 Nanostructured ceramic coatings

Nanoceramic coatings are attractive in terms of enhancement of mechanical properties and bioactivity. The most intensively investigated class among them is nano-HA coatings. Nanostructured metalloceramic coatings (Cr–Ti–N) are extensively investigated as they significantly enhance the wear and corrosion resistance. It is known that nanostructured surface coatings such as diamond and diamond-like coatings have extreme hardness, wear resistance and low friction. Such coatings increase the corrosion resistance of stainless steels and cobalt-based alloys (Catledge *et al.*, 2004; Saji *et al.*, 2007). This section mainly discusses the novel strategies in producing nano-HA coatings and their behaviour as a corrosion-resistant barrier.

Biomedical applications of HA, $Ca_{10}(PO_4)_6(OH)_2$, have been researched extensively due to its analogy to the inorganic component of natural bones and teeth (LeGeros, 2002; Kalita *et al.*, 2007). Although HA does not have the mechanical strength to enable it to succeed in load-bearing applications, implant materials such as stainless steels and titanium alloys are coated with HA for its high biocompatibility and good bio-affinity. HA coating not only increases the bone bioactivity of the metallic implants and facilitates bonding with the surrounding bone tissue, but also enhances the corrosion resistance. Coatings of HA on metal substrates have been widely studied for the past few decades;

however, nano-HA coatings have gained interest more recently because of their better biological properties compared with those of micro particles. A variety of coating methods, such as sol–gel, electrophoretic and electrolytic deposition, high-velocity oxy-fuel process, electrohydrodynamic spray deposition, ion implantation, cathodic arc plasma deposition, RF magnetron sputtering and pulse laser deposition, have been tried for achieving high performance nano-HA coatings.

The electrochemical deposition method is one of the cheapest and easiest methods of coating HA onto metallic materials. Another advantage of this method is the feasibility of coating complex structures. In regards to achieving corrosion resistance, a uniform coating is critical; otherwise localized corrosion such as crevices could potentially occur. Hu *et al.* prepared a novel porous nano-HA coating on CP-Ti by a modified electrochemical deposition method (Fig. 15.6). The micrographs of the coating show a uniform microporous morphology consisting of wire-like crystals at the nanometre scale. They observed that, under controlled deposition conditions, the primary HA nanowires grow and self-assemble to construct an ordered microporous nest-like morphology. Their *in vitro* studies indicated excellent biocompatibility and bioactivity for the nano-HA coating (Hu *et al.*, 2010).

Narayanan *et al.* electrochemically coated nanograined calcium phosphate on Ti–6Al–4V alloy using aqueous electrolyte maintained at acidic pH. They reported that an ultrasonic bath produced coatings containing dicalcium phosphate dehydrate and the grain sizes were in the range of 50–100 nm (Narayanan *et al.*, 2007). Lobo *et al.* (2011) developed a nano-HA crystalline film on Ni–Ti shape memory alloy by the electrodeposition method. It was reported that the nano-HA film was homogeneous and highly crystalline and possessed bioactivity properties.

Recently, Hu *et al.* produced nano-HA on titanium (sandblasted and acid etched) by hydrothermally treating the material in a simple suspension of HA.

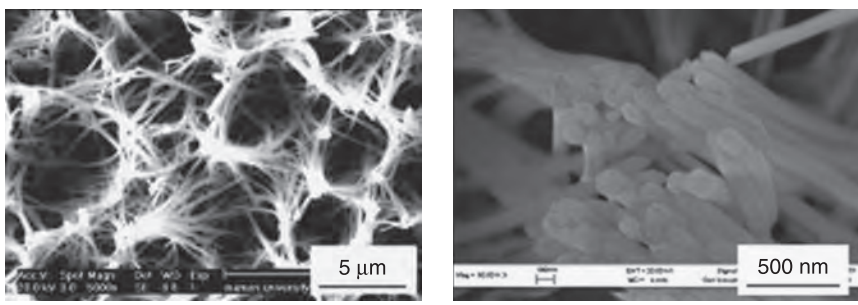

(a) (b)

15.6 SEM micrographs of the electrochemically deposited calcium phosphate coating: (a) microporous structure, (b) nanometre-scale crystal grains (Hu *et al.*, 2007).

The increase in hydrothermal treatment temperature and time enhanced the formation of nano-HA. The bonding strength of the nano-HA coating formed by hydrothermal treatment was higher than that of a HA coating generated directly by HA suspension deposition. *In vitro* testing showed a more favourable cell attachment for a nano-HA coating formed by hydrothermal treatment than for the directly generated HA suspension coating (Hu *et al.*, 2010). Xiong *et al.* also produced nano-HA coating on a titanium–niobium (Ti–Nb) alloy substrate using a hydrothermal coating process. It was reported that, during the hydrothermal process, TiO_2 and Nb_2O_5 formed on the Ti–Nb alloy surface and hydrated to $Ti(OH)_4$ and $Nb(OH)_5$, respectively, and calcium phosphate nucleated and grew into a layer of nano-HA particles on the surface of Ti–Nb alloy under the hydrothermal conditions. They found that the crystallinity of the nano-HA coating was improved with the increase in hydrothermal treatment temperature and coating time (Xiong *et al.*, 2010). Nanocrystalline fluoridated HA (FA) powders and coatings with a chemical composition of $Ca_{10}(PO_4)_6OH_2$–xF_x (where x values were selected equal to 0.0, 0.5, 1.0, 1.5 and 2.0) were prepared by Zahrani *et al.* (2010) through a modified simple sol–gel technique. TEM analysis revealed that FA powder was composed of nanosized particles, ~25 nm in size.

Great effort is being undertaken in producing different HA-based composite coatings. Kaya *et al.* coated Ti6Al4V alloy with carbon nanotube (CNTs)-reinforced HA employing electrophoretic deposition (EPD) and found that the addition of CNTs increased the bonding strength of the EPD formed layers to the metallic substrate (Kaya *et al.*, 2008). Kwok *et al.* (2009) reported that a CNTs-reinforced HA coating exhibited increased coating hardness without compromise in the adhesion strength as compared with a monolithic HA coating. Importantly, the corrosion current was lower, suggesting better corrosion protection for the CNTs-reinforced HA coating as compared with the other coatings.

15.6 Resorbable biomaterials: nanoscale approaches

Metallic materials such as stainless steels, Ti and Co–Cr based alloys are currently used as permanent implant materials. These alloys are also used for temporary implant applications in the form of plates, screws and pins, for the repair of bone fracture. However, these metal implants have to be removed by a second surgical procedure after the tissues have healed sufficiently, since they pose a risk of releasing toxic metallic ions and/or particles through corrosion or wear processes. The second surgical procedure adds to the cost and burden to the patients. Identification of implants to support tissue regeneration and healing in specific applications by material corrosion and simultaneous implant replacement by the surrounding tissues is an important area of research.

Magnesium (Mg) is a potential material for temporary/resorbable bio-implant applications because Mg corrodes in the physiological environment and the

corrosion product is non-toxic and soluble in body fluid (Staiger *et al.*, 2006). However, the major problem in the application of Mg for temporary bio-implant applications is the corrosion rate. Pure Mg corrodes too quickly in the pH level (7.4–7.6) and high chloride level of the physiological environment. The extremely high corrosion rate of Mg in body fluid not only dissolves the implant before the tissues sufficiently heal, but it also creates hydrogen (a cathodic reaction) gas pockets which potentially affect the healing process (Witte *et al.*, 2008).

In recent years, a number of Mg alloys have been tested under *in vitro* and *in vivo* conditions to understand their corrosion behaviour and mechanisms (Witte *et al.* 2006; Kannan and Raman, 2008, 2010; Kannan, 2010; Walter and Kannan, 2011). AZ series alloys show a lower corrosion current than that of pure Mg. However, aluminium-containing Mg alloys may not be the ultimate choice, simply because of the potentially toxic effects of high aluminium levels in body fluid. The influence on corrosion properties of calcium and rare-earth elements added to Mg and its alloys has been investigated, but the improvement was not significant.

The low solubility of HA and its high osteoconductivity make it a very attractive material for coating on Mg alloys. Wen *et al.* deposited a bone-like nanowhisker HA coating on AZ31 by an electrochemical deposition method (Fig. 15.7). The as-deposited HA coating exhibited plate-like particles arranged in a flower pattern on the substrate. These particles contained calcium phosphates, whereas the post-treated coating was HA doped with Na^+, Mg^+, HPO_4^{2-} and CO_3^{2-}, presenting needle-like particles of 1000 nm in length and 35 nm in diameter. They also found that the E_{corr} of the substrate shifted by 180 mV towards the noble direction in simulated body fluid after treatment and hence suggested that the coating could protect the substrate effectively (Wen *et al.*, 2009).

Razavi *et al.* (2010) evaluated the effect of fluoroapatite (FA) nanoparticle content on the microstructure, mechanical properties and bio-corrosion behaviour of a nanocomposite made of AZ91 Mg alloy as matrix, and FA nanoparticles as

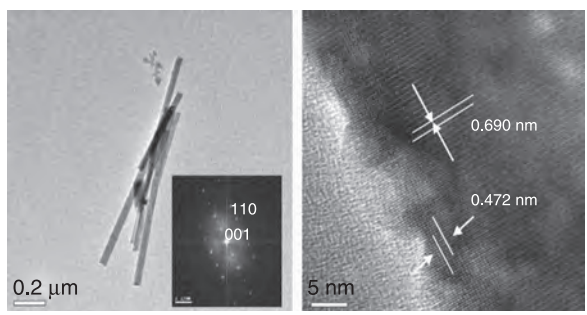

15.7 TEM images of nanowhisker HA particles on AZ31 alloy (Wen *et al.*, 2009).

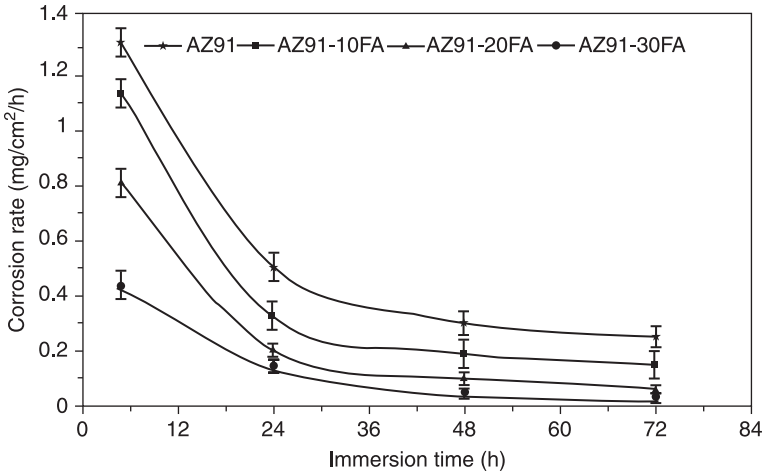

15.8 Corrosion rate of immersed AZ91 Mg alloy and AZ91-FA nanocomposites in simulated body fluid as a function of immersion time (Razavi *et al.*, 2010).

reinforcement, for load-bearing applications. They produced the nanocomposites (with 10 wt%, 20 wt% and 30 wt% of FA) by mixing AZ91 Mg alloy powders and FA nanoparticles using a blend press-sinter powder metallurgy method. The presence of FA nanoparticles in the Mg alloy matrix not only led to significant improvement in hardness and elastic modulus but also increased the corrosion resistance. An AZ91-FA nanocomposite with 20 wt% of the FA nanoparticles showed optimum mechanical properties as well as corrosion resistance (Fig. 15.8).

Meng *et al.* reported that fluorine-doped nano-HA coating on Mg–Zn–Ca alloy by pulse electrodeposition was dense and uniform than the conventional electrodeposition method. The potentiodynamic polarization experiment indicated that pulse electrodeposited coating effectively protects the material from corrosion (Fig. 15.9). They also found that pulse electrodeposition coating induces precipitation of Mg^{2+}, Ca^{2+} and PO_4^{3-} more effectively in comparison with conventional electrodeposition coating, because the nanophase had comparatively high specific surface area (Meng *et al.*, 2011).

Gao *et al.* used micro-arc oxidation to fabricate a porous coating on Mg–Zn–Ca alloy, and then electrochemical deposition of rod-like nano-HA on the porous coating. Atomic force microscopy observation of the composite coatings showed that the diameters of HA rods varied from 95 nm to 116 nm. Interestingly, the bonding strength between the HA–film and micro-arc oxidation coating increased almost two times higher than that of the direct electrochemical deposition coating. The corrosion current density of the alloy decreased significantly when the porous structure was coated with nano-HA (Fig. 15.10)

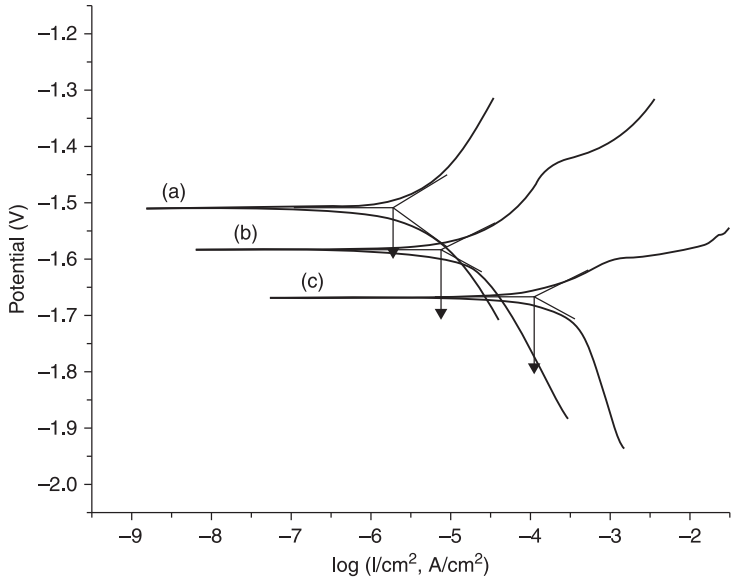

15.9 Polarization curves in simulated body fluid of (a) pulse-electrodeposition, (b) traditional electrodeposition and (c) bare Mg alloy (Meng *et al.*, 2011).

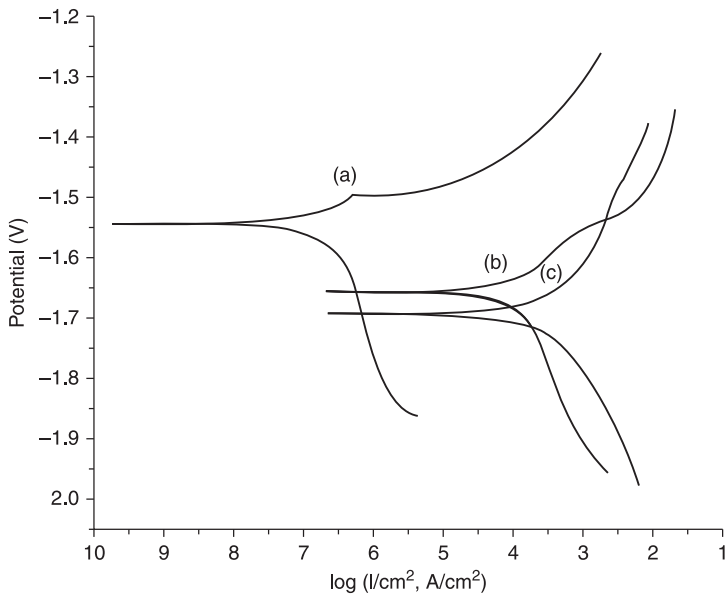

15.10 Polarization curves of coated and bare Mg–Zn–Ca alloy in simulated body fluid: (a) micro-arc oxidation coating and rod-like nano-HA deposition, (b) micro-arc oxidation coating and (c) bare alloy (Gao *et al.*, 2011).

and that has been attributed this to the enhancement of bonding strength and rod-like nano-HA. The rod-like nano-HA induced a rapid precipitation of calcium orthophosphates in comparison with conventional HA coatings (Gao *et al.*, 2011).

15.7 Conclusions

Currently, widespread investigations are being made into producing nanostructured bulk materials and nanostructured surface modifications on metallic implants for orthopaedics and dental applications. Nanostructured diamond and metalloceramic coatings are well known as wear and corrosion resistance coatings. While bioactive nanostructured hydroxyapatite coatings have constructive impact on the general corrosion resistance, a recent report on nanotubular oxide layer formation on titanium-based alloys was found to have a negative impact on the overall corrosion resistance. Fortunately, heat-treatment procedures can tailor the corrosion performance of the nanotubular oxide layer coated titanium alloys. Bulk nanocomposites (e.g. titanium–ceramic nanocomposites) and nanocomposite coatings are the current focus areas. Nanohydroxyapatite coatings on magnesium alloys are promising for their potential applications in biodegradable implant applications. Corrosion resistance assessment is critical before clinical application of any such nanostructured biomaterials.

15.8 References

Aliev, M. Kh. and Saboor, A. (2007), 'Pulsed nanocrystalline plasma electrolytic boriding as a novel method for corrosion protection of CP-Ti', *Bulletin of Materials Science*, **30**, 601–5.

Azar, V., Hashemi, B. and Yazdi, M. R. (2010), 'The effect of shot peening on fatigue and corrosion behaviour of 316L stainless steel in Ringer's solution', *Surface and Coatings Technology*, **204**, 3546–51.

Azevedo, C. R. F. (2003), 'Failure analysis of a commercially pure titanium plate for osteosynthesis', *Engineering Failure Analysis*, **10**, 153–64.

Bobby Kannan, M. and Singh Raman, R. K. (2008), 'In vitro degradation and mechanical integrity of calcium-containing magnesium alloys in modified-simulated body fluid', *Biomaterials*, **29**, 2306–14.

Bobby Kannan, M. (2010), 'Influence of microstructure on the in-vitro degradation behaviour of magnesium alloy', *Materials Letters*, **64**, 739–42.

Bobby Kannan, M. and Singh Raman, R. K. (2010), 'A mechanistic study on in vitro degradation of magnesium alloy using electrochemical techniques', *Journal of Biomedical Materials, Research Part A*, **93A**, 1050–5.

Catledge, S. A., Fries, M. and Vohra, Y. K. (2004), 'Nanostructured surface modifications for biomedical implants', in Nalwa, H. S. (Ed.) *Encyclopedia of Nanoscience and Nanotechnology*. California: American Scientific Publishers, pp. 741–62.

Gao, J. H., Guan, S. K., Chen, J., Wang, L. G., Zhu, S. J. *et al.* (2011), 'Fabrication and characterization of rod-like nano-hydroxyapatite on MAO coating supported on Mg-Zn-Ca alloy', *Applied Surface Science*, **257**, 2231–7.

Giordani, E. J., Guimaraes, V. A., Pinto, T. B. and Ferreira, I. (2004), 'Effect of precipitates on the corrosion–fatigue crack initiation of ISO 5832-9 stainless steel biomaterial', *International Journal of Fatigue*, **26**, 1129–36.

Hu, R., Lin, C. J. and Shi, H. Y. (2007), 'A novel ordered nano hydroxyapatite coating electrochemically deposited on titanium substrate', *Journal of Biomedical Materials Research Part A*, **80A**, 687–92.

Hu, X., Shen, H., Cheng, Y., Xiong, X., Wang, S. *et al.* (2010), 'One-step modification of nano-hydroxyapatite coating on titanium surface by hydrothermal method', *Surface and Coatings Technology*, **205**, 2000–6.

Jager, M., Zilkens, C., Zanger, K. and Krauspe, R. (2007), 'Significance of nano- and microtopography for cell-surface interactions in orthopaedic implants', *Journal of Biomedicine and Biotechnology*, 1–19.

Jakubowics, J. (2008), 'Formation of porous TiO*x* biomaterials in H_3PO4 electrolytes', *Electrochemistry Communications*, **10**, 735–9.

Kalita, S. J., Bhardwaj, A. and Bhatt, H. A. (2007), 'Nanocrystalline calcium phosphate ceramics in biomedical engineering', *Materials Science and Engineering C*, **27**, 441–9.

Karlsson, M., Palsgard, E. P., Wilshawb, P. R. and Di Silvio, L. (2003), 'Initial in vitro interaction of osteoblasts with nano-porous alumina', *Biomaterials*, **24**, 3039–46.

Kaya, C., Singh, I. and Boccaccini, A. R. (2008), 'Multi-walled carbon nanotube-reinforced hydroxyapatite layers on Ti6Al4V medical implants by electrophoretic deposition', *Advanced Engineering Materials*, **10**, 131–8.

Khan, M. A., Williams, R. L. and Williams, D. F. (1999), 'The corrosion behaviour of Ti-6Al-4V, Ti-6Al-7Nb and Ti-13Nb-13Zr in protein solutions', *Biomaterials*, **20**, 631–7.

Kubota, S., Johkura, K., Asanuma, K., Okouchi, Y., Ogiwara, N. *et al.* (2004), 'Titanium oxide nanotubes for bone regeneration', *Journal of Materials Science. Materials in Medicine*, **15**, 1031–5.

Kumar, S. and Sankara Narayanan, T. S. N. (2008), 'Corrosion behaviour of Ti-15Mo alloy for dental implant applications', *Journal of Dentistry*, **36**, 500–7.

Kwok, C. T., Wong, P. K., Cheng, F. T. and Man, H. C. (2009), 'Characterization and corrosion behaviour of hydroxyapatite coatings on Ti6Al4V fabricated by electrophoretic deposition', *Applied Surface Science*, **255**, 6736–44.

LeGeros, R. Z. (2002), 'Properties of osteoconductive biomaterials: calcium phosphates', *Clinical Orthopaedics and Related Research*, **395**, 81–98.

Li, X., Wang, J., Han, E. H. and Ke, W. (2007), 'Influence of fluoride and chloride on corrosion behaviour of NiTi orthodontic wires', *Acta Biomaterialia*, **3**, 807–15.

Liu, Y., Chen, W., Yang, Y., Ong, J. L., Tsuru, K. *et al.* (2008), 'Novel fabrication of nano-rod array structures on titanium and in vitro cell responses', *Journal of Materials Science. Materials in medicine*, **19**, 2735–41.

Lobo, A. O., Otubo, J., Matsushima, J. T. and Corat, E. J. (2011), 'Rapid obtaining of nano-hydroxyapatite bioactive films on NiTi shape memory alloy by electrodeposition process', *Journal of Materials Engineering and Performance*, **20**, 793–7.

Macak, J. M., Tsuchiya, H., Ghicov, A., Yasuda, K., Hahn, R. *et al.* (2007), 'TiO_2 nanotubes: self-organized electrochemical formation, properties and applications', *Current Opinion in Solid State and Materials Science*, **11**, 3–18.

Mareci, D., Chelariu, R., Gordin, D. M., Ungureanu, G. and Gloriant, T. (2009), 'Comparative corrosion study of Ti–Ta alloys for dental applications', *Acta Biomaterialia*, **5**, 3625–39.

Mendonca, G., Mendonca, D. B. S., Aragao, F. J. L. and Cooper, F. L. (2008), 'Advancing dental implant surface technology-From micron to nanotopography', *Biomaterials*, **29**, 3822–35.

Meng, E. C., Guan, S. K., Wang, H. X., Wang, L. G., Zhu, S. H. *et al.* (2011), 'Effect of electrodeposition modes on surface characteristics and corrosion properties of fluorine-doped hydroxyapatite coatings on Mg-Zn-Ca alloy', *Applied Surface Science*, **257**, 4811–16.

Narayanan, R., Seshadri, S. K., Kwon, T. Y. and Kim, K. H. (2007), 'Electrochemical nano-grained calcium phosphate coatings on Ti-6Al-4V for biomaterial applications', *Scripta Materialia*, **56**, 229–32.

Ogawa, T., Saruwatari, L., Takeuchi, K., Aita, H. and Ohno, N. (2008), 'Ti nano-nodular structuring for bone integration and regeneration', *Journal of Dental Research*, **87**, 751–6.

Oh, S. H., Finones, R. R., Daraio, C., Chen, L. H. and Jin, S. (2005), 'Growth of nanoscale hydroxyapatite using chemically treated titanium oxide nanotube', *Biomaterials*, **26**, 4938–43.

Olmedo, D. G., Duffo, G., Cabrini, R. L. and Guglielmotti, M. B. (2008), 'Local effect of titanium implant corrosion: an experimental study in rats', *International Journal of Oral and Maxillofacial Surgery*, **37**, 1032–8.

Park, J. B. and Bronzino, J. D. (2003), *Biomaterials – Principles and applications*. Florida: CRC Press.

Razavi, M., Fathi, M. H. and Meratian, M. (2010), 'Microstructure, mechanical properties and bio-corrosion evaluation of biodegradable AZ91-FA nanocomposites for biomedical applications', *Materials Science and Engineering A*, **527**, 6938–44.

Reclaru, L., Lerf, R., Eschler, P. Y. and Meyer, J. M. (2001), 'Corrosion behaviour of a welded stainless-steel orthopaedic implant', *Biomaterials*, **22**, 269–79.

Richert, L., Vetrone, F., Yi, J. H., Zalzal, S. F., Wuest, J. D. *et al.* (2008), 'Surface nanopatterning to control cell growth', *Advanced Materials*, **20**, 1488–92.

Saji, V. S. and Thomas, J. (2007), 'Nanomaterials for corrosion control', *Current Science*, **92**, 51–5.

Saji, V. S. and Choe, H. C. (2009), 'Electrochemical corrosion behaviour of nanotubular Ti-13Nb-13Zr alloy in Ringer's solution', *Corrosion Science*, **51**, 1658–63.

Saji, V. S., Choe, H. C. and Brantley, W. A. (2009), 'An electrochemical study on nanoporous and nanotubular Ti-35Nb-5Ta-7Zr alloy for biomedical applications', *Acta Biomaterialia*, **5**, 2303–10.

Saji, V. S., Choe, H. C. and Yeung, K. W. K. (2010), 'Nanotechnology in biomedical applications – a review', *International Journal of Nano and Biomaterials*, **3**, 119–39.

Sivakumar, B., Kumar, S. and Sankara Narayanan, T. S. N. (2011), 'Fretting corrosion behaviour of Ti-6Al-4V alloy in artificial saliva containing varying concentrations of fluoride ions', *Wear*, **270**, 317–24.

Staiger, M. P., Pietak, A. M., Huadmai, J. and Dias, G. (2006), 'Magnesium and its alloys as orthopaedic biomaterials: A review', *Biomaterials*, **27**, 1728–34.

Walter, F. and Bobby Kannan, M. (2011), 'In-vitro degradation behaviour of WE54 magnesium alloy in simulated body fluid', *Materials Letters*, **65**, 748–50.

Wen, C., Guan, S., Peng, L., Ren, C., Wang, X. *et al.* (2009), 'Characterization and degradation behaviour of AZ31 alloy surface modified by bone-like hydroxyapatite for implant applications', *Applied Surface Science*, **255**, 6433–8.

Williams, D. F. (1987), *Definition of Biomaterials*, Amsterdam: Elsevier.

Witte, F., Fischer, J., Nellesen, J., Crostack, H. A., Kaese, V. *et al.* (2006), 'In vitro and in vivo corrosion measurements of Mg alloys', *Biomaterials*, **27**, 1013–18.

Witte, F., Hort, N., Vogt, C., Cohen, S., Kainerc, K. U. *et al.* (2008), 'Degradable biomaterials based on magnesium corrosion', *Current Opinion in Solid State and Materials Science*, **12**, 63–72.

Xiong, J., Li, Y., Hodgson, P. D. and Wen, C. (2010), 'Nanohydroxyapatite coating on a titanium-niobium alloy by a hydrothermal process', *Acta Biomaterialia*, **6**, 1584–90.

Yan, Y., Neville, A. and Dowson, D. (2007), 'Biotribocorrosion of CoCrMo orthopaedic implant materials – Assessing the formation and effect of the biofilm', *Tribology International*, **40**, 1492–9.

Zahrani, E. M., Fathi, M. H. and Alfantazi, A. M. (2011), 'Sol-gel derived nanocrystalline fluoridated hydroxyapatite powders and nanostructured coatings for tissue engineering applications', *Metallurgical and Materials Transactions A*, **42**, 3291–309.

Index